EUROPEAN ATOMIC ENERGY COMMUNITY — EURATOM

ISPRA NUCLEAR ELECTRONICS SYMPOSIUM

May 6-9, 1969

EUROPEAN ATOMIC ENERGY COMMUNITY — EURATOM

ISPRA NUCLEAR ELECTRONICS SYMPOSIUM

May 6-9, 1969

Europäische Atomgemeinschaft
Communauté Européenne de l'Energie Atomique
Comunità Europea dell'Energia Atomica
Europese Gemeenschap voor Atoomenergie
European Atomic Energy Community

EURATOM

Sitzungsberichte | Actes officiels
Atti ufficiali | Handelingen
Proceedings

ISPRA NUCLEAR ELECTRONICS SYMPOSIUM

6-9.5.1969

1969

Veröffentlich von der Kommission
der Europäischen Gemeinschaften
Generaldirektion Verbreitung
der Kenntnisse
Zentralstelle für Information
und Dokumentation - CID

Publié par la Commission
des Communautés Européennes
Direction générale
Diffusion des Connaissances
Centre d'Information et de
Documentation - C.I.D.

Pubblicato dalla Commissione
della Comunità Europee
Direzione generale
Diffusione delle Conoscenze
Centro d'Informazione e di
Documentazione - C.I.D.

Gepubliceerd door de Commissie
van de Europese Gemeenschappen
Directoraat-generaal
Verspreiding van Kennis
Centrum voor Informatie en
Documentatie - CID

Published by the Commission of the European Communities
Directorate-General for Dissemination of Information
Centre for Information and Documentation - CID
Brussels, June 1969.

ISPRA NUCLEAR ELECTRONICS SYMPOSIUM

Organisiert unter Forderung von Organisé sous les auspices de Organizzato sotto gli auspici di Opgesteld onder auspiciën van Organized under the sponsorship of	IEEE	North Italy Section
	IEEE	Nuclear Science Group
	CNR	Consiglio Nazionale delle Ricerche
	CNEN	Consiglio Nazionale per l'Energia Nucleare
	AEI	Associazione Elettrotecnica ed Elettronica Italiana
	SIF	Società Italiana di Fisica

Ausschuß für die Auswahl der Artikel
Comité de Sélection des Articles
Comitato di Selezione degli Articoli
Keuzecomité van de Artikelen
Paper Selection Committee

E. Gatti, Chairman — E. Baldinger — R.L. Chase — K. Kandiah — J. Pottier — B. Souček and L. Stanchi.

Price : DM 48 FB 600 FF 60
Lit. 7 500 Fl. 43,50 $ 12

EUR 4289 e

Foreword

High level scientists and engineers met at Stresa to attend the Ispra Nuclear Electronics Symposium. This International Symposium was organized by the Euratom Joint Nuclear Research Center of Ispra and sponsored by the Institute of Electrical and Electronics Engineers (North Italy Section and Nuclear Science Group). Co-sponsors were four Italian Institutes: CNR (Consiglio Nazionale delle Ricerche), CNEN (Comitato Nazionale per l'Energia Nucleare), AEI (Associazione Elettrotecnica ed Elettronica Italiana), SIF (Società Italiana di Fisica).

Outstanding papers were presented and I wish to thank all the authors for their contributions. The complete manuscripts of three among the papers announced, were not presented for various reasons. I would apologize to the reader for the fact that he has found only summaries. The accepted papers were carefully selected by an international committee and I think that the choice was well made indeed. Naturally the choice based on summaries can lead to improper results and perhaps some rejected paper deserved better attention. In addition several papers arrived after the selection was made and had no possibility to be accepted. There are some minor variations in the program due to the fact that some people invited, only sent their acceptance after the program had been printed.

The Symposium had originally been planned to last for three days, but it became opportune to add a fourth day to the program, in order to deal with the subject of modular instrumentation with particular emphasis on the new CAMAC standard. From this the title of the CAMAC-day was derived. A panel discussion on future trends had already been scheduled for that same day at Ispra. I must therefore once more apologize for some misunderstanding caused by this, and explain that the panel discussion was quite independent of the Symposium. This latter ran up to the fourth day as foreseen by the program.

I wish to thank all the people who contributed to the organization as well as the many participants who wished amiably to congratulate me on the success of the Symposium.

L. STANCHI

Préface

Des savants et ingénieurs hautement qualifiés se retrouvaient à Stresa pour partioiper au Congrès "Ispra Nuclear Electronios Symposium". Cette manifestation était organisée par le Centre Commun de Recherche Nucléaire de Ispra sous l'égide par l'IEEE(Institute of Electrical and Electronics Engineers) et ses deux sections (North Italy Section et Nuclear Science Group) avec le concours de quatre instituts italiens: CNR (Consiglio Nazionale delle Ricerche), CNEN (Comitato Nazionale per l'Energia Nucleare), AEI (Associazione Elettrotecnioa ed Elettronica Italiana), SIF (Società Italiana di Fisica).

Des communications de grand intérêt étaient présentées et je désire en remercier tous les auteurs. Pour différentes raisons trois manuscrits prévus au programme n'étaient pas présentés; aussi je prie le lecteur de m'excuser s'il n'en trouve que les résumés.
Les articles furent soigneusement sélectionnés par un comité international et je pense que le choix fut réellement judicieux. Evidemment, étant basé sur des résumés, il aura pu être un peu arbitraire et des articles rejetés auraient sans doute mérité d'être mieux considérés. Par ailleurs plusieurs résumés sont arrivés en retard et n'ont pu malheureusement être acceptés. Quelques invités ayant répondu affirmativement seulement après l'impression du programme, il y eut quelques modifications dans son ordonnancement.

Le Symposium était prévu à l'origine pour trois jours, mais il parut opportun de le prolonger d'une journée pour traiter le problème de la standardisation des appareillages et tout particulièrement du système modulaire CAMAC. C'est ainsi que naquit le "CAMAC-day". Une table ronde sur les perspeotives futures avait déjà été organisée à Ispra pour le même jour. Je voudrais m'excuser encore une fois pour les quelques malentendus qui ont surgi à ce propos et souligner que cette table ronde était indépendante du congrès lui-même, qui s'est poursuivi jusqu'au quatrième jour comme prévu.

Je désire remercier toutes les personnes qui ont participé à l'organisation de ce congrès ainsi que les participants qui ont eu l'obligeance de me féliciter pour le succès de ce Symposium.

L. STANCHI

Vorwort

Im Mai 1969 fand in Stresa das "Ispra Nuclear Electronics Symposium" statt, zu dem sich nahmhafte und qualifizierte Wissenschaftler und Ingenieure zusammenfanden. Organisator des Treffens war das Forschungszentrum Ispra der Europäischen Atomgemeinschaft und das Institute of Electrical and Electronics Engineers (North Italy Section and Nuclear Science Group) unter Patenschaft von vier italienischen Instituten: CNR (Consiglio Nazionale delle Ricerche), CNEN (Comitato Nazionale per l'Energia Nucleare), AEI (Associazione Elettrotecnica ed Elettronica Italiana), SIF (Società Italiana di Fisica).

Ich möchte allen Referenten und Autoren für ihre Beiträge danken. Alle präsentierten Manuskripte sind im Nachfolgenden abgedruckt. Allerdings fehlen - aus unterschiedlichen Gründen - drei der angekündigten Referate. Ich bedauere sehr den Umstand, dass von ihnen nur Zusammenfassungen gegeben werden können.

Die gehaltenen Referate bzw. veröffentlichten Manuskripte wurden sorgfältig von einem internationalen Programmausschuss ausgewählt und ich glaube, dass die Auswahl gut war. Es ist allerdings möglich, dass angebotene Beiträge zu Unrecht zurückgewiesen wurden, da als Beurteilungsgrundlage nur jeweils die Zusammenfassung des Referates diente. Eine Reihe von Beiträgen musste zurückgewiesen werden, da sie zu spät - erst nach Beginn der Auswahlprozedur - eintrafen.

Ursprünglich war das Symposium für eine Dauer von drei Tagen geplant. Es wurde aber dann ein vierter Tag hinzugenommen, der der Information und den Problemen von Funktions- und Baugruppen elektronischer Instrumentierungen (modular instrumentation) gewidmet war. Besonderer Nachdruck wurde hierbei auf das neue CAMAC-System gelegt, weshalb dieser Tag auch als CAMAC-day bezeichnet wurde. Eine Paneldiskussion über zukünftige Entwicklungsrichtungen war am gleichen Tag in Ispra vorgesehen. Ich möchte mich noch einmal entschuldigen für einige Missverständnisse, die dieser Umstand verursachte; diese Diskussion war völlig unabhängig vom Symposium, das am vierten Tag wie im Programm vorgesehen ablief.

Ich möchte allen denen danken, die die Organisation des Treffens besorgten, sowie auch den vielen Teilnehmern, die mich freundlicherweise zum Erfolg des Symposiums beglückwünschten.

L. STANCHI

Prefazione

Scienziati e tecnici di alto livello convennero a Stresa per partecipare al Congresso "Ispra Nuolear Electronics Symposium". Questo congresso internazionale organizzato dal Centrò Comune di Ricerohe Nucleari di Ispra era patrocinato dall'IEEE (Institute of Electrical and Electronics Engineers) con le sue due ramificazioni: la sezione Nord Italia e il gruppo "Nuclear Science". Patrocinatori associati erano quattro istituzioni italiane: CNR (Consiglio Nazionale delle Ricerche), CNEN (Comitato Nazionale per l'Ensrgia Nucleare), AEI (Associazione Elettrotecnica ed Elettronica Italiana), SIF (Società Italiana di Fisica).

Articoli di elevato valore sono stati presentati ed io desidero pertanto ringraziare tutti gli autori per le loro contribuzioni. I manoscritti oompleti di tre fra gli articoli annunciati non sono stati presentati per differenti ragioni. Vorrei scusarmi ool lettore per il fatto che troverà solo i riassunti. Gli articoli aocettati furono selezionati accuratamente da un comitato internazionale. Ed io penso che la scelta fu fatta in effetti molto bene. Naturalmente, la scelta basata su sommari, può portare a risultati imperfetti e forse qualche articolo respinto meritava una migliore attenzione. Inoltre parecchi articoli pervennero dopo la selezione e non ebbero la poseibilità di essere aocettati.

Il congresso era stato previsto originariamente per tre giorni ma si trovò opportuno aggiungere un quarto giorno al programma, dedicato alla strumentazione modulare con particolare enfasi al nuovo standard CAMAC. Da ciò fu derivato il titolo "CAMAC-day". Una discussione ad invito sulle tendenze future era stata già programmata per questo stesso giorno a Ispra. Vorrei ancora scusarmi per qualche incomprensione causata da questo motivo e spiegare che la discussione era indipendente dal congresso. Quest'ultimo ha prooeduto sino al quarto giorno oome previsto dal programma.

Vorrei ringraziare tutte le persone che contribuirono all'organizzazione e tutte le persone che ebbero l'amabilità di congratularsi con me per il successo della manifestazione.

L. STANCHI

Voorwoord

Wetenschapsmensen en technici kwamen in Stresa bijeen teneinde het "Ispra Nuclear Electronics Symposium" bij te wonen. Dit internationale Symposium werd georganiseerd door het Gemeenschappelijk Centrum voor Atoomonderzoek van Euratom te Ispra en stond onder auspicien van het "Institute of Electrioal and Electronics Engineers (North Italy Section and Nuolear Soience Group) met medewerking van vier Italiaanse instituten, te weten: CNR (Consiglio Nazionale delle Ricerche), CNEN (Comitato Nazionale per l'Energia Nucleare), AEI (Associazione Elettrotecnica ed Elettronica Italiana), SIF (Società Italiana di Fisica).

Interessante artikelen werden gepresenteerd en ik dank alle schrijvers voor hun medewerking. De complete teksten van drie der aangekondigde artikelen werden om verschillende redenen niet gepresenteerd. De lezer excusere mij, dat hij alleen samenvattingen aantreft. De geaccepteerde artikelen werden door een internationaal comité geselecteerd en ik meen, dat de keuze een goede is geweest. Het is duidelijk, dat een selectie, welke is gebaseerd op samenvattingen, tot onjuiste resultaten kan leiden en misschien hadden enkele afgewezen artikelen een betere aandacht verdiend. Bovendien kwamen meerdere artikelen binnen, nadat de keuze reeds gemaakt was en deze konden daardoor niet meer geaccepteerd worden. Het programma onderging enkele kleine wijzigingen omdat enige genodigden hun bevestiging inzonden nadat het programma reeds gedrukt was.

Oorspronkelijk was vastgesteld, dat het Symposium drie dagen zou duren, maar het bleek nuttig een vierde dag aan het programma toe te voegen, teneinde ook het onderwerp gestandaardiseerde apparatuur en in het bijzonder de nieuwe 'CAMAC-standard" te kunnen behandelen. Een bespreking te Ispra, onder speciaal hiervoor uitgenodigde personen, over toekomstige ontwikkelingen was voor dezelfde dag reeds vastgesteld. De lezer verzoek ik mij te willen verontschuldigen voor enkele misverstanden, welke hierdoor zijn ontstaan, doch deze bespreking was volledig onafhankelijk van het Symposium. Deze laatste viel samen met de vierde dag, zoals voorzien was in het programma.

Ik dank alle personen, die medewerkten aan de organisatie en eveneens de vele deelnemers, die mij gelukwensten met het sucoes van het Symposium.

L. STANCHI

PAPERS PRESENTED AT THE
ISPRA NUCLEAR ELECTRONICS SYMPOSIUM

SESSION 1: AMPLIFICATION AND ANALOG SIGNAL PROCESSING

CHAIRMAN : K. KANDIAH

1/f Noise in Physical Measurements.
V. Radeka (invited paper) 1

FET Preamplifiers for Semiconductor Radiation Detectors.
E. Elad 21

The Development of "n" Channel FET's for Low Noise Nuclear Pulse Amplifiers.
J.H. Howes 35

Realization of Optimum Pulse Shaping Filter.
M. Oda 43

Minimum-Noise Filters with Good Low-Frequency Rejection.
M.O. Deighton 47

Mismatch Oriented Circuit Design and its Application to Nuclear Electronics.
A.F. Arbel 55

Signal Shaping, Transformation and Generation, Using Basing Elements of Analog and Digital Computers.
K. Čuljat, B. Souček, V. Bonačić, B. Matić 67

Maximum Loop Gain of Feedback Amplifiers with Monotonic Step Response.
H. Babić 73

An Operational Pulse Amplifier with FET-Input.
R. Patzelt, R. Posch 81

Design of a Wideband Pulse Amplifier with Linear Circuit μA 702A Using Frequency Compensation Technique.
N. P. Lero, P.B. Frantlović 85

SESSION 2: TIMING

CHAIRMAN : E. GATTI

Shaping and Timing Circuits with Alternative Symmetric and Asymmetric Input and Output Configurations.
P. Horváth, L. Ondriš 93

Influence of the Compensated Thickness of Coaxial Ge(Li) Detectors and of Noise Sources on Timing Properties.
J.A. Miehé, P. Siffert, R. Stuck, A. Coche 95

Plasma Effects for α-Particles and O^{16} Ions in Silicon Detectors.
P.A. Tove, W. Seibt, K.E. Sundström 101

Digital, Analog and Program Techniques for On-Line Computer Control of Phased Neutron Choppers.
M.C.B. Russell, D.B.J. Smith 107

Time-of-Flight Instrumentation for a Quasielastic Critical Neutron-Scattering Experiment.
E.M. Christiansen, P. Christensen 111

Differential Linearity Testing and Precision Calibration of Multichannel Time Sorters.
M. Bertolaccini, S. Cova 119

A Weighted Chronotron for Time-Digit Conversion.
M. Feran, E. Katz, R. Papina 127

Fast Time Marking Discriminator Circuit.
N. Fiebiger, P. Elzer, W.D. Emmerich, A. Hofmann, J.W. Klein 137

SESSION 3: SPECTROMETRY

CHAIRMAN: R.L. CHASE

System Requirements for High Resolution Gamma-Ray Spectrometry at High Counting Rates.
L.O. Johnson, R.L. Heath (invited paper) 141

State of Art in Multichannel Pulse Data Analysis.
B. Souček 149

Performance Tests for Ge(Li) Spectrometers.
H. Meyer, H. Verelst 171

Fast ADC for Pulse Height Analysis.
R. Kurz 179

Analysis of Nonlinear Feedback Loops in Pulse Stretchers.
I. Alleva, I. De Lotto, P.F. Manfredi, P. Maranesi 193

An Analogue-to-Digital Converter Employing Recycled Successive Approximations.
K. Kandiah, A. Stirling, D.L. Trotman 205

A Normalizing ADC for Use with Position Sensitive Detectors.
G.L. Miller, A. Senator 211

Direct Digitalization of the Quotient of Two Pulse Heights.
W.M. Carpay, S.S. Klein 217

An Analog Spectrum Stabilizer.
T. Friese 221

SESSION 4: MISCELLANEOUS TECNIQUES

CHAIRMAN: J. POTTIER

A Data-Handling System for Large-Scale Space Radiation Experiments.
J.B. Reagan, R.D. Reed, J.C. Bakke, J.D. Mattews 225

Compensation of Pulse Deterioration in Miniature Cables by Means of Switching Transistors.
D. Maeder, G. Vuilleumier 231

Deadtime Corrections in a Two-Parameter System Containing Four Detectors.
G. Grosshög 237

A Data Collecting System for Pulse Radiolysis Experiments.
K.E. Neisig, S.O. Nielsen 243

Wire Proportional Counter Arrays with Fast Digital Arithmetic for Decision Making.
L.J. Koester, R.M. Brown, U. Kötz, T. Clark, S. Segler, R. Taylor 247

Nucleonic Applications of E^2CL Monolithic Integrated Circuits.
Z.H. Cho 251

Multiparameter Analysis and Recording System (MARS) for Isotopes Identification of Transuranium Elements.
B. V. Fefilov, L.P. Chelnokov 259

A Programmed Control and Instrumentation System for a Nuclear Reactor.
J.R. Kosorok (Summary) 263

Digital High-Voltage Supply for Automatic Testing and Regulation of Photomultiplier Gain.
D. Maeder 265

SESSION 5: COMPUTER ON LINE AND DATA REDUCTION IN NUCLEAR EXPERIMENTS

CHAIRMAN: B. SOUČEK

A Computerized Data Acquisition System for High Event Rates from Many Sources.
D.G. Dimmler 269

Computer System for On-Line Neutronic Noise Analysis and Calculation of Nuclear Reactor Parameter.
M. Čarapić, D. Velašević, S. Stanković 277

A Computer On-Line in Activation Measurements.
L. Arcipiani, U. Farinelli, A. Gibello 283

Use of a Computer On Line in Experiments at the Fast Critical Assembly SNEAK.
P.L. van Velze, H. Walze 291

NUDIAC-Data Acquisition and Processing System Applied to Physics Experiments and to Nuclear Measurements.
J. Moisset, M. Barthélémy 293

An On-Line Data Handling System for Physics Experiments at the Swiss Federal Institute for Reactor Research.
J.B. Bossel, W.Hälg 299

A CAMAC Multi-User System.
G.C. Best, I.N. Hooton 305

The "ESTER" System for Simultaneous Running of Several On-Line Multiparametric Experiments.
J. Zen, A. Muser, J.D. Michaud, F. Scheibling 307

Data Acquisition and Reduction in Activation Analysis by On-Line Computer.
G. Di Cola, F. Girardi, G. Guzzi, A. Termanini 313

Data Handling System for Activation Analysis by Means of a Small Process Computer.
P. Christensen, E.M. Christiansen 317

A Display Terminal for On-Line Nuclear Experiments.
H.L. Klessmann, J. Zahn 321

Computer Controlled Dataway for Nuclear Informations.
J.F. Gilbert, J.J. Girod, J.L. Lecomte, M. Lesourne (Summary) 331

SESSION 6: STATISTICS AND MATHEMATICAL METHODS

CHAIRMAN: E. BALDINGER

Methods of Reducing the Number of Binary Digits Required to Convey Random Counting-Rate Information.
E.H. Cooke-Yarborough 333

Improvement of Sliding-Scale Analog-to-Digital Converters through Weighted Averaging.
E. Gatti, V. Svelto, P.F. Manfredi, P. Thieberger 339

Optimum Statistical Equalization in Controlled Analog to Digital Converters.
N. Abbattista, B. Marangelli, D. Marino, V.L. Plantamura (Summary) 347

Statistical Errors of Direct Pulse Rate Ratio Measurement.
M. Konrad 349

The Measurement of Autocorrelation and Crosscorrelation Functions in the Fast Domain and its Application to Nuclear Electronics.
G. Amsel, R. Bosshard, R. Rausch, M. Sauce, C. Zajde 355

A New General Purpose Correlation Function Computer.
I.H. Quayle 363

Switching Circuits Optimal Configuration for Amplitude Discrimination and Timing.
N. Abbattista, V.L.Plantamura, G. Giannelli, M. Coli 371

A Method for the Analysis of Complex Gamma-Ray Spectra Using a Computer.
T. Inouye 375

SESSION 7: CAMAC AND MODULAR INSTRUMENTS

CHAIRMAN: H. BISBY

The CAMAC System of Modular Instrumentation.
R.C.M. Barnes, I.N. Hooton 379

Project AGORA. Adaptive Network for Data Collection and Transmission.
J.F. Mougel 385

CAMAC Crate Control for a PDP8 and a CAMAC 2^4 Bit Counter.
W. Attwenger, W. Egl, F. May, R. Patzelt, K. Petreczek, J. Schwarzer 391

Programmed Control of Autonomous Transfers in a CAMAC System.
J.M. Richards, L.D. Ward 395

CAMAC and Modular Instrumentation (A report on the discussion).
H. Bisby, W. Becker, R.C.M. Barnes 399

LIST OF PARTICIPANTS

ABEND K. - KFA Jülich, Postfach 365 - 517 JÜLICH, Germany.

ACERBONI G. - Hewlett-Packard S.A., 7 rue du Bois-du-Lan - 1217 MEYRIN, Switzerland.

ADORJAN B. - Central Research Institute for Physics of the Hungarian Academy of Sciences, P.O. 49 - BUDAPEST 114, Hungary.

ALBERTI G. - LABEN, Via Bassini, 15 - MILANO, Italy.

ALBERIGI QUARANTA A. - University of Modena, Via Vivaldi, 70 - 41100 MODENA, Italy.

ALLEN K.W. - University of Oxford, Dept. of Nuclear Physics, Keble Road - OXFORD, U.K.

ALLEVA I. - CISE, Casella postale 3986 , 20100 MILANO, Italy

ALOIA A. - ENEL, Via G. B. Martini, 3, ROMA, Italy.

AMSEL G. - Groupe de Physique du Solide, 9, Quai Saint-Bernard - PARIS Ve, France.

ANTHONY . - CITEC/GIE, 17 route de la Reine - PARIS

AQUILI A. - CNEN CASACCIA, Casella Postale 2400 - 00100 ROMA, Italy.

ARBEL Arie - Technion Israel Institute of Technology , P.O.Box 4910 - HAIFA,Israel.

ASSADOULAH . - Laboratoires de Marcoussis, C.G.E., route de Nozay - 91 MARCOUSSIS, France.

ATTWENGER W. - Öster. Studiengesellschaft für Atomenergie, Reaktorzentrum Seibersdorf, Lenaugasse 10 - 1082 WIEN VIII, Austria.

AUDEBEAU J.P. - C.C.R. EURATOM - 21020 ISPRA, Italy.

BABIĆ H. - Institute "Ruder Bošković" Bijenicka 54, ZAGREB, Yugoslavia.

BALDINGER E. - Inst.für Angew.Physik der Universität Basel, Klingelbergstr. 82 - 4000 BASEL, Switzerland.

BALLAND J.C. - Institut de Physique Nucléaire 43, Bd. du 11 Novembre 1918 - 69 VILLEURBANNE, France.

BANERJEE B.M. - SAHA Institute of Nucl.Physics 92, A.P.C. Road - CALCUTTA, India.

BANERJEE P. - SIEMENS A.G., Gellertstrasse 38, 75 KARLSRUHE, Germany.

BARBIEUX Ph.- Cie Internationale pour l'Informatique, 68 route de Versailles - 78 LOUVECIENNES, France.

BARNES R.C. - A.E.R.E., HARWELL, Didcot, Berks., U.K.

BARTHELEMY M. - C.E.A.-C.E.N./SACLAY, B.P. N.2 - 91 GIF-sur-YVETTE , France.

BATTISTA A. - TENNELEC Inc., P.O.B. D - OAK RIDGE, TENN. 37830, U.S.A.

BECKER L. - C.C.R. EURATOM - 21020 ISPRA , Italy

BECKER W. - C.C.R. EURATOM - 21020 ISPRA, Italy

BERANGER R. - INTERTECHNIQUE - 78 PLAISIR,France.

BERNEDE M. - C.C.R. EURATOM - 21020 ISPRA, Italy.

BERTOLACCINI M. - Istituto di Fisica del Politecnico, P.zza Leonardo da Vinci, 32 - 20133 MILANO, Italy.

BISBY H. - A.E.R.E. HARWELL, Didcot, Berks., U.K.

BOCCIOLINI M. - Istituto Nazionale Fis.Nucl. Largo E. Fermi, 2 - FIRENZE, Italy.

BONNAURE P. - C.C.R. EURATOM - 21020 ISPRA,Italy.

BONSIGNORI C. - LABEN, Via Bassini 15 - 20133 MILANO, Italy.

BORER A. - BORER & CO., ELECTRONICS, 45 SOLOTHURN 2 , Switzerland.

BOSSEL J.B. - Swiss Fed.Inst. Reactor Research 5303 WÜRENLINGEN, Switzerland.

BOSSHARD R. - Accélérateur Linéaire - Bât. 200 91 ORSAY, France.

BOUCKE G. - AEG-TELEFUNKEN, Forschungsinstitut Elisabethenstr. 3 - 79 ULM, Germany.

BOUSSARD D. - C.E.R.N. - 1211 GENEVA 23, Switzerland.

BOYCE D.A. - A.E.R.E., HARWELL, Didcot, Berks., U.K.

BREHM H. - Inst. für Angew. Physik, Universität Frankfurt/M. Am Forsthaus Gravenbr.28 - 6078 NEU ISENBURG 2, Germany.

BRET A. - C.C.R. EURATOM - 21020 ISPRA, Italy.

BRISCOE W.L. - Los Alamos Laboratory - LOS ALAMOS/NEW MEXICO, U.S.A.

BROOKS J.R. - Science Research Council,Daresbury Nuclear Physics Lab. WARRINGTON/Lancs. U.K.

BÜSCHING E. - Labor Prof.Dr. Berthold, Postfach 160 - 7547 WILDBAD, Germany.

CARAGHEORGHEOPOL G. - Institute for Atomic Physics BUCHAREST, Rumania.

ČARAPIĆ M. - Nucl.Sci.Inst. "Boris Kidrich" P.O.B. 522 - VINCA-BEOGRAD,Yugoslavia.

CERVELLATI R. - CNEN CASACCIA, Casella Postale 2400 - 00100 ROMA, Italy.

CHASE R.L. - Brookhaven National Lab. UPTON L.I. N.Y. 11973, U.S.A.

CHISMON N. - Electronic Assocates Ltd. Victoria Rd. BURGESS HILL/Sussex , U.K.

CHO Z.H. - Institute of Physics, Stockholms University - STOCKHOLM, Sweden.

CHRISTALLER G. - Wenzel-Elektronik, Lamontstr. 32 MÜNCHEN, Germany.

CHRISTENSEN P. - Danish Atomic Energy Commission Risö - 4000 ROSKILDE, Denmark.

CHRISTIANSEN E.M. - Danish Atomic Energy Commission Risö - 4000 ROSKILDE, Denmark.

CINISELLI C. - C.C.R. EURATOM - 21020 ISPRA,Italy.

COIANTE D. - CNEN CASACCIA, Casella Postale 2400 00100 ROMA, Italy.

COLI M. - Laboratori Nazionali di Frascati del CNEN, C.P. 70 - 0044 FRASCATI, Italy.

COLLINSON A.J.L. - Borough Polytechnic, Borough Road - LONDON S.E.1, U.K.

COLOMBO A. - C.C.R. EURATOM - 21020 ISPRA, Italy.

COLOMBO G. - C.C.R. EURATOM - 21020 ISPRA, Italy.

CONRAD R. - HAHN-MEITNER INSTITUT, Glienicker Str. 100 - 1 BERLIN 39, Germany.

COOK A.D. - Cambridge Scientific Inst. Co., Chesterton Road, CAMBRIDGE, UK.

COOKE-YARBOROUGH E. - A.E.R.E., HARWELL, Didcot, Berks., U.K.

COPPO N. - C.C.R. EURATOM - 21020 ISPRA, Italy.

COTTINI C. - CISE, Casella Postale 3986 , 20100 MILANO, Italy.

COURBOIS Th. Harshaw Chemie N.V. Strikjkviertel 95 - DE MEERN, Netherlands.

COVA S. - Istituto di Fisica del Politecnico, P.zza Leonardo da Vinci, 32, 20133 MILANO, Italy.

COWAN R.C. - Precision Metal Fabricators, 540 Lewelling Blvd. SAN LEANDRO, CALIF. U.S.A.

CUBIOTTI G. - Istituto di Fisica, Università di MESSINA, Italy.

ČULJAT K. - Institute "Ruder Boskovič", Bijenicka c. 54 - ZAGREB, Yugoslavia.

DE BRUIN M. - Reactor Institute, Berlagweg 15, DELFT, Netherlands.

DE AGOSTINO E. CNEN CASACCIA, Casella Postale 2400 - 00100 ROMA, Italy.

DEIGHTON M.O. - A.E.R.E. HARWELL, Didcot, Berks., U.K.

DE JONGE S. - B.C.M.N. EURATOM GEEL, Steenweg naar Retie, Belgium.

DE LOTTO I. - CISE, Casella Postale 3986, 20100 MILANO, Italy.

DEMARCHI G. - GAMMATOM S.p.A., via 25 aprile, 22070 GUANZATE. Italy.

DEMUYNCK J. - University Ghent, K. van de Woestynestr. 12 - ZWYNAARBE,Belgium.

DIETTRICH O. - C.C.R. EURATOM - 21020 ISPRA, Italy.

D'OLEON F. - INTERTECHNIQUE - 78 PLAISIR, France.

DOTTI D. - CISE, Casella Postale 3986 - 20100 MILANO, Italy.

DRUŽETA A. - Institute "Ruder Boskovič ", Bijenicka c. 54 - ZAGREB, Yugoslavia.

DURCANSKY G. - KFA Jülich, Postfach 365, 517 JÜLICH, Germany.

EDER J. - C.C.R. EURATOM - 21020 ISPRA, Italy.

ELAD E. - Nuclear Diodes Inc. P.O.B. 135 - PRAIRIE VIEW, ILL., U.S.A.

ELEK G. - Central Research Institute for Physics P.O.Box 49 - BUDAPEST 114, Hungary.

EQUILBEY S. - Ministère de l'Education Nationale CNRS, 15 rue G. Clémenceau - 91 ORSAY, France.

FARAGO H.- Central Research Institute for Physics P.O.Box 49 - BUDAPEST 114, Hungary.

FEFILOV B.V. - Joint Inst.for Nucl. Research DUBNA, P.O.B. 79 MOSCOW, USSR.

FELLMANN S. - Physikalisches Institut der Universität Marburg/Lahn, Renthof 5 MARBURG/ Lahn, Germany.

FESTA E. - Institut de Physique Nucléaire, B.P. 1 91 ORSAY, France.

FIEBIGER N.- Physik.Inst. der Universität 852 ERLANGEN, Germany.

FIEGNA G. - Ist. Fisica Tecnica del POLITECNICO Corso Duca degli Abruzzi, TORINO, Italy.

FINZI S. - C.C.R. EURATOM - 21020 ISPRA, Italy.

FIORONI F. - CNEN CASACCIA, Casella Postale 2400, 00100 ROMA, Italy.

FISCHER P.M. - Gesellschaft für Kernforschung Lab. f. Elektr. u. Messtechnik , Weberstr. 5 - 75 KARLSRUHE, Germany.

FRANTLOVIĆ P. - Nucl.Sc.inst. "Boris Kidrich" P.O.B. 522 - VINCA-BEOGRAD, Yugoslavia.

FREYCENON J. - C.E.N. - Cadarache, B.P. N.1 - ST-PAUL les DURANCE, France.

FRIANT . - C.E.A. - C.E.N. Saclay, DEG/SER B.P. N.2 - 91 GIF-sur-YVETTE, France.

FRIESE Th. - Hahn-Meitner Institut, Glienicker Str. 100 - 1 BERLIN 39 , Germany.

FRUMAU C.F.A. - Reactor Centrum Nederland, PETTEN (N.H.) Netherlands.

GANSS B. - C.C.R. EURATOM 21020 ISPRA, Italy.

GARAGNANI G.C. - ENEL, V.le Regina Margherita 137 - ROMA, Italy.

GATTI E. - CISE and POLITECNICO di Milano, C.P. 3986 - 20100 MILANO, Italy.

GEDCKE D. - ORTEC Inc. 100 Midland Road, OAK RIDGE, TENN. U.S.A.

GIACOMICH R. - Istituto di Fisica, Via Valerio 2 TRIESTE, Italy.

GIBELLO A. - CNEN CASACCIA, Casella Postale 2400, 00100 ROMA, Italy.

GOLDER J. - Institut für Angew.Physik der Universität Basel, Klingelbergstr. 82, 4000 BASEL, Switzerland.

GOLUTVIN I.A. - Joint Inst. for Nucl. Research DUBNA - P.O. Box 79 - MOSCOW, USSR.

GOYOT M. - Institut de Physique Nucléaire , 43 Bd. du 11 novembre 1918 - 69 VILLEURBANNE, France.

GRANATA L. - Istituto di Fisica, Via Valerio 2 34100 TRIESTE, Italy.

GRECO G. - Istituto Applicazioni e Impianti Nucleari - 90100 PALERMO, Italy.

GUILLON H. - C.E.A.-C.E.N. Saclay B.P. N.2. 91 GIF-sur-YVETTE, France.

GUREWITSCH A.M. - GENERAL ELECTRIC CO. USA Research & Development Center Löwenstr. 29 - 8001 ZÜRICH, Switzerland.

GUYON .- Institut de Physique Nucléaire, 43 Bd.du 11 Novembre 1918 - 69 VILLEURBANNE, France.

GUZZI G. - C.C.R. EURATOM - 21020 ISPRA, Italy.

HALLER E. - Institut für Angew. Physik der Universität Basel, Klingelbergstr. 82 4000 BASEL, Switzerland.

HARGROVE C.K. - National Research Council of Canada, 100 Sussex Drive - OTTAWA, CANADA.

HAURIE Y. - C.C.R. EURATOM - 21020 ISPRA, Italy.

HEATH R.L. - Idaho Nuclear Corporation, P.O. Box 1845, IDAHO FALLS, IDAHO 83401, U.S.A.

HEELAS . - Dynatron Electronics, St. Peters Road - MAIDENHEAD, U.K.

HØY-CHRISTENSEN P. - Danish Atomic Energy Commission Risö - 4000 ROSKILDE, Denmark.

HOLMQVIST B. - A.B. Atomenergi, Studsvik, NYKÖPING, Sweden.

HORVATH P. - Joint Inst.for Nucl.Research DUBNA, P.O.B. 79 MOSCOW, USSR.

HOWES J.H. - A.E.R.E., HARWELL, Didcot, Berks., U.K.

HRISOHO .- Institut de Physique Nucléaire, B.P. N.1 91 ORSAY, France.

HUGHES G. - Science Research Council, DN.P.L DARESBURY - WARRINGTON, U.K.

IDZERDA A.B. - B.C.M.N. EURATOM GEEL, Steenweg naar Retie, Belgium.

INOUYE T. - Central Research Lab. Tokyo Shibaura Electric Co., Ltd. 1 Komukai Toshiba-Cho, Kawasaki-Shi, Kanagawa-Ken, Japan.

ISELIN F. - C.E.R.N. NP. Div. - 1211 GENEVA 23 Switzerland.

JACQUIN M. - Institut de Physique Nucléaire, 43, Bd. du 11 Nov. 1918 - 69 VILLEURBANNE, France.

JEDLOVSZKY R. - National Office of Measures XII. Németvölgyi ut 37-39 - BUDAPEST, Hungary.

JONSSON G. - AB Atomenergi - Studsvik - NIKÖPING Sweden.

JOVIC F. - Institute "Ruder Boskovid " Bijenicka c. 54 - ZAGREB, Yugoslavia.

KADJAR .- 38 rue Gabriel Crié, SAIP - 92 MALAKOFF, France

KANDIAH K. - A.E.R.E., HARWELL, Didcot, Berks., U.K.

KATKIEWICZ W. - Central Radiological Protection Laboratory, Modlinska 15 - WARSAW, Poland.

KEDDAR A. - I.A.E.A. Kärntnerring 11-13 , 1010 VIENNA, Austria.

KEROE E. - I.A.E.A. Kärntnerring 11-13 - 1010 VIENNA, Austria.

KESSEL W. - Institut für Kernphysik , Aug.Eulor-str. 6 - FRANKFURT/M., Germany.

KISLEV A. - Nuclear Research Centre-Negev , P.O.B. 9001 - BEER SHEVA, Israel.

KLEIN J.W. - Frieseke u. Hoepfner - 852 ERLANGEN-BRUCK, Germany.

KLEIN S.S. - Technological University, Insulinde-laan ,(P.B.513) EINDHOVEN, Netherlands.

KLESSMANN H. - Hahn-Meitner Institut, Glienicker-Str. 100 - 1 BERLIN 39, Germany.

KOBUS L. - C.C.R. EURATOM - 21020 ISPRA, Italy.

KOECHLER C. - C.C.R. EURATOM - 21020 ISPRA, Italy.

KOEMAN H. - I.K.O. Ooster Ringdijk 18, AMSTERDAM-O Netherlands

KOESTER J. - Physics Department, University of Illinois - URBANA, ILL. 61801, U.S.A

KOLBE W. - Labor. Prof. Dr. Berthold, Postfach 160 - 7547 WILDBAD, Germany.

KONRAD M. - Institute "Ruder Boskovic' " Bijenicka c. 54 - ZAGREB, Yugoslavia.

KONY J. - C.E.A.-C.E.N. SACLAY - D.C.E. B.P. N.2 91 GIF-sur-YVETTE, France.

KORTHOVEN P.J.M. - Reactor Institute, Berlageweg 15 DELFT, Netherlands.

KOSSIONIDES E. - G.A.E.C. 7, Sandileigh Ave. MANCHESTER 20, U.K.

KOUVARAS N. - N.R.C. DEMOKRITUS, Aghia Paraskevi-Attikis - ATHENS, Greece.

KOVACS E.- Central Research Inst. for Physics P.O.Box 49 - BUDAPEST 114, Hungary.

KRUISKAMP M. - KEMA Suspension Test Reactor, Monnikensteeg 108, ARNHEM, Netherlands.

KUMPF S. - C.C.R. EURATOM -21020 ISPRA, Italy.

KURZ R. - TENNELEC, P.O.Box D, OAK RIDGE, TENN. 37830, U.S.A.

LAGONEGRO M. - Istituto di Fisica di Trieste Via Valerio, 2 - 34100 TRIESTE, Italy.

LAGOYANNIS D. - N.R.C. DEMOKRITUS, Aghia Paraskevi-Attikis - ATHENS, Greece.

LANGKAU R. - I. Inst. für Experimentalphysik Jungiusstr. 9 - 2 HAMBURG 36, Germany.

LECLERC J. - CITEC/G.I.E. 17, route de la Reine 92 BOULOGNE, France.

LECOMTE J. - C.E.A.-C.E.N.G. - CEDEX N. 85 - GRENOBLE-GARE, France.

LEPERS A.- C.C.R. EURATOM - 21020 ISPRA, Italy.

LERO N. - Nucl.Sci.Inst. "Boris Kidrich" , P.O.B. 522 - VINČA-BEOGRAD, Yugoslavia.

LEVY J. - CITEC/G.I.E., 17 route de la Reine, 92 BOULOGNE, France.

LIDOFSKY L. - Pegram Nuclear Physics. Lab., Columbia University, 538, West 120th Street, NEW YORK, N.Y. 10027, U.S.A.

LOURENS W. - Technische Natuurkunde, Lorentzweg 1 - DELFT, Netherlands.

LUGOL J.C. - C.E.A.-C.E.N. SACLAY, B.P.N.2 , 91 GIF-sur-YVETTE, France.

MACLENNAN D.N. - D.A.F.S. MARINE Lab., Victoria Road, P.O.B. 101, ABERDEEN, U.K.

MAEDER D.G. - Ecole de Physique, Univ. de Genève, Bld. d'Ivoy 32, 1211 GENEVA 4, Switzerland.

MALOSTI D. - CNEN CASACCIA, Casella Postale 2400 00100 ROMA, Italy.

MANDL V. - C.C.R. EURATOM - 21020 ISPRA, Italy.

MANFREDI P.F. - CESNEF, Politecnico di Milano, Via Pascal 3, MILANO, Italy.

MARACCI G.C. - C.C.R. EURATOM - 21020 ISPRA, Italy.

MARANESI P. - CESNEF, Politecnico di Milano, Via Pascal 3, MILANO, Italy.

MASKELL S. - Science Research Council Rutherford Lab. CHILTON, Berks., U.K.

MEILING W. - Zentralinstitut für Kernforschung Postfach 19 - 8051 DRESDEN, Germany.

MERDINGER J.C. - Université de Strasbourg, Inst. de Recherches Nucléaires, B.P. N. 16 CR 67 STRASBOURG 3, France.

METZDORF J. - C.C.R. EURATOM - 21020 ISPRA, Italy.

MEY J. - C.E.A.-C.E.N.G. CEDEX N. 85 - 38 GRENOBLE-GARE, France.

MEYR H.P. - Swiss Federal Institute for Reactor Research - 5303 WÜRENLINGEN, Switzerland.

MEYER H. - B.C.M.N. EURATOM GEEL, Steenweg naar Retie, Belgium.

MICHAUD J.D.- Université de Strasbourg, Institut de Recherches Nucléaires, B.P. N. 16 CR 67 STRASBOURG 3, France.

MIEHÉ J.A. - C.R.N. Physique des Rayonnements et Electronique Nucléaire, Rue du Loess, 67 STRASBOURG-CRONENBOURG, France.

MILLER G.L.-Bell Telephone Lab. Mountain Avenue, MURRAY HILL, N.J. 07974, USA

MOLINARI M.A. - Université de Strasbourg, Inst. de Recherches Nucléaires, B.P. N.16 CR 67 STRASBOURG 3, France.

MOL M. - C.C.R. EURATOM - 21020 ISPRA, Italy.

MOLL G. - TOTAL - 6802 LADENBURG, Germany.

MOUGEL J.F. - C.E.A.-C.E.N. SACLAY, B.P. N2. 91 GIF-sur-YVETTE, France.

MÜLLER K.D. - KFA Jülich, Postfach 365 - 517 JÜLICH, Germany;

MUSER A. - Université de Strasbourg, Institut de Recherches Nucléaires, B.P. N. 16 CR 67 STRASBOURG 3, France.

NAJZER M. - Nucl.Institute "J. Stefan" Jamova 39 LJUBLJANA, Yugoslavia.

NEISIG K.E. - Danish Atomic Energy Commission Risö - 4000 ROSKILDE, Denmark.

NETZBAND D. - ZfK Rossendorf, Postfach 19 - 8051 DRESDEN , Germany.

NIESTROJ D. - Frieseke & Hoepfner GmbH, Tennenloher Strasse - 852 ERLANGEN, Germany.

ONDRIS L. - Joint Inst.for Nucl. Research DUBNA, P.O.B. 79 MOSKOW, USSR.

OTTES J. - Ges. für Kernforschung, Lab. für Kernforschung Lab. f. Elektr. u. Messtechnik, Weberstr. 5 - 75 KARLSRUHE, Germany.

PAGNOTTE .- Institut de Physique Nucléaire, 43 Bd. du 11 Novembre 1918, 69 VILLEURBANNE France.

PAIN J. - C.E.A.-C.E.N. SACLAY , B.P.N. 2 , 91 GIF-sur-YVETTE, France.

PATRUTESCU M. - Institute for Atomic Physics P.O.B. 35, BUCHAREST, Rumania.

PATZELT R. - Österr. Studienges. für Atomenergie Lenaugasse 10 - 1082 WIEN VIII, Austria.

PEDRINI A. - C.C.R. EURATOM - 21020 ISPRA, Italy.

PELLEGRINI U. - LABEN, Via Bassini 15 - 20133 MILANO, Italy.

PETEL M. - C.E.A. B.P. N. 510, 75 PARIS XVe, France.

PETERSEN J. - Danish Atomic Energy Commission Risö - 4000 ROSKILDE, Denmark.

PHILIPPE A. - C.C.R. EURATOM - 21020 ISPRA, Italy.

PIRRONE G. - AMP ITALIA, Corso F.lli Cervi, 15 10093 COLLEGNO (TO), Italy.

PLATTNER R. - ORTEC - Am Birkicht 6 MÜNCHEN, Germany.

POENARU D.N. - Institute of Atomic Physics, P.O.B. 35 - BUCHAREST, Rumania.

POTTIER J. - C.E.A.-C.E.N. - SACLAY, B.P. N.2 91 GIF-sur-YVETTE, France.

PRATO A. - ENEL , via G.B. Martini, 3 ROMA, Italy.

PREZZI C. - Laboratori Nazionali di Frascati del CNEN, Casella Postale N. 70 - 00044 FRASCATI, Italy.

PRIOR G.M. - Nuclear Enterprises Ltd. Bath Rd. BEENHAM (Reading), U.K.

QUAYLE I.H. - AIM ELECTRONICS Ltd., Barhill, CAMBRIDGE, U.K.

RADEKA V. - Brookhaven National Laboratory, UPTON, N.Y. U.S.A.

RAUSCH R. - Accélérateur Linéaire - Faculté des Sciences - 91 ORSAY, France.

REAGAN J.- Lockheed Missile and Space Co. 3251 Hanover Street, PALO ALTO, CALIF. 94304, U.S.A.

RICHARD A. - Institut de Physique Nucléaire B.P. N. 1 91 ORSAY, France.

RICHARDS J.M. - A.E.R.E., HARWELL, Didcot, Berks. U.K.

RIGHINI B. - C.E.R.N. 1211 GENEVA 23, Switzerland.

ROBERTS C. - Victoreen Instrument, Co. Arndale House, High Street - EGHAM, Surrey. UK

ROEHMER F.C. Laboratory for High Energy Physics Gloriastr. 35, ZÜRICH, Switzerland.

ROS D. - Central Laboratorium T.N.O. P.O.B. 217 DELFT, Netherlands.

ROUGER M. - C.E.A.-C.E.N. SACLAY, B.P. N. 2, 91 GIF-sur-YVETTE, France.

ROUSEK J. - Nuclear Research Institute of Academy Rez u Prahy - PRAGUE

RUSSEL M.C.B. - A.E.R.E., HARWELL, Didcot, Berks., U.K.

SABBAH B. - ELSCINT Ltd. P.O.B. 5258 - HAIFA, Israel.

SALOMONI A. - C.N.E.N. Via Mazzini 2 - BOLOGNA, Italy.

SAMUELI J.J. - Institut de Physique Nucl. 43 Bd. du 11 Novembre 1918 - 69 VILLEURBANNE France.

SARGENT T.D. - Department of the Army I.G. Farben-Hochhaus - FRANKFURT/M. , Germany.

SAUCE M. - Accélérateur Linéaire, Faculté des Sciences - 91 ORSAY, France.

SAUNDERS P. - DYNATRON ELECTRONICS, St.Peters Road - MAIDENHEAD, U.K.

SAWICKI A. - Institute of Nuclear Research Zaklad Elektroniki, SWIERK K/OTWOCKA Poland.

SCHEIBLING F. - Université de Strasbourg, Institut de Recherches Nucléaires, B.P.N .16 CR 67 STRASBOURG 3, France.

SCHNEIDER W. - Hans Wiener K.G. Neuenhaus 106 - 5675 HILGEN, Germany.

SCHOEPS W.-Laboratorium für Hochenergiephysik Eidg. Technische Hochschule - 8006 ZÜRICH, Switzerland.

SCHOLTZEL P. - HEWLETT-PACKARD GmbH, 110 Herrenberger Str. 703 BÖBLINGEN, Germany.

SCHULTZ A. - Université de Strasbourg, Institut de Recherches Nucléaires, B.P.N.16 CR 67 STRASBOURG 3, France.

SCHUSTER .- Phys.-Techn. Bundesanstalt Deutschland, Bundesallee 100 - BRAUNSCHWEIG, Germany.

SCINTEI N. - Institute for Atomic Physics, P.O.B. 35, BUCHAREST, Rumania

SECCHIA S. - NUCLEAR MILANO, 33 Via Teodosio - 20131 MILANO.

SENS .- Université de Strasbourg, Institut de Recherches Nucléaires, B.P. N. 16 CR 67 STRASBOURG 3, France.

SERVENT J.M. - S.A.I.P., 38 rue Gabriel Crié 92 MALAKOFF, France.

SIFFERT P. - C.R.N. Physique des Rayonnements et Electronique Nucléaire, rue du Loess 67 STRASBOURG-CRONENBOURG, France.

SINAEV A.N. - Joint Inst. for Nuclear Research DUBNA, P.O.B. 79 MOSCOW, USSR.

SINDERMAN J. - Comision Energia Atomica, Avda Libertador 8250, BUENOS AIRES, Argentina.

SMILJANIĆ G. - Institute "Ruder Boskovid" Bijenicka c. 54 ZAGREB, Yugoslavia.

SMIT T. - C.C.R. EURATOM - 21020 ISPRA, Italy.

SMITH W. - VICTOREEN Instrum. Co., Arndale House High Street - EGHAM, Surrey, U.K.

SNAIJDER J. - Nucl.Instr. "J. Stefan" Jamova 39 LJUBLJANA, Yugoslavia.

SOREL F. - C.C.R. EURATOM - 21020 ISPRA, Italy.

SOSO F. - Laboratori Nazionali di Frascati del CNEN, Casella Postale N.70 - 00044 FRASCATI, Italy.

SOUČEK B. - Institute "Ruder Boskovic' " Bijenicka 54 - ZAGREB, Yugoslavia.

SPASOV A.Y.- Bulgarian Academy of Sciences, Lenin Street 72 - SOFIA 13, Bulgaria.

STANCHI L. - C.C.R. EURATOM - 21020 ISPRA, Italy.

STENSGAARD R. - Institute of Physics, University of Aarhus - AARHUS, Denmark.

ST.JACQUES J. - AMP INC., Terminal House, STANMORE, Middlesex, U.K.

STRUVING J.N. - PHILIPS Natuurkundig Laboratorium N.V. Philips , Gloeilampenfabrieken EINDHOVEN, Netherlands.

STÜBER W. - B.C.M.N. EURATOM GEEL, Steenweg naar Retie, Belgium.

STUCK R. - C.R.N. Physique des Rayonnements et Electronique Nucléaire, rue du Loess, 67 STRASBOURG-CRONENBOURG, France.

SVELTO V. - CISE, Casella Postale 3986, 20100 MILANO, Italy.

SZABO L. - Central Research Institute for Physics XII. Konkoly Thege u. BUDAPEST, Hungary.

SZAVITS O. - Institute "Ruder Boskovic' "Bijenicka c. 54 - ZAGREB, Yugoslavia.

SZIGETI B. - Central Research Institute for Physics P.O.B. 49 - BUDAPEST 114 - Hungary.

SZLAVIK F. - Central Research Institute for Physics P.O.B. 49 - BUDAPEST 114 - Hungary.

SZPIRO S. - C.C.R. EURATOM - 21020 ISPRA, Italy

TARAS A. - IBM - ENDICOTT U.S.A.

TENTEN W. - KFA Jülich, Postfach 365 - 517 JÜLICH Germany.

TERMANINI A. - C.C.R. EURATOM - 21020 ISPRA, Italy.

THIELMANN R. - Physikalisches Institut der Universität MARBURG/Lahn Renthof 5, MARBURG/ Lahn, Germany.

TISHIN V.G. - Joint Inst. for Nuclear Research DUBNA, P.O.B. 79 MOSCOW, USSR.

TOLLAN O. - Institutt for Atomenergi, P.O.B. 40 KJELLER, Norway.

TOVE P.A. - Institute of Physics, Box 530, 75121 UPPSALA, Sweden.

TRADOWSKY K. - Gesellschaft für Kernforschung Lab. für Elektr. und Messtechnik, Weberstr. 5, 75 KARLSRUHE, Germany.

TURALA M. - Joint Inst. for Nuclear Research DUBNA, P.O.B. 79 - MOSCOW,USSR.

UYTTENHOVE J. - University GHENDT, Lockaertstraat 16 - ANTWERPEN, Belgium.

VACCAREZZA J. - C.C.R. EURATOM - 21020 ISPRA, Italy.

VAN DEN BERG P.C. - Reactor Centrum Nederland PETTEN, Netherlands.

VAN MONTFOORT J.E. - EURATOM - PETTEN, Netherlands.

VAREKAMP P. - C.C.R. EURATOM - 21020 ISPRA, Italy.

VÖLPEL R. - Strahlenzentrum Giessen, Leihgesternerweg 217 - GIESSEN, Germany.

VUILLEUMIER G. - Ecole de Physique, Univ. de Genève, Bld. d'Ivoy 32, 1211 GENEVA 4, Switzerland.

WALZE H. - Institut für Angewandte Reaktorphysik Kernforschungszentrum - 75 KARLSRUHE, Germany.

WEHRLE G. - SIEMENS A.G., Lassalle Str. 21 - 75 KARLSRUHE, Germany.

WENDEL P. - Université de Strasbourg, Institut de Recherches Nucléaires, B.P. N.16 CR 67 STRASBOURG 3, France.

WEYMANN J.P. - Université de Strasbourg, Institut de Recherches Nucléaires, B.P.N. 16 CR 67 STRASBOURG 3 France.

WINTER J. - B.C.M.N. EURATOM GEEL, Steenweg naar Retie, Belgium.

WÖLCKEN K. - Strahlenzentrum, Leihgesternerweg 217 - 63 GIESSEN, Germany.

ZACHAROV B. - Science Research Council, Daresbury Nuclear Physics Lab., DARESBURY, Nr. Warrington (Lancs.) U.K.

ZAJDE C. - Accélérateur Linéaire, Faculté des Sciences - 91 ORSAY, France.

ZAMBONI F. - Physik. Institut der Universität Zürich, Schönberggasse 9, ZÜRICH, Switzerland.

ZAMPACH J. - C.R.N. Physique des Rayonnements et Electronique Nucléaire, rue du Loess 67 STRASBOURG CRONENBOURG, France.

ZANDER K. - Hahn-Meitner Institut, Glienicker Strasse 100 - 1 BERLIN 39, Germany.

ZEN J. - Université de Strasbourg, Institut de Recherches Nucléaires, B.P.N.16 CR 67 STRASBOURG 3, France.

ZSDANSZKY K. - National Office of Measures XII. Nemetvölgyi ut 37/39, BUDAPEST, Hungary.

1/|f| NOISE IN PHYSICAL MEASUREMENTS *

Veljko Radeka
Brookhaven National Laboratory
Upton, N. Y.

Summary

The purpose of this paper is to provide an insight into low frequency divergent noises with spectral density $|f|^{\alpha}$, where $\alpha \leq -1$, and into their effect on physical measurements, with special reference to $1/|f|$ noise. This class of noise is widespread in nature, and it presents unique limitations to the measurement accuracy. In an attempt to present a picture of this class of noise with regard to the measurements of observable physical quantities, the questions about generation of noise, its divergence, correlation properties and measurements of variance are discussed.

A statistical model for generation of low frequency divergent noises is used to consider the divergence problem in both the frequency and time domain. It is shown that $1/|f|$ noise is "weakly divergent," and that power limitation presents no reason to impose a low frequency limit within time intervals observable in nature. Correlation properties are discussed in terms of the time-dependent correlation function, using an ideal impulse response which generates low frequency noise from white noise. Two general models for generation of $1/|f|$ noise are summarized and discussed. Generation of $1/|f|$ noise from white noise over a limited frequency range by distributed and lumped-parameter filters is described.

It is shown that the variance (i.e. mean square noise) is determined by the frequency limits of the observation method. The variance is independent of the low frequency limit of noise, if such a limit exists, and if the frequency limit of noise is lower than the low frequency limit of the measurement process. If the ratio of the high frequency limit and the low frequency limit of the measurement process is constant, the variance is a function of one parameter, τ, which is proportional to the "measurement time." For power-law noises, the variance $\sigma \propto \tau^{-1-\alpha}$. Variance in the case of a general power spectral density function can be represented by the power series, where each term $\tau^{-1-\alpha}$ may be associated with a power-law noise component. Thus, the measurement of variance as a function of measurement time represents a method for identification of power-law noises, and their effect under actual measurement conditions.

1. Introduction

The purpose of this paper is to provide an insight into low frequency divergent noises with spectral density $|f|^{\alpha}$, where $\alpha \leq -1$, and into their effect on physical measurements, with special reference to $1/|f|$ noise. The class of noise $|f|^{\alpha}$ with α close to minus one is widespread in nature and it presents unique limitations to the measurement accuracy. Even in cases where the signal energy can be increased arbitrarily by extending the measurement time, the accuracy of the measurement of the signal magnitude cannot be improved by increasing the measurement time.

The basic distinction between white noise and $1/|f|$ noise is that the span of interdependence between samples is very large for $1/|f|$ noise, while sufficiently spaced samples for white noise (and for bandlimited white noise) are independent. This can be expressed in terms of correlation functions, that, while the correlation function for white noise is the delta function (in the limit of infinite bandwidth), the correlation function for

*This work was performed under the auspices of the U.S. Atomic Energy Commission.

low frequency noises (to the extent that it can be defined) decreases only very slowly with the interval between samples. The basic feature of any noise-generating mechanism for low frequency divergent noises is an "infinitely long memory" for individual independent perturbations.

Integration of white noise generates noises with spectral density $|f|^{\alpha}$, where $\alpha = -2i$, and i is the order of integration. One "integer-order" integration converts white noise into $1/f^2$ noise, or "random walk." One "half-order integration" is required to obtain $1/|f|$ noise from white noise. Noises which are related to white noise by an "integration" of a fractional-order are sometimes referred to as "fractional noises." Noises with spectral density $|f|^{\alpha}$, where $-\alpha$ is close to unity, observed over a certain frequency region, have been referred to as "flicker effect," "excess noise," "low frequency noise," "contact noise," and "pink noise."

$1/|f|$ noise has been observed as electrical noise or as fluctuations of some other physical quantity, or, more generally, of a "process variable" in a number of different devices and physical and other systems. It was discovered in electron tubes as "flicker effect."[1,2] It was also observed in all semiconductor devices which could have any application for amplification and detection of small signals.[3,4,5] Some semiconductor devices have particularly large $1/|f|$ noise, for example, MOS transistors as compared to junction field-effect transistors. Noise in MOS transistors has recently been a subject of extensive studies.[6,7,8,9] Low frequency fluctuations appear to be the principal limiting factor on the accuracy of frequency and time measurements and on the stability of precision signal generators.[10,11,12,13,14] $1/|f|$ fluctuations have been found also in a biological system.[15] Fluctuations in the frequency of rotation of the earth[16,17,14] appear to have a frequency spectrum with $\alpha = -2$ over a certain region. The concept of fractional noises has also been invoked to study the fluctuations of variables in economics.[18] It is also known that nuclear reactors with their feedback control exhibit power fluctuations which have $1/|f|$ spectral density over a range of frequencies. This noise presents a limitation in some nuclear physics experiments. Noises with spectral density represented approximately by the sum of white, $1/|f|$ and $1/f^2$ densities impose a limit on the measurement resolution of charge-sensitive amplifiers for nuclear radiation detectors. One source of $1/|f|$ noise in this case seems to be frequency-dependent thermal noise of solid dielectrics.[20]

The mechanisms of generation of $1/|f|$ noise in particular physical situations have been little understood. In the vast amount of literature on observed low frequency noises a satisfactory explanation of mechanisms was provided only in a few cases. Recently more insight has been gained as to how $1/|f|$ noise could be generated, and several models and interpretations have been proposed.[13,14,19] The most general model is the mechanical model proposed by Halford,[14] in which broad classes of perturbations are shown to be able to generate a given spectrum. This model leads also to analog and digital schemes for generation of low frequency noise for simulation purposes.

$1/|f|$ noise has received very little attention from the point of view of signal processing in the literature on statistical communication theory. Some mathematical studies of fractional noises have been published (other references are given in Ref. 18), where a number of problems of mathematical nature have been raised.

Measurements of physical quantities in the presence of low frequency fluctuations have been considered in greater detail in some special areas. The measurements of frequency and time have been analyzed extensively,[10-14,16,17] and will not be discussed here. In pulse amplitude measurements a general low

frequency spectrum represented by a negative power series has been considered by Gatti and Svelto.[21] Dependence of the noise power (variance) on the measurement time has been used for some time in this field to identify $|f|^{\alpha}$ noise components with different exponents. Consideration of dependence of noise on other variables has led to identification of physical sources of noise in charge amplifiers.[20] The effect of $1/|f|$ noise on nuclear magnetic resonance (NMR) measurements was discussed by Klein and Barton.[22]

In this paper an interpretation of low frequency noises and of the divergence problem is presented. A note is made on the difficulties with the definition of the correlation function for divergent noises, and on the characterization of their correlation properties. Models and mechanisms for generation of $1/|f|$ noise are reviewed, and an example of a circuit is given for generation of $1/|f|$ noise. Some effects of $1/|f|$ noise on the pulse amplitude measurements and on repetitive measurements in NMR are discussed. The method for identification of power-law noises based on time domain measurements is described. The interpretation and the models discussed here are based on linear superposition of perturbations generated by a stationary process, which should result in a divergent noise process with stationary increments. Problems arising from more complex processes with non-stationary behaviour are indicated.

2. An Interpretation of Low Frequency Divergent Noises

Representation of Noise and Divergence Tests

Power-law noises are represented as

$$w_{\alpha}(f) = |f|^{\alpha} \qquad (1)$$

$w_{\alpha}(f) = W_{\alpha}(f)/W_{\alpha}(0)$ is the normalized one-sided spectral density as a function of cycle frequency. ($W_{\alpha}(0)$ is the mean square value of the fluctuating variable at 1 Hz per $Hz^{\alpha+1}$; for voltage $1/|f|$ noise $w_{-1}(f) = v^2(f)/A_f$, where $A_f = W_{-1}(0)$ is expressed in volts^2.) Of particular interest here are the cases of white noise ($\alpha=0$), $1/|f|$ noise ($\alpha = -1$), and "random walk" ($\alpha = -2$), since they appear most frequently and since white noise and random walk represent interesting limit cases for comparison with $1/|f|$ noise. Power-law noise can be considered as being generated by a Poisson process acting upon an appropriate filter.[13] In the frequency domain, the transfer function of the filter which converts white noise into power-law noise is

$$H(\omega) = (j\omega)^{\frac{\alpha}{2}} \qquad (2)$$

In the time domain, we think of the power-law noise as being generated by the random sequence of impulses, each impulse generating at the output of the filter an impulse response, $h(t)$, which is the Fourier transform of the frequency domain transfer function $H(\omega)$,

$$h(t) = \frac{2^{\frac{-\alpha-1}{2}}\,(\pi)^{-\frac{\alpha}{2}}}{\Gamma(\frac{\alpha}{2})}\, t^{-\frac{\alpha}{2}-1} \qquad (3)$$

(Campbell and Foster,[23] pair 516.) For $\alpha = -2$, $\Gamma(\frac{\alpha}{2}) = 1$, for $\alpha = -1$, $\Gamma(\frac{\alpha}{2}) = \pi^{1/2}$. (The coefficient $2^{(-\alpha-1)/2}\cdot\pi^{-\alpha/2}$ is due to the normalization of all the variances, calculated in the following, to the one-sided spectral density $W_{\alpha}(0)$ at 1 Hz.)

If the input white process is $x(t)$, the process at the output of the filter is convolution $y(t) = x(t) * h(t)$,

$$y(t) = \frac{2^{\frac{-\alpha-1}{2}}\,(\pi)^{-\frac{\alpha}{2}}}{\Gamma(\frac{\alpha}{2})} \int_0^t (t-u)^{-\frac{\alpha}{2}-1}\, x(u)\,du \qquad (4)$$

Thus power-law noise can be obtained by fractional-order integration of white noise.[13] (For $\alpha = -2$, random walk is obtained by 1st order integration.) For $\alpha = -1$, $1/|f|$ noise is obtained by half-order integration,

$$y(t) = \int_0^t \frac{1}{(t-u)^{1/2}}\, x(u)\, du \qquad (5)$$

The impulse response of the filter for conversion of white noise into $1/|f|$ noise is

$$h(t) = \frac{1}{t^{1/2}} \quad \text{for } t > 0$$
$$= 0 \quad \text{for } t \le 0 \qquad (6)$$

The concept of the generation of various basic noises by a Poisson process is illustrated in Fig. 1. Fig. 1(b) shows the physical white noise - with high-frequency cutoff [impulse response $\frac{1}{\tau_h} \exp(-t/\tau_h)$ is shown resulting in the spectrum $1/(1 + \omega^2\tau_h^2)$ and autocorrelation function $r(\tau) = \exp(-|\tau|/\tau_h)$.] The main distinction of low-frequency noises is that each impulse of the random process produces an effect of infinite duration (constant for random walk, and a slowly decaying one for $1/|f|$ noise).

As a divergence test in the frequency domain, total power (variance) in the frequency band limited by frequencies f_ℓ and f_h can be calculated

$$\sigma^2(f_h, f_\ell) = \int_{f_\ell}^{f_h} |f|^\alpha \, df$$
$$= \begin{cases} \frac{1}{1+\alpha}\left[f_h^{1+\alpha} - f_\ell^{1+\alpha}\right] & \text{for } \alpha \neq -1 \\ \ell n \frac{f_h}{f_\ell} & \text{for } \alpha = -1 \end{cases} \qquad (7)$$

Extending the frequency band $f_\ell \to 0$ and $f_h \to \infty$, the total power tends to infinity, at the low frequency limit for $\alpha < -1$, at the high frequency limit for $\alpha > -1$, and at both limits for $\alpha = -1$. Thus, the unique place of $1/|f|$ noise among power-law noises is that it is divergent at both frequency limits. Low frequency divergent noises are characterized by $\alpha \le -1$. The high frequency divergence presents no actual problem, since in any physical system there is a high frequency limit, and infinite power at high frequencies cannot exist. For analytical purposes it can be handled by introducing an approperiate high frequency cutoff (which is a realistic solution, since any method for observation of noise introduces a high frequency limit).

To get closer to the substance of low frequency divergence, a time domain divergence test can be applied. In this test we imagine that the Poisson process is switched-on at the input of the filter $h(t)$, which converts it into power-law noise, and then we observe the output mean square noise power (variance) as a function of time, as illustrated in Fig. 2. There are a number of different approaches to calculate this. The most plausible one in this case is to apply Campbell's theorem,[24] and to determine the effect of input impulses occurring in the interval $0,t$ on the output at time t, as the sum of mean square contributions by independent impulses. The output due to a single impulse $q\cdot\delta(\lambda)$ will be $q\cdot h(\lambda)$ at a time (λ) after the impulse occurred. For the random sequence with mean rate $\bar{n}$, the mean square output due to $\bar{n}d\lambda$ impulses in the interval $d\lambda$ will be $\bar{n}q^2h^2(\lambda)\,d\lambda$, and the output for the whole interval $(0,t)$ is obtained by the integral[26]

$$\sigma_w^2(t,0) = \bar{n}q^2 \int_0^t h^2(\lambda)\, d\lambda \qquad (8)$$

Noting that $\bar{n}q^2$ is the (two-sided) power spectral density of the input process, the normalized output variance is

$$\sigma^2(t,0) = \int_0^t h^2(\lambda)\, d\lambda \qquad (9)$$

For power-law noise, using Eq. (3), it follows,

$$\sigma^2(t,0) = \frac{2^{-\alpha-1}\pi^{-\alpha}}{[\Gamma(\frac{\alpha}{2})]^2}\int_0^t \lambda^{-\alpha-2}\,d\lambda$$

$$= \frac{2^{-\alpha-1}\pi^{-\alpha}}{[\Gamma(\frac{\alpha}{2})]^2}\,\frac{1}{-\alpha-1}\,t^{-\alpha-1} \quad \text{for } \alpha < -1 \tag{10}$$

For $\alpha = -1$, integral (10) gives $\ell n\ \lambda\Big]_0^t$, and the lower limit presents a problem due to infinite power of $1/|f|$ noise at high frequencies. This can be solved by introducing a high frequency cutoff. One way is to introduce averaging over a short time interval δ. The "smoothed" impulse response for $\alpha = -1$ is

$$h(t,\delta) = \frac{1}{\delta}\int_t^{t+\delta} h(u)\,du$$

$$= \frac{2}{\delta}\left[(t+\delta)^{1/2} - t^{1/2}\right] \tag{11}$$

Impulse response $(t/\delta)^{-1/2}$ and the "smoothed" response $h(t,\delta)$ are shown in Fig. 3, curves a and c. While Eq. (11) gives the effect of sampling with a finite integration time δ, a function similar to this (curve b) can be used, as it results in somewhat simpler calculations. (Both curves affect only the high frequency response.)

Variance as a function of time for $1/|f|$ noise is then

$$\sigma^2(t,0) = \frac{1}{\delta}\int_0^t d\lambda + \int_\delta^t \frac{1}{\lambda}\,d\lambda$$

$$= \begin{cases} t/\delta & \text{for } t \le \delta \\ 1 + \ell n(t/\delta & \text{for } t \ge \delta \end{cases} \tag{12}$$

Thus, for various low frequency divergent noises, we have:

$w_\alpha(f)$ =	α =	$\sigma^2(t,0) \propto$
$1/\|f\|$	-1	$\ell n(t/\delta)$
$1/f^2$	-2	t
$1/\|f\|^3$	-3	t^2
$1/f^4$	-4	t^3

(13)

For low frequency divergent noise, the variance increases in time without limit. This brings up the question of the existence of the low frequency limit. Must it exist? The divergence of the $1/|f|$ noise is so weak that the variance increases very little over a large range of time. According to the argument of Flinn,[25] if the low frequency limit corresponds to current estimates of the age of the universe ($\sim 10^{-17}$ Hz), and the highest frequency to the time taken for light to traverse the classical radius of the electron ($\sim 10^{23}$ Hz), this would represent 40 decades, and in that time the rms noise would increase only $\sqrt{40}$ times the value for one decade. In many measurements the averaging time δ is increased with the observation interval t (the ratio of cutoff frequencies remains the same). In that case one measures a constant power for $1/|f|$ noise.

Noises with $\alpha = -2$ and $\alpha = -3$ are strongly divergent, and they cannot exist without a low frequency limit for any variable which has an upper bound, or a dynamic range limit in the sense of electronic systems. However, they can exist if the variable has no such bound (variables accumulated in time, phase of an oscillator, for example).

Among these noises there is a distinct difference in the ratio of power contained at high and at low frequencies. This is apparent also from sample waveforms shown

in Fig. 4. An interesting effect is that the appearance of $1/|f|$ changes little with time scale, Fig. 5. $1/|f|$ noise in this case was generated by an MOS transistor. The divergence of some noises is shown in Fig. 6, which presents a demonstration of the experiment in Fig. 2. According to relations (13), rms noise increases as $t^{1/2}$, t, $t^{3/2}$ respectively for the three types of noise presented. The low frequency limit of the circuits used to generate these noises was about 2 orders of magnitude lower than the inverse of the (gating) time interval shown on Fig. 6, and the high frequency limit was about 3 orders of magnitude higher.

A Note on the Autocorrelation Function of Divergent Noises

According to the Wiener-Khintchine theorem, the autocorrelation function of a random process is the Fourier transform of its power spectrum. For the spectral density obtained by passing a uniform spectral density (white noise) through a power-law filter according to Eq. (2)

$$R(\tau) = 2\,\frac{1}{(2\pi)}\int_0^\infty H^2(\omega)\,\cos\,\omega\tau\,d\omega \qquad (14)$$

for $\tau = 0$, $R(0) = 2\,\frac{1}{(2\pi)}\int_0^\infty H^2(\omega)\,d\omega$ is the total noise power, which for low frequency divergent noises tends to infinity in the sense discussed in the preceding section. An alternative way of defining the autocorrelation function is based on the concept of the filter autocorrelation function, which is defined as,[27,28]

$$R(\tau) = \int_0^\infty h(u)\cdot h(u+\tau)\,du \qquad (15)$$

where h(t) is the impulse response of the filter. If R_x is the autocorrelation function of the process at the input of the filter, the autocorrelation function of the output process is given by the convolution of the input correlation function and the filter correlation function,

$$R_y(\tau) = \int_0^\infty R_x(\tau-\lambda)\cdot R_h(\lambda)\,d\lambda \qquad (16)$$

For white noise $R_x(\tau) = \delta(\tau)$, and the autocorrelation function of the output process equals the autocorrelation function of the filter.

Relation (15) is of no help, however, since it is equivalent to (14). The problem is only a little better illustrated if one tries to calculate $R(\tau)$ for $1/f^2$ and for $1/|f|$ noise using Eq. (15), as shown in Fig. 7. It is obvious that $R(\tau)$ is undefined for any impulse response which results in $\sigma^2(t,0) \to \infty$.

A somewhat better insight into the correlation properties of low frequency divergent noises can be gained by using the concept of the "time-dependent autocorrelation function." The time-dependent autocorrelation function was introduced by Lampard.[28] The time-dependent autocorrelation function is based on the assumption of a finite observation interval, and can be defined as follows,

$$R(t,\tau) = \int_0^{t-\tau} h(u)\cdot h(u+\tau)\,du \qquad (17)$$

For the case of a random walk, $\alpha = -2$, the impulse response of the filter which converts white noise into $1/f^2$ noise is the unit step function $\sqrt{2\pi}\,U(u)$, Eq. (3), and the function $R(t,\tau)$, according to Fig. 7(a), is

$$R(t,\tau) = (2\pi^2)(t-|\tau|) \qquad (18)$$

$$\text{For } \tau = 0 \quad R(t,0) = (2\pi^2)\,t\,, \qquad (19)$$

which is the variance as a function of time, as derived from Eq. (10). However, the quantity

$$R(t,0) - R(t,\tau) = (2\pi^2)\,|\tau| \qquad (20)$$

is independent of t.

For $1/|f|$ noise, $\alpha = -1$, the impulse response $h(u) = u^{-1/2}$ can be used to determine $R(t,\tau)$.

The high frequency limit can be handled in one of the ways discussed in the previous section. Using the function b in Fig. 3, the calculation of $R(t,\tau)$ can be performed according to Fig. 7(b) and Eq. (16). An unimportant term results from the part of the function $0 < u < \delta$, so that this part can be ignored, and the integration carried on from δ to $t-\tau$. (δ corresponds to the inverse of the high frequency limit and can be made arbitrarily low.) Then,

$$R(t,\tau) = \int_{\delta}^{t-\tau} \frac{1}{u^{1/2}(u+\tau)^{1/2}}\, du \qquad (21)$$

The result of this integration (Peirce,[29] integral 160) is

$$R(t,\tau) = \ell n \frac{(t^2-t\tau)^{1/2} + t - \frac{\tau}{2}}{(\delta+\delta\tau)^{1/2} + \delta + \frac{\tau}{2}} \qquad (22)$$

It is reasonable to assume that $t \gg \tau$, so that

$$R(t,\tau) = \ell n \frac{2t}{(\delta+\delta\tau)^{1/2}+\delta+\frac{\tau}{2}} \qquad (23)$$

Several results are of interest. For $\tau = 0$,

$$R(t,0) = \ell n\left(\frac{t}{\delta}\right) \qquad (24)$$

which equals the noise power (variance) as a function of time, Eq. (12).

$$R(t,0) - R(t,\tau) = \ell n \frac{(\delta+\delta\tau)^{1/2}+\delta+\frac{\tau}{2}}{2\delta} \qquad (25)$$

For $\delta \ll \tau$, the expressions assume a simple form,

$$R(t,\tau) = \ell n 4 + \ell n(t/\delta) - \ell n(|\tau|/\delta) \qquad (26)$$

$$R(t,0) - R(t,\tau) = \ell n(|\tau|/\delta) - \ell n 4 \qquad (27)$$

Both in the case of $1/f^2$ noise and of $1/|f|$ noise, the quantity characteristic of correlation, $R(t,0)-R(t,\tau)$ is independent of t, and therefore of the "age" of the process. This quantity is significant for the calculation of the differences of instantaneous values of noise spaced by τ, since

$$\overline{[x(t+\tau)-x(t)]^2} = 2[R(t,0)-R(t,\tau)] \qquad (28)$$

One assumes here (without proof!) that the translation of the values of x in time is justified since $R(t,0)-R(t,\tau)$ is independent of t. Finite differences as statistically well-behaved quantities for low frequency divergent noise have been used by Barnes[12] and Allan.[11] Barnes[12] was the first to introduce and make use of the function $R(t,0)-R(t,\tau)$. It has been shown,[31] that in these cases[30] the generalized Fourier transform of the generalized spectral density function gives formally $R(t,0)-R(t,\tau)$. This does not imply that the term $R(t,0)$ is not significant. The significance of $R(t,0)$ as considered above is that it represents the variance of the process at time t after the inception of the process. While the knowledge of $R(t,0)$ is not necessary for analysis of differences, it may be required for solution of some time domain problems.

3. Generation of $1/|f|$ Noise

Distributed RC-line Model (Diffusion Model)

The filter which converts a Poisson process into noise with $1/|f|$ spectral density has transfer function $(j\omega)^{-1/2}$, and impulse response $t^{-1/2}$, according to Eqs. (2) and (3). This also represents the required relation between the voltage and current (impedance) for a two-pole (single port) network. It can be shown[32,31] that an "infinitely long" distributed RC line has such an impedance. Referring to Fig. 8(a) and (b), one can write for an infinitesimal section of the line, which is followed by the remainder of the line with line impedance Z,

$$Z = r\delta x + \frac{1}{j\omega c\delta x} \;||\; Z, \qquad (29)$$

where r and c are resistance and capacitance per unit length. The equation for Z is then,

$$Z^2 = Zr\delta x + \frac{r}{j\omega c} \qquad (30)$$

For $\delta \to 0$, it follows,

$$Z = \sqrt{\frac{r}{j\omega c}} \qquad (31)$$

If a noise current is applied to the driving point (input), the mean square noise voltage is, Fig. 8(c),

$$v_n^2 = i_n^2 \,|Z|^2 = i_n^2 \cdot \frac{r}{c} \cdot \frac{1}{|\omega|} \qquad (32)$$

Thus, for a uniform spectral density of the current, $1/|f|$, spectral density is obtained for the voltage.

We can consider now the noise of the RC-line itself. The noise current of the line, which is in thermal equilibrium, is determined by the real component of its admittance,

$$Y = G+jB = \frac{1}{Z} = \left(\frac{\omega c}{r}\right)^{1/2} \cdot j^{1/2}$$

$$= \left(\frac{\omega c}{r}\right)^{1/2} \frac{\sqrt{2}}{2}(1+j) \qquad (33)$$

The mean square noise current density is then

$$\overline{i_n^2} = 4kT\,G(\omega) = \frac{\sqrt{2}}{2} 4kT\left(\frac{c}{r}\right)^{1/2} \cdot |\omega|^{1/2} \qquad (34)$$

The mean square noise voltage at the driving point, Fig. 8(d) is then,

$$\overline{v_n^2} = \frac{\sqrt{2}}{2} \cdot 4kT\left(\frac{r}{c}\right)^{1/2} \frac{1}{|\omega|^{1/2}} \qquad (35)$$

If this noise current flows into a large capacitance C_o, Fig. 8(e), such that $\frac{1}{\omega C_o} << |Z|$, then the voltage on that capacitance is

$$\overline{v_n^2} = \frac{\sqrt{2}}{2} 4kT\left(\frac{c}{r}\right)^{1/2} \frac{1}{C_o^2} \cdot \frac{1}{|\omega|^{3/2}} \qquad (36)$$

Thus, a number of different fractional noises may result from the RC-line noise, depending on the impedance of the input termination.

An RC-line is an electrical equivalent to the diffusion process, and to the heat conduction process. They are all described by the same differential equation, which can be written in the normalized form as

$$\frac{\partial^2 v(x,\theta)}{\partial x^2} - \frac{\partial v(x,\theta)}{\partial \theta} = 0 \qquad (37)$$

where v is the variable equivalent to potential (temperature, concentration of ions), x is distance, and θ is normalized time.

It is of interest to determine the validity of the above expressions and conclusions for a line of finite length (diffusion over a finite distance). Detailed behavior as a function of end termination is quite complicated and has been treated in the literature from various aspects (temperature,[33] impedance,[34] and, recently, impulse response[35,36]). Fortunately, a simple orientative rule can be developed. An RC-line of finite length, Fig. 8(f), is characterized by the time constant $R_\ell C_\ell$, where $R_\ell = r\cdot\ell$ and $C_L = c\cdot\ell$. It can be shown[34] that the impedance of the finite-length line follows the relation for the infinite line, Eq. (31), independently of the end termination, above a lower limit frequency, which is given by

$$\frac{1}{\omega_\ell} \approx \frac{R_\ell C_\ell}{10} \qquad (38)$$

(It may be interesting to note that $R_\ell C_\ell/\pi^2$ appears as a dominant time constant in the expressions for the propagation time of such a line.)

This parameter is significant since it determines the low frequency limit of

$1/|f|$ noise generated by such a network or physical process.

The diffusion model for generation of $1/|f|$ noise is very attractive since it covers a wide range of physical systems, and since various interactions among electrical, thermal and chemical quantities could be considered in some systems in the analysis of the noise generating process. However, detailed analysis and justification of this mechanism in particular cases is quite difficult.

Halford's Mechanical Model

The model which assumes impulse response $t^{-1/2}$ is too restricted in the sense that each perturbation constituting a white process produces the same effect, which has a particular shape in time.

In some studies of noise in solid-state devices (Refs. 3, 4, 5, and others) it has been recognized that $1/|f|$ can be generated by perturbations occurring randomly in time which have certain specific distributions of lifetimes. Halford[14] has proposed a general model in which broad classes of perturbations are found to satisfy the criteria for generation of $1/|f|$ noise. This model is summarized in the following.

According to this model, any class of "reasonable perturbations" occurring at random, under certain constraints, generates random noise having a spectral density $|f|^{\alpha}$ over an arbitrarily large range of frequency only for $-2 \leq \alpha \leq 0$. A class is the set of all perturbations which are equivalent under some individual independent scaling of amplitude, scaling of time and translation of time. A subclass of perturbations is characterized by $P(\tau)$ and $A^2(\tau)$, where $P(\tau)$ is the probability density of perturbations with lifetime τ, and $A^2(\tau)$ is a mean-square amplitude of perturbations having lifetime τ. For a given class, $|f|^{\alpha_\infty}$ and $|f|^{\alpha_o}$ are the frequency-smoothed laws in the limits of infinite and zero frequencies which specify the cutoff properties. Any reasonable perturbation must have $\alpha_\infty \leq -2$ and $\alpha_o \geq 0$, which means that there should be no divergence at either the low or high frequency limit. To generate random noise having an $|f|^{\alpha}$ law over an arbitrarily large range of f from a subclass chosen from any class characterized by α_∞ and α_o, it is necessary that $\alpha_\infty \leq \alpha \leq \alpha_o$. For $P(\tau)$ and $A^2(\tau)$, it is then necessary and sufficient to satisfy the condition,

$$P(\tau) \cdot A^2(\tau) \approx B\tau^{-\alpha-3} \qquad (39)$$

where B is a constant. This condition should be satisfied over a range of τ, which determines the range of f over which the $|f|^{\alpha}$ law is obeyed. Outside of this range of τ, the condition

$$P(\tau)A^2(\tau) \leq B \cdot \tau^{-\alpha-3} \qquad (40)$$

should be satisfied. A reasonable perturbation is any perturbation which satisfies the requirements that it is everywhere finite, and that it has a finite integral, finite energy and finite nonzero lifetime.

For $1/|f|$ noise $\alpha = -1$, and the condition (39) can be satisfied over an arbitrarily large range. This can be illustrated by the example of a very common perturbation $A(\tau)\ U(t)\ \exp(-t/\tau)$, which represents a step change with exponential decay. The condition (39) for $1/|f|$ noise is

$$P(\tau)A^2(\tau) \approx B\,\frac{1}{\tau^2} \qquad (41)$$

Assuming a restricted case where all lifetimes are equally probable, $P(\tau) = 1$, it follows

$$A(\tau) \propto \frac{1}{\tau} \qquad (42)$$

The spectral density of the perturbations $\frac{1}{\tau}\exp(-t/\tau)$ for the values of lifetime between τ and $\tau+d\tau$ is $d\tau/(1+\omega^2\tau^2)$. Then the spectral density for the perturbations over the range of τ from 0 to ∞ will be

$$\int_0^\infty \frac{1}{1+\omega^2\tau^2}\,d\tau = \frac{1}{|\omega|}\tan^{-1}(\omega\tau)\Big]_0^\infty = \frac{\pi}{2}\,\frac{1}{|\omega|}$$

(The same result is obtained in this example for $A(\tau)$ = const. and $P(\tau) \propto 1/\tau^2$). It should be noted here that in any class of perturbations the low frequency limit of the spectral density is determined by the maximum value of lifetime τ.

The mechanism of $1/|f|$ noise in MOS transistors has been recently described[6,7] in terms which fall within the frame of this model. The particular mechanism is explained in terms of tunneling of carriers at the silicon-silicon oxide interface to traps located inside the oxide. The dispersion of the time constant was found to be 10^{17}, and the low frequency limit corresponds to $\tau \approx 10^9$ sec ($\approx$ 30 years).

An interesting case of this model is for constant amplitude perturbations, $A(\tau) = 1$. Then, for $1/|f|$ noise, the condition to be satisfied is,

$$P(\tau) \propto \frac{1}{\tau^2} \qquad (43)$$

This case is suitable for simulation of $1/|f|$ noise on the computer, although an amplitude distribution may also be used.

The models described in this section are elegant and analytically neat. The actual physical mechanisms in particular cases might be considerably more involved. Some complex mechanisms are discussed in Ref. 15.

Lumped-Parameter Approximations of Impulse Response $t^{-1/2}$

The realization of impedances and filters with transfer functions with $(j\omega)^{-1/2}$ frequency dependence ($t^{-1/2}$ impulse response) by using distributed and lumped parameter networks to approximate this law over a limited range of frequencies for various purposes has received much attention in the literature (further references are given in Ref. 34 of this paper). These networks are variously referred to as "constant-argument impedance," "constant-angle impedance," "fractional capacitance," "fractional integral and derivative operators," or "power-law magnitude impedance." Each of these terms is meaningful in some way of representing $1/|f|$ noise.

For generation of $1/|f|$ noise in the low frequency range, digital circuits, or digital computers, are more suitable because perturbations (impulse responses) with arbitrarily long lifetimes can be realized, aside from other processing advantages. Analog circuits are generally simpler, but unsuitable for the low frequency range. The choice between them is somewhat arbitrary in the frequency range where both can be realized. Analog circuits are the only solution in the frequency range where the speed of digital circuits is not sufficient. (The high frequency limit of the noise generated by digital operations is about an order of magnitude lower than the rate of digital operations, if gaussian distribution of amplitudes is to be achieved.)

An example of a lumped-parameter network is shown in Fig. 9. The ratio of time constants is the same between successive RC networks. A large value was selected for this ratio to emphasize the effects of the lumped-parameter approximation, as shown in Fig. 10. In spite of this, the departure of the spectral density from the $1/|f|$ law is no larger than 0.7 dB over 4 decades (Fig. 10). An advantage of this circuit is that independent adjustment of the attenuation coefficients and the time constants is possible. Switches (realized by junction field-effect transistors) are included for time-domain and time-variant filter studies. A point sometimes neglected in realizations of such circuits is that the resistors which cover a wide range of values should be real (a ladder network attenuator may be necessary, as shown in Fig. 9, to avoid the effect of stray capacitances, which can be significant in the range above 10^5 Hz).

4. Conclusions on Measurements

From the discussion about power-law noises $|f|^{\alpha}$, the conclusion is that $1/|f|$

noise occupies a central place between the noises which are high frequency divergent ($\alpha \geq -1$) and the noises which are low frequency divergent ($\alpha \leq -1$). The unique property of $1/|f|$ noise is that it is divergent at both limits. The relations derived for the variance in the frequency domain, Eq. (7), and in the time domain, Eqs. (10) and (12), and the relations describing correlation properties, are important in the measurements of physical quantities in the presence of noise and in the measurements of noise. In the case of narrow-band measurements, where $\Delta f = f_h - f_\ell \ll \frac{1}{2}(f_h + f_\ell)$, an obvious result follows for the variance

$$\sigma^2(f, \Delta f) \approx |f|^\alpha \Delta f \qquad (44)$$

For a given bandwidth, the variance is determined by the spectral density.

In the case of wide-band measurements, the variance is determined by both frequency limits. In the case of wide-band measurements where $f_\ell \ll f_h$, the variance is determined by the low frequency limit for low frequency divergent noises $\alpha < -1$, and by the high frequency limit for high frequency divergent noises $\alpha > -1$. Both limits should always be considered when α is close to -1.

In the time domain measurements, the length of the measurement interval T, or, in other words, the observation time [0,t in Eqs. (10) and (12)] corresponds to the low frequency limit. In the time domain measurements, instantaneous values are observed by some sampling method. Each sample represents some averaging function of all the instantaneous values in a short time interval δ, which then corresponds to the high frequency limit. The variance is then determined by T and δ.

The class of measurements which is of particular interest is the one where the ratio of the high frequency limit and the low frequency limit is maintained constant (f_h/f_ℓ = const., or T/δ = const.) as the limits are varied. The frequency limits are characterized by one parameter, τ, which is related to $1/f_\ell$ and $1/f_h$ (T and δ) by a constant. Using the relation (7), the relation of the variance to the parameter τ ("measurement time") is determined for power-law noises,

$$\sigma^2(\tau) = K_\alpha \tau^{-1-\alpha} \qquad (45)$$

K_α is a constant determined by α from Eq. (7) and by the relation of τ to the frequency limits. More generally, K_α is a constant characteristic of the impulse response of the particular bandpass filter, or of the weighting function in pulse measurements and for time-variant filters.

The importance of the relation (45) is that the observed dependence of variance as a function of measurement time τ can be used to identify a particular noise component, which would otherwise be impossible to measure separately. Any physical power spectral density function can be represented by the power series,

$$W(f) = \cdots + W_1 |f|^1 + W_0 f^0 + W_{-1} |f|^{-1} + W_{-2} f^{-2} + \cdots \qquad (46)$$

The corresponding power series for variance as a function of τ is

$$\sigma^2(\tau) = \cdots + K_1 \tau^{-2} + K_0 \tau^{-1} + K_{-1} \tau^0 + K_{-2} \tau^1 + \cdots \qquad (47)$$

The meaning of this power series is not the mere approximation of a continuous function. Each term is meant to correspond to a particular physical source of noise or to a group of sources. To fulfill this, in some cases, a power series with fractional exponents may be more appropriate. As an example, the noise of the feedback resistor in charge amplifiers can be considered. A resistor in the range of 10^9 - 10^{10} ohms represents a distributed RC-line due to its stray capacitance. Its noise current is integrated on the amplifier input capacitance, and, according to Fig. 8(e) and Eq. (36), it produces $|f|^{-3/2}$ noise in the frequency range of interest in that case.[39] The term $K_{-3/2} \cdot \tau^{1/2}$ added to the series (47) would in such a case result in a better agreement with the measured function $\sigma^2(\tau)$.

This method, based on three terms of a power series ($\alpha = 0, -1, -2$), was first used in measurements with charge amplifiers for nuclear radiation detectors.[37,38] It has been used extensively in frequency and time data analysis and measurements.[10,11,12,17] If this method is extended to measure $\sigma^2(\tau)$ as a function of some other system variables (temperature of input amplifier components), as has been done with charge amplifiers,[20] it can be a powerful tool in identifying some physical sources of noise. The parameter τ is equivalent to various commonly used terms in different areas of measurements. It is referred to as "filter time-constant" in pulse amplifiers for nuclear detectors. It corresponds to the "sweep time," or to the "filter integration time-constant" in nuclear magnetic resonance and in electron paramagnetic resonance measurements.

Relation (45) was derived from Eq. (7), and it holds for any α. However, it must be noted that the bandpass frequency characteristic implied by the integral (7) is a "window" limited by frequencies f_ℓ and f_h. If the lowest order bandpass filter is used with one pole and one zero (one RC integration and one RC differentiation), the variance for that filter would not converge for $\alpha \geq 1$ at the high frequency limit, and for $\alpha < -2$ at the low frequency limit. The relation (45) holds for this range of α, and such a filter is in most cases satisfactory. If noises beyond this range of α are expected, filters with a sharper cutoff (multiple poles and zeros) should be used. In time domain measurements, sampling with simple integration of instantaneous values in each sample represents a first order filter, which is not sufficient for noises with $\alpha > 1$. If f^2 noise is expected, instantaneous values from the interval δ should be passed through a second order low-pass filter, which can be realized in a number of ways. These remarks about the sampling apply also to the derivation of Eq. (45) from the time domain expression (10), where higher-order smoothing should be applied to $h(u)$ for high frequency divergent noises with $\alpha > 1$.

Having the noise defined, the usual procedure is to find an optimum filter for a given signal (filter matched to signal and noise). One of the most common signals is a step function (or a dc quantity resulting from rectification of an ac signal), the amplitude of which is to be measured in the presence of noise. An intuitive step usually undertaken is to integrate this signal and noise. This is a correct procedure for white noise since integration represents a matched filter for this case. If $1/|f|$ noise is present, the variance decreases as τ^{-1} until the variance due to $1/|f|$ noise is reached, which is independent of τ. Little advantage can be gained by changing the ratio f_h/f_ℓ since variance is a logarithmic function of this ratio. Thus, in the case of $1/|f|$ noise, the most important aspect is to find its physical source, with the aim of reducing it at the source if possible.

According to relation (7) the variance is a function of the frequency limits of the measurement for a given type of noise. In the measurements of differences, Eq. (28), the variance is determined by the observation interval τ and by the averaging interval δ (for noises where averaging or smoothing is important), Eqs. (20) and (27); that is, by the time domain equivalents of the frequency limits. This also applies to the general relation (45) for power-law noises in all the frequency domain and time domain measurements in which the ratio of the high frequency limit and the low frequency limit is constant (or where one of the limits is unimportant). For low frequency noise, this means that the part of the spectrum below the low frequency limit of the measurement process is unimportant (paying attention to the exact nature of the low frequency cutoff in relation to the power-law exponent α). For an imagined truly divergent low frequency noise (where the spectrum

follows the power-law to zero frequency), the variance in such measurements would be independent of the "age" of the noise process. Thus, for purposes of the measurements, that is, for physical observations, it is unimportant whether the low frequency noise has a low frequency limit or not (whether it is convergent or divergent), provided that it obeys its power-law within the observable frequency range. Consequently, all physical evidence relating to low frequency noises is limited by the low frequency limit of the measurement process; that is, by the maximum observation time.

Some Further Questions about $1/|f|$ Noise

In this paper the qualification of $1/|f|$ noise as being stationary or non-stationary has not been explicitly considered so far. We can first specify that in the representation in Section 2 the imagined Poisson process which generates $1/|f|$ noise is stationary in time (in the strict sense) and that the parameters of the "transforming filter" are constant (in the case of Halford's model, for example, we assume that the distribution functions remain constant in time). The resulting low frequency divergent process cannot be called stationary in the strict sense since its variance increases with time. Some of its features are stationary, however. From the discussion of the correlation function it follows that finite differences of $1/|f|$ noise are stationary. From this, and from the fact that the underlying mechanism which generates $1/|f|$ noise by a linear transformation is stationary, one can consider this case as a "divergent process growing in a stationary way" or as a divergent process with "stationary increments."[31]

A stationary characteristic of such a process can be expressed in the following way. The true variance (mean value of noise power) for a given frequency range is given by Eq. (7), or more generally, including time domain measurements by Eq. (45). An estimate of this variance is obtained by measurements in which the noise power (variance) is averaged over a measurement time T_m. An underlying assumption in this procedure is that the spectral density function of the fluctuations of the variance is white, which should be the case for a stationary process. This should apply to finite-bandwidth measurements on low frequency noises, since these measurements involve only the noise increments which are stationary. In such a case the variance of these fluctuations ("variance of variance") should decrease with the measurement time as $\sim 1/T_m$. [In the case where variance (mean square noise) is determined from a number of samples, N, the "variance of variance" should decrease as $\sim 1/N$] $1/|f|$ noise satisfying this requirement would correspond to what is sometimes vaguely referred to as "well-behaved" $1/|f|$ noise.

There is some evidence that there are noises whose spectral density function is generally categorized as $1/|f|$ noise (under unspecified measurement conditions in many cases), and which are not "stationary" or "well-behaved" in the sense discussed above. Brophy[40,41,42] has reported more detailed measurements on $1/|f|$ noise in carbon resistors, in which he finds the fluctuations of the variance to be larger than for white noise under equivalent measurement conditions. He also finds the dependence of variance of these fluctuations on the measurement interval to be different from $1/T_m$.

For such noises, one is led to assume that there might be some low frequency fluctuations in the parameters of the process generating $1/|f|$ noise. Alternatively, a nonlinear mechanism may be involved, where low frequency components would cause variations in the amplitude of the high frequency components.

There is too little statistically meaningful experimental evidence on such behavior so far. To specify the noise more precisely, the measurements of "variance of variance" should be performed as a function of measurement time, after the essential noise components have been

identified by spectrum measurements or by the method discussed in the preceding section. Such measurements are easier for the high frequency portion of the spectrum, since the large amount of data required can be collected in a shorter time. In these measurements it becomes increasingly difficult to separate "causal" changes in process parameters (due to temperature) from random changes. Nevertheless, the significance of such information is that it would lead closer to the sources of the fluctuations, whether they are random or not, and thus increase the possibility of their reduction.

In some particular cases of measurements of physical quantities, the knowledge of the spectrum of fluctuations of the variance may result in better optimization of measurement and data processing procedures than by just assuming that the spectrum of fluctuations of the variance is white.

Acknowledgements

It is a pleasure to acknowledge many discussions with R. L. Chase and M. J. Rosenblum. A useful discussion with J. A. Barnes and D. Halford of NBS, Boulder, Colorado is gratefully acknowledged.

DISCUSSION

S. S. Klein : - I understand from Mr. Radeka's talk that there is an optimal time for the minimal variance of a meaurement. However, it is necessary to indicate the accuracy of the measurement. As I understand it now, you are not sure the value obtained from any measurement will be repeated to a given accuracy in ten years or in thirty years or in a time comparable to the age of the universe, so leading to a state of despair about ever measuring anything with any accuracy at all.

Radeka : - Well, I understand this more as a comment than as a question.

S. S. Klein :-Give me hope, please.

Radeka : - Well, the things may be not so bad as I presented them. We hare still making some measurements within the time which is available to us and the effects of noise with the different power laws is a matter for a longer discussion. The effects, of any variance in the noise power as a function of measurement parameters would depend on a specific case. In some cases the $1/f^n$ noise may be quite stationary and in some other cases it may not be. If they are stationary then, any measurement that we make with the measurement time of one second would always give the same probability distribution of results now and after ten years. If however we have a process which is not stationary in this sense, that is a process which generates low frequency noise, then, it may not be so.

References

1. J. B. Johnson, "The Schottky Effect in Low Frequency Circuits," Phys. Rev. 26, 71 (1925)

2. W. Schottky, "Small-Shot Effect and Flicker Effect," Phys. Rev. 28, 75 (1926)

3. A. van der Ziel, Fluctuation Phenomena in Semiconductors, Academic Press, New York 1959

4. A. L. McWhorter, "1/f Noise and Related Surface Effects in Germanium," M.I.T. Lincoln Lab., Lexington, Mass., Tech. Rep. 80, May 1955

5. A. L. McWhorter, "1/f Noise and Germanium Surface Properties," Semiconductor Surface Physics, R. H. Kingston, Ed., Philadelphia, Pa., Univ. of Pennsylvania Press, 1957, pp. 207-228

6. C. Christensson, I. Lundström and C. Svensson, "Low Frequency Noise in MOS Transistors-I," Solid-State Electronics 11, 797 (1968)

7. S. Christensson and I. Lundström, "Low Frequency Noise in MOS Transistors-II," Solid-State Electronics 11, 813 (1968)

8. I. R. M. Mansour, R. J. Hawkins and G. G. Bloodworth, "Digital Analysis of Current Noise at Very Low Frequencies," The Radio & Electronic Engineer, 35, 201 (1968)

9. I. R. M. Mansour, R. J. Hawkins and G. G. Bloodworth, "Measurement of Current Noise in M.O.S. Transistors from $5X10^{-5}$ to 1 Hz," The Radio and Electronic Engineer, 35, 212 (1968)

10. L. S. Cutler and C. L. Searle, "Some Aspects of the Theory and Measurement of Frequency Fluctuations in Frequency Standards," Proc. IEEE 54, 136, Feb. 1966

11. D. W. Allan, "Statistics of Atomic Frequency Standards," Proc. IEEE 54, 221 (1966)

12. J. A. Barnes, "Atomic Timekeeping and the Statistics of Precision Signal Generators," Proc. IEEE 54, 207 (1966)

13. J. A. Barnes and D. W. Allan, "A Statistical Model of Flicker Noise," Proc. IEEE 54, 176 (1966)

14. D. Halford, "A General Mechanical Model for $|f|^{\alpha}$ Spectral Density Random Noise with Special Reference to Flicker Noise $1/|f|$," Proc. IEEE 56, 251 (1968)

15. H. E. Derksen, "Axon Membrane Voltage Fluctuations," Acta Physiol. Pharmacol. Neerl. 13, 373 (1965)

16. D. Brouwer, "A Study of the Changes in the Rate of Totation of the Earth," Astron. J. 57, 125 (1952)

17. J. A. Barnes and D. W. Allan, "An Approach to the Prediction of Coordinated Universal Time," Frequency, pp 3-8, Nov./Dec. 1967

18. B. B. Mandelbrot and J. W. van Ness, "Fractional Brownian Motions, Fractional Noises and Applications," Siam Rev. 10, No. 4, 422 (Oct. 1968)

19. B. B. Mandelbrot, "Noises with an 1/f Spectrum, a Bridge Between Direct Current and White Noise," IEEE Trans. Information Theory, IT-13, 289 (1967)

20. V. Radeka, "State of the Art of Low Noise Amplifiers for Semiconductor Radiation Detectors, Proc. Internat. Symposium on Nuclear Electronics, Versailles, 1968, p. 46-1

21. E. Gatti and V. Svelto, "Resolution as a Function of Noise Spectrum in Amplifiers for Particle Detection," Energia Nucleare, 8, 505 (1961)

22. M. P. Klein and G. W. Barton, Jr., "Enhancement of Signal-to-Noise Ratio by Continuous Averaging: Application to Magnetic Resonance, Rev. Sci. Instr. 34, 754 (1963)

23. G. A. Campbell and R. M. Foster, "Fourier Integrals for Practical Applications," D. Van Nostrand Co., Inc., New York, 1961

24. N. Campbell, Proc. Cambridge Phil. Soc. 15, 117 (1909)

25. I. Flinn, "Extent of the 1/f Noise Spectrum" Nature, 219, 1356, Sept.28,1968

26. J. S. Bendat, "Principles and Applications of Random Noise Theory, John Wiley & Sons, Inc., New York 1958

27. J. R. Schwarz and B. Friedland, Linear Systems, McGraw-Hill, New York, 1965

28. D. G. Lampard, "The Response of Linear Networks to Suddenly Applied Stationary Random Noise," IRE Trans. on Circuit Theory, CT-2, 43 (1955)

29. B. O. Peirce, A Short Table of Integrals, Ginn & Co., New York 1929

30. M. Lighthill, Introduction to Fourier Analysis and Generalized Functions, New York: Cambridge 1962

31. J. A. Barnes, Private Communication

32. O. Heavyside, Electromagnetic Theory, Dover Publications, New York 1950

33. H. S. Carslaw and J. C. Jaeger, Conduction of Heat in Solids, Clarendon Press, Oxford, 1947, p. 76

34. S. C. Dutta Roy and B. A. Shendi, "Distributed and Lumped RC Realization of a Constant Argument Impedance," Jour. of the Franklin Institute, 282, No. 5, 318 (1966)

35. W. W. Happ and S. C. Gupta, "Time-Domain Analysis and Measurement Techniques for Distributed RC Structures. I. Analysis in the Reciprocal Time Domain," Jour. Applied Phys. 40, 109 (1969)

36. R. C. Perison and E. C. Bertnulli, "Time-Domain Analysis and Measurement Techniques for Distributed RC Structures. II. Impulse Measurement Techniques," Jour. Applied Phys. 40, 118 (1969)

37. A. B. Gillespie, Signal, Noise and Resolution in Nuclear Counter Amplifiers, Pergamon Press, London, 1953

38. E. Baldinger and W. Franzen, Advances in Electronics and Electron Physics, Vol. 8, 256 (1956)

39. V. Radeka, to be published

40. J. J. Brophy, "Statistics of 1/f Noise," Phys. Rev. 166, 827, (1968)

41. J. J. Brophy, "Zero-Crossing Statistics of 1/f Noise," J. Appl. Phys. 40, 567 (1969)

42. L. J. Greenstein and J. J. Brophy, "Influence of Lower Cutoff Frequency on the Measured Variance of 1/f Noise," J. Appl. Phys. 40, 682 (1969)

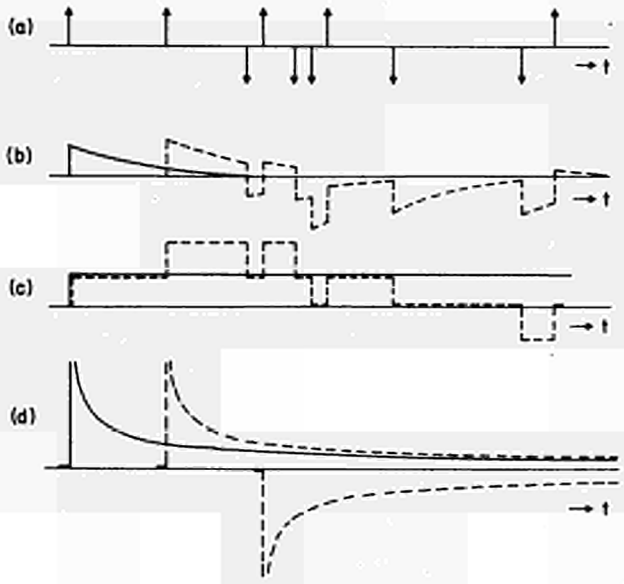

Fig. 1 - Generation of $1/|f|$ noise and $1/f^2$ noise from a Poisson process by a filter with appropriate impulse response. a) Poisson process, random sequence of impulses ; b) Band-limited white noise ; c) $1/f^2$ noise (random walk) ; d) $1/|f|$ noise.

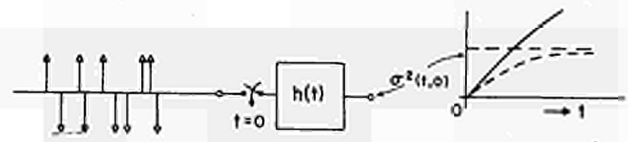

Fig. 2 - Time domain divergence test.

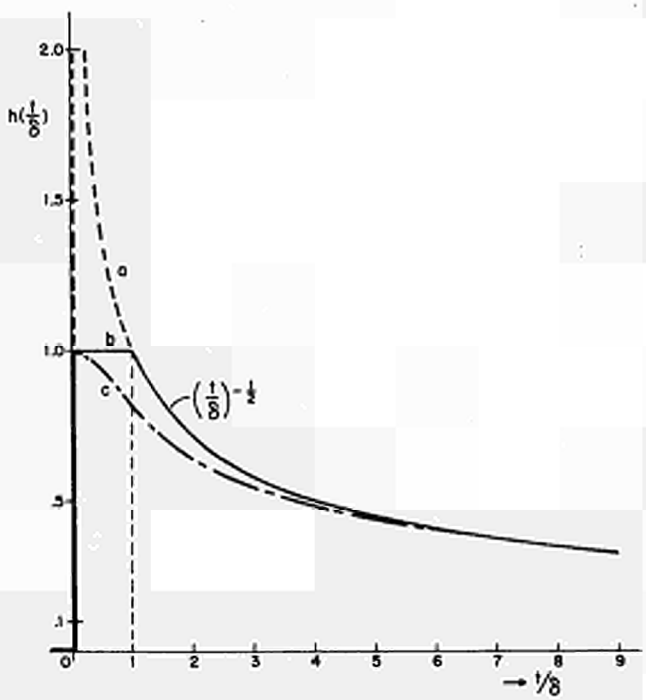

Fig. 3 - Impulse response for generation of $1/|f|$ noise (curve a) , and with high frequency cutoff (curves b and c);

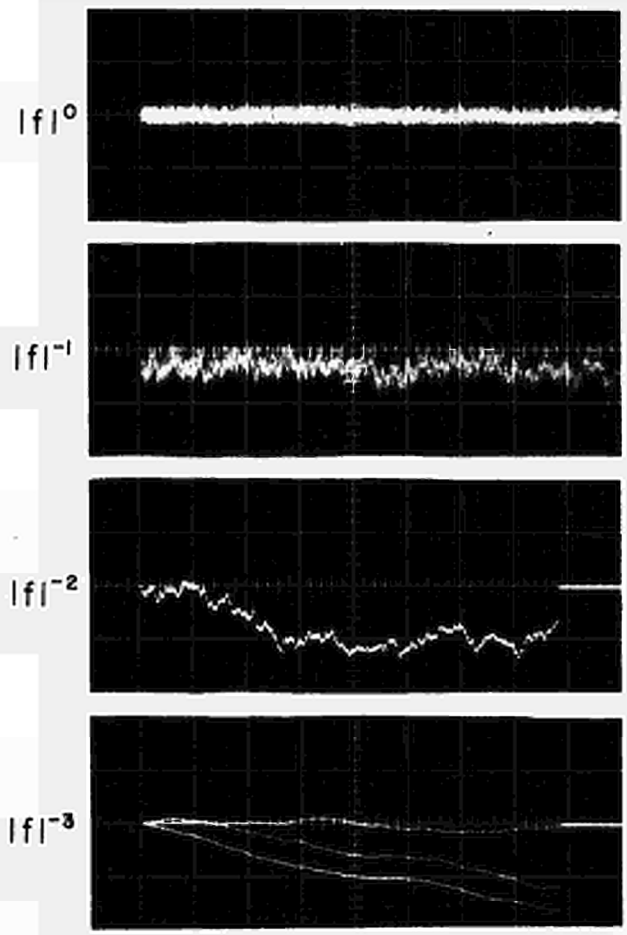

Fig. 4 - Samples of noise waveforms for α = 0, -1 , -2, -3 (white noise, $1/|f|$ noise, random walk, $1/|f|^3$ noise)

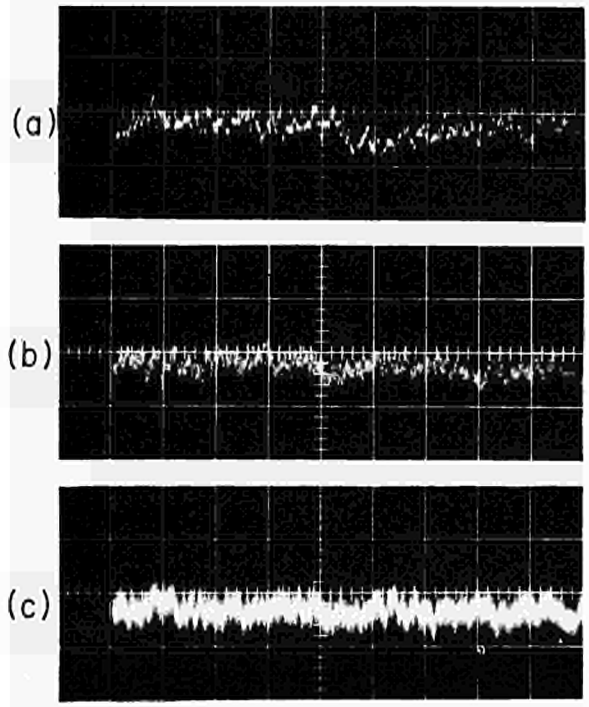

Fig. 5 - Samples of noise waveforms for $1/|f|$ noise at different time scales : a) 10 µsec/div. , b) 50 µsec/div. , c) 500 µsec/div. .

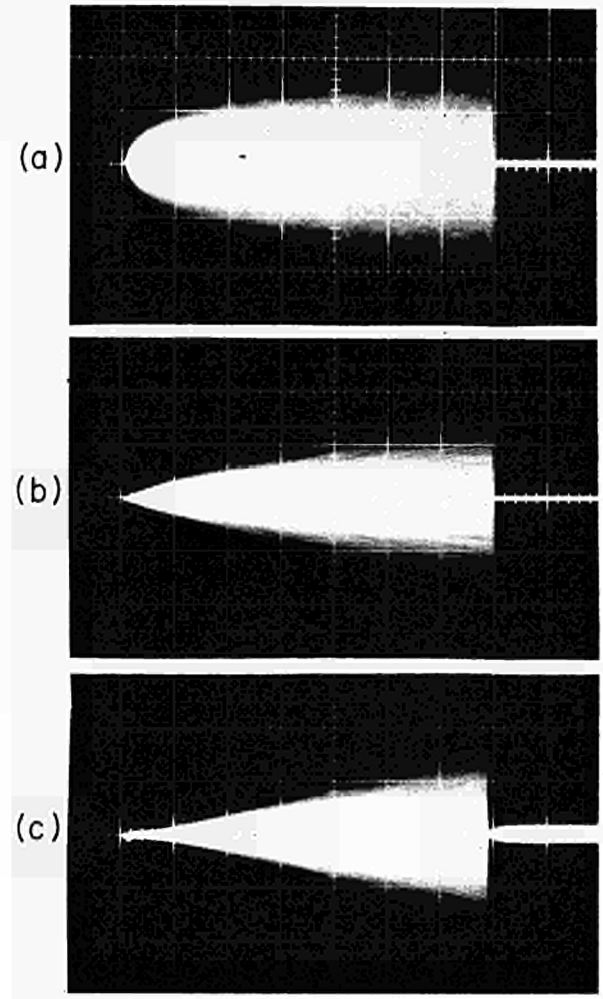

Fig. 6 - Standard deviation (rms noise) as a function of time for some low frequency divergent noises. (envelope of bright area $\approx \sigma(t,0)$). a) $1/f^2$ noise ; white noise switched into an integrator, $h(t) = U(t)$; b) $1/f^3$ noise switched on $h(t) = t^{1/2}$; c) $1/f^4$ noise ; white noise switched on $h(t) = t$.

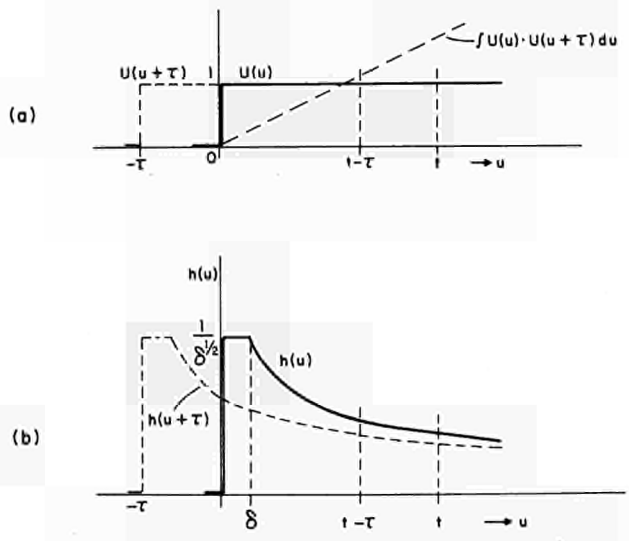

Fig. 7 - Calculation of "time-dependent correlation function", a) $h(u) = \sqrt{2\pi}\, U(u)$ for $1/f^2$ noise ; b) $h(u) = u^{-1/2}$ for $1/|f|$ noise.

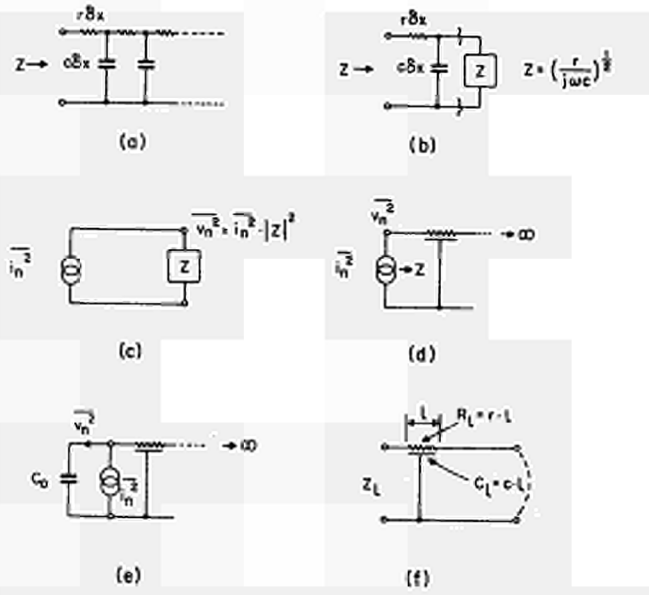

Fig. 8 - Distributed RC-line model for generation of $1/|f|$ noise , a) Distributed RC-line ; b) Impedance of distributed RC-line ; c) Noise voltage-current relation for impedance Z ; d) Thermal noise of RC-line acting upon the line itself ; e) Thermal noise of RC-line acting upon a capacitance ; f) RC-line of finite length.

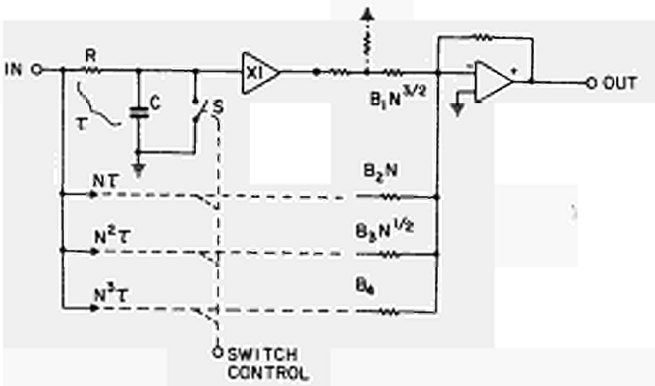

Fig. 9 - A lumped parameter circuit for generation of $1/|f|$ noise from white noise. N - ratio of time constants.

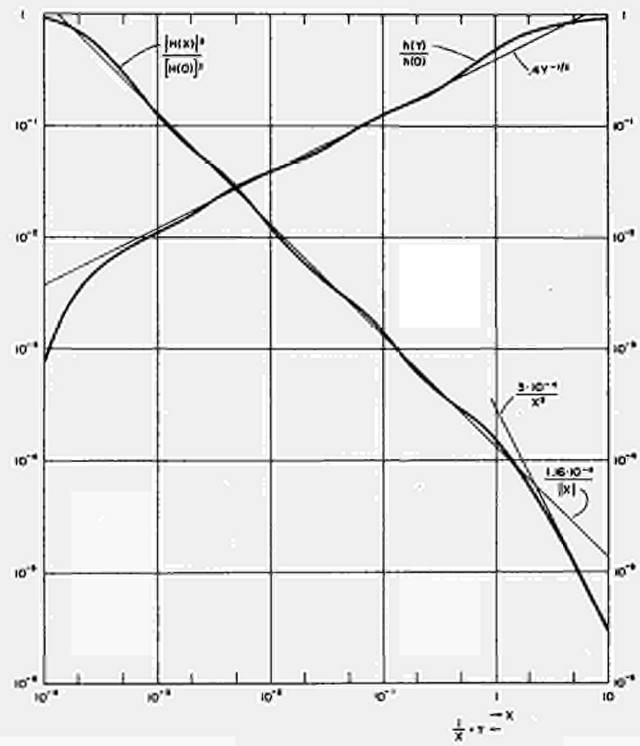

Fig. 10 - Spectral density $|H(X)|^2$ and impulse response h(Y) for the filter in Fig.9. Coefficients $B_1 = B_4 = 1$, $B_2 = B_3 = .7$; ratio of time constants $N = 15$; $X = \omega\tau$; $Y = t/\tau$.

FET PREAMPLIFIERS FOR SEMICONDUCTOR RADIATION DETECTORS

Emanuel Elad,
Nuclear Diodes, Inc.
Prairie View, Illinois

Abstract

A summary of the state-of-the-art of FET preamplifiers for X-ray and γ-ray spectroscopy is presented. Mainly noise considerations for cryogenic operation are analyzed, both from the device and circuit point of view. A comparison is made between various types of FET's differing in channel material, geometrical structure and operating conditions. Some previously unpublished results on GaAs FET's are given. The noise of the input stage and especially its temperature dependence is analyzed and some optimum measuring conditions are derived. Input stage configurations, detector-preamplifier coupling methods and microphonic generation are discussed, emphasizing low temperature operation. Finally, future possibilities in the development of low noise amplifiers are assessed in view of the growing scientific and industrial applications of high resolution semiconductor spectrometers.

Introduction

Semiconductor nuclear particle detectors registered phenomenal progress in the first decade of their existence. Most of the work in the first part of this decade, 1958-1964, has concentrated upon improving the detector performance and developing new types of detectors. However, only with the introduction of the lithium-drifted germanium detector with satisfactory depletion depth in 1963[1], semiconductor gamma ray spectroscopy has been converted from a laboratory curiosity to a productive area of nuclear physics and chemistry. The most important advantage of semiconductor detectors over scintillators and gaseous detectors is their excellent resolution, stemming from the small amount of energy needed to produce one electron-hole pair. With the increased use of semiconductor detectors, it was quickly understood that the reduction of the electronic noise associated with the preamplifier is the key to successful realization of the resolving capabilities of such detectors. Therefore, it is to no one's surprise that during the last 3-4 years a lot of effort was concentrated in that area. In the following, the milestones in the development of preamplifiers for semiconductor radiation detectors are summarized. No attempt is made to list all the various valuable contributions in the field.

The first preamplifiers used in conjunction with semiconductor detectors were vacuum tube type units[2-4]. The resolution of the best units was in the vicinity of 2 keV with a slope of 50 eV/pf, and to keep it at that level, the tubes had to be carefully selected and be replaced nearly every six months. Although nowadays the noise properties of these preamplifiers are not impressive, the ground work for charge-sensitive preamplifiers was laid by their designers.

Following the technological progress in fabrication of semiconductor active devices, preamplifiers were designed using such devices in their input stages. Bipolar transistor preamplifiers were attempted with disappointing results (25 keV)[5], which should have been expected due to the high noise figure of bipolar transistors for high source resistances.

The era of FET preamplifiers began around 1964 with the appearance of the first commercial FET units. The early results[6-7] (3-5 keV) were not very encouraging as the designers could not even equal the performance of vacuum tube preamplifiers. However, the theory predicted that the FET should have much smaller noise than the vacuum tube and the designers did not give up. Cryogenic operation was attempted[8-10] and for the first time noise performance was better than that of the vacuum tube preamplifiers. Blalock[8] reported resolution of 1.6 keV (Si) with a slope of 60 eV/pF and Nybakken[9] 0.98 keV (Si). However, the actual system resolutions for low energy gamma rays (10-100 keV) were still in the region between 2 to 3 keV comparable to the results obtained with vacuum tube preamplifiers.

VHF field effect transistors became commercially available in 1965, initially the 2N3823, followed by many other types. Subsequently, Elad[11] reported a cooled preamplifier with 0.7 keV resolution. The detector-input stage configuration was optimized using dc coupling, minimizing the stray input capacitance, providing effective electrostatic shielding and using low capacitance, low leakage germanium detector. Resolution for Co^{57} γ-rays was 1.1 keV, almost a factor of 2 better than previously obtained with vacuum tube preamplifiers. These results were subsequently improved[12-13] to 0.4 keV + 38 eV/pF coupled with a 0.8 keV resolution for Co^{57} γ-rays, by careful selection of the critical components.

To compensate for the relatively low efficiency of semiconductor detectors large volume detectors have to be used in numerous applications. Unfortunately, that means high detector capacitance and consequently high system noise. Preamplifiers with low sensitivity to input capacitance are thus required. Paralleling FET's in the input stage was suggested by Smith and Cline[14] as a possible solution. They reported resolution of 0.62 keV + 17 eV/pF with four paralleled FET's. At the present, better results (10-15 eV/pF) are obtained using large area chopper type FET's, as reported in the following and by others.[15]

In the search for lower and lower noise preamplifiers, FET's from other materials than silicon were investigated. Elad and Nakamura[16] using a germanium FET at 4.2° K obtained resolution of 280 eV with a slope of 18 eV/pF. Less successful results were obtained by Elad[17] for GaAs FET, although theoretically FET's from this material should be superior to the germanium transistor.

This paper will summarize the state-of-the-art of FET preamplifiers for X-ray and γ-ray spectrometers. Mainly noise considerations for cryogenic operation will be analyzed, both from the device and circuit point of view. A comparison will be made between various types of FET's differing in channel material, geometrical structure and operating conditions. Some previously unpublished results on GaAs FET's will be presented. The various noise sources of the input stage, and especially their temperature dependence, will be analyzed and some optimum measurement conditions will be derived. Input stage configurations and their passive elements, detector-preamplifier coupling methods and microphonic generation will be discussed, emphasizing low temperature operation.

Finally, future possibilities in the development of low noise amplifiers will be assessed in view of the growing scientific and industrial applications of high resolution semiconductor spectrometers.

General Considerations

Block diagram of a typical FET preamplifier used in conjunction with semiconductor radiation detectors is given in Fig. 1. The charge signal from the detector is amplified by two cascaded feedback amplifiers. The first amplifier which has an FET input stage followed by a high voltage gain (A_1) unit, is normally operated in the charge-sensitive mode determined by the capacitive character of Z_{f1}. The second amplifier is usually voltage sensitive and it boosts the analyzed signals to a level which can be transmitted through long cable without large deterioration of the signal-to-noise ratio. The second amplifier is normally omitted in preamplifiers for high energy spectrometers.

The main requirement from a preamplifier for high resolution spectroscopy is low noise. The noise of the detector-preamplifier unit is determined by the detector, the FET stage, and the feedback network Z_{f1}. The contribution of A_1 is negligible due to the high power gain of the FET stage. The same is true for A_2, especially when the output impedance of A_1 is low and the main differentiator is in the following amplifier.[18]

Other requirements from the preamplifier are gain stability, linearity, wide bandwidth and sufficient dynamic range. Gain stability of feedback amplifiers depends on the stability of the feedback network and the open-loop gain of the amplifier. Temperature stable capacitor and resistor are therefore required for Z_{f1} and Z_{f2}, respectively. High frequency response, required mainly for coincidence experiments, necessitates the use of high frequency FET's as well as bipolar transistors in A_0, A_1 and A_2. With presently available active components, however, timing limitations are mainly due to the detector itself. Large dynamic range dictates the use of transistors with high breakdown voltage, which normally agrees with the speed requirement.

The heart of an FET amplifier is obviously the FET itself. Therefore, a thorough discussion of their temperature characteristics and noise considerations will be presented. This will be followed by an investigation of noise aspects of various input stage configurations, detector-preamplifier coupling configurations, microphonic generation and passive components of the input stage and the feedback network.

Field Effect Transistors

The principles of field effect transistors were introduced by Shockley[19] in 1952 before the first bipolar transistors were devised. Unfortunately the early devices were of the metal-oxide-semiconductor (MOS) type and surface contamination prevented their successful operation. The first commercial field effect devices appeared in the early 60's with the fast advancing semiconductor technology after the invention of the bipolar transistor.

The field-effect transistors may be divided into two general groups known as the junction field-effect transistors (JFET's) and the insulated gate field-effect transistors (IFGET's). Up to now only JFET's were used in low noise preamplifiers for semiconductor detectors, but it seems appropriate to mention some of the cryogenic properties of IGFET's, especially with their recent incorporation in low noise preamplifiers operated at 4.2°K.[20] The two types of FET's are illustrated in Fig. 2. Junction FET's (Fig. 2(a)) operate through modulation of a current path, the channel, by the depletion region of a reverse-biased rectifying junction. That junction may be a semiconductor to semiconductor p-n structure or a metal-semiconductor Schottky barrier junction. Junction FET's are majority carrier devices and they can operate in the depletion mode only. In the IGFET's the semiconductor channel is insulated from the metal gate by a layer of oxide (MOS) or nitride (MIS). The channel may be metallurgically built-in (Fig. 2(b)) or induced by an electric field (Fig. 2(c)). The first is a majority carrier device which may operate in the depletion and the enhancement modes. The second is a minority carrier device operating in the enhancement mode only.

The equivalent circuit of an FET is given in Fig. 3, the derivation of which is described in most textbooks on semiconductor circuits. The transconductance g_m for an n-channel device is given by

$$g_m = G_o\left[1-\left[\frac{8K_s\varepsilon_o(\phi_o-V_G)}{qN_D d^2}\right]^{\frac{1}{2}}\right] \quad (1)$$

where $$G_o = \frac{Zq\mu_n N_D d}{L} \quad (2)$$

is the conductance of the metallurgical channel.

$K_s\varepsilon_o$ - dielectric constant of the material

ϕ_o - contact potential of the gate junction

V_G - gate voltage

q - charge of an electron

N_D - impurity concentration in the channel

d - thickness of the channel

Z - width of the channel

μ_n - bulk electron mobility

L - length of the channel

R_s and R_d are the parasitic resistances of these portions of the channel which are not covered by the gate. The source resistance R_s constitutes internal negative feedback decreasing the g_m of the JFET.

$$g_m \text{ (observed)} = \frac{g_m}{1+g_m R_s} \quad (3)$$

C_{gs} and C_{gd} are the gate-to-source and gate-to-drain capacitances, respectively. In case of a JFET these are approximately the capacitances of reverse biased graded p-n junctions given by

$$C_{gs} = A\left[\frac{qK_s\varepsilon_o N_D}{2(\phi_o-V_{gs})}\right]^{\frac{1}{3}} \quad (4)$$

where

A - is the area of the junction

It was assumed that the gate impurity concentration is much higher than that of the channel. It has to be realized that (4) is a simplication because in reality C_{gs} and C_{gd} are distributed capacitances. Current generators I_{gs} and I_{gd} represent the leakage currents of the two junctions.

The maximum frequency of operation of an FET is given by

$$f_o = \frac{g_m}{C_{gs}+C_{gd}} = \frac{g_m}{C_g} < \frac{q\mu_n N_D d^2}{4K_s\varepsilon_o L^2} \quad (5)$$

As will be clarified below, f_o is an important factor for low noise FET's. For IGFET's the equivalent circuit is very similar with the capacitances being those of the MOS structures.

Our interest in the equivalent circuit is mainly in the temperature dependence of the different parameters, and ultimately the cryogenic performance of FET's. The temperature behavior of the transconductance (1), (2) will follow that of the conductance of the channel. Thus the two variables here are the mobility μ_n and the availability of free carriers. The mobility of Si, Ge and GaAs at cryogenic temperatures is determined by lattice and impurity scattering mechanisms.[16, 17] Due to their opposite temperature dependence, the mobility of these three materials peaks in the region 10-150° K depending on the material and its impurity concentration. Analytical expressions for the mobility and the optimum temperature at which its maximum is obtained may be found in references 16 and 17. The density of free electrons n (which at low temperatures substitutes N_D in (2) is given by

$$n = B(N_D)^{\frac{1}{2}}\exp\left(-\frac{E_d}{2kT}\right) \quad (6)$$

where

B = a weakly temperature dependent function;

E_d = ionization energy of the impurities;

k = Boltzman's constant

T = absolute temperature.

From the behavior of the mobility and the density of free carriers, we would expect the transconductance to peak at some cryogenic temperature and then to decrease exponentially in the deionization region. From the preceding discussion, it should be clear that the maximum transconductance that can be obtained for an FET depends strongly on the material of the channel. To compare the capabilities of FET's from various materials some relevant properties of Si, Ge, GaAs and InSb are listed in

Table 1. The materials are listed in order of the level of their technological development, but unfortunately their promise for cryogenic performance is according to their reverse order. From columns 2 and 4 of Table 1, we would expect silicon FET's to have their maximum g_m in the region 100-150° K, germanium devices 20-40° K, GaAs 85-115° K, and InSb 30-55° K. The last three types of devices should have still fairly high g_m at 4.2° K. By comparing μ_n and μ_h for the various materials, it is clear why n-channel devices have higher f_o's for similar geometries.

The transconductance of silicon, germanium and GaAs JFET's versus temperature is given in Figs. 4-6. For silicon (Fig. 4) experimental results confirm theoretical predictions. Maximum g_m is obtained at 110° K (2N3823) and it is approximately twice than the g_m at 300° K. Optimum g_m and T of other low noise silicon JFET's are given in Table 2. The sharp decrease of g_m below the optimum temperature is typical for silicon devices and is due to carrier freeze-out (6). Fig. 5 demonstrates the advantage of germanium JFET over its silicon counterpart at cryogenic temperatures. The g_m of a p-channel device (TIXM12) increases with decreasing temperature down to 4.2° K. Although it levels off at the very low temperatures, it does not decrease sharply below 20-30° K, as predicted. This behavior of the transconductance appears to be a result of the impurity impact ionization taking place in the channel of the FET and providing the necessary free carriers for conduction.[17] The transconductance of an experimental n-channel GaAs device*[21] is given in Fig. 6. It increases continuously down to 4.2° K, where the maximum observed is 12.3 mA/V. This feature contradicts the predicted temperature behavior according to which the g_m should peak around 85 to 115° K (Table 1). This is caused by impurity impact ionization in the channel as evidenced by the I_d-V_d curve.[17,22] Also, the mobility of GaAs given in Table 1 is the bulk mobility of compensated GaAs and its behavior may not follow that of a thin epitaxial layer. The calculated g_m for the GaAs JFET is 140 mA/V (T=300°K, μ=8000 cm^2/Vsec), but we observe transconductance of only 4 mA/V. The reason for that small g_m is large source resistance (3) and smaller mobility for epitaxial layers of GaAs. The main additional factor which causes deterioration of the g_m is the trapping of carriers, obviously decreasing the density of free carriers and their mobility through increased impurity scattering (type 2 device at room temperature). The small geometry device shows an anomaly in the transconductance as a function of the gate voltage with maximum g_m obtained at V_{gs}= -2v. Fig. 7 shows the temperature dependence of the drain current of the GaAs FET. As expected, the drain current and the g_m show similar thermal behavior.

Temperature dependence of the other elements of the equivalent circuit (Fig. 3) is as follows: The parasitic resistances R_s and R_d exhibit opposite thermal behavior to that of the transconductance, junction capacitances decrease with temperature 20% for Si between 300 and 110° K and 40% for Ge between 300 and 4.2° K (ϕ_o increases), the leakage currents I_{gd}, I_{gs} decrease exponentially. For good silicon FET's R_s is smaller than 10 ohm and the leakage currents (at low V_D are smaller than 1pA. The tested GaAs FET had R_s = 45 ohm. More detailed discussion of these parameters is given in references 16, 17 and 23.

The IGFET's have identical equivalent circuit to that of JFET's (Fig. 3), but their different construction determines some basically different temperature dependence. This is true in particular for the enhancement type MOSFET's. Fig. 8 exhibits the transconductance of experimental enhancement type MOSFET's* versus temperature. The p-channel units have a similar temperature dependence to silicon JFET's, but it must not be taken as completely indicative of p-channel MOSFET's because the tested units had a thick oxide layer. To the contrary, the thermal behavior of g_m of the n-channel units is surprising. The high transconductance at 4.2° K points to the possibility that the conduction at the very low temperatures is by surface state changes in the oxide or hot carriers generated by some type of avalanche mechanism. High temperature coefficient of the turn-on voltage[24] and field dependence of the mobility[25] in the hypercryogenic region may support previous suppositions. Undoubtedly, further investigation of enhancement type MOSFET's at cryogenic temperatures is needed.

The purpose of this lengthy section was to establish the temperature dependence of FET parameters relevant to low noise operation, the importance of the channel material and the geometrical structure of the device.

Noise Properties of FET's

Noise properties of FET's, especially JFET's have been investigated by many workers.[26-28] The main noise source of a JFET is the thermal noise of its channel, though other noise sources, which cannot be neglected in most cases of high resolution

*Courtesy Fairchild Semiconductor, Palo Alto, CAlifornia

*Supplied by Fairchild Semiconductor.

spectroscopy are: shot and thermal noise of the gate, thermal noise of the parasitic source and drain resistances and the generation-recombination type low frequency noise. The main difference between the noise of JFET's and MOSFET's is in the low frequency region where the MOSFET's have additional noise sources arising from the fluctuations in the occupancy of the SiO_2-Si interface states.

The channel noise of JFET's was analyzed by Van der Ziel[26], assuming an abrupt gate junction and considering only the unsaturated mode of operation. The channel thermal current generator is given by

$$\overline{i_d^2} = 4kTg_m Q(V_D; V_G)df \qquad (7)$$

where df is the frequency increment of measurement and $Q(V_D;V_G)$ a complicated function of drain and gate voltages and a weak function of temperature. The function Q ranges from 0.5 to 0.67 as V_G varies from zero to pinch-off voltage. Subsequent derivations of (7) for graded-junction JFET's and MOS structures show that for the first Q varies from 0.57 to 0.67 and is constant - 0.67 for MOSFET's. The thermal noise referred to input is given by

$$\overline{v_{th}^2} = \frac{4kT}{g_m} Qdf \qquad (8)$$

Equation (8), with the information on g_m from the preceding section, points out the advantage in cryogenic operation of FET's for low noise applications, as could have been expected from the physical principles of the device.

The parasitic drain and source resistances, R_s and R_d, constitute additional thermal noise sources. However, the influence of these sources is normally small as can be seen from the modified expression for $\overline{i_d^2}$

$$\overline{i_d^2} = 4kT\frac{g_m Q + g_m^2 R_s + g_d^2 R_d}{(1+g_m R_s + g_d R_d)^2} df \qquad (9)$$

At cryogenic temperatures this influence diminishes even further with the decrease of both resistances.

In the gate of an FET there are two noise sources: the shot noise of the reverse-biased gate-to-channel junction and thermal noise capacitively coupled from the channel. The first noise source is given by

$$\overline{i_{go}^2} = 2q(I_{gd} + I_{gs})df \qquad (10)$$

This noise source decreases considerably with temperature.[23]

The second noise source is significant at high frequencies[29]

$$\overline{i_g^2} = \frac{4kT}{g_m}\omega^2 C_{gs}^2 P(V_D; V_G)df \qquad (11)$$

where $w=2\pi f$ and P is a complicated function weakly temperature dependent. For practical bias voltages in the saturation mode P is 0.15 to 0.2. The temperature dependence of this noise source will follow that of the thermal noise of the channel (8).

Low frequency noise is caused mainly by recombination-generation trapping processes both in the bulk and on the surface of the semiconductor.[27] These processes result in charge fluctuations in the depletion layer of the gate junction and consequently modulation of the width of the channel. This type of noise can be represented by current noise generator

$$\overline{i_l^2} = \frac{h\ df}{1+\omega^2\tau^2} \qquad (12)$$

where h is a constant and τ the trapping time-constant. τ increases sharply at cryogenic temperatures and therefore a decrease in the low frequency noise should be expected.

The power spectrum of the low frequency noise of FET's can be represented by[17]

$$S(f) = \frac{g(I_D;T)}{f^n} = \frac{A I_D^m T^\alpha}{f^n} \qquad (13)$$

where A is a constant and I_D the drain current. The parameters m, α and n are found experimentally.

Summarizing, it can be said that all the noise sources of the FET decrease with temperature, and therefore cryogenic operation of FET preamplifiers is very desirable. Silicon devices have an optimum operating temperature above liquid nitrogen temperature (100-160°K). FET's from other materials, like Ge and GaAs, may and should be operated at much lower temperatures (approx. 10°K) to obtain their best performance.

Experimental noise results for various types of FET's will be presented in the next section. Optimum operating conditions of the FET will also be discussed.

Noise of the Preamplifier

The various noise sources of the FET and the other noise generators of the input stage of the preamplifier, including the detector, are summarized in Fig. 9. Using that equivalent noise circuit, the output noise voltage (V_{no}) may be calculated by summing the

contributions of the individual sources. For a charge-sensitive preamplifier

$$\overline{V_{no}^2}=4kT\left[\frac{1}{g_m}\left[Q\left(\frac{C_g+C_d+C_f}{C_f}\right)^2+P\left(\frac{C_{gs}}{C_f}\right)^2\right]+\frac{1}{\omega^2C_f^2}\left[\frac{1}{R_L}+\frac{1}{R_f}+\frac{q(I_g+I_l)}{2kT}\right]\right]df+\frac{A\,I_D^m T^\alpha}{f^n}\left(\frac{C_g+C_d+C_f}{g_m C_f}\right)^2 df \quad (14)$$

For most cases Q and P may be taken as Q=0.6 and P=0.15. The parameters of the $1/f^n$ noise have to be determined experimentally although for most low noise FET's that contribution is negligible.

The noise voltage of the preamplifier (14) is frequency dependent, as expected. The charge signal from a semiconductor detector is limited in bandwidth and therefore filtering the signal of the preamplifier will improve its signal to noise ratio. Extensive work has and is being done on optimization of filters for high resolution nuclear spectroscopy.[30-33] Simple passive circuits and complex time-variant networks have been designed, but the practical gains in signal-to-noise ratio have not been dramatic. In order to explore the relative significance of the various noise sources (14) and derive possible optimum operating conditions, let us calculate the equivalent noise charge (ENC) of an FET preamplifier with the simple CR-RC pulse shaping network. From (14)

$$\overline{V_{no}^2}(\omega)=a^2+\frac{b^2}{\omega^2}+\frac{c^2}{\omega^n} \quad (15)$$

The transfer function of the filter network with equal differentiation and integration time constants (τ) is

$$G(\omega)=\frac{1}{1+j\omega\tau}\cdot\frac{j\omega\tau}{1+j\omega\tau} \quad (16)$$

The noise voltage at the output of the filter

$$\overline{e_{no}^2}=\int_0^\infty \overline{V_{no}^2}\,\overline{G(\omega)}^2 d\omega=\frac{\pi}{4}\left(\frac{a^2}{\tau}+b^2\tau\right)+\frac{c^2}{2} \quad (17)$$

assuming n=1.

It is clear that for n<1 the $1/f^n$ noise will have $1/\tau^K$ dependence on τ (with K<1) and for $1<n<2$ the dependence will be τ^K (with K<1).

$$ENC^2=\frac{\overline{e_{no}^2}}{A_c^2}=\frac{e^2}{2}\left[\frac{0.6kT}{\tau g_m}(C_g+C_d+C_f)^2+\frac{0.15kT}{\tau g_m}C_{gs}^2+kT\tau\left(\frac{1}{R_L}+\frac{1}{R_f}\right)+\frac{\tau}{2}q(I_g+I_l)+A\,I_D^m T^\alpha\frac{(C_g+C_d+C_f)^2}{g_m^2}\right] \quad (18)$$

where Ac is the gain of the preamplifier and the filter and e=2.712.

Expression (18) points out to the existance of τ τ_{opt} at which ENC is minimum.

$$\tau_{opt}=\left[\frac{0.6C_{in}^2+0.15C_{gs}^2}{g_m\left[\left(\frac{1}{R_L}+\frac{1}{R_f}\right)+\frac{q}{2kT}(I_g+I_l)\right]}\right]^{\frac{1}{2}} \quad (19)$$

For a typical silicon X-ray spectrometer, C_{in}=6pF, C_{gs}=3.5pF, $R_f=10^{10}\ \Omega$, I_g+I_l=1pA, T=120° K, g_m=10 mA/V,

and therefore $\tau_{opt} \cong 4\mu$sec

Also from the expression for the ENC we can obtain the noise sensitivity for input capacitance

$$\frac{d(ENC)}{dC_d}=\frac{e^2}{2(ENC)}\left[\frac{0.6kT}{\tau g_m}+\frac{A\,I_D^m T^\alpha}{g_m^2}\right](C_g+C_d+C_f) \quad (20)$$

In most cases the thermal noise coupled to the gate (11) and the $1/f^n$ noise may be neglected and then

$$\frac{d(ENC)}{dC_d}=e\left(\frac{0.6kT}{\tau_{opt}\cdot g_m}\right)^{\frac{1}{2}} \quad (21)$$

From (21) we observe that the slope, like the absolute value of the noise (18), depends on the ratio T/g_m and therefore will decrease considerably with temperature. That points out the definite advantage of cryogenic operation for silicon FET preamplifiers and even more that of the hypercryogenic operation for germanium and GaAs FET preamplifiers.

Using a charge-sensitive preamplifier low temperature performance of various JFET's and MOSFET's was measured and compared with the theoretical predictions of the expression for ENC (18). Fig. 10 shows the temperature dependence of the thermal noise of silicon and germanium JFET's of which the transconductance curves were given in Figs. 4 and 5. The thermal noise is close to the theoretically predicted value and its minimum for the silicon units is obtained at a higher temperature than the maximum g_m. The germanium JFET, TIXM12, operated at 20-40°K is clearly superior to the silicon devices. Fig. 11 shows the "white noise" of the experimental GaAs JFET's. The agreement between the experimental results and theoretical predictions is not particularly good, especially in the temperature region of 200 to 300°K and around liquid helium temperature. The increased noise at high temperature may be explained by the existence of large amount of deep level trapping centers with short characteristic lifetimes and the resulting high frequency generation-recombination noise. This type of noise is strongly temperature dependent as the probability of detrapping decreases exponentially with temperature. The increased departure from the theoretical noise at the very low temperatures is caused by the avalanche type conduction in the FET, similarly to the behavior of the germanium FET.

The I-V characteristics of the tested GaAs JFET's are not stable with time. When kept at 77° K the I_{dss} and pinch-off voltage increase slowly and the g_m decreases. Two of the three tested FET's exhibited large changes in their characteristics during thermal cycling with the original characteristics restored after 20 to 30 hours at 300°K.

The MOSFET's examined (Fig. 8) have larger high frequency noise than predicted by (8), especially for the n-channel units, suggesting contributions from other sources in addition to the thermal noise of the induced channel. The thermal behavior of the high frequency noise agrees generally with the theory and the noise attains a minimum value in the cryogenic range.

The parameters m, α, and n of the $1/f^n$ noise (13) were measured using a low frequency spectrum analyzer. The spectra of all tested devices (silicon and germanium) showed $1/f^n$ behavior with n ranging from 0.5 to 1.6 and being not particularly consistent for the same type of device. The same is true about the corner frequencies of the $1/f^n$ noise. For the n-channel 2N3823 "low noise" units, corner frequencies of 3-7 kHz were obtained, but some units showed corner frequencies as high as 100kHz. The germanium devices TIXM12 showed particularly high $1/f^n$ noise (at 300°K), most of them up to 5 MHz. The MOSFET's examined have very high $1/f^n$ noise with corner frequencies above 1 MHz.

The drain-current dependence (I_D^m) of the low-frequency noise appeared to be much more regular between one unit and another. The power m was 1-1.15 for 2N3823, 0.75-0.9 for 2N2608 and 1.1-1.4 for TIXM12.

Fig. 12 shows the temperature dependence of the low-frequency noise. The noise, for constant current, decreases with temperature according to a varying power low. For both silicon devices the noise decreases as T^α (α-1.17-2.1) in the temperature range 300-140° K. The rate of decrease becomes slower at lower temperatures. The noise of the germanium device decreases much faster ($\alpha \sim 3$) between 300-200° K, and then follows the pattern of silicon devices. The low requency noise of the germanium JFET at 4.2°K is lower than that of the n-channel silicon JFET at 77°K.

Concluding, it must be said that temperature is perhaps the most important parameter influencing the noise properties of an FET. Other parameters include the gate voltage V_G, the drain voltage V_D and the drain current I_D. In the early stages in the development of FET preamplifiers, it was common to operate the gate-to-source junction under significant reverse bias,[7,10] sacrificing transconductance apparently in an attempt to decrease the input capacitance. This approach is not effective because with the FET well in the saturated mode its input capacitance depends only weakly on V_{GS}. Still today many designers operate the FET's with some reverse V_{GS} as they find it to be the optimum operating point.[15] Actually the optimum V_{GS} is tied indirectly with the temperature of the FET as can be seen from Fig.13. Here the noise of a charge-sensitive preamplifier is given as a function of V_{GS} for high and low thermal resistance between the case of the FET and the thermal "ground". Reducing the V_{GS} increases the dissipation of the FET (V_{DS} is kept constant) and therefore in the case of high thermal resistance its temperature increases. The higher temperature, which by itself means higher noise, decreases and even nullifies the expected increase in the g_m. The minimum noise is obtained at negative V_{GS}. However, it is clear from Fig. 13 that when the temperature of the FET is not allowed to vary considerably the optimum V_{GS} may be even positive.

The optimum V_{DS} should be obviously above the pinch-off voltage of the transistor to ensure small junction capacitances C_{gd} and C_{gs}. However, it should not be too high because of increased dissipation and increased avalanche generation in the depletion region of the channel. This kind of generation becomes more signifcant at low temperatures as the breakdown fields in semiconductors decrease with temperature.[17] Good example of the described effect is the germanium JFET (TIXM12 which has to be operated at 4.2°K with V_{DS} of only 2V.[16]

The drain current I_D should be low to keep the $1/f^n$ noise small, but unfortunately transistors with small I_{DSS} have also small g_m.

Input Stage Configurations

The performance of the very high resolution systems is determined not only by the FET, but also by the passive elements of input stage, the detector-preamplifier coupling network, and microphonic generation in the system. These topics will be discussed in the following.

Two basic input stage configurations are used in preamplifiers for semiconductor radiation detectors: the charge-sensitive (Fig. 14 a, b, c) and the voltage sensitive[34] (Fig. 14 d, e). The charge-sensitive configuration, which is the more popular, is necessary in all cases where the capacitance of the detector is not constant. This was true for the early versions of semiconductor detectors, but is not true for today's p-i-n detectors. It is also convenient, with the charge-sensitive configuration, that the gain and its stability depend only on one passive component. The normally used configuration (Fig 14a) provides also dc feedback to stablize the operating points of the amplifier. However, the input stage of a cooled preamplifier operates under well controlled environment, constant temperature,

vacuum conditions (10^{-6}mm Hg) and good electrostatic shielding and therefore short term variations in its parameters are not likely. It is thus possible to remove the full loop dc feedback and use local feedback for A, (Fig. 1) if necessary. The disadvantages of that configuration (Fig. 14a) are additional noise caused by the feedback elements R_f and C_f as demonstrated by (18). These contributions may be significant in x-ray spectrometers where minimum noise level is sought and therefore configurations (b)-(e) may prove advantageous. Additionally to its thermal noise contribution, which may be reduced by cooling, the resistor (R_f ($>10^9$ Ω) poses few more problems. It has stray capacitance of 0.25 to 0.5 pF and its resistance decreases with increasing frequency[15]. Both effects cause an increase in noise and deterioration of system resolution. The high value resistors used in low-noise amplifiers are made from glass compounds and metal-oxide films and therefore may exhibit properties of semiconducting thin films. The pyroelectric effect may be significant in configuration (a) where the two ends of the resistor are at different temperatures and from here possible noise advantage of configuration (b).[14] The voltage sensitive configuration[34] (Fig. 14e) avoids the use of high value resistor and consequently its associated noise. The gate circuit of the FET is closed through the radiation detector and its operating point may be adjusted with the drain supply. In cases where the leakage currents of the FET and the detector are not close in magnitude, configuration (d) may be used. The voltage sensitive configuration operated properly, gives the best resolution possible for a given FET and detector, because the noise of a feedback amplifier is always larger than that of the unfedback amplifying chain. However, the voltage sensitive circuit is limited to low-leakage low-capacitance detectors and low counting rate situations, conditions which are independently imperative for very high resolution, low energy applications.

Another solution avoiding the high value feedback resistor was proposed recently by Goulding et al[35]. They use an opto-electronic feedback by varying mainly the leakage currents of the FET (I_{gs} and I_{gd} (Fig. 3)) with light emitted by a GaP diode powered by the output voltage of the preamplifier. The idea of an opto-electronic feedback is interesting in general, but at the present time it seems practically too complicated for the merits it offers. Although the resolution of the opto-electronic preamplifier is 150 eV, similar results of 185 eV were obtained with a conventional type preamplifier (see next section). The difference between the two results is due mainly to further decrease in stray capacitance of the FET (FET was removed from its metal case to apply the optical feedback), the use of higher equivalent R_f of 10^{11} Ω in the opto-electronic preamplifier and accordingly, the use of the resulting higher optimum pulse shaping time constants (19).

The coupling between the detector and the preamplifier affects (often significantly) the noise properties of the system. Two basic methods exist - ac and dc coupling, as demonstrated in Fig. 15. AC coupling technique provides the convenience in detector mounting (one side may be grounded), but is inherently noisier and therefore used mainly in room temperature operated preamplifiers. In the dc coupled configuration the following noise sources are eliminated: the bias resistor R_L (thermal noise and stray capacitance) and the high voltage coupling capacitor C (stray capacitance to ground, shot noise from leakage current and microphonics due to vibrations). Also, microphonic generation is reduced by removing the high voltage from the input of the preamplifier. Additionally, the detector leakage current can be monitored by measuring the output voltage of the preamplifier. The dc coupling configuration should definitely be used in high resolution systems.

A significant noise source in high resolution systems, which received relatively little attention, is the microphonic generation. In every high impedance, capacitance transducer, a charge or voltage signal will be generated with variations of the capacitance according to

$$dQ = V\,dc \qquad (22)$$

In cryogenic systems mechanical vibrations inside the cryostat are induced by the bubbling of liquid nitrogen and the environmental noise. Vibrations of the coupling network between the detector and the preamplifier will cause variations in the input capacitance and subsequently generate the noise signal dQ. The microphonic signal is proportional to the voltage at the point at which it is generated (22) and therefore the definite advantage of the dc coupling method. The optimum condition is obviously V_{GS}=0. To realize the seriousness of the problem, we observe (22) that to generate a microphonic signal with the amplitude of 1 keV (Si) at the input of the preamplifier held at 100 mV a change of capacitance of only 0.0005 pF is needed. Fortunately, the frequency of the mechanical vibrations is inherently small, normally below 1kHz. Assuming a triangular microphonic signal with amplitude A and period 2T, it may be decomposed into its Fourier constituents:

$$\text{Microphonic signal} = \frac{8A}{\pi^2 n^2} \sum_{n=1,3,5,\ldots} \sin \frac{n\pi x}{2T} \qquad (23)$$

The frequency region of interest determined by the band-pass of the amplifier is around 100 kHz. The effect of the microphonic

signal is therefore reduced by a factor of 10^4 (according to eq. 23). In spite of the fortuitous frequency region of the microphonics, their amplitude should be kept small in high resolution, low energy spectrometers.

Results and Applications

In previous sections noise considerations of FET preamplifiers were discussed. In the following, circuit and system resolutions will be presented and then compared with theoretical capabilities of semiconductor radiation detectors. Also, some applications of high resolution FET preamplifiers will be discussed.

Noise contribution of FET preamplifiers may be approximated (from eq. 18) by

$$\text{Noise} = a + bC_d \qquad (24)$$

where the intercept a is determined by the parallel noise sources (Fig. 9) and slope b by the series ones and C_d is the capacitance of the detector. The relative importance of the intercept and the slope depends on the application. For α and high energy γ-ray spectroscopy where high capacitance detectors (shallow surface barrier and high volume Ge(Li), respectively) are used, low slope is essential. For x-ray and low energy γ-ray spectroscopy where low capacitance Si(Li) and Ge(Li) detectors are used, low intercept is obviously important. Both the intercept and the slope decrease with temperature and therefore cooled preamplifiers are advantageous in all types of nuclear spectroscopy. As an example of state-of-the-art results for various types of FET preamplifiers, the noise of Nuclear Diodes Models 101A, 102 and 104 will be given. For room temperature preamplifiers (101A) the noise is 700 eV + 18 eV/pF, for liquid nitrogen cooled instruments (104 for high capacitance detectors) 420 eV + 10 eV/pF and 185 eV + 30 eV/pF (102 for low capacitance detectors). All these preamplifiers use n-channel silicon junction FET's. A liquid helium cooled preamplifier using p-channel germanium junction FET has noise of 280 eV + 18 eV/pF.[16,23,36] This preamplifier combines a relatively low intercept and slope. It is believed that the intercept of that preamplifier may be improved by using a gate resistor exhibiting smaller frequency dependence. The reported results were obtained with Allen-Bradley carbon composition resistors. Using the experimental GaAs FET at 77° K and 4.2° K resolutions of 1.25 and 1.05 keV respectively were obtained with a slope of 40 eV/pF.

It is well known that for the uncorrelated noise sources of a nuclear spectrometer

$$\text{Noise}^2_{\text{total}} = \text{Noise}^2_{\text{electronics}} + 5.52\ FE\varepsilon \qquad (25)$$

where the second term is the statistical contribution, F is the Fano factor, E energy of the analyzed particle and ε the mean energy required to generate an electron-hole pair.

Fig. 16 shows the contribution of the statistical fluctuations in charge production which cause the basic resolution limitation of semiconductor nuclear spectrometers. With ε equal to 2.96 eV for germanium and 3.81 eV for silicon (at 90°K)[37] and the Fano factor of 0.13 for germanium[38] and 0.1 for silicon[39] the contribution of statistics is almost equal for silicon and germanium detectors. Experimental results obtained with the 104 and 102 preamplifiers are also plotted in Fig. 16. The results at high energies (>60 keV) were obtained with a 25 cc Nuclear Diodes Ge(Li) detector (27pF and 0.1 na leakage current) and the 104 preamplifier. For Co^{60} 1.33 MeV γ-ray, the best resolution obtained with room temperature (dc coupled) preamplifier is 2.2 keV (101A) and with the cooled preamplifier 1.95 keV (104). The results at low energies were obtained with a 25 mm^2 x 3 mm Nuclear Diodes Si(Li) detector (1 pF) and 102 preamplifier. Comparing the theoretical limits and experimental results, it is clear that the noise of the preamplifier limits the system resolution only for x-rays below 10 keV. Figs. 17 and 18, containing the spectra of Mn and Np x-rays, respectively, demonstrate the state-of-the-art resolution capabilities of x-ray spectrometers. From Fig. 17, we see that Kα and Kβ lines of Mn, 600 eV apart, are completely resolved, and the Kα line 5.89 keV is measured with 242 eV resolution. The neptunium Lβ lines are almost completely resolved (5:1 peak to valley ratio for $L_{\beta 1}$ and some of its weak lines like $L_{\beta 6}$, L_{η}, $L_{\beta 3}$) are resolved from the background. Detection limit of present x-ray spectrometers is around 1 keV, which means that K x-rays of elements as low in Z number as sodium (Z=11) may be detected.

The improving noise properties of FET preamplifiers create an increasing number of new applications for semiconductor radiation spectrometers, especially x-ray spectrometers. By far the most significant of these applications is the non-dispersive fluorescence analysis of materials[40]. In that method, characteristic x-rays, excited by a radioactive source, are emitted by each chemical element in the sample, then resolved and identified by a high resolution x-ray spectrometer. The method is quantitative as the area under the individual peaks is proportional to the amount of each element. Variations of this method are applied in electron scanning microscopy,[41] geological explorations, archeological investigations[42] and criminalistics[43]. For example, in electron scanning microscopy used for testing of semiconductor devices, the attached x-ray spectrometer may provide very valuable information on the contents of the

non-desirable sodium element. Recently the fluorescence technique was applied successfully in medicine for thyroid scanning[44] and blood analysis. With further improvements in resolution, many biological applications will become possible.

CONCLUSIONS

During the last few years, continuous improvement of FET preamplifiers caused a tenfold decrease of resolution limits for semiconductor spectrometer systems. This progress is due to better understanding of FET characteristics, development of improved transistor types for low-noise amplication, search for optimum materials and geometrical configurations for our application and improved techniques of circuit configurations and signal processing. Cryogenic FET preamplifiers constitute definitely the state-of-the-art low-noise amplifying units for semiconductor spectrometers.

Although nowadays in most cases of nuclear spectroscopy the detector is the limiting factor, there are two areas where further improvement of the low noise amplifier will be welcomed. The main area is the x-ray region below 10 keV in which the electronics limits the resolution and even the detection (<1 keV), in spite of the fact that some improvements are also needed in detectors for that energy region. The FET's desirable for that application are VHF transistors with f_o above 1 GHz. Although such devices are feasible in silicon by the optimization of the chip (5) and the parasitic noise sources due to the packaging of the transistor, our best hope for the future are FET's from other materials than silicon. There are clear possibilities for improvement in the field of germanium FET's which already proved its advantages for low noise cryogenic operation. The III-V compound semiconductors like GaAs and InSb have very high electron mobilities and low ionization energies (Table 1) and thus are very promising for low noise cryogenic applications. However, before these properties may be fully utilized, further progress is needed in the development of processing methods and growth of epitaxial layers for these materials.

With the successful development of improved FET's for hypercryogenic temperatures operation of the detector at these temperatures[23] will obtain new impetus because lowering its leakage current will mean significant decrease of the parallel noise, larger τ_{opt} and consequently lower total noise.

The second area where improved preamplifiers may be advantageous is in spectrometers with high efficiency high capacitance germanium detectors (>50 pf). Here the development of well optimized low noise power FET's will be needed to provide relatively low noise level for the growing area of very large volume detectors.

The rapid progress in low noise amplication renewed the interest in further development of semiconductor radiation detectors. Already some significant improvements have been made in reducing the leakage current due to thermal radiation[45] and in developing high-volume low-capacitance geometrical structures.[46] In view of the basic resolution limitations due to statistical fluctuations, a search for new materials with lower ε's for future radiation detectors seems logical.

The progress made in the field of low noise FET preamplifiers for semiconductor radiation detectors will have a definite impact on other areas where low noise amplification at cryogenic temperatures is desirable like infrared radiation detection or superconducting sensors.

ACKNOWLEDGMENTS

Large part of the described work was done by the author at the Electrical Engineering Department of the University of California, Berkeley, and at the Lawrence Radiation Laboratory, Berkeley. Consequently, contributions of Prof. G. A. Rigby and Mr. M. M. Nakamura are gratefully acknowledged. The author would like to thank M. Nakamura and A. Sandborg for reviewing the manuscript. Thanks are also due to many members of the Nuclear Diodes, Inc. team, especially to J. A. Koontz and G.M.B. Wason for their technical help and Mrs. D. Moore for typing the manuscript.

REFERENCES

1) A. J. Tavendale and G. T. Ewan, Nucl. Inst. & Meth. 25 (1963) 185.

2) E. Fairstein, IRE NS-8, No. 1 (1961), 129.

3) R. L. Chase, W. A. Higinbotham and G. L. Miller, IRE NS-8, No. 1 (1961), 147.

4) J. L. Blankenship, IEEE NS-11, No. 3 (1964), 373.

5) T. L. Emmer, IRE NS-9, No. 3 (1962) 305.

6) L. G. Jonasson, Nucl. Inst. & Meth. 26 (1964), 104.

7) V. Radeka, IEEE NS-11, No. 3 (1964), 358.

8) T. V. Blalock, IEEE NS-11, No. 3 (1964), 365

9) T. W. Nybakken and V. Vali, Nucl. Inst. & Meth. 32 (1965), 121.

10) O. Meyer, Nucl. Inst. & Meth. 33 (1965), 164.

11) E. Elad, Nucl. Inst. & Meth. 37 (1965), 327.

12) E. Elad and M. Nakamura, Nucl. Inst. & Meth. 41 (1966), 161.

13) E. Elad and M. Nakamura, IEEE NS-14, No. 1 (1967), 523.

14) K. F. Smith and J. E. Cline, IEEE NS-13, No. 3 (1966), 468.

15) V. Radeka, Brookhaven National Laboratory, BNL-12748 (1968).

16) E. Elad and M. Nakamura, IEEE NS-15, No. 1 (1968), 283.

17) E. Elad, Ph.D. Thesis, U. of California, Berkeley, June 1968.

18) A. F. Arbel, IEEE NS-15, No. 5 (1968), 2.

19) W. Shockley, Proc. IRE 40 (1952), 1365.

20) D. S. Miyoshi and R. M. Cotts, Rev. of Sci. Inst. 39 No. 12 (1968), 1881.

21) W. W. Hooper and W. I. Lehrer, Proc. IEEE 55 (1967), 1237.

22) R. A. Reynolds, Solid State Electronics 11 (1968), 385.

23) E. Elad and M. Nakamura, IEEE NS-15, No. 3 (1968), 477.

24) H. C. Nathanson et al, IEEE Trans. of Elect. Dev. ED-15, No. 6 (1968) 362.

25) F. F. Fang and A. B. Fowler, Phys. Rev. 169 No. 3 (1968), 619.

26) A. Van der Ziel, Proc. IRE 50 (1962), 1808.

27) C. T. Sah, Proc. IEEE 52 (1964), 795.

28) I. Flinn et al, Solid State Electronics 10 (1967), 833.

29) A. Van der Ziel, Proc. IEEE 51 (1963), 461.

30) M. Tsukuda, Nucl. Inst. & Meth. 14 (1961) 241.

31) V. Radeka, IEEE NS-15, No. 3 (1968), 455.

32) E. Fairstein and J. Hahn, Nucleonics 23, No. 11 (1965), 50.

33) M. Oda and M. O. Deighton, (two papers) ISPRA, Nuclear Electronics Symposium, this issue.

34) E. Elad and M. Nakamura, Nucl. Inst. & Meth. 42 (1966), 315.

35) F. S. Goulding, J. Walton and D. F. Malone LRL, U. of California, Berkeley, Report UCRL-18698 (Jan. 1969).

36) E. Elad and M. Nakamura, Nucl. Inst. & Meth. 54 (1967), 308.

37) R. H. Pehl, et al, Nucl. Inst. & Meth. 59 (1968), 45.

38) H. R. Bilger, Phys. Rev. 163, 238 (1967).

39) H. R. Zullinger, L. M. Middleman and D. W. Aitken, IEEE NS-16, No. 1 (1969), 47.

40) H. R. Bowman, et al, Science 151 (1966) 562.

41) J. C. Russ and A. Kabaya, Proceedings of the 2nd Annual Scanning Electron Microscope Symposium, April 29-May 1, 1969, Chicago, Ill. p.57.

42) F. Asaro, private communication on non-destructive analysis of ancient sculpture.

43) Report No. OR03561-1, Clearinghouse, U.S. Dept. of Commerce, Springfield, Va. 22151.

44) P. B. Hoffer, Radiology 90 No. 2 (1968), 342.

45) R. J. McIntyre, IEEE NS-15, No. 5 (1968), 6.

46) G. Armantrout, IEEE NS-14, No. 1 (1967), 503.

DISCUSSION

Kandiah : - May I make a comment on one point Mr. Elad raised. This is the question of noise of insulated gate FET at cryogenic temperatures. There has been a report, which has not yet been published but is due to be published soon which indicates that p channel enhancement types MOST's at 4°K can consistently give lower noise than n channel MOST's. Little more can be added at the moment but there is evidence that there is a tendency of this sort.

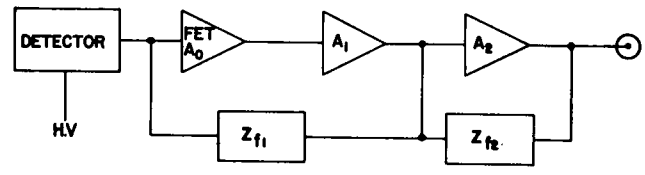

Fig. 1) Block diagram of an FET preamplifier.

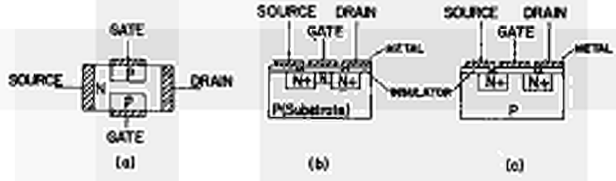

Fig. 2) Cross-section of field-effect devices.
a) n-channel junction FET.
b) n-channel depletion type IGFET.
c) n-channel enhancement type IGFET.

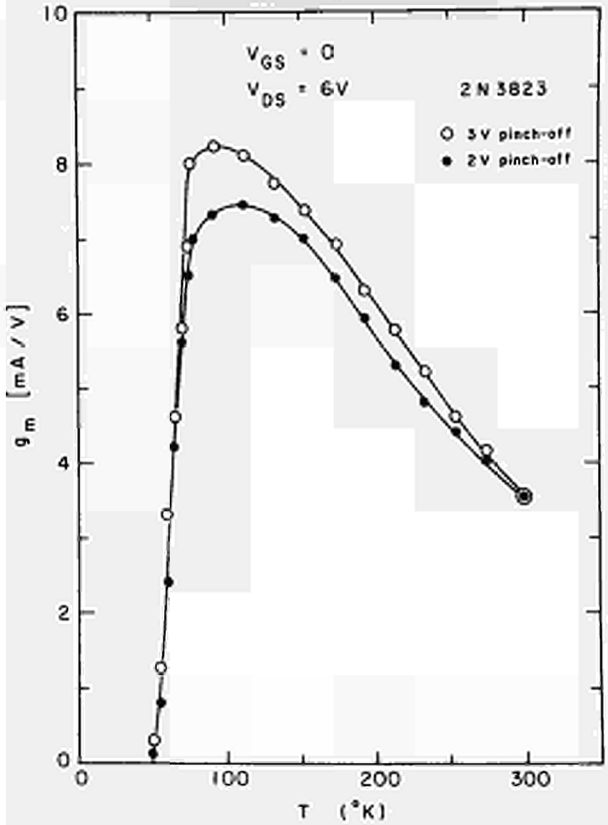

Fig. 4) Transconductance of a silicon JFET vs. temperature. (T).

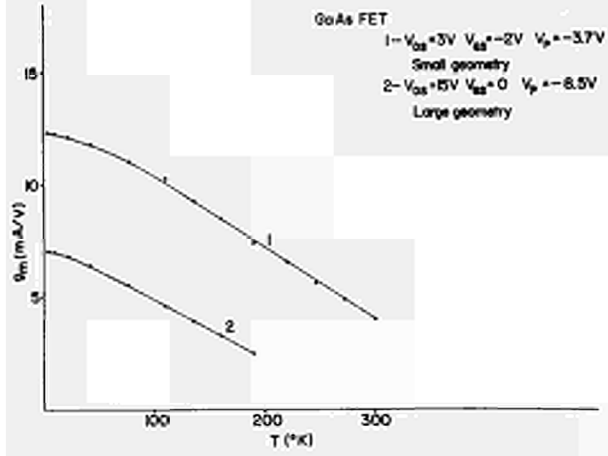

Fig. 6) Transconductance of a GaAs FET vs. T.

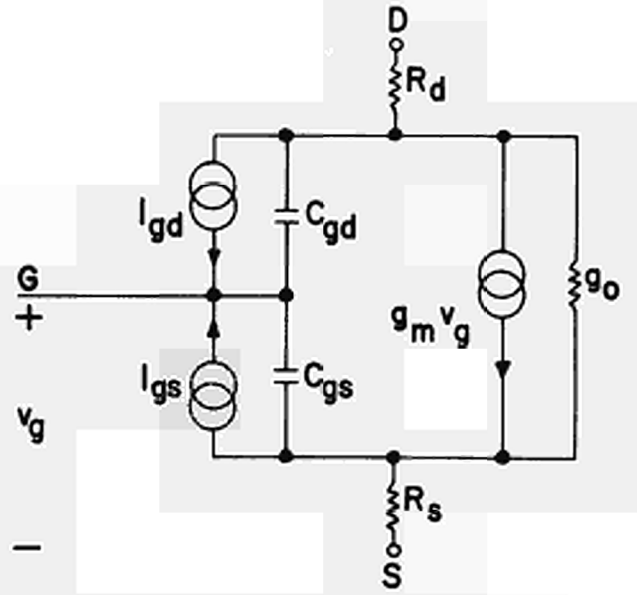

Fig. 3) Equivalent circuit of an FET.

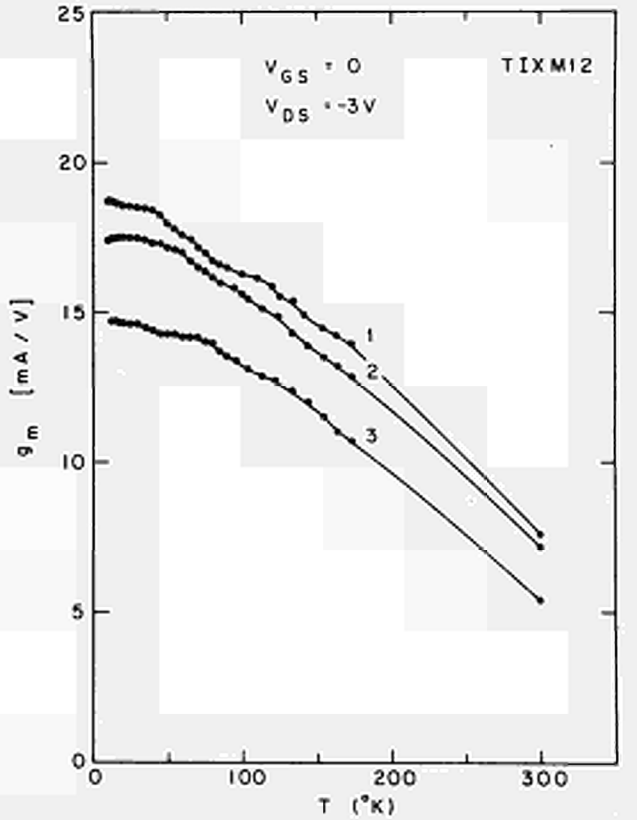

Fig. 5) Transconductance of a germanium JFET vs. T.

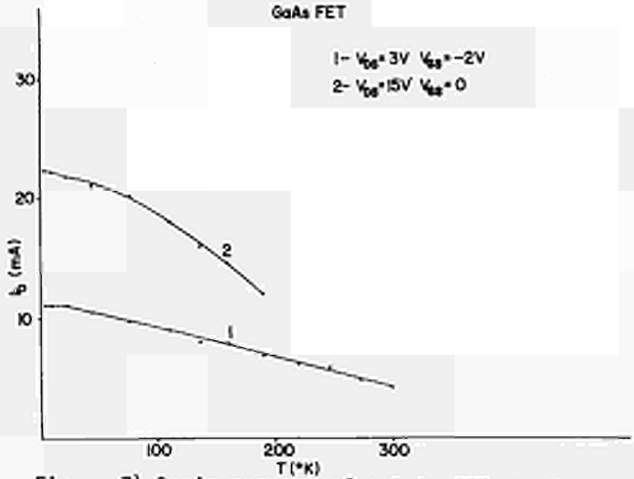

Fig. 7) Drain current of a GaAs FET vs. T.

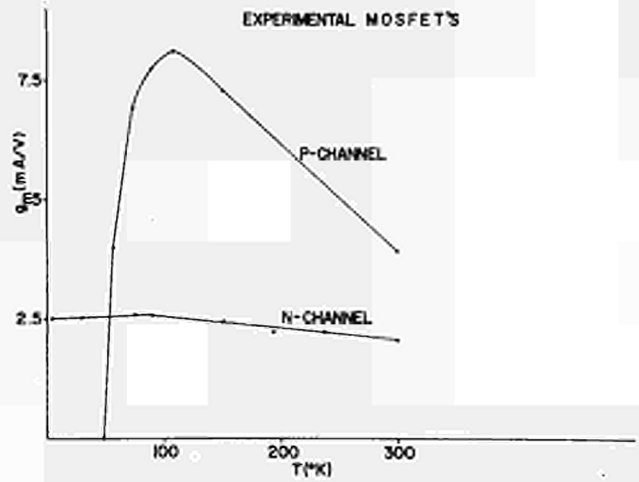

Fig. 8) Transconductance of experimental type MOSFET's vs.T.

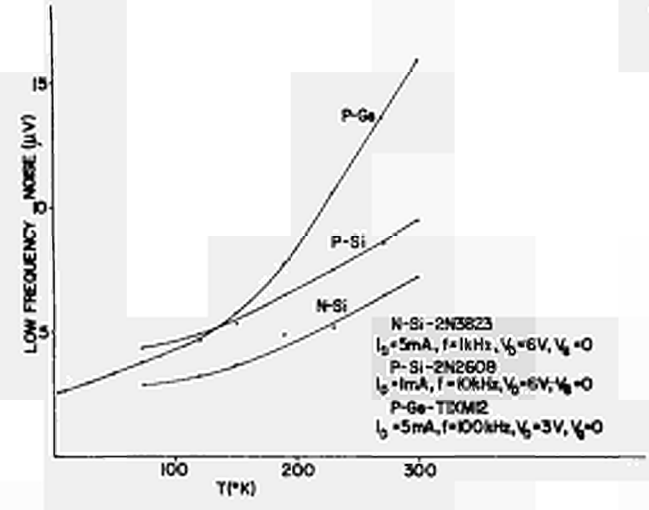

Fig. 12) Low frequency noise vs. T

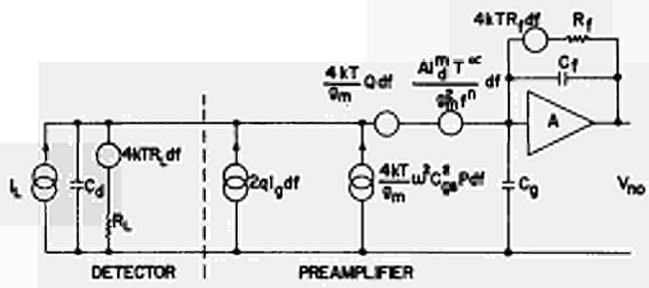

Fig. 9) Equivalent noise circuit of a charge-sensitive preamplifier.

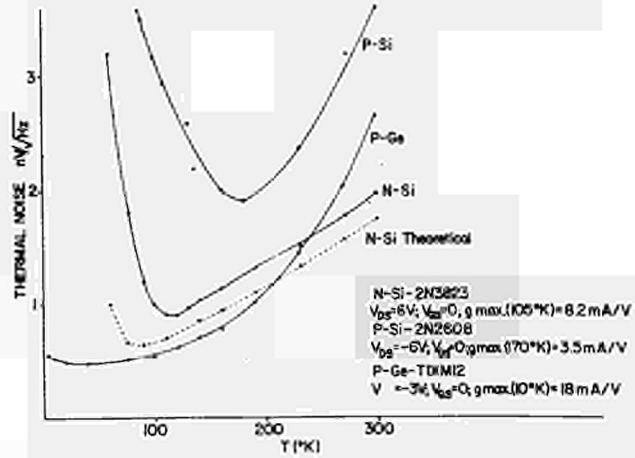

Fig. 10) Thermal noise of Si and Ge JFET's vs. T.

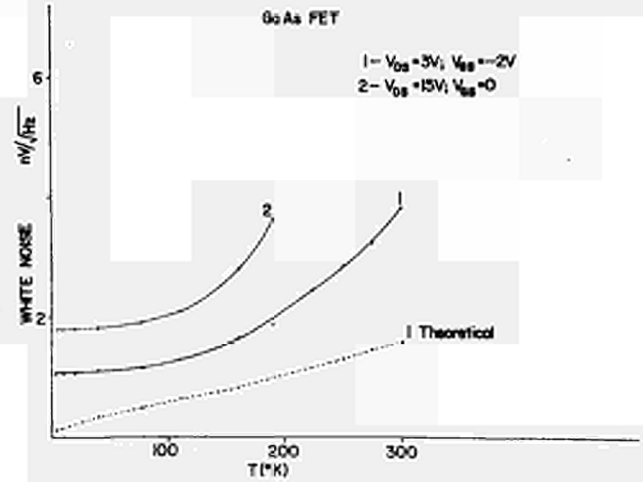

Fig. 11) White noise of the GaAs FET vs. T.

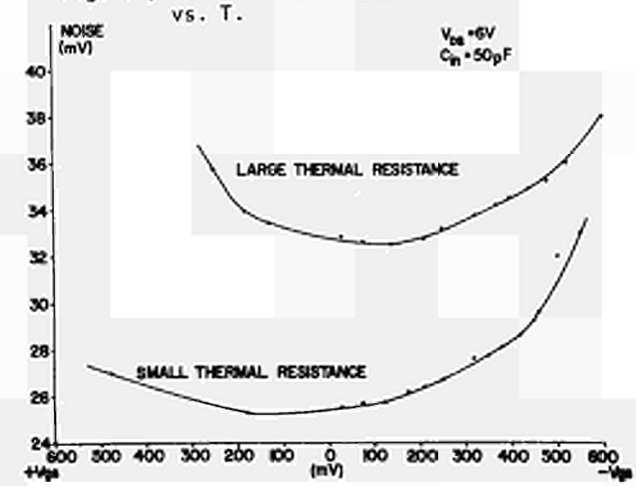

Fig. 13) Noise of an FET vs. gate-to-source voltage.

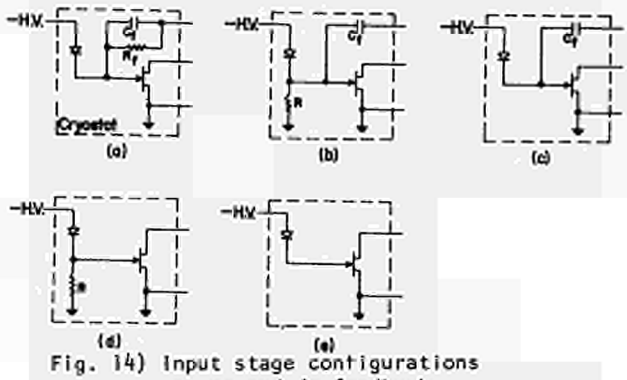

Fig. 14) Input stage configurations
a. ac and dc feedback
b. ac feedback charge sensitive
c. ac feedback
d. voltage sensitive
e. voltage sensitive

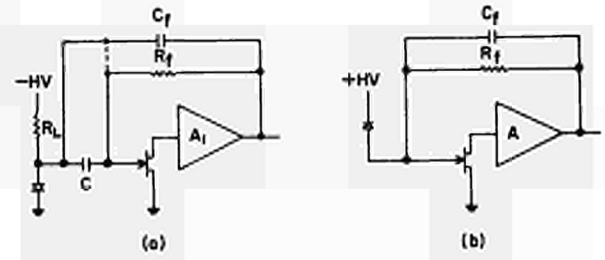

Fig. 15) Coupling mehtods of the detector and the preamplifier.
a. ac coupling
b. dc coupling

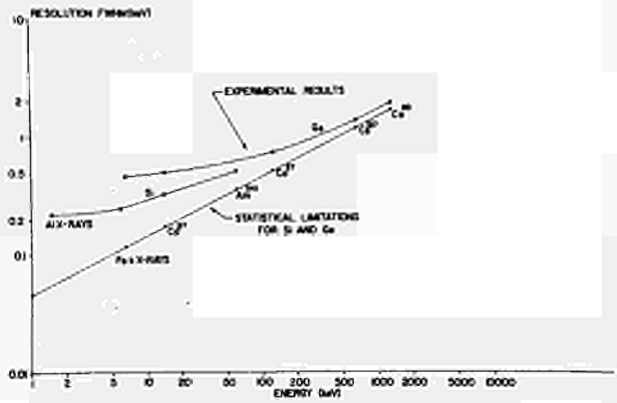

Fig. 16) Theoretical limitations and experimental results for state of the art x-ray and γ ray spectrometers.

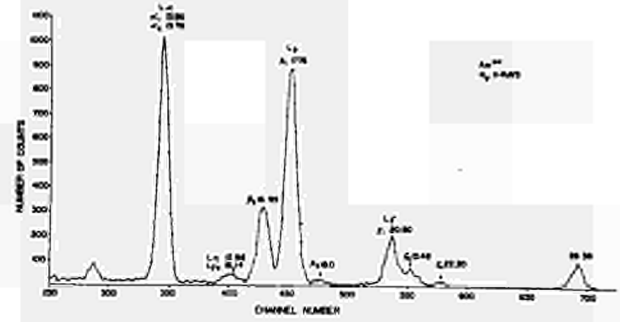

Fig. 18) Spectrum of Np L x-rays.
Energy in KeV.

	1		2		3	4	5
	μ (cm^2/Vsec)(300°K) μ_n	μ_h	μn max (Nd=5.10^{15} cm^3	at T(°K)	E_d(eV)	$T=\frac{E_d}{6K}$	K_s
Si	1350	480	~15000	65-90	0.045	~90	11.7
Ge	3900	1900	n 80.000	10-20	0.01	20	16.3
			p 25.000	20-35			
GaAs	8600	250	22.000	85-115	0.006	12	12
InSb	75.000	—	200.000	35-55	0.0006	12	17

SOME PROPERTIES OF Si,Ge,GaAs AND InSb

TABLE 1

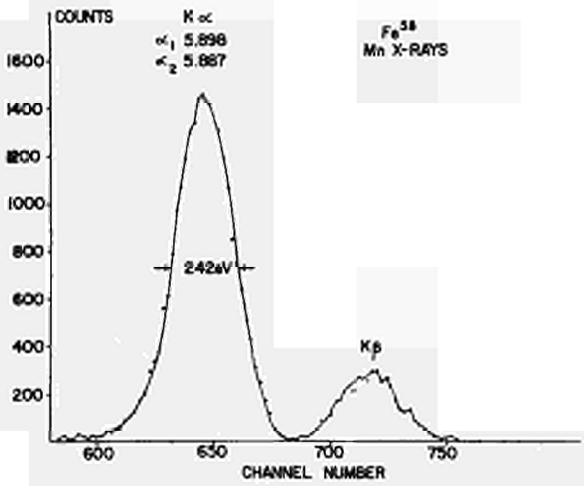

Fig. 17) Spectrum of Mn K x-rays.
Energy in KeV.

FET Type	Optimum g_m (mA/V)	at T(°K)	C_{in} (pF)
2N3823	10	110	6
2N4223	9	85	6
UC210	9	77	7
2N5105	9.5	125	5
2N4416	10.5	100	4
2N2608	3.5	170	17
TIS75	45	85	18
ND-104	60	145	25

Optimum g_m and operating temperature for various FET's.

TABLE 2

THE DEVELOPMENT OF 'n' CHANNEL FET'S FOR LOW NOISE NUCLEAR PULSE AMPLIFIERS

by

J. H. Howes
Electronics & Applied Physics Division,
U.K.A.E.A. Research Group,
Atomic Energy Research Establishment,
Harwell.

Abstract

This paper discusses some aspects of the development and characteristics of two types of low noise 'n' channel field effect transistors developed on U.K. government contracts, placed by the C.V.D. organisation on Texas Instruments Ltd., Bedford, England, and supervised by A.E.R.E. Harwell. The transistors were developed to meet a general circuits requirement for high input impedance, low noise transistors for following nuclear particle detectors, infra-red detectors and acoustical transducers. The paper also describes the application of the transistors to the design of low noise pulse amplifiers for very high resolution nuclear particle and gamma-ray spectrometry.

Introduction

In recent years improvements in the design of semiconductor radiation detectors have made greater demands on the performance of the input amplifying stage of nuclear pulse amplifiers. Effort has been concentrated on the development of a device for the input amplifying stage, since this stage is the most significant in determining the equivalent input noise level and hence the contribution of amplifier noise to the energy resolution of the complete spectrometer system. The thermionic valve had been developed to its limit of noise performance some ten or fifteen years ago. With the advent of the 'n' channel field effect transistor (FET) a new type of device became available for development as a low noise high input impedance amplifier. Up to about four years ago the thermionic valve was possibly still comparable in noise performance to the junction FET at room temperature, but more recently FET designs have been developed to the stage where they have a noise performance superior to that of the best thermionic valve.

A problem which has existed in designing low noise amplifiers is the absence of specified FET characteristics in terms which will give a guaranteed noise performance over a wide range of frequencies. An endeavour to overcome this problem has been made on a U.K. government contract placed via the C.V.D. Organisation with Texas Instruments Ltd., Bedford, England and supervised by A.E.R.E. This paper deals with aspects of the development for which A.E.R.E. has been directly responsible, i.e. the specification of performance and means of evaluation and testing of development models. Two distinct types of 'n' channel FET were specified. The design of one of these (VX286) has been optimised for low input capacitance systems and has an operating frequency range up to 400 MHz. The second device (VX9305) has a higher mutual conductance to meet the requirement of high input capacitance systems. An important factor was to have a good understanding of noise correlation in terms of e_n, the equivalent input noise voltage generated per unit bandwidth (the transistor specification is in terms of e_n/root cycle) and of equivalent noise charge when used in a wide band amplifier for nuclear pulse amplifier applications.

Factors influencing noise in junction field effect transistors

One of the factors limiting noise of the junction FET at low frequencies is the thermal noise of the channel resistance. Sah[2] and Van der Ziel[1] have shown that the noise can be represented by a current generator i_d where

$$\overline{i_d^2} = 4\ KT\ g_{max}\ Q(Vg, Vd)\Delta f,$$

K is Boltzmann's constant, T is the absolute temperature, g_{max} is the mutual conductance of the channel in saturation, Δf corresponds to the bandwidth of the amplifier, and $Q(Vg, Vd)$ a complex function of the gate and drain voltages; this is unity at zero gate voltage and less than unity for all other values of Vg and Vd and a typical value is 0.7, i.e. in typical operation the fluctuation in source to drain current is

$$i_d^2 = 2.8\ KT\ g_{max}\Delta f.$$

The generation of $1/f$ type of noise has been discussed by Sah[2]. The voltage variations across the channel are due to fluctuations in carriers arriving at the source and drain contacts. These fluctuations are due to the generation and recombination of carriers at centres in the "depletion layer" or "transition region" between the gate and channel. Fluctuations in the rate of generation of hole-electron pairs in the depletion-layer cause corresponding changes in the width of the depletion layer and hence of the channel. These centres are mainly due to imperfections in the silicon crystal lattice, surface imperfections and metal ions which have diffused into the crystal. Sah[2] gives the noise voltage from this source as

$$\overline{e^2} = 4\ KT\ R_n\Delta f,$$

where R_n is a function of the density of generation and recombination of centres (often referred to as Shockly-Read-Hall centres) in the space change region as distinct from the channel. This noise source can be very much more serious than that from the SRH centres in the channel. The methods of controlling this source of noise

in order to obtain a consistent device in production will be described elsewhere by K. Maddex of Texas Instruments, Bedford, England.

The magnitude of shot noise is given by

$$i_{sh}^2 = 2qI_{gss}\Delta f$$

where $q = 1.6 \times 10^{-19}$ coulomb, and I_{gss} is the gate leakage current. The shot noise component arising from I_{gss} can be very small in n channel FETs, since I_{gss} is often only a few picoamps, at 295°K in a device in which the manufacturing processes are under close control.

One source of low frequency excess noise has been shown to arise from imperfections in the epitaxial layer from which the channel is formed. Examination of channel profiles by use of a scanning electron microscope* operating in the conductivity or emissive modes have shown that in transistors exhibiting higher than average low frequency noise, there are localised regions of high conductivity in the channel and in the space charge volume. Transistors with low noise of the same geometry are comparatively free of the "pipes" of high conductivity. An example of this phenomenon is shown in Fig. 1c.

Figs. 1a and b show regions of low conductivity under the silicon oxide between the gate and drain electrode; transistors showing this type of imperfection often exhibit high gate current and high e_n noise at low frequencies. Fig. 1a is taken in the emissive mode indicating the region under the surface of SiO_2, and Fig. 1b is a conductive mode photograph showing where the corresponding imperfection occurs. It is not entirely clear how this condition arises. Fig. 1c shows regions of high conductivity in the channel and space charge regions of a transistor which exhibited higher than average noise. Fig. 1d is a conductive mode photograph of part of the channel/space charge region of a low noise specimen which is free of excessively high conductivity regions. The scanning electron microscope has proved to be a powerful tool for examining the behaviour of various solid state electronic devices.

A phenomenon which was predicted by Dacey and Ross[3] in 1954 and further noted by Fowler in 1968[4] can influence low frequency noise of the FET. This is excess gate current which flows at high channel voltages. It is suggested by K. Maddex[5] that the electron current flowing from the source to drain can result in a small hole current being generated from the region of the drain. The holes would normally recombine within a short distance of the drain because they are majority carriers, with a lifetime τ and a mean free path λ. As the drain to source voltage V_{DS} is increased, the space charge from the gate widens until the gate begins to collect holes. In devices which have a compact geometry the threshold for hole collection is about 12V and a further increase in source to drain voltage causes an exponential increase in the number of holes collected. This effect is significant when considering operating conditions to minimise gate current generated noise.

*Stereoscan Electron Microscope. Cambridge Instrument Co., Cambridge, England.

Noise characteristics of VX9286 and VX9305

The specified limit of equivalent input noise voltage e_n for the VX9286 and VX9305 are shown in Fig. 2 together with e_n measurements which are typical of the two types of transistor. Noise above 10Hz is measured by incorporating the FET under test in a charge-sensitive amplifier, with facilities for setting the drain current and voltage at various values. After preliminary amplification, the noise signal is fed through a frequency selective filter ($Q \simeq 7.5$) and then through a second amplifier to a r.m.s. thermal noise voltmeter. By selecting filters spot measurements of e_n can be made at ten points in the frequency range 10Hz to 300KHz. The overall accuracy of the measuring system is better than 5% and the most sensitive range permits the measurement of e_n down to 0.3 $nV\sqrt{\sim}$.

The measurement of noise below 10Hz uses a digital analysis technique. Filtered noise is sampled periodically and stored on paper tape, and is then analysed in a digital computer. This technique was developed by G.G. Bloodworth[6] and co-workers. It is interesting to note from Fig. 2 that neither type of transistor exhibits a $1/f$ dependency.

Established practice in non-nuclear work is to specify noise in terms of e_n, since commercially available equipment exists for this type of measurement. The method of equivalent noise charge is more commonly used in the field of nuclear electronics. The relation between the two methods of specifying noise has been considered by M.O. Deighton[7], among others, who shows the general relationship that one would expect to exist between equivalent noise charge (ENC) and e_n measurements.

Figs. 3, 4, show ENC results obtained with the two types of transistors at 295°K and 120°K. These transistors were selected to have a e_n noise at 1KHz equivalent to the limits of the specifications indicated in Table I. These results were obtained using a circuit similar to that shown in Fig. 5, however, transistors J_2 and J_3 are selected for low $1/f$ noise and high current gain for low emitter current to ensure that the base current shot noise is not a significant noise source. The more significant characteristics of the VX9286 and VX9305 are given in Table I.

Application of the FET to nuclear pulse pre-amplifiers for high resolution spectrometry

In order to achieve a consistent performance from solid state detectors when used as high resolution spectrometers, it is necessary to consider the optimum conditions for the pre-amplifier, main amplifier and pulse shaping networks. The basic arrangement for pulse amplifying systems used with semi-conductor detectors is shown in Fig. 6. The signal produced by the collection of carriers generated by an ionising event constitutes a current pulse whose shape and duration depends on the size and geometry of the detector and electric field distribution. The signal rise-time can vary

from a few nanoseconds for small planar detectors to tens of nanoseconds in large coaxial Ge(Li) detectors.

Figure 6 shows the main features of the detector amplifier feeding a pulse shaping system, also indicating the main parameters of interest, including the equivalent noise generators due to detector and various components of the amplifier. When a total charge Q is collected across the terminals of the detector (Capacitance C_{det}), the charge Q_f flowing into the feedback capacitor Cf is

$$Q_f = \frac{Q}{1 + C_{det}\left(\frac{C_o + C_{in}}{C_o C_{in}}\right)} \cdot \frac{(A_1 + 1)C_f}{C_{in}},$$

where C_o is the isolating capacitor used to isolate the amplifier from the polarising voltage applied to the detector, C_{in} is the total input capacitance of the current integrator stage and $C_{in} = C_s + C_f (1 + A_1)$. C_s represents the total capacitance due to the cold capacitance of the input device plus all the stray capacitance to ground of components connected to the input terminal.

If Q_f is to be nearly equal to Q and be independent of changes in C_d, then

$$\frac{C_{det}}{C_{in}} + \frac{C_{det}}{C_o} << 1$$

i.e. C_o must be >> C_{det} and $C_{in} = C_s + A_1 C_f$ must be >> C_{det}. Since C_f must itself be small to make the output voltage signal of the current integrator ($= Q/C_f$) as large as possible, it follows that a high value of A_1 is required and in practice it is in the range 1000 to 10,000.

The principle sources of electrical noise in the detector/pre-amplifier system are those associated with reverse bias current in the detector (bulk generated and surface leakage currents) and noise associated with the input FET device. In Fig. 6 the detector noise is represented by an r.m.s. noise current generator i_{det}; E.N.C. is $\propto\sqrt{I_{det} \times T}$, where I_{det} is the detector current and T is the time constant of the pulse shaping circuits. Detector generated noise in a detector operated at liquid nitrogen temperature can be negligible compared with FET generated noise when i_{det} is < 50pA. The equivalent noise generators associated with the FET input stage are shown in Fig. 6 as a current generator i_g related to leakage current in the FET gate, and an equivalent voltage generator e_n in series with the gate which represents fluctuations in the source to drain current of the FET. The current noise i_g is analogous to detector current noise, i.e. E.N.C. $\propto\sqrt{i_g \times T}$, but the equivalent r.m.s. noise charge due to e_n is

$$\propto \frac{C_{det} + C_S + C_f}{(g_m T)^{\frac{1}{2}}}.$$

Both these sources of noise can be reduced if the FET can be operated at a low temperature but the e_n term is usually dominant, at any rate for input capacitances < 10pf. it is obvious that the stray capacitance C_s should always be made small in relation to C_{det} to obtain minimum E.N.C.

Sources of noise other than the FET are thermal or Johnson noise in the detector load resistor R and in the resistor R_f used in parallel with the feedback capacitor C_f to maintain necessary quiescent operating conditions in amplifier A_1. With very careful design both these noise sources can be reduced to negligible proportions by choosing resistors of sufficiently high values. The characteristics of R_f at high frequencies and the quality of the dielectrics associated with the input circuitry are very critical as the value of C_{det} becomes very small. This problem is discussed in a paper by V. Radeka[8].

The noise sources already discussed produce a spread in pulse amplitudes which limits the ultimate energy resolution of the system. Another source of spread is incomplete collection of the primary carriers generated in the detector and the magnitude of this effect is governed by the properties of the starting material from which the detector is manufactured. Another important source of spread is the effect of "pile up" of one pulse on the tail of a proceeding pulse and other 'base line' shift effects, all of which become more predominant at high count rates. K. Kandiah[3] has described a directly coupled counting system which overcomes many of the problems arising from the more conventional shaping networks. This system can operate satisfactorily at counting rates of 1MHz.

Operation of FETs at temperatures below 295°K

The principal advantage of operating field effect transistors attemperatures below 295°K is the reduction in noise. The principal source of noise of the FET in the range of frequencies applying the nuclear pulse amplifiers is the thermal noise of the conducting channel. This noise source can be shown to be equivalent to an input voltage generator

$$\overline{e_n^2} = \frac{2.8KT\Delta f}{g_m}$$

where Δf is the effective bandwidth. From this it follows that e_n will be reduced by reducing temperature T or increasing g_m (mutual conductance). The increase of g_m is dependent on the electrical conductivity of the channel which in turn depends on the mobility and density of free carriers. In the case of the n-type channel, conductivity $\sigma = q\mu_e n$ where q = electronic charge, μ_e = electron mobility and n the free electron density. The mobility of free carriers in the channel has an acoustic lattice vibration component μ_a, with a temperature dependance approximating to $T^{-3/2}$ where T is absolute temperature. The component μ_i due to scattering of ionized impurities is given approximately by $n^{-1} T^{3/2}$, where n is a constant relating to the impurity concentration. The total mobility μ_T is given by

$$\frac{1}{\mu_T} = \frac{1}{\mu_a} + \frac{1}{\mu_i}.$$

The temperature dependence of the combined scattering processes will be determined mainly by the smaller of the two components μ_a, μ_i. Further, the temperature dependence of the two scattering processes are opposite so a maximum will occur in the mobility/temperature curve. The temperature T_{max} at which the mobility is maximum will be dependent to a large degree on impurity concentration in the channel. The mutual conductance maximum will roughly correspond to the same T_{max}, so for temperatures above T_{max} the mobility is determined by lattice scattering. For temperatures less than T_{max} impurity scattering is predominant. In intrinsic n-type silicon T_{max} would be expected to be in the region of 60-70°K but in the more highly doped n-channel FETs the maximum mobility can occur over a wide range of temperatures. In the case of the VX9286 and VX9305 T_{max} occurs in the region of 100-120°K.

From the above it can be concluded that the lower limit of temperature for optimum signal-to-noise ratio in a silicon n-channel FET could be as low as 60°K, however, in practice it is more likely to be in the region of 90-140°K. An exception to this has been noted by V. Radeka[10] where the noise increases giving a maximum at about 180°K and then decreases to a value lower than that at 295°K. This effect is most probably due to some particular impurity which "freezes out" and thus permits the channel mobility to increase as the temperature further decreases. The properties of a p-channel germanium planar FET (T1X301) have been described by E. Elad[11] showing its ability to operate down to 4°K. Experience at A.E.R.E., Harwell would confirm E. Elad's results using the Ge FET below 100°K.

The VX9286 and VX9305 both have g_m maxima in the temperature range 100-130°K and Fig. 7 shows the ratio of noise at a given temperature to the noise at room temperature. The amplifier used for low temperature operation is shown in Fig. 5. The input stage can be detached for use in various types of cryostat. The choice of input circuit configuration is largely determined by the characteristics of the detector. In the case of low capacitance detectors (< 20pf) the D.C. coupldding method shown in Fig. 5, Inset B is used, since this condition gives the lowest stray input capacitance, i.e. the stray capacitance associated with the coupling capacitor and load resistor are absent. To realise fully the advantage of D.C. coupling the reverse leakage current of the detector should be small (< 0.5nA) to enable the feedback resistor to be of sufficiently high value not to contribute excessive parallel noise. In the case of the larger volume higher capacity detectors, the advantages of D.C. coupling are not quite so great, since the bulk generated current in the detector is often larger and the mean signal current at high counting rates is such that the dynamic range of the pre-amplifier is exploited better by using A.C. coupling.

One of the advantages of a cooled input amplifier stage is the long term gain stability that a well designed system can achieve. The stability of a cooled amplifier system is demonstrated by Fig. 8, showing the gamma ray spectrum of ^{56}Co for a counting period of 20 hrs, where at 3.25MeV the FWHM is maintained at 3.0keV. The stability limitation is in the electronics following the pre-amplifier.

When operating detectors with low input capacitance (< 5pf), sources of noise are apparent which are not related to the FET. These fall into four main categories:-

1) microphony due to very small movement of input circuitry attached to the input stage; also in this category are piezo-electrically generated signals arising from shock applied to the detector and insulators connected to the input stage; this effect can be observed by applying low level signals in the pass frequency of the amplifier to various parts of the cryostat using a Piezoelectric transducer. To reduce this source of noise, electrical insulators attached to the input should be reduced in volume to a minimum,

2) dielectric losses of insulators in the proximity of and connected to the input stage; these include insulators supporting components, capacitor dielectrics and FET header insulators,

3) resistors attached to the input stage which have a frequency dependence of resistance resulting in a lower value of resistance at the pass frequency of the amplifier than at D.C.,

4) fluctuating magnetic fields inducing current in the input amplifier stage is a further source of spurious noise.

When operating at noise levels below equivalent noise charge of 150 ion pairs these four effects can severely limit the ultimate performance of a high resolution spectrometry system.

Conclusions

The VX9286 and VX9305 represent a significant advance of FET development in terms of specified noise parameters and gate current limits which enable the circuit designer to calculate the worst noise performance over a wide range of frequencies. The specification of noise is a problem that has existed in many fields of circuit design involving the amplification of small signals from high impedance transducers. In the present designs the gate current limit is 30pA; it would be desirable to reduce this limit to about 1pA, which would in turn reduce the shot noise. Texas Instruments Ltd. are investigating techniques to reduce gate current and initial results are promising. The designs discussed in this paper are very near to the limit of development using current techniques, which are limited by the channel length, which in turn is limited by current photomasking and diffusion techniques.

Further development of the FET is possible by using techniques which would enable gate lengths of less than 1μm to be produced. This would make it possible to produce transistors

which would have a mutual conductance/input capacitance ratio over three times greater than present designs, with a very low value of gate to drain capacitance. Other developments[12] involving silicon Schottky barrier FETs show promise in terms of high frequency performance (>5GHz). Such devices require gates 1μm long using a projection masking technique. Experience with GaAs Schottky barrier FETs on a semi-insulating substrate have not been encouraging in view of the excessive low frequency noise (at 10Hz 6μV$\sqrt{\sim}$). The performance of the silicon Schottky barrier transistors might well be more satisfactory than the GaAs FET. Developments along these lines are being investigated at A.E.R.E., Harwell.

References

1. A van der Ziel "Thermal Noise in FETs" Proc. IRE 50 Aug. 1962. p.1808-12.

2. C. T. Sah "Theory of Low Frequency Generation Noise in Junction Gate FET's. Proc. IEEE. July, 1964. p.794.

3. G. C. Dacey and I. M. Ross "The Field Effect Transistor". Bell System Tech. J. 1955. 34 pp 1151-1158.

4. E. F. Fowler. Electronic Letters 31. May 1968. Vol. 4 No. 11.

5. K. Maddex. Private communication. Texas Instruments Ltd., Bedford, U.K.

6. I.R.M. Mansour, R.J. Hawkins, G.G. Bloodworth. Electronic Engineer Vol. 35 No. 4, 1968.

7. M. O. Deighton. "The Simple Theory of Noise in Nuclear Pulse Amplifiers". A.E.R.E., Harwell. R5439, 1967.

8. V. Radeka. IEEE Trans. Nuc. Sci., Nis 15 No. 3 455, 1968.

9. P. E. Gibbons, J. H. Howes, R. B. Owen, IEE Conference Publication No. 47, 152, 1968.

10. V. Radeka. Brookhaven National Laboratory BNL 12798, 1968.

11. E. Elad and M. Nakamura. UCRL 17818. 1967.

12. K. E. Drangeid et al. Electronic Letters, 23rd August, 1968. Vol. 4 No. 7.

13. K. Kandiah. Proceedings of Gatlinburg Conference, 1967.

TABLE I

Characteristics of VX9286 and VX9305

Parameter	VX9286	VX9305	Units
e_n equivalent noise voltage 10Hz	20	16	nV$\sqrt{\sim}$ max
" " 120Hz	10	8	" "
" " 1KHz	5.0	4	" "
" " 10KHz	3.0	2.0	" "
" " 100KHz	1.5	1.1	" "
" " 500KHz	1.5	1.1	" "
I_{g} Gate leakage Current	30	100	pA. max
Y_{fs} Mutual Conductance	7.5	20	mA/v mean
C_{iss} Common source input capacitance	8.5	10.5	pf. max
C_{rss} Common source, short circuit, reverse transfer capacitance	1.2	2.7	pf. max
I_{DSS} Zero gate voltage Drain current limits	5-20	10-30	mA

If the VX9286 is operated with the source and drain terminals reversed, without any alteration to other specified parameters the capacitance limits become C_{iss} = 5pf max, C_{rss} = 1.5pf max.

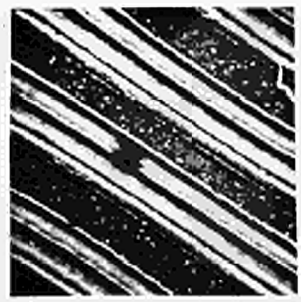

Fig. Ia. Emissive mode photograph showing surface imperfection between gate and drain. Mag. x 1750

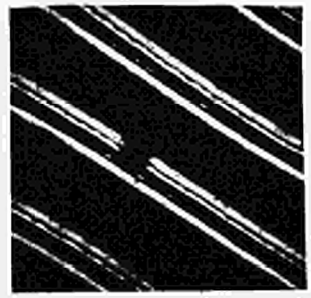

Fig. Ib. As Fig. Ia. but conducting mode. Mag. x 1750

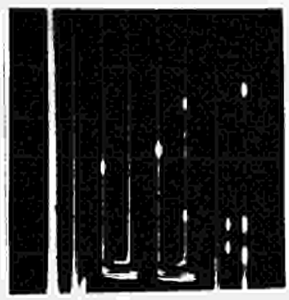

Fig. Ic. Conductive mode photograph of channel and space charge region of a noisy specimen of the VX9286. Mag. x 500

Fig. Id. Conductive photograph of space charge and channel region in a low noise specimen of the VX9286. Mag. x 1155

FIG.1 SCANNING ELECTRON MICROSCOPE PHOTOGRAPHS

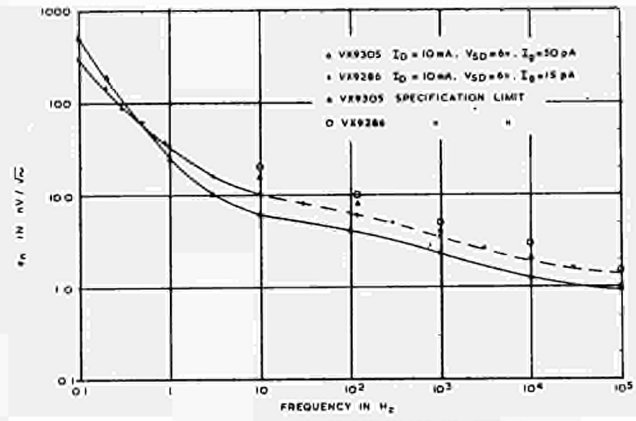

FIG 2 e_n VALUES FOR VX9286 AND VX9305

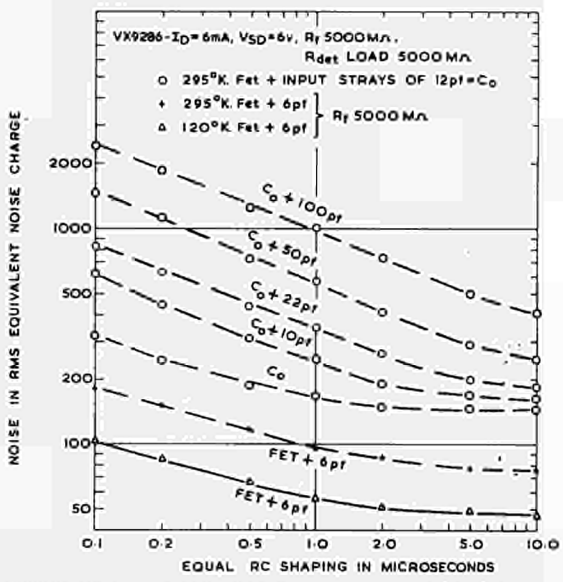

FIG. 3 EQUIVALENT RMS NOISE CHARGE FOR VARYING CAPACITANCE (VX9286)

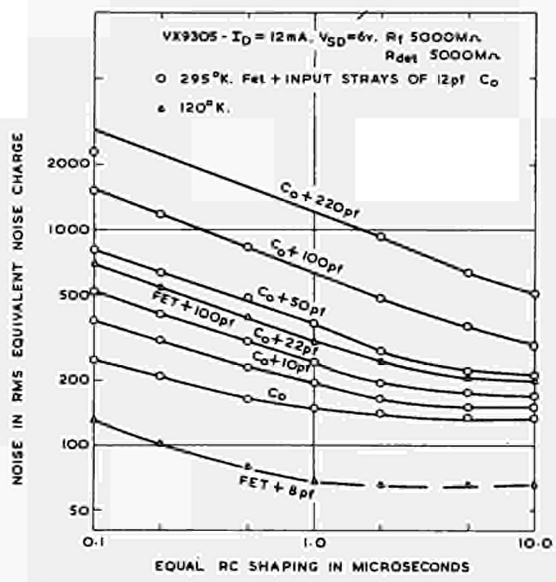

FIG. 4 EQUIVALENT RMS NOISE CHARGE FOR VARYING CAPACITANCE (VX9305)

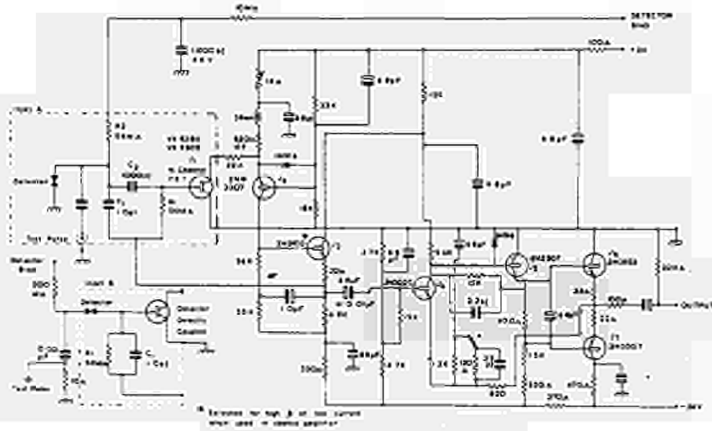

FIG 5 LOW NOISE PRE-AMPLIFIER

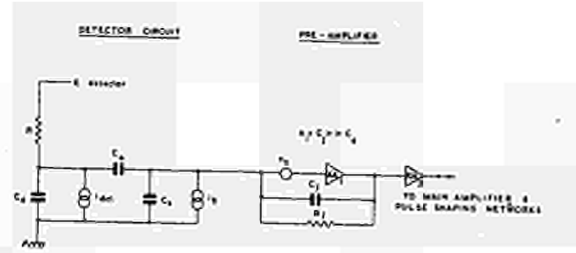

FIG. 6. The charge-sensitive amplifier, showing noise sources.

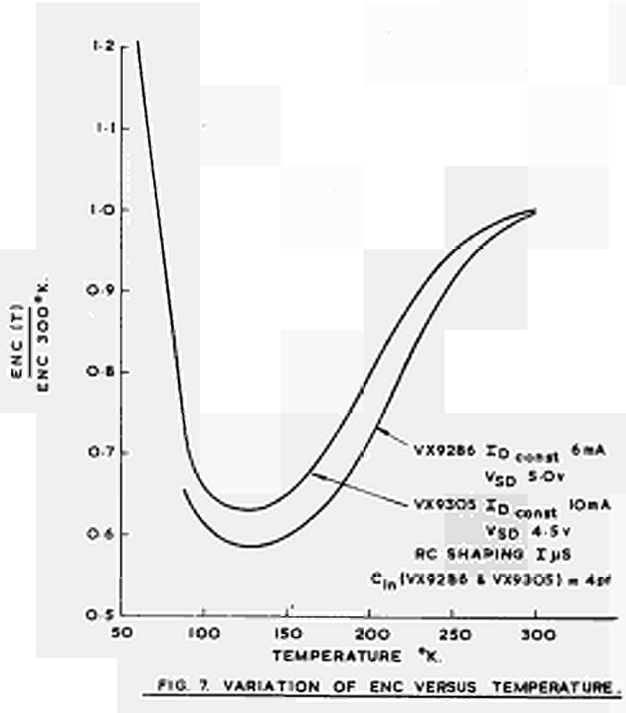

FIG. 7. VARIATION OF ENC VERSUS TEMPERATURE.

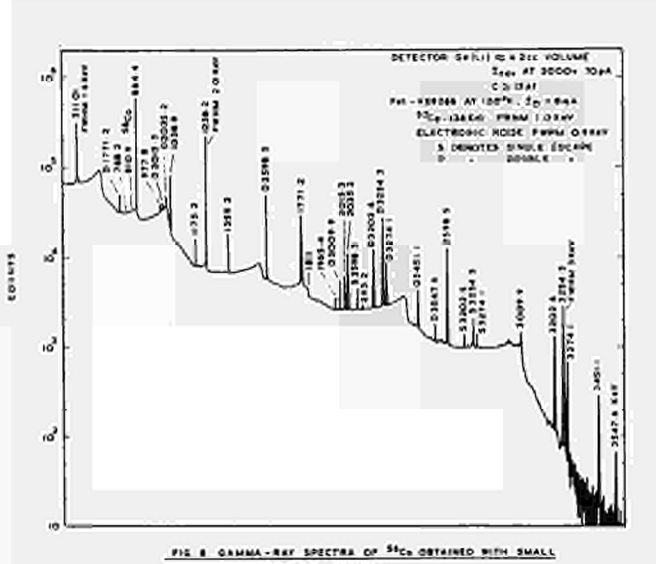

FIG. 8 GAMMA-RAY SPECTRA OF ^{56}Co OBTAINED WITH SMALL Ge(Li) DETECTOR

Realization of Optimum Pulse Shaping Filter

Minoru Oda
Central Research Laboratory
Mitsubishi Electric Corporation
Amagasaki, Japan

Presented by G. Colombo

Summary

In this paper, a close approximation method of theoretically optimum filter is reported. The principle of this method is the subtraction of delayed single CR integrated pulse from multiple integrated pulse. Approximation accuracy is excellent and the calculated NF is 1.015. The effect of band width limitation of delaying elements is not a serious problem on the filter NF.
Also reported is a method of eliminating the degradation of resolution due to the risetime spread of input signals. The risetime sensitivity is eliminated by this method with slight sacrifice of noise performance.

1. Introduction

Prior to the detailed description, some definitions and assumptions are briefly explained. The noise figure (or factor) of a pulse shaping filter is the capability of separating step signal pulses from the noise whose power spectrum is $A+B/\omega^a$, where A and B are constants. Generally following index NF is used with normalization of AB=1.

$$NF=\frac{\text{noise gain}}{\text{signal gain}}=\frac{\left\{\frac{1}{2\pi}\int_0^\infty |F(\omega)|^2\left(A+\frac{B}{\omega^2}\right)d\omega\right\}^{\frac{1}{2}}_{min}}{\text{signal gain}} \quad \cdots (1)$$

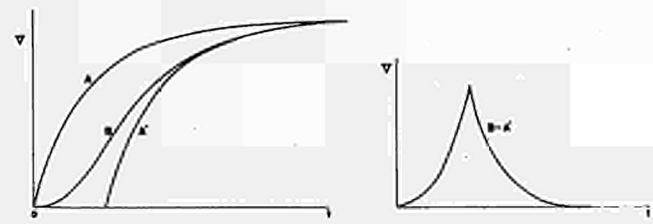

Fig. 1. Principle of cusp shaping.

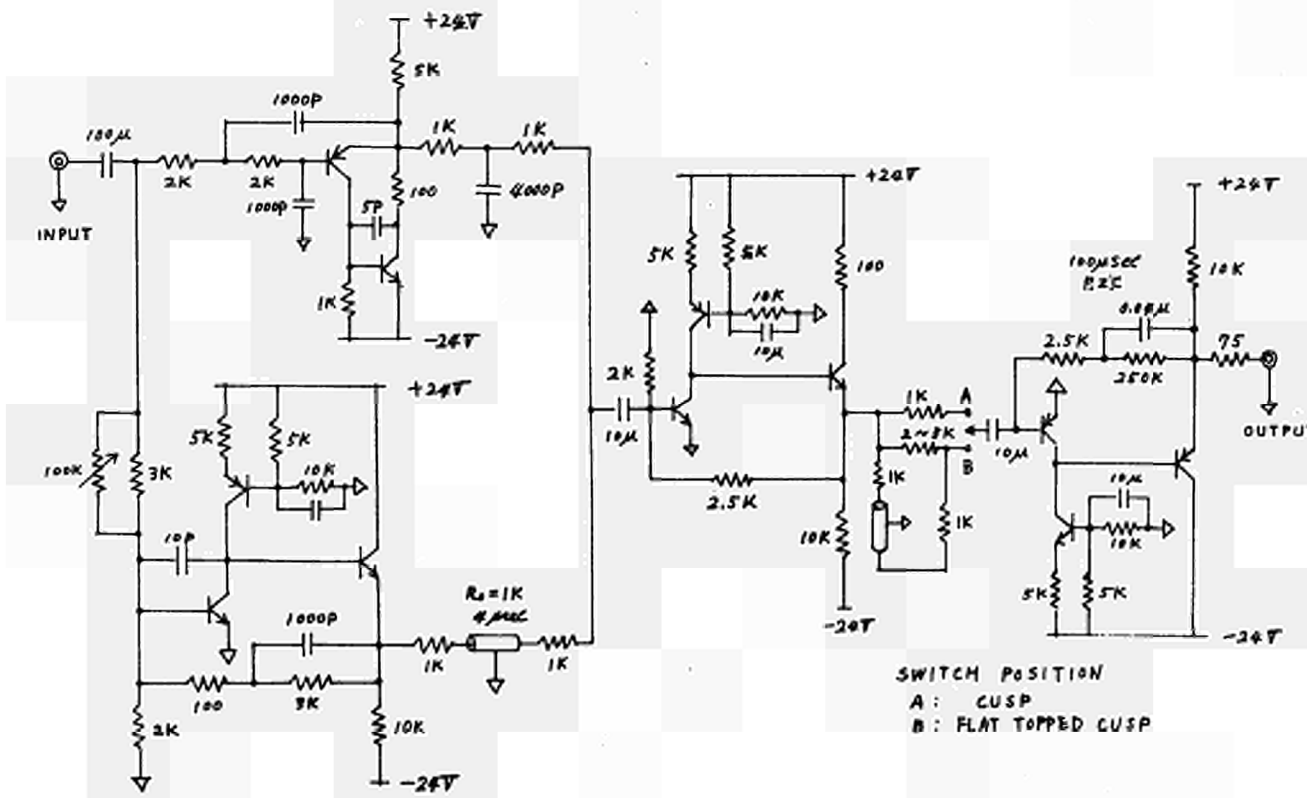

Fig. 2. Cusp shaping circuit.

where $F(\omega)$ is the frequency responce of the shaping filter. Theoretical minimum value of NF is unity, and for the ordinary CR filter, NF is 1.36. Optimum filter is theoretically proven to have cusp responce ($V(t)=e^{-|t/\tau|}$). One of the remaining problem is how to realize a close approximation with simple circuit.

2. Approximation of cusp shaping

The principle of this method is shown in Fig. 1. In Fig. 1, A is obtained by CR integration of step signal, while B is obtained by multiple CR integration, and A' is obtained by delaying A. Cusp shape responce is obtained by making B-A'. Actual circuit diagram and output pulse shape are shown in Fig. 2 and Fig. 3 respectively. On designing actual circuit, optimum combination of integrating time constants and delaying time have to be determined. To simplify the integration of Eq. (1), Parseval's equation was utilized. This method not only simplifies the integration but also clarifies the relation between output pulse shape and NF in geometrical concept. Deighton et al, have reached the same conclusion from different basis by assuming noise model, whereas there no additiona assumption is necessary from this point of view, and so mathematically clearer. In the case of triple integration of B in Fig. 1, the optimum combination is as follows.

$$\tau_A/\tau_B = 1.5 \qquad Td/\tau_B = 2 \qquad \text{----(2)}$$

(Effective time constant with regard to noise corner is $0.8\tau_B$.)
The circuit in Fig. 2 is designed with this conditions.
Thus the inditial responce function is as follows. (Fig. 3)

$$V(t) = 1 - \left\{1+\frac{t}{\tau_B}+\frac{1}{2}\left(\frac{t}{\tau_B}\right)^2\right\} e^{-t/\tau_B} \quad (0 \leq t \leq 2\tau_B)$$

and

$$V(t) = e^{-2/3(t/\tau_B-2)} - \left\{1+\frac{t}{\tau_B}+\frac{1}{2}\left(\frac{t}{\tau_B}\right)^2\right\} e^{-t/\tau_B} \quad (t > 2\tau_B) \qquad \text{---- (3)}$$

Fig. 3. Output pulse shape of cusp

In this case NF=1.015, which is almost equal to the theoretical limit. Experimental results are shown in Table 1.
Calculated NF in Table 1 is including the effect of band width of delaying element. Approximate evaluation of this effect is shown in Appendix. In spite of probable presence of 1/f noise, experimental results are close to theoretical calculation.

3. Risetime compensation method

Signal risetime of Ge (Li) detectors has not usually a difinite value. Spread of risetime causes pulse height spread to degradate resolution. The pulse shaping method to be described is to prevent this deffect by realization of insensitive characteristic of output pulse height ti input signal risetime. The principle of this method is as follows.
If the filter responce has a flat portion at the top, and maximum risetime is less than the duration of flat portion, maximum value of following equation is kept constant.

$$V_{out}(t) = \int_0^\infty f(t-\tau)\,\frac{ds(t)}{d\tau}\,d\tau \qquad \text{----(4)}$$

Where $f(t)$ is the inditial responce of the filter with flat portion of ΔT, $S(t)$ is input signal with risetime spread of Δt. ($\Delta T \geq \Delta t$). Because

Table 1
Noise Figure of Cusp Shaping Method

Noise Source	NF		
	PHA	VTVM	Calculated
FET	1.02-1.06	1.05	1.03
FET+SSD	1.02-1.06	1.05	1.03

1. In case of PHA, γ-ray source is ^{57}Co.
2. Band width of VTVM is 4Mhz
3. NF of CR filter of the same time constant is taken as a reference.

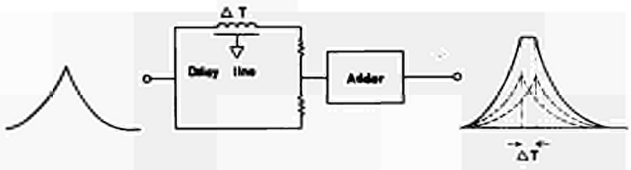

Fig. 4. Principle of flat topped cusp shaping.

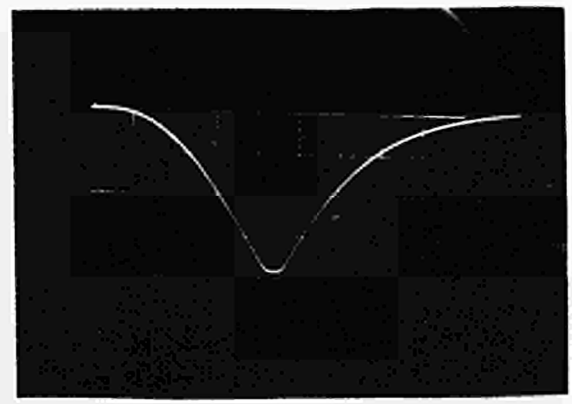

Fig. 5. Output pulse shape of flat topped cusp shaper.

duration of S'(t) is less than ΔT, interval of convolution is limited within ΔT, and so, maximum value of Eq. (4) is kept unaffected though pulse shape is varied with Δt. Principle of flat topped cusp shaping is illustrated in Fig. 4. Flat portion at the top of pulse causes degradation of noise performance. If original pulse shape is of perfect cusp, NF is given by the following equation.

$$NF = \sqrt[4]{1+\alpha} \qquad \text{----(5)}$$

where $\alpha = \Delta t/\tau$. If this method is applied to the approximate cusp of present approach, it approximately leads to

$$NF = \sqrt[4]{(1.015)^4+\alpha} \qquad \text{--- (6)}$$

where $\alpha = \Delta T/0.8\tau_B$. ΔT should be chosen so as to involve risetime of most pulses, so that α of 0.1~0.2 is considered to be practical. Substituting α =0.1 and 0.2 into Eq. (6), NF results in 1.04 and 1.06 respectively. Experimental result is shown in table 2. γ-ray source used is ^{137}Cs. Effect of flattened peak is clearly appeared, and this effect seems to exeed the sacrifice of NF in high energy γ-ray measurement. Output pulse shape in the case of α =0.2 is shown in Fig. 5.

Table 2
Effect of Risetime Compensation Method

Det. Bias \ Shaping	Cusp	Flat topped Cusp	CR-CR
500 V	2.5-2.6KeV	2.2-2.3	2.8-2.9
1000 V	2.1-2.2	2.2-2.3	2.7-2.8
Channel Shift	1/790	0/790	0/790

γ-Ray Source; ^{137}Cs

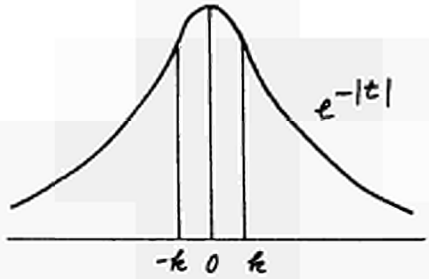

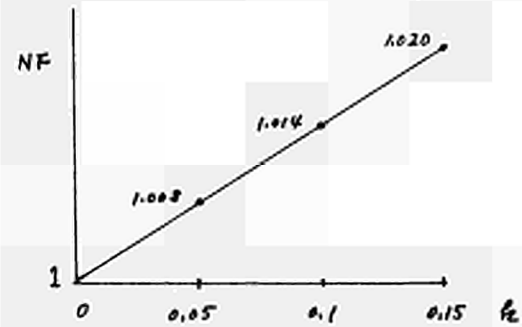

Fig. 6 NF degradation as a function of K

4. Conclusion

Cusp approximation approach presented here is considered to be practical. Band width limitation of delaying element and ADC is not a serious problem in this approach. Even if the responce speed of ADC is not sufficient to analyze cusp pulses, providing some suitable pulse stretcher is not difficult. Risetime compensation method considerably lessens the risetime sensitivity of cusp shaping, and seems to be important in practical use.

Appendix.

Approximate evaluation of the effect of band width limitation of delaying element

The effect of band width appears as the peak rounding effect. The degradation of NF by this effect can be approximately evaluated in the following way. To evaluate this effect alone, true cusp is assumed for the basis, and round portion is assumed to be parabolic. (Cf Fig. 6) Calculation of NF by time domain method leads to

$$NF=\sqrt[4]{1+\frac{8}{3}k+2k^2+\frac{4}{9}k^3}\ /1+\frac{k}{2} \qquad ----(7)$$

where 2k is the duration of round portion, and time constant of cusp is taken to be unity. NF degradation as a function of k is shown in Fig. 6. Assuming k=0.1, total NF in the case of present approach results in 1.03. This evaluation seems to be valid in NF measurement under additional integration.

Reference

1. M. O. Deighton
   A time domain method for calculating noise of active integrators used in pulse amplitude spectrometry. Nuclear Instruments and methods . 58 (1968) 201-212

2. M. Tsukuda
   IRE Trans. Neclear Sci. NS-9, 63 (August, 1962)

DISCUSSION

Stanchi : - Thank you but I am afraid that the construction of the signal which will be evident from figure 1 which was reversed in projection, was not completely understood and also the unability of the author to come makes this problem more difficult. So, please repeat figure 1.

Kandiah : - Thank you Mr. Colombo. First I could make a comment adding to the description of this method of obtaining an approximate cusp shape. The method apparently is a very simple one of obtaining a cusp shape, which gives a nearly theoretical signal to noise performance.

P. Banerjee : - Is it true to assume that although you have a better energy resolution with this form of shaping, the pulses would be much longer than for semi gaussian shaping ?

G. Colombo : - I want to apologize because we only received yesterday the paper and we hardly had time to prepare slides. Perhaps somebody is ready to answer to such problem. For instance Mr. Deighton or somebody else I beg to help me.

Deighton : - Could you repeat your question ?

P. Banerjee : - Yes, the reason why I asked this question is that with semi-gaussian shaping using n integrators and one RC differentiator the shot noise is selectively reduced which permits using a short pulse with a good resolution. Delay line differentiation with an RC integration does not reduce the shot noise as effectively as semi-gaussian filter does and this make me think that although the ultimate resolution of the pulse shaping described here would be better the impulse would be much longer than for semi-gaussian filtering.

Deighton : - I find difficult to answer your question without thinking about it and without making some analysis but certainly the semi-gaussian filtering you mention has inferior noise figure. There is no doubt about this. I think it might well be a slightly shorter pulse but I don't think there will be much difference. This is my feeling.

MINIMUM-NOISE FILTERS WITH GOOD LOW-FREQUENCY REJECTION

by

M.O. Deighton
Electronics & Applied Physics Division, U.K.A.E.A. Research Group,
Atomic Energy Research Establishment, Harwell, U.K.

Summary

A nuclear pulse spectrometer should have both low noise and minimal sensitivity to slow disturbing signals, e.g. base-line fluctuations due to long CR-couplings. A bipolar filter weight-function (or step response) with area balance is advantageous for the latter, but generally involves increased noise and/or resolving time. This paper derives the optimum area-balanced waveform giving least noise for a defined overall width. Optimum waveforms are illustrated and the noise/signal performance is compared with that of the finite-width unipolar cusp and also with several practical bipolar systems in common use.

1. Introduction

In an idealised nuclear pulse amplifier-spectrometer the noise/signal ratio depends on the total capacity at the input, the equivalent noise generators at the input and the nature of the pulse shaping or processing, as distinct from amplification. Fig. 1 shows the relevant parts of the system, in a simplified form in which the functions of pulse shaping and amplification are separated. The (passive) filter characteristics are completely determined from its time response, $F(t)$, to a unit input step at $t = 0$ and it is convenient to assume unity pulse gain here, i.e. a unit-amplitude pulse output in response to unit-step input; the value of G then allows for any numerical attenuation of a practical filter. Clearly G amplifies both signals and noise equally, hence the noise/signal ratio of the system is equal to that at terminals aa'; here the signal pulse height in response to instantaneous charge Q in the detector is always Q/C_d, hence one can compare N/S ratios of different filters by comparing noise magnitudes at terminals aa'. Noise is assumed to arise from two uncorrelated sources at the input, e_n and i_n, each of which generates white noise of spectral density as indicated in Fig. 1.

In filter optimisation problems one assumes C_d, e_n and i_n are given and the form of $F(t)$ has to be optimised, subject to various constraints, so as to yield the best noise/signal ratio. Van Heerden[1] was the first to show that such an optimum exists, with no constraints; assuming instantaneous charge collection, the solution is the 'ideal cusp' response given by $F(t) = \exp[-|t/T_o|]$, where $T_o \equiv C_d\sqrt{2kT_aR_n/qI_g}$, the noise-corner time constant. Baldinger and Franzen[2] give a detailed analysis of this problem taking into account a variety of possible signal current waveforms in the particle detector. Most of these solutions, however, involve responses with (theoretically) infinite extent for negative as well as positive times, hence they cannot be realised in actual physical systems. Gatti and his co-workers[3] therefore considered the case when $F(t)$ is constrained to lie entirely within a given interval $0 \leqslant t \leqslant T$, i.e. $F(t) = 0$ everywhere outside this interval. This yields a modified cusp, each edge of which is a portion of a sinh-curve instead of an exponential. For this width, the best noise/signal ratio (N/S) is $[\coth(T/2T_o)]^{\frac{1}{2}}$ times that of the ideal cusp.

Nowadays many experimenters, perhaps a majority, use bipolar pulse shaping, e.g. by double CR-differentiation or double-delay-line shaping or by double (or multiple) sampling schemes[4] which are effectively equivalent. All these methods yield an effective response function $F(t)$ having equal areas above and below the zero level, the prime advantage being that base-line disturbances introduced by long coupling time-constants present in a.c.-coupled amplifiers, or by the leakage time-constant of the feedback capacitor in the head amplifier, are thereby substantially reduced. The combined effect of these disturbances from many signal pulses otherwise constitutes a base-line fluctuation which seriously limits the high-rate energy resolution of low-noise systems. Another advantage of any area-balanced (A-B) response is that it strongly attenuates other unwanted low-frequency signals at the input, such as excess noise, microphonics, a.c. hum and spurious charge released slowly in the detector. These are merely two facets of a fundamental property of A-B waveforms, namely that the energy density in the low-frequency region of their Fourier spectra is small compared with that at frequencies near $1/T$, in contrast to unipolar waveforms, whose energy density is substantially uniform over most of this range. The price paid for these advantages in practical bipolar systems is a worsening of noise/signal ratio and/or resolving time. One is thus led to ask what is the optimum waveform of prescribed width T and having area balance, in order to assess how much of this noise increase is inevitable and whether it is worthwhile to try to improve existing bipolar techniques. This paper is concerned with analysis of this problem and not with the physical means of realisation of the optimum $F(t)$ obtained. The method of solution is different from those used by previous authors, but with one change it also gives the known solutions of the earlier problems.

2. Derivation of Optimum F(t)

Referring to Fig. 1, the two noise voltage components at terminals aa' are V_{ng} and V_{ns}, given by

$$\overline{V_{ng}^2} = \frac{qI_g}{C_d^2} \int_o^\infty [F(t)]^2 dt$$

and $$\overline{V_{ns}^2} = 2kT_a R_n \int_o^\infty [F'(t)]^2 dt,$$

where the constants have the significance indicated in Fig. 1 and F'(t) denotes the time-derivative of F(t), i.e. the filter response to a unit impulse function. These expressions result from decomposing the white noise from each source into a random sequence of impulses and then applying Campbell's theorem to the randomly superimposed noise pulses at the filter output. It can be shown[5], however, that they apply also to any linear active filter, of which multiple sampling is one example, provided F(t) is interpreted as the reversed integral weight-function, i.e. F(t) is the effect at the measuring instant of a unit step at the input which preceded that instant by the arbitrary amount t. Total noise can be written

$$\overline{V_n^2} = a \int_o^T [F(t)]^2 dt + b \int_o^T [F'(t)]^2 dt, \qquad .....(1)$$

where a, b are constants of the input circuit and the upper limit of each integral is now T, since F and F' both vanish outside the range 0 - T.

The object of the analysis is to minimise the expression on the right-hand side of eqn. (1), with the constraints:-

$F(t) = 0$ for $t \leqslant 0$ and for $t \geqslant T$,

$F(T_1) = 1$ where T_1 is the instant of the pulse peak,

$$\int_o^T F(t)dt = 0.$$

It turns out that the positive peak at $t = T_1$ is a cusp and the mathematical form of F(t) is different on the two sides of the peak, as in the ideal cusp. It is therefore convenient to distinguish between these two parts, by using $F_1(t)$ and $F_2(t)$. Also waveform optimisation is achieved in two stages; first the optimum shape is obtained for any given value of T_1 and then one examines the variation with T_1, keeping T constant, of the resulting expression for minimum noise. This variation exhibits a central maximum with two minima, one on each side. The latter pair of values of T_1 define two (mirror image) solutions for the absolute optimum pulse shape, with a common absolute minimum N/S ratio.

Variational analysis (Appendix 1) shows that an optimum area-balanced waveform (or indeed one having a given fixed area) must be of the form

$$F(t) = Ae^{t/T_o} + Be^{-t/T_o} + C,$$

where $T_o \equiv \sqrt{b/a}$,

the noise-corner time constant, A and B are arbitrary constants and C is constant throughout the pulse. To meet the boundary conditions, A and B are different in the two portions of the waveform, a fact which does not invalidate the solution. This is therefore

$$\left.\begin{aligned} F_1(t) &= A_1 e^{t/T_o} + B_1 e^{-t/T_o} + C \\ \text{and } F_2(t) &= A_2 e^{t/T_o} + B_2 e^{-t/T_o} + C. \end{aligned}\right\} \qquad .....(2)$$

The boundary conditions are dictated by the need to avoid step-discontinuities in F(t) and are $F_1(0) = 0$, $F_1(T_1) = 1$, $F_2(T_1) = 1$, $F_2(T) = 0$. The area-balance condition is

$$\int_0^{T_1} F_1(t)dt + \int_{T_1}^T F_2(t)dt = 0.$$

The first four conditions easily determine the A's and B's, in terms of C, and C is then found for overall area balance. Writing $e^{T/T_o} = \alpha$ and $e^{T_1/T_o} = \beta$, for brevity, the values of the constants are:-

$$\left.\begin{aligned} A_1 &= \frac{\beta}{\beta^2-1} - \frac{C}{\beta+1}, \qquad B_1 = -\frac{\beta}{\beta^2-1} - \frac{\beta C}{\beta+1}, \\ A_2 &= -\frac{\beta}{\alpha^2-\beta^2} - \frac{C}{\alpha+\beta}, \qquad B_2 = \frac{\alpha^2\beta}{\alpha^2-\beta^2} - \frac{\alpha\beta C}{\alpha+\beta} \\ \text{and} \quad C &= -\frac{\gamma}{\log_e \alpha - 2\gamma}, \\ \text{where } \gamma &\equiv \frac{\beta-1}{\beta+1} + \frac{\alpha-\beta}{\alpha+\beta} = \tanh\left(\frac{T_1}{2T_o}\right) + \tanh\left(\frac{T-T_1}{2T_o}\right). \end{aligned}\right\} \qquad .....(3)$$

These results determine the constants in the solution, in terms of T and T_1. Table 1 gives specimen values, for overall pulse widths of $2T_o$, $5T_o$ and $10T_o$ and with the peak (T_1) either central or at one of the optimum positions, in each case. Notice that C is always negative, while the A's and B's are always positive. This means that the curve on either side of the peak is concave

upwards. The general character of the waveforms, for the last and first pair in the Table, is illustrated by solid curves plotted in Fig. 2, (a) and (b). The best pulse shape with central peak is tripolar and symmetrical about the centre with equal negative lobes on each side. These approach one third of the positive pulse height, for short pulses, becoming progressively less as overall pulse width increases. The best possible pulse, however, is that shown with peak at the left of each diagram, with the equally good mirror-image pulse shown dotted. For comparison, the optimum unipolar finite-width cusp is also included (dot-dashed curve), and all curves are annotated with their values of N/S ratio, taking that of the ideal cusp as unity.

Table 1. Coefficients for Optimum Waveforms

T	T_1	A_1	B_1	A_2	B_2	C	N/S Ratio
$2T_o$	T_o	2.066	4.033	0.5459	15.26	-6.099	2.033
	$0.416T_o$*	2.437	0.7559	0.3296	5.599	-3.193	1.787
$5T_o$	$2.5T_o$	0.1627	0.8931	6.018×10^{-3}	24.15	-1.056	1.382
	$0.969T_o$*	0.6229	0.0290	4.196×10^{-3}	4.323	-0.6519	1.277
$10T_o$	$5T_o$	8.92×10^{-3}	0.3171	1.44×10^{-5}	196.5	-0.3260	1.150
	$1.61T_o$*	0.2497	2.8×10^{-4}	1.133×10^{-5}	6.257	-0.2500	1.118

*optimum value of T_1

It may be observed that, for moderately large pulse widths, the unipolar finite cusp is much closer to the ideal cusp than any of the bipolar waveforms and this is reflected in the relative noise values. Ultimately, however, as overall width is increased to large values, all the pulse shapes become indistinguishable, the bipolar ones showing extended flat negative lobes of very small amplitude, as one might expect. The opposite extreme, viz. $T \ll T_o$, has special relevance to high-rate pulse spectrometry and is treated separately in Section 4.

3. Noise/Signal Ratio as a function of T_1 and T

To obtain the total noise $\overline{V_n^2}$, one substitutes the functions of eqns. (2) in eqn. (1), using the values of constants given in eqns. (3). Each integral in eqn. (1) has to be broken in two parts, one from 0 to T_1 and one from T_1 to T. After considerable manipulation and collection of terms, one obtains

$$\overline{V_n^2} = \sqrt{ab}\left\{\frac{\beta^2+1}{\beta^2-1} + \frac{\alpha^2+\beta^2}{\alpha^2-\beta^2} + \frac{\gamma^2}{\log_e\alpha-2\gamma}\right\}.$$

Using the identity $\frac{\alpha^2+\beta^2}{\alpha^2-\beta^2} \equiv \frac{1}{2}\left[\frac{\alpha+\beta}{\alpha-\beta} + \frac{\alpha-\beta}{\alpha+\beta}\right]$ and the corresponding one for $\frac{\beta^2+1}{\beta^2-1}$, this reduces to the simpler form

$$\overline{V_n^2} = \frac{\sqrt{ab}}{2}\left\{\frac{\beta+1}{\beta-1} + \frac{\alpha+\beta}{\alpha-\beta} + \frac{\gamma\log_e\alpha}{\log_e\alpha-2\gamma}\right\}. \quad .....(4)$$

Now the mean square total noise for an ideal cusp filter of the same unity gain is easily shown to be $2\sqrt{ab}$. Hence the relative r.m.s. N/S ratio for the area-balanced cusp is given by

$$\left(\frac{N}{S}\right)^2 = \frac{1}{4}\left\{\coth\left(\frac{T_1}{2T_o}\right) + \coth\left(\frac{T-T_1}{2T_o}\right) + \frac{\gamma T/T_o}{T/T_o-2\gamma}\right\}, \quad .....(5)$$

where γ is defined in eqns. (3). N/S is plotted in Fig. 3 as a function of relative position of T_1 within T, for several values of T. These curves are clearly symmetrical about the half-way position, where each has a maximum. As the pulse peak moves to either side of the mid-position, N/S decreases at first, passes a minimum and then rapidly increases to large values as T_1 approaches 0 or T; at these limits the waveform has a very steep rise or fall and hence generates a large shot noise component. Notice that, for a width $10T_o$, although the optimum peak positions are about 1/6 or 5/6 of the way through the pulse, there is only a slight increase in noise with optimum A-B pulses peaking at intermediate times. Conversely, with short pulses, the hump in the curve becomes more noticeable. Section 4, however, shows that, even for very short pulses, N/S at the maximum is only $2/\sqrt{3}$ times that at either minimum, a ratio closely approached by the uppermost curve in Fig. 3.

Curves B and C in Fig. 4 show the N/S ratio, relative to the ideal cusp, for the optimum bipolar waveform and for the symmetrical tripolar waveform, respectively, as a function of overall width expressed in units of T_o. These may be compared with curve A, which shows the performance of the unipolar finite-width cusp. (Explicit expressions for N/S for curves B and C are derived in Appendix 2.) The difference between A and B ordinates represents the necessary increase of noise associated with the area-balance property, while the difference between B and C, which is quite small, represents the minimum price to be paid for a further order-of-magnitude improvement in attenuation of low-frequency signals, which one

achieves with a symmetrical area-balanced waveform. (See Section 4, low-frequency response.)

The broken curves D-G show the calculated performance of some practical bipolar systems in common use, as listed on the diagram. All these waveforms have theoretically infinite width, hence for present purposes 'width' is arbitrarily defined as that between extreme points where the waveform departs from zero by 1% of the main pulse amplitude. For curve F, the system comprises a conventional single-CR pulse shaper, with facilities for sampling a signal pulse just before it commences and again at the peak; the pulse measure is the difference of the samples. The 'filter' function to be used is thus:-

$$F(t) = \frac{t}{T_1}\, e^{1-t/T_1}, \qquad \text{for } 0 \leqslant t \leqslant T_1$$

$$F(t) = \frac{t}{T_1}\, e^{1-t/T_1} - \left(\frac{t}{T_1} - 1\right) e^{2-t/T_1}, \qquad \text{for } t \geqslant T_1.$$

Noise is calculated from eqn. (1) with this function and using limits 0 and ∞ in the two integrals. T_1 is the value of the shaping time constants and also the time to the positive peak of unit height. The broken curves (Fig. 4) relate to filters which generate waveforms of fixed shape, only the time-scale being variable; they therefore all exhibit noise minima at certain widths, unlike the theoretical filters (A, B and C), whose pulse shapes are changing with width. Curve G is included since this gives the limiting performance of a filter comprising two CR-differentiators and n CR-integrators, all of the same time-constant, as n tends to infinity. The minimum noise here is $\frac{1}{2}e\sqrt{2}.(6\pi)^{1/4} = 1.718$ absolute units, and is rather poor, largely because of the 100% undershoot.

Comparing the first three practical systems with curve B, they all give around 25% more noise than the area-balanced optimum of the same pulse width. Alternatively, ideal systems with the same noise levels as the minima of curves D, E, F would have pulse widths of only a quarter to a third of the practical systems and hence could cope with pulse rates some 3-4 times higher.

4. The Case of a Very Short Pulse ($T \ll T_o$)

This case is best treated by recognising that shot (or f.e.t. channel) noise is entirely dominant, hence gate-current noise can be neglected. Putting a = 0 in Appendix 1, the differential equation to be satisfied becomes $-bF''(t) = \text{constant}$. The solution is thus two parabolic segments of the form

$$F(t) = At^2 + Bt + C,$$

where A is common to both portions, while B and C have different values in each. Putting in the four boundary conditions and the area-balance condition, the optimum pulse shape for given T, T_1 is:-

$$\left.\begin{aligned} F_1(t) &= \frac{3\lambda x^2 + (1-3\lambda)x}{\lambda(1-3\lambda+3\lambda^2)} \\ \text{and } F_2(t) &= \frac{3(1-\lambda)x^2 - (4-3\lambda)x + 1}{(1-\lambda)(1-3\lambda+3\lambda^2)} \end{aligned}\right\} \quad \ldots\ldots(6)$$

where $x \equiv t/T$, $\lambda \equiv T_1/T$ and F_1 is to be used for $t < T_1$, F_2 for $t > T_1$.

This pulse is illustrated for several values of λ in Fig. 5, which shows the progressive change in optimum shape, with peak position, and the appearance of the initial negative lobe when λ exceeds 1/3. The expression for shot noise, for any such waveform, is obtained from eqn. (1) and is

$$\overline{V_{ns}^2} = \frac{b}{T} \cdot \frac{1}{\lambda(1-\lambda)(1-3\lambda+3\lambda^2)};$$

this can be compared with noise for the unipolar cusp of the same width, which is now a symmetrical triangle and gives mean square noise of $4b/T$. Values of N/S indicated in Fig. 5 are normalised to that for the triangle and it is noteworthy that they vary only between $\sqrt{3}$ and 2 over the range of λ from 0.1 to 0.9. The optimum values of λ, for least noise, are $(3 \pm \sqrt{3})/6$ and the optimum shape for one of these is included (dashed line) in Fig. 5. This curve has undershoot of 50%, while the symmetrical tripolar optimum pulse has undershoots of exactly 1/3, with each positive or negative portion occupying one third of the total duration. A notable feature of these curves is their very close similarity to those in Fig. 2(b); evidently a pulse width of $2T_o$ can be regarded as 'short' in this context.

These diagrams illustrate one unfortunate feature of the area-balanced pulse, namely the very narrow peak which is only about 0.25-0.35 of the width of that of a unipolar cusp of the same overall width (if T is fairly short). Besides demanding a very high bandwidth in any peak-measuring circuit, the system would also be very sensitive to charge collection-time in the detector and thus show a considerable 'ballistic deficit'. One remedy would be to impose a short flat top on the peak, which would not entail much sacrifice of N/S ratio, even if area balance were strictly preserved.

Low-frequency Response

Because of their relatively simple algebraic form, the curves in Fig. 5 provide a convenient vehicle for analysis of the low-frequency response of such filters; results so obtained are substantially accurate for pulse widths up to about $4T_o$.

First one obtains the filter transfer function f(p) as the Laplace transform of the unit-impulse response F'(t),

$$\text{i.e.} \quad f(p) = \int_0^\infty F'(t)e^{-pt}dt. \qquad .....(7)$$

Replacing p by jω then gives the frequency response f(jω) and interest centres mainly on the magnitude of this when $\omega << 1/T$.

For the unipolar triangular pulse in Fig. 5, F'(t) is a bipolar rectangular waveform of total width T and, from eqn. (7), the filter transfer function is

$$f(p) = \frac{2}{pT}\left(1-e^{-pT/2}\right)^2.$$

Replacing p by jω, one obtains

$$f(j\omega) = \frac{8j}{\omega T}\sin^2\left(\frac{\omega T}{4}\right).e^{-j\omega T/2},$$

whence $|f(j\omega)| \simeq \frac{1}{2}\omega T$, if $\omega T << 1$.

Turning to the bipolar cusp waveforms given by eqns. (6), a similar procedure yields the following filter transfer-function:-

$$f(p) = \left[\frac{6(1-e^{-pT})}{p^2T^2} + \frac{(3\lambda^2-4\lambda+1) + (3\lambda^2-2\lambda)e^{-pT} - e^{-\lambda pT}}{\lambda(1-\lambda)pT}\right] \Big/ (1-3\lambda+3\lambda^2).$$

Replacing p by jω, expanding the resulting trigonometric terms in powers of ωT and retaining terms up to $(\omega T)^4$, one obtains

$$f(j\omega) = -\frac{10(1-2\lambda)(\omega T)^2 - j(4-5\lambda-5\lambda^2)(\omega T)^3 - (1-\lambda-\lambda^2-\lambda^3)(\omega T)^4}{120(1-3\lambda+3\lambda^2)}.$$

Thus, for values of λ other than 0.5, the first term is dominant, if $\omega T << 1$, and

$$|f(j\omega)| \simeq \frac{|1-2\lambda|}{12(1-3\lambda+3\lambda^2)} \cdot (\omega T)^2 .$$

By an odd coincidence, this response is greatest when $\lambda = (3 \pm \sqrt{3})/6$, the same values that yield the lowest N/S ratio. Even then, however, the magnitude of $f(j\omega)$ is less than $1/10(\omega T)^2$, which is a marked reduction on $\frac{1}{2}\omega T$. If $\lambda = 0.5$, the term in $(\omega T)^2$ vanishes and the second term then dominates, giving $|f(j\omega)| \simeq (\omega T)^3/120$, which is at least an order of magnitude smaller still. Thus the symmetrical waveform with central peak has only third-order sensitivity to disturbing l.f. signals. Note that all the filters are, however, equally sensitive to the wanted signal pulse.

5. Conclusions

The mathematical form of the optimum bipolar cusp, for minimum noise/signal ratio, has been derived and illustrated graphically. This waveform is required to have a finite width T and overall area balance, the latter property being advantageous when such a filter is incorporated in an a.c.-coupled amplifier or when spurious low-frequency signals (e.g. microphonics) are present at the input. The best noise performance is obtained when the peak is offset a certain amount from the centre of the interval T and the minimum N/S ratio is then $\left[\coth\left(\frac{T}{2T_o}\right) - \frac{2T_o}{T}\right]^{-\frac{1}{2}}$, relative to the ideal cusp. This may be compared with $\left[\coth\left(\frac{T}{2T_o}\right)\right]^{\frac{1}{2}}$, the value for the optimum unipolar cusp of the same overall width. (T_o = noise corner time constant.) The optimum waveform with central peak is symmetrical about the centre. Despite a small increase of N/S ratio, it therefore offers a further considerable reduction of l.f. sensitivity.

Comparison with the calculated performance of some practical bipolar systems shows that the best of these (double CR-diff^n, double CR-integ^n) gives about 25% more noise for comparable overall width or some 3-4 times the pulse width for comparable noise performance. At least in some applications, therefore, it would seem worthwhile to try to improve on existing bipolar techniques. The problem of realising a practical filter approximating to the ideal F(t) is not considered here, but the best approach may well be a time-variable filter with switched parameters.

References

1. Van Heerden, Dissertation (Utrect) 1945.
2. E. Baldinger and W. Franzen, "Advances in electronics and electron physics", 8, p. 255 , (Academic Press, New York, 1956).
3. F.T. Arecchi, G. Cavallari, E. Gatti and V.Svelto, "Signal-to-noise ratio and resolving time in pulse amplifiers",Energia Nucleare, 7 p. 691 (1960).
4. M. Bertolaccini, C.Bussolati.and E.Gatti "Signal-to-noise ratio in nuclear pulse amplifiers with high repetition rates". Nucl.Instr. and Meth., 42 , p. 286 (1966).
5. M.O.Deighton, "A time-domain method for calculating noise of active integrators used in pulse amplitude spectrometry",Nucl.Instr.and Meth., 58, p. 201 (1968).

Appendix 1

Optimum Pulse Shape for a Given T_1

Consider the class of all area-balanced pulses* of overall width T and having a positive peak of unit height at a given time T_1. One of these waveforms, which we denote by F(t), gives less noise than all the others and hence constitutes the required optimum shape, for this particular T and T_1. Any neighbouring curve of the class can be described by the modified function $F(t) + \phi(t)$, where $\phi(t)$ is subject to the constraints

$$\phi(0) = \phi(T_1) = \phi(T) = 0 \quad \text{and} \quad \int_0^T \phi(t)dt = 0.$$

The modified function must always give an increase in total noise, such increase being moreover only of the second order in ϕ, if ϕ is everywhere small, since noise is a continuous 'function' of pulse shape.

Replacing F(t) by $F(t) + \phi(t)$ and also F'(t) by $F'(t) + \phi'(t)$, the derivative of the modified function, eqn. (1) gives the increase in total noise:-

$$\overline{\Delta V_n^2} = \{2a \int_0^T F(t)\phi(t)dt + 2b \int_0^T F'(t)\phi'(t)dt\} +$$

$$+ \{a \int_0^T [\phi(t)]^2 dt + b \int_0^T [\phi'(t)]^2 dt\}.$$

The second bracket consists of second-order terms which are always positive, whatever the nature of $\phi(t)$; the first bracket (denoted by $\Delta_1 V_n^2$) consists of first-order terms in ϕ, both of which change sign if ϕ reverses its polarity. It follows that $\Delta_1 V_n^2 = 0$, for any ϕ which satisfies the constraints above, if F(t) is the optimum waveform.

Now both integrals in $\Delta_1 V_n^2$ must be broken in two parts if F(t) changes its form at $t = T_1$, the limits for the first part being 0 and T_1 and for the second part T_1 and T. In particular, the first part of the second integral can be written

$$\int_0^{T_1} F'(t)\phi'(t)dt = \left[F'(t)\phi(t)\right]_0^{T_1} - \int_0^{T_1} F''(t)\phi(t)dt,$$

integrating by parts and using the double prime to denote the second time derivative. The first term vanishes, since F'(t) is everywhere finite and $\phi(t) = 0$ at both limits.

Therefore $\int_0^{T_1} F'\phi'dt = -\int_0^{T_1} F''\phi dt$, and likewise

$$\int_{T_1}^{T} F'\phi'dt = -\int_{T_1}^{T} F''\phi dt.$$

Hence $$\int_0^T F'(t)\phi'(t)dt = -\int_0^T F''(t)\phi(t)dt.$$

The condition $\Delta_1 \overline{V_n^2} = 0$ thus becomes

$$2\int_0^T [aF(t) - bF''(t)]\phi(t)dt = 0,$$

which must be satisfied for <u>any</u> area-balanced $\phi(t)$.

Therefore $aF(t) - bF''(t) = K$, a constant, throughout the waveform. [Exceptions occur at $t = 0$, T_1 and T, where F(t) may have slope discontinuities and therefore F''(t) impulse-type discontinuities of finite area. However $\phi(t)$ is zero, by definition, at each of these points, hence they make no contribution to the integral above and can be disregarded.]

It follows that

$$F(t) = Ae^{t/T_o} + Be^{-t/T_o} + C,$$

where $T_o = \sqrt{b/a}$, the noise-corner time constant, A and B are constants within each interval $0 < t < T_1$ and $T_1 < t < T$, but may differ as between the two, while $C = K/a$, another constant which must be the same in both. The determination of the constants consists in imposing the known boundary conditions and the area-balance condition on F(t).

It is interesting to see how the analysis above is varied, if one drops the area-balance restriction on F(t). This condition then no longer applies to $\phi(t)$ either, so the integral equation above has to be satisfied for any ϕ, subject only to the boundary conditions at 0, T_1 and T. The bracket [aF-bF''] is thus zero and the solution consists of two segments of the form

$$F(t) = Ae^{t/T_o} + Be^{-t/T_o}.$$

Imposing the boundary conditions, each segment becomes part of a sinh-curve, with an appropriate vertical scale-factor, and total noise is found to be least when $T_1 = \frac{1}{2}T$. This is the simple finite-width cusp, which degenerates to the ideal cusp as $T \to \infty$.

*excluding those with step discontinuities, which give infinite noise.

Appendix 2

Optimisation of T_1 for Least N/S Ratio

Equation (4) gives the minimum total noise $\overline{V_n^2}$ as a function of $\alpha(=e^{T/T_o})$ and $\beta(=e^{T_1/T_o})$. Minimisation of this with respect to T_1 is thus the same as minimisation with respect to β. We therefore differentiate with respect to β, keeping α constant and remembering that γ is also β-dependent, and set the result equal to zero.

This gives

$$\frac{\partial(\overline{V_n^2})}{\partial\beta} = \sqrt{ab}\cdot\frac{(\alpha-1)(\beta^2-\alpha)}{(\alpha+\beta)^2(\beta+1)^2}\ x$$

$$x\ \left\{\left[\frac{(\alpha+\beta)(\beta+1)}{(\alpha-\beta)(\beta-1)}\right]^2 - \left[\frac{\log_e\alpha}{\log_e\alpha-2\gamma}\right]^2\right\} = 0.$$

One zero of this expression is clearly at $\beta = \sqrt{\alpha}$, i.e. $T_1 = \frac{1}{2}T$; this gives the central maximum with respect to T_1 already noted in Fig. 3. The other zeros are obtained by equating the two expressions in square brackets, since both are positive. This yields a simple quadratic in β, the roots of which give the noise minima and are

$$\beta_{opt} = \frac{\alpha-1}{\log_e\alpha} \pm \sqrt{\left(\frac{\alpha-1}{\log_e\alpha}\right)^2 - \alpha}.$$

These two values of β are always real and different*, for any finite T; their product is seen to be α, hence the sum of the corresponding optimum values of T_1 is T and the optimum peak positions are equally displaced on either side of the centre. It can be shown that the optimum waveforms are mirror images of each other.

To determine the minimum N/S ratio, one can use the equality of the two square brackets above to simplify the third fraction in eqn. (4). This becomes

$$\gamma\cdot\frac{(\alpha+\beta)(\beta+1)}{(\alpha-\beta)(\beta-1)} = \frac{\beta+1}{\beta-1} + \frac{\alpha+\beta}{\alpha-\beta}$$

so $$\overline{V_{n,min}^2} = \sqrt{ab}\cdot\left(\frac{\alpha+\beta}{\alpha-\beta} + \frac{\beta+1}{\beta-1}\right).$$

Inserting either value of β_{opt}, this simplifies to

$$\overline{V_{n,min}^2} = 2\sqrt{ab}\Big/\left(\frac{\alpha+1}{\alpha-1} - \frac{2}{\log_e\alpha}\right),$$

i.e. $\left(\frac{N}{S}\right)_{min} = \left[\coth\left(\frac{T}{2T_o}\right) - \frac{2T_o}{T}\right]^{-\frac{1}{2}}$, relative to the ideal cusp.

The N/S ratio with the central peak position is given by substituting $T_1 = \frac{1}{2}T$ in equation (5). Thus

$$\left(\frac{N}{S}\right)^2_{sym} = \frac{1}{2}\left[\coth\left(\frac{T}{4T_o}\right) + \frac{\frac{T}{T_o}\tanh\left(\frac{T}{4T_o}\right)}{\frac{T}{T_o} - 4\tanh\left(\frac{T}{4T_o}\right)}\right]$$

Using the identity $\coth x + \tanh x \equiv 2\coth 2x$ with $x = T/4T_o$, this reduces to

$$\left(\frac{N}{S}\right)_{sym} = \left[\frac{\frac{T}{2T_o}\coth\left(\frac{T}{2T_o}\right) - 1}{\frac{T}{2T_o} - 2\tanh\left(\frac{T}{4T_o}\right)}\right]^{\frac{1}{2}}.$$

*this can be proved by substituting $x = \frac{1}{2}\log\alpha$ in the inequality $\sinh x > x$, which is true for all positive x.

DISCUSSION

Gatti : - I would like to ask if you tried to synthesize by some practical circuits your asymmetrical bipolar shaping.

Deighton : - I have done very little in this direction. One could derive the optimal waveform by generating a triangular and a partly parabolic shape and combining the two.

Radeka : - I would just like to open a comment. It appears that it is only a matter of preference of an experimenter whether one chooses a bipolar shaping or a unipolar type with a base line restorer. There is one instance where a method of shaping similar to that described may be essential. If one has low frequency noise in the detector leakage current which when integrated on the input capacity of the preamplifier gives $1/f^3$ law then unipolar shaping gives very high noise. Calculation will show that it is not convergent and in that case one needs a second order shaping as Deighton described.

Deighton : - This is rather a comment than a question. I would agree certainly with the speaker that where you have $1/f^3$ noise power relationship it would strongly indicate the use of something equivalent.

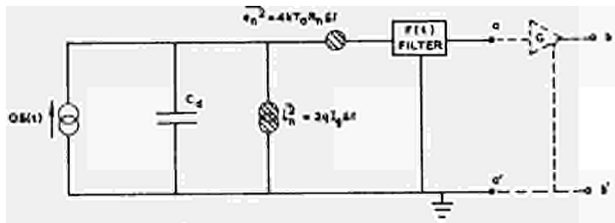

FIG. 1. IDEAL NUCLEAR PULSE AMPLIFIER

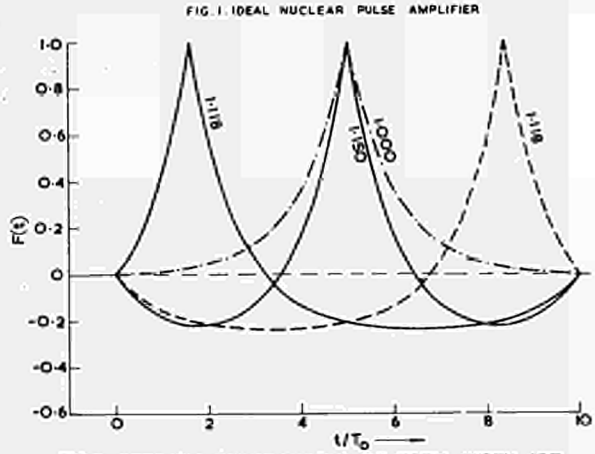

FIG.2a OPTIMUM PULSE SHAPES OF TOTAL WIDTH $10T_0$

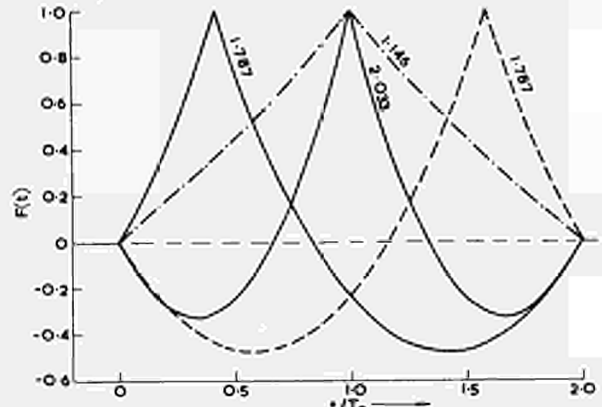

FIG.2b OPTIMUM PULSE SHAPES OF TOTAL WIDTH $2T_0$

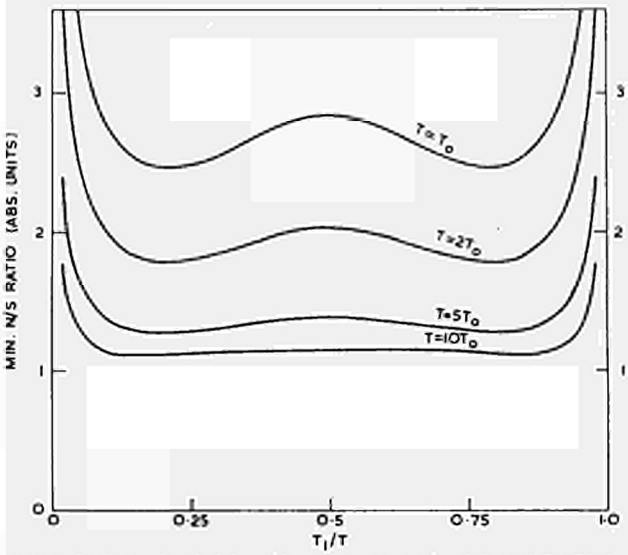

FIG. 3. VARIATION OF $(N/S)_{min}$ FOR AREA-BALANCED PULSE, WITH TIME OF PEAK

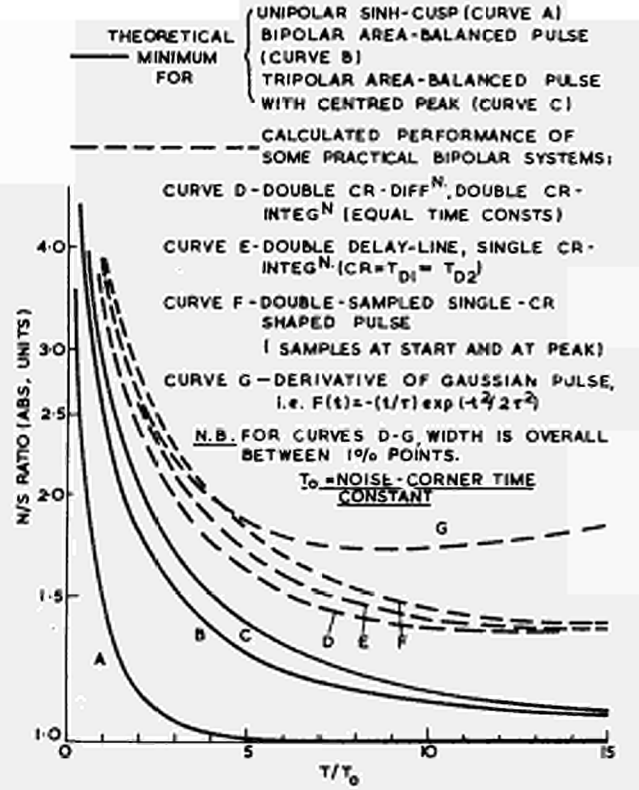

FIG.4. NOISE/SIGNAL RATIO vs. PULSE LENGTH FOR VARIOUS PULSE SHAPES

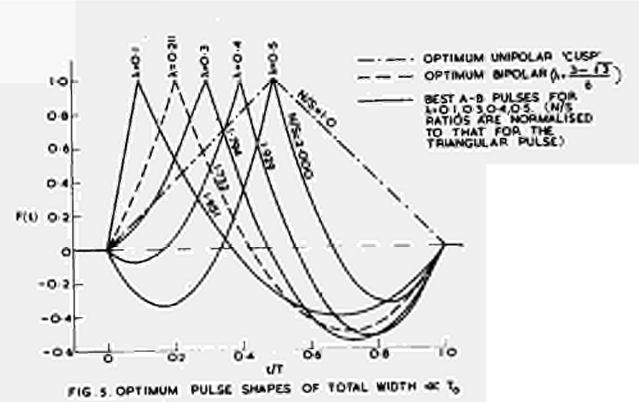

FIG. 5. OPTIMUM PULSE SHAPES OF TOTAL WIDTH $\propto T_0$

MISMATCH ORIENTED CIRCUIT DESIGN AND ITS APPLICATION TO NUCLEAR ELECTRONICS

Arie F. Arbel,

Department of Physics, Technion-Israel Institute of Technology
P.O.B. 4910, Haifa, Israel.

Summary

Consistent application of mismatch between source and load is shown to lead to the design of feedback amplifiers, whose characteristics closely approach those of idealized "black boxes" exhibiting zero or infinite input and output impedance levels. The resulting configurations are shown to employ enhancing combinations between four kinds of basic amplifiers and series or shunt feedback applied to their input and output, respectively. Depending upon the signal parameter employed, the input and output terminals of the "black boxes" will operate in the voltage or in the current mode, each emerging in its own rights as the preferable technique if employed under proper conditions. Enhancing combinations result in greater flexibility of usable gain values and functions, and in reduced noise contribution to the preceding stage.

Further extension of mismatch to active circuit design makes it possible to employ a greatly simplified transistor model, and restricts the dominant poles to those which are unavoidably introduced by the active elements. The resulting "standard" circuits are readily reproducible by conventional manufacturing methods, and further improvement of their performance is predicted through the application of microcircuit techniques. The design of a high resolution spectrometer is described, which employs enhancing combinations of such standard circuits. The choice of the most suitable circuit for each stage depends on the preferred signal parameter, noise considerations, and gain requirements.

1. Introduction

The synthesis of circuits has always been a largely heuristic process. The method of design presented in this paper represents an attempt at a systematic approach. It is based on the principle of mismatch, which in itself is not a new idea[1]. Its consistent application is shown to offer guide lines for the most suitable circuit configuration to be used in certain well defined applications, and for the elimination of insignificant parameters in computing their response. Thus, mismatch oriented circuit design is meant to serve as an aid rather than as a substitute for computer aided circuit design and analysis. Such an approach is of particular importance in view of the increasing use of microelectronics, which requires the use of advanced circuit techniques in order to utilize its full potentialities

2. Matching Versus Mismatching Between Load & Source

There are two ways of connecting a load to a source: One is based upon matching to ensure maximum power transfer, which is achieved by maximizing the product between the two signal parameters (voltage and current). In order to extend the range of operation to the highest frequencies at which power amplification is still feasible, both kinds of reactances (L and C) play an important part. Their combined use results in a band pass response for which matching is ensured over a limited range of frequencies.

The second method of interconnecting load and source is based upon deliberate mismatch. A low impedance source will be connnected to a high impedance load and vice versa, in order to ensure maximum transfer of the chosen signal parameter between source and load. The result is a broad band frequency response extending to frequencies at which the circuit reactances become significant. Either voltage or current may be chosen as the information carrying signal parameter between source and load. Thus, we arrive at a definition of the voltage or current mode with respect to a particular point in a circuit: The input or output mode of an active element or amplifier is defined by the respective signal parameter accepted by its input or delivered by its output. Once a particular mode has been chosen, the other parameter must be regarded as undesirable and should be minimized by proper circuit design.

Considering the limitations imposed upon the circuit response by parasitic reactive elements, we shall assume that the physical size of the circuit has been reduced to the practical minimum by employing such techniques as hybrid or integrated circuits. This reduces the interstage capacitances to the lower limit for the capacitance associated with the fastest available active devices, which is of the order of a few tenths of picofarads, and to inductances of less than 5×10^{-9} Hy, the latter constituting the inductance of a conductor of approximately 0.2" length. The resonant frequency for reactances of this order of magnitude is well above the gain band-width product of the circuits considered. Hence, the nature of the circuit impedances is capacitive over the range of frequencies affecting the transient response of the circuit we are concerned with.

The foregoing considerations lead to two conclusions: First, voltage swings throughout the circuit should be kept as small as possible, in order to reduce slewing due to undesirable parasitic currents through circuit capacitances; this leads to a reduction in impedance levels and thereby to the desirable decrease of voltage swings, and to the preferred use of the current mode whereever feasible.

Second, it is advantageous to reduce the out-

put resistance of voltage sources and the input resistance of current sinks to a possible minimum, in order to make the unavoidable interstage RC time constant as short as possible; this brings us back to the principle of mismatch, which is the main subject of the present article.

The principal benefit derived from consistant application of mismatch in active circuit design is the possibility of employing a greatly simplified transistor model, and of avoiding introduction of dominant poles in addition to those which are unavoidably introduced by the active elements. Moreover, the reduced impedance levels result in increased gain flexibility, and - in certain applications - in reduced noise contribution[2]. The latter is due to heavier loading of the preceding stage, and a favourable effect of the low impedance levels on the spectral distribution of the noise current components of the feedback network.

3. Synthesis of Feedback Circuits

Consider basic amplifiers whose input and output impedance approaches, in accordance with the principle of mismatch, either zero or infinity. The resulting four alternatives lead to an equal number of idealized transfer functions, which are tabulated in Table 1: The voltage amplifier A_V, the current amplifier A_C, the transimpedance amplifier Z_T, and the transadmittance amplifier Y_T. Each basic amplifier will necessarily consist of one or several suitably interconnected active elements. Feedback will be employed in order to stabilize its response and at the same time to modify its impedance levels in a desirable way. In combining feedback with the four basic kinds of amplifiers we have the choice of applying to their input and output either shunt or series feedback, yielding four possible combinations for each kind of amplifier or 16 combinations altogether. The resulting closed loop response is determined solely by the nature of feedback employed: Shunt-Shunt feedback yields a Z_T, amplifier, Series - Series a Y_T one, Series Shunt an A_V one, and Shunt - Series an A_C one. Moreover, in order to obtain optimum results we shall choose intuitively a combination in which the input and output impedance levels of the basic amplifier are enhanced by the feedback. This leads to four combinations which may be shown to exhibit properties preferable to the remaining ones, such as higher possible loop-transmission and less direct signal transmission between input and output. In chapter 5 this will be proved by comparison between two shunt-shunt combinations, one enhancing, and the other non-enhancing.

The proof for the remaining combinations may be left to the reader.

Common to the four enhancing combinations is the law of combination between feedback and basic amplifier: AN "ENHANCING COMBINATION" RESULTS IF THE KIND OF FEEDBACK EMPLOYED ENHANCES THE IMPEDANCE LEVELS OF THE BASIC AMPLIFIER. As an example, consider a basic voltage amplifier exhibiting high input and low output impedance: The proper kind of feedback to be applied will be series - shunt, the series feedback further increasing the input impedance, and the shunt feedback reducing the output impedance of the basic amplifier.

In figures 1 to 4, the four preferred combinations are shown together with the idealized relationships describing their behaviour, and the mismatch conditions necessary for deriving them. These relationships have been arranged in such a way as to facilitate comparison between the four enhancing combinations. To this end, the transfer functions T have been brought into the form

$$T(s) = \frac{1}{B(s)} \frac{LT(s)}{[1 - LT(s)]} \qquad (1)$$

Thus, we have defined the desirable feedback stabilized response as $1/B(s)$. The second factor in eq. (1) contains the information about the undesirable properties of the feedback system and is conventionally analyzed by the root-locus method. The resulting expressions bring out the following important points:

First, the various relationships actually constitute an approximation to the case in which the input and output impedance levels of the basic amplifier approach the idealised values indicated in Table 1. They are still true in the sense of a practical engineering solution, if the relations between input and output impedance of the basic amplifier and the feedback elements satisfy the conditions for mismatch indicated in each case. Hence, these conditions constitute the concise relationships which enable us to identify the basic amplifiers in Fig. 1-4 with one of the idealized elements of Table 1; by satisfying these mismatch conditions, we have practically eliminated the undesirable influence of the input and output impedance levels exhibited by the basic amplifier, on the properties of the feedback amplifier.

Second, the loop transmission LT has been factorized into two factors. Consider, for instance, the expression for LT in Fig. 1: This has been factorized into the dominant term Z_T/Z_1, multiplied by a factor which differs from unity by a complex term. This term arises due to direct transmission between input and output. It is inversely proportional to the active short circuit transadmittance Y_a of the basic amplifier, and its mathematical form shows that it introduces at least one zero into the right hand side of the complex frequency plane.

Fig. 2 shows series-series feedback applied to a basic transconductance amplifier. Direct transmission from input to output does not enter LT. Although not shown, it is present in 1/B and should be taken into account in an accurate analysis. We note that a signal is present at all three terminals of the basic amplifier, which enables us to utilize this particular combination in three different ways: As transadmittance amplifier (T_1), as voltage follower (T_2), and as current follower (T_3). If properly designed, this combination constitutes a powerful and most versatile circuit element.

4. Enhancing Configurations for Operational Amplifiers

The realization of a dimensionless transfer function by a feedback stabilized amplifier leads to the concept of an operational amplifier, whose transfer function is determined by the ratio between two impedances. Figs. 3 and 4 are examples of such amplifiers, but their characteristics

exhibit certain undersirable properties in spite of their employing enhancing combinations: Consider, for instance, that we wish to perform differentiation: In order to avoid the use of a choke in the feedback path, we shall choose $Z_1 = R_1$ and $Y_2 = sC_2$, yielding $(Z_1+Z_2)/Z_2=(1+sC_2R_1)$ as the $1/B(s)$ term in T(s) of both amplifiers, and a dominant loop transmission term $LT(s) = -A_v/(1+sC_2R_1)$ for Fig. 3, or $LT(s) = -A_c/(1+sC_2R_1)$ for Fig. 4, respectively.

These expressions bring out the following disadvantages: First, we would like to move the zero in T(s) from the negative real axis into the origin, in order to obtain ideal differentiation; second, the pole $-1/R_1C_2$ in the expression for LT(s) introduces a phase lag and therefore restricts the maximum value of LT at high frequencies compatible with stability conditions. Both disadvantages may be overcome, converting the enhancing combination of Fig. 1 into an operational differentiator by connecting a capacitor as Z_2 in series with its input as shown in Fig. 7: Now, the $1/B(s)$ term in T(s) indicates perfect differentiation, whereas phase lag due to Z_2 is entirely eliminated in the dominant loop transmission term $LT(s) = -Z_T/R_1$. This is due to the low input impedance of the basic Z_T amplifier, which practically separates Z_1 from Z_2 and makes the loop Z_T/Z_1 completely self-contained and independent of Z_2. In the next chapter, Fig. 7 will be discussed in greater detail.

The question now arises how to synthesize an operational current amplifier. The disadvantages which were shown to be associated with the operational voltage amplifier of Fig. 3 apply equally to the operational current amplifier of Fig. 4. Apparently we ought to look for some kind of configuration employing the remaining enhancing combinations of figures 1 and 2.

That question is neatly resolved by connecting combination 1 and 2 in cascade, as shown in Fig. 5. The use of the two cascaded enhancing combinations ensures completer separation between Z_1 and Z_2 in T(s), and the loop transmission of each may be independently designed for stability. The only objection one could raise is the need for <u>two</u> separate feedback loops in cascade instead of one, in order to realize an operational amplifier. It may however be shown that it is possible to combine the Z_T with the Y_T amplifier in a single feedback loop, at low frequencies, while separation between them is maintained at high frequencies at which stability conditions do not allow the inclusion of both Z_T and Y_T in a single loop (See Fig. 11).

5. Enhancing Versus Non-Enhancing Combinations

Let us now demonstrate the advantages of an enhancing combination, as compared with a non-enhancing one. Consider Figs. 6 and 7: Both show a shunt-shunt feedback combination employed as an operational voltage amplifier, by connecting an impedance Z_2 in series with its input. But, where-as the combination in Fig. 7 is an enhancing one with respect to both the input and output impedance levels of the basic amplifier, the one in Fig. 6 is non-enhancing as far as the input impedance level is concerned.

The two diagrams have been arranged in such a way as to facilitate a comparison of their characteristics: To this end, the basic transimpedance amplifier of Fig. 7 has been synthesized from the basic voltage amplifier of Fig. 6 by adding a current follower in front of it. This is not quite in accordance with the practical case, in which the gain stage following the current follower would be classified as transimpedance - rather than voltage - amplifier; but it serves well the purpose of demonstrating the advantage of adding a current follower in front of an operational amplifier of conventional design.

Comparison between Fig. 6 and 7 shows an increase in the loop transmission of the latter by a factor $(Y_1+Y_2)/Y_{oc}$, and a decrease in the direct transmission through Z_1, from input to output, due to an increase in Y_a by a factor Z_{oc}/Z_{ic}. Further, the dominant loop-transmission term for Fig. 6 introduces, in the case of an operational differentiator, an integrating time constant R_1C_2, which imposes severe restrictions on the value of loop transmission at high frequencies and thereby increases the sensitivity of the closed loop response to circuit parameter changes, for fast signals. No such restrictions exist in the circuit of Fig. 7, where the dominant loop transmission is a function of Z_T and Z_1 only. Last but not least, the impedance levels of the feedback elements may be considerably reduced in the enhancing combination, enabling one to use larger gain factors and - under certain circumstances - to reduce the noise contribution through heavier loading of the preceding stage. If, moreover, we note that a current follower is realized by a common base connected transistor, which adds only an insignificantly short time constant to the loop transmission, then the advantage of the circuit of Fig. 7 over that of Fig. 6 may be considered to be well established.

In spite of these advantages it is not always desirable to employ enhancing combinations: Consider again the transimpedance amplifier of Fig. 1. The input active element of the basic amplifier exhibits a low input impedance, which makes it impossible to accurately define the current flowing into the feedback resistor R_1. This limits practical maximum values for R_1 to about 5KΩ. Wherever a higher valued feedback resistor is required, one may either employ an auxiliary circuit to stabilize the output voltage of the amplifier, or use as input element an active device exhibiting a high input impedance, which therefore allows the current flowing into R1 to be defined with great accuracy. Another case in point is the need to choose a high input impedance active device such as an F.E.T. as input element for the basic amplifier, due to overriding noise considerations. Both cases lead to the non-enhancing combination shown in Fig. 6.

Let us mention, for completeness, the existence of circuits which serve to stabilize the DC level of an enhancing shunt-shunt combination: An early attempt at stabilizing a preferred Z_T combination DC wise has been made by the author[4]. A more sophisticated circuit has been employed by Waldhauer[5], who connects a high input impedance DC stabilized Y_T amplifier in series with a low input impedance Z_T amplifier. At high frequencies, where stability problems exist, the DC amplifier is effectively by-passed by a capacitor, and the shunt-shunt feedback enhances the impe-

dance levels of the basic Z_T amplifier. At low frequencies, the Y_T in series with the Z_T amplifier constitutes an A_V amplifier, which makes possible accurate control of the input and output DC levels of the complete amplifier.

6. The Synthesis of Basic Amplifiers

In synthesizing the four basic amplifiers from active devices we extend the principle of mismatch to interconnections between the active devices constituting a basic amplifier. This leads to a non-ambiguous solution for each case.

The design process is as follows: We have at our disposal two basically different three terminal devices. i.e. the FET and the bipolar transistor. Identification of the respective terminals as input, output and reference terminal leads to six possible combinations for each device, among which only those three which exhibit power gain are of any practical interest. In the design procedure we shall first identify each of the three alternatives with one or more basic building blocks, several of which are then suitably combined into complete amplifiers.

Table 2 represents the first step. The first two alternatives are classified as voltage follower and as its dual - the current follower. These two serve as impedance converters operating in the voltage or current mode, respectively. Their transfer function is dimensionless, and its value is close to unity - hence, the term "follower".

The third alternative (terminal 2 to ground, 1 input-and3 output-terminal) has been classified in 4 different ways as a Y_T, Z_T, A_V or A_C amplifier. Identification with one of these transfer functions depends upon the input and output mismatch conditions. Table 3 defines these four basic transfer functions for a bipolar transistor, and indicates for each case the necessary mismatch conditions. These functions have been derived from the simplified transistor model shown in Fig. 8, which accounts satisfactorily for the behavior of mismatch oriented circuits, at high frequencies.

The combination of these basic building blocks into the four basic amplifiers will be demonstrated. In synthesizing a basic Z_T amplifier we start with a C.E. connected transistor, whose DC input and output impedance levels are $h_{fe}(0)r_e'$ and $r_c'/h_{fe}(0)$, respectively. Both these levels are too high for the low input and output impedance desirable for a basic Z_T amplifier, which makes it only natural to add impedance converters to the input and output.

Fig. 9 shows the resulting circuit, in which Q_{1a} serves as input current follower, and Q_3 Q_4 as output push pull voltage follower. Q_{1b} is inoperative, and for the purpose of analysis we assume a single output stage Q_3 only. Input and output impedance of the basic Z_T amplifier are now r_{e1a}' and $r_{c2}'/h_{fe2}h_{fe3}$ and will be further reduced by a factor proportional to the inverse loop-transmission LT, after closing the loop. The open loop transfer resistance equals r_{c2}', whose practical value is of the order of $10^6\Omega$.

In the equivalent diagram, Q_{1a} is assumed to exhibit zero input and infinite output impedance; it introduces a pole $-1/\tau_{b1}$; the transfer function of Q_2 is taken from Table 3; in computing the pole introduced by the output stage Q_3, we note that the asymptotic loop transmission of an emitter follower fed from a capacitive source and loaded by a resistor R_1, may be shown to approach $LT = -R_1/sr_{b3}'\tau_{b3}$ (6). Hence, evaluating the voltage follower response LT/(1-LT), the output stage is found to introduce a pole $-R_1/r_{b3}'\tau_{b3}$. Thus we obtain for the transimpedance of the complete basic Z_T amplifier.

$$Z_T \approx \frac{-r_{c2}' \exp(-s\tau_d)}{[1+sr_{c2}'(C_{c2}'+C)](1+s\tau_{b1a})(1+s\tau_2)(1+s\tau_3)} \quad (2)$$

where τ_d is the total time delay around the loop including excess phase shift in the transistors,

$$\tau_2 = [1 + \frac{C_s}{(C_{c2}'+C)}]\,\tau_{b2}, \text{ and } \tau_3 = \frac{r_{b3}}{R_1}\,\tau_{b3}.$$

A practical difficulty arises if one tries to evaluate stability conditions from relationship (2), due to the ill-defined value of the dominant time constant $r_{c2}'(C_{c2}'+C)$. This may be overcome by applying the "Gain Bandwidth Theorem" (6), which replaces the dominant pole by the unity-gain bandwidth, as factor determining the conditions for stability. This simplification is permissible under certain conditions which have been defined in(6). The simplified looptransmission now equals

$$LT = \frac{-Z_T}{R_1} = \frac{-\exp(-s\tau_d)}{sR_1(C_{c2}'+C)(1+s\tau_{b1a})(1+s\tau_2)(1+s\tau_3)} \quad (3),$$

from which one may easily derive the conditions for stability. The dominant closed loop response is obtained as

$$\frac{e_o}{i_s} \approx \frac{-R_1}{[1 + s(C_{c2}' + C)\,R_1]} \quad (4)$$

Particular attention is drawn to the way in which the stray capacitance C_s and the collector capacitance C_{c2}' in parallel with C enter relationship (3): C_s increases the value of τ_2, which is a non-dominant but significant time constant, and thereby adversely affects the stability conditions and monotony. On the other hand, C_{c2}' and C reduce this particular time constant and simultaneously reduce the value of the unity-gain bandwidth $1/2\,\pi\,R_1(C_{c2} + C)$, thereby twice affecting stability conditions in a favorable way. Hence, care should be taken to design the physical layout of this amplifier in such a way that C_s is reduced as much as possible. Any remaining stability problems may then be solved through reduction of the unity-gain bandwidth, either by increasing R_1, or by connecting C between base and collector of Q_2, which for a transistor fed by a current source is to a first approximation equivalent to connecting it in parallel with C_{c2}'.

Another practical design consideration is the need to reduce the stray capacitance between emitter and ground of Q_{1a}, because that capacitance increases the time constant τ_{b1a}. This makes it inadvisable to employ the emitter of Q_{1a} directly as input terminal. Instead, a resistor

should always be connected in series, which may in the current mode serve as termination for an interconnecting cable.

The simple input circuit to Q_2 imposes certain restrictions upon its maximum achievable current gain, and upon the noise contribution of R. Both restrictions may be overcome by increasing the value of R and returning it to a higher voltage. D_1 - D_6 are not an essential part of the circuit; they merely improve the recovery from positive and negative overload signals.

The right hand side of Fig. 9 shows the suggested packaging of the circuit and its connection as inverting (Z_T) and non-inverting (A_V) amplifier. Note that connection of the feedback to terminal 2(Q_{1b} inoperative) results in an enhancing combination, in both cases. Connection to 3 provides moderately accurate DC stabilization.

Fig. 10 shows the practical realization of a Y_T amplifier. As the loop-transmission achievable with a single Y_T active element is insufficient, it is only natural to boost the current output of the Y_T element by a transistor operating as current amplifier. A detailed stability analysis of this circuit is beyond the scope of this paper.

Fig. 11 shows the realization of a current amplifier, in accordance with Fig. 5. It has been derived from the Z_T amplifier of Fig. 9 by extending the use of its voltage follower output stage: Being a basic Y_T amplifier, its third terminal is utilized to provide the current output. The use of two output transistors connected in series is required in the current amplifier in order to prevent loading of the collector of Q_2 by R_2, whose value is of the order of a few ohms for high gain factors. At the same time, Q_3 returns the base current of Q_4 to its emitter [7] and thereby increases the effective h_{fb} of Q_4 to $h_{fe4}(1 + h_{fe3})/[1 + h_{fe4}(1 + h_{fe3})]$. Thus, the total current flowing through R_1 and R_2 is routed into the output, except for the base current of Q_3, which is negligible. DC wise, the collector voltage of Q_4 is stabilised by Q7 - Q8. The diodes D_1 - D_4 improve the recovery of the amplifier from overload signals. This kind of current amplifier is capable of providing variable gain factors between unity (R_1 = 200 Ω, R_2 = ∞) and 10^3 (R_1 = 3 KΩ, R_2 = 3Ω).

7. The Design of a High Resolution Spectrometer

The effect which the use of enhancing configurations has on the design of the various circuit blocks, in a high resolution spectrometer, will now be discussed by describing a complete amplifier chain. The system employs a combination between conventional circuits and novel techniques. Noise considerations, gain requirements and the necessary signal shaping determine the choice of configuration in each stage.

Consider first Fig. 12. The low noise preamplifier needs hardly any comment. The choice of an FET as a low noise input device classifies the basic amplifier as A_V. The shunt-shunt capacitive feedback applied to the A_V amplifier constitutes a non-enhancing combination with respect to the input whose use is necessitated in this case owing to noise considerations.

Let us now examine the need for an additional gain stage in front of the main amplifier. The present practice of using such a stage is justified for two reasons:

First, it provides an additional gain factor without introducing parallel noise, because the latter is eliminated by the following short differentiator. This reduces the parallel noise contribution of the main amplifier by an equal factor, which is important in most presently used main amplifiers.

Second, it boosts the signal with regard to interference pick up in the interconnecting cable between pre- and main amplifier. This is, however, true only for a certain range of frequencies: We denote τ_a and τ_b as the decay time constants of the low noise charge sensitive and of the 2nd stage, respectively, and A as the gain of the 2nd stage. Then, due to greater pre-emphasis of low frequencies by the charge amplifier, than by the 2nd stage, relative interference pick up may be shown[3] to be less without a 2nd stage over a frequency spectrum between DC and $1/2\ \pi\ A\ \tau_b$, and to be more beyond that frequency. The total resulting gain in the signal to interference ratio due to a 2nd stage is a factor of A, but only for frequencies beyond $1/2\pi\ \tau_b$; at frequencies below $1/2\pi\ \tau_a$, the use of a 2nd stage results in a loss in this ratio by a factor of $\tau_a/A\ \tau_b$.

An inherent disadvantage of a conventionally designed 2nd stage preceding the main amplifier is the series noise contribution of R_o, which is part of its differentiating input network. In order to accomodate pile up, this is usually chosen of the order of 500Ω, which always exceeds the equivalent series noise resistance of the active circuit. The resulting dominant series noise contribution due to R_o is not eliminated by the following short differentiator.

In the presently described system, the series noise contribution of the resistor R_2 in the input differentiating network, plus parallel and series noise of the main amplifier, are minimized by appropriate design[2] without employing a 2nd stage preceding it. Hence, the only justification for a 2nd stage would be the presence of strong interferences beyond $1/2\pi\ \tau_b$. Such a stage is shown schematically in Fig. 12, and its design is considered in greater detail elsewhere[3].

The preamplifier feeds two channels - the energy and the timing channel. The latter is possible because careful design of the preamplifier[8] and second stage high frequency response makes it possible to amplify the detector signal without significant loss of timing information. Pulse - shortening methods[9] enable one to compensate for the dominant integration introduced by the preamplifier and thus to further improve the timing performance.

The preferred input mode for the main amplifier has been shown to be current[2], which leaves us a choice between a Z_T or an A_C amplifier as the gain stage. An A_C amplifier has been chosen for both the timing and energy channel owing to its superior speed, higher gain capacity, and an advantage of current as output parameter in both channels: In the timing channel, current makes possible further signal processing at maximum speed and minimum slewing; in the energy channel,

this enables one to cover a wide range of gain values by switching the feedback network. The high output impedance of the current amplifier also enables one to employ a long output coupling time-constant, which is of importance in a high resolution spectrometer. C_2 and C_3 are varied as a function of the shaping time constant, whereas R_2 is kept constant in order not to increase its series noise contribution at long time constants.

An alternative method enables one to extract the timing information directly from the preamplifier[10]; it employs a Y_T amplifier connected to the output of the preamplifier, which performs differentiation by its Y_T shaping network.

Between the input of the preamplifier and the output of the main amplifier gain stage, the gain of the system is defined as charge gain and equals $Q_3/Q_s = (C_o/C_f)(C_2/C_1)A_c$ (preamp. 2nd stage inverting), or $Q_3/Q_s = [(C_o + C_1)/C_f](C_2/C_1)A_c$ respectively (preamp. 2nd stage non-inverting). Due to the inherenly high gain of the system it is insufficient, at high energies, to reduce the gain of the current amplifier to unity. Further gain reduction is possible, decreasing the valueof C_2.
Thus, except for the presence of high frequency pick up by the interconnecting cable between pre- and main amplifier, the additional amplification of the 2nd gain stage in the preamplifier is not only necessary but even excessive, because the necessary gain reduction of the main amplifier at high energies creates problems.

Regarding the use of an enhancing combination with respect to the main amplifier input, the current mode requires the use of a common base input stage. Note that the parallel noise of the C.E. and C.B. configuration referred to their respective input is the same in both, namely $\overline{i_N^2} = 2eI_e[1-h_{fb}(0)]df = 4KTdf/R_p$, from which the equivalent parallel noise resistance of a transistor obtains as $R_p = 2r_e'[1 + h_{fe}(0)]$.

The only difference between the C.E. and the C.B. configuration is the way in which the parallel noise of the next transistor in the loop affects the noise performance: If the input stage is C.B., then the parallel noise R_{p2} due to the second transistor in the loop is <u>not</u> reduced with respect to the R_{p1} of the first one, but adds as $1/R_p = 1/\Sigma R_{pi}$, where R_{pi} includes in addition to R_{p1} and R_{p2} also the resistors supplying the emitter and collector current of the first one. Hence, the difference between C.B. and C.E. parallel noise is, for an identical first and second transistor in the loop and equal collector currents, a factor of $\sqrt{2}$ in favour of the C.E. Current supply resistors should not contribute, in a proper design.

These considerations confirm the use of an enhancing input combination employing a C.B. connected input transistor, which leaves complete freedom of choice for the most suitable values for R_2 and C_2: The low input impedance of the C.B. transistor provides effective separation between the input differentiating network and the feedback resistor and makes therefore possible the design of the loop transmission independently of R_2C_2, without affecting the stability conditions. Hence R_2 and C_2 may be chosen for equal parallel and series noise contribution of the main amplifier, for which condition it has been shown[2] that the total noise contribution of the main amplifier to the noise of the preceding stage approaches a minimum if R_2C_2 is much shorter than the shaping time constant.

It may be noted in passing, that if one employs such a short time constant, then the integration in the noise whitening filter is necessarily placed after the main amplifier. This further reduces slightly the noise contribution of the main amplifier and tends to offset the previously mentioned factor of $\sqrt{2}$ due to using the C.B. configuration. As a fringe benefit, this also enables one to connect a photomultiplier through a terminated interconnecting cable directly to the virtual ground of the main amplifier; the frequency response between the low noise preamplifier input and the output of the gain stage will only be affected by the natural bandwidth limitations of the various amplifiers. This means that signal shaping is exclusively by the filter following the gain stage of the main amplifier.

The output stage employs the enhancing A_v combination of Fig. 9 and needs no further comment.

8. Practical Results

Considerable experience has been gained with enhancing combinations using discrete components. Some results on these have been reported before in[6],[10]. Provided that an effective ground plane is provided and the circuits are carefully laid out, performance is in accordance with theoretical predictions. Certain means necessary to prevent oscillations, such as connecting resistors in series with the base of transistors serving as voltage followers, are ascribed to excessive circuit inductances due to the physical size of the circuits, which cannot be reduced below a certain minimum. These undesirable correcting networks limit the maximum unity-gain bandwidth of the resulting circuits.

Initial results obtained with hybrid circuits indicate that the further reduction in physical size achieved by this technique indeed makes possible the elimination of such undesirable correcting networks. The ex-tend to which the circuit miniaturization will push the frequency limits of the closed loop towards those predicted by theory is the subject of a current investigation.

The spectrometer has been realized, using conventional circuit construction techniques. Except for the low noise input stage, it employs enhancing combinations throughout. Owing to practical considerations, certain deviations from the optimal design have been made: a) An isolating voltage follower in front of the main amplifier,to make possible interconnection by cable between pre- and main - amplifier, and b) Time constant switching by R_2 instead of C_2 and C_3, for simplicity. The penalty for this is a certain increase in main amplifier noise contribution above the theoretical minimum, at long time constants. Theoretical predictions of speed, stability, and noise performance have been verified by practical results.

9. Conclusions

The use of enhancing combinations between feedback and a basic amplifier has been shown to result in increased loop transmission, in reduced direct signal transmission from input to output, in greater flexibility of usable gain functions and values, and in a significant reduction in the impedance levels of the feedback networks. The resulting four kinds of feedback amplifiers may by synthesized employing only two basic amplifiers, namely the Z_T and the Y_T one: The basic A_V amplifier (non-inverting) is obtained by shifting the ground connection of the Z_T, amplifier, and the A_C one by combining a Z_T with a Y_T amplifier. The reduced impedance levels of the feedback networks have been reported elsewhere[2] to result in reduced noise contribution to the preceding stage, in cetain well defined cases.

The extension of the principle of mismatch to interconnections between active devices leads to a non-ambiguous realization of the four basic amplifiers. Circuit examples are given for each kind of amplifier.

The application of the foregoing design principles to the various stages of a nuclear high resolution spectrometer is demonstrated. The use of an enhancing combination as main amplifier is shown to make unnecessary the use of a 2nd stage preceding the main amplifier. Resulting benefits are a significant reduction of noise contribution by the shaping network, and also a reduction of interference pick up by the interconnecting cable between pre- and main amplifier below a certain frequency. The use of a 2nd gain stage of modified design is only recommended in presence of strong interferences at frequencies above that frequency.

The technique employed also enables one to place the noise whitening filter after the main amplifier, which makes possible the connection of a photomultiplier through a terminating interconnecting cable directly to the virtual ground of the main amplifier.

10. Acknowledgements

Helpful discussions on the spectrometer design with D. Inbar* are gratefully acknowledged. The circuits have been built and tested by I. Klein*. Thanks are also due to the management of Elron Electronic Industries for granting permission to publish certain details of the spectrometer.

* Elron Elctronic Industries.

References

1. Cherry, F.M. and Hooper, D.E. "The Design of Wide-Band Transistor Feedback Amplifiers", Proc. I.E.E. London 110, No. 2 (1963), 375-389.

2. Arbel, A.F. "The Second Stage Noise Contribution of Nuclear Pulse Amplifier", I.E.E.E. Trans. Nu. Sci. NS-15, Oct. 1968.

3. Arbel, A.F. "A Further Note on the Second Stage Noise Contribution", in preparation.

4. Arbel, A.F. "The Current Routing Amplifier - a Novel Circuit Element", Proc. Sympos. Nucl. Instrum., Harwell 1961, London, Heywood and Co Ltd., (1962), 210-219.

5. Waldhauer, F.D., "Analog Integrated Circuits of Large Band-Width", IRE Conv. Rec. (1963) 200-207.

6. Arbel, A.F., "Multistage Transistorized Current Modules", I.E.E.E. Trans. Circuit Theory, CT-13, No. 2 (1966), 302-310.

7. Personal Communication from S. Fargeon.

8. Radeka, V. "State of the Art of Low Noise Amplifiers for Semiconductor Detectors". International Symposium on Nuclear Electronics, Versailles, Sept. 1968, Published by Documentation Francaise, 31 Quai Voltaire, Paris, Vol. 1, paper 46.

9. Amsel et al., "Pulse Shortening of Detector Signals by Passive Filters for the Reduction of Pile Up," same publication as (8), Vol. 1, paper 63.

10. Arbel, A.F. "Progress Report on Current Modules", Conference on Semiconductor Nuclear Particle Particle Detectors and Circuits,Gatlinburg, 1967. In Print.

11. A. Arbel, "Transistorized Circuit Modules for Pulse Height Analysis", U.S. National Academy of Sciences Publ. 1184, p. 79-87.

12. Gilbert, B. "A New Wide-Band Amplifier Technique", I.E.E.E. Jour. Sol. St. Circ. SC-3 No. 4, Dec. 1968 (353-365).

	Idealized		Practical	
T	Z_i	Z_o	Z_i	Z_o
Z_T	0	0	$\leq 10\Omega$	$\leq 10\Omega$
Y_T	∞	∞	$\geq 10K\Omega$	$\geq 10K\Omega$
A_v	∞	0	$Z_i \geq 10^3 Z_o$	
A_c	0	∞	$10^3 Z_i \leq Z_o$	

Table 1. Idealized and practical characteristics of the four basic amplifiers.

Device	Index 1	2	3
Bipolar Transistor	Base	Emitter	Collector
F E T	Gate	Source	Drain

Configuration:

C.E. Common Emitter
C.B. Commmon Base
C.C. Common Collector
C.S. Common Source
C.D. Common Drain

Configuration	Basic Building Block	Terminal Connection: Common	In	Out	Preferred Device:	Application
C.C. C.D.	Y_T	3	1	2	Both	Volt follower
C.B.	Y_T	1	2	3	Trans.	Curr. follower
C.S.	Y_T	2	1	3	F E T	Low Noise Device
C.E.	Y_T	2	1	3	Trans.	Tu. Di. Discr.[11]
C.E.	Z_T	2	1	3	Trans.	High Gain Device
C.E.	A_v	2	1	3	Trans.	High Gain Device
C.E.	A_c	2	1	3	Trans.	2nd Stage of Y_T amp.; Curr.ampl.[12]

Table 2. Classification of amplying devices into basic building blocks.

MISMATCH CONDITIONS		TRANSFER FUNCTION
INPUT	OUTPUT	T(s)
$[1+h_{fe}(0)]r'_e<<r'_b + R_s$	$R_o << \tau'_b/C'_c$ $C_o << h_{fe}(0)\ C'_c$	(a) $\frac{i_o}{i_s} \simeq \frac{-h_{fe}(0)\ \exp(-s\tau_d)}{[1 + s\ h_{fe}(0)\ \tau'_b][1 + s\ (1 + \frac{C_o}{C'_c})R_o\ C'_c]}$
	$R_o >> r'_c/h_{fe}(0)$ $C_o << h_{fe}(0)\ C'_c$	$\frac{e_o}{i_s} \simeq \frac{-r'_c\ \exp(-s\tau_d)}{(1 + s\ r'_c\ C'_c)[1 + s\ (1 + \frac{C_o}{C'_c}\ \tau'_b]}$
$[1+h_{fe}(0)]r'_e>>r'_b+R_s$	$R_o << r'_c\ (r'_e/r'_b)$	(b) $\frac{i_o}{e_s} \simeq \frac{-\exp(-s\tau_d)}{r'_e\ [1 + s\ (C'_e + C'_c)\ r'_b][1 + s\ (C'_c + C_o)R_o]}$
	$R_o >> r'_c$	(c) $\frac{e_o}{e_s} \simeq \frac{-r'_c\ \exp(-s\tau_d)}{r'_e\ [1 + s\ r'_c(C'_c + C_o)][1 + s\ (C'_e + C'_c)r'_b]}$

(a) $\tau'_b = r'_e\ (C'_e + C'_c)$

(b) Simplified, assuming $r'_e\ (C'_c + C_o) >> r'_b\ C'_c$

(c) Simplified, assuming $r'_e >> r'_b$

Table 3. The Four idealized transfer-functions of the bipolar transistor.

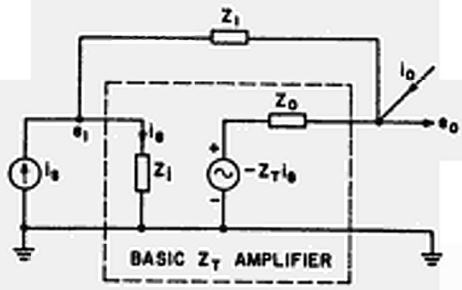

$$T = \frac{e_o}{I_s} = Z_f \frac{LT}{(1 - LT)}$$

$$LT = \frac{-Z_T}{Z_f}\left(1 - \frac{1}{Y_a Z_i}\right)$$

$$Y_a = \frac{Z_T}{Z_i Z_o}$$

$$Z_{IN} = \frac{e_i}{I_s} = \frac{Z_i}{(1 - LT)}$$

$$Z_{OUT} = \frac{e_o}{I_o} = \frac{Z_o}{(1 - LT)}$$

Mismatch Conditions:

$Y_f \gg Y_i$; $Y_o \gg Y_i$

Fig. 1 - Shunt-shunt feedback, applied to a basic Z_T amplifier.

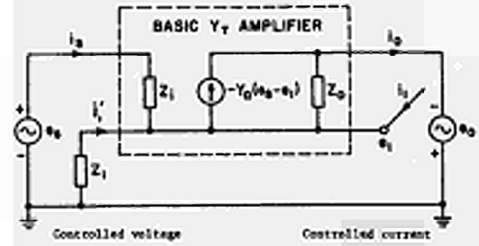

Controlled voltage source:

$$T_1 = \frac{i_o}{e_s} = Y_f \frac{LT_2}{(1 - LT_2)}$$

$$T_2 = \frac{e_i}{e_s} = \frac{-LT_2}{(1 - LT_2)}$$

$$LT_1 = -Y_a Z_i$$

$$Z_{IN} = \frac{e_s}{I_s} = Z_i (1 - LT_1)$$

$$Z_{OUT2} = \frac{e_i}{I_i} = \frac{Z_f}{(1 - LT_1)}$$

$$Z_{OUT1} = \frac{e_o}{I_o} = Z_o (1 - LT_1)$$

Controlled current source:

$$T_3 = \frac{i_o}{i_i} = \frac{-LT_2}{(1 - LT_2)} = h_{fb}$$

$$LT_2 = -h_{ie}$$

$$Y_a = 1/r_e$$

Mismatch Conditions:

$Y_i \ll Y_f$; $Y_o \ll Y_a$

Fig. 2 - Series-series feedback, applied to a basic Y_T amplifier.

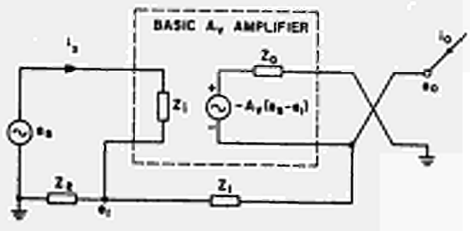

$$T = \frac{e_o}{e_s} = \frac{(Z_f + Z_s)}{Z_s} \frac{(1 - LT)}{(1 - LT)}$$

$$LT = \frac{-A_v Z_i}{(Z_f + Z_s)}\left(1 - \frac{1}{Y_a Z_i}\right)$$

$$Y_a = \frac{A_v}{Z_o}$$

$$Z_{IN} = \frac{e_s}{I_s} = Z_i (1 - LT)$$

$$Z_{OUT} = \frac{e_o}{I_o} = \frac{Z_o}{(1 - LT)}$$

Mismatch Conditions:

$Y_i \ll Y_f + Y_s$; $Y_o \ll Y_f$

Fig. 3 - Series-shunt feedback, applied to a basic A_v amplifier.

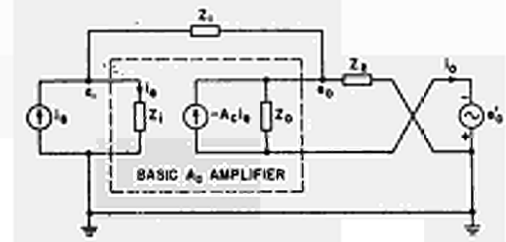

$$T = \frac{i_o}{i_s} = \frac{(Z_f + Z_s)}{Z_s} \frac{(1 - LT)}{(1 - LT)}$$

$$LT = \frac{-A_c Z_s}{(Z_f + Z_s)}\left(1 - \frac{1}{Y_a Z_i}\right) \; ; \; Y_a = \frac{A_c}{Z_f}$$

$$Z_{IN} = \frac{e_s}{I_s} = \frac{Z_i}{(1 - LT)}$$

$$Z_{OUT} = \frac{e_o'}{I_o} = Z_o (1 - LT)$$

Mismatch Conditions:

$Y_i \ll Y_f$; $Y_o \ll Y_f + Y_s$

Fig. 4 - Shunt-series feedback, applied to a basic A_c amplifier.

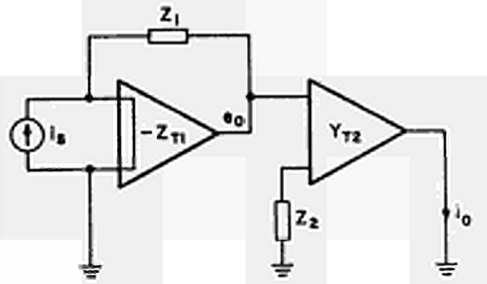

$$T_1 = \frac{e_0}{i_s} = Z_1 \frac{LT_1}{(1 - LT_1)}; \quad LT_1 = -\frac{Z_{T1}}{Z_1}$$

$$T_2 = \frac{i_o}{e_o} = \frac{1}{Z_2} \frac{LT_2}{(1 - LT_2)}; \quad LT_2 = -Y_{T2} Z_2$$

$$\frac{i_o}{i_s} = T_1 T_2 = \frac{Z_1}{Z_2} \frac{LT_1}{(1 - LT_1)} \frac{LT_2}{(1 - LT_2)}$$

Fig. 5 - Operational current amplifier, consisting on one Z_T and one Y_T amplifier in cascade.

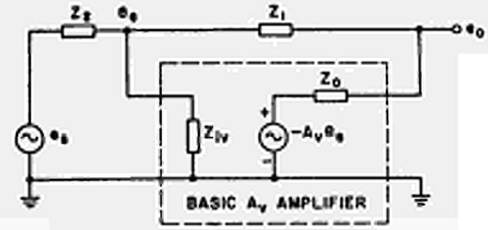

$$T = \frac{e_o}{e_s} = \frac{Z_1}{Z_2} \frac{LT}{(1 - LT)}$$

$$LT = \frac{-A_v Z_2}{(Z_1 + Z_2)} \left(1 + \varphi \frac{1}{A_v Z_1}\right)$$

$$Y_o = A_{v1} Y_o$$

Mismatch Conditions:

$$Y_{iv} \ll Y_1 + Y_2; \quad Y_o \gg Y_1$$

Fig. 6 - Operational voltage amplifier, applying shunt-shunt feedback to a basic A_v amplifier (non-enhancing with respect to input).

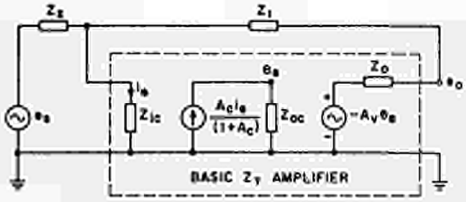

$$T = \frac{e_o}{e_s} = \frac{Z_1}{Z_2} \frac{LT}{(1 - LT)}$$

$$LT = \frac{-Z_T}{Z_1} \left(1 + \varphi \frac{1}{A_v Z_1}\right)$$

$$Z_T = A_v Z_{oc}; \quad Y_o = \frac{Z_1}{Z_{oc} Z_o}$$

Mismatch Conditions:

$$Y_{ic} \gg Y_1 + Y_2; \quad Y_o \gg Y_1$$

Fig. 7 - Operational voltage amplifier, applying shunt-shunt feedback to a current follower cascaded with a basic A_v amplifier (enhancing).

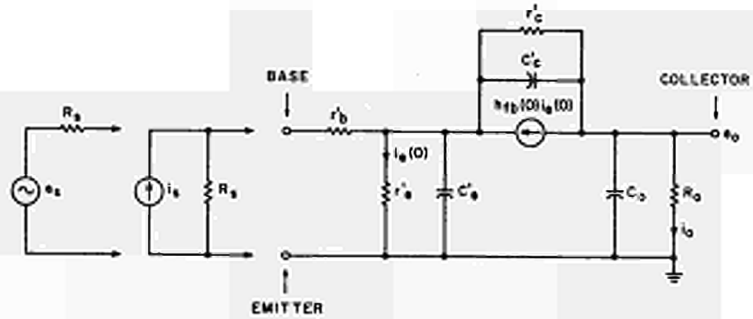

Fig. 8 - Simplified transistor model.

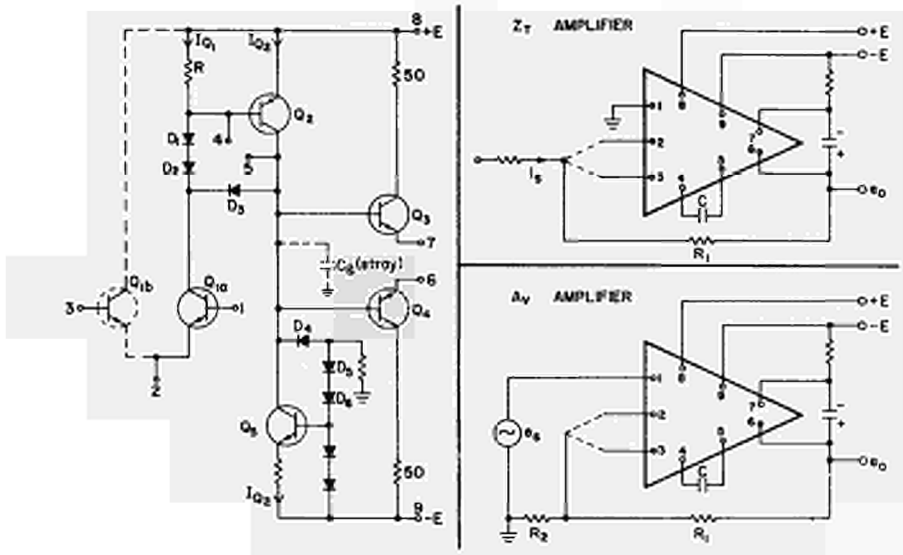

Fig. 9 - Realization of Z_t amplifier and proposed packaging as integrated circuit.

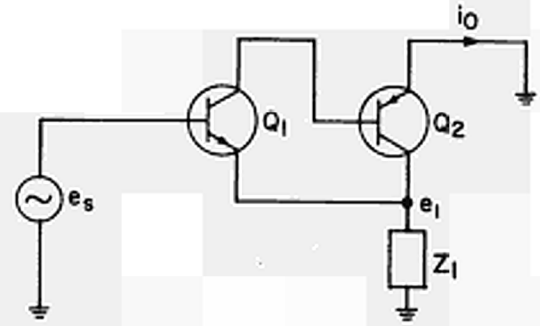

Fig. 10 - Practical configuration for Y_T amplifier, disregarding DC conditions.

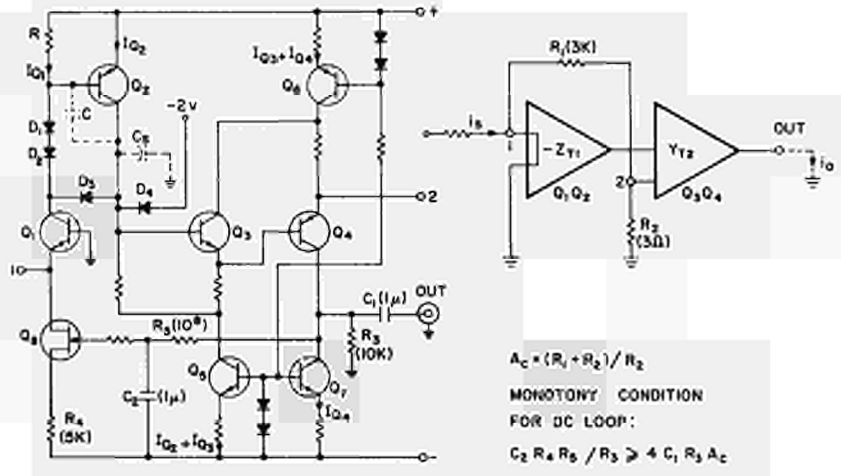

Fig. 11 - Realization of A_c amplifier.

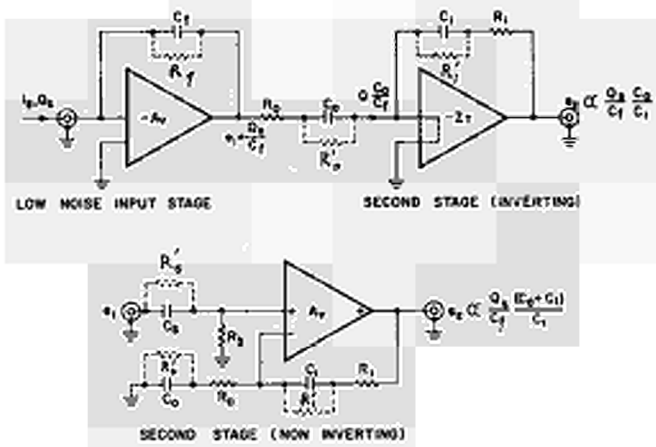

Fig. 12 - Low noise preamplifier.

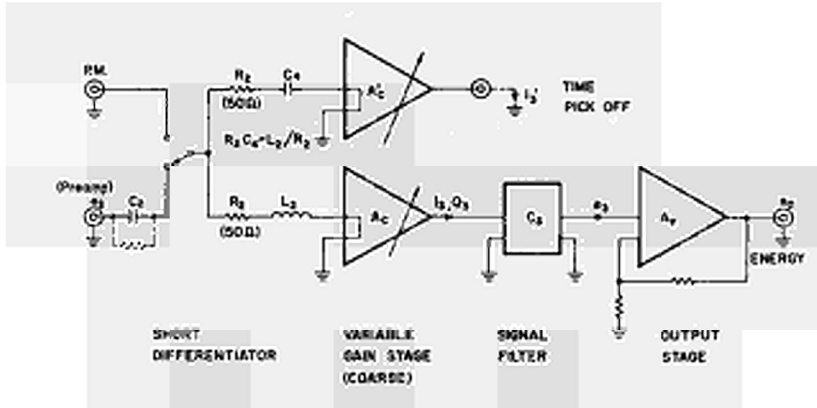

Fig. 13 - Main amplifier.

SIGNAL SHAPING, TRANSFORMATION AND GENERATION, USING BASIC ELEMENTS OF ANALOG AND DIGITAL COMPUTERS

K. Čuljat, B. Souček, V. Bonačić, B. Matić
Institute "Rudjer Bošković", Zagreb, Yugoslavia

1. INTRODUCTION

To realize some analog and digital functions, it is very useful to use integrated operational amplifiers and digital integrated elements. Using such elements, design problems are reduced. Owing to the improvement of their properties, these elements will make it possible to solve more and more sophisticated problems. Such circuits could be applied for educational purposes: to show students how to use "elements" (such as operational amplifiers, comparator, integrator in linear field, and gate, bistable, univibrator in digital field) in designing complicated functional "circuits" (such as function generators, multipliers, random and pseudo-random noise generators). These circuits could be also used for real time analog and digital computing functions in laboratory applications.

In this paper some examples of functional circuits are described.

2. SOME CIRCUITS FOR ANALOG SIGNAL GENERATION AND TRANSFORMATION [1]

2.1. Analog bistable multivibrator

An "analog" bistable is realized with two operational amplifiers, one is used as a summing circuit, the other as a comparator function, Fig. 1a. Figure 1b shows the waveforms, the upper e_0 and the lower e_1. Trigger pulses are of opposite polarity, and e_1 is the sum of e_0 and these pulses. A positive feedback and a comparator make it possible that an analog bistable multivibrator shows the same behaviour as a "digital" bistable. Operational amplifiers are Fairchild μA 741 as in all other analog circuits.

2.2. Analog astable multivibrator

The main parts of an analog astable multivibrator are an integrator and a hysteresis generator, Fig. 2a. The hysteresis generator is composed of a comparator and an inverter. The waveforms e_i and e_0 are shown in Fig. 2b.

2.3. Square function generator

Figure 3a shows a diode square function generator and Fig. 3b an input triangle waveform and an output square waveform.

2.4. Indirect multiplier

This multiplier is based on the relation

$$x \cdot y = \frac{1}{4} [(x+y)^2 - (x-y)^2]$$

and is shown in Fig. 4a. Figure 4b shows the output of the multiplier $x \cdot y$ (upper) and the output of the square function generator $\frac{1}{4}(x+y)^2$ (lower). The input waveforms are sinewave and triangular with frequency ratio 5:1 and similar amplitudes. Figure 4c shows the same input waveforms with frequency ratio 20:1 and amplitude ratio 1:3. The upper part is the multiplier output $x \cdot y$ and the lower part is the sum of the input waveforms. These figures show the well-known amplitude modulation due to multiplication process, (without carrier).

3. ANALOG RANDOM NOISE GENERATION AND TRANSFORMATION [2-5]

Analog random noise could be generated using many different physical phenomena as a primary noise source. A few examples are: thyratron, thermo-

ionic diode, radioactive source, photomultiplier tube, semiconductor diode and transistor. This primary noise could be amplified and transformed to obtain random noise with suitable characteristics.

In this section two generators are described. The only purpose was to generate a suitable amplitude probability density function or the so-called amplitude distribution. Distributions are measured by means of a PDP-8 pulse height analyzer. The sampled analog noise is used for measuring directly or transformed by the square function generator.

3.1. Semiconductor diode as a primary noise source

In this generator, Fig. 5, a semiconductor diode GA 203 is reverse biased. It generates random noise which is amplified 800 times with the first amplifier stage. The second stage is an a.c. coupled amplifier with amplification 100 times. These two stages give amplification about 80.000 and amplify the noise from ^{RMS}100 μV to 8 V. The noise level of the diode GA 203 is at least 100 times higher than the unwanted noise of the amplifier.

3.2. Primary noise from a radioactive source

Pulses generated by a radiation detector which occur at random in time are a very useful primary noise source. Figure 6 represents such a generator. After passing through a Schmitt trigger pulses have constant amplitude but random occurrences. They complementary trigger a flip-flop which gives a telegraph signal with pulses of random durations. Applying this signal to a low-pass filter, random noise is obtained with a similar amplitude distribution as the generator previously mentioned.

3.3. Amplitude probability density functions

After sampling the noise generated by the generators from Figs. 5 and 6 and after measuring their amplitude distribution, a Gaussian density function is obtained, as shown in Fig. 8a. If the generated noise has a distribution more or less different from the Gaussian, the latter one could be generated from the former by selecting the sampling frequency low in comparison with the rate of the noise waveform fluctuation. This requirement is opposite to the sampling theorem for good reconstruction of the waveform sampled but is necessary to obtain independent samples to fulfil the central limit theorem.

If the generated noise is transformed before sampling, different density functions could be produced. If the square function generator from Fig. 3a is used as transformer, the Gaussian distribution could be transformed into the χ^2 distribution, Fig. 8b. It could easily be shown that the random process x(t) with a normal amplitude density function

$$f_x(x) = \frac{1}{\sigma\sqrt{2\pi}} e^{-\frac{x^2}{2\sigma^2}}$$

transforms with the square function $y = x^2$ into the y(t) process with the χ^2 density function

$$f_y(y) = \chi^2 = \frac{1}{\sigma\sqrt{2\pi}} \cdot \frac{e^{-\frac{y}{2\sigma^2}}}{\sqrt{y}}$$

This function is shown in Fig. 8b.

4. DIGITAL PSEUDORANDOM NOISE GENERATION [6-7]

Figure 7 shows a pseudorandom signal generator with a 10-bit shift register and two exclusive-or gates. Any starting number could be set by the set logic, which is shown in the lower position of Fig. 7. The feedback polynomial of the maximum degree 10 has two coefficients different from zero. They are given by two feedback lines with exclusive or gates EOR 1 and EOR 2. Switching off SW1, the degree of the polynomial can be decreased to any value. The pseudorandom sequence can be stopped after one period through the stop logic by switch SW 2. The generator is realized by digital DTμL integrated elements family SGS 946, 932, 936, 9097.

By filtering a pseudorandom binary sequence by different low-pass analog filters, random processes with different amplitude density functions were pro-

duced, Fig. 9. If the clock frequency f_0 is very small in comparison with the filter cut-off frequency f_f, the distribution tends to the non-filtered distribution with two amplitudes only, Fig. 9a. By increasing the clock frequency the distribution changes, Fig. 9b, and approaches the Gaussian, as the clock frequency is higher than f_f.

References

1. H.D. Huskey, G.A. Korn: Computer Handbook, Mc Graw Hill, New York 1962
2. V.N. Zovinskij: Generating Noise for Automatic Systems Research, ed. by "Energija", Moskva, in Russian.
3. R.R. Bannett, A.S. Fulton: Journal of Appl. Physics, 22, No 9, Sept. (1951), 1187.
4. J.B. Manelis: Electronics, Sept. 8, 1961, 66.
5. J. Havel: Transactions of the Second Prague Conference on Information Theory and Random Processes, Prague 1959, 219.
6. W.W. Peterson: Error-Correcting Codes, M.I.T. Press, 1961.
7. R.P. Gilson: IEEE Trans. on Electronic Computers, EC-15, No 6, Dec. 1966, 926.

DISCUSSION

S. S. Klein : Do you have any data concerning accuracy and speed of the multipliers ?
Čuljat : - Yes we have, we have been using in this multiplier µA741 operational amplifiers which are limited in frequency and we can multiply signals to only 20 Kc/s with accuracy about 4 %.
Deighton : - In your description of the "quarter-squares" multipliers you had two circuits one of which generated -(x+y) and the other one which generated -(x-y) and the two circuits looked identical to me. Could you explain how they function ?
Čuljat :- In the first amplifier we only used one input, while in the lower part we used a differential amplifier and we used two inverting and non-inverting inputs. By suitably connecting the inverting and non-inverting inputs we can produce the difference.
Deighton : - I see, thank you.

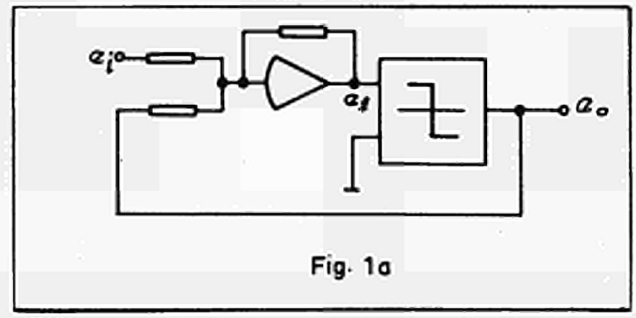

Fig. 1a

Fig. 1b

Fig. 1 - Analog bistable multivibrator a) circuit, b) waveforms.

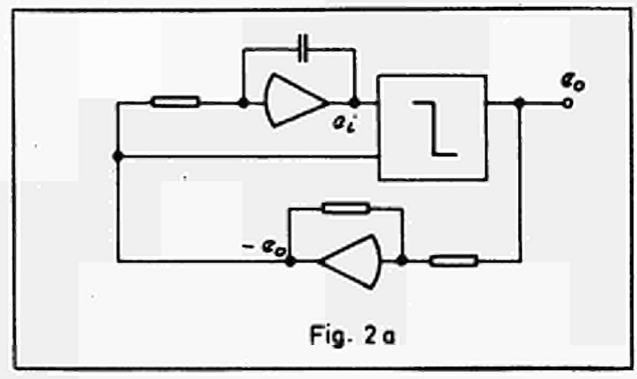

Fig. 2a

Fig. 2b

Fig. 2 - Analog stable multivibrator a) circuit b) waveforms.

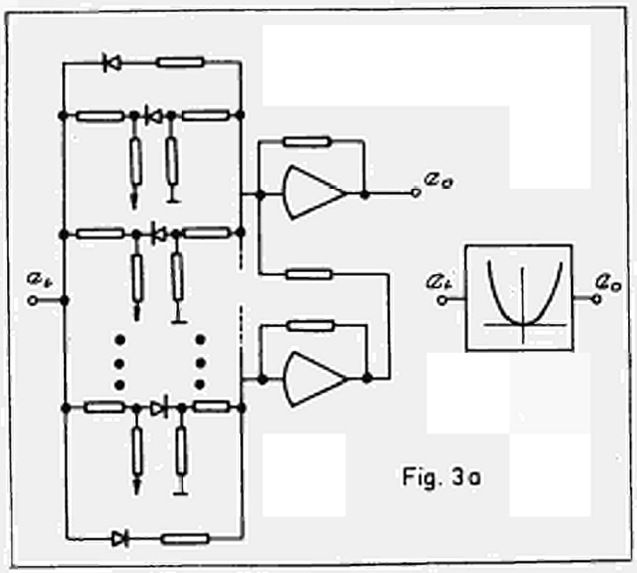

Fig. 3a

Fig. 3b

Fig. 3 - Square function generator a) circuit, b) waveforms.

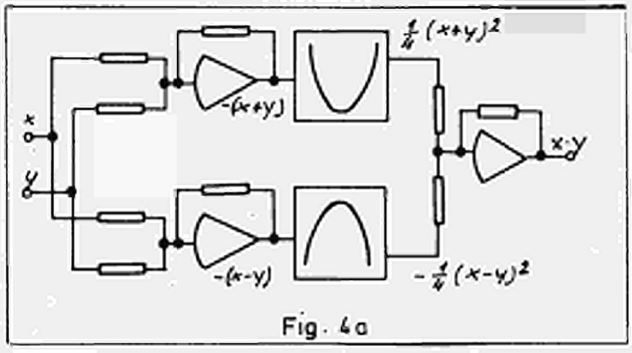

Fig. 4a

Fig. 4b

Fig. 4c

Fig. 4 - Indirect multiplier a) circuit, b) and c) waveforms.

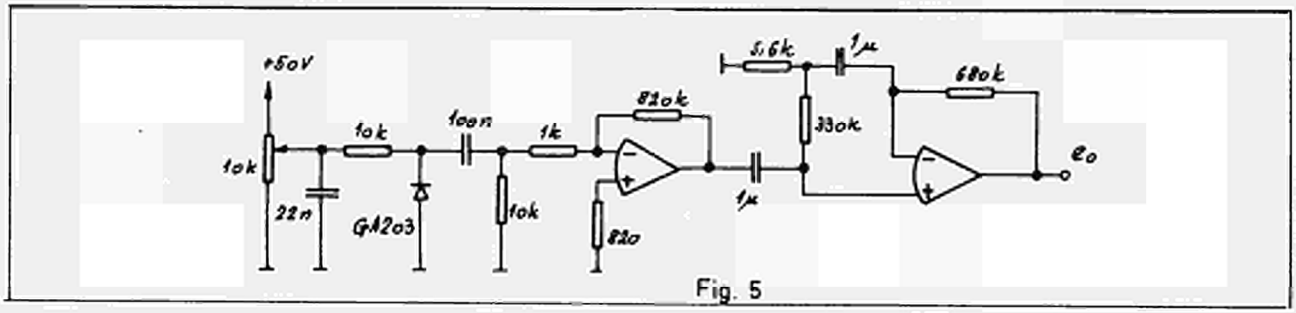

Fig. 5

Fig. 5 - Semiconductor diode noise generator.

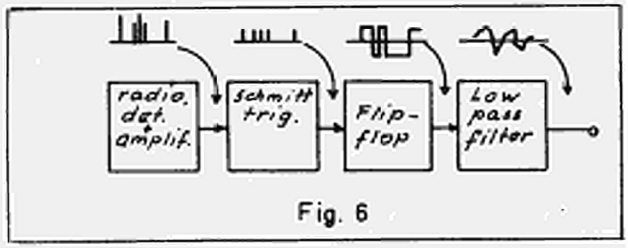

Fig. 6

Fig. 6 - Noise generator with radioactive primary source.

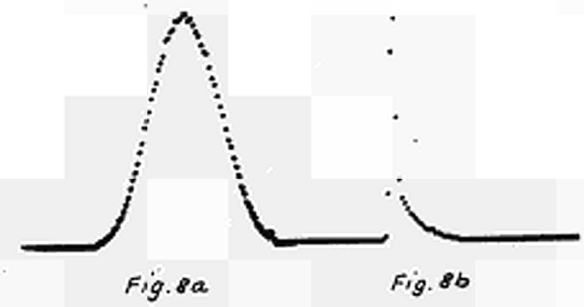

Fig. 8 - Amplitude distribution functions a) Gaussian b) χ^2.

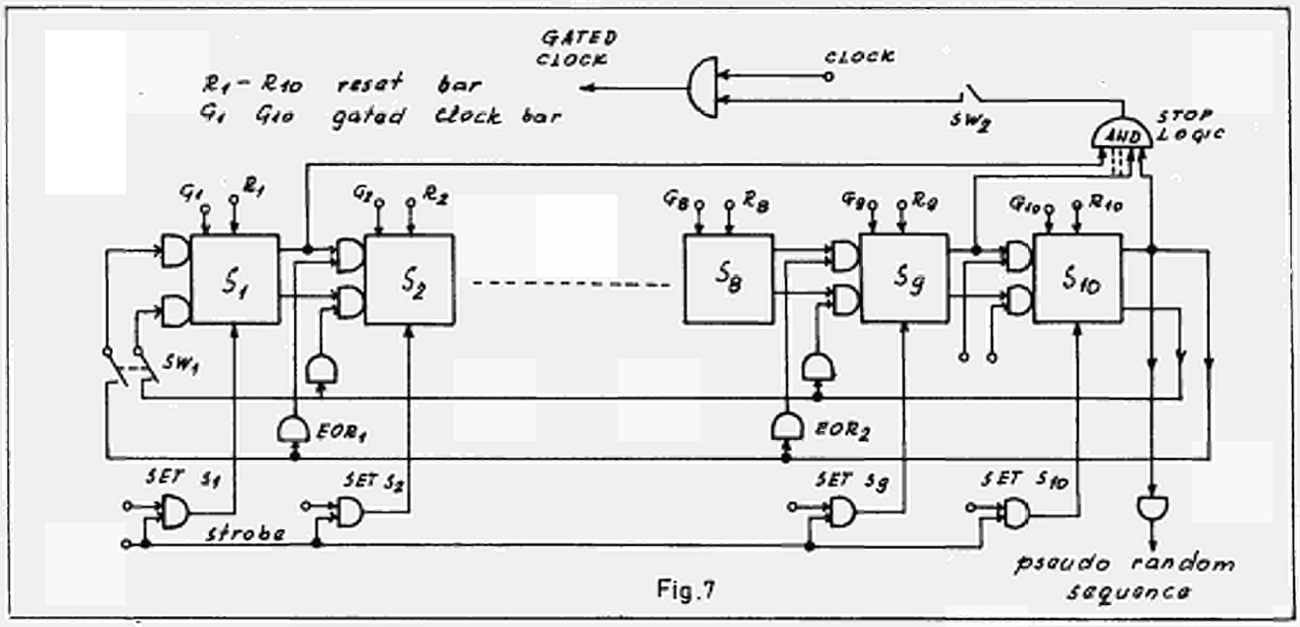

Fig. 7 - Digital pseudorandom noise generator.

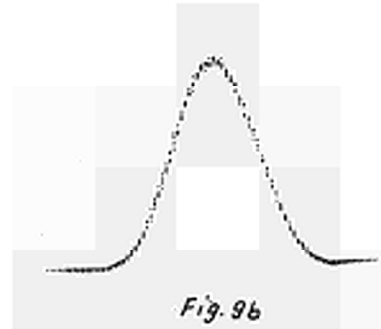

Fig. 9 - Amplitude distribution functions of filtered pseudorandom noise a) $f_o/f_f \ll 1$, b) $f_o/f_f \approx 1$.

MAXIMUM LOOP GAIN OF FEEDBACK AMPLIFIERS WITH MONOTONIC STEP RESPONSE

H. Babić
Institute "Rudjer Bošković", Zagreb, Yugoslavia

A class of transfer functions for feedback amplifiers, which allow high loop gain is considered.

With real poles only in the closed loop amplifier transfer function it follows that the optimum denominator of the open loop transfer function is a Chebishev's polynomial.

Conditions for the realization of the pulse amplifiers with feedback pairs together with a high gain overall feedback are given.

Introduction

Linear pulse amplifiers consist usually of cascaded feedback stages and feedback pairs to avoid stability and response problem. The gain stability and linearity is better if overall feedback with high loop gain is used[1]. A designing technique of the stable feedback system is the use of integrating and differentiating circuits in the amplifier-feedback loop what is usually far from optimum solution.

A multistage amplifier transfer function can be simplified enough to make optimisation possible.

In order to optimize an amplifier one has to define the requirements. Such an amplifier fulfil the requirements in "the best way" under given constrants. Two different but common requirements for amplifiers will be mentioned. One, common for pulse amplifiers, is to obtain the shortest possible rise time for a given overshoot, gain and specified electronic element parameters. The other, typical for feedback amplifiers, is to obtain maximum open loop gain, for a given dominant time constant, rise time, gain and specified electronic element parameters.

An amplifier with a maximum loop gain was obtained by Fränz[4]. The constaint to RC amplifiers with real poles only in the open loop transfer function was substantial. The resulting amplifier has a wide closed loop pole region and therefore a rather long rise time and small loop gain for a given dominant time constant.

The maximum loop gain amplifiers without mentioned constraint will be considered in this paper. The open loop transfer function with a dominant time constant and complex poles is assumed, to allow the maximum loop gain. The position of complex poles have to be determined to meet the latter requirement.

The closed loop transfer function was assumed with real poles only, what is a sufficient condition for a monotonic step response[5]. This results in a class of transfer function which is not limited to real poles only. These transfer functions give amplifiers with nearly the same rise time as fast amplifiers without feedback.

Maximum loop gain transfer function

The transfer function of an open loop amplifier is assumed without zeros what is a satisfactory approximation for DC-amplifier, i.e.

$$A(p) = \frac{A_o}{a_n p^n + a_{n-1} p^{n-1} + \ldots + 1} = \frac{A_o}{P_n(p)} \qquad (1)$$

The polynomial $P_n(p)$ of the n-th degree with roots ϱ_k has at least one real root $p_1 = -\varrho_1$ if n is odd, and two real roots are assumed if n is even.

Let us take that one real root corresponds to the maximum, i.e. dominant time constant $\varrho_1 = 1/\tau_1$ and another to the minimum time constant $\varrho_n = 1/\tau_n$. We assume in fact that real parts of all other complex roots $\varrho_k + j\omega_k$ lay between these limits.

$$-\varrho_n < -\varrho_k < -\varrho_1 , \qquad (k=2,3,\ldots n-1) \qquad (2)$$

The last term of the polynomial is taken $a_o=1$ to obtain $A(o)=A_o$.

A graph of the function $z=P_n(\varrho)$ in ϱ,z coordinate system will pass points $B(-\varrho_n,0)$, $C(-\varrho_1,0)$, $D(0,1)$ in Figure 1a. All crossings of the $\varrho=\mathrm{Re}[p]$ axis and also the maxima and minima of the polynomial will lay inside the limits $(-\varrho_n,-\varrho_1)$.

The closed loop transfer function for a real feedback factor $\beta \neq f(p)$ is also a function without zeros

$$G(p) = \frac{A(p)}{1+\beta A(p)} = \frac{A_o}{P_n(p)+A\beta} = \frac{A_o}{Q_n(p)} \qquad (3)$$

The closed loop amplifier gain or simply amplifier gain is

$$G(0) = G_o = \frac{A_o}{Q_n(0)} = \frac{A_o}{P_n(0)+\beta A_o} = \frac{A_o}{1+\beta A_o} \qquad (4)$$

It depends on the term $\beta A_o = L$ known as the loop gain of amplifier..

Our assumption about polynomial $Q_n(p)$ is that its roots q_k are all real to ensure a monotonic step response. This condition is sufficient for a monotonic response but not a necessary one[5]. A more general approach to the problem is difficult mainly because of a lack of suitable condition for a monotonic response[5] relating zeros and poles of the transfer function. The relation between polynomials $P_n(p)$ and $Q_n(p)$ is according to (3), i.e.

$$Q_n(p) = P_n(p) + L \tag{5}$$

They differ by constant L only. One can obtain the roots of polynomial $Q_n(p)$ from the condition $Q_n(q_k) = 0$, what gives

$$P_n(q_k) = -L \tag{6}$$

If roots q_k are real, the polynomial $z=P_n(p)$ will cross or touch the line $z=-L$ as shown in Figure 1b (with line $z=-L_{min}$). For polynomial of the n-th degree it must be n solutions of equation (6) If ν is the number of crossing points and μ their multiplicity and

$$\sum_{1}^{\nu} \mu_k = n \tag{7}$$

all roots of (6) are real as shown in Figure 1b. Otherwise some roots will be complex as shown in Figure 1a.

Let us suppose now that the poles of the amplifier transfer function must remain real for a loop gain change ΔL. The value of ΔL depends on design precision and parameter variation in amplifier application. In amplifiers with nonlinear electronic elements and large signal the loop gain depends also on the signal amplitude.

The real poles q_k for the loop gain L in the interval $[L_{min}, L_{max}]$ cannot be obtained if some of the points have multiplicity $\mu > 2$. If we assume a tangent point on $z=-L_{min}$ line with a multiplicity $\mu=4$ then a small increase of the loop gain from that point will give only two real poles but not 4. Other two poles will be complex. Thus the real poles in the interval $[L_{max}, L_{min}]$ can be obtained only if the crossing points for any L are simple crossings or simple maxima or minima ($Q'(q_k) \neq 0$). Therefore for any loop gain L in the interval (L_{min}, L_{max}) it must be n-crossings of the polynomial with the line $z=-L$. The difference between the line L and the polynomial, i.e. the polynomial $Q_n(p)$, ($Q_n = P_n - (-L)$) must change the polarity n-times. That will be the case for example of the polynomial in Figure 1b, if polynomial is of 6th degree. Such a polynomial passing through the points B,C,D, Figure 1b, will give real roots in the interval $[L_{min}, L_{max}]$.

Our intention is to find the polynomial which will allow the highest possible loop gain, i.e. a polynomial which will allow the lowest position of the line $z=-L_{max}$. We may start by considering a polynomial with a fixed L_{min}. Changing the parameters of the polynomial one can shift away the nearest peak and therefore the allowed L_{max}. By this change the other peaks will approach the line L_{max}. The limiting case of such a repeated procedure will be when all peaks are equal. Then the distance from the line L_{min} to the nearest peak is maximum. In the same time the distance to the farthest peak is minimum (Figure 1b, dashed). Polynomial of n-th degree with such properties and which change the polarity on a middle line n-times is the Chebishev's polynomial[6].

We may suppose that there is a better polynomial of the n-th degree $S_n(p)$ than the Chebishev's $T_n(p)$ passing through the points B,C,D (Figure 1c, dashed) and having a lower line L'_{max}. Such a polynomial must have with line L'_{max} n common points (7). It will cross L'_{max} at least n+1 times the Chebishev's polynomial, Figure 1c. The difference $R_n(p)$ between such polynomial and Chebishev's

$$S_n(p) - kT_n(p) = R_n(p)$$

is also a polynomial of n-th order and cannot have n+1 root. $R_n(p)$ is therefore identical to zero. Thus the Chebishev's polynomial is the best one.

It gives the highest possible L_{max} and the widest tolerancies for the loop gain L.

Open and closed loop amplifier pole distribution

The transcendent form of the Chebishev's polynomial is

$$T_n(s) = \cos(n \arccos s) \tag{8}$$

$$|s| \leq 1$$

$$T_n(s) = \mathrm{ch}(n \operatorname{Arch} s) \tag{9}$$

$$|s| \geq 1$$

The polynomials $P_n(p)$ and $Q_n(p)$ in the denominator of the transfer functions may be written with parameters a,b,c,d to obtain a general form, i.e.

$$Q_n(p) = cT_n(ap+b)$$

$$P_n(p) = cT_n(ap+b)-d$$

From extrems of polynomials $(T_n)_m = \pm 1$ it follows for $P_n(p)$, (Figure 1c)

$$-L_{min} = c-d \; ; \quad -L_{max} = -c-d$$

$$2c = L_{max}-L_{min} \; ; \; 2d = L_{max}+L_{min}$$

Using the relative deviation of the loop gain as parameter

$$\varepsilon = \frac{L_{max}-L_{min}}{2L_o} \; ; \quad L_o = \frac{L_{max}+L_{min}}{2} \qquad (10)$$

one obtains

$$Q_n(p) = \varepsilon L_o T_n(s) \; , \quad s = ap+b \qquad (11)$$

$$P_n(p) = \varepsilon L_o T_n(s)-L_o \qquad (12)$$

The roots p_k of $P_n(p_k) = 0$ which follows from (12) are determined by

$$ch(n \; Arch \; s) = 1/\varepsilon, \quad |1/\varepsilon| \geq 1 \qquad (13)$$

$$ch(u+jv) = 1/\varepsilon$$

$$s_k = (ap_k+b) = (ch u/n)\cos(v/n) + j(sh\, u/n)\sin(v/n),$$

where

$$u = Arch \; 1/\varepsilon ; \qquad (14)$$

$$v = 2k\pi ; \quad k=1,2,\ldots,n. \qquad (15)$$

A polynomial of an even degree n=2m has two real roots $-\varrho_n$, $-\varrho_1$, passing the points B and C. These roots are obtained for k=n/2 and k=n, what gives

$$-a\varrho_1+b = ch\, u/n \; ; \quad -a\varrho_n+b = -ch\, u/n$$

The constant b and a are thus

$$b = a(\varrho_n+\varrho_1)/2 = a\varrho_o \qquad (16)$$

$$a = (\varrho_o-\varrho_1)^{-1} \; ch(n^{-1} \; Arch \; 1/\varepsilon) = 1/\mathfrak{a} \qquad (17)$$

Instead of $\varrho_n-\varrho_1$ we introduced $2\varrho_o-2\varrho_1$, where $-\varrho_o$ is the abscissa of the polynonimal centre s=0. Having ϱ_o in all relations they will be valid also for odd degrees of the polynomial, i.e. n=2m+1.

The open loop pole distribution is thus

$$p_k = -\varrho_o+(\varrho_o-\varrho_1)\cos 2k\pi/n + j\sqrt{(\varrho_o-\varrho_1)^2-\mathfrak{a}^2} \cdot \sin 2k\pi/n \qquad (18)$$

The poles are located on ellipse in the p-complex plane with $(\varrho_o-\varrho_1)$ as minor and $\sqrt{(\varrho_o-\varrho_1)^2-\mathfrak{a}^2}$ as major axis, Figure 2a.

The closed loop poles follow from (11) as

$$q_k = -\varrho_o + \mathfrak{a}\cos(\pi/2+2k\pi)/n \qquad (19)$$

We see that the parameter $\mathfrak{a}$ presents the width of the amplifier pole region, Figure 2a.

Since the polynomial is passing through the point D(0,1), it follows from (12) and $b = a\varrho_o = \varrho_o/\mathfrak{a}$

$$P_n(0) = \varepsilon L_o T_n(b) - L_o = 1$$

$$ch(n \; Arch \; \varrho_o/\mathfrak{a}) = (1+1/L_o)/\varepsilon \qquad (20)$$

and using (17) and (20) we obtain the required time constant for a given loop gain L_o

$$\frac{\varrho_1}{\varrho_o} = 1 - \frac{ch(n^{-1}Arch\; 1/\varepsilon)}{ch(n^{-1}Arch(1+1/L_o)/\varepsilon)} = \frac{\tau_o}{\tau_1} \qquad (21)$$

or approximately for $\mathfrak{a}/\varrho_o < 1/3$ the loop gain for a given dominant time constant ($L_o \gg 1$)

$$L_o = \frac{1}{n}\left(\frac{\tau_1}{\tau_o} - 1\right)\frac{(2/\varepsilon)^{2/n} - 1}{(2/\varepsilon)^{2/n} + 1} \qquad (22)$$

An interesting special case[b] is for $\varepsilon = 0$. Then pole region $\mathfrak{a} = 0$ and the open loop poles are located on the circle.

$$p_k = -\varrho_o+(\varrho_o-\varrho_1)\cos 2k\pi/n + j(\varrho_o-\varrho_1)\sin 2k\pi/n \qquad (23)$$

All amplifier poles q_k are then at the same point

$$q_k = -\varrho_o , \qquad (24)$$

giving the transfer function with a multiple pole. The polynomial $P_k(p)$ takes the form

$$P_n(p) = \lim_{\mathfrak{a}\to 0} P_n(\mathfrak{a},p) = (1+L_o)(p+\varrho_o)^n/\varrho_o^n - L_o \qquad (25)$$

The dominant time constant is simply ($L_o \gg 1$)

$$\frac{\varrho_1}{\varrho_o} = 1-(1+1/L_o)^{-1/n} \; ; \quad \frac{\tau_1}{\tau_o} = n(1+L_o) \qquad (26)$$

or for given τ_1/τ_o the loop gain is

$$L_o = \frac{1}{n}\left(\frac{\tau_1}{\tau_o} - 1\right) \qquad (27)$$

This value of L_o is apparently higher than in the case with allowed tolerancies $\varepsilon \neq 0$, (22), as is shown for an example in Figure 2.

Another special case is for $\varepsilon = 1$ which was solved by Fränz[4]. The open loop transfer function has real poles only, what can be realized by simple cascaded stages. The amplifier poles are real and have a wide pole region $\alpha = \varrho_o - \varrho_1$, so that system of an order $n > 2$ gives long rise time. On the hand the maximum loop gain is also small for $n > 2$

$$L_{max} = 2L_o \sim \frac{2}{n^2}\frac{\tau_1}{\tau_o}$$

and it is falling proportional to n^2.

Further deformation of the open loop pole ellipse from a circle to an ellipse with major axis parallel to the imaginary axis, gives an interesting transfer function (case c))

$$Q_n(p) = \varepsilon L_o \, sh(n \, Arsh(p+\varrho_o)/\lambda) \qquad (28)$$

It does not represent a conventional Chebishev polynomial but has a similar transcendental form (9).

The open loop pole distribution

$$p_k = -\varrho_o + (\varrho_o - \varrho_1)\cos 2k\pi/n + j\sqrt{(\varrho_o-\varrho_1)^2 + \lambda^2}\,\sin 2k\pi/n \qquad (29)$$

is on ellipse, Figure 2c.

The amplifier pole distribution is

$$q_k = -\varrho_o + j\lambda \sin 2k\pi/n \qquad (30)$$

i.e. on a line parallel to the imaginary axis.

Parameter λ represents the amplifier pole region and it is given by

$$\varrho_o/\lambda = sh(n^{-1}Arsh(1+1/L_o)/\varepsilon) \qquad (31)$$

This equation is obtained in the same way as (20). The dominant pole is

$$\frac{\varrho_1}{\varrho_o} = 1 - \frac{sh(n^{-1}Arsh\ 1/\varepsilon)}{sh(n^{-1}Arsh(1+1/L)/\varepsilon)} = \frac{\tau_o}{\tau_1} \qquad (32)$$

The loop gain is approximately ($L_o \gg 1$)

$$L_o = \frac{1}{n}\left(\frac{\tau_1}{\tau_o} - 1\right)\frac{(2/\varepsilon)^{2/n} + 1}{(2/\varepsilon)^{2/n} - 1} \qquad (33)$$

what is even higher than in the special case for $\varepsilon = 0$. Fig.2.

The parameter ε has not the same meaning here, but determines all other parameters by relations similar to (20), (21) and (22).

The amplifier pole distribution in the latter case is very similar to the pole distribution of a transfer function which fulfills Lucacs-Szasz condition of monotonic response[5]. Such a function has equidistant poles on the line. Thus the overshoot in the last case with complex poles cannot be very large.

A practical question arrises what will happen when the loop gain falls outside prescribed the limits $\Delta L = L_{max} - L_{min}$, which is $\Delta L = 0$ for the last two considered cases.

For a moderate gain departure from the limits $(0, 2L_o)$ the pole distribution will change into a thin ellipse with its major axis parallel to the real axis in case a) into a small circle with a centre at $-\varrho_o$ in case b), and into thin ellipse with its major axis parallel to the imaginary axis in case c).

Thus one cannot expect a radical change the step response in spite of a qualitative change of the pole distribution. This makes all considered cases suitable for amplifier realization.

Rise time and gain of amplifiers

The simplest way to determine the rise time of considered amplifiers is to use the Elmore's definition but expressed by poles[3]. It can be applied also in the last considered case in spite of complex poles because the expected overshoot cannot be very high.

The rise time is given by

$$\tau^2 = 2\pi \sum_1^n \frac{1}{q_k^2}$$

from which it follows:

a) for real poles

$$\tau^2 = 2\pi \frac{1}{\varrho_o^2} \sum_1^n \frac{1}{(1-(\alpha/\varrho_o)\cos 2k\pi/n)^2} \qquad (34)$$

$$\tau^2 \doteq \frac{2\pi n}{\varrho_o^2}\left(1 + \frac{3}{2}\left(\frac{\alpha}{\varrho_o}\right)^2\right) \qquad (35)$$

b) for the special case $\varepsilon = 0$; $\alpha = 0$

$$\tau^2 = \frac{2\pi n}{\varrho_o^2} \qquad (36)$$

c) for complex poles (n=2m+1)

$$\tau^2 = \frac{2\pi n}{\varrho_o^2}\left[1+2\sum_1^m \frac{1-(\lambda/\varrho_o)^2\sin^2 2k\pi/n}{(1+(\lambda/\varrho_o)^2\sin^2 2k\pi/n)^2}\right] \quad (37)$$

$$\tau^2 \doteq \frac{2\pi n}{\varrho_o^2}\left(1 - \frac{3}{2}(\frac{\lambda}{\varrho_o})^2\right) \quad (38)$$

The pole region æ and λ influence rise time. However this influence is small for $æ < 0{,}3\,\varrho_o$. A wider pole region in case a) is not interesting. However in case c) rather fast amplifiers are obtained using a wide complex pole region ($\lambda > \varrho_o$). The allowed loop gain is then higher since it is increasing with λ.

For the determination of the required number of stages of an amplifier with a given rise time and gain, the figure of merit of the electronic elements is essential. The amplifier transfer function can be expressed by

$$G(p) = \frac{K}{\prod_1^n (p-q_k)} = \frac{K}{Q_n^*(p)} \quad (39)$$

where $Q_n^*(p)$ is a polynomial with leading coefficient $a_n=1$. Such a function for $p\to\infty$, behaves like $G(p)\sim K/p^n$. For a cascade of stages or feedback pairs the transfer function will behave in the same way. The coefficient K will have a value

$$K = F_1\cdot F_2 \ldots . F_k = F^n \quad (40)$$

where F_k are electronic element figures of merit and F is their geometrical average value. The amplifier gain is then

$$G_o = G(0) = \frac{F^n}{Q^*(0)} \quad (41)$$

A transformation of polynomial $Q_n(p)$ to $Q^*(p)$ with $a_n^*=1$ may also be made by letting $p\to\infty$, what gives for the polynomial $Q_n(p) = \varepsilon L_o T_n(ap+b)$ the form

$$Q_n(p)\sim \varepsilon L_o a_n a^n p^n$$

This determines the coefficient of the highest degree term. Thus

$$Q^*(0) = \frac{Q_n(b)}{\varepsilon L_o a_n a^n} = \frac{T_n(b)}{a_n a^n} \quad (42)$$

Using relation (20) and $a_n=2^{n-1}$ one obtains

$$G_o \doteq \frac{a_n a^n\cdot F^n}{T_n(b)} = \frac{F^n}{\varrho_o^n}\,\frac{(2\varrho_o/æ)^n}{2\mathrm{ch}(n\,\mathrm{Arch}\,\varrho_o/æ)} \quad (43)$$

or more approximately for case a)

$$G_o \doteq \frac{F^n}{\varrho_o^n}\,\frac{1}{1-n(æ/2\varrho_o)^2}\,, \quad (44)$$

case b)

$$G_o = \frac{F^n}{\varrho_o^n}\,, \quad (45)$$

case c)

$$G_o \doteq \frac{F^n}{\varrho_o^n}\,\frac{(2\varrho_o/\lambda)^n}{2\mathrm{sh}(n\,\mathrm{Arsh}\,\varrho_o/\lambda)} \doteq \frac{F^n}{\varrho_o^n}\,\frac{1}{1+n(\lambda/2\varrho_o)^2} \quad (46)$$

Using the expressions for the rise time and gain one determines a parameter required for amplifier design. Let us take special case b) of an amplifier with multiple pole, one obtains using (36) and (45)

$$G_o = (F\tau_o)^n = (\frac{F}{\sqrt{2\pi n}})^n \text{ or } (\frac{F}{\sqrt{2\pi}}) = nG^{1/n} \quad (47)$$

The system order or number of stages is implicit in this relation. A diagram based on this relation is given in Figure 3 from which the required number of stages can be determined. Once n is obtained from specified electronic element parameters and all other amplifier parameters can be determined from relations in the text.

An interesting conclusion follows from consideration of the optimum number of stages. By maximizing the loop gain for a given dominant time constant. Using (45) and (26) one obtains

$$G_o = (\frac{F}{\varrho_o})^n = (\frac{F}{n\,\varrho_1 L})^n \text{ or } L = \frac{F/\varrho_1}{nG^{1/n}} \quad (48)$$

The maximum L is for

$$n_o = \ln G \quad (49)$$

The fastest conventional cascade of stages has a double number of stages, i.e. $n_o = 2\ln G$. It follows that feedback amplifier with a multiple pole has a $\sqrt{1/2}\,e^{1/2} = 1{,}17$ times larger rise time than a cascade amplifier for the same gain. The fastest stage in feedback amplifier has a gain ($L_{omax} = F/\varrho_1 n_o e$)

$$A_n \doteq \frac{F}{2\varrho_o} = \frac{F}{\varrho_1 2n_o L_{omax}} = \frac{e}{2} = 1{,}36\,.$$

Calculation of amplifiers in case a) c) could be based on the given calculation

for a multiple pole if $\alpha/\varrho_o < 1/2$ and $\lambda/\varrho_o < 1/2$ using the corrected values for the rise time which are

a)

$$\tau_c^2 = \frac{\tau^2}{1+3(\alpha\tau_o)^2/2} \quad \text{or}$$

c) (50)

$$\tau_c^2 = \frac{\tau^2}{1-3(\alpha\tau_o)^2/2}$$

and the corrected values for the gain.

a)

$$G_c = (F\tau)^n(1-n(\alpha\tau_o)^2/4) \quad \text{or}$$

c) (51)

$$G_c = (F\tau)^n(1+n(\lambda\tau_o)^2/4) \ .$$

Conclusion

The considered transfer functions enable a comparatively simple realization of feedback amplifiers with a high loop gain, short rise time and a monotonic response.

The open loop amplifier can be realized by a cascade of stages, Figure 4b. The required complex poles can be obtained by shunt inductive peaking. The transfer function zero of such a stage has to be cancelled by one stage without peaking.

A more convenient realization of the open loop amplifier is a cascade of feedback pairs which have a two pole transfer function. The required complex poles are obtained with a proper feedback of each pair. The stage with the dominant time constant is a stage with a high DC gain. The block diagram of such an amplifier is shown in Figure 4c. Such design has the advantage of a partial ellimination of parameter variations already by local feedbacks and a realization without inductances. The latter makes an integrated circuit realization of such amplifiers possible.

The use of local feedback together with the maximum loop gain of the overall feedback results in very linear amplifiers with a high gain stability.

References

1. Truxal J.G., Automatic Feedback Control System Synthesis, McGraw Hill Co., N.Y., 1955.
2. Fränz K., Gegenkoppelte überschwingfreie Widerstandsverstärker, Archiv der Elektr.Übertragung, Band 11 (1957)Heft 4.
3. Babić H., An Optimum Transfer Function for Amplifiers with Nondecreasing Step Response, Proc. of Int.Symp. on Network Theory, Belgrade 1968, p. 66.
4. Cauer W., Synthesis of Linear Communication Networks, McGraw Hill Co.,N.Y.1958.
5. Zemanian A.H., The Properties of Pole and Zero Location for Nondecreasing Step Responses, Trans. AIEE, Commun. and Electronics, Sept. 1960.

DISCUSSION

Koeman :- Can you tell me something about practical results you have obtained on rise--time, gain -bandwidth product and maximum gain that can be used with 100% feedback ? I would suggest that your analysis would fail when there is time delay in the amplifier, for example when using transistors. The root-locus method, as an analysing procedure, to locate the poles of the closed loop function, will give information about the location of these poles. Generally speaking, the gain-bandwidth product determines the stability of an amplifier with feedback, neglecting the stability of the feedback loop. It appears that you need a large number of poles for realising your theory.

Babić : - The analysis is purely theoretical and I have not attempted to make transistor amplifiers of this form. One will encounter difficulties when time delay exists. However it should be clear that local feedback simplifies the problems in a multistage amplifier with overall feedback. In order to be able to analyse the problem and derive the optimum condition it was necessary to consider only an ideal situation in which the number of poles and zeros was arbitrarily defined. This is nearer the practical situation when using vacuum tube amplifiers than when using transistors. The solution in the paper then gives a feedback amplifier which is as fast as a cascade of RC amplifiers without feedback. In a complicated situation, as in the case of transistor amplifiers, the proposed solution of the optimum number of stages my not apply.

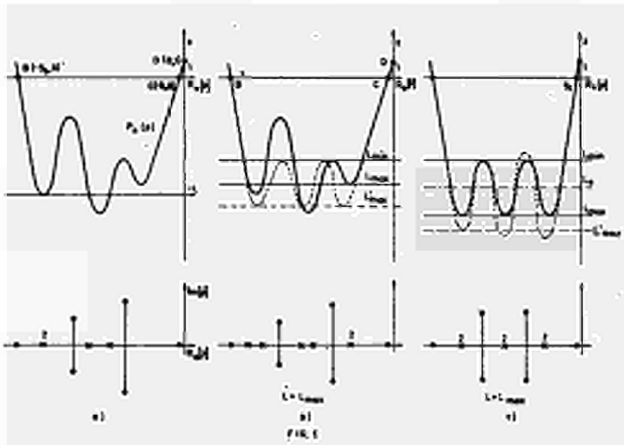

Fig. 1 - Maximum loop gain of feedback amplifiers.

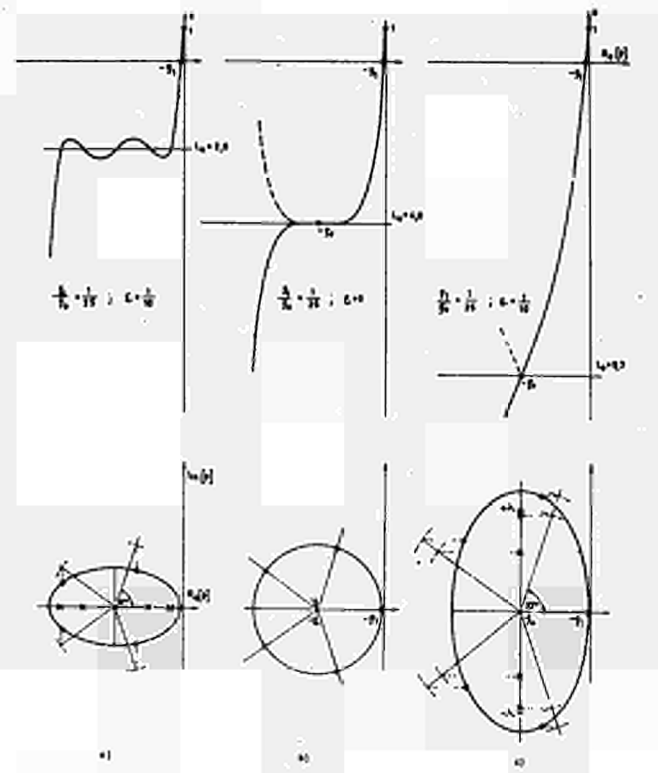

Fig. 2 - Maximum loop gain of amplifiers.

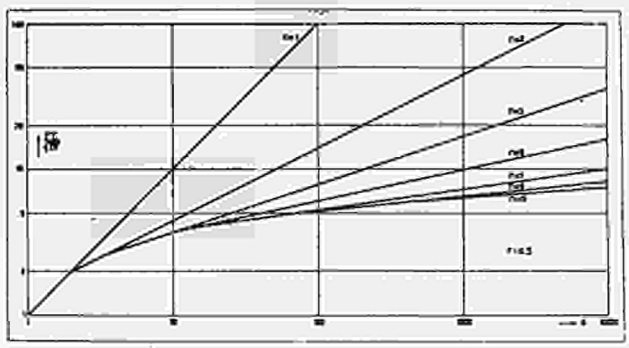

Fig. 3 - Maximum loop gain of amplifiers.

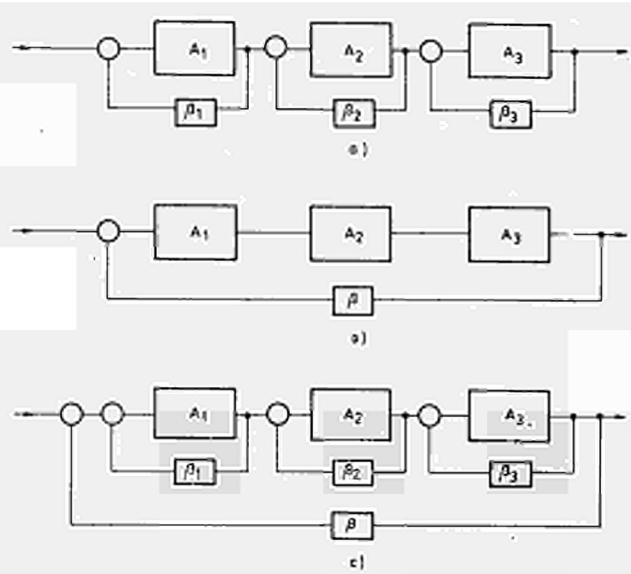

FIG. 4.

Fig. 4 - Maximum loop gain of amplifiers.

AN OPERATIONAL PULSE AMPLIFIER WITH FET INPUT

R.Patzelt, R.Posch

Österreichische Studiengesellschaft für Atomenergie
Reaktorzentrum - Seibersdorf, Elektronik - Institut

Abstract:

The important characteristics of a linear pulse amplifier are defined. An operational pulse amplifier with FET-input has been designed. The differences and advantages compared to similar transistor circuits are discussed. The FET circuit is suitable for general applications because of its high input impedance, dynamic stability, linearity of open loop gain and overload characteristics.

1. Definitions of important characteristics:

Linear and stable pulse amplifiers consist of an operational amplifier circuit with appropriate feedback. The important characteristics and specifications of the operational amplifier for this purpose are the following:

1. Open loop gain, as function of the frequency.
2. Useful output signal range (voltage- and currentswing).
3. Output slew-rate (maximum voltage change per unit-time).
4. Input-drift for constant output (versus temperature, supply voltage, time).
5. Nonlinearity, e.g. gain as a function of output level.
6. Gain-stability, gain as a function of temperature, supply voltage, time.
7. Input common mode rejection ratio.
8. Permissible input voltage range, differential and common mode.
9. Input-characteristics: impedance, leakage current, capacity.
10. Signal-delay between input and output.
11. Overload-recovery-time.

Generally the specifications of the feedback circuit are improved with respect to the open loop-circuit by a factor equal to the excess amplification (the ratio between open loop gain and closed loop gain sometimes called loop-gain). A more thorough treatement shows that the other specifications have also an important influence. The input drift for instance depends on the drift of each single stage, divided by the preceeding gain.

For the amplification of narrow pulses containing frequencies in a narrow band, only the excess gain in this frequency range is important. The nonlinearity of the open loop circuit is also very important, since the nonlinearity of the closed loop amplifier is given by the openloop-nonlinearity divided by the excess gain. The limit for the rise time at full output amplitude is given by the slew-rate and the output voltage-range.

2. Bode-Plot (gain/frequency):

Practically a pulse amplifier consists in most cases of a differential amplifier as a first stage, a buffer stage, a second amplifying stage and an output buffer stage. The two buffers may be ommitted. For a bipolar output range the second stage must be symmetrical with two complementary transistors. In this case the characteristics gain versus frequency (Bode-Diagramm) of the open loop circuit shows normally a constant gain up to a first cut-off-frequency. Towards higher frequencies the gain decreases with a slope of 20 db per decade until a second cut-off-frequency. This is followed by a portion with a slope of 40 db per decade. This is true, when the two amplifying stages have two different time-constants and the other time-constants of the buffer stages etc. are insignificant. The corresponding characteristic phase-shift versus frequency has three portions with a phase-shift of zero, 90 and 180 degrees. The transitions between these parts correspond to the two cut-off-frequencies mentioned above.

As it is well known, it is impossible to reduce the gain of the feedback circuit below the value for the open loop-gain at the second cut-off-frequency (without additional frequency compensation), if overshoot or oscillations are to be avoided. The open loop gain divided by the feedback ratio must not be higher than 1 at the frequency, at which the phase shift exceeds 180 degrees. Practically there is always an additional phase-shift, that increases linearly with the frequency caused by the propagation delay through the stages of the amplifier. If the conditions mentioned above are not fulfilled, so called frequency-compensation is to be applied. Especially series combinations of R and C are used to decrease the gain and to improve the phase-shift-characteristics in a certain frequency domain.

From that it follows, that the open loop circuit should be designed so that the second cut-off-frequency is as high as possible. The gain at this point should be equal to the gain of the feedback-circuit.

From this frequency downwards the gain increase with 20 db per octave. Pulse amplifiers are used normally for pulses, that have a width of ten to hundred times the rise time of the amplifier. The frequencyband used is therefore very near to the second cut-off-frequency. The excess gain in this frequencyband is given by the ratio of the second cut-off-frequency to this frequencyband, since the open loop gain must not increase by more than the same ratio, as mentioned above.

the open loop gain must not increase by more than the same ratio, as mentioned above.

The value of the open loop gain at lower frequencies has only an indirect influence on the dc-stability of the circuits. In pulse amplifiers normally only the value of the input drift is an important specification, the actual dc amplification being of no interest.

Since all drift values must be referred to the input the amount of feedback has no influence, the values for the open loop and closed loop configuration are the same. Primarily the input drift is given by the first stage. The effect of the both following stages (first buffer, second amplifier) is reduced by the gain of the first stage only that of the output buffer by the full open loop gain.

The design of the circuit is strongly influenced by the slew rate that is necessary to obtain the rise time for full output-amplitude. If the output-buffer can deliver a high current and the capacitive load at the output is not too high, the slew-rate is defined by the values of the second amplifier stage. The slew-rate in volts per µsec is given by the maximum current in µA divided by the capacitive load given in pF. Typically the gainband-width-product of fast transistors has a high value only in the range from ten to twenty mA collectorcurrent. Therefore the capacitive load of the output point of the second amplifier stage must be very low, to obtain a slew-rate above 100V/µsec. From that the value of the collector load resistor of the second stage is practically determind and gain and cut-off-frequency as well.

The ratio of both cut-off-frequencies must be larger than the dc-excess-gain. It is practically impossible to obtain a sufficiently high value of open-loop-gain, if the first amplifier stage is designed so as to have a cut-off-frequency high above that of the second stage. Therefore the frequency-characteristics of the first stage governs the important part of the Bode-Plot of the open-loop-gain. The frequency-compensation is preferably to be applied at this point, if the exact values are not to be adjusted very critically.

3. Other design parameters (linearity, drift, stability).

The one big difficulty in the design of amplifiers is the fact, that the input and the output impedance as well as the gain (transconductance) of transistor-stages are even in the unsaturated range a function of the emitter-current. Also the input-capacitance base-emitter has a high not clearly defined and current-dependent value. Only with special precautions it can be avoided, that the dc-open-loop-gain A_o (w = o) and the cut-off-frequencies in the Bode-plot change their values by a factor of 2 or even more within the output-signal-range.

Following to this considerations the cut-off-frequencies of the open loop gain must not change with the output amplitude. If this is fulfilled, also the nonlinearity of the open loop gain is small. Therefore the excess gain at low freuqencies need not be very high, to obtain a good linearity for the closed loop circuit. As mentioned earlier the effective excess gain for fast pulses can not be very high (because of the shape of the Bode-plot). In this frequency range near the second cut-off-frequency a good linearity is only obtainable if the nonlinearity of the open loop gain is not too high. These facts are very important for the use of FET stages, since the transconductance and the gain of FET stages are much smaller, but also the nonlinearity is smaller by about the same factor. Typical values for the change of the gain per millivolt input voltage are 40% for transistors and 0,1% for FET. The transconductance at comparable conditions is 100 mA/V for transistors and 5 mA/V for FET. These effects can cel each other and the advantage remains that the FET has a very high input impedance given by its gate-capacitance of a few pF.

The overload characteristic of an amplifier is also extremely important for pulse measurements. The requirements are not easy to define and it is very difficult to obtain good results. The input should withstand overloading signals, at least up to the full amplitude range of the output. When the overloading input signal has disappeared the circuit should recover into its linear regime within a short time. There exist two primary sources for the delay of the recovery: changes of the "dc-working-conditions" during the overloading-signal and saturation effects in the transistors. The first effect can be avoided, if no coupling and smoothing capacitors are used, that can change their voltage during the time the input is overloaded. Saturation is difficult to avoid in the input stage if transistors are used. With FET it becomes easy, since they do not show saturation effects themselves and additionally passive limiting networks can be used at the inputs because of the very high input-impedance. By proper design of limiting networks with diodes it can be prevented that the following stages are driven into saturation at all.

The dc drift of the amplifier must be small, preferably 0,1 mV or less per °C. The input drift of FET is different from that of transistors. It depends strongly on the difference of the actual gate source voltage from the cut-off (pinch-off) voltage. Since this value differs for a given source current up to 1 V or more for different FET of the same type, matched temperature compensated pairs of FET must be used for the input stage. Additionally the common source current must be stabilized to obtain a good stability and a good common mode rejection ratio. Practically matched pairs of transistors and FET have equivalent drift-characteristics and component prices. The only important difference is, that matching of the two transistors for the differential amplifier is much more

important for FET than for transistors.

4. Design of the actual circuit:

According to all the principles mentioned above two versions of an operational amplifier for pulse amplification have been designed and tested. Both consist of a differential amplifier as first stage, an emitter-follower as buffer stage, and a complementary pair of pnp and npn transistors driving a common load resistor through their collectors, as second amplifier stage. The second version that has been designed as high current output buffer has an additional complementary output emitter follower.

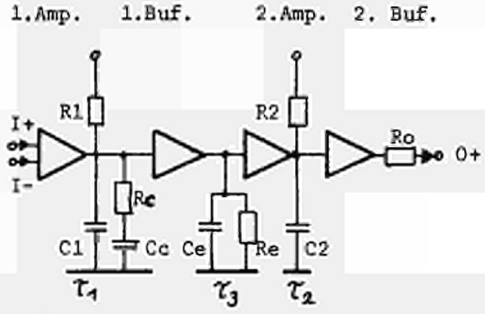

Fig. 1. Block-diagram, with time-constants

Fig. 1 shows the block-scheme with the resistor, capacitor and stray-capacitances, that define the gain/frequency-characteristic. Both amplifier-stages are to be considered as current-sources, the buffers as voltage-sources. The first buffer is a normal emitter-follower, its output-impedance is neglected; 3 becomes effective only for steep negative going signals, that cut 4 off. C1, Ce, C2 are the stray-capacitances connected to the corresponding outputs. Rc, Cc are applied for frequency compensation, the combination with R1, C1 defines the shape of the Bode-plot up to the second cut-off-frequency (corresponding to R2, C2).

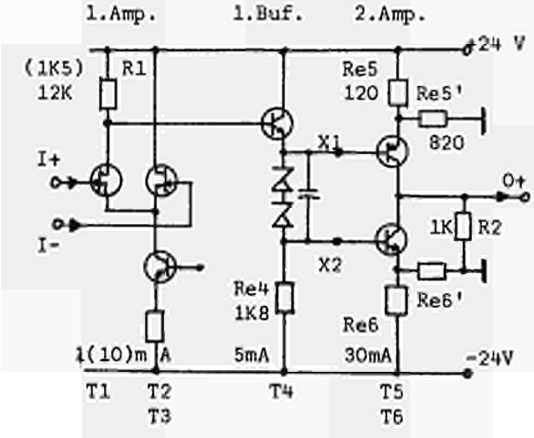

Fig. 2. Amplifier without second buffer

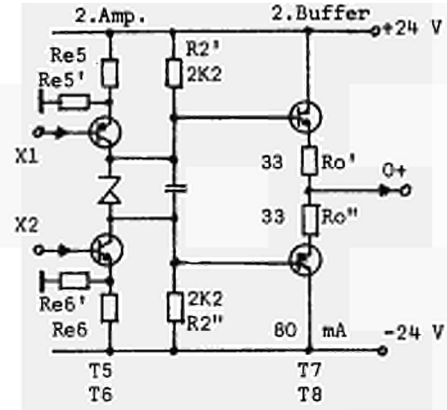

Fig. 3. Second amplifierstage with output-buffer.

The circuits (fig. 2 and 3) are dc-coupled throughout to keep the recoverytime after overloading signals short. The emitter-follower (T4) between the both amplifier-stages ensures, that the loading impedance for the first stage is high and constant. The chain of Z-diodes allows to shift the level 30 V downwards for the npn-transistor (T6) of the complementary second stage. By that the limiting levels for the output-voltage are as high as ± 14V and the output-range of ± 10 V can be used without any restrictions.

Both transistors of the second stage (T5,T6) have an unbypassed voltage divider (Re5 + Re5' and Re6 + Re6') in the emittercircuit with an output-resistance of 100 Ohm. The stage-gain is therefore only 20, but the cut-off-frequency is high, input-impedance and gain do not change very much in the specified output-range. Also beyond the limiting output-level the saturation of the transistors is kept low, since the emitter-current is limited.

The current in the emitter-follower between both stages must be high enough, that it is not turned off by negative-going signals (positive signals at the output). The Z-diodes must have a low temperature-coefficient, since the gain of the first stage is not high.

The first stage consists of a differential amplifier, because only so a low temperature-drift can be obtained and two equivalent inputs are available. Also the nonlinearity of this stage is small, because changes of the transconductance in the both transistors compensate each other as long as the currents are nearly equal. A current-generator is used in the common-source circuit to obtain a good common-mode-rejection.

Different elements for this differential pair have been tested:

1. A low-current, medium gain, matched FET-pair type TIS 69.
2. Two high-current, high gain FET, type 2N 3972.
3. A high frequency transistor pair 2 C 111 for comparison.

Used as noninverting feedback-circuit they have the following common characteristics: Amplification: + 10, linear output range from + to - 10 V, permissible output-load 1 kOhm or more, permissible input-range ± 10 V, wideband-noise about 70 µVeff.

The first configuration is very well suited for general applications. The risetime is a bit slower (60 nsec) as for the transistor-stage, but input drift and linearity are practically the same. The second circuit is slightly faster than the transistor stage, but a bit worse in the drift; it has an extremely high slew-rate of 600 V/µsec.

The important property of the FET-stages is their very high and constant input-impedance, well above 100 MOhm, parallelled by a few pF. This allows a very simple design of attenuators RC/CR and DL frequency-filters between the stages in an amplifier. No current flows into an overload input causing dc-shifts. By a proper design of internal diode-limiters the saturation of anyone of the transistors can be avoided reducing the recovery-time to a minimum. In active, feedback filter-circuits much higher R-values and much lower C-values can be used than with the usual transistor-stages.

The circuit shown in Fig. 3 has an additional symmetrical emitter-follower as output-buffer. With 100% voltage feedback it delivers through 50 Ohm into a load of 50 Ohm up to 100 mA at both polarities with a linearity of about 3.10^{-4}. The input-impedance has the same high value as the first circuit mentioned above. It is therefore very useful as buffer for precision pulse-generators, linear gates, etc.

Acknowledgement:

Mr. Waschka and Mr. Fritz designed and tested some of the circuits; the theoretical considerations include work of Mr. Drimmel, Mr. Attwenger Mr. Buschbeck, Mr. Halling, Mr. May and Mr. Moder.

Typical characteristics of the 3 versions

	1.: TIS 69	2.:2x2N3972	3.: 2C 111
Open loop gain	225	120	580
Open loop cut-off frequency MHz	0,8	2	1,8
Input voltage drift temperature µV/°C	80	700	60
Slew-rate V/µsec (+/-)	310/140	450/660	330/300
Risetime nsec (A_{CL} = +10)	60	30	30
Linearity (integral) 10^{-3}	<0,5	<0,5	0,7
dc-common mode rejection ratio	45.000	600	2.300
common mode feedthrough (open loop)	0,2	0,3	0,3

DESIGN OF A WIDEBAND PULSE AMPLIFIER WITH LINEAR INTEGRATED CIRCUIT μA 702A USING FREQUENCY COMPENSATION TECHNIQUE

N.P.Lero , P.B.Frantlović
Institute of Nuclear Sciences "Boris Kidrich"
Vinča-Beograd , Yugoslavia

The possibility has been considered to use a commercial linear integrated device for amplification of proportional radiation detector pulses in pulse counting assemblies. Principal requirements with respect to the amplifier gain and bandwidth have been specified, and choice has been made of the most suitable linear integrated device. Stability analysis of the chosen device has been carried out,and appropriate frequency compensation made it possible to satisfy the imposed requirements. Experimental results are in good conformity with analytical conclusions.

1. Introduction

Counting assemblies with proportional pulse radiation detectors are in wide use for various nuclear measurements. Digital operations in these assemblies are performed recently using digital integrated circuits. It is reasonable,therefore,to consider the use of adequate integrated circuits to perform the necessary linear operations (amplification,pulse discrimination) within the counting system. Authors have been concerned in this paper with the problem of amplification of pulses from proportional radiation detectors. Taking into account all the requirements which the pulse amplifier included in the counting system should satisfy,the device μA 702A has been chosen among the SGS-Fairchild linear integrated circuits as the most convenient. All further investigations have been carried out on this device,in order to obtain gain and bandwidth required for the intended application.

2. Detector signal considerations and choice of the integrated amplifying device

Fig.1 represents the block-diagram of a typical pulse-counting assembly,with specified blocks for appropriate linear and digital operations.

The operation of counting is preceeded by the linear treatment of the detector signal,in order to obtain standardized signal suitable for driving a scaler or a counting-rate meter. If a fixed discriminator sensitivity is assumed,basic amplifier characteristics can be defined considering only the detector signal.

Proportional pulse radiation detector can be regarded as a current source,and the primary form of its output signal is a current pulse :

$$I = I(t) \qquad (2.1.)$$

The information about the energy of radiation,absorbed within the sensitive volume of the detector,which is of interest in nuclear spectrometry,can be obtained employing the linear relationship with the electrical charge developed within the detector :

$$E_A \sim \int_{t_1}^{t_2} i(t)\,dt = Q \qquad (2.2.)$$

where E_A denotes the energy of radiation absorbed in the detector due to the impact of a nuclear particle. The time interval (t_2-t_1) denotes the total duration of the resulting current pulse. The integration denoted by Eq.2.2. is usually performed by the detector output circuit with sufficiently long RC constant.

In case of pulse counting,where the information on radiation energy is not of primary importance,the detector signal can be treated either in its primary form (Eq.2.1.) (Fig.2a) or in the integral form (Eq.2.2.)(Fig.2b).

2.1. Treatment of the detector signal in its integral form

Due to RC time constant of the detector output circuit,which can be made sufficiently long,the obtained voltage pulse may have considerably longer duration than the primary detector current pulse. Further treatment of the voltage pulse can be carried out with an amplifier having moderate bandwidth, of the order of 2-3 MHz,but a relatively high amplifier input impedance is required. A serious drawback of this method is the pile-up effect at higher counting rates.

2.2. Treatment of the detector signal in its primary form

If the detector pulse is treated in its primary form,without preliminary integration,pile-up condition cannot occur even with very high counting rates,and a low input impedance amplifier can be employed. However,the amplifier bandwidth of about 20 MHz is required with typical detectors[1].

Having in mind characteristics and performances of available linear integrated devices (as well as some application reasons),this second method of detector signal treatment has been accepted here. In that way a low input impedance device can be used,and the requirements for gain and bandwidth have been fixed at 30-40 dB and 20 MHz,respectively,taking into account character-

istics of the typical radiation detectors and the input sensitivity of available integrated discriminators (e.g. 2 mV for the μA 710 SGS-Fairchild differential comparator). The device μA 702A (SGS-Fairchild)[2] has been accepted to perform the required pulse amplification , and the appropriate analysis has been carried out in order to achieve the imposed performance characteristics[2].

3. μA 702A Stability Analysis and Bandwidth Limitations

The amplitude vs.frequency characteristics of the integrated amplifier μA 702A , supplied by the manufacturer (Fig.3),can be approximated,using Bode method,by straight-line segments differing in slope by 6 dB/oct. Break points on the approximated characteristic designate the transfer function poles (the concerned transfer function does not contain zeros,due to negligibly short time constants of the interstage coupling elements within the integrated circuit). According to the above consideration the open-loop transfer function of the integrated amplifier μA 702A may be written as follows :

$$A = A(s) = \frac{A_o}{(S-S_1)(S-S_2)(S-S_3)} = \frac{K_1 A_o}{(S+2\pi\cdot 0.8)(S+2\pi\cdot 4)(S+2\pi\cdot 40)} \qquad (3.1.)$$

where $A_o = 2600$; $f_1 = 0.8\,MHz$; $f_2 = 4\,MHz$; $f_3 = 40\,MHz$

$K_1 = 8\pi^3 \cdot f_1 f_2 f_3 = 128\cdot 8\pi^3$

Introducing the negative feedback with the feedback factor β , the closed-loop voltage gain is given by :

$$A_r = \frac{A}{1+\beta A} \qquad (3.2.)$$

where A is defined by Eq.3.1.

With purely resistive feedback used in this case, β is a real number. The device μA 702A operates in operational amplifier configuration (Fig.4.).

For the amplifier stability analysis graphoanalytical root-locus method has been adopted. The initial expression on which the method is based is the so-called characteristic equation :

$$1 + A\beta = 0 \qquad (3.3.)$$

(A β - loop gain).

The denominator of the expression (3.2.) appears at the left side of this expression.It can be shown that the zeros of the expression (3.3.) are at the same time poles of the A_r function[3,4]. The equation (3.3.) may be represented in the following form :

$$Fe^{-j\varphi} = e^{j(2k+1)\pi}$$

$$k = 0, \pm 1, \pm 2, \ldots; \quad A\beta = Fe^{-j\varphi} \qquad (3.4.)$$

Values of s which satisfy the characteristic equation must satisfy the following conditions :

$F = |A\beta| = 1$ (magnitude cond.) (3.5.)

$-\varphi = (2k+1)\pi$ (angle cond.) (3.6.).

The root-locus represents a plot of all the s-plane points which satisfy conditions (3.5.) and (3.6.),with the gain A as a variable parameter. The plot can be calibrated in terms of βA,and the range of the loop-gain,in which the amplifier is stable,can be read directly from the diagram. Geometrically,it is that part of the plot which lies in the left s-halfplane. An advantage of the root-locus method lies in the fact that it is possible to determine directly from the plot what kind of corrections one should make on the amplifier in order to have it meet the defined requirements.

Root-locus diagram has been obtained by the routine method for the integrated amplifier μA 702A without frequency compensation. From the obtained plot (Fig.5) it can be concluded that the maximum allowable degree of feedback which can be used,if the amplifier is to remain stable,is 36,5 dB. This means that the uncompensated amplifier with purely resistive feedback can satisfy the requirement with respect to gain,put in Sec.2. From the amplitude and phase plot (Fig.3) it can be concluded,however,that the maximum allowable phase-shift of 180° is reached at the frequency of 14 MHz,so that the requirement of Sec.2 with respect to bandwidth cannot be satisfied with uncompensated amplifier.

4. Obtaining the Required Bandwidth Using Frequency Compensation Technique

It is evident from the previous section that the requirement for 20 MHz bandwidth can be satisfied only if some kind of frequency compensation is applied,which would result in convenient reduction of the natural roll-off in amplitude characteristic,followed by the appropriate reduction of the phase lag. Under these conditions it would be possible to obtain the required bandwidth, keeping the amplifier in the stable domain.

In this case the "lead" compensation technique has been chosen,because the device μA 702A is supplied with terminals convenient for such type of compensation. Compensation network is formed by putting an adequate capacitor across terminals (5) and (6) of the integrated circuit.(Fig.6). This capacitor with the resistive elements incorporated in the integrated circuit forms a high-pass filter network with the equivalent circuit shown in Fig.7. Transfer function of this network may be represented by :

$$A_F(s) = \frac{V_{out}(s)}{V_{in}(s)} = \frac{s+1/T}{s+1/\alpha T} \qquad (4.1.)$$

where $T = R_1'C$ (4.2.)

and $\alpha = \frac{R_2'}{R_1' + R_2'}$ (4.3.).

The amplifier and the compensation network are practically cascaded, so that the resultant transfer function may be written as :

$$A_k(s) = A(s)A_F(s) \qquad (4.4.)$$

where A(s) is defined by Eq.3.1.

Resultant closed-loop gain can be obtained by substituting $A_k(s)$ instead of A(s) in Eq.3.2.

In Bode approximation amplitude characteristic of the compensating network is represented by three straight-line segments with zero,6 dB/oct,and constant attenuation,respectively,and the respective corner frequencies are given,in terms of T and α ,by :

$$f_1 = \frac{1}{2\pi T} \qquad (4.5.)$$

$$f_2 = \frac{1}{2\pi\alpha T} \qquad (4.6.)$$

These corner frequencies can be appropriately positioned by proper choice of two variable circuit parameters. The only variable parameter in the case of the integrated amplifier is the external capacitor C , so that it is practically possible to choose independently only the first corner frequency f_1 , while the other is then automatically determined :

$$f_2 = f_1/\alpha \qquad (4.7.)$$

having in mind that α (4.3.) is invariable for a given integrated amplifier.

For optimum positioning of the corner frequency f_1 it is convenient to use the open-loop root-locus diagram of the µA 702A amplifier (Fig.5.). Corner frequencies f1 and f_2 of the compensation network insert a zero and a pole (respectively) into the resultant characteristic. Consideration has shown that it is convenient to determine the position of the corner frequency f_1 in such a manner that the introduced zero cancels out the pole at 4 MHz in the amplifier transfer function,because this pole,being near the origin,is of considerable influence on the shape of the root-locus diagram. The pole introduced by the corner frequency f_2 has no considerable influence on the shape of the root-locus diagram,being far-off from the origin. Fixing the value of f_1 at 4 MHz and taking into account the values R_1' and R_2' in the compensating circuit,the external capacitor C acquires the value of 11,7pF (α = 0,1 ; f_2 = 40 MHz). With the new pole configuration root-locus diagram for the compensated amplifier has been drawn (Fig.8). It can be seen from the diagram that,with the required closed-loop gain,bandwidth of about 20 MHz can be obtained with the amplifier operating in the range of absolute stability (dominant complex poles of the compensated amplifier are considerably far-off in the left half-plane).

In Fig.9 Bode approximations of the following characteristics are given :

a. Uncompensated µA 702A amplifier open-loop amplitude characteristic;
b. Compensated µA 702A amplifier open-loop characteristic;
c. Compensated µA 702A closed-loop amplitude characteristic;
d. Compensating network amplitude characteristic;

as well as the corresponding phase characteristics. Phase characteristics for cases b. and c. are identical,because the applied feedback is purely resistive.

Resultant characteristics are obtained by algebraic addition of the corresponding log-amplitude and phase characteristics of the amplifier proper and the compensating network.

With the required bandwidth of 20 MHz , the phase margin of 20° and module margin of 5 dB are obtained,which is considered in amplifier theory as quite satisfactory to ensure amplifier stability in case of predictable environmental or component variations.

5. Experimental Results

The results of the above analysis have been verified on the realized amplifier,shown in Fig.10 with indicated component values. Measured amplitude and phase characteristics are in good conformity,in the limits of measuring errors, with those obtained in Sec.4 and given under c. in Fig.9.

Having in mind the intended use of the amplifier,its pulse response characteristics have been separately measured,and the following results have been obtained :

	input	output
rise time	10 ns	19 ns
overshoot	0%	5%
undershoot	0%	10%
voltage gain	/	36 dB

Amplifier bandwidth,calculated on the basis of these results,is approximately 21,6 MHz. Amplifier linear operating range (measured at the output) :

- with negative input signal:0-3000 mV
- with positive input signal:0-800 mV.

Amplifier equivalent noise voltage,reffered to the input,is less than 15 µV r.m.s.

Measurements have been carried out with TEXAS INSTRUMENTS Mod.6605 Pulse Generator and TEKTRONIX Type 661 Sampling Oscilloscope.

6. Conclusion

The results of the analysis, as well as the obtained experimental results, show that the integrated amplifier uA 702A with the appropriate frequency compensation may be used as a wideband amplifier, with the closed-loop gain approximately 40 dB and bandwidth of about 20 MHz. It is suitable for the amplification of pulses from proportional nuclear detectors, and can be used in pulse counting assemblies.

REFERENCES

1. Miwa, H., Kasai, T., Hayashi, H. ; Journal of Nuclear Science and Technology 2 (5) (1965) 183.
2. SGS-Fairchild, The Application of Linear Microcircuits (Handbook) (1966)
3. S.S.Hakim : Feedback Circuit Analysis (book) Iliffe Books, London, 1966.
4. J.J.D'Azzo, C.H.Houpis: Feedback Control Systems Anal. & Synth. (book) Mc.Graw-Hill, New York, 1960.

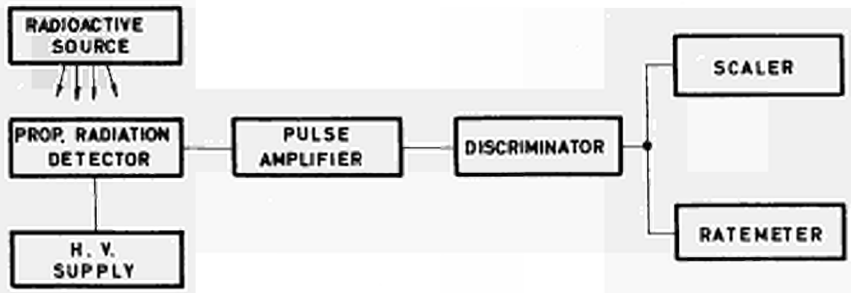

Fig. 1 - Typical pulse-counting assembly block-diagram.

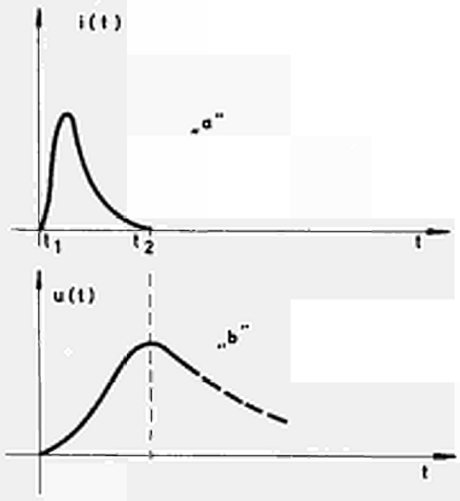

Fig. 2 - a. Pulse radiation detector current signal ; b. integral form of the pulse radiation detector voltage signal.

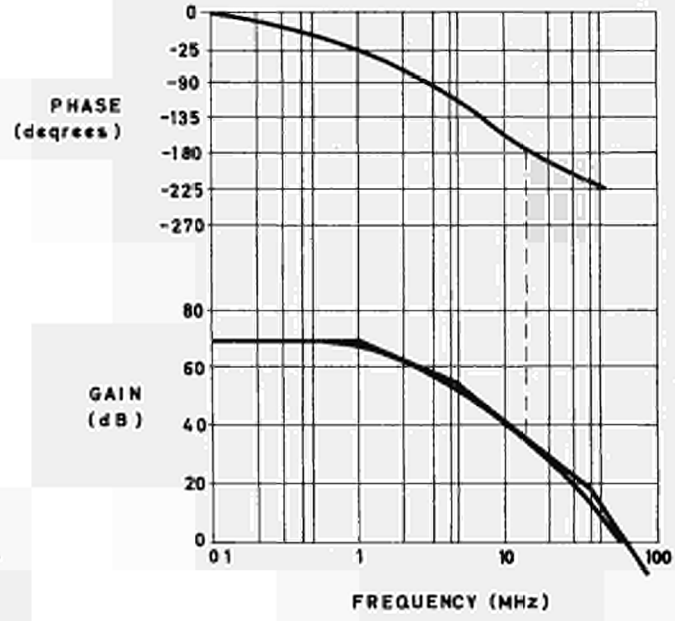

Fig. 3 - µA 702A open-loop amplitude and phase characteristics.

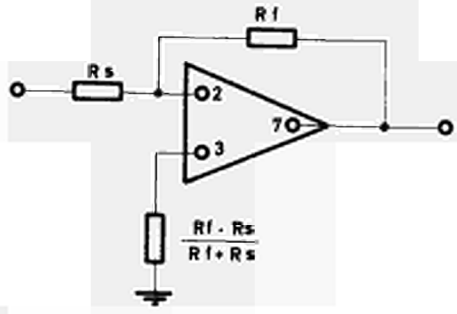

Fig. 4 - µA 702A in operational amplifier configuration.

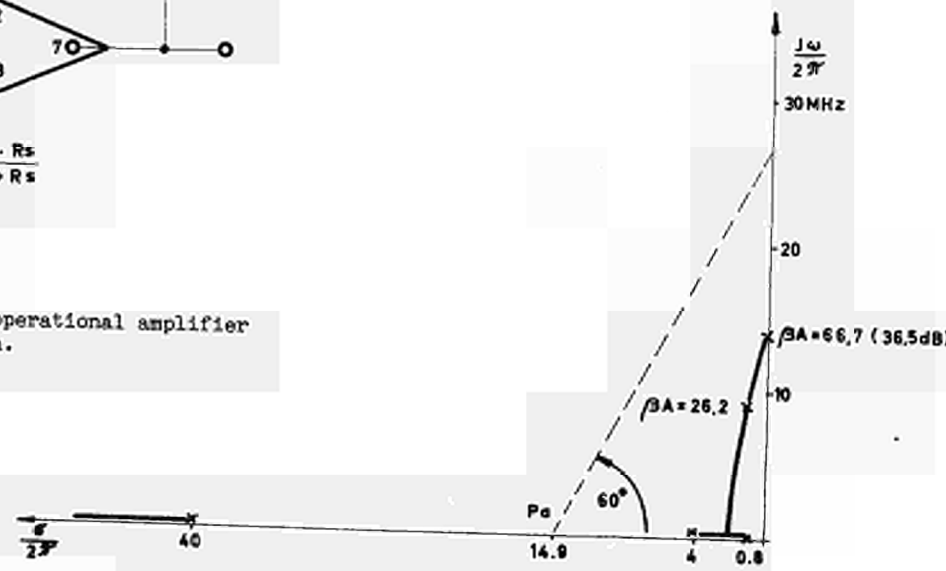

Fig. 5 - Uncompensated amplifier root-locus plot.

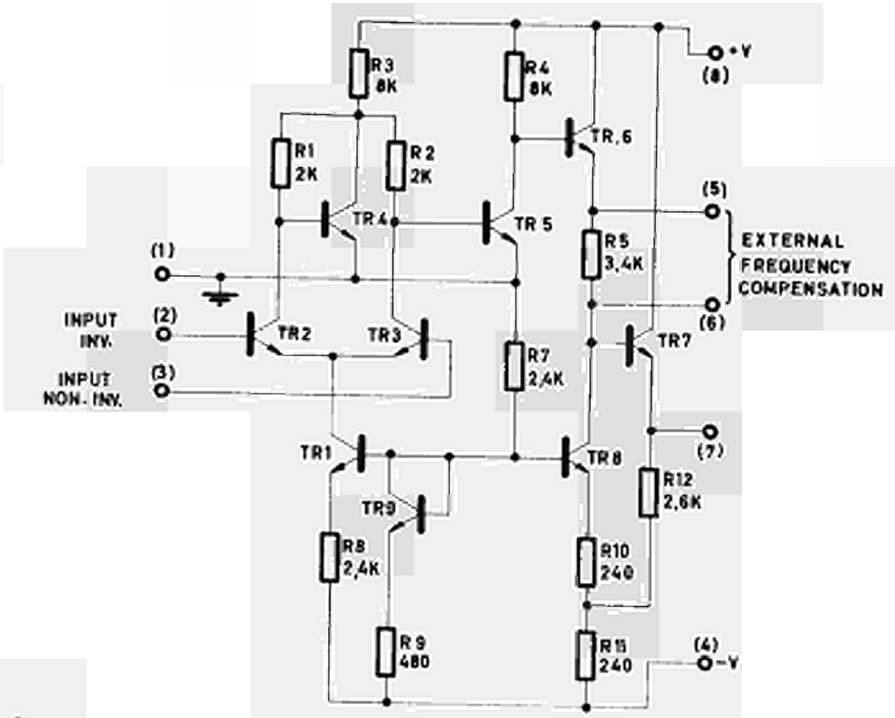

Fig. 6 - µa 702A circuit diagram.

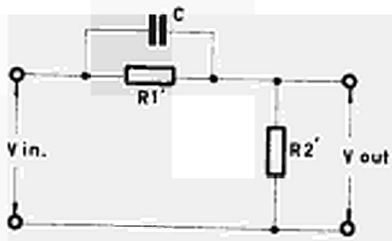

Fig. 7 - Compensating network equivalent diagram

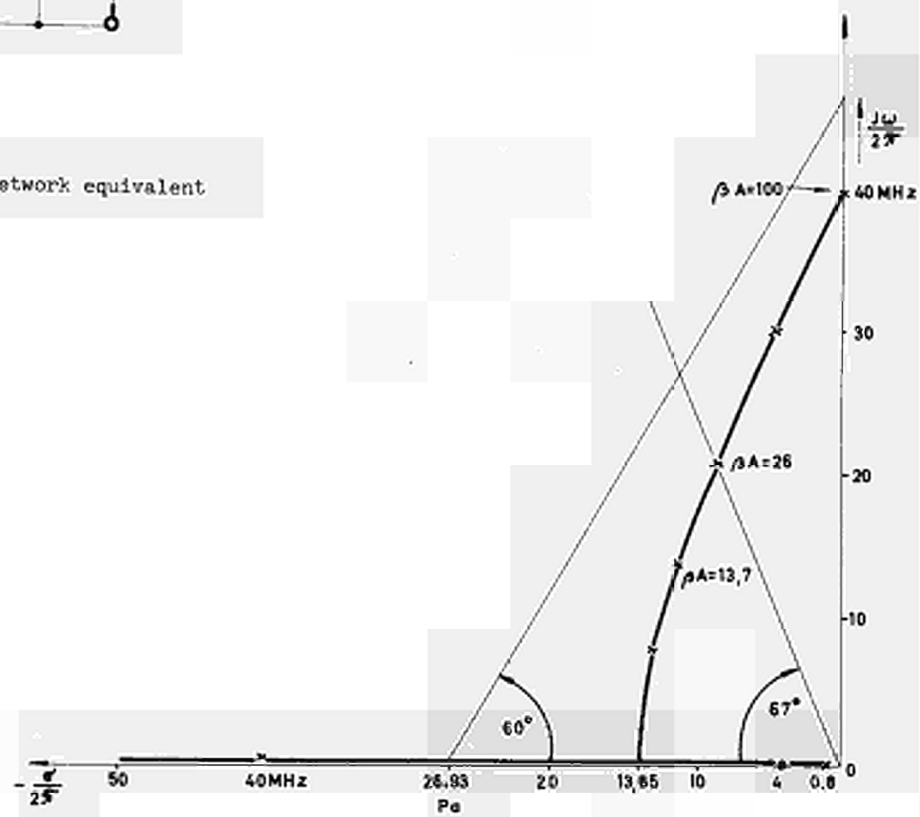

Fig. 8 - Compensated amplifier root-locus plot.

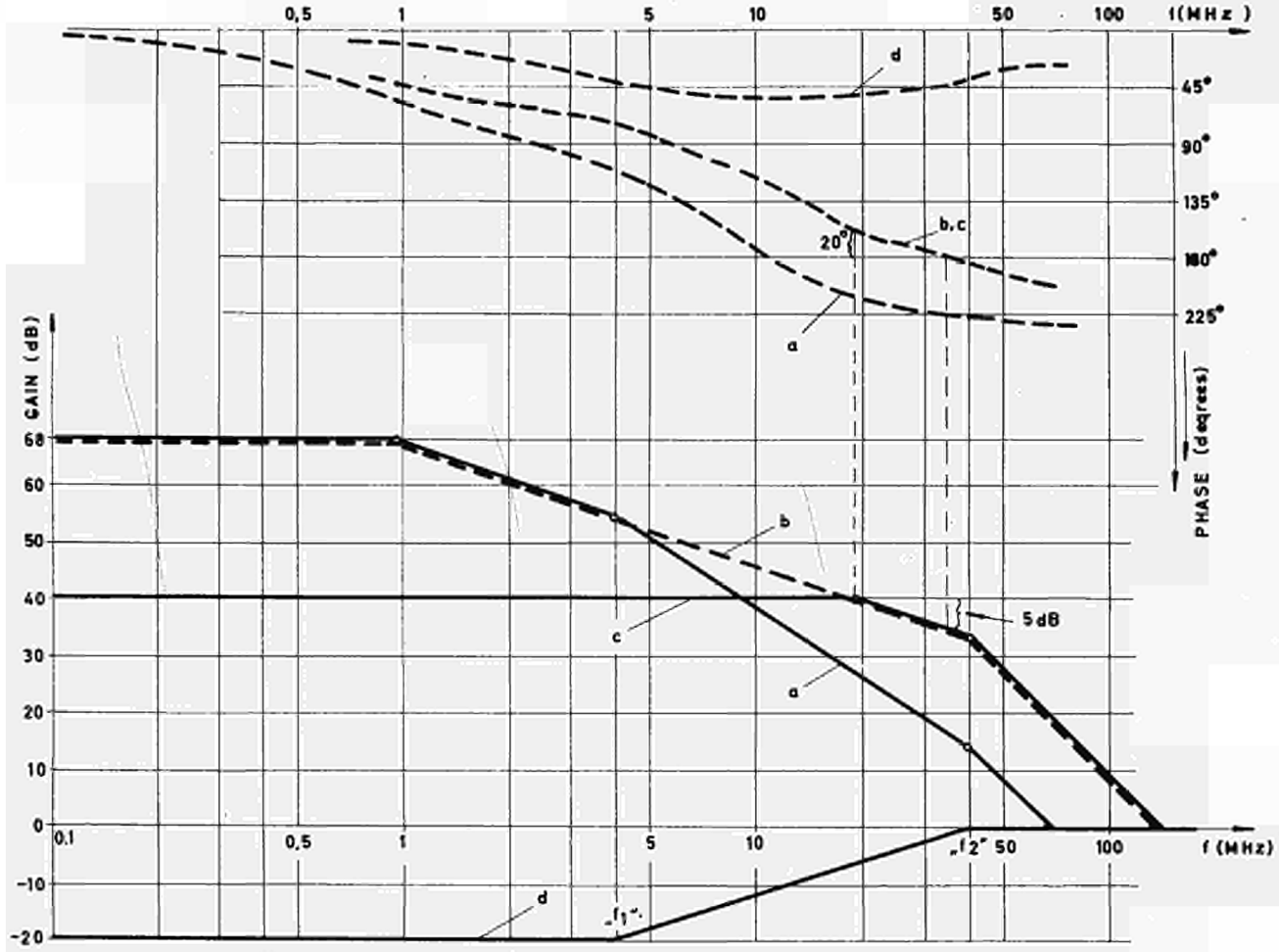

Fig. 9 - Log-magnitude and phase amplifier diagram : a.uncompensated open-loop characteristics ; b. compensated open-loop characteristics ; c) compensated closed-loop characteristics ; d. compensating network characteristics.

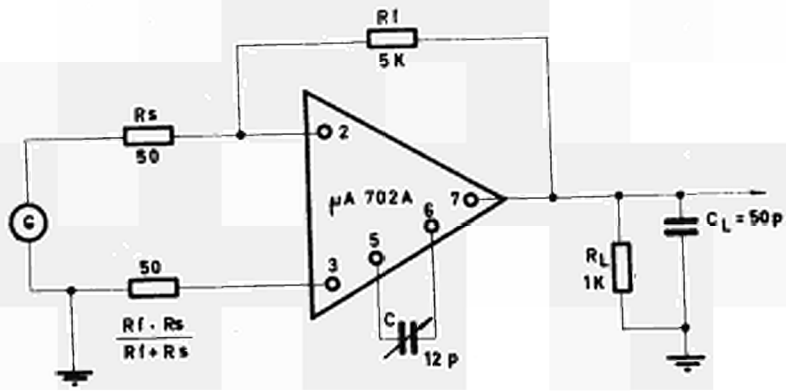

Fig. 10 - Realized amplifier configuration.

SHAPING AND TIMING CIRCUITS WITH ALTERNATIVE SYMMETRIC AND ASYMMETRIC INPUT AND OUTPUT CONFIGURATIONS

Pavel Horváth[+], Lubomir Ondriš[++]

Joint Institute for Nuclear Research, Dubna, U.S.S.R.

ABSTRACT

Shaping and timing circuits with both symmetric input and asymmetric output and the inverse configuration are described. Good rejection of undesired signal components, which appear at the output as a result of coupling effects and of non-ideal circuit element properties, is achieved.

—

In fast circuit techniques, especially in some fast computer applications the advantages of circuits which employ either an asymmetric input and a symmetric output or the inverse configuration are well established.

This method can be used also for synthesizing various new circuits for the purpose of shaping and timing of scintillation pulses.

The examples which will be considered here are very simple and rather obvious.

1. Symmetric bilateral clipper (Fig. 1). Backward diodes are used in this circuit to form two nonlinear bipoles, (two-terminal elements) for example D_1 and C or D_2 and D_3 in Fig. 1 a.

The V-I characteristics of the diode D_1 and of the antiparallel connection of the diodes D_2 and D_3 are given in Fig. 1b. For positive V and I the characteristics are relatively displaced. For negative V and I both characteristics are practically the same. Thus, for sufficiently large positive V and I we obtain an output voltage $V_{out} \cong \frac{1}{2}(V_2 - V_1)$, which is practically constant and greater than zero. For negative V and I, V_{out} is practically equal to zero. Fig. 1c shows a photomultiplier pulse excited by a light pulse generator and also the pulse clipped by a bilateral symmetrical clipper.

There are various configurations in which diodes, tunnel diodes, backward diodes and certain other elements may be connected to form nonlinear bipoles: antiparallel connection, antiseries connection, etc. This gives a large variety of proper bipole V-I characteristics so that one can obtain circuits acting as bilateral clippers, unilateral clippers, with a choice of circuits to obtain an arbitrary polarity of output pulses.

2. Symmetric tunnel diode discriminator (Fig.2). This circuit combines properties of a biased tunnel diode discriminator and a symmetric clipping circuit. The V-I characteristics of a both biased tunnel diode D_1 and the antiparallel connection of tunnel diodes D_2, D_3 are given in Fig. 2b.

A bipolar pulse is applied at the input. As the bipolar pulse crosses the zero-point, the tunnel diode D_1 goes to its peak level I_{pk} and switches to the high-voltage state.

The bipolar photomultiplier pulse and the output pulse from the symmetric discriminator are shown in Fig. 2c.

3. Symmetric true zero-crossing discriminator (Fig. 3).

Two biased tunnel diodes are used in this circuit.

In the time interval during which the bipolar pulse is rising and positive, the tunnel diode D_1 moves to its peak level I_{pk}, and the diode D_2 is forced in the opposite direction (Fig. 3b). After the diode D_1 switches to the high-voltage state, the diode D_2 gets a pedestal current I_{pd} so that, at the instant when the bipolar pulse goes through zero, the tunnel diode D_2 switches.

Fig. 3c shows the bipolar photomultiplier pulse and the output pulse from the symmetric true zero-crossing discriminator.

A time shift less than 150 ps was achieved over a 50.1 dynamic range.

We note, that both the symmetric clipper and the symmetric discriminator may operate in the inverse direction.

Fig. 4 shows the symmetric bilateral clipper in reverse operation.
In this case, in the symmetric input of the rejector, the undesired components of signals appear as in-phase waveforms and the clipped pulse as antiphase waveforms. Oscillograms are given in the Fig. 4c, showing the input signals of the rejector and the output pulse, namely the resulting clipped pulse after rejection of undesired signal components.

[+] On leave from Technical University, Bratislava, CSSR.

[++] On leave from Institute of Electronics, Slovak Academy of Sciences, Bratislava, CSSR.

DISCUSSION

Arbel : - *In the practical circuits do you have any provisions to prevent the tunnel diodes from oscillating ? If the answer is yes do they in any way limit the speed of the circuit ?*

Horvath : - *The main property of these circuits is the great sensitivity and the very good rejection of nondesired signals e.g. of signal components which appear at the output in consequence of coupling effects and of nonideal circuit elements properties.*

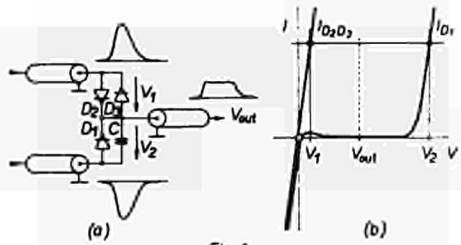

Fig. 1.

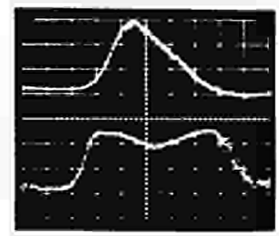

(c) time base 2 ns/cm
vertical sensitivity 2V/cm
100 mV/cm

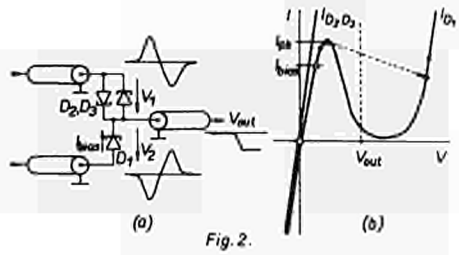

Fig. 2.

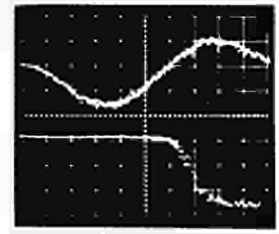

(c) time base 1 ns/cm
vertical sensitivity 2V/cm
100 mV/cm

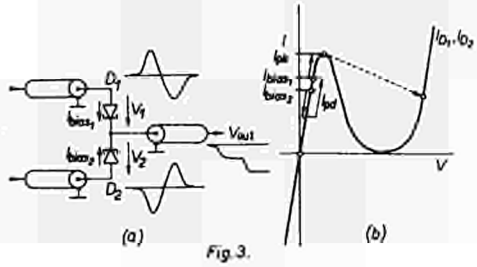

Fig. 3.

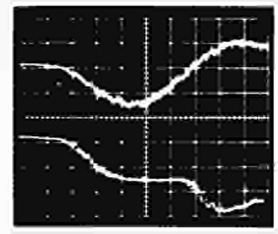

(c) time base 1 ns/cm
vertical sensitivity 2V/cm
100 mV/cm

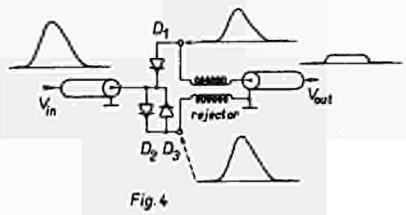

Fig. 4

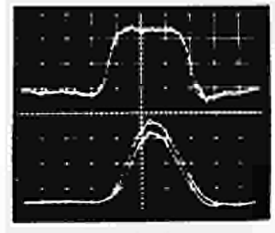

(c) time base 2 ns/cm
vertical sensitivity 100 mV/cm
1V/cm

INFLUENCE OF THE COMPENSATED THICKNESS OF COAXIAL Ge(Li) DETECTORS AND OF NOISE SOURCES ON TIMING PROPERTIES

J.A. MIEHE, P. SIFFERT, R. STUCK and A. COCHE

Centre de Recherches Nucléaires
Laboratoire de Physique des Rayonnements
et d'Electronique Nucléaire
Strasbourg - Cronenbourg
France

SUMMARY

Starting with equal diameter germanium crystals, we have fabricated double open ended Ge(Li) coaxial diodes, in which the compensated region is varied by 2 mm steps. The spread of the charge collection times and the time resolution are studied simultaneously. The influence of other parameters, such as the triggering level of the fast discriminator are analyzed. The results are compared to those of a planar counter having the same sensitive thickness.

The influence of parallel and series noise sources are studied.

In a previous paper [1] we have studied the influence of the external radius r_e of true coaxial Ge(Li) detectors, all having the same sensitive thickness W (9 mm), on the charge collection fluctuations and the resolution of the prompt coincidence curves. We showed that for a given W the charge collection fluctuations and the FWHM of the prompt coincidence curves decrease when the external radius of the device is increased. As an example when r_e rises from 12 to 22 mm, the FWHM of the prompt coincidence curve drops from 6.4 to 3.2 ns for a ^{60}Co source. Other parameters like noise, discriminator threshold... can contribute to the curve broadening.

In this paper we are concerned with the influence of other parameters on the timing properties of Ge(Li) counters, namely the compensated thickness W for a given r_e value in coaxial detectors, and the different noise sources.

We have examined the timing properties of true coaxial counters having constant external radii r_e and increasing depletion layer thickness W. In order to avoid any differences in the properties of the germanium material, we used during the whole study the same vertically pulled samples. These samples were drifted to a preliminary thickness W_1 and the characteristics of the counter were determined. Subsequently the detectors were put again under drift until thicknesses W_2 were obtained, and again the timing performances were investigated...

The results are compared with those obtained with a planar detector.

Some experimental results lead us to define more accurately the influence of the different noise sources on the timing properties of the Ge(Li) detectors. The main results are presented in the second part of this work.

I - EXPERIMENTAL CONDITIONS

1. Detectors.

All the detectors were made from two germanium cylindrical samples (D_1 , D_2) of external radius r_e = 20 mm , and 10 mm length in which counters having thicknesses of 2, 4, 6, 8 and 10 mm were successively prepared. The principal characteristics of the counters are summarized in table I. When the depletion layer reached 8 mm, we increased the leakage current of the detector by means of a special surface treatment, as a consequence the energy resolution was decreased (this new detector is called D_1' in table I).

2. Electronic set-up.

The experimental set-up for the determination of the pulse shape distribution was described previously [1] and is based on the Strauss method [2].

The delayed coincidence circuit for the measurement of the prompt coincidence curve uses in one path a fast photomultiplier XP 1020 coupled with a NE 102 scintillator, whereas the other path consists of the Ge(Li) counter under test. The slow circuitry selects from the pulses coming from the photomultiplier those corresponding to the Compton edge. In a similar manner, the pulses coming from the Ge(Li) counter are selected only if theycorrespond to the full energy peak.

The fast circuitry consists of a voltage preamplifier with a field effect transistor input stage. It has a rise time of 20 ns and an energy resolution (FWHM) of 2 keV for a detector capacitance of 25 pF.

II - INFLUENCE OF THE DEPLETION LAYER THICKNESS.

At each stage of the successive drifts we have analyzed the following characteristics :

- the pulse shape distribution at different detector bias voltages for a ^{137}Cs γ-ray source.
- the prompt coincidence curves as a function of different fast discriminator threshold levels, for the 0.511 MeV γ-rays from ^{22}Na and also for the 1.33 γ-rays from ^{60}Co.

Spectra of the pulse amplitude distribution obtained after 50 ns [2] for different W values between 0.2 and 1 cm and for an electric field of about 100 V/mm, are given on figure 1. As expected from the theory [1] a broadening of the pulse distribution appears when the thickness of the depletion layer increases. Prompt coincidence curves obtained with a ^{22}Na source and optimal threshold level setting (leading to minimal FWHM) for different W are plotted in figure 2. Optimal values of the threshold levels and results for a ^{60}Co source can be found in table I.
Following observations can be made :

- the FWHM of the prompt coincidence curve is not increased by more than 1.5 ns when W increases from 2 to 10 mm, in spite of a large increase in the spread of the charge collection times.

- the energy resolution does not seem to have any influence on the time resolution. This can be illustrated by the counters D_1 and D_2 (each with a sensitive thickness of 2 mm) and also by D_1 and D'_1 each of 8 mm depletion layer thickness. In the latter example, when the FWHM of the pulse height distribution curve is increased by a factor 4, the FWHM of the timing curve is not altered.

III - COMPARISON OF TIMING PROPERTIES FOR PLANAR AND COAXIAL COUNTERS.

With the same experimental set-up as described above, we have studied the charge collection and the time resolution for a planar detector, the principal characteristics of which are presented in table I

Prompt coincidence curves obtained, with a ^{22}Na source, for the planar detector and two coaxial counters D_1 and D_2 having approximately the same depletion layer thickness are shown in figure 3. The discriminator level is fixed at the optimal value, giving the best timing resolution. Table II summarizes the results for ^{22}Na and also for ^{60}Co.

The influence of the fast discriminator threshold level on the FWHM and FW(0.1)M of the prompt coincidence curve for ^{22}Na is shown in figure 4.

The following remarks can be made :

- By plotting the FWHM of the prompt coincidence curve as a function of the fast discriminator threshold, a minimum in the curve appears [3,4] for a certain threshold level. This minimum is more pronounced for coaxial than for planar detectors. At FW(0.1)M a similar behaviour is observed for both kinds of counters.

- For a given depletion layer thickness, the timing characteristics are better in a planar than in a coaxial detector, even if all carriers are moving at the saturation velocity. But, as we have shown earlier, the increase of the charge collection time fluctuations when W is increased, has only a small effect on the FWHM of the coincidence curve. It seems then, that the differences in the pulse shapes between the planar (fig. 5a) and the coaxial (fig. 5b) detectors at low threshold levels are responsible for the broadening in the timing curve for coaxial counters. In planar detectors the majority of pulses commence with the same fast risetime.

IV - THE INFLUENCE OF SERIES AND PARALLEL NOISE SOURCES ON THE PROMPT COINCIDENCE CURVES.

The noise equivalent input circuit of Ge(Li) detector-voltage sensitive preamplifier system is shown in figure 6. Thus, the

noise power spectrum is given by :

$$S(\omega) = 2kTR_s + \frac{2kT}{R_p C^2 \omega^2}$$

where R_p is the equivalent parallel noise resistance, R_s the equivalent series noise resistance, C the input capacitance of the preamplifier, K the Boltzmann constant and T the Kelvin temperature.
In the same figure is shown a simplified schematic of the experimental set-up including detector, preamplifier, discriminator and pulse shape amplifier.

The input stage of the preamplifier is a low noise field effect transistor. At the output there are two pulses $S_T(t)$ and $S_E(t)$ which convey, respectively, the time and energy information. The principal electrical characteristics of these pulses are presented in table III.

TABLE III

Time constant	Preamplifier		Amplifier
	$S_T(t)$	$S_E(t)$	$\tau_i = \tau_d = \tau$
Integration τ_i	10 ns	10 ns	3 µs
Differentiation τ_d	1 µs	40 µs	3 µs

If it is assumed that the transfer function of the preamplifier is these of an integrating and differentiating circuit with time constants τ_i and τ_d respectively, then the average noise power at the output can be written :

$$\overline{v^2} = KT \frac{\tau_d}{\tau_d + \tau_i} \left[\frac{R_s}{\tau_i} + \frac{\tau_d}{R_p C^2} \right]$$

In other respects, the noise power output of an RC-CR shaping amplifier is given by :

$$\overline{V^2} = \frac{KT}{2} \left[\frac{R_s}{\tau} + \frac{\tau}{R_p C^2} \right]$$

This noise power characterizes the contribution of the electronic system to the energy resolution.

The same increase ΔV can be caused by a corresponding increase in the value of R_s or a decrease in R_p i.e. :

$$\Delta V^2 = \overline{V_1^2} - \overline{V^2}$$

where

$$\overline{V_1^2} = \frac{KT}{2} \left[\frac{R_{S_1}}{\tau} + \frac{\tau}{R_p C^2} \right] = \frac{KT}{2} \left[\frac{R_S}{\tau} + \frac{\tau}{R_{p_1} C^2} \right]$$

In the first case, noise power at the output of the preamplifier can be written :

$$\overline{v_1^2} = \overline{v^2} + \frac{\tau}{\tau_i} \cdot \frac{\tau_d}{\tau_d + \tau_i} \Delta V^2$$

$$\simeq \overline{v^2} + \frac{\tau}{\tau_i} \Delta V^2$$

In the second case :

$$\overline{v_1^2} \simeq \overline{v^2} + \frac{\tau_d}{\tau} \Delta V^2$$

From these expressions and from the shaping time constants in table III, the following conclusions can be drawn : for a given worsening ΔV of the energy resolution, the corresponding average noise power at the output of the preamplifier increases markedly only in the case of series noise. Therefore the time resolution is less affected by parallel than by series noise.

Experimentally, this has been proved by increasing the noise in two different ways.

1) Series noise.

Noise available at the output of a large band amplifier (300 MHz) was applied to the gate of the field effect transistor through the test capacitor of the preamplifier.

2) Parallel noise.

A modification of the gate resistor of the field effect transistor lead to a change in the parallel noise level.

Energy spectra for a ^{57}Co source without external noise (curve I), with series noise (curve II), and with parallel noise (curve III), measured with the planar detector are plotted on figure 7. For these 3 experimental conditions prompt coincidence curves utilizing a ^{22}Na source have been obtained.

Figure 8 shows that worsening the energy resolution (from 2.5 keV to 11 keV) with parallel noise does not affect the prompt coincidence curve, but worsening the energy resolution (from 2.5 keV to 10 keV) with series noise makes the FWHM of the coincidence curve increase from 1.6 ns to 4.1 ns.

Identical experiments have been performed with the coaxial detector D_1 with W = 10 mm. Coincidence curves are shown in figure 9 and the effect of series noise is shown to be the same.

ACKNOWLEDGMENT

We wish to thank J. Gsell for the care with which he has fabricated the Ge(Li) detectors as well as J.P. Oberlin who has developed the preamplifier.

REFERENCES

1. R. Stuck, J.A. Miehe, E. Ostertag, P. Siffert and R. Henck. Colloque International sur l'Electronique Nucléaire, Versailles 1968, Tome I, 27.
2. M.G. Strauss, R.N. Larsen and L.L. Sifter, I.E.E.E. Trans. Nucl. Sci., NS 13, (No 3), 265 (1966).
3. J.C. Balland, M. Goyot, I. Guyon, J. Pigneret, J.J. Samueli and A. Sarazin. Colloque International sur l'Electronique Nucléaire, Versailles 1968, Tome I, 28.
4. T.D. Douglass and C.W. Williams. Colloque International sur l'Electronique Nucléaire, Versailles 1968, Tome I, 66.

DETECTOR SHAPE	THICKNESS	TIME RESOLUTION					
		^{22}Na				^{60}Co	
		DISCRI THRES (%)	FWHM (ns)	FW0.1M (ns)	CURVE ON FIGURE	DISCRI THRES (%)	FWHM (ns)
PLANAR	7-8 mm (V = 1300 V)	25	3	5.1	A	10	1.1
COAXIAL	8 mm D_1' (V = 800 V)	4	4.4	10.5	B		
	8 mm D_2 (V = 1 500 V)	7	3.4	7.5	C	20	1.8

TABLE II

DETECTOR SHAPE	SENSITIVE THICKNESS (mm)	DETECTOR	CAPACITY (pF)	REVERSE CURRENT (A)	ENERGY RESOLUTION ^{22}Na FWHM (keV)	AMPLITUDE OUTPUT PREAMPLI ^{22}Na (V)	TIME RESOLUTION ^{22}Na DISCRI THRES (mV)	^{22}Na FWHM (ns)	^{22}Na FW0.1M (ns)	^{22}Na CURVE (Fig 1)	^{60}Co DISCRI THRES (mV)	^{60}Co FWHM (ns)
COAXIAL TWO OPEN ENDED	2	D_1	75	2×10^{-10}	6.2	1 (900 V Bias)	180	3.1	7	A	400	1.8
		D_2	80-100	1.2×10^{-9}	12.8	0.8 (900 V Bias)	180	3	6.5	B	400	1.9
	4	D_1	50	5.2×10^{-10}	7.7	1.2 (900 V Bias)	90	3.1	6.8	C	280	1.8
	8	D_1	23	5×10^{-10}	2.6	2.9 (900 V Bias)	110	4.4	10.5	D		
		D_1'	24	2×10^{-9}	10	2.9 (900 V Bias)	180	4.4	10.9			
		D_2		2×10^{-10}	2.5	2.4 (1300 V Bias)	220	3.4	7.4	E	300	1.8
	10	D_1	20	1×10^{-10}	2.6	2.6 (900 V Bias)	180	4.5	11.4	F	300	2.3
PLANAR	7-8		18	1.7×10^{-10}	2.2	2.9 (1200 V Bias)						

TABLE I

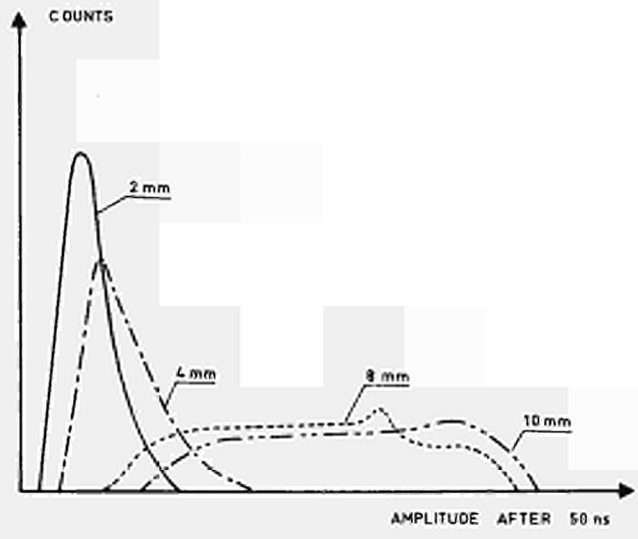

Fig.1

Fig. 1 Pulse amplitude distribution after 50 ns for different values of the compensated thickness W and for a 661 keV γ-ray (^{137}Cs).

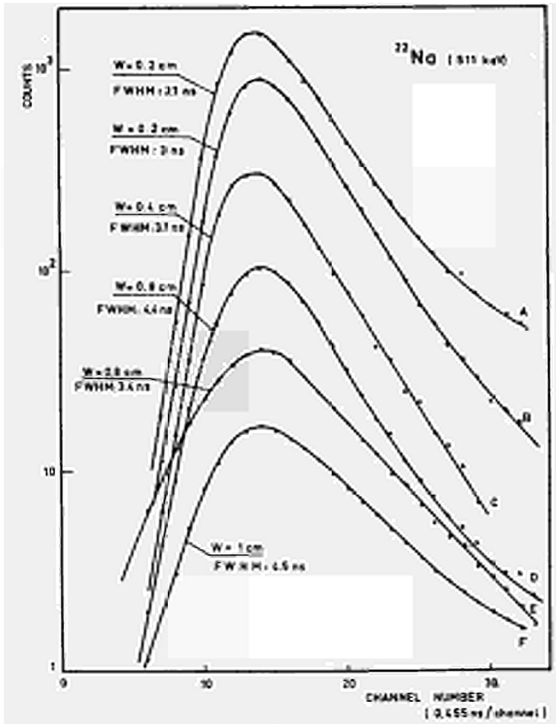

Fig. 2 Prompt coincidence curves for different values of the compensated thickness W and for a 511 keV γ-ray (^{22}Na).

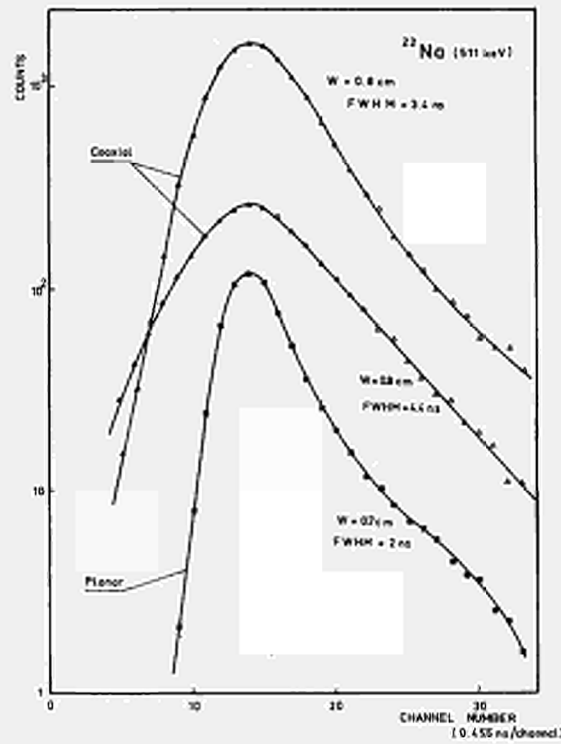

Fig. 3 Comparison of ^{22}Na time spectra obtained with planar and coaxial detectors.

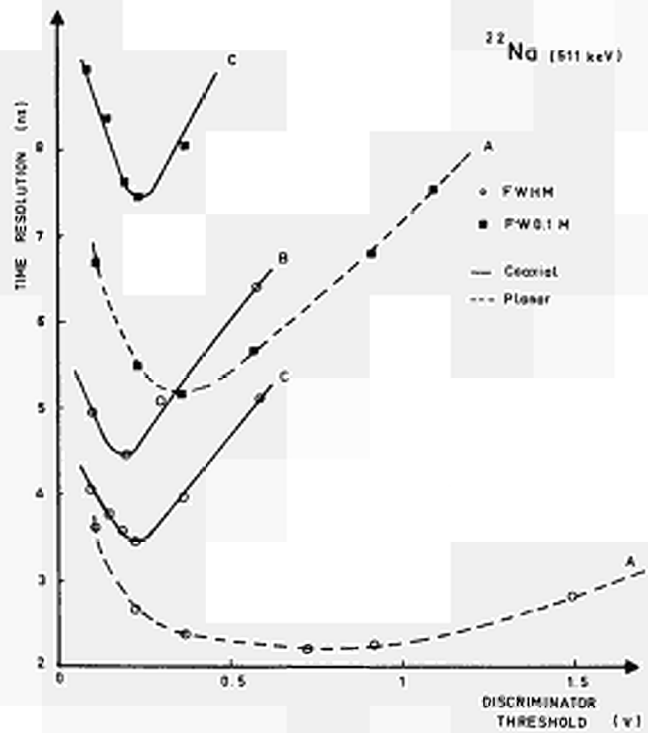

Fig. 4 FWHM and FW(0.1) M as a function of discriminator threshold level.

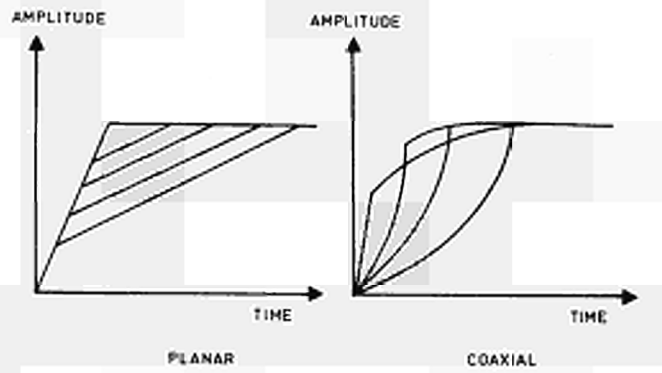

Fig. 5 Pulse shape differences between planar and coaxial detectors.

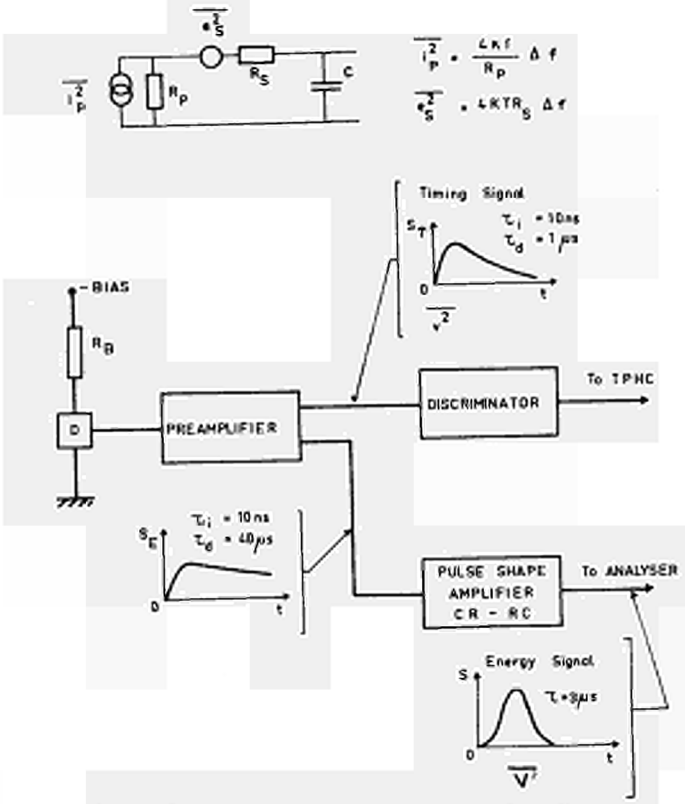

Fig. 6 Equivalent noise input circuit. Timing circuit.

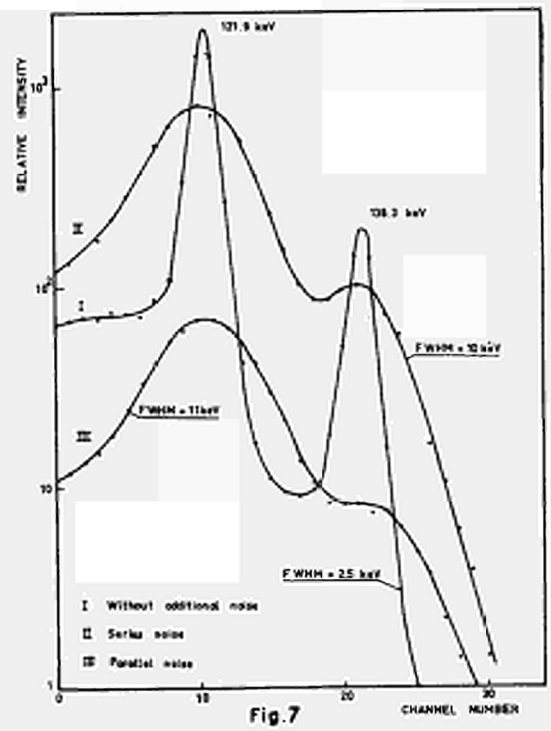

Fig. 7 The effect of series and parallel noises on the energy spectrum of ^{57}Co.

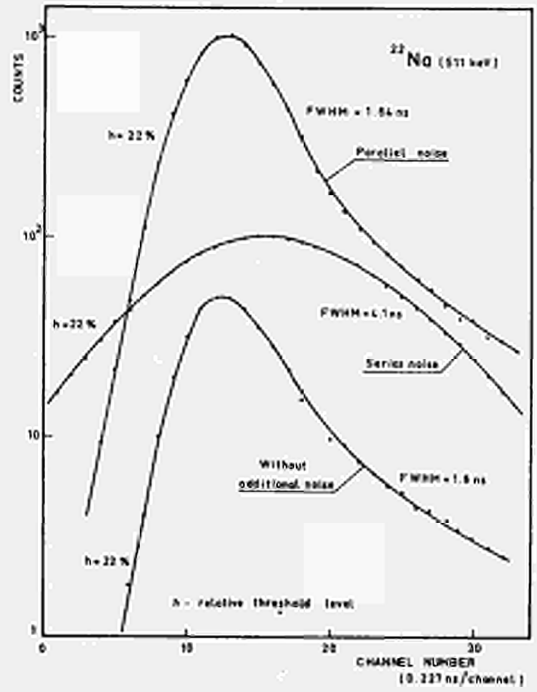

Fig. 8 The effect of series and parallel noises on the ^{22}Na time spectrum obtained with a 8 mm planar detector.

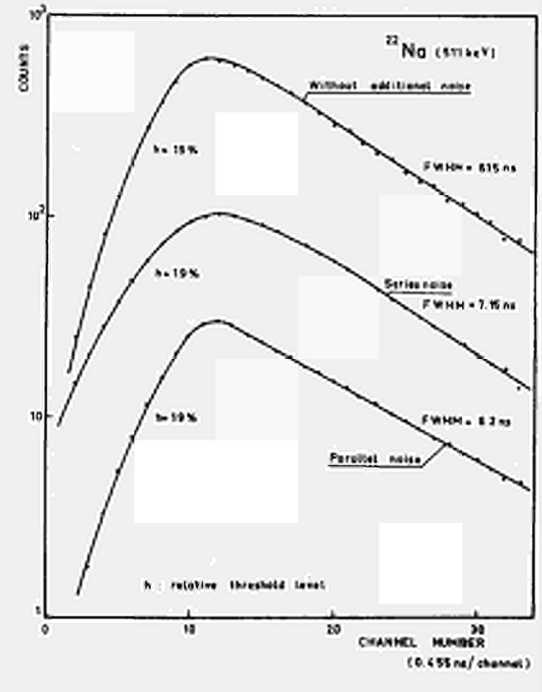

Fig. 9 The effect of series and parallel noises on the ^{22}Na time spectrum obtained with a 8 mm coaxial detector.

PLASMA EFFECTS FOR α-PARTICLES AND O^{16} IONS IN SILICON DETECTORS

P.A. Tove, W. Seibt, K.E. Sundström

Electronic Department, Institute of Physics, Uppsala, Sweden

ABSTRACT

Injection of strongly ionizing particles such as α-particles and oxygen ions into semi-conductor detectors give rise to plasma effects which change the simple picture of charge collection valid for lightly ionizing particles, e.g. protons. The observable current pulse in the detector therefore becomes different in the mentioned three cases. Measurements results are compared with a previously designed theoretical model which assumes that erosion of the created plasma is caused by transient space charge limited currents from the plasma edge.

SUMMARY

Semiconductor detectors for nuclear radiation have several advantages compared with previous types of detectors. One of these is the high energy resolution, another the very high accuracy possible in determining the time position for a nuclear event. The latter is especially true for planar detectors at high applied voltages while cylindrical lithium-drifted germanium detectors can show rather bad timing properties, appreciably worse than scintillation detectors. One problem connected with the utilization of the high timing accuracy (pulse rise times of the order of 10^{-9} sec. practically without the statistical straggling in the number of charge pairs which exists e.g. in scintillation detectors) is that the detector pulses are very small. Existing coincidence or time-to-pulse-height converters require larger pulses. Thus one has to use fast pulse amplifiers, which on the present status of technical development hardly have sufficient gain-bandwidth products.

If we disregard this latter "electronic" limitation one may also in semiconductor detectors have a delay of the detector-pulse which is of physical origin and may increase and cause spread in the pulse rise time. This effect is present especially for highly ionizing particles, α-particles or heavier, and is caused by plasma creation in the ionization track. This occurs when the ionization density becomes so high that the collecting field does not instantaneously reach all charge carriers.

Rise times measurements performed by different authors on integrated pulses from the detectors show that the collection time for α-particles and fission fragments is longer than what the simple charge collection theory indicates. In the analysis of experimental data one often uses the formula $t_p = t_m^2 - t_c^2$. Here t_m is the total measured rise time of the voltage pulse (integrated current) and t_c is the collection time calculated from simple theory. In this way the value for t_p, the so-called "plasma time" is defined. The dependence of this on ionization intensity and electrical field strength in the detector has then been the object of study.

It is difficult to relate the plasma time defined in this way to the physical behaviour in the detector. In order to reach this aim we have studied the current pulse from the detector, i.e. the pulse obtained when the detector is connected through a very low-ohmic system (50Ω) to a fast oscilloscope. By studying the shape of this pulse it is possible to obtain more information than from the measurement of the rise time of the integrated pulse.

Theoretical model for plasma effect in the detector

In a previous publication [1] we discuss a model for the erosion of a plasma track by space charge limited currents from the plasma edge. In this way we obtained a theoretical value for the time needed to dissolve the plasma by an electrical field, disregarding spreading by diffusion.

A very simple model of the erosion process is shown in Fig. 1. Assume the plasma is created

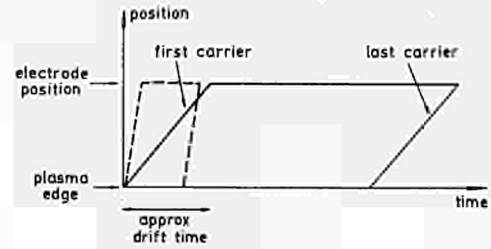

Fig.1

close to one electrode. Carriers then travel from the edge towards the other electrode. If this is positive (anode) the carriers are electrons, if it is negative, they are holes. The plasma time is the separation between the first carriers leaving the plasma and the last ones leaving the track passing towards the collecting electrode. We see that when studying cur-

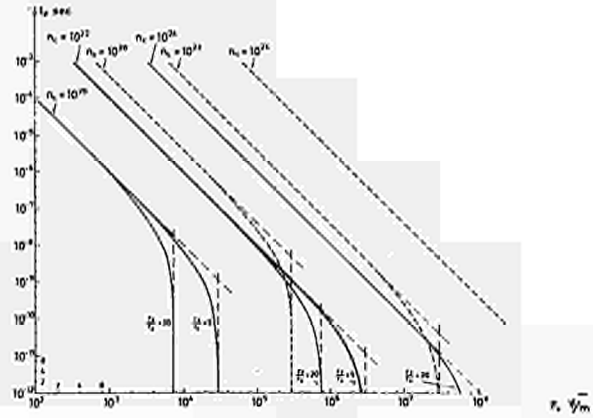

Fig.2

rent pulses, this gives an argument for linear superposition of t_p and t_c, the drift time, i.e. $t_m = t_p + t_c$ where t_m is the duration of the current pulse (and also a measure of the rise time of the voltage pulse).

The result of the calculations in ref. 1) is seen in Fig. 2 where the solid line shows the expected variation of plasma time for α-particles, as a function of the strength of the eroding field.

Experimental arrangement

To study t_p by measuring the current pulse shape in the detector, the set-up in Fig. 3 was

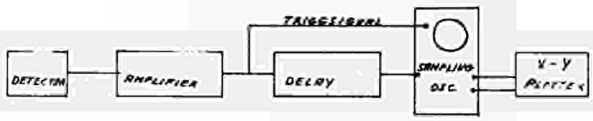

Fig.3

used. A surface barrier detector was exposed to α-particles, O^{16}-ions, or fission fragments. In order to study the behaviour when no plasma effect is expected, measurements with protons were also done. The sampling oscilloscope was a Tektronix type 661 with 4S1 plug-in. Because of the small size of the current pulse a fast Hewlett-Packard pre-amplifier with a voltage amplification $\approx$ 100 and 50 Ω inputimpedance was used. The output was fed to the direct input on the oscilloscope. External triggering from a cathode follower connected to the input of the preamplifier was used. A system rise time of $\approx$ 3.5 n sec was measured. A 50 Ω delay cable was inserted between the preamplifier and the signal input of the oscilloscope.

Experimental results for different particles

a) Current pulses for α-particles

Most measurements were done with 8.8 MeV α-particles from a ThB source. These have a penetration depth of about 55 microns in silicon. In order to enhance the appearance of plasma effects, which requires low electric field, the detectors were bombarded from the back-side where the field can be made to have all values from zero, for an applied voltage equal to V_d, to high values when $V \gg V_d$. Here V_d is the depletion voltage. Results are seen in Fig. 4, lower left corner. The theoretically expected pulse shape when no plasma effects are present, for the case of incidence from the back side, is shown in Fig. 4, bottom center. This is drawn for the case where the ionization track is short compared to the detector thickness. The increase of current with time is caused by the fact that the holes, which are responsible for the current pulse in this case, are travelling into successively higher fields when they approach the cathode (front contact).

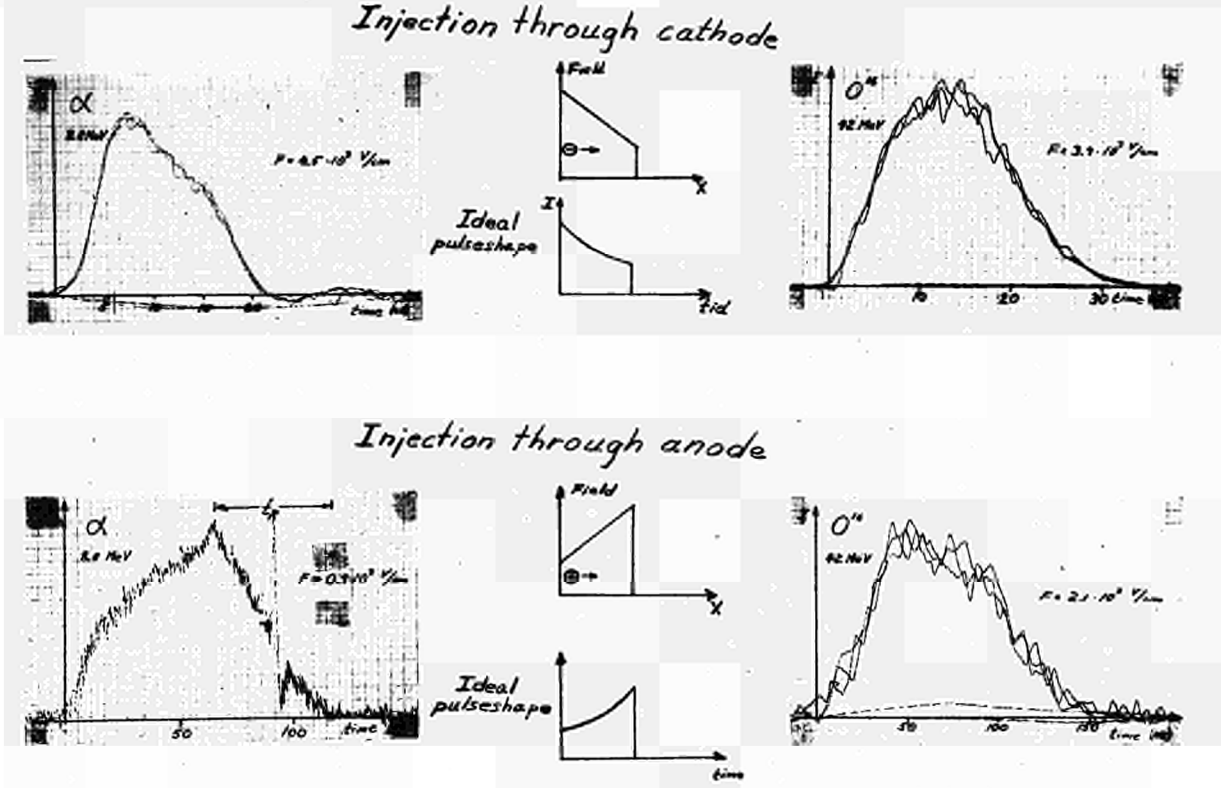

Fig.4

The current pulse is a cut exponential (see e.g. 2) 8)).

The experimental current pulse deviates markedly from the theoretical shape. The first, fast part of the pulse rise is attributed to the rise-time of the electronic system. The subsequently following slower rise to the peak (cusp) corresponds to the condition that the charges that have left the plasma enter a region of higher field. Also, new carriers eroding from the plasma contribute to the current rise. The current maximum corresponds to the time when the first charges leaving the now dissolved plasma arrives to the cathode. The time from the beginning of the pulse to the cusp is approximately equal to the nominal transport-time. With respect to the interesting later occurring slow decay of the pulse, the following can be said:
The cusp occurs when the first particles arrive at the cathode. The end of the pulse occurs when the last particles leaving the plasma arrive at the cathode. The transport-time for the first and the last carriers should be approximately equal. Because the last particles leave the plasma at a time equal to the plasma time after the first particles the decay time of the pulse becomes equal to the plasma time.

We have for α -particles a case when the plasma time is shorter or at least not longer, than the transport-time which is the basis for the above discussion. We have neglected eventual spreading effects due to diffusion.

To check the above interpretation, values of the transport time t_t, deduced from the current pulse as the time between the start and the cusp were compared with theoretical values calculated from

$$\text{Eq.(1)} \quad t_c = \frac{w^2}{2\mu V_d} \ln \frac{V+V_d}{V-V_d} \quad \text{(see e.g. ref. 8)}$$

where w is the detector thickness and V applied voltage. Good agreement is obtained, especially if we take into account that the first carriers start a small distance in from the surface (the penetration depth of the particle). Values of t_p (in nanoseconds) deduced from the length of the pulse decay were plotted in Fig. 5 (points marked ThB RB for straight incidence from the back and marked ThB SB for slanting incidence). Also shown are points for lower energy P_o α's, which have been corrected for the decay time of the system. In this case perpendicular front incidence was used (marked RF). The pulse shape for front (cathode) incidence is shown in Fig. 4, upper left corner. Now electron current is mainly responsible for the erosion, contrary to the case of incidence from the anode where holes are responsible. We note that the ratio of erosion time (plasma time) for the two cases is not very different from the ratio of mobilities (≈ 3). This is expected from the drift current erosion model [1]. However, a somewhat similar dependence could also be expected if diffusion is important, because the diffusion constant is proportional to the mobility, according to the Einstein relation $\mu/D = e/KT$. Similar results are shown for another detector in Fig. 6. We note that the difference between straight and slanting incidence in this case is negligible, while it amounts to $\approx 10\%$ for Fig. 5, a not significant difference. Deduction of t_p from pulse shapes for RF incidence, is more difficult than for the RB case as seen from Fig. 4, because in the former case the end of the travel of the first carriers only gives rise to a not too sharp break in the current. Because of this the alternative procedure of calculating the transport time from Eq. (1) and subtracting from the total pulse length, to obtain t_p, was used. The results, including those for ^{p}ThB α's (not shown) indicate that the field dependence is the same as for RB incidence. Also, these t_p values tend to be a factor 2 - 2.5 shorter than for the RB case.

The fact that the variation of t_p with field strength F is weaker,

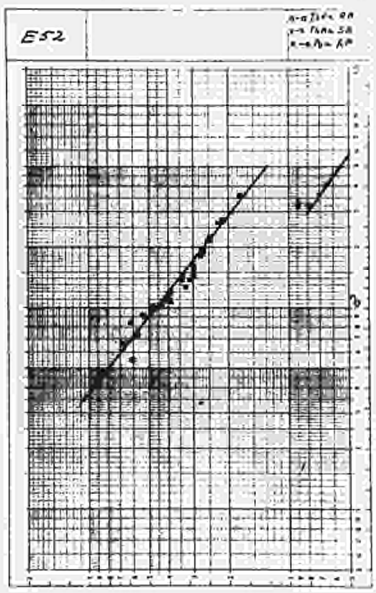

Fig.5

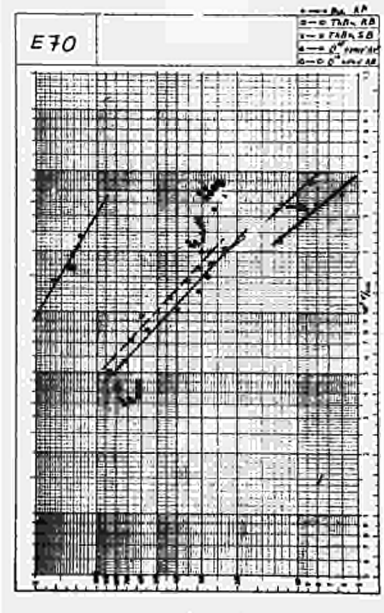

Fig.6

$$t_p \sim \frac{1}{F^{\approx 0.8}}$$

than predicted by the drift-current erosion model of ref 1),

$$t_p \sim \frac{1}{F^2} ,$$

may indicate that diffusion effects are of importance. The field strength plotted in Figs. 5 and 6 is the value appropriate to the position of the centroid of the track, cf. 3). As seen from Figs. 5 and 6, the absolute values of t_p for the two detectors are nearly the same.

b) Current pulses for 42 MeV O^{16} ions*

We have here a case when the calculated plasma-time is longer than the nominal transport time of carriers. This leads to a different current pulse shape which is seen in Fig. 4. A possible interpretation is the following (we consider first the RB case); The rising part of the wave-form is due to injection of space-charge-limited erosion current from the small-size ionization track (length approximately 25 microns) into the depleted volume of the detector. This could be said to have a "transfer function", for injection of a "Dirac current impulse", of the shape in the center of Fig. 4. At time $t = t_t$ we have the entire width of the detector filled by carriers due to erosion current. Because the erosion current during this first period of the erosion period is high we now have a maximum number of carriers in transit between the electrodes and hence the current has its maximum value. During the subsequent time interval up to $t = t_p$ (the point of relatively sharp decrease of the pulse) we continue to have injection of erosion current into the "transfer function". If the erosion current remains constant the current up to $t = t_p$ should hence be constant. This is not the case. A slight decrease is observed and may be explained by the fact that the erosion current decreases with time, as the plasma spreads out.

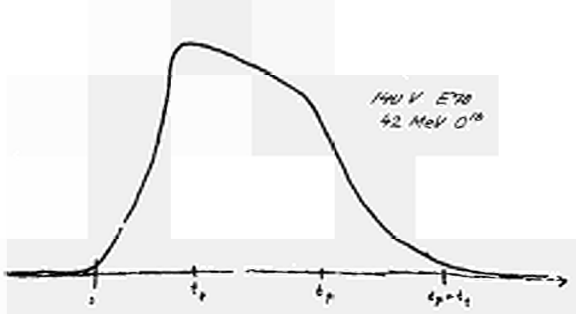

Fig.7

* These measurements were done in the Tandem Van de Graaf accelerator of the Danish Atomic Energy Commission. We want to thank Dr. B. Elbek and his co-workers for putting this facility to our disposal.

At $t = t_p$ the plasma is fully eroded and the current starts decreasing henceforth as the carriers in travel vanish into the cathode. At $t = t_t + t_p$ the last carriers eroded from the plasma have reached the cathode and the time between the end of the pulse and the decreasing "knee" should hence be approximately equal to the transit time of the carriers. Thus the rise and the decrease time of the pulse should be approximately equal. See Fig. 7. The rise time of the pulse is observed to be somewhat longer than the calculated transit time (about a factor 1.4).

Thus, quantitative agreement is not obtained but the general features of the pulse shape follow the given discussion. For RF incidence Fig. 4, upper right corner, the shape is changed because the carriers (in this case electrons) move into a region of higher field strength.

In connection with the above discussion assuming an erosion current that decreases with time, we may refer to another experiment, undertaken to study more directly, plasma erosion and transient SCLS's in silicon 4). Here the detector was exposed to a very intense (up to 100-1000 W peak power), short ($\approx$ 1 nsec) light pulse from a superradiant laser 5). The arrangement is seen in Fig. 8. From a study of the resulting current pulses, Fig. 9, we may note two features. The two top rows of pulses corresponds to fully developed SCLC conditions and show the pulses under different time scales.

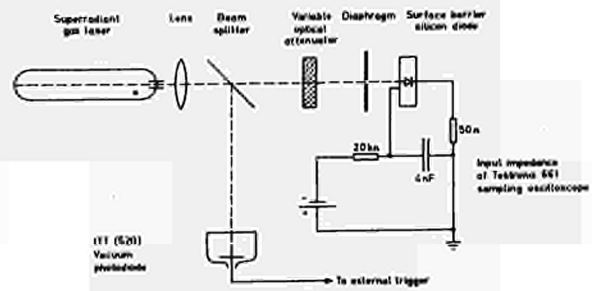

Fig.8

We observe that the reservoir of charge built up during the laser pulse is not sufficient to maintain the SCLC at a constant value but the current decreases continuously during the last part of the pulse. From a study of the ratio of currents at the cusp and at the beginning we may also conclude that we have contribution from diffusion. This follows because this ratio in Many and Rakavy's 6) drift-current model for transient SCLC is $\approx$ 2.7 while the ratio is smaller, $\approx$ 1.5, in Fig. 9, indicating a contribution from diffusion to the start current. The concentration gradient, and hence the diffusion contribution, can be expected to be higher for a dense particle track than for the laser pulse. The current rise between start and cusp (separated $\approx 0.8\ t_t$) is not expected to show up in the particle case, because SCLC conditions are believed to exist only in a very small region (with short transit time), cf. 1)

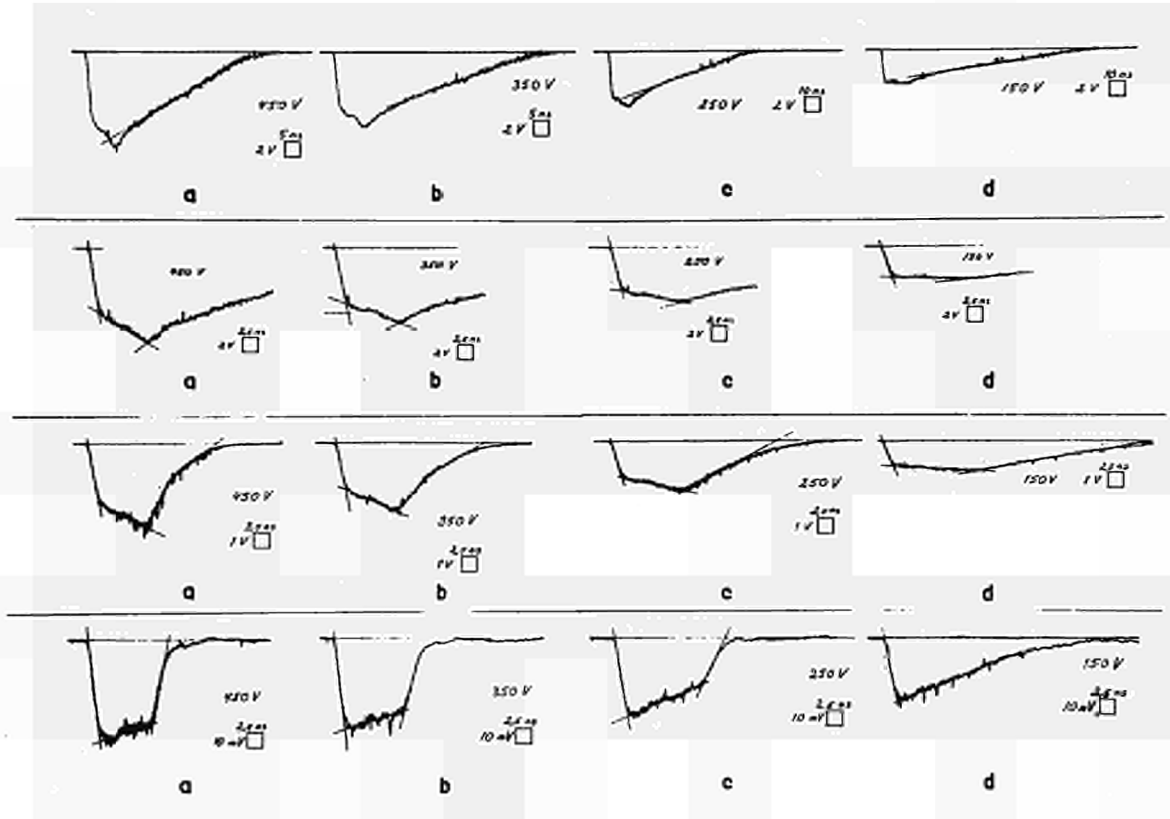

Fig.9

The evaluation of t_p from the O^{16} pulses was done by subtracting calculated values of t_c, the drift time, using eq. (1), from the measured pulse length. The results are given in Fig. 5 for one detector and are 4-5 times as large as for the α-case. The field dependence is seen to be weaker. The ratio between $(t_p)_{RB}$ and $(t_p)_{RF}$ is about the same as the ratio of mobilities, 3.

c) Current pulses for Cf^{252} fission fragments

Preliminary experiments have given pulse shapes shown in Fig. 10. The field dependence

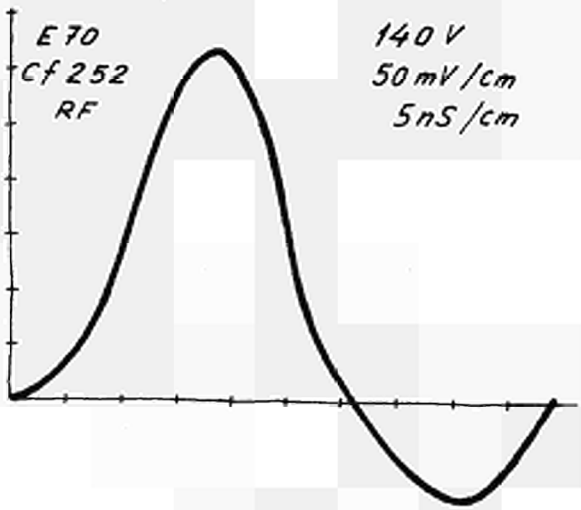

Fig.10

in this case seems to be even weaker than for the O^{16} case, possibly indicating a still more important contribution from diffusion current. An unexplained feature is the undershoot of the pulse. It has not been possible to trace back this as originated in the electronic system.

Implications of the plasma effect

For a consideration of the influence on timing properties one would normally be especially interested in a possible spread in plasma time. The results from experiments with straight and slanting incidence of the particles indicate that no appreciable difference exists. The field dependence of t_p may show up if particle tracks are created in different field strengths. There is also a difference if they are created close to the cathode or at the anode. This condition would, however, normally also lead to different rise times even if only transit time contributes to the rise time.

Study of the current pulse for protons (negligible plasma effects)

The pulse shape for RF incidence at $V = V_d$ for 5 MeV protons was measured. If the penetration depth of the particles is small compared with w this should give an exponentially decaying pulse

$$\sim e^{-t/\tau_e}$$

according to the "Ramo principle" of calculation of the pulse. (τ_e is the dielectric relaxation time constant). However, the penetration depth of 5 MeV protons was about w/2. A

very simplified picture of the influence of this can be obtained if we consider all carriers to be created at $X_o = w/4$.
Then, in accordance with the reasoning leading to the pulse shapes in the center of Fig. 4, the electrons will give an exponentially decreasing pulse, while the holes give a slightly increasing pulse. The contribution of the electrons to the charge will be approx. three times that of the holes and the pulse duration for the latter will be smaller. The net effect of

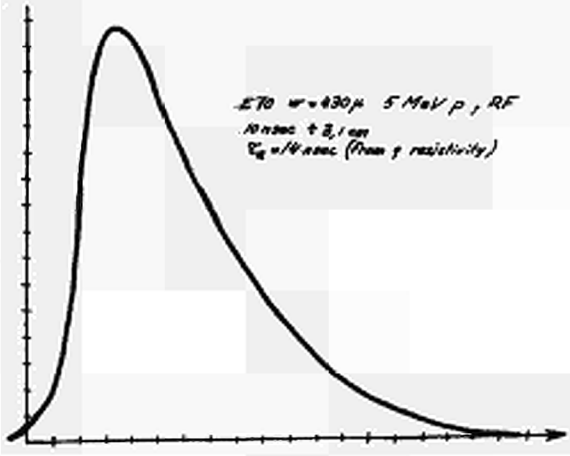

Fig.11

this is to "spoil" the exponential current shape by a "filling-in" effect, due to hole current, at the first section of the exponential.

The length of the pulse is not changed very much. These considerations are in agreement with the observed pulse shape in Fig. 11 and the length is in agreement with the Ramo principle rather than half this value which should be expected using a simple energy balance [2)7)].

Bibliography

1) P.A. Tove, W. Seibt, Nucl. Instr. & Meth., 51 (1967) 261-269
2) P.A. Tove, K. Falk, Nucl. Instr. & Meth., 29 (1964) 66-68
3) A. Alberigi Quaranta, A. Taroni, G. Zanarini, Nucl. Instr. & Meth., in process of publication
4) P.A. Tove, G. Andersson, to be published
5) G. Ericsson, R. Lidholt, in process of publication
6) A. Many, G. Rakavy, Phys. Rev. 126 (1962) 1980
7) M. Martini, G. Ottaviani, Nucl. Instr. & Meth. 67 (1969) 177-178
8) G. Bertolini, A. Coche (editors): Semiconductor Detectors, North-Holland Publishing Co., Amsterdam, 1968

DISCUSSION

Miller : - Could you explain the last remark about the mentioned undershoot on the fission fragment pulses ?

Tove : - Well, I am not prepared to explain it because of its very preliminary results as I said but I think it we may have competition between two effects diffusion and drift. We may think that the diffusion is acting very fast in the beginning and may cause a charge distribution which causes the current to the electrodes (including displacement current) for a certain time to change direction but this is not worked out in any way. It is not impossible to think about it but we don't believe it is due to our short clipping time, for instance, which is the first thing you suspect. Further experiments should however be done to verify the results.

Addendum

The author made new tests and sent a new fig. 10 which does not display the mentioned undershoot. So the last three lines of the paragraph under fig. 10 should be neglected.
The above discussion becomes pleonastic.

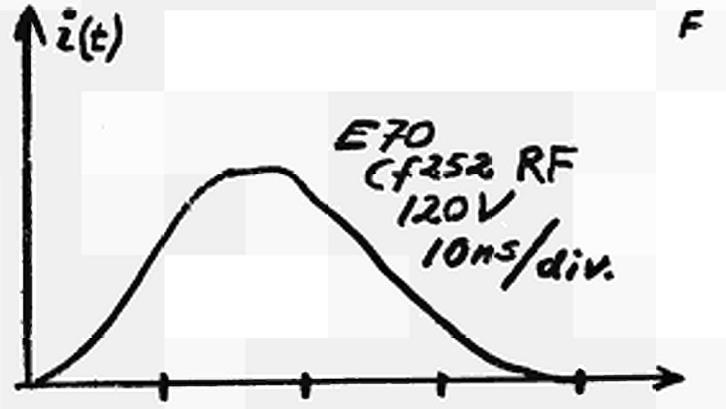

Fig.10

DIGITAL, ANALOG AND PROGRAM TECHNIQUES FOR ON-LINE COMPUTER CONTROL OF PHASED NEUTRON CHOPPERS

by M. C. B. Russell and D. B. J. Smith

Atomic Energy Research Establishment,
Harwell, Didcot, Berkshire, England.

Summary

A new system has been developed at Harwell for driving phased neutron choppers. It provides a general solution to the need for a power source with digital control, on-line from a computer, of the relative phase angle of any number of rotors whose parameters, for example speed, inertia, stiffness or electromechanical transfer characteristics, are not the same. Various ways are described for reaching synchronous speed and a simple way has been found for accelerating a 3-phase synchronous motor at zero slip frequency.

1 Introduction

New techniques have been developed for driving phased neutron choppers at high speed. For this purpose a solid state alternator has been designed which provides a means for setting up, directly from memory, both the speed and the relative phase angle of motor shafts. Some of these developments have already been described[1] and a detailed description has now been published of recent developments of the Harwell chopper system[2]. The purpose of this paper is to include fresh material on other means for phase control and acceleration of rotors and to report on the accuracy of timing.

The static alternator is a three-phase sine wave power source which has essentially no inertia and is a fast link between the low power digital circuits controlled by the computer, and the high analog power requirements of each spinning rotor.

In its simplest form the control program sends out a combined sub-address and binary number for setting up the phase and speed of each shaft in turn on buffer registers. The program may be extended to simplify the requirements of digital circuits or to assist the user, for example, by changing speed or phase in ways which depend on time-of-flight data as it is analysed by the computer. Alternatively, fast changes of relative phase angle may be planned by program to control either neutron burst energy or the interval between bursts.

2 Electronic Drive System

In developing the new drive system we had five objectives:

(a) An independent drive power for each neutron rotor, controlled in phase steps of 100 nanoseconds.

(b) To provide a 3-term analog control of all mechanical instabilities, independent of the means of phase angle control and without need to look at the rotor position.

(c) To use a means of phasing which does not require rotors to spin at the same frequency.

(d) To ensure that no electronic instabilities cause observable changes of phase the motor is driven by a rotating field whose speed stability is 1 part in 10^{10} and jitter less than 10 nanoseconds.

(e) To set up the speed and relative phase as binary numbers direct from memory into CAMAC modules.

A circuit of the alternator is shown in Fig. (1). It consists of six thyristors which are fired in sequence to connect the power supply to class C tuned circuits. The conduction of each switch extinguishes current in one previously conducting, so only one of the thyristors is conducting at a time, and effectively the direct current is routed in turn through each phase of the motor field winding in alternate directions to provide a rotating sine wave field for the motor.

The thyristors were not chosen for their high speed of operation, there is a delay of about 2 microseconds between their gate pulses and full anode conduction. But this delay is free of jitter when the gate pulse is fast, and so the three sine waves are effectively locked to the digital input with a variation of about 1 nanosecond if the motor load is constant.

Also shown in Fig. (1) is the means for turning on and off the power output to the motor by means of a seventh thyristor which extinguishes current in the alternator. Power is turned on by resuming the commutation of the six.

3 Speed Stabilisation

A large range of power, from 20 to 500 watts, may be required to drive each rotor. We have found it convenient to phase shift the drive power as the means for both digital and analog control of the angles of rotors and to remove incipient instabilities of the rotor assembly. As the alternator is an efficient power converter, the current which it takes from its source accurately represents the net load on the shaft and includes all the mechanical instabilities. This current vector, after band pass amplification and phase angle correction of each unstable mode, controls the delay of pulses which commutate the alternator. Such an arrangement, a low power digital means of controlling a large torque, should be adaptable to the particular constants of inertia, stiffness and electro-mechanical transfer characteristic of any neutron rotor system.

4 Phase and Speed Control

A general purpose module, in the format of

CAMAC, has been designed in which a 15-bit buffer register sets up either the number, (N + 4), which divides the frequency of a clock pulse source, or the quantised number, (N + 4), of clock pulse intervals by which an input pulse is delayed. In these two alternative ways the module is used to determine respectively the speed or phase of pulses which drive the alternator. The relative phase of rotors is retarded or advanced automatically, in increments of one clock pulse interval, by circuits which set the number, which controls speed, momentarily to either (N + 3) or (N + 5). Several aspects of these digital circuits, and of those which commutate the alternator, are logical or arithmetical and need not be very fast, so there is the choice of using computer program in their place.

When a rotor has constant acceleration (f) its position is changing, with respect to a constant speed reference of the same frequency by an amount ($\frac{1}{2}fT^2$) in each revolution where (T) is the period of rotation. For values of (f) and (T), which are typical of neutron rotors, it is possible to detect the moment when both speed and phase reach the required condition with a phase error less than 1 microsecond. If the speed of the rotating field is changed at this moment to coincide with the speed of the rotor then the rotor is aligned to the required phase when it first reaches synchronous speed. That is a rapid means of forming the hysteresis motor poles into the right position on the rotor.

The alternative electronic means of phasing rotors is to allow the poles to form in an arbitrary position relative to the neutron rotor slot and then to rotate the field relative to the speed reference. This means of phasing compares the timing of rotor pulses with that of reference pulses and automatically shifts the field in increments of 1 clock pulse intervals until they coincide. The rotation must not be too fast or the available synchronous torque of the motor is exceeded, and that causes the magnetic poles to slip to a new position. As is shown in Fig. (3), the relative phase of rotors may be adjusted either by changing the angle θ of the pick-up coil or by delaying the coil pulse by a quantised number of clock pulse periods. In either case the control loop is closed to remove the effects of changes in friction.

5 Synchronous Acceleration of Motors

The Harwell choppers spin in vacuum but their drive motors are at atmospheric pressure and so there is no problem in cooling them. For some purposes it is an advantage if the whole rotor is in vacuum. The armature, which is outside the vacuum, is readily cooled, but heat loss in the rotor itself can be a serious disadvantage. The heat generated in a rotor which is synchronous to its rotating field depends on the amplitude of components of the field which rotate at other frequencies, and these are small if the alternator provides current of sine wave shape. There remains the problem of providing torque for acceleration.

We have normally accelerated rotors from standstill by providing a fixed frequency of rotating field to the hysteresis motor. If it is essential to reduce rotor losses during acceleration then the rotating field can be programmed to exceed rotor speed by a small margin. Maximum torque is then obtained with only a small slip frequency. This can be done by program control of the number which divides the clock frequency input to the alternator.

An alternative method has now been developed (Fig. 2) which accelerates the rotor at zero slip frequency. The alternator is used to provide a rotating field which is locked to the frequency of the rotor. For this purpose (2p) marks are required on the rotor for each phase of the motor winding, where (p) is the number of poles. The pulses either feed separate thyristors in the alternator or else are commutated in the normal way. The motor then accelerates but remains synchronous to its field, so there are no slip losses in the rotor. The torque provided by this means depends on the angle between the field and the position of the magnetic pole in the rotor. This is controlled by a module which delays the mark pulses by a quantised number set by program. Alternatively the angle may be changed by moving the pick-up coil.

The control of torque during synchronous acceleration is shown in Fig. (3). The delayed coil pulses drive the alternator which provides a motor field which leads the magnetic pole by an angle α. The motor torque, which is proportional to sin α, is controlled by variation of the delay Δt of coil pulses which are the input to the commutator. When the loop is closed in this way a change of the delay causes a change of (α + β) equal to $2\pi\Delta t/T$ where T is the period of the rotor. The stability of this arrangement is due to the large inertia of the rotor compared to that of the electronic circuit and to the variation of β, a characteristic of the alternator, which reduces the changes in α.

The synchronous torque available from hysteresis motors is not as great as that obtained during non-synchronous acceleration. If necessary a greater accelerating torque may be obtained without significant slip loss by continuously rotating the pick-up coil against the direction of the rotor, and this arrangement removes the need for a controllable delay.

6 Digital Control

The digital control of rotors is easy once the design of a suitable alternator is completed. This provides both the power and the means of control of speed and phase. It is the interface between digital circuits and the power requirements of the rotor system, and it effectively has no inertia.

Many of the functions of the circuits required for phase and speed control are too fast to be conveniently done by program. But program control is a means for routing signals between modules, setting up digits in divide or delay circuits, and requesting a change of mode, which is conditional on coincidence checks. For example, the change from synchronous phase control to synchronous acceleration requires a smooth transition from one pulse source to another in phase with it.

Once the decision is made to use digital circuits for speed and phase control, and to follow the rules of CAMAC, it is a simple matter to design the logical circuits for either program or switch control. The divide by N module which also serves to delay a signal by N clock pulses is designed so that a request for N to change by plus or minus one digit is stored until this has happened for one delay or divide cycle only.

7 Performance

The accuracy of phasing of rotors depends in practice on the rate of change of drive torque which is required to keep the shaft aligned to the reference clock pulses. It depends how well the 3 term analog control circuit is adjusted to overcome the DC and AC components of the torque changes required for a particular rotor system.

Fig. (4) demonstrates that the sine wave outputs of the 3-phase alternator can be very accurately locked to the digital input. The chart recording shows the difference in time between a 1 MHz clock pulse source, and the pulses picked up from a magnetic mark on the rotor. For this recording the rotor was spinning in air at atmospheric pressure and supported by air bearings, the rotor was not connected to a neutron shutter, and there was no direct coupled analog control of phase.

The recorded noise and drift include contributions from the mark pulse generator circuit, from the circuit which converts time differences into an analog for the recorder, and from the variations in delay of conduction of thyristors, in addition to the variations in angle between the rotor and its rotating field. These variations of angle are caused either by changes in friction or in the torque required to keep the rotor in step with small variations of the clock pulse frequency. The recording shows that when changes in load torque are small the shaft can be controlled with an rms variation of about 1nS, equivalent in this instance to 0.3 seconds of angle. The mean speed can be controlled at least to 1 part in 10^{10} of the reference frequency but there may be short term variations greater than this which are not revealed, as the period is being measured only once per revolution.

8 Acknowledgement

The amplitude/time converter circuit, which is used in the loop which controls the alternator, was designed by Roger Martin, who also gave us useful advice on logic circuits.

References

1. Russell, M. C. B., and Smith, D. B. J. Proceedings of Nucleonics Conference, IEE Publication No. 47, pages 186-191, September 1968.

2. Bedford, L. A. W., Dyer, R. F., Hall, J. W. and Russell, M. C. B. Nuclear Engineering International, pages 330-337, April 1969.

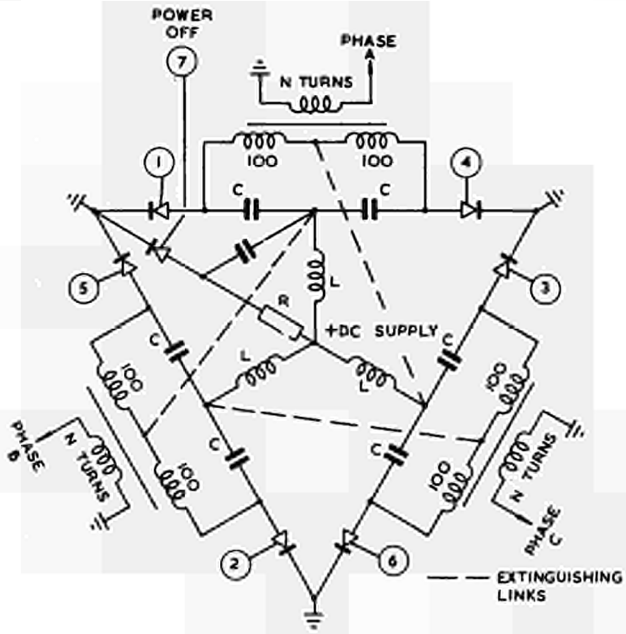

FIG. 1 . THREE-PHASE ALTERNATOR USING SIX THYRISTOR SWITCHES FIRED IN SEQUENCE

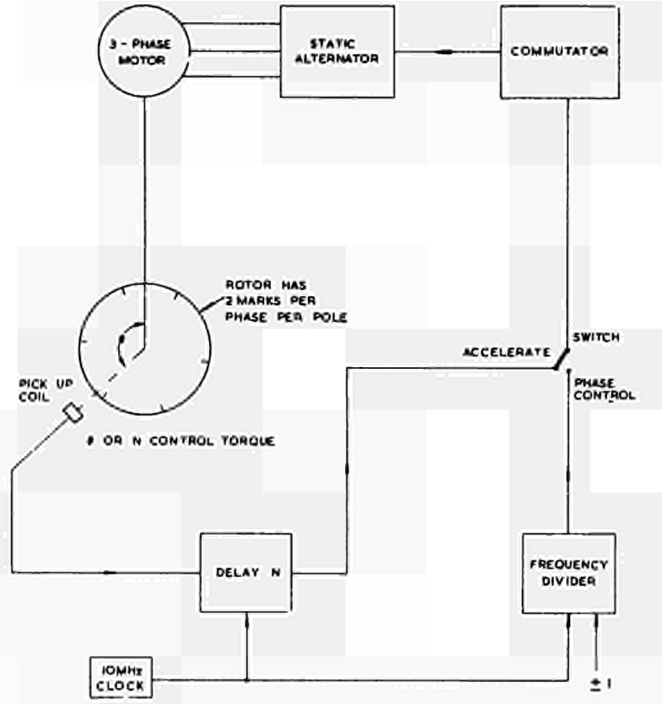

FIG. 2 CONTROL OF SYNCHRONOUS ACCELERATION OR PHASING OF ROTORS

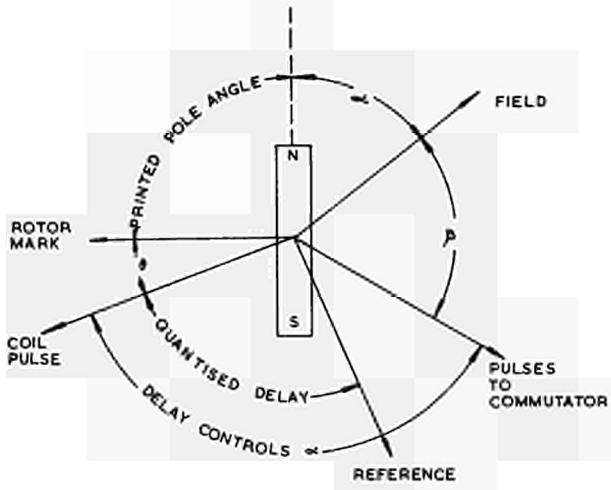

FIG. 3. VECTOR DIAGRAM OF ALTERNATOR AND HYSTERESIS MOTOR

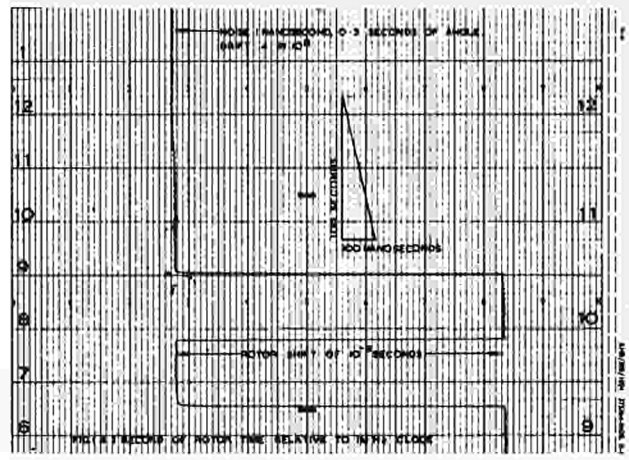

TIME-OF-FLIGHT INSTRUMENTATION FOR A QUASIELASTIC CRITICAL NEUTRON-SCATTERING EXPERIMENT

by

E. Mose Christiansen, Palle Christensen

Danish Atomic Energy Commission
Research Establishment Risö
Electronics Department

Summary

The instrumentation for a quasielastic critical neutron time-of-flight experiment is described. On the basis of an experiment using a sinusoidal modulating chopper and a position-sensitive neutron detector, a combined time-of-flight and scattering-angle analysis is performed by means of a 1024-channel analyser. A digital delay generator delays the phase reference pulses from the chopper for a period equal to the mean flight time of the neutrons. As this may be much longer than the time separation between the reference pulses a special working principle was required. This paper describes in some detail the delay generator and the changes made in the standard pulse-height analyser to perform the position- and the time-of-flight analysis.

Introduction

In a quasielastic critical neutron-scattering experiment a monochromatic neutron beam is directed at the sample, and the scattered neutrons are analysed according to their energy and scattering angle. With the instrumentation described herein the energy analysis is performed by the time-of-flight technique, a sinusoidal modulated neutron beam being used, while the scattering angles are determined by means of a position-sensitive neutron detector.

During the last few years various methods[1,2] of increasing the low efficiency of the standard time-of-flight technique have come into use. One of these methods involves the use of a sinusoidal modulated neutron beam. The standard time-of-flight spectrum may be regarded as the response of the scattering system to an impulse signal, and the scattering parameters are determined from this response function, f(t), but they may be equally well determined from the response of the system to a number of different impressed sinusoidal signals, that is, from the frequency response, $F(\omega)$, of the system.

The method is fully exploited by the use of several neutron detectors or, as in the present work, a position-sensitive neutron detector making simultaneous analysis of the scattering angles possible.

This paper describes the experimental equipment, particularly the electronics used for the time-of-flight- and the scattering-angle analysis.

Experimental Equipment

General Arrangement

Fig. 1 shows a functional diagram of the experimental arrangement. The sinusoidal intensity modulation of the monochromatic neutron beam is effected by means of a high-speed chopper, the rotor disk of which contains a total of 24 uniformly spaced neutron-absorbing sections. The neutrons are detected by the position-sensitive neutron detector after they have been scattered by the sample and have passed through the flight path. This detector is of the type that employs a resistive anode as charge divider, and the position of impact of a neutron is determined from the ratio of the charge accumulated at one end of the detector to the total charge generated by the detection process. The detector[3] consists of a 50 cm long cylindrical brass tube with an anode of 0.3 mm glass wire, coated with colloidal carbon giving a resistance of approximately 45 kilo-ohms. The detector gas is a mixture containing He^3.

The signals from the two ends of the detector are each amplified by a charge-sensitive preamplifier (Nuclear Enterprises, type NE 5287). One signal is further amplified and shaped before being sent to the analogue-to-digital converter (ADC) of the 1024-channel analyser (TMC type CN-1024). The sum of the signals from the two preamplifiers is shaped and amplified in the same way to go finally to the ADC of the analyser.

The ADC was modified to analyse the two signals according to their ratio and thus according to the position of impact of the detected neutron. A single-channel pulse-height selector operating on the sum signal excludes, in connection with the coincidence facility of the ADC, signals that do not originate from the detection of neutrons. Suitable delays were inserted in the two signal paths to give the coincidence circuit of the analyser time for its operation. 128 channels, employing the seven least signifi-

cant bits of the address, are used for the position analysis. The last three bits are set according to time, making up eight phase channels representing in all one period of the modulating signal. From the contents of the phase channels the attenuation and phase shift of the modulating signal are determined.

The phase counter is advanced by pulses generated by the chopper system. A pattern engraved along the rim of the rotor disk is detected by an opto-electronic system giving out eight pulses per period of the modulating signal. To ensure timing accuracy, a balanced detector-amplifier system was used in connection with a zero cross-over trigger. A second pattern and opto-electronic system generate a reset pulse for every eighth pulse from the first pattern to preserve the synchronism between the chopper and the phase counter. The flight time of the neutrons will contribute to the phase shift a term that increases linearly with frequency. In order to compensate for this and thereby reduce the stability demand on the chopper, the reference pulses from the chopper are delayed for a period equal to the mean flight time of the neutrons. A digital delay generator provides this delay.

To take full advantage of the resolution capabilities of the measuring facility, modulation frequencies up to 20 kHz are required. With the 24 periods per revolution this gives a chopper speed of 50 000 r.p.m. The chopper is actuated by a high-frequency motor (C.O. Öberg and Co., type VM 17), fed from a rotating high-frequency generator. The stability obtained by this system without any feedback is 0.5% for several hours. At the lower modulation frequencies this will be sufficient. At the higher frequencies a better stability may, however, be required in order that the delay generator may function correctly. A voltage generated by the delay generator may be used for the stabilization of the chopper.

Digital Delay Generator

Design Parameters. The mean flight-time of the neutrons is a few milliseconds with the present flight path. To fit in with this and also to comply with future requirements, the delay generator was given a maximum delay of 10 msec, adjustable in steps of 1 μsec. The delay generator must be able to delay all the pulses from the chopper by the set period, even though for most modulation frequencies this will be much longer than the time separation between the pulses. Because of the special operating principle needed to achieve this, and in order to keep the time jitter of the delay within a fraction of the setting accuracy, a clock frequency of 10 MHz was chosen. Thus the time jitter will be within 0.3 μsec. The clock oscillator is crystal controlled, giving the delay generator a long-term stability of 20 p.p.m.

Operating Principle. In order to delay pulses for periods longer than those that separate them, the digital delay generator currently measures the difference between the set delay and the total of pulse periods that is just less than the delay. This difference is then used as the preset for the delay counter operating on every input pulse. A specific value of the difference is used as the preset for the delay counter until a new measurement of the difference has been performed, whereupon the preset is corrected in accordance with this. The principle outlined above will delay all pulses for the correct time provided that the totals of any fixed numbers of pulse periods are equal and only change slowly.

A functional diagram of the delay generator is shown in fig. 2. The time difference used as the preset for the delay counter is measured by a five-decade up/down synchronous counter. By pushing the CLEAR- and START-buttons the control logic is reset, and the counter is preset with the delay, set in a four-decade thumb-wheel switch register. The first reference pulse to arrive from the chopper initiates counting-down by clock pulses. If no more reference pulses have arrived when the counter passes zero, an output pulse is generated, the counter is preset with the delay, and the procedure is repeated for every reference pulse from the chopper.

If one or more reference pulses have arrived during the counting-down to zero, the counting is continued. At the arrival of the first reference pulse from the chopper after the expiration of the delay, the counting direction is reversed, and during the following period until the next reference pulse arrives, the clock pulses count the up/down counter up. Then the counting is stopped, and the contents of the counter, which are now equal to the difference between the set delay and the total of reference pulse periods that is just less than the delay, are transferred to a five-decade memory register. The up/down counter is preset to the delay, and the whole procedure is restarted at the next reference pulse.

From the memory register the difference is transferred to the five-decade delay counter. At every reference pulse the counting-down by clock pulses is started. When the contents of the register equal zero, an output pulse is generated, and the delay counter is again preset with the difference contained in the memory register.

The time required for the operation of the control logic and for the transfer of the measured time difference from the up/down counter to the memory register and from this to the delay counter, in-

hibits the generation of an output pulse a few tenths of a microsecond about the time of arrival of the reference pulses. This limits the allowable relative variations of the chopper speed to the ratio between one period of the reference pulse signal and the total delay. Only at the higher speeds may the stability of the chopper be inadequate. An error voltage may, however, be derived from the control logic of the delay generator to be used for the stabilization of the chopper.

The reset pulse for the phase counter in the multi-channel analyser is generated synchronously with the delayed reference pulse that follows next to the arrival of the reset pulse from the chopper system. This means that the measured phase may be wrong by one to seven eighths of a period of the modulating signal. It will, however, always be possible to correct this when the delay and the modulation frequency are known.

Design. The circuits[4] are based on the application of the transistor-transistor-logic integrated digital networks. The two counters as well as the control logic were designed for synchronous operation. Fig. 3 shows the up/down counter, and fig. 4 shows the connections between the registers for a single decade. The design of the decades is approximately as found[5] by using the 1, 2, 4, 8 code. Fig. 5 shows the control logic. A total of 108 dual-in-line network packages were applied, all mounted on a single printed circuit board.

Multichannel Analyser

Position Analysis. The calculation of the charge ratio for determination of the position of impact of a detected neutron is performed by means of the analogue-to-digital converter (ADC, TMC model 213) of the multichannel analyser. The converter is of the Wilkinson type in which a capacitor is charged to a voltage proportional to the pulse to be analysed and then discharged by a constant current. The discharge time and thus the number of gated address advance pulses is then proportional to the pulse height. For the computation of the charge ratio the ADC is altered in such a way that the capacitor is discharged by a current proportional to the denominator of the ratio. The number of address advance pulses is now proportional to the charge ratio.

To make the discharge current proportional to the denominator of the charge ratio, that is the sum pulse, a linear gate, a pulse stretcher and a current generator were added to the ADC (see fig. 6). The linear gate is controlled by the same UNCLAMP signal that controls the gate at the input of the converter circuit. The output from the pulse stretcher and thus the discharge current are sustained until the end of the conversion process. In order to make this particular ADC work, the current generator must supply it with at least 0.2 mA. This sets a lower limit for the sum pulses that might be accepted for analysis. As, however, the minor sum pulses have to be rejected because they do not originate from detected neutrons, this limit is unimportant for our purpose.

The charge ratio is digitized with a resolution of seven bits. Fig. 7 shows the results of a linearity test on the converter. The 128 channels used for the position analysis should be compared with the approximately 2% spatial resolution of the detector. This is illustrated in fig. 8, which shows the performance of the total position analysis system, using a narrow, collimated beam of thermal neutrons. The different intensities of the particular peaks are due to varying gas multiplication along the detector.

Phase Analysis. A separate three-bit phase counter was added to the computer unit to perform the phase analysis. The counter is advanced by the delayed phase reference pulses. At every eighth pulse the counter is reset by the delayed reset pulse in order to keep up the synchronism with the chopper. When a detector pulse has been accepted for analysis, the state of the phase counter is transferred to the three last bits of the address register. The first seven bits are set according to the charge ratio as determined by the ADC. As in normal pulse-height analysis, the memory cycle is initiated at the end of the conversion process. If a detector pulse is coincident with a phase reference pulse, the memory cycle is inhibited as the state of the phase counter is indefinite at that moment. This is effected by using the late anticoincidence facility of the ADC in connection with two one-shot multivibrators to define the resolution time. The multivibrators are triggered by the phase reference pulses and by the phase transfer pulse respectively. The memory cycle is also inhibited by the address overflow signal, taken from the seventh binary.

Conclusion

The instrumentation has been in operation for only a short time, so its performance has not yet been completely evaluated. It has, however, proved its capability in giving spectra with a spatial resolution equal to the theoretically possible for the detector. Fig 9 shows an example of the type of spectra measured by the instrumentation. The individual peaks represent the angular distribution of neutrons scattered by the sample, while the ensemble of peaks gives

the distribution according to the phase. The flight path was 4.45 m, and the measurement was performed at a modulation frequency of 4444 Hz.

Extension of the instrumentation is already foreseen as the instrumentation is going to be governed from the control system of an automatic neutron spectrometer. The stabilization of the chopper as mentioned in this paper is also being prepared in connection with a system to change the chopper speed on command from the control system.

Acknowledgements

The authors wish to thank J. Kjems of the Physics Department for the encouraging co-operation and the patience with which he has awaited the completion of this instrumentation, as well as for the results presented in figs. 8 and 9. Thanks are due to T. Hviid for the design of the logic and the circuitry of the delay generator and for helpful suggestions and assistance with the work. We also wish to acknowledge the work of A. Sloth on the opto-electronic system for the reference pulse generation.

References

1. I.F. Colwell et al., A New High Efficiency Time-of-Flight System. IAEA Symposium, Copenhagen 1968. Paper SM-104/77.

2. F. Gompf et al., The Use of a Pseudostatistical Chopper for Time-of-Flight Measurements. IAEA Symposium, Copenhagen 1969. Paper SM-104/67.

3. I. Kjems, Risö, Denmark, personal communication, 1969.

4. T. Hviid, Risö, Denmark, unpublished work 1969.

5. Texas Instruments: Integrated Circuits Applications Manual.

DISCUSSION

Miller : - I would like to ask what is the limit for accuracy of your dividing circuitry for using it for seven decades of accuracy.

Christensen : - 2% .

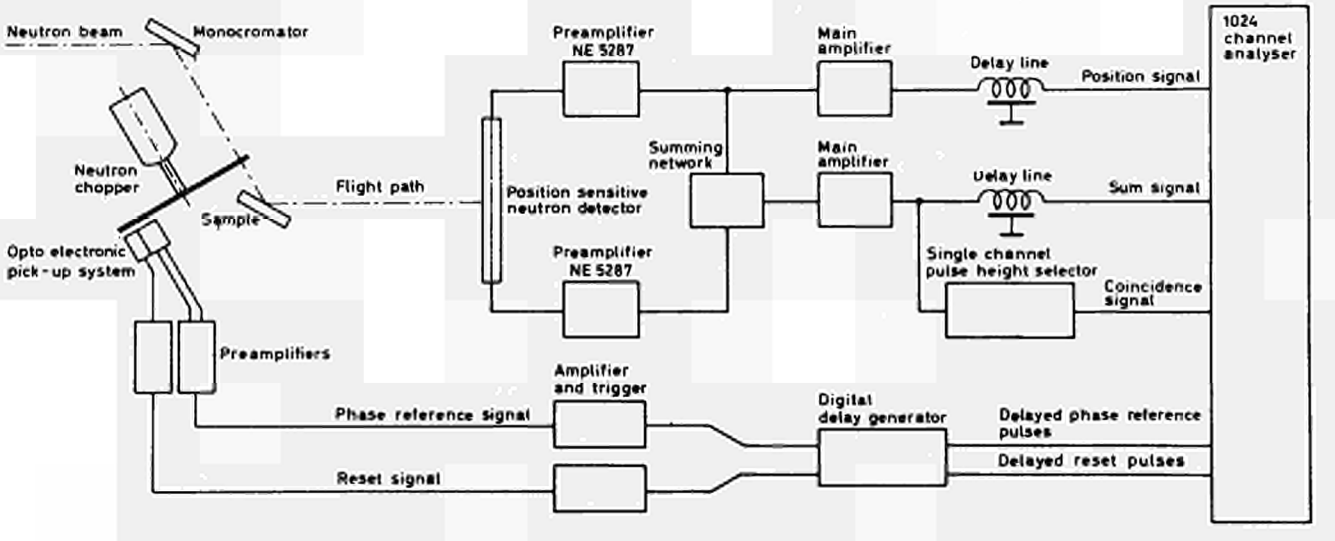

Fig. 1 - Experimental arrangement, functional diagram.

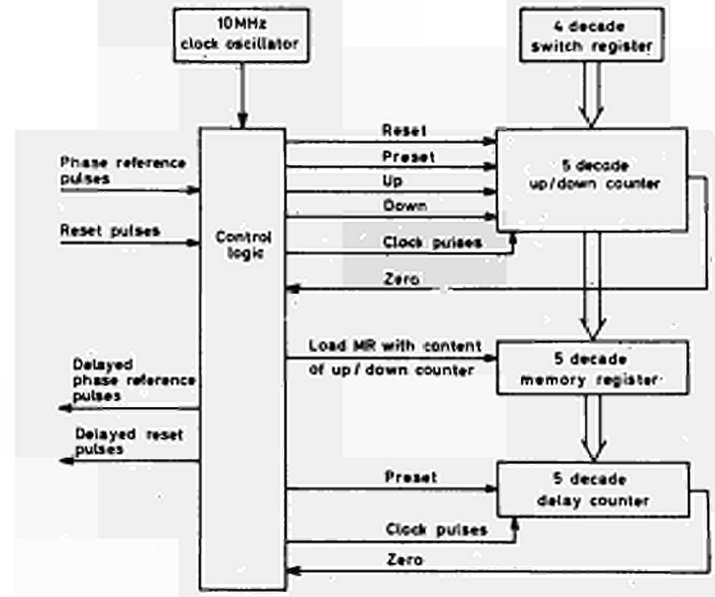

Fig. 2 - Delay generator, functional diagram.

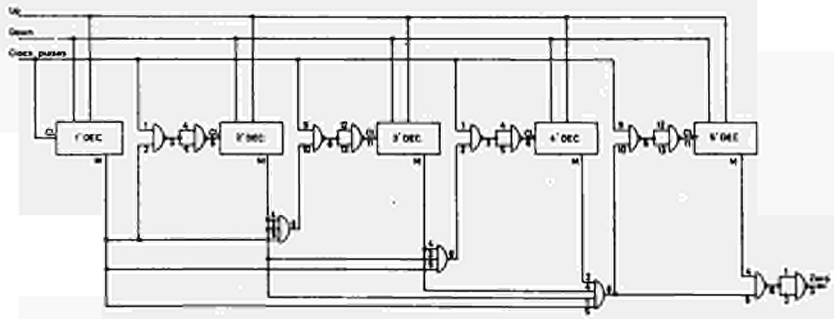

Fig. 3 - Delay generator, block diagram of up/down counter.

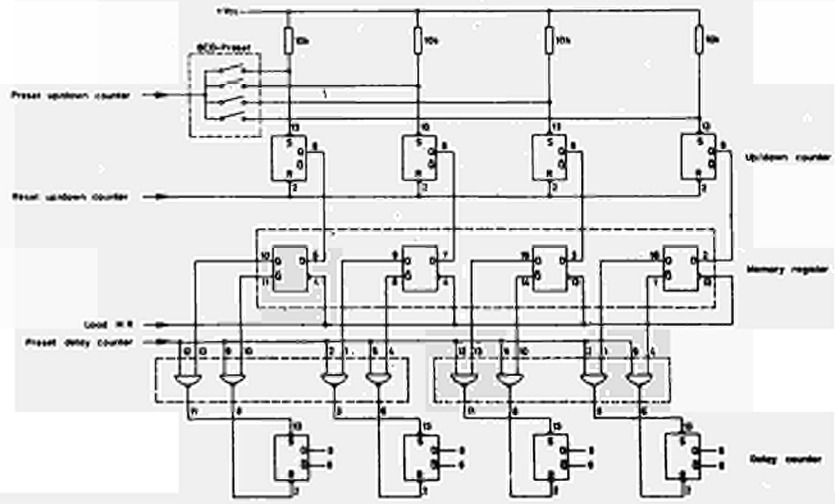

Fig. 4 - Delay generator, block diagram of connections between the registers, one decade shown.

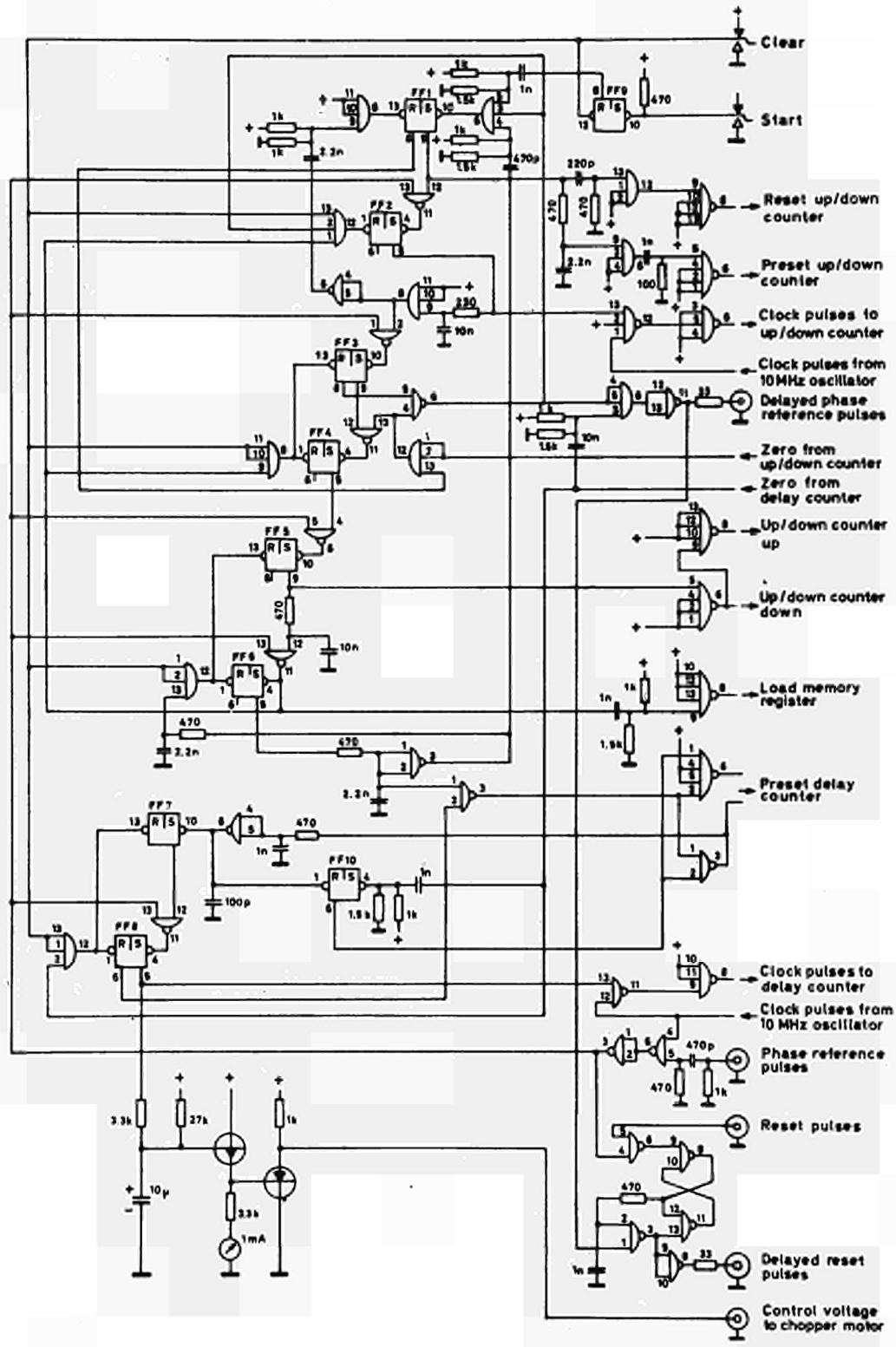

Fig. 5. Delay generator, block diagram of control logic.

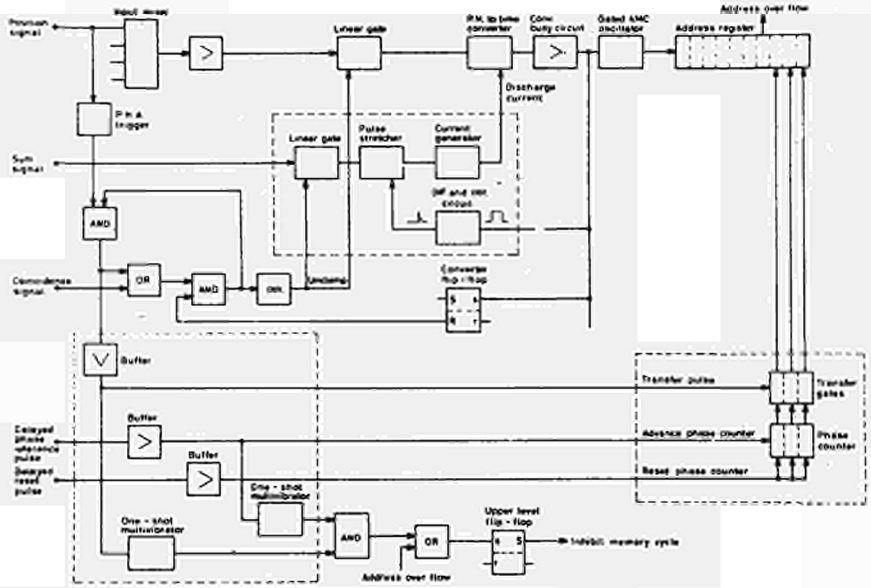

Fig. 6.

1024-channel analyser, simplified block diagram of circuits used for position and phase analysis. The circuits added to the original design are surrounded by a dashed line.

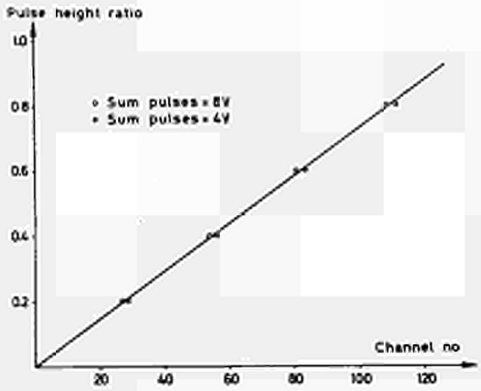

Fig. 7.

Result of linearity test on the pulse-ratio converter.

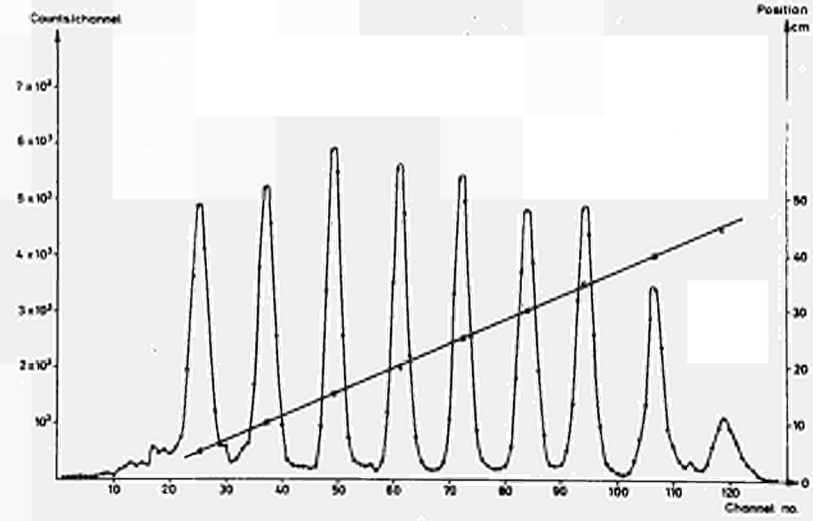

Fig. 8. Result of linearity test on the total position-analysis system by means of a 3 mm collimated beam of thermal neutrons.

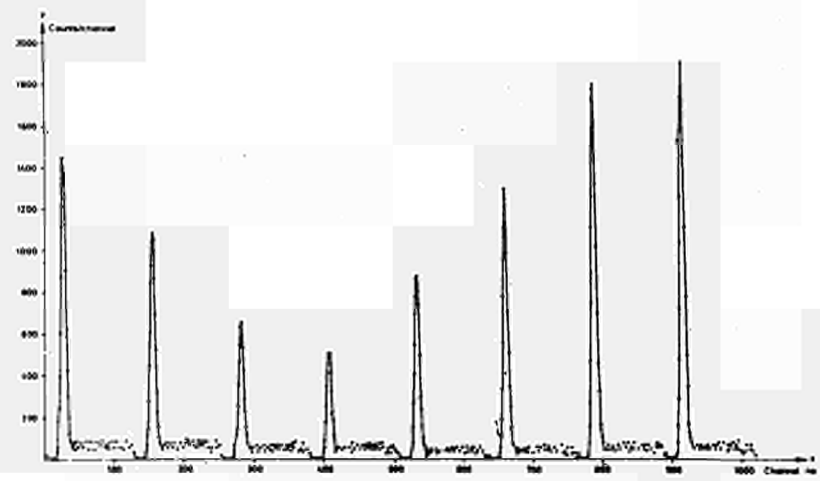

Fig. 9.

Scattering angle/phase spectrum. Flight path 4.45 m; modulation frequency 4444 Hz.

DIFFERENTIAL LINEARITY TESTING AND PRECISION CALIBRATION OF MULTICHANNEL TIME SORTERS.

M. Bertolaccini and S. Cova - Istituto di Fisica del Politecnico, Milano, Italy.

Summary

The requirements for accurate differential linearity measurements of multichannel time sorters are discussed, and it is shown that these measurements can be practically done in reasonable counting time and employing standard laboratory instrumentation. Methods for absolute calibration are also considered, and a technique which is accurate and suitable for routine use is examined in detail.

1. Introduction

The high accuracy required for the analysis of complex time spectra with many different components, as measured by multichannel time sorters, requires an accurate knowledge of the width of each channel. Let us call t_k the time corresponding to the upper border of channel k, $\Delta t_k = t_k - t_{k-1}$ the time interval corresponding to this channel. In a real instrument Δt_k usually differs slightly from channel to channel: if we call Δt_a the constant value which best fits the real Δt_k versus K distribution, the differential non linearity l_k of channel K is defined as

$$l_k = \frac{\Delta t_k - \Delta t_a}{\Delta t_a} \qquad (1)$$

So in a real instrument $t_k = t_o + \sum_1^k \Delta t_r$ differs somewhat from $t_o + K \Delta t_a$, and one defines the integral non linearity L_{1k} from channel 1 to channel K as

$$L_{1k} = \frac{t_k - (t_o + K \Delta t_a)}{K \Delta t_a} = \frac{\sum_1^k l_r}{K} \qquad (2)$$

If the instrument presents differential non linearities, the spectrum shape will be distorted: if distortions are to be avoided or corrected all l_k should be negligibly small or very accurately known. An accurate determination of l_k is usually thought to require careful and time consuming operations or very special equipment. We want to show that it is not necessarily so and that a satisfactory differential linearity test can be performed with standard laboratory instrumentation in reasonable counting times.

Spectra with decay components of very different lifetimes are usually obtained by separate measurements on various time ranges. This means that different portions of the spectrum are measured with different channel widths Δt_a. Now when putting together these results in order to analyse the whole spectrum, we must know very accurately the ratios between the different Δt_a. Small errors in the evaluation of Δt_a may cause considerable errors in the evaluation of low intensity components. So it is often required to calibrate different time ranges with an accuracy better than 1% for the absolute values of Δt_a and even higher for their ratios. Therefore we shall also discuss methods of calibration to evaluate their accuracy and suitability for routine experimental work.

2. Differential linearity testing

We shall make reference in our analysis to the most widely used time sorter, that is a time to pulse hight converter (TPHC) of the start-stop type, followed by a multichannel pulse height analyzer: however extension to other types, such as pulse overlap converters or digital instruments, is not difficult.

If we want to measure an l_k of the order of 10^{-2} we need a delay spectrum known to better than 10^{-2}. An uniform spectrum is not necessary, but it is the most practical. We have to accumulate Q counts per channel, and because of statistical fluctuations Q must be high to determine l_k with sufficient precision, let us say more than 10^4 counts.

If we have C channels, the total number of measurements to be recorded is M = CQ. If the dead time of the analizer is T_{da}, the minimum counting time L_{min} required is

$$L_{min} = MT_{da} \qquad (3)$$

We shall compare with this limit the time actually required by practical methods of testing. For istance if C = 500 and T_{da} = 50 micros, $Q = 10^4$ means $M = 5 \cdot 10^6$ and L_{min} = 250 s, about 4 minutes, which would be practical.

Actually one can almost reach the limit L_{min} by the use of specialized apparatus [1, 2], that is

delayed pulse generators with linearly modulated delay. However such instruments are not common in standard laboratory instrumentation, so we shall suppose to use two separate pulse sources, A for start, B for stop, and see how the measured spectrum depends on the characteristics of the two sources and of the time sorter.

Let us consider one cycle of operation of a start-stop TPHC. At time y = O the instrument becomes ready to operate, and at time y an A pulse starts an operation. B pulses which occur before time y have no effect at all, as the TPHC is supposed to be the start-stop type. If a B pulse occurs after y with a delay $t \leq T_{ma}$ (T_{ma} is the measurement range of the time sorter), that is at time y+t, a measurement is accomplished and the instrument is not able to begin another cycle until a dead time T_{dm} has elapsed. T_{dm} is usually made slightly larger than T_{da}, to ensure correct pulse height analysis for all pulses. If a B pulse does not arrive before time $y + T_{ma}$, operation ends at this time, and following it the instrument is dead for a time T_{dr}.

Some TPHC give in this case a saturated output pulse and have $T_{dr} = T_{dm}$, while in improved ones no output pulse is produced and $T_{dr} < T_{dm}$, usually $T_{dr} \cong 0.1\ T_{dm}$.

Now if we denote by

$p_{A1}(o, y)$ the probability density of having the first A pulse after time y = O at time y.

$p_{B1}(y, y+t)$ the probability density of having the first B pulse after time y at time y+t

the probability density q (t) of having a measurement corresponding to delay t in one cycle of operation is given by

$$q(t) = \int_0^\infty p_{A1}(O, y)\, p_{B1}(y, y+t)\, dy \qquad (4)$$

Note that in general p_{A1} and p_{B1} are not independent; and that the beginning of the cycle, i.e. y = O may be correlated to A or B. For instance if the input of the TPHC is gated, an operation cycle begins when a gating pulse arrives. Suppose this pulse arrives from the output of a supervisory fast coincidence which receives pulses from sources A and B: in general it will be synchronous to the second pulse arrived at the coincidence within the resolving time. Now if the propagation delays from the sources to the coincidence and to the TPHC are so adjusted that A and B pulses have the same relative delay for the coincidence and for the converter, y = O will be correlated to B, that is B will always arrive at a certain time $y+t = y_B$

If no input gating is used y = O corresponds to the end of the dead time of the preceding cycle, and will be in many cases not correlated to A or B. So we shall consider two cases, supposing that A and B are stationary sources

a) B is not correlated to y=O, so that p_{B1} does not depend on y, but only on t. Then

$$q(t) = p_{B1}(t) \int_0^\infty p_{A1}(y)\, dy = p_{B1}(t) \qquad (5)$$

Note that in this case q(t) does not depend on the type of source A: it depends on the type of source B and on its correlation to source A.

b) B may arrive only at a definite time $y+t = b \leq T_{ma}$, with probability P_B ($P_B = 1$ being also possible)

Then

$$p_{B1}(y, y+t) = P_B\, \delta(y+t-b) \qquad (6)$$

and

$$q(t) = P_B\, p_{A1}(b-t) \qquad (7)$$

In this case q(t) does not depend on the type of source B, but just on the type of source A and on its correlation to B.

So in both these cases q(t), that is the shape of the delay spectrum, will depend on the correlation between the two sources and on the type of only one of them. The other source will contribute to determine the counting rate of measurements. A first requisite on the two sources to obtain an uniform q(t) is therefore that they are not correlated. Provided we fulfill this condition, one of them may be selected rather arbitrarily, so we shall take it with high repetition rate to have a high counting rate of measurements.

Let us consider case a), and suppose A has a high repetition rate N_A. The effective start repetition rate is limited by the mean time interval T_d after an operation is started, during which the instrument is busy. Now T_d depends on the measurement time $t \leq T_{ma}$ and on the following dead time T_{dr} (without stop B) or T_{dm} (with stop B). Let us denote by $P_{Bo}(T_{ma})$ the probability of having no B events with $t \leq T_{ma}$, and suppose $T_{ma} \ll T_{dr}$, so that

$$T_d \cong \left[1 - P_{Bo}(T_{ma})\right] T_{dm} + P_{Bo}(T_{ma})\, T_{dr} \qquad (8)$$

If we have $N_A \gg 1/T_d$ the rate at which measurements will be started is

$$N_A' \cong \frac{1}{T_d} \qquad (9)$$

and the rate at which measurements are performed is

$$N_m = N_A' \left[1 - P_{Bo}(T_{ma})\right] \cong \frac{1 - P_{Bo}(T_{ma})}{T_d} \qquad (10)$$

so that the counting time required will be

$$L = \frac{M}{N_m} = \frac{M\, T_d}{1 - P_{Bo}(T_{ma})} \qquad (11)$$

Now let us consider source B.

Suppose first that B gives pulses randomly distributed in time, and is not correlated to A. Let us call $P_{Bo}(t)$ the probability of having no B pulses in an interval t and $p_B = \frac{1}{\tau_B}$ the probability density of having a B pulse at time t.

Then

$$q(t) = p_{B1}(t) = P_{Bo}(t)p_B = \frac{e^{-t/\tau_B}}{\tau_B} \qquad (12)$$

So if q(t) must be constant to better than 10^{-2} up to $t = T_{ma}$, we need

$$1-P_{Bo}(T_{ma}) < 10^{-2} \qquad (13)$$

and therefore

$$T_d \simeq T_{d2}$$
$$L > 10^2 T_{dr} \qquad (14)$$

that is with $T_{dr} \simeq 0.1\, T_{dm} \simeq 0.1\, T_{da}$ one has $L > 10\, L_{min}$, and with $T_{dr} = T_{da}$ one arrives to $L > 100\, L_{min}$.

In the numerical example previously given this means more than 40 minutes in the first case, more than 7 hours in the second.

So a random source has the disadvantage of requiring a long counting time. However there is one advantage: that it is not difficult in practice to have two uncorrelated random spurces, for istance using two scintillation detectors with separate sources and placed some distance apart.

Suppose now that B is periodic, with period τ_B, and not correlated to A. We have then

$$\begin{cases} p_{B1}(t) = \frac{1}{\tau_B} & \text{for } t \leq \tau_B \\ p_{B1}(t) = 0 & t > \tau_B \end{cases} \qquad (15)$$

$$\begin{cases} 1-P_{Bo}(T_{ma}) = \frac{T_{ma}}{\tau_B} & \text{for } T_{ma} \leq \tau_B \\ 1-P_{Bo}(T_{ma}) = 0 & \text{for } T_{ma} > \tau_B \end{cases} \qquad (16)$$

So, taking τ_B slightly larger than T_{ma}, we shall have in principle an uniform q(t) over the range T_{ma}, and $1-P_{Bo}(T_{ma}) \simeq 1$, so that $T_d \simeq T_{dm}$ and

$$L \simeq M\, T_{dm} \simeq M\, T_{da} \simeq L_{min} \; ; \qquad (17)$$

In practice two pulse generators will almost certainly be more or less correlated, it they are not expressely designed with special precautions in power supply filtering and R F shielding and q(t) will be not uniform and quite impredictable.

Let us now suppose that we take as B the output of a tigger circuit with a fixed dead time T_1; triggered by pulses from a random source which has probability density $p_B = \frac{1}{\tau_B}$ of having a pulse at time t. It is easy to show (see Appendix) that if B pulses are not correlated to A, i.e. B pulses are not correlated to time t = O,

$$\begin{aligned} q(t) = p_{B1}(t) &= \frac{1}{T_1 + \tau_B} && \text{for } t \leq T_1 \\ q(t) = p_{B1}(t) &= \frac{1}{T_1 + \tau_B} e^{-\frac{t-T_1}{\tau_B}} && \text{for } t \geq T_1 \end{aligned} \qquad (18)$$

So to take $T_1 \geq T_{ma}$ will be sufficient for our purpose. We have in this case

$$1-P_{Bo}(T_{ma}) = \frac{T_{ma}}{T_1 + \tau_B} \qquad (19)$$

This probability may be made close to 1 using a high repetition rate random source and we can obtain co obtain counting times L not far from L_{min}. From a practical standpoint, by the use of two uncorrelated random sources giving high level pulses (scintillation detectors), it is not difficult to avoid correlation between the trigger circuits fed by such pulses.

As a conclusion an accurate linearity test may be performed on a time sorter without using input gating, and employing as start A a high repetition rate random source, as stop B another high repetition rate random source not correlated to the first and coupled to a trigger circuit with dead time greater than the delay range to be tested.

For short time ranges (of the order of some tens of nanoseconds) it is easy to show (see case b) that, if input gating by a fast coincidence as previously described is used, reasonable counting times may also be achieved using as stop B a high repetition rate random source, as start A another random source uncorrelated to B and with mean interval between pulses $\tau_A > 10^2 T_{ma}$.

3. Calibration

A calibration method suitable for routine use should be highly accurate and versatile over various time ranges; it should not require very special or cumbersome apparatus and allow calibration to be performed in a short time.

Let us review the various methods known.

a) Use of calibrated delay cables. The drawbacks are well known. The accuracy is often unsatisfactory, as the propagation characteristics of coaxial cables are frequency dependent[3], and the effective delay depends on the pulse shape and on the characteristics of the trigger circuit which receives the pulse. With some circuits it is possible to use a simple and elegant method[4] to calibrate directly the cables connected to the circuits to be used, making a non linear closed loop oscillator and measuring its period. However calibration of the time sorter requires many cables, is quite tedious and long and is practically not possible for ranges greater than one microsecond. For short delay ranges (tens of nanoseconds) special delay lines of complicated mechanical construction have also been used[5].

b) [illegible] ray times of flight over accurately known

distances, usually employing positron annihilation sources. The method is suitable only for nanosecond ranges, the accuracy is not high and systematic errors may be caused by counting rate variation when changing source-detectors distances.

c) The uniform delay spectrum method. Let us consider a linearity test made in one of the ways corresponding to case a) of the preceding paragraph. If p_B is the probability density of having a pulse B with delay t, that is if source B has mean repetition rate $N_B = p_B$, the probability of getting a count in channel K in one cycle of operation is

$$q(K) = N_B \Delta t_K \qquad (20)$$

But if during one measurement we had n'_A effective starts and we find Q_K counts in channel K

$$q(K) = \frac{Q_K}{n'_A} \qquad (21)$$

So if one measures N_B, n'_A and Q_K, one can obtain the absolute value Δt_K. However precision and accuracy are not very high, and in any case one has to rely on a linearity measurement, while it would be advisable to obtain the calibration independently.

d) A radio frequency technique introduced by De Waard[6], employing a pulse mixer receiving pulses from two sources A and B a precision tuned U. H. F. radio receiver that selects those couples of A and B pulses spaced by multiples of a known period. This technique is very ingenious but nevertheless not versatile over many time ranges.

e) Methods employing a precision clock pulse generator, with a very stable and accurately known period (usually quartz controlled, and therefore accurate to better than 10^{-3}). This period is the calibration interval, and by demultiplication many time ranges may be easily covered, with very high precision in the ratios of the calibration on different ranges. The basic idea is to select in two different ways some of the pulses from the clock and thus obtain at two outputs A and B couples of pulses spaced by many different multiples of the period. The calibration spectrum consists of a series of lines spaced by one period. In a first scheme by Hatcher[7] A was just the clock demultiplied, while B was the output of a coincidence receiving the clock pulses and auxiliary pulses not correlated to the clock. In a subsequent application by Cho et al.[8] even A was obtained by another coincidence and another auxiliary A pulse, not correlated to the clock and to the auxiliary B pulse. Other instruments based on the same scheme have been described[9], differing in the choice of auxiliary pulses, which may be any couple of A and B suitable for a linearity test.

Only method e) seems to us to combine all the requisites. The required apparatus may be readily assembled from standard laboratory instrumentation, oscillators with accuracy and stability better than 10^{-3} are quite common and the operation requires a few minutes. However we recognized the opportunity of introducing two further improvements.

The first one concerns the precision on nanosecond ranges. As the clock pulse has a non zero width it happens sometimes that the leading edge of the auxiliary pulse falls between the leading and the trailing edge of the clock pulse. In this instance the output of the coincidence is not properly synchronized to the clock, and it has an error of the order of the width of the clock pulse, that is at least a few nanoseconds. This means that on nanosecond ranges the shape of the calibration lines will be considerably wider than the intrinsic resolution of the time sorter. This error can be corrected very simply, as shown in Fig. 1.

A second coincidence is employed, which receives the output pulse of the first one, shaped in a rectangular shape of about 20 ns duration, and the clock pulse train suitably delayed, so that a clock pulse falls aproximately in the middle of the rectangular pulse. The error of some nanoseconds in the rectangular pulse position has therefore no effect on the synchronization of the output pulse from coincidence 2 to the clock. In Fig. 2 a comparison is made of the shapes of the calibration lines without and with the correction by coincidence 2: the corrected line is consistent with instrumental resolution of the time sorter.

The second modification concerns versatility over various time ranges. If the resolving time of coincidence 1 in Fig. 1 is much less than the clock period, the probability of having an output pulse corresponding to an auxiliary pulse is low, and this increases the counting time for calibration. On the other side, if the resolving time is greater than the clock period, one can have more than one output pulse for each auxiliary pulse, which may be undesiderable. So it is often advisable to readjust the resolving time when the clock period is changed. This readjustment is avoided if one substitutes a bistable to coincidence 1, as shown in Fig. 3. The auxiliary pulse resets and holds in the lower state the bistable, even if clock pulses are present. The first clock pulse after the end of the auxiliary pulse sets the bistable in the upper state. This transition is shaped and used as an output, so to each auxiliary pulse there always corresponds one output pulse.

The output from bistable 1 is subject to the same error as that of coincidence 1 and this may be corrected by a coincidence, as in the scheme in

Fig. 1. However inf Fig. 3 the second coincidence is substituted by an alternative solution, which gives equivalent results and is somewhat simpler to be adjusted in practice. The reset transition of bistable 1 sets bistable 2 in the upper state and this acts as a gating on the output tunnel diode, allowing it to be triggered by the next clock pulse. The output pulse resets bistable 2 and therefore the output tunnel diode.

These modifications allow to perform in a few minutes calibrations with clock periods from about 10 ns upward: practically no readjustment other than the clock period is needed when the range is changed. The narrow line width even on nanosecond ranges allows to obtain calibration lines spaced by known fractions of nanoseconds if one employs successively two clock generators with a known small difference in their periods(*). Only very short term stability is required for the circuits utilizing the clock waveform, which determines the accuracy and stability of the calibration.

In Fig. 4 a calibration and a differential linearity test on the same time sorter are shown. We note that calibration is complementary to the linearity measurement. This is not only because the number of counts in the various lines gives a fast rough evaluation of linearity, provided that auxiliary A and B satisfy the requisites of a differential linearity test. More important is the fact that even if A or B are somewhat correlated the number of counts in the lines are affected, but not their channel position. Therefore if we consider the integral of the differential linearity curve, as shown in Fig. 5, if start-stop correlations have been present in the measurement, not all the calibration points will fall on the curve. So an indepenent check of the linearity measurement is possible.

Appendix

Let us consider a stationary source of pulses randomly distributed in time, with $p = \frac{1}{\tau}$ probability density of having a pulse at a given time. These pulses trigger a circuit which gives an output pulse and is then insensitive for a fixed dead time T_1 to following pulses.

We call p_s the probability density of having an output pulse at time y; p_{s1} the probability density of having the first output pulse after y = O; $P_{so}(y_1, y_2)$ the probability of having no output pulses from y_1 to y_2.

So we have

$$p_{s1}(y) = p_s = P_s(y-T_1)p \qquad \text{for } y \leq T_1$$
$$p_{s1}(y) = P_{so}(O,y)p \qquad \text{for } y \geq T_1 \qquad \text{(A1)}$$

Let us consider the case in which the time origin y = O is not correlated to output pulses, and therefore $P_{so}(y-T_1, y)$ does not depend on y $P_{so}(y-T_1, y) = P_{so}(O, T_1)$ for $y \leq T_1$ we have

$$1 - P_{so}(O,y) = \int_0^y p_s \, dx = P_{so}(O,T_1) \int_0^y p \, dx =$$

$$= P_{so}(O,T_1)py \qquad \text{(A2)}$$

so we get

$$P_{so}(O,T_1) = \frac{1}{1+pT_1} = \frac{\tau}{\tau+T_1} \qquad \text{(A3)}$$

$$1 - P_{so}(O,y) = \frac{y}{\tau+T_1} \qquad \text{(A4)}$$

For $y > T_1$ we have

$$dP_{so}(O,y) = -p_{s1}(y)\,dy = -P_{so}(O,y)p\,dy \qquad \text{(A5)}$$

$$P_{so}(O,y) = P_{so}(O,T_1)\, e^{-\frac{y-T_1}{\tau}} \qquad \text{(A6)}$$

so that

$$p_{s1} = \frac{1}{\tau + T_1}$$

$$p_{s1} = \frac{1}{\tau + T_1} e^{-\frac{y-T_1}{\tau}} \qquad \text{(A7)}$$

References

(1) M. Birk, Q. A. Kerns and T. A. Nunamaker: Rev. Scient. Instr. 34 (1963), 1026.

(2) S. Cova and M. Bertolaccini: to be published

(3) G. Fidecaro: Nuovo Cimento 15, suppl. 2 (1960) 254

(4) B. Kiesler, B. Righini: Boll. Soc. Italiana Fis. no. 55 (1967) 23.

(5) R. L. Graham, J. S. Geiger, R. E. Bell and R. Barton: Nucl. Instr. 15 (1962) 40.

(6) H. De Waard and H. Beekhuis: Proceed. 1961 Gatlinburg Conf. Electromagn. Lifetimes and Properties of Nuclear States, publ. 974 Nat. Acad. Sci., Nat. Res. Council (1962) Washing.. H. De Waard: Rev. Scient. Instr. 20 (1949) 911.

(7) C. Hatcher, E. G. &G. Nanonotes 1, no. 2 (1964)

(8) Z. H. Cho, L. Gidefeldt and L. Eriksson: Nucl. Instr. 52, (1967) 273

(9) A. Lansfard and P. E. Dolley: Nucl. Instr. 59 (1968) 120.
C. A. Baker, C. J. Batty and L. E. Williams: Nucl. Instr. 59 (1968) 125.

(10) F. A. Johnson: Nucl. Instr. 59 (1968) 237.

(*) A scheme proposed by Johnson[10] employs a clock generator and another one of about the same frequency to obtain calibration lines spaced by a known fraction of the clock period, but it suffers from even small relative drifts of the two generators being thus not very practical.

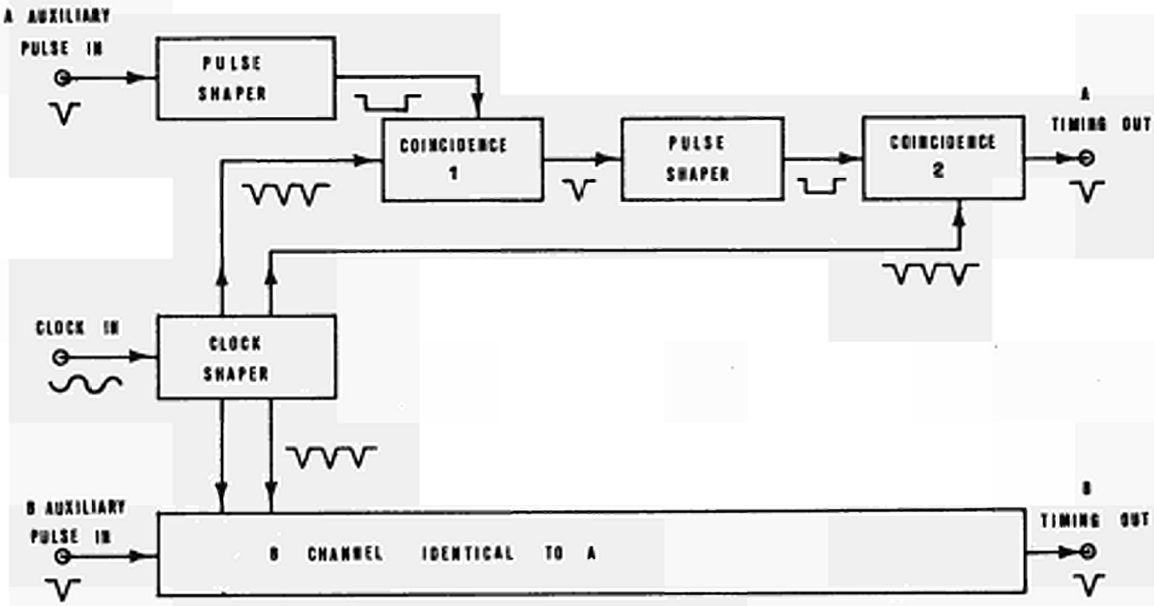

Fig. 1 - Experimental set up to obtain a a calibrated delay spectrum from a clock waveform. Coincidence 2 provides correct synchronization of output pulses to the clock.

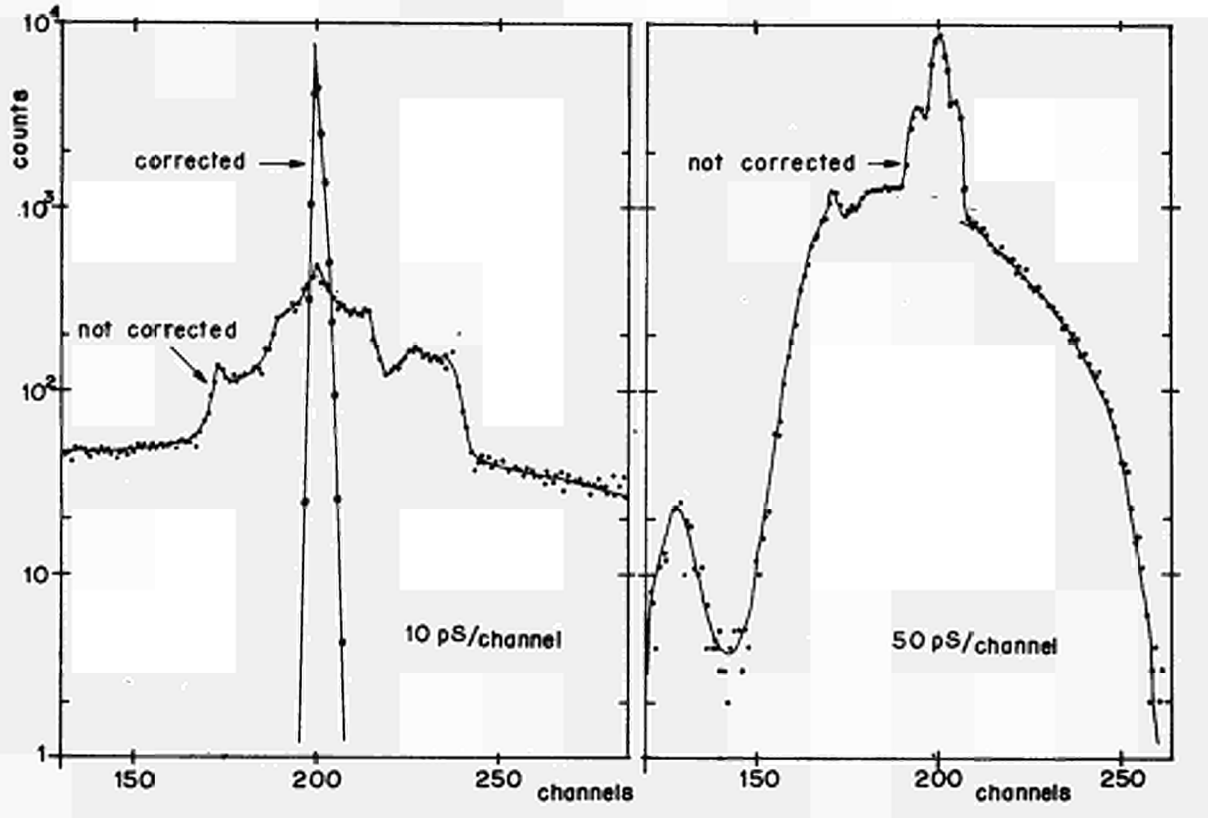

Fig. 2 - Line shapes in the calibration spectrum with and without the syncronization correction by the second coincidence.

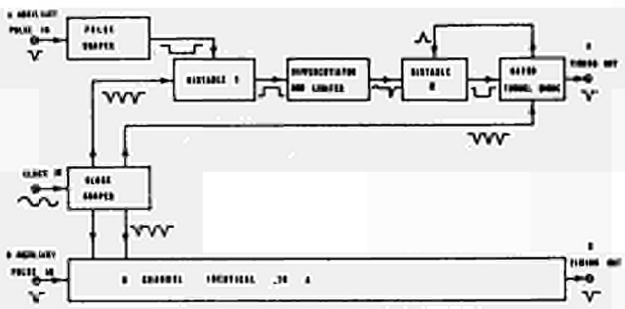

Fig. 3 – Modified experimental set up: bistable 1 instead of coincidence 1 in Fig. 1. allows higher counting rate without readjustments when calibration is made with longer clock periods (microseconds or more).

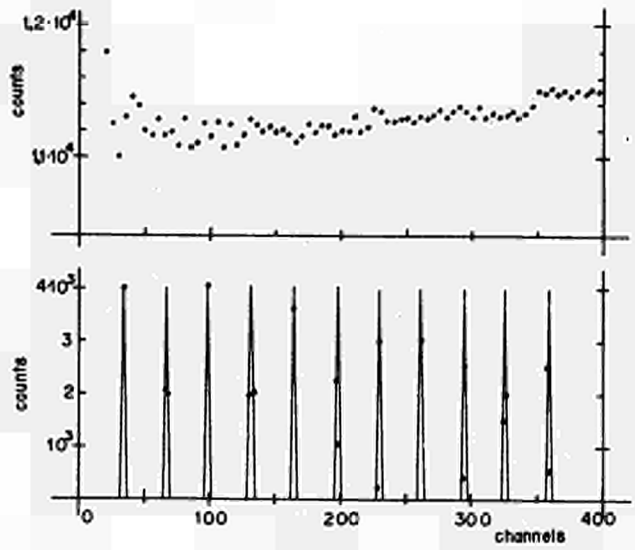

Fig. 4 – Differential linearity measurement and calibration of a time sorter.

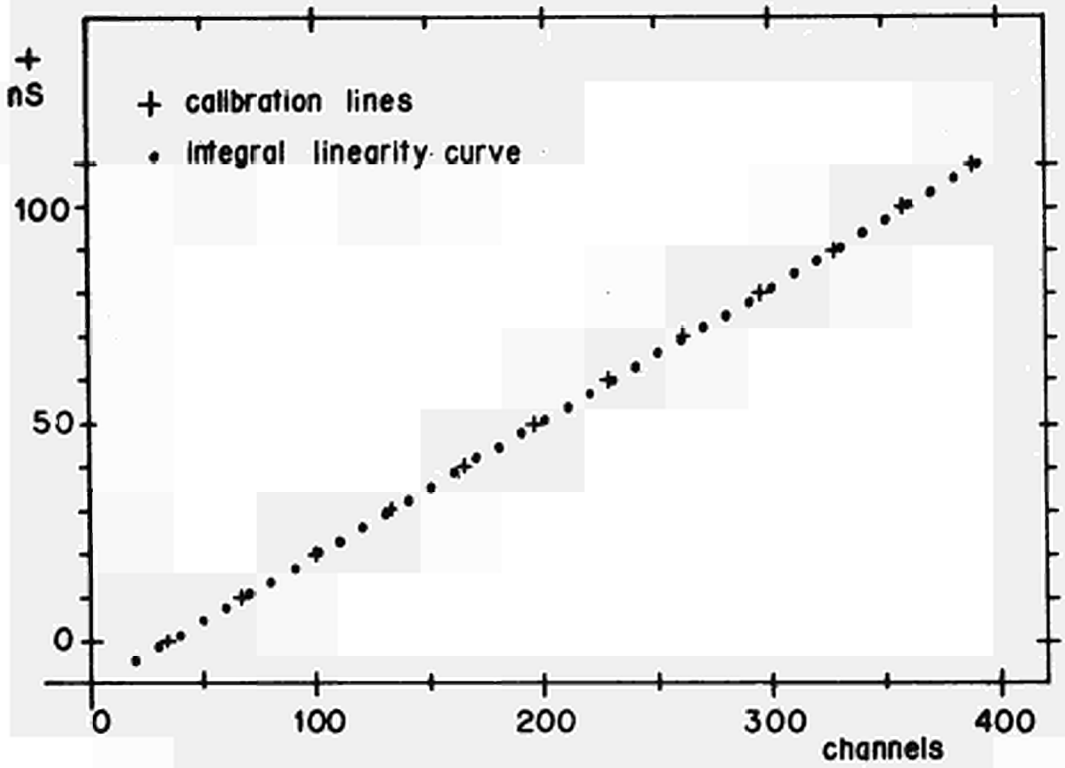

Fig. 5 – Comparison between calibration points and the integral of the differential linearity curve of Fig. 4. The agreement confirms absence of start-stop correlations in the differential linearity measurement.

A WEIGHTED CHRONOTRON FOR TIME-DIGIT CONVERSION

Monica Feran, Eli Katz, Radu Papina,
Institute of Atomic Physics, Bucharest - Rumania

Summary

A time interval is measured by counting the integer number of periods of a delay line generator with taps at weighted intervals, iteratively swept by a START pulse. The remainder of the time interval is measured by iteratively circulating START and STOP pulses through the weighted portions of the line and succesively subtracting and registering them.

1. Introduction

Progress in improving particle detector performances and continuous increase in the volume of information to be processed have led to a continuous development of analog to digital converters with respect to speed, channel width, number of channels and differential linearity. Special care has been given to time-digital converters used in determining the distributions of time intervals occurring between succesive events. The use of the proposed weighted chronotron allows : a) A smaller number of circuits proportional to the logarithm of the number of channels contained in the period of the chronotron, thus allowing the reduction of channel width by only slightly increasing the number of circuits. b) A scaler with a substantially lower resolution than the corresponding channel.width. c) A relatively simple logic based on a small number of circuit types. d) Mean conversion time slightly greater than that of the simple chronotron.

2. The instrument

The basic idea consists in first recording the number of integer periods of the chronotron contained in the time interval to be measured and then in measuring the remainder using weighted fractions of the chronotron period, as usual in the succesive approximation method of the amplitude digital conversion.

A delay line with taps, DL (fig. 1), gives the period of the chronotron. The taps are at weighted distances from the input-port D of the line, i.e. at distances $D_k = 2^k . \tau . v$, where $k = 0,1..,$ n, τ = channel width, v = propagation speed on the line. Besides this taps these are n-1 supplementary taps, D'_k, placed at a distancesbefore taps D_k, (it is seen that D'_0 coincides with D, and D'_1 with D_0) and one compensation tap, D_0. Summing up, there are $2(n+1)$ taps for 2^n channels in comparison with 2^n+1 taps used in the conventional method with uniformly distributed taps.

The START pulse passes through the normally open gate P_{st}, and through OR-1 gate, and starts the generator G_{st}, which through OR-2 gate and the initially open C gate, sends through the line a pulse of duration τ_i, so that $\tau < \tau_i \leq 1,5\,\tau$.
The START pulse suitable delayed (Δ) also closes the P_{st} gate as well as the C gate, (through flip-flop B_B). The leading front of the pulse determines its

position on the line. For this purpose, each D'_K tap is linked to one of the coincidence inputs of the coincidence-anticoincidence circuits CA_k , while the D_k taps are linked to the anticoincidence inputs of the same circuits, CA_k. Thus the CA_k circuits are sensibilised in the moment when the leading edge of the pulse reaches the D'_k tap, and blocked when it reaches the D_k one, the total duration of sensibilisation beeing τ . In this manner, the presence of the pulse in the channels 2^k (K = 0,1 ....n), which are the last of the respective weighted fractions of the line, is determined. The presence of the pulse in the channels comprised between D_{k-1} and D'_k (K = 3,4,....n) is determined by the flip-flop circuits $M_{(k-1),k}$ and by the their associated coincidence-anticoincidence circuits, $CA_{(k-1),k}$. When the leading edge reaches the tap D_{k-1}, thus when it passes in the channel $2^{k-1}+1$, it sets the $M_{(k-1),k}$ flip-flop in position "1" and this one sensibilises one of the coincidence inputs of the correspondind $CA_{(k-1),k}$ circuit. When the leading edge reaches the D'_k tap, thus passing into channel 2^k, it resets $M_{(k-1),k}$ flip-flop and thus the $CA_{(k-1),k}$ circuit is blocked. So, the $M_{(k-1),k}$ circuits act as memory cells beeing set in state "1" for the time the pulse is somewhere between channels 2^{k-1} and 2^k. For the purpose of compensating the delay due to switching time of the $M_{(k-1),k}$ circuits, the $CA_{(k-1),k}$ circuits are also directly blocked by D'_k taps through one of the anticoincidence inputs. For the interval D_1 - D'_2 (channel 3) there is no flip-flop necessary and the $CA_{1,2}$ circuit is directly linked to taps D_1 and D'_2. Summarizing, the position of the pulse on the delay line is dedetermined by the fact that only one of the CA_k or $CA_{(k-1),k}$ circuits is sensibilised at one moment, the former indicating the presence of the pulse in the last channel of the weighted portions and the latter indicating its presence in the interior of these portions. After travelling through the line, the START pulse passes on one hand through the delay circuit I and the normally open gate R to a binnary scaler N recording the passage of 2^n channels: on the other hand, it returns through the normally open gate P to the OR-1 gate and from it repeats the cycle. The output to the N scaler is taken from the D'_n tap, the passage of which means that the pulse has entered the 2^n channel of the line. The output for the recycling is taken from the compensation tap D_c leading by a time δ the final tap, δ beeing so chosen as to compensate the time necessary for the pulse to pass through the circuits P, OR-1, G_{st}, OR-2 which return and reshape the pulse from the output to the input of the delay-line. The reshaped pulse which exists at the correspondind input of gate C is sent on the line at the instant at which the leading edge of the pulse which already exists on the line, reaching its end-tape D_n-, opens through OR-5 the gate C. In this manner: a) the delay determined by the reshaping circuits is eliminated from the chronotron period, thus improving the stability of the chronotron frequency, b) the channels which are integer multiples of 2^n are correctly determined. The differential distorsion which would appear if the 2^n channels should be determined (fig.2) by taps D'_n and D_n (the respective channels should be longer than τ i.e. $\tau + \delta$) as well as the integral distorsion which would appear if this channels should be determined by taps D'_n and D (after each group of 2^n channels should appear a shift δ) are eliminated. After the elapsing of the time interval T, whose conversion is to be done, interval in which

m pulses corresponding to $m.2^n$ channels ($T = T_i + T_f = m.2^n.\tau + T_f$, where $T_f < 2^n.\tau$) are recorded in scaler N, the pulse STOP appears. It passes through a normally open gate P_{sp}; through the circuit OR-3, to a generator G_{sp} which generates a standard pulse of duration τ_s ($\tau < \tau_s \leq 1,5\tau$) This pulse is simultaneously fed to the second coincidence inputs of all the CA circuits. During the STOP pulse, while the START pulse progresses on the line, one or more of the circuits CA give succesively coincidence signals. For the purpose of selecting the first (in time) of them - that one which corresponds to the coincidence of the leading edges of the START and STOP pulses - a series of selecting circuits CS_K, $CS_{K-1,k}$ are introduced which permit the passage of the signal generated by a coincidence circuit only if the preceding coincidence circuits have not been actuated (CS_o, the first selection circuit is blockable by the last coincidence circuit, CA_n). As a result, when the STOP pulse appears, a signal is obtained at the output of only one of the selective circuits. The subsequent processing depends on which of the CS circuits has been actuated. If it is a CS_k circuit which gives the signal, then it means that the START-STOP coincidence occurred when the START pulse was inside one of the separating channels of the weighted fractions of the line. The pulse from the output of the actuated CS_k circuit closes the analysis recording through a circuit $OR\text{-}I_k$ a logic "1" in flip-flop B_K. The B_K flip-flops form a register, N_o, for the small figures of the number obtained by conversion.. The closing of the conversion is made by the same CS_k pulse which through the OR-6 circuit actuates a circuit END, which resets in their initial position the gates and the flip-flops of the converter. The last coincidence-anticoincidence circuit, CA_n does not need a selection circuit because the recording in its case is at any rate made in the scaler N. The pulse of the CA_n circuits blocks the selecting circuit CS_o, thus avoiding the recording of one channel in excess (since, due to the duration of the START and STOP pulses, a coincidence in CA_n is followed by a coincidence in CA_o); however the pulse of the CA_o circuits bypasses in its way to the OR-6 and END circuits, the selection circuit CS_o. As a result, the coincidence in CA_o stops the conversion in both cases, without recording a "1" in B_o (when the first coincidence occurred in CA_n), or with a recording a "1" in B_o, when the first coincidence occurred in CA_o.

If the actuated selection circuit was a $CA_{k-1,k}$ circuit, that means a STOP pulse occurred while the START pulse was somewhere on the weighted portion of the line, between channels 2^{k-1} and 2^k. The pulse from the output of the circuit $CS_{k-1,k}$ has two effects: first, through the circuit $OR\text{-}I_{k-1}$ it sets the flip-flop B_{k-1} in state "1", thus recording that the START pulse has already travelled across the weighted portions of the line preceding the one in which it was at the moment the STOP pulse appeared. Second, for the purpose of converting also the remainder, T_R (fig.1) the pulse from the output of $CS_{k-1,k}$: a) opens for a time equal to the sum of the preceeding weighted portions, the gates P_k and S_k ; b) passes through the OR-4 circuit and starts the monopulse generator G_{sr} which through OR-2 sends a reshaped STOP-pulse on the line (the C gate has been previously opened by the STOP, through B_B flip-flop); c) blocks also, for a time equal with the sum of the preceeding weighted portions, all the circuits (beginning with $CA_{k,k+1}$) which follow the actuated circuit $CA_{k-1,k}$ avoiding the possible coincidence between

the START pulse which continues to travel across the line and the reshaped STOP-pulse; d) blocks the P gate.

Starting from this moment two pulses travel across the line, one START and one STOP. The START pulse continues its way reaching the tap D_k (after a time $t = 2^{k-1} \cdot \tau - T_R$) then passes through a delaying circuit I_k and the gate P_k previously opened by $CS_{k-1,k}$, and by OR-1 starts G_{st} which through OR-2 sends a new START pulse on the line. In this time the STOP pulse which covered on the line a distance corresponding to the time $2^{k-1} \cdot \tau - T_R$ continues to travel down the line and after a time T_R reaches the tap D_{k-1} to which gate S_s is linked. Passing through this gate the STOP pulse starts through OR-3 the G_{sp} generator, which simultaneously applies a pulse to the inputs of all CA circuits. In this time the START pulse has covered on the line an interval corresponding to the time T_R. The new coincidence between the reshaped START and STOP pulses measures the time interval, T_R. Depending on the kind of circuits CS_k or $CS_{k-1,k}$ in which the new selection occurred the analysis and conversion stops or restarts, for measuring the new remainder time-interval, T'_R. This operation repeats itself until the actuated selection circuit is a CS_k one which is linked to the END circuit. The delaying circuits I_k were introduced for equalizing the different delays for different ways of the START and STOP pulses.

At the end of the conversion the B_k flip-flop register, N_o, contains in binary form the duration corresponding to the position of the START pulse on the line at the moment of the occurring of the STOP pulse while scaler N contains the integer number of periods 2^n. elapsed between the START and STOP pulses.

Differential nonlinearity

If we assume an ideal compensation of all the differences between START and STOP pulse paths, systematic inequalities between channel widths result only from the imprecision in positioning the taps D_k. (as it will be seen later it is possible to position the D'_k taps (K = 3,4..,n) so that they do not influence the channel width). Since the recirculations reduce the channel determination to a coincidence in the first four channels of the line or in the last channels of the weighted fractions, we shall have for 2^n channels per period, n+1 different widths (τ_1 - given by taps D-D_o, τ_2 - by taps D_o - D_1, τ_3 - by taps D_1 - D'_2, τ_4 - by taps D'_2 - D_2 and τ_K given by a combination of τ_1, τ_2, τ_3 and tap D_K, for K = 3,4...n). Thus the mean channel width will result from an average of these n+1 kinds of channels. It is evident that the smaller the width of a channel, the bigger the differential nonlinearity produced by the error in positioning the taps. The thermal variations of the line will not affect the differential linearity due to the fact that the weighted portions which determine the time standards form constructively a monolithic block and the START and STOP pulses travel across the same line. The threshold fluctuations will have the same influence as in the case of other types of chronotrons.

The weighted chronotron has however its own differential nonlinearity sources, which result, as one could suppose, from the incomplete compensation of the differences in START and STOP paths.

Let's suppose conventionally that if the STOP pulse path is shorter than that of the START pulse, the paths difference is positive, $\delta_K > 0$. Let's also suppose a uniform distribution of the time intervals to be measured. In these

conditions, let us determine the density of the record in different channels, operation consisting evidently in the determination of the width of the channels.

It will be shown: a) that a difference in path lenghts δ_K affects the width of only two channels, $2^{k-1}+1$ and 2^k, respectively the first and the last of the portion $2^{k-1} \sim 2^k$, which determines the recirculation on the preceding weighted portions; b) that the sum of the width of the two affected channels is constant and thus independent of δ_K.

Let us consider channel $2^{k-1}+1$. Its lower limit is obviously $2^{k-1}.\tau$ determined by tap D_{k-1}. Its upper limit due to the recirculation is $2^{k-1}.\tau + \tau_1 + \delta_K$. In fact if $\delta_K = 0$ the START pulse which at the advent of the STOP pulse is at a distance t ahead of tap D_{k-1}, after recirculation, will be found by the reshaped stop pulse at the same distance t ahead of the input tap D. If $t = \tau_1 - \varepsilon$ the pulse is recorded in channel $2^{k-1}+1$; if $t = \tau_1 + \varepsilon$ it is recorded in channel $2^{k-1}+2$. But if there exists a path difference δ_K (be it positive, i.e. the START pulse lags) the last START pulse recorded in channel $2^{k-1}+1$, will be that which was met by the STOP pulse at a distance $t = \tau_1 + \delta_K - \varepsilon$ ahead of tap D_{k-1}, the START pulse met at $t = \tau_1 + \delta_K + \varepsilon$ beeing already recorded in channel $2^{k-1}+2$. If $\delta_K < 0$ (i.e. the STOP pulse lags) the upper limit becomes obviously $2^{k-1}.\tau - \tau_1 + \delta_K$. The width of channel $2^{k-1}+1$ is given by the difference between the upper and lower limits, $\tau_{2^{k-1}+1} = \tau_1 + \delta_K$ where δ_K is to be taken with its conventional sign, i.e. channel $2^{k-1}+1$ has the same width as the first channel but affected by the path difference δ_K. The width of the following channel, $2^{k-1}+2$, is obviously not affected by δ_K, since both upper and lower limits are shifted in the same direction with the same quantity, δ_K. The same is true for all the following channels situated in the portion $2^{k-1} \sim 2^k$, except for the last channel, 2^k. In fact, its upper limit is given by tap D_k. Its lower limit (supposing that all other path differences are fully compensated) is given by $(2^{k-1} + 2^{k-2} + \ldots + 2^3)\tau + \tau_1 + \tau_2 + \tau_3 + \delta_K$, with the condition of correct positioning D'_K (fig.3, $\Delta_K > |\delta_{K\max}|$). If at the advent of the STOP pulse, the START one has already passed tap D'k, it is recorded in channel 2^k, without recycling (flip-flop B_k is set in position "1"). If it is somewhere on the portion Δ_K, the B_{k-1} flip-flop is set in "1" and recycling begins. If, after recycling, the STOP pulse meets the START pulse before the latter has reached tap D'2, the pulse is recorded in channel 2^{k-1}, since all flip-flops from B_0 to B_{k-1} inclusive are set on "1". If however the meeting occurs after the START pulse has passed D'2 tap, the actuated circuits will be CA_2 followed by CS_2 which reset the flip-flop B_2 in "0" state, this one in its turn sets B_3 in "0" state, and so on until the B_{k-1} flip-flop going to "0" state sets B_K in state "1" and the pulse is recorded in channel 2^k. The lower limit of this channel will be shifted by $+\delta_K$ since the upper limits of all the preceding channels were shifted by $+\delta_K$. The resulting width for the channel 2^k is $\tau_K = \tau - \delta_K$. It is obvious that the sum of the widths of the two channels affected by error δ_K is independent of this error.

It should be mentioned that the above described positioning of taps D'k solves at the same time the problem of correct measuring in the case in which due to independent random fluctuations and drifts, the remainder which is to be reanalysed is greater than the sum of inferior weights.

Accounting for the fact that the determination of the limits of the 2^n

channels of the chronotron's period is made without, with one or with more recyclings, the following distribution of errors due to path differences results:

1) The channels affected by a conventionally positive error form a set $M+\left\{2^n - 3 - m.2^2\right\}$ where m takes the values $m = 0,1... 2.(2^{n-3} -1)$, in all $2^{n-2} -1$ channels (with a periodicity of four, fig.4). This set divides in n-2 subsets, each of them beeing marked by the same error δ_k, where k = n-s, s = n-3,n-4,... 1,0. In each subset, M^s+, are included those channels from M+ for which m takes the values $m = 2^{n-(s+3)} - [1+r.2^{n-(s+2)}]$ where r takes the values $r = 0,1,...,$ 2^s-1.

2) The channels affected by a conventionally negative error form another set, $M-\left\{2^n-m.2^3\right\}$ where m takes the values $m = 0,1,2..., 2^{n-3}-1$, in all 2^{n-3} channels (with a periodicity of eight, fig.4). This set divides into n -3 subsets each of them beeing marked by the same error $\Delta t_k = \sum_{k=3}^{s} \delta_k$, where k = n-s and s takes the values s = n-3, n-4, ...1,0. In each of these subsets, M^s are included those channels of M-, for which m takes the values $m = 2^{n-3} - [1+2k].2^{(n-3)-s}$ where k takes the values $k = 2^{s-1}, 2^{s-1} -1, ..., 1,0$ (for s = 0,k equals zero).

It is seen that the conventionally positive errors are non cumulative, while negative ones are cumulative. The most affected channels are the multiple of 2^n channels, namely by an error $\Delta t_n = \sum_{k=3}^{n} \delta_k$. Its results a) that it is necessary for the D'k taps to be positioned (fig.3) with $\Delta_k > |\Sigma \delta_{k\,max}|$ and b) it would be advantageous to so adjust the instrument that the path differences during the recycling be alternativelly positive and negative, otherwise the differential nonlinearity could assume big values.

Reducing the differential nonlinearities

It is obvious that the compensation by adjusting the signs and values of δ_k is difficult and nonr liable. A very interesting way for sensibly reducing the differential nonlinearities is given by a method similar to that proposed by Gatti[1,2]. In fact, adding in analog form a time interval comprised between zero and z.τ , noncorellated with the time interval to be measured, and subtracting the same interval digitally, the measurement of the same time interval will be done in z+1 different channels, the resulting widths of these channels beeing averaged and correspondingly the differential nonlinearities beeing reduced.

An essential feature, specific to the weighted chronotron is the fact that if $z+1 = 2^k$, the averaging is done on a group of channels in which necessarily enter the sum the pairs of channels affected by the error δ_k, sum which, as it has been shown, is principially independent of the error δ_k. In other words the averaging of 2^k channels principally excludes the recycling errors δ_{k-i}, where i ==0,1,2... and reduces by a factor 2^k all the errors δ_{k+i} where i = 1,2..., since in a group of 2^k channels there is one single channel affected by error δ_{k+i} ; which by averaging is distributed over 2^k channels.

By the same method the differential nonlinearity resulting from the inaccurate positioning of the taps and of the groups of 2^n channels is also reduced. As it is seen, Gatti's method in this case is very efficient.

The second feature is the relatively simple way in which averaging may be obtained by delaying the stop pulse with a time interval comprised between zero and z.τ . This delay, $\nu \cdot \tau$ is controlled through the matrix M_z by the state of the scaler Z which at the same

time triggers the scalers N and N_0 in a state corresponding to the number $\bar{\nu} = -\nu$ (fig.1). At the end of the conversion the figure obtained is the necessary one, ν beeing automatically subtracted. The coupling and triggering into initial states of the scalers N_0 and N (fig.1) assure the correct recording of the resulted figure, including the case in which during recycling the remeasured interval happens to be greater than the sum of inferior weights.

Attention must be paid to the correct delaying of the STOP pulses by a multiple of τ . It is worth mentioning that the positioning errors of the taps on the delay line of the STOP pulses are also averaged by the same procedure, the discrete delaying of the stop pulse. A possible difference between the mean channel width in the converter and the mean width of the discrete STOP delays leads to a loss of resolution which, however, remains small as long as the difference remains itself small.

The third feature is the extremely small supplementary time necessary for the averaging procedure.

A constructive alternative

If the channel width is greatly reduced it is possible that the time necessary to reshape the START pulse be comparable if not greater than the channel width which evidently impedes the correct positioning of the compensating tape D_0. One solution to this problem would be the attachement of a portion of four channels at the end of the delay line which would have the same purpose as the four channels at the front end of the line. The recycling would begin at D_n tap and the opening of the gate C, linked to tap D_2, would be conditioned by the final tap of the attached portion. In this manner one has for the reshaping of the START pulse a time equivalent to four channels. A corresponding altering of the logic is necessary.

Conclusions

The weighted chronotron may be an alternative with remarcable advantages in constructing wide range small channel width time - digit converters.

These advantages consist in reduced necessary speed of the scaler, relatively simple logic, and improvement of differential nonlinearity by adapting in a very simple and convenient manner Gatti's method.

References

1 C.Cottini, E.Gatti, V.Svelto: Nucl. and Meth. 24, 241 (1963)

2 C.Cottini, E.Gatti, V.Svelto: Proceedings of the international symposium on Nuclear Electronics. Paris, Novembre 1963, pag.309.

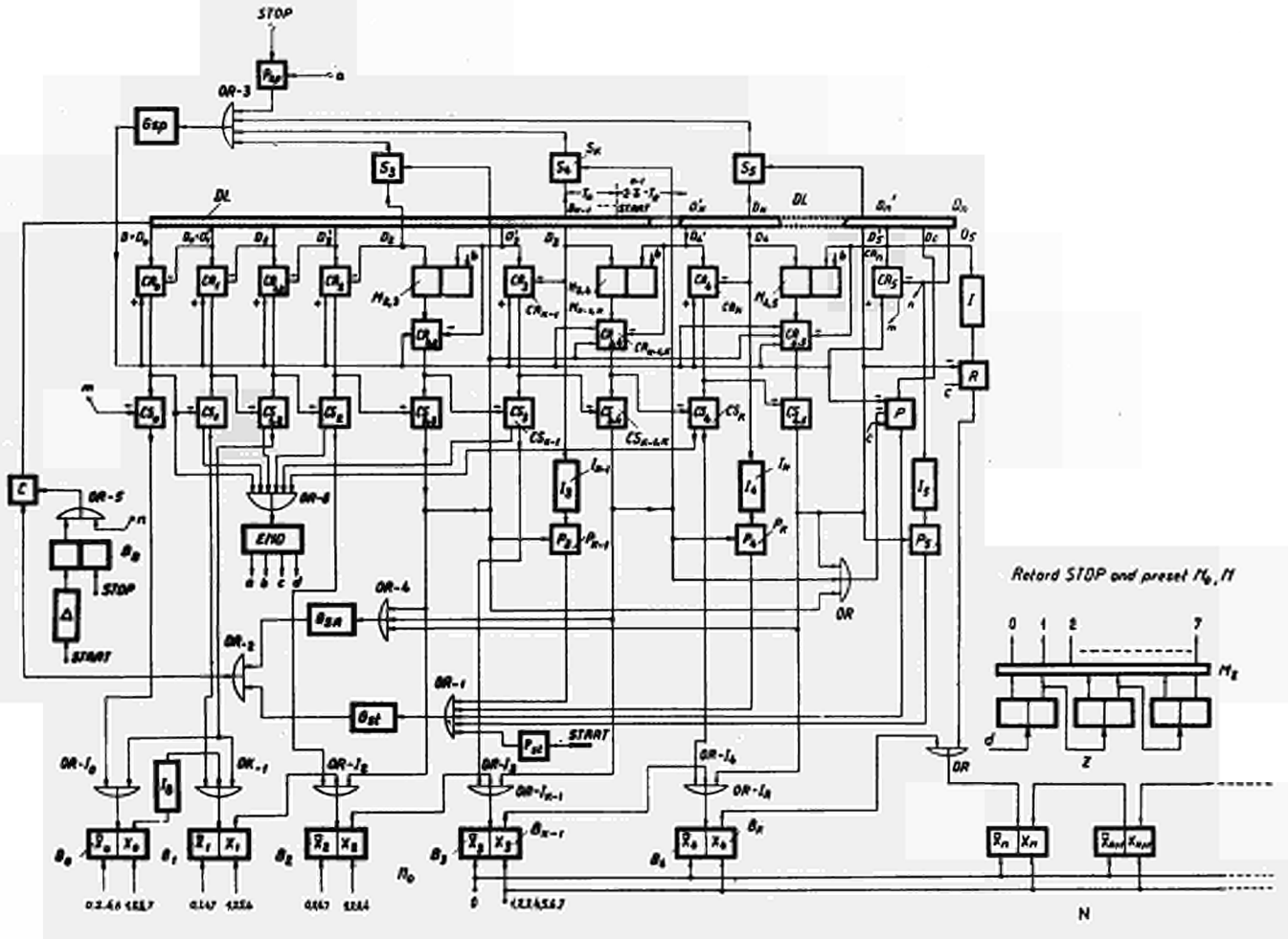
STOP
OR-3
6sp
DL
OR-5
OR-6
END
STOP
START
OR-4
OR-2
OR-1
OR
Retard STOP and preset M_0, M
N

Fig. 1

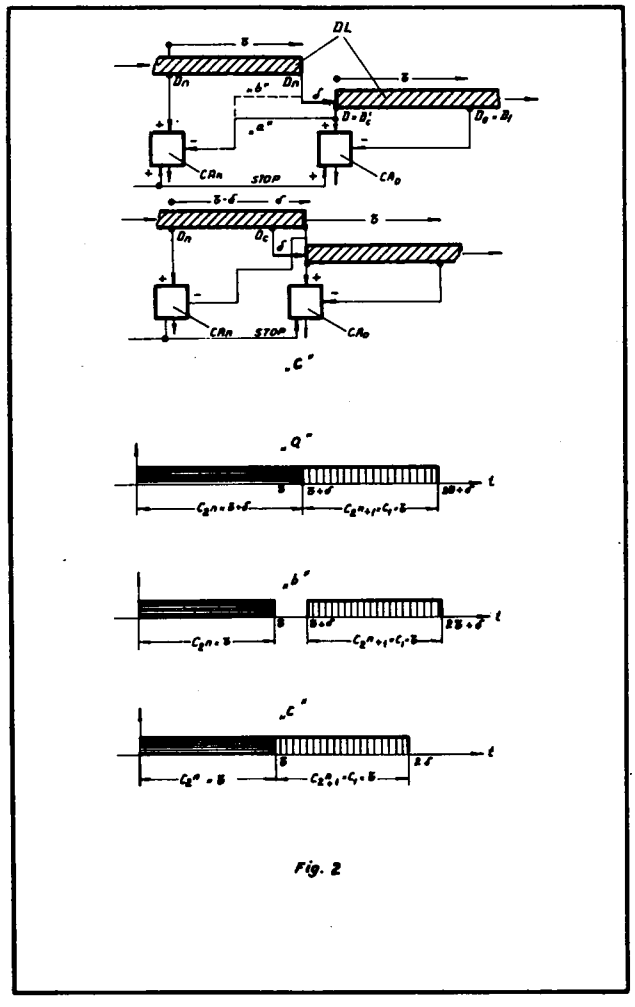

Fig. 2

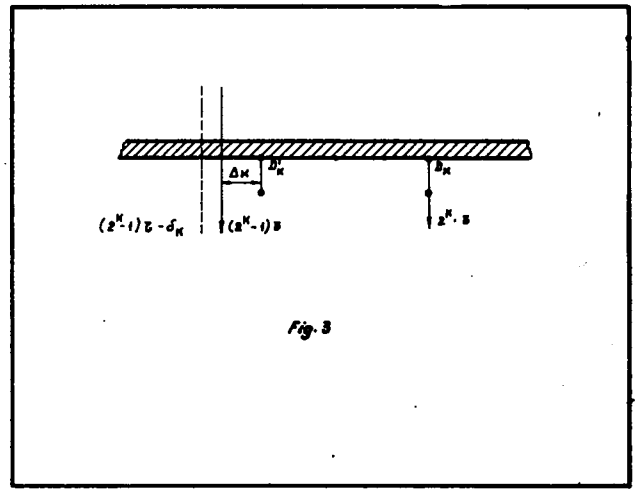

Fig. 3

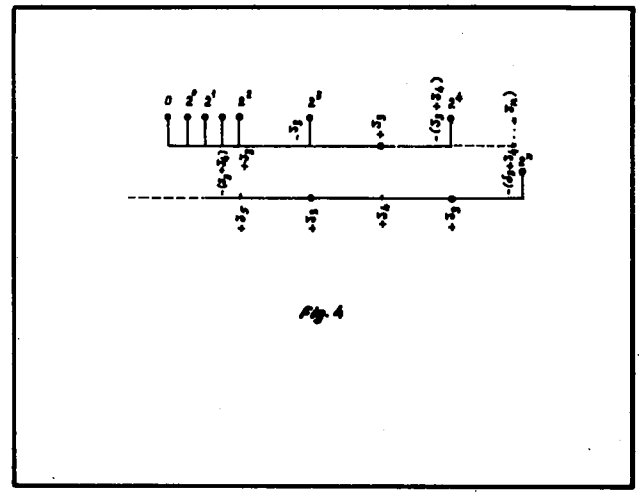

Fig. 4

FAST TIME MARKING DISCRIMINATOR CIRCUIT

N. Fiebiger, P. Elzer, W. D. Emmerich, A. Hofmann
Physikalisches Institut der Universität Erlangen-Nürnberg

J. W. Klein, Frieseke & Hoepfner GmbH, D 852 Erlangen, Germany

given by J. W. Klein

A leading edge threshold discriminator with 60 dB threshold range, a time walk of less than 0.1 ns/dB and 10^8 pps repetition rate making use of linear integrated circuits is described. It is designed for time measurement with coincidence stage or TPC with signals from solid state detectors via charge amplifiers or scintillation counters.

The problem of time measurement in the nanosecond range can be divided into two parts:

1. fixing a time significant point on the signal wave form

2. time coding or digitalizing.

This paper deals with the first part of the time measurement problem. The fixing of a significant point on the wave form is done by so-called time marking discriminators or time pick-off circuits which give digital signals directly correlated to the pick-off point of the input wave form. As most of the detector signals are also carrying other information as for example amplitude information or pulse shape information, the timing point has to be almost independent of the other pulse qualities. As the timing point of an event is physically given by the moment a particle or quantum enters the radiation detector, the ideal electric timing point is the moment the first charge carrier reaches the collecting electrode or any other point directly correlated to this moment. The time inaccuracy of the output signal with respect to this ideal timing point is given by the time walk and jitter as a function of the amplitude, the pulse rise time or other pulse parameters. Generally speaking it can be said that all time marking circuits or time pick-offs can be divided into two categories:

1. leading edge discriminators and

2. zero crossing discriminators.

The leading edge type is especially useful in cases where pulse rise time is not constant, which may happen with solid state detectors. On the other hand the zero crosser needs pulses with constant rise time but in this case is useful for a wide dynamic range.

The more sophisticated types of discriminators, as e.g. the constant fraction type, can also be regarded as modifications of these two principles. Therefore it may be interesting to know what minimum value of time walk could be achieved in an industrial series production of a simple leading edge time marker which has an input sensitivity of about $\pm$ 1 mV.

For making the time marker useful for different types of detectors, as scintillation counters as well as solid state detectors with fast charge sensitive amplifiers, the input sensitivity can be varied between + 1 mV and + 1 V in steps by the factor of three. The threshold stability in series production can be held better than 2×10^{-3}/°C. This threshold stability can be improved by matching the integrated circuits as to provide all the amplifier stages running in the same working point.

The whole circuit is dc coupled and base line restored to prevent base line shift in cases of capacitive input and drift in offset voltage or offset current up to a duty cycle of 50 %. An overload of 100 times the threshold voltage gives a recovery time of less than 5 ns. Provisions are made that there is no doubling of the digital output pulses, independent of the input pulse width. The output pulse width is variable by an internal interchangeable cable. The time walk is about 0.1 ns/dB amplitude variation for input amplitudes of more than 25 % over threshold up to about 10 times the threshold voltage. Between 10 times and 25 times the threshold overload, the time walk is about 0.06 ns/dB and for higher input amplitudes the further time walk is negligible. This is even true for a threshold voltage setting of 1 mV. Fig. 1 shows the time walk as a function of input voltage at a threshold setting of 1 mV. The input was fed by rectangular pulses with a rise time of about 1 ns.

As the block diagram in fig. 2 shows, the circuit consists of an input attenuator, a limiter, four amplifier stages with an overall gain of about 300 and a total rise time of 2.5 ns, a base line restorer, a tunnel diode threshold discriminator, an intermediate storage flip-flop with delay line pulse former, two fast fan-out stages, and one slow fan-out stage.

Figs. 3 and 4 show the detailed circuit diagrams. The input attenuator is constructed in 50 ohms strip line technique with printed line. This gives reflexions less than 5 % for input pulses with 0.7 ns rise time. The limiter consists of the two fast diodes d_1 and d_2.

The limiter is followed by the four amplifier stages $E_1 \ldots E_4$. Each stage consists of an integrated linear circuit of the RCA type CA 3005 with an emitter follower at its output. The integrated circuit itself is a differential amplifier long tailed pair and a constant current source in the common emitter. The emitter follower uses a transistor of the type BFY 90. These emitter followers are necessary for decoupling between the output of each stage and the input reverse capacitance of the following stage and for correcting the dc potentials. Because of transient time reasons feedback loops could only be built within the stages themselves.

The output of the fourth stage feeds both the base line restorer and the threshold discriminator. The base line restorer consists of two long tailed pairs with the transistors 5, 6, 7 and 8. This circuit works as a bipolar clipper. The output current of transistor 7 is integrated by the capacitors C 32, 3, 4, 5, 6. This voltage is fed to the differential input of the first amplifier stage as a control signal proportional to the deviation of the base line at the amplifier output (test point at R 65), compared to the given value at the base of transistor 6. The threshold discriminator consists of another long tailed pair E 5 which is of the same type as the amplifier stages. It works as a fast comparator driving the tunnel diode D_{16} in the collector circuit of the right transistor. The whole circuit which has Schmitt trigger characteristics with an internal dead time of about 5 ns fires the tunnel bistable multivibrator D_{23} via the transistors 9, 10 and 12. This bistable multivibrator is reset by the same signal, delayed by the delay line v_1 and amplified by transistor 11. So the output pulse width is given by the delay time of v_1. As the reset pulse for the tunnel diode bistable multivibrator is in any case higher than the set pulse, the reset signal is dominant, independent of whether the triggering signal is still there or already off at the moment of reset. This kind of circuit prevents multiple triggering for long input pulses. The digitalized signal is fed to the two fast fan-out stages transistor 13 and 14 respectively 15 and 16. Each one forms a long tailed pair and is capable of delivering 25 mA into a 50 ohm's load. These current sources give the possibility of another cable pulse shape at the output with an amplitude high enough to fulfill the AEC NIM standards. Finally there is an additional slow output stage which consists of the transistors 20 and 21, forming a one shot multivibrator which delivers a negative or positive output signal via the transistors 18 and 19. The whole unit is mounted in AEC NIM module of one unit's size.

Acknowledgements:

The authors are grateful to Mr. J. Bosch for useful discussions. They also acknowledge that this work could only be done with the assistance of Messrs. H. Faatz and A. Dittner who did the main part of the circuitry layout.

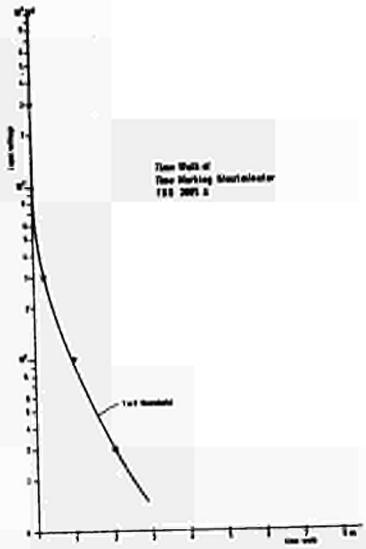

Fig. 1 Time Walk vs. Input Amplitude

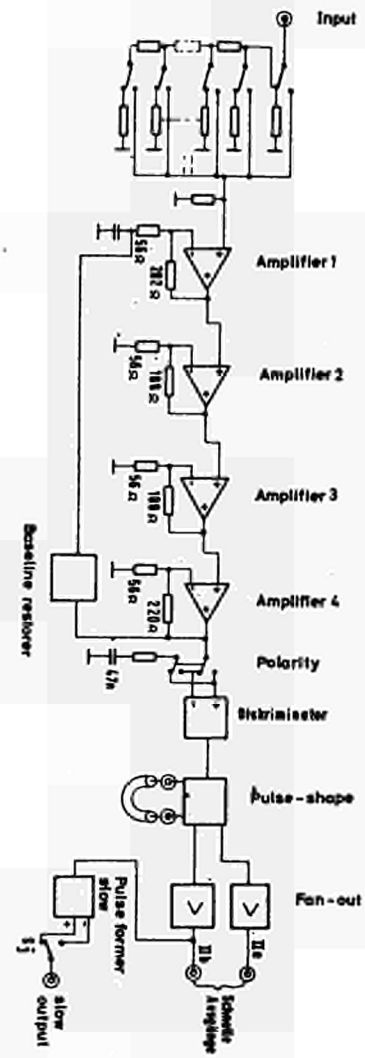

Fig. 2 Block Diagram

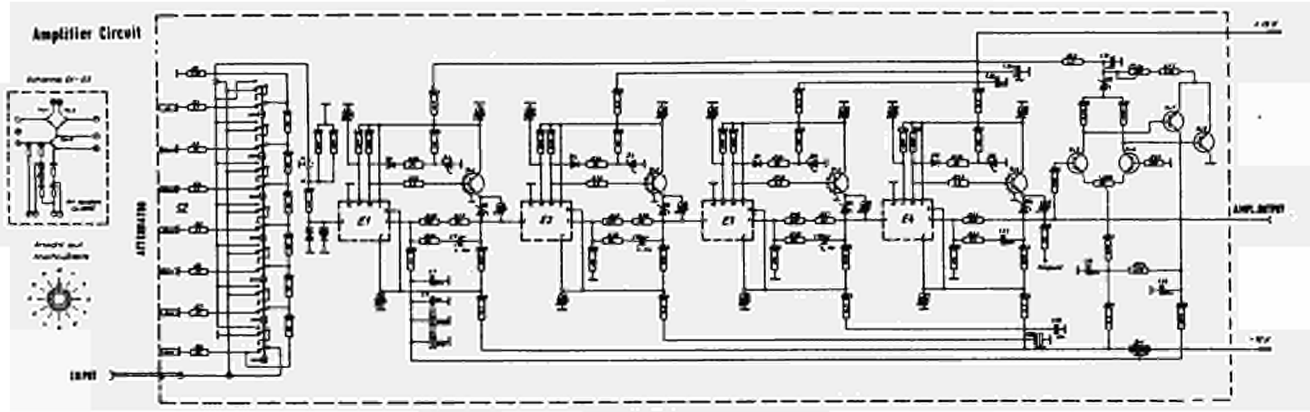

Fig. 3 Amplifier Circuit

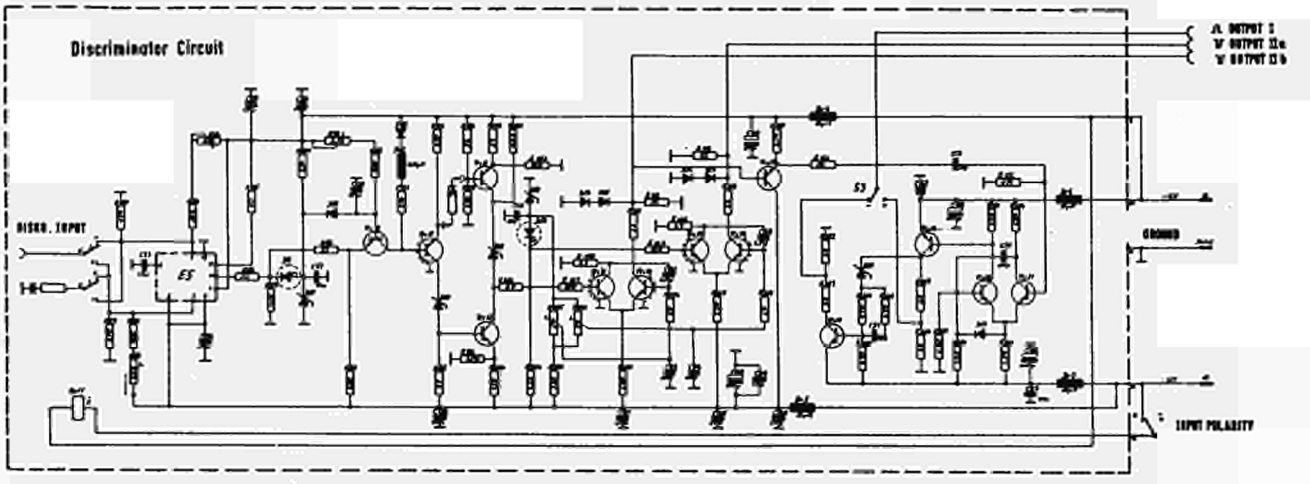

Fig. 4 Discriminator Circuit

SYSTEM REQUIREMENTS FOR HIGH-RESOLUTION GAMMA-RAY SPECTROMETRY AT HIGH COUNTING RATES†

R. L. Heath and L. O. Johnson

National Reactor Testing Station
Idaho Nuclear Corporation
Idaho Falls, Idaho

Summary

The full potential of high-resolution gamma-ray spectrometers has been severely hampered by degradation in the quality of the pulse-height spectrum at high input data rates. Over the past year or two considerable effort has been expended in the examination of this problem[1-3]. This paper will briefly review the nature of these instrumental difficulties, define realistic experimental requirements, and illustrate state-of-the-art solutions to these problems. A DC-coupled system which has been developed in our laboratory for high-rate applications will be described and performance presented.

Introduction

The wide application of high-resolution pulse-height spectrometers employing solid-state detectors and cryogenic FET preamplifiers places stringent requirements on the electronic systems employed. At the present time experimental requirements for laboratory systems demand negligible degradation in the quality of the data at high counting rates (up to 50,000 pulses/sec as a practical limit) over a dynamic range from few kilovolts to 10 MeV. Without special consideration in the design of electronic systems for such applications, serious shifts in zero and system gain and degradation in the shape and width of peaks in the pulse-height distribution will result. Most of these effects are the result of random fluctuations in the zero reference baseline at the input to the analogue-to-digital converter.

To provide some insight into these effects and the requirements for specialized circuitry to eliminate these problems let us examine part (a) of Figure 1. To achieve optimum signal-to-noise ratios in high-resolution systems, a monopolar pulse shape achieved by suitable RC integration and differentiation networks is usually employed. As indicated in part (a) of the figure, the output pulse shape from such networks will be more-or-less Gaussian in shape with equal rise and fall times. Following the pulse, there will be a negative undershoot with a long recovery time constant (generally in the order of several hundred microseconds). At low counting rates the baseline will have returned to its original value prior to the arrival of a succeeding event at the input of the ADC, and the undershoot will have no influence on the analysis of succeeding pulses. If, however, at high rates, another pulse (indicated by the dotted line in the figure) occurs a short time after the first, the negative tail of the preceding pulse will result in a reduced amplitude measurement by the ADC. At reasonable rates (a few thousand pulses per second) the net effect of this will be an observed asymmetry in the peaks of the pulse-height distribution as indicated at the far right of the figure.

Established practice in AC-coupled amplifier systems at the present time is to eliminate this undershoot by the technique of pole-zero cancellation. Using suitable networks this technique can effectively reduce the undershoot from a monopolar pulse. The net effect of pole-zero cancellation is shown in part (b) of Figure 1. Here we see that the undershoot returns quickly to the original baseline, thus pulses following will be unaffected. It should be pointed out that pole-zero cancellation must be accomplished on all elements of the complete amplifier-preamplifier system.

At high input data rates (in excess of 5,000 counts/sec), we still have problems from fluctuations in the baseline as shown in part (c) of Figure 1. In this figure we have reduced the time scale to show the long-term character of the baseline shift. As a result of residual charge on coupling capacitors within an AC-coupled amplifier system, the baseline will vary in a random manner producing a net negative shift in the zero reference and a general broadening of peaks in the spectrum as indicated on the extreme right side of the figure. In AC-coupled systems this effect can be reduced by the use of DC restorers such as the simple Robinson circuit[4] or the more sophisticated circuits which have been developed by Chase and Poulo[5] and Gere and Miller[6]. The action of these circuits is to remove the random fluctuations in the zero reference level. It should be stated that the input time constant of the restorer must be optimized for best performance at high counting rates. The net effect of this will be that the restorer will restore on noise and a small loss in resolution at low rates will result. It is now common practice to include a switch selection of the restorer in system to permit optimization of performance for a given experiment. The result of proper DC restoring action is illustrated in part (d) of Figure 1. Here we see that the zero reference baseline has been maintained at a constant level and the degradation seen without the restorer has been largely removed.

† Work performed under the auspices of the U. S. Atomic Energy Commission.

DC-Coupled Amplifier System

Over the past two years we have been investigating at our laboratory the possibility of achieving improved performance at high input rates through the use of an entirely DC-coupled system. The essentials of the approach are illustrated in Figure 2. This block diagram illustrates the basic approach. The system incorporates a DC-coupled charge-sensitive FET preamplifier which has been DC drift compensated. This is followed by a DC-coupled shaping amplifier which is input by DC coupling directly to the linear gate of the ADC. As indicated, the differentiation with pole-zero correction is accomplished in two separate stages. The shaping amplifier uses commercially available chopper-stabilized operational amplifiers.

Preamplifier

The charge-sensitive preamplifier design is illustrated in Figure 3. This basic circuit configuration, which has been in general laboratory use for several years at this laboratory[7], is a rather standard high-gain FET preamplifier with front-end DC stabilization. Feedback elements used in this typical example were a 0.24 pF Vitramon capacitor and a 2×10^9 ohm (room temperature value) Victoreen epoxy encapsulated resistor. The FET used in this particular unit was a selected TIS-75 (Texas Instruments). Noise performance of this particular unit (cooled) was 0.4 + 0.015 keV/pF FWHM Ge equivalent. Risetime of this preamplifier is typically 20 nanoseconds with 0 external capacity on the input and 80 nanoseconds with 100 pF external capacity. Risetime characteristics are essentially the same for either polarity input and are uniform up to a full 10 V output pulse amplitude.

The primary DC stability requirement is met by establishing and holding an optimum operating temperature (from noise considerations) of the input FET and feedback components internal to the detector cryostat. Minimizing drift in the FET drain voltage and drain current is accomplished by establishing the emitter voltage of the cascode transistor Q-1 through the matched emitter-base junctions of Q-1 and Q-2. Q-1 and Q-2 are inserted in a common heat sink for this purpose. The entire front end voltage supply is regulated by temperature compensated zener diodes D-1 and D-2. These components plus all associated resistors, capacitors, and coils are included inside a common temperature-controlled oven. The DC voltage gain through the cascode stage is given by: $g_m \times 10K \approx 200$. Thus, any drift referred to the input stage of the following voltage amplifier is divided by 200 when referred to the input of the preamplifier. FET's Q-3 and Q-4 form a high-impedance complimentary input to a voltage amplifier comprised of Q-3, Q-4, Q-5, Q-6, and their associated components. Q-3 and Q-4 provide the high-current capability necessary to produce high slewing rate in the preamplifier. Q-5 and Q-6 in the common-base configuration provide impedance transformation to enable high open-loop gain through to the collectors of Q-5 and Q-6. Depending on the quality of transistors used, operating temperature, etc., the open-loop gain may vary between 10^5 and 10^6.

Diodes D-3, D-4, D-5, D-6, and a 91-ohm resistor provide biasing for the bipolar output driver consisting of Q-7, Q-8, Q-9, Q-10, and their associated components. C-1, C-2, and P-1 are response-trim elements that reduce the high frequency open-loop gain to prevent oscillation. The preamplifier has multiple outputs terminated in 91 ohms.

Shaping Amplifier

The shaping amplifier utilizes four (4) Analogue Devices Inc. chopper-stabilized amplifiers. These amplifiers were selected for this application because of their excellent DC drift characteristics (0.2 microvolts/°C), slewing rate (100 V/μsec), and noise performance. To enhance the current driving capabilities of these amplifiers, bipolar class-A drivers were added to the output and included in the feedback loop. Including these drivers in the loop does not degrade the overall DC stability of the amplifier stage. All resistors used as gain or zero determining elements were high-stability metal-film resistors. Variable resistors were cermet elements. Capacitors employed in the shaping networks were all silver-mica units.

The first stage of the amplifier is a pole-zero corrected differentiator which cuts the decay time of incoming signals to approximately 50 microseconds with no undershoot. As shown in Figure 3, P-1 is the adjustable element in the pole-zero correction network comprised of C-1, P-1, and R-1. P-2 compensates for DC offset at the preamplifier output. The voltage references for P-1 are temperature compensated zener diodes D-1 and D-2. Coarse gain control No. 1 switches feedback resistors to give a pulse gain selection over a range from 1 to 8. DC gain varies from 0.2 to 1.6 over this range of adjustment.

Since single-ended chopper-stabilized amplifiers were used instead of differential amplifiers, it was necessary to add one amplifier stage for inversion capability. The input to the integrator stage is switch selectable either from the first differentiator output or the output of the inverting stage. The third stage amplifier is a Tennelec-type integrator. The feedback network comprised of C-2, C-3, R-2, and R-3 yields a transfer function essentially equal to two 1.6 microsecond integrations. P-3 as a series input resistor serves as a fine-gain control. Pulse gain of stage 3 is variable from 1 to 2. DC gain is 2 to 4.

A second pole-zero corrected differentiation is included in stage 4. This cuts the pulse decay time constant from 50 microseconds to 1.6 microseconds. Potentiometer P-4 sets the output zero level. It derives its reference voltages from zener diodes D-1 and D-2. Coarse gain control No. 2 switches feedback resistors to give a pulse gain 1, 2, 4, and 8. DC gain is 1/40, 1/20, 1/10, and 1/5, respectively.

The overall pulse gain of the amplifier is continuously variable from 1 to 125 with corresponding DC gains of 0.01 to 1.25. Multiple outputs are provided.

Pile-up Effects at High Rates

At high input counting rates pulses are arriving closely spaced in time at the input of the ADC. To simplify a discussion of these effects it is most convenient to divide such effects into two classes: peak pile-up, which occurs when two pulses arrive within the time that the linear gate of the analogue-to-digital converter is open, thus yielding a stored pulse amplitude which is related to the sum of the two pulses; and tail pile-up, which results from a situation where the ADC has completed a conversion, stored the resulting address in memory, and reset the ADC. If any deviation from the baseline as a result of a signal which was presented to the linear gate by the amplifier shortly before ADC reset exists and a second pulse arrives, the linear gate will then open and the resultant amplitude will again be related to the sum of the preceding pulse and the new event. A block diagram of a complete spectrometer system which includes rejection circuitry for eliminating questionable events is shown in Figure 5.

Tail Pile-up Rejection

Tail pile-up rejection is normally accomplished by including in the ADC input circuitry an "inspection circuit" which requires that the reference baseline be identically zero before a new pulse can be accepted by the ADC. As shown in the figure, the shaping amplifier output is fed into a sensitive baseline discriminator whose threshold is preferably set in the middle of the baseline noise band. The discriminator output and the ADC-busy signal feed a gated bistable whose output controls the ADC linear gate. The condition that must be satisfied to open the linear gate are ADC-not-busy and baseline restored. The only condition that will close the linear gate is the presence of the ADC-busy signal.

Peak Pile-up Rejection

Peak pile-up rejection is generally accomplished by special external circuitry which incorporates fast differentiating networks which inspect short intervals of time to determine whether or not two pulses have occurred during the time an ADC conversion has been requested. If this is the case, a reject signal will be generated and the event rejected by the ADC. As indicated in Figure 5, we are presently accomplishing this without delaying the signal pulse train by utilizing the ADC reject circuitry. Occurrence of a second pulse from the amplifier in a time period starting 50 nanoseconds after the primary pulse rise and ending at the time the ADC detects the peak amplitude of the primary pulse will cause a reject pulse to be generated. The reject pulse will then inhibit storage of the rundown capacitor information and cause an internal reset of the ADC.

To accomplish this, pulses from the output of the preamplifier are clipped to a 50 nanosecond width and amplified in a fast delay line amplifier. The delayed output from this amplifier is then noise discriminated such that the output of the discriminator in the peak pile-up rejector produces pulses of uniform amplitude and whose widths are equal to the noise baseline width of the delay-line amplifier pulses. The discriminator output feeds an anti-coincidence circuit along with the ADC-busy signal. If the ADC is not busy, an anti-coincidence pulse is generated whose width is equal to the noise baseline width of the delay-line amplifier output pulse. The trailing edge of the anti-coincidence pulse sets a 3-microsecond single shot. The outputs of this single-shot and the anti-coincidence circuit, in turn, feed a fast coincidence network. If a discriminator signal passes through the anti-coincidence gate while the 3-microsecond single-shot is set, a reject pulse is then generated.

System Performance

The performance of the DC-coupled amplifier system incorporating tail pile-up rejection is illustrated in Figures 6 and 7. The system used to obtain these data employed a 3.5-cc planar detector. The two figures indicate the shape of the 1.33-MeV photopeak from a ^{60}Co source for input counting rates varying from 2,000 pulses/sec to 75,000 pulses/sec. It is important in considering the degradation in resolution shown, that the system resolution is essentially intrinsic (i.e., limited almost entirely by detector statistics). If the resolution of a system employed to demonstrate high-rate performance does not meet this requirement, the relative peak widths as a function of input counting rates may be somewhat deceiving. Observing Figure 6, we see that the system resolution at 2,000 c/sec is 1.92 keV (FWHM). Beneath each set of peak shapes are listed the conditions (baseline inspection in or out), input rate, resolution at both half-height and one-tenth of the maximum peak amplitude, and the peak center location in channels. Proceeding upward in counting rate, we note that essentially no change in resolution or peak shape has occurred at a counting rate of 25,000 pulses/sec. The peak width has increased by about 0.2 keV (10%). The peak location has essentially remained unchanged. The difference of one channel represents a long-term drift in the system since the data were taken on a different day from the two preceding runs. At 50,000 pulses/sec we see a further slight increase in peak width. It should be noted that at this rate, the effect of baseline inspection is becoming significant. Without the baseline inspection circuitry in operation, the peak is somewhat asymmetric on the high-energy side and the resolution is somewhat degraded from that which was measured with the tail pile-up rejection circuitry in operation. At 75,000 pulses/sec this effect is even more dramatic. This is also attributed to long-term DC drift. In short-term measurements we have seen no observable drift in zero up to input rates of 100,000 pulses/sec. Observing the general character of the spectra at high rates we see no asymmetry on the low-energy side of the peaks, which would normally be the case even with the best baseline DC restorer in an AC-coupled system. The general rise in the continuum relative to the peak is attributed to peak pile-up. This results from the fact that random coincidences will remove pulses from the peak to distribute them over the continuum.

In summary, we feel that this is a reasonable demonstration of the capabilities of DC-coupled systems at high input rates. Using such a system, which is simple in concept, one can achieve excellent performance over a wide range of input counting rates.

Pulse Shape Discrimination

In any discussion of high-resolution systems there is one additional effect which should be considered. When one considers charge collection problems in lithium-ion drifted detectors it has been established that many events which occur within the intrinsic volume of the detector do not produce an amount of charge which truly represents the energy of the particle produced within the sensitive volume of the detector. Such events include the following: (1) events which lose some hole-electron pairs to trapping or competitive processes within the detector, (2) events which produce energetic electrons whose range exceeds their path length within the intrinsic volume, and (3) events which produce some pairs in regions of low field, resulting in a slow component to the charge collection current pulse arriving at the input to the filter network in the pulse amplifier. Because of the finite integration time of the filter network, the resultant pulse amplitude will be less than that required for a true representation of collected charge. It is this latter class of events which lend themselves to electron rejection schemes. Studies of this problem have been made by a number of investigators. Sakai[8] has demonstrated that charge produced in the regions of the junctions exhibit an abnormally long collection time.

A block diagram of a conventional pulse rise-time rejection system employed at our laboratory is shown in Figure 8. In this system, output pulses from the preamplifier are inspected and a pulse developed whose amplitude is proportional to the time for the leading edge of the pulse to reach a maximum, thus measuring effective rise time. This is accomplished with zero-crossing pick-off circuitry and a time-to-amplitude converter. Appropriate signals are then generated to reject pulses which exhibit long rise times. Figure 9 illustrates the performance of this system. In this figure we have plotted the spectrum of capture gamma rays from the Fe(n,γ) reaction obtained with a small Ge(Li) detector with and without rise-time rejection. This is an extreme case, where large numbers of high-energy electrons are being created within the intrinsic volume with a high probability of escape with less than full-energy loss. The marked reduction in the unwanted continuum with rise-time rejection circuitry in operation serves as a dramatic demonstration of the value of such techniques in special circumstances. For example, in a large coaxial detector (35 cc), the rejection rate at 1.3 MeV is about 10%. At 8 MeV, the rejection rate for the same detector is about 30%. For a 3-cc planar device, the corresponding rejection rates are about 15% and 50%, respectively.

Acknowledgments

The work reported in this paper represents contributions from many members of our staff. The development of low-noise cryogenic preamplifiers and detector systems was largely the responsibility of J. E. Cline and C. T. Howard. The work on rise-time rejection systems and measurements in this area were contributed by J. E. Cline. Special thanks are extended to Mrs. Carol Ball who prepared the manuscript.

References

1. V. Radeka, "Optimum Signal-processing for Pulse-amplitude Spectrometry in the Presence of High-rate Effects and Noise", IEEE Trans. on Nucl. Science, Vol. NS-15, No. 3, p. 455, (June 1968).

2. S. J. Rudnick and M. G. Strauss, "The Relative Importance of Various Rate-oriented Design Features of High-resolution Spectrometers", Semiconductor Nuclear Particle Detectors and Circuits, proceedings of Gatlinburg Conference, NAS Publication 1593, (1969).

3. F. S. Goulding, D. A. Landis, and R. H. Pehl, "The Design and Performance of a High-resolution, High-rate Amplifier System for Nuclear Spectrometry", Semiconductor Nuclear Particle Detectors and Circuits, proceedings of Gatlinburg Conference, NAS Publication 1593, (1969).

4. L. B. Robinson, Rev. Sci. Instr. 32, 1057 (1961).

5. R. L. Chase and L. R. Poulo, IEEE Trans. on Nucl. Science, NS-14, 83 (February 1967).

6. E. A. Gere and G. L. Miller, IEEE Trans. on Nucl. Science, NS-14, 89 (February 1967).

7. K. F. Smith and J. E. Cline, IEEE Trans. on Nucl. Science, NS-13, 468 (June 1966).

8. E. Sakai, IEEE Trans. on Nucl. Science, NS-15, 310 (1968).

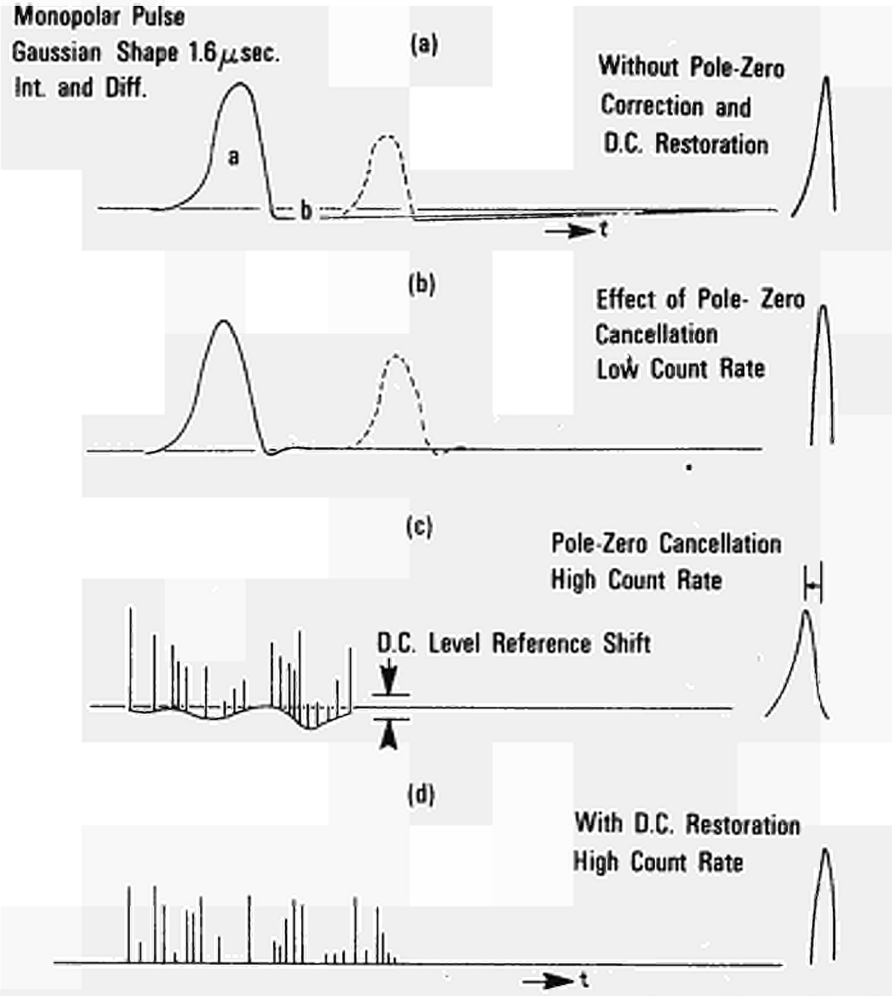

Fig. 1. Pictorial representation of problems which result in distortion of peaks in pulse-height spectra as a function of input signal rate: (a) system without pole-zero cancellation networks in amplifier at low input rate, (b) system with pole-zero cancellation networks in amplifier at low input rate, (c) system at high input rates with no DC restoration, and (d) system at high input rates with both pole-zero and DC restorer circuits optimized.

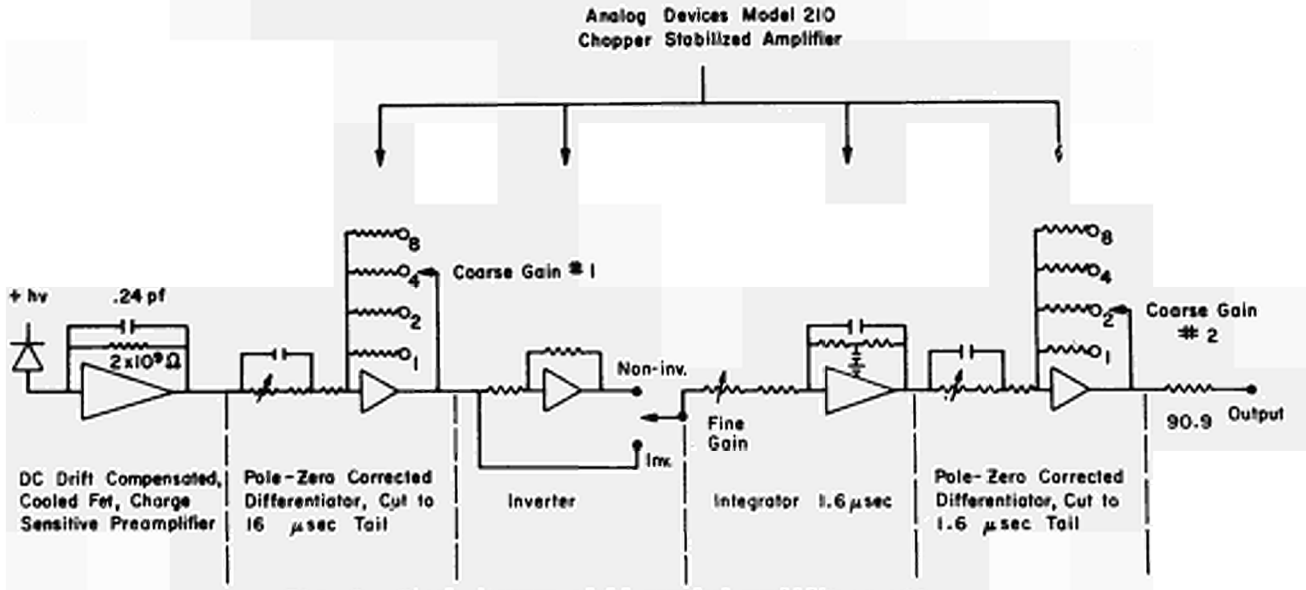

Fig. 2. Block diagram of DC-coupled amplifier system.

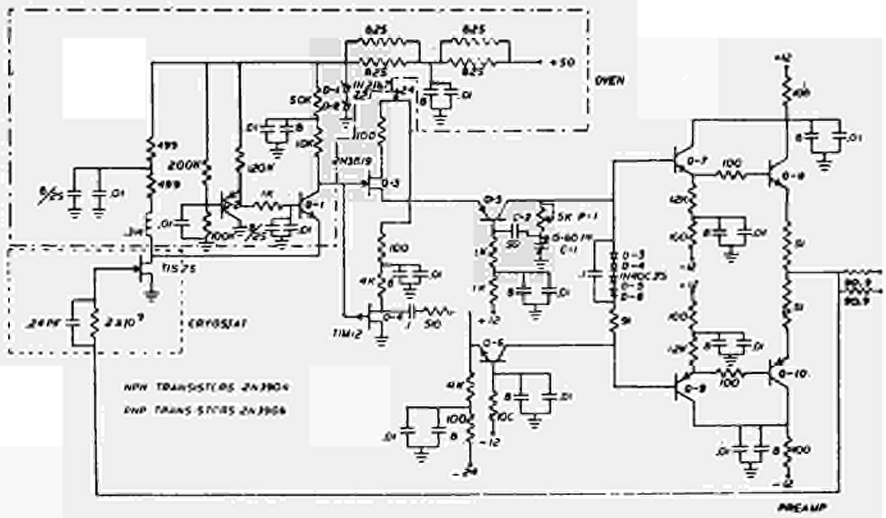

Fig. 3. Circuit schematic of DC-coupled low-noise FET preamplifier.

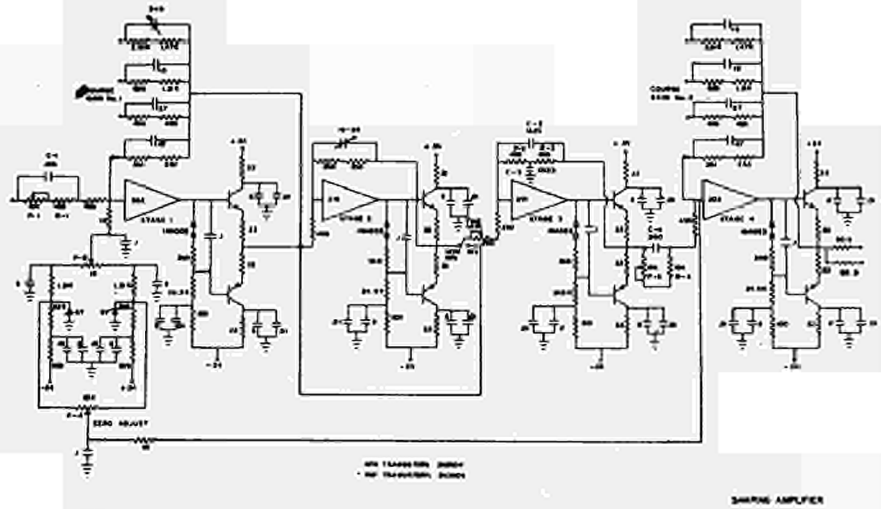

Fig. 4. Schematic diagram of shaping amplifier circuit.

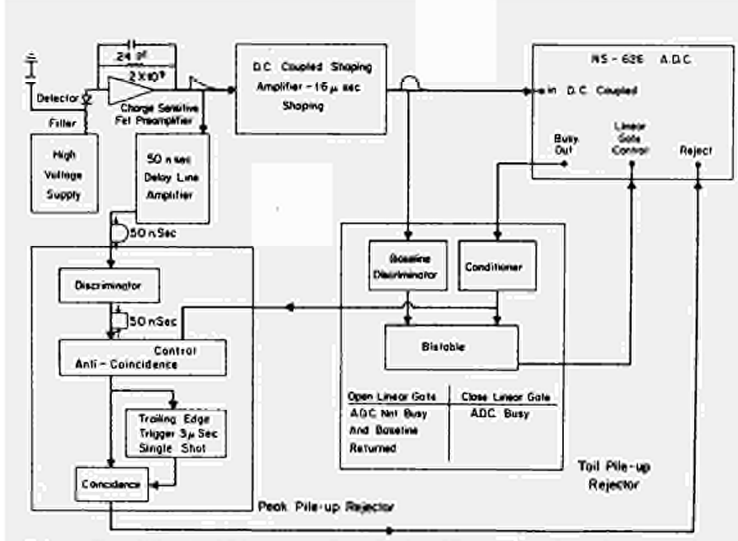

Fig. 5. Block diagram of pulse pile-up rejection system.

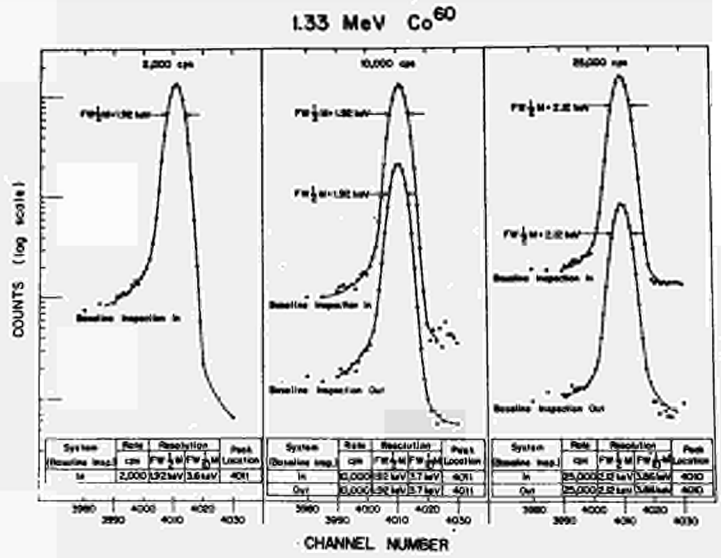

Fig. 6. Performance of DC-coupled system as a function of input counting rate showing the 1.33-MeV peak of ^{60}Co at input rates of 2,000, 10,000, and 25,000 pulses/sec.

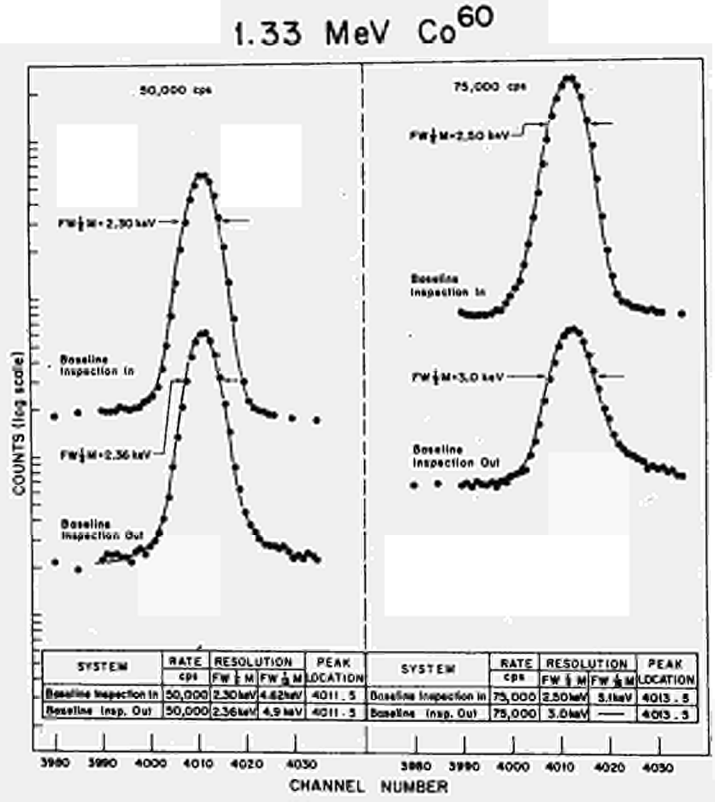

SYSTEM	RATE	RESOLUTION		PEAK
	cps	FW $\frac{1}{2}$ M	FW $\frac{1}{10}$ M	LOCATION
Baseline Inspection In	50,000	2.30 keV	4.62 keV	4011.5
Baseline Insp. Out	50,000	2.36 keV	4.9 keV	4011.5

SYSTEM	RATE	RESOLUTION		PEAK
	cps	FW $\frac{1}{2}$ M	FW $\frac{1}{10}$ M	LOCATION
Baseline Inspection In	75,000	2.50 keV	5.1 keV	4013.5
Baseline Insp. Out	75,000	3.0 keV	——	4013.5

Fig. 7. System performance for ^{60}Co at input rates of 50,000 and 75,000 pulses/sec. For comparison, spectra are shown with and without tail pile-up rejection system in operation.

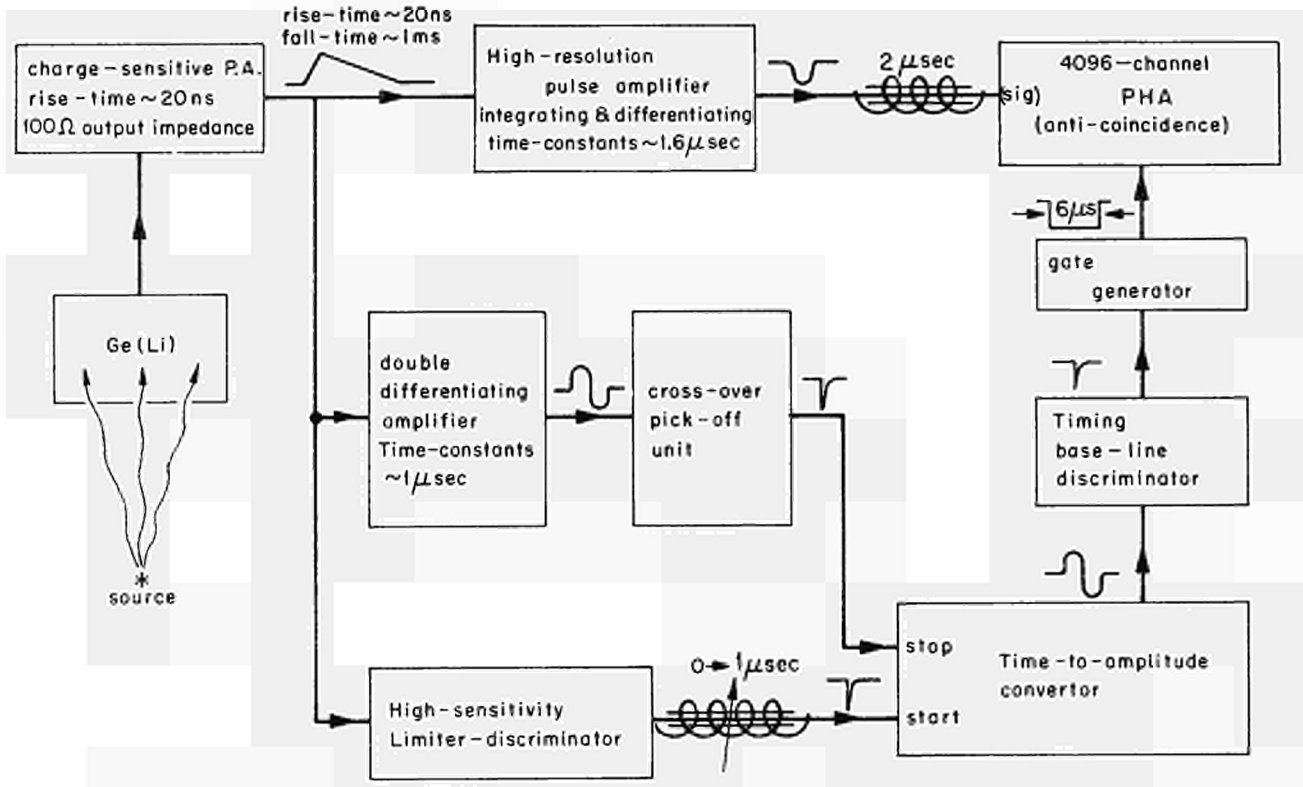

Fig. 8. Block diagram of pulse rise-time rejection system employed to improve quality of spectra by elimination of events which lead to the escape of electrons from the intrinsic volume of the detector.

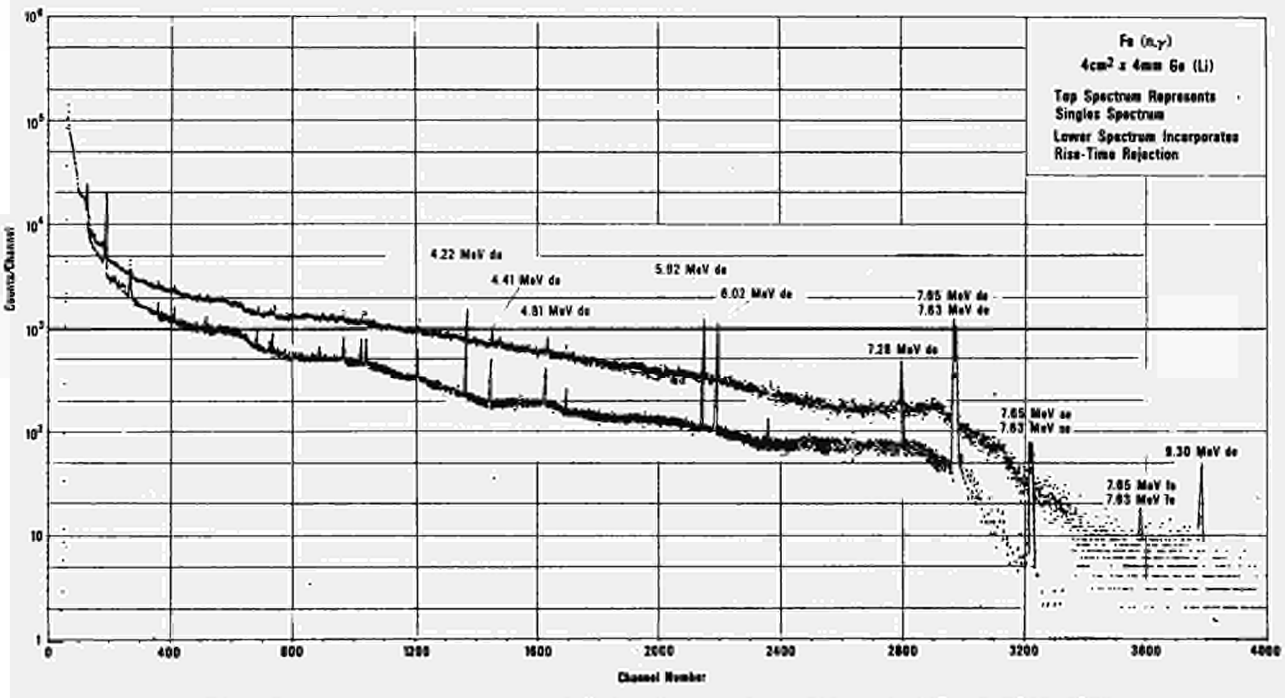

Fig. 9. Gamma-ray Spectrum of Fe(n,γ) reaction with and without rise-time rejection system in operation. The reduction in the intensity of the background continuum results from the elimination of events which produce electrons that lose energy in the region of the p and n junctions of the detector.

STATE OF ART IN MULTICHANNEL PULSE DATA ANALYSIS

B. Souček
Institute "Ruđer Bošković", Zagreb, Yugoslavia

In many nuclear physics, biology and engineering experiments it is important to measure the probability distribution function of random processes. In this paper a survey and comparison of different measuring techniques are given. The following systems and their basic principles of operations are described:

Single channel and multidiscriminator analyzers without memory. Systems with fast digital memories and computer oriented systems. Mean rate analyzer. Multiparameter analyzers. Analog memory analyzers with capacitors and with storage tubes. Associative megachannel analyzers. Most active zone encoder. Pseudo-random transformation mode megachannel analyzer. Window preselection. Event recording analyzers. Spectrum stabilization. Trends in probability distribution measurements.

1. INTRODUCTION

In analyzing nature one finds that many results indicate that the subject of measurements belong to the class of random physical phenomena. In a descriptive manner, randomness means that the data are nonperiodic, exhibit no explicit time trend, bias or regularity, cannot be precisely defined for all the time by any simple analytic function. Many random processes belong to the class of stationary processes. Stationarity means that certain statistical properties of the data do not change with time, and will be the same in the future as they are at present.

There are three main types of general statistical analysis which should be carried out for the data verified as random and stationary:

- amplitude probability density functions
- correlation functions
- power spectral density functions.

Those three classes of functions describe a random process in a similar way as the amplitude, waveform and Fourier frequency spectrum describe a deterministic process.

In this paper we shall deal with methods for measuring amplitude probability density functions.

Five important examples of processes that could occur in practice, singly or in various combinations, will now be considered:

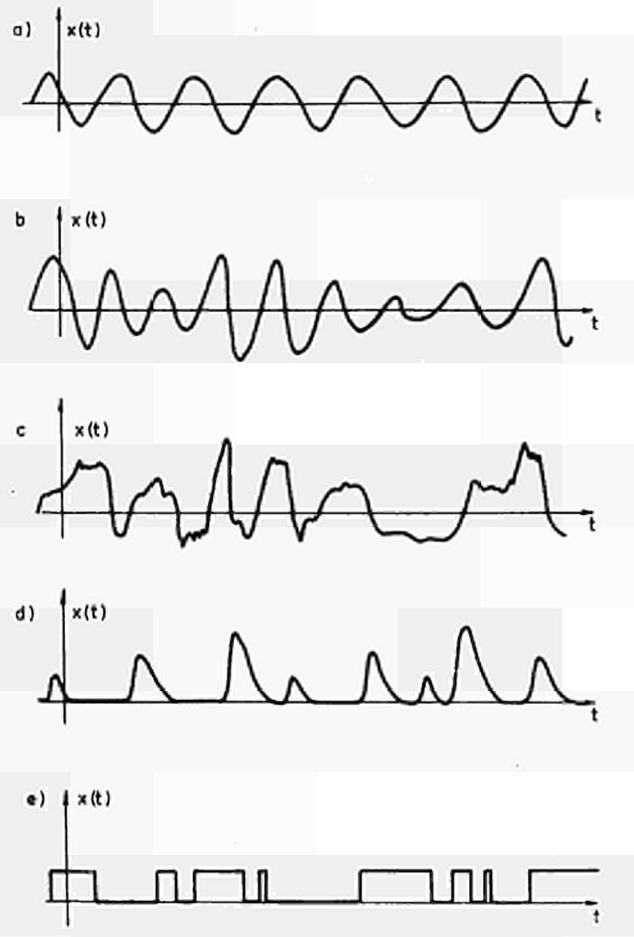

Fig. 1. Five special time histories. (a) Sine wave. (b) Narrow band noise. (c) Wide band noise. (d) Discrete random pulses. (e) Discrete random time intervals.

a. sine wave
b. narrow-band noise
c. wide-band noise
d. discrete random pulses
e. discrete random time intervals.

For each of these waveforms the following discussion will develop its appropriate probability density functions. Five waveforms are pictured in Fig. 1. The instantaneous amplitude $x(t)$ of the sine wave can be described by

$$x(t) = A \cdot \sin(2\pi \cdot f_o t + \Theta) \qquad (1)$$

where A = maximum amplitude, f_o = frequency, Θ = initial phase angle.

For narrow-band noise (which can be considered in some cases as a combination of a sine wave plus noise) a possible representation for the instantaneous amplitude $x(t)$ would be

$$x(t) = A(t) \cdot \sin[2\pi f_o t + \Theta(t)] \qquad (2)$$

where $A(t)$ and $\Theta(t)$ indicate that the amplitude factor and phase factor vary (relatively slowly) in some random fashion with time. However, the centre frequency f_o is still assumed to be the same as it was for the original sine wave. The frequency spread associated with $x(t)$ is assumed to be small compared with f_o. Such records occur when random noise is passed through a filter whose band-width is small compared with its centre frequency.

An alternative and approximate expression for (2) is given by the formula $x(t) = s(t) + n(t)$, where $s(t) = A \sin(2\pi f_o t + \Theta)$ is the fixed sine wave of (1), while $n(t)$ is a random noise record whose power spectral density function is confined to a relatively narrow frequency band about the sine-wave frequency f_o.

For wide-band noise no analytical representation is possible. All frequencies are theoretically possible in the record. The proportion of time spent in any frequency band is variable. The knowledge of instantaneous amplitude values associated with any narrow frequency band generally gives no information about the amplitudes to be associated with any adjacent narrow frequency band.

The probability density functions to be described will be applied to instantaneous amplitude values for the first three processes in Fig. 1; for the peak values of pulses in the fourth process and for the duration of pulses in the last process. Similar probability density functions can be developed for other parameters of interest.

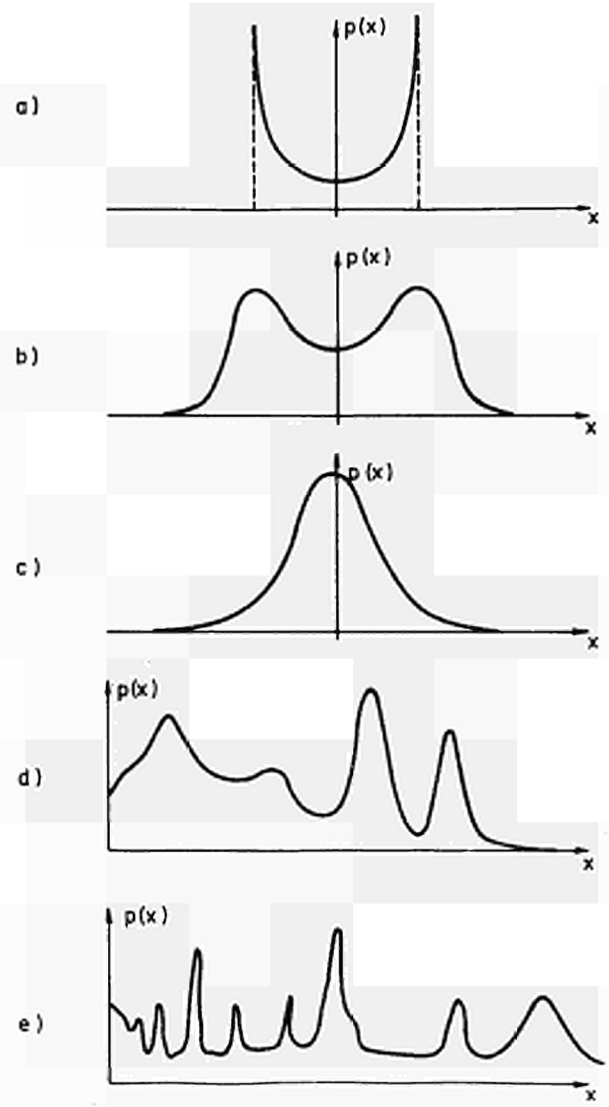

Fig. 2. Probability density functions: (a) Sine wave. (b) Narrow-band noise. (c) Wide-band noise. (d) Discrete random pulses (e.g. ^{60}Co spectrum). (e) Discrete random time intervals (e.g. Capture gamma-ray events vs time-of-flight).

Pictures of appropriate probability density functions for a sine wave, narrow-band noise and wide-band noise, where the mean value is assumed to be zero, are shown in Fig. 2a,b,c.

It is proved that the probability density function $p(x)$ of a sine wave is concave at $x=0$ and approaches infinity

asymptotically at $x = \pm A$. The probability density function $p(x)$ is 0 for x greater than +A or less than -A, since the instantaneous amplitude is always restricted to the range from -A to +A.

The probability density function shown in Fig. 2b is for narrow-band noise when a sine wave component is present. This curve is double-peaked, with a minimum at x=0 and with tails rapidly approaching zero. The probability density function shown in Fig. 2c for wide-band noise is of the well-known normal (Gaussian) type, with tails that are asymptotic to the x axis as x approaches $\pm \infty$.

Fig. 2d shows the probability density function of the peak values for discrete random pulses obtained from radioactive source ^{60}Co. Fig. 2e shows the capture gamma ray events vs time of flight. Such "spectra" give an insight into the nuclear process under consideration.

From the knowledge of a probability density function one can compute the probability that the amplitude values will lie in any specified range, and this may be a very significant parameter for particular applications. For example, one may be interested in estimating the probability of excessive high amplitudes as an indication of an abnormal condition in an electroencephalogram data analysis, or in predicting structural failures under random vibration, discovering clipping or nonlinearities of a system etc. Of special importance is the application in nuclear pulse spectrometry. Most of measuring systems are developed primarily for nuclear fields but can usually be used for other applications as well.

Many discussions of work in this area are available in the literature. In particular, one can consult excellent books by Chase[1], Korn[2], Bendat and Piersol[3]. A review paper by Bendat[4] covers the application in biomedical electronics, similar papers by Souček and Spinrad[5,6] are concerned with the application in nuclear spectrometry, mainly summarizing the developments before 1965. Here we shall mostly concentrate on systems and principles developed after that time.

2. SYSTEMS WITHOUT MEMORY

An estimate of the probability that x(t) assumes particular amplitude values between a and b for a record of finite lengh T may be obtained by taking the ratio $\Delta t/T$, where Δt is the total amount of time that x(t) falls within the range $a < x \leq b$. For this measurement we generate the functions

$$f[x(t)] = \begin{cases} 1 & [a < x(t) \leq b] \\ 0 & \text{otherwise} \end{cases} \qquad (3)$$

Such a function can be generated by a "dual slicer" circuit composed of an ideal diode and a comparator[2].

Averages of $f[x(t)]$ serve as estimates of Prob $[a < x(t) \leq b]$, While continuous averaging is readily possible, the digital nature (0 or 1) of $f[x(t)]$ makes it especially convenient to compute the sampled-data averages by counting 1 s, Fig. 3

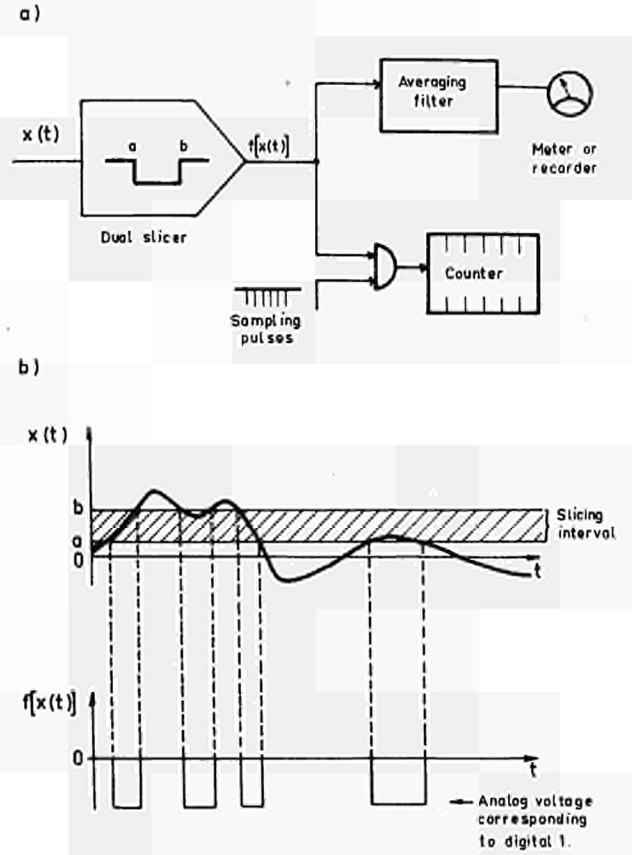

Fig. 3. Basic probability estimation scheme using dual slicer circuit (a). and waveforms (b).

$$\bar{f} = \frac{1}{n} \sum_{k=1}^{n} f[x(t_k)] \qquad (4)$$

As an important special case, a simple analog comparator with the input x(t)-X produces the output

$$f[x(t)] = \begin{cases} 1 & x(t) \leq X \\ 0 & \text{otherwise} \end{cases} \qquad (5)$$

which, when suitably averaged yields estimates of the cummulative distribution function $P(X,t) \equiv \text{Prob}\,[\,x(t) \leq X\,]$. An array of such comparators can estimate 10-100 values $P(X_1,t)$, $P(X_2,t)$... of the distribution function, and the addition of simple digital logic circuits produces simultaneous estimates of a set of probabilities Prob $[X_k < x(t) \leq X_{k+1}]$, as shown in Fig. 4.

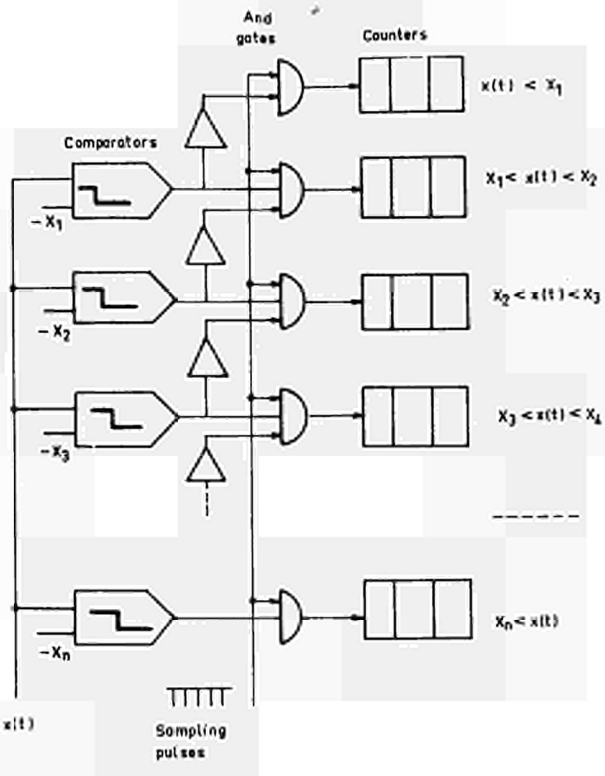

Fig. 4. Multidiscriminator amplitude--distribution analyzer.

3. SYSTEMS WITH FAST DIGITAL MEMORIES

Figures 3 and 4 show single channel and multidiscriminator pulse-height analyzers, respectively. If one wants to measure a fine structure of probability density functions, it is necessary to use instruments with hundreds of channels. In this case it is important that the widths of all channels are the same. The percentage deviation of the nominal channel width is called the differential nonlinearity. Such analyzers

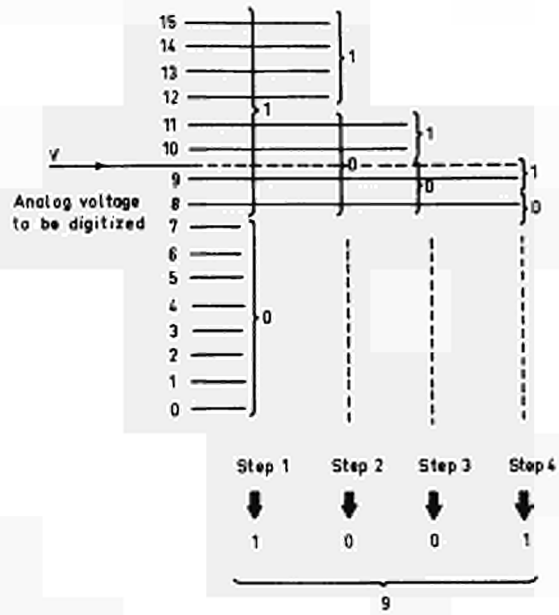

b)

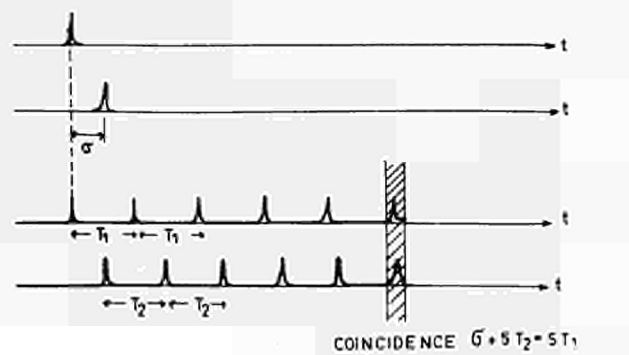

Fig. 5. (a) Analog-to-digital conversion by successive approximations. The analog voltage is quantized by making a series of binary decisions. (b) Vernier time expansion technique. The time period σ is extended to the period $5T_1$.

are in general composed of analog to digital converters and some kind of memory.

A converter takes an analog signal and converts it to a digital number, which is used to address the memory. Then one is added to the addressed memory location. This procedure is repeated for each input item and in this way a picture of probability distribution function is formed in the memory. Conversion is a separate field beyond the scope of this paper[7-15], and we shall only outline the principles of the basic techniques. Review papers on the subject are given by Chase[7], Bonitz[8] and others.

One of the simplest techniques for voltage digitization is to use successive approximation, Fig. 5a.

A voltage V (approx. 9.1 Volts in the figure) is to be digitized to the nearest integral voltage between 0-15 V. The digitization is accomplished by a series of test steps. The first step tests whether V is greater or less than 7.5 V (i.e. the voltage range is divided in half). It is greater so the most significant output binary digit is set equal to one. Next, the upper half of the range is itself divided in half and a test made to see which of these quarters contains V. In this example V is located in the range 7.5 to 11.5 Volts, so a binary zero is entered as the next significant digit. The procedure continues through steps three and four, yielding a binary zero and one as the two succeeding digits. Thus, after four steps an unknown voltage is placed in channel 9 of 16 possible channels. In general, it takes only n steps to quantize an unknown voltage into one of 2^n channels. This technique is rapid, but requires special care to achieve good differential linearity[9,10].

If the probability distribution of time intervals has to be measured, time digitizing equipment is needed.

For long time periods, direct gating of clock pulses is possible. For shorter periods, one can convert time to amplitude[11], and then use a standard pulse height digitization technique. Finally, there are "time expansion" or "vernier technique"[12,13], Fig. 5b.

The time period to be measured σ, is bracketed by two pulses. The arrival of the first pulse starts clock c_1 going; the arrival of the second pulse starts clock c_2 going. The time coincidence between a pulse from c_1 and a pulse from c_2 marks the completion of the expanded time period. The proportionality constant for the expansion $T_o/(T_1-T_2)$ of about 100 can be achieved[14].

The predominant technique for the quantization of pulse height (voltage or charge) derives from a method originated by Wilkinson[15] in 1950. It consists of first converting the height into a time interval and then counting clock pulses to measure that interval. The count is then directly proportional to the original pulse height to the precision of clock intervals and within the accuracy of the pulse to time converter. After conversion the obtained information is used to address the memory.

The first memories were acoustic delay line, Hutchinson & Scarrot[16]. At a later time electrostatic memories and magnetic drums appeared, Higinbotham[17]. Ferrite core memories first came into use in 1955 and 1956, Byington and Johnsone[18], Schumann and Mc Mahon[19]. Recently, real time computers are directly connected to the analog to digital converters and work as multichannel analyzers. One of the major advantages of the computer oriented, stored-program system is that both the sequencing of the functions and their detailed makeup are readily alternable (by programming) to meet the individual requirements of any given situation.

The first computer-analyzer systems[20-33] were published in 1962-1963.

Figure 6 shows a typical pulse-height analyzer using the Wilkinson type converter directly connected to the computer equipped with CRT display.

The pulse-to-time conversion is accomplished by the technique of charging a capacitor to a voltage proportional to the maximum excursion of the signal pulse, and then discharging it linearly in time, using a constant current. The counting of clock pulses is started at the beginning of the run down and stopped at the time that the capacitor voltage reaches zero. Those pulses are counted in an ADC register, which is used to address the computer memory.

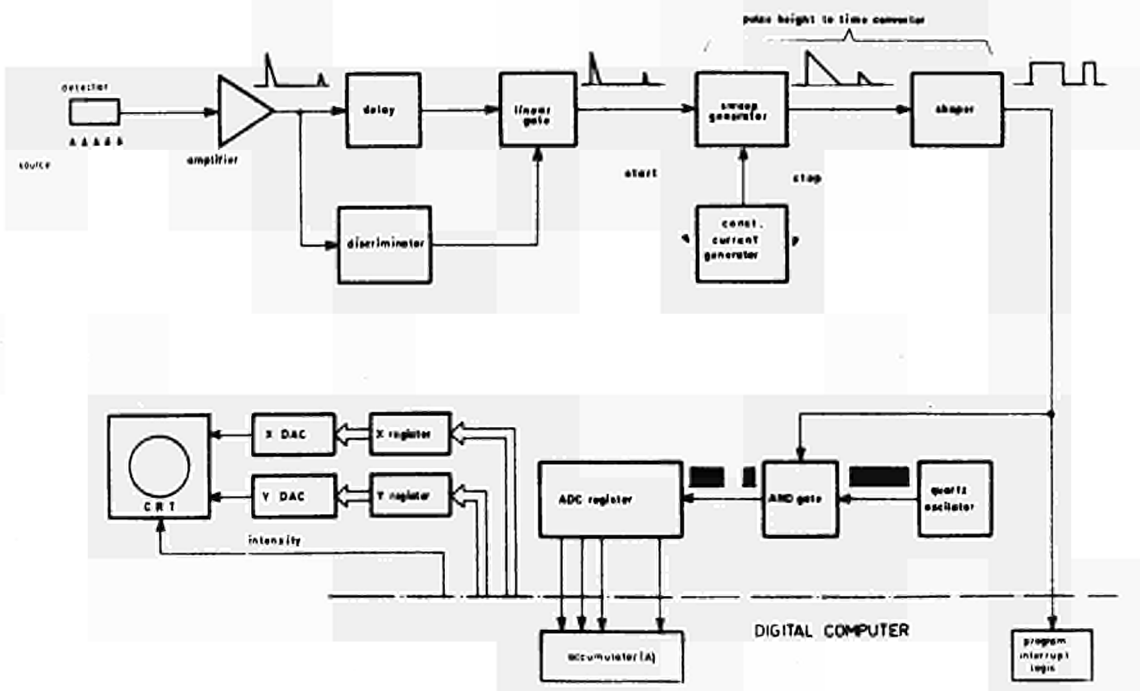

Fig. 6. Typical pulse-height analyzer system using the Wilkinson type converter directly connected to the computer, equipped with a CRT display.

The computer is used to display the data on CRT, and a flow diagram of the display programme is shown on the left side of Fig. 7. It should be mentioned that the x coordinates come here from the memory address A_x but the y coordinate is the contents of the A_x address. The flow diagram of the display programme consists of two loops: an inner loop for point display and an outer loop for picture display. After the abscissa has reached the maximum value x_{max} the x value is reset, i.e. x=0, and the picture display starts again.

During the display of every point interrupt is made possible. The display programme is interrupted with the appearance of new data and the computer jumps to another, "interrupt programme", the right side of Fig. 7. The computer saves the accumulator contents and commences the datum transfer, i.e. taking of a new item. The ADC transfers the register contents (it has a new item accepted at the end of ADC conversion) to the computer accumulator and afterwards this contents is used as memory address. The contents of that location is incremented, which means that a new descriptor is stored together with some others. Afterwards the computer restores the AC contents, clears the ADC register and tests if a sufficient number of data has been taken. If so, the computer continues displaying the collected data. If not, a new interrupt is made possible and the display continues waiting for new data.

Figures 8a,b,c show the progressing in measurement of 1024-channel ^{60}Co spectra, using a PDP-8 laboratory computer[34]. It is obvious that the spectrum is increased with time by an increasing number of input data.

Since 1963 a large number of computer-analyzer systems has been published. They differ in many aspects,

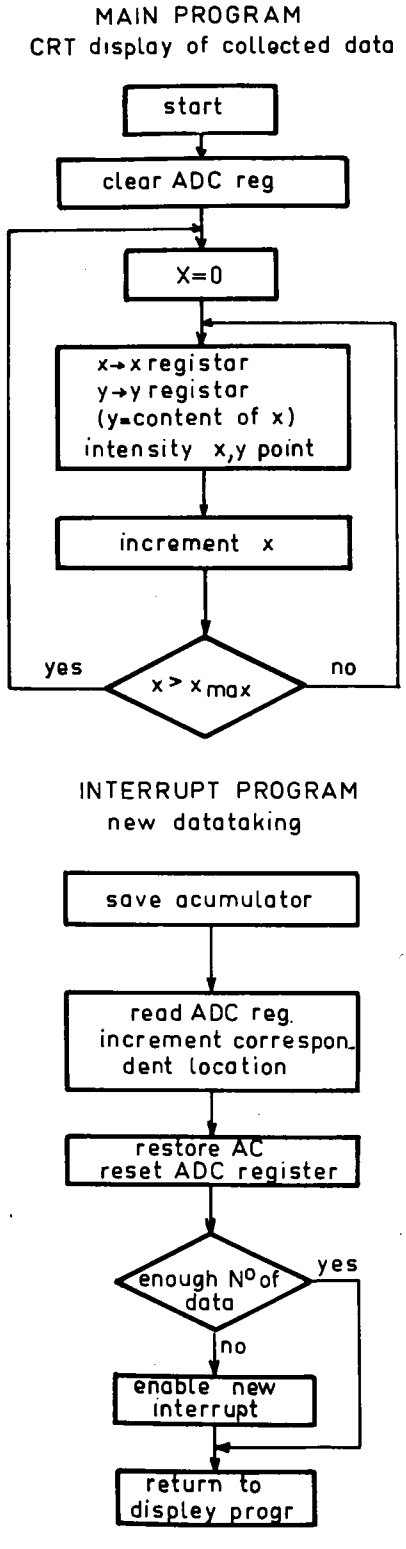

Fig. 7. Flow diagram of display and data taking routine.

but the basic principle is the same.

4. MEAN RATE ANALYZERS

The shape of the spectra in Fig. 8 is unchanged, but statistical fluctuations in the distribution curve are diminished as the number of data is increased. If M_i is the average rate of data belonging to the channel i, then after the time T in the i-th channel there might be on an average $S = M_i \cdot T$ data.

The process of measuring is binomial (the probability that some event belongs to the channel i is $k \cdot M_i$ and that it belongs to any other channel is $(1-k \cdot M_i)$. Hence the deviations around the mean value will be S .

Having a computer, one can make a programme for direct measuring of mean rates. Such a method was first proposed by Hooton and Best[35,36]. In mean rate analysis two independent locations are alloted to each descriptor. The descriptor is a digital equivalent to the input signal amplitude . One of these locations, the "MEAN" location, holds the last value of mean rate as counts per interval. The contents of the rate locations, averages, are taken over all completed intervals. They are continually updated and fed to the display system, which presents a histogram of the mean rate against the channel number. This display therefore maintains the amplitude approximately constant but improves in precision in the course of experiment. The other storage location, the "COUNT" location contains the count collected in the channel within the current interval together with any remainder from the previous mean rate calculation.

The whole experiment is divided into a sequence of intervals. The number n of completed intervals so far elapsed is held in a common register. The time interval is determined by total counts over all channels at the initial run of the experiment.

Assume that at the end of the n-th interval the rate location for one channel contains M_{n-1}, the mean rate observed in that channel over (n-1) tests, and the corresponding count location contains P_n, i.e. the previous remainder (<0) and new counts ($P_n = Q_{n-1} + C_n$). Thus the total count in this channel during n intervals S, is

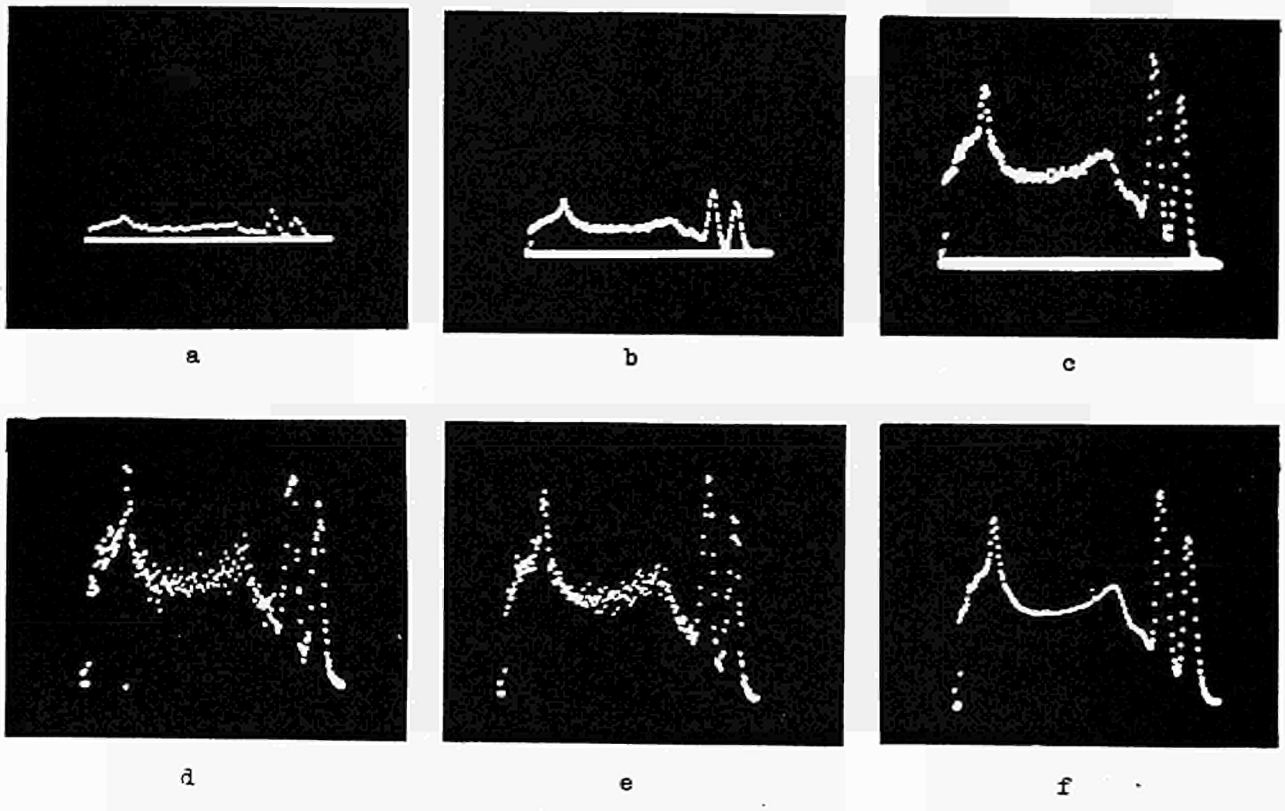

Fig. 8. Course of measurement of Co^{60} spectrum on the CRT screen, after 1, 3 and 820 time intervals; a, b, c conventional analysis; d, e, f mean rate analysis.

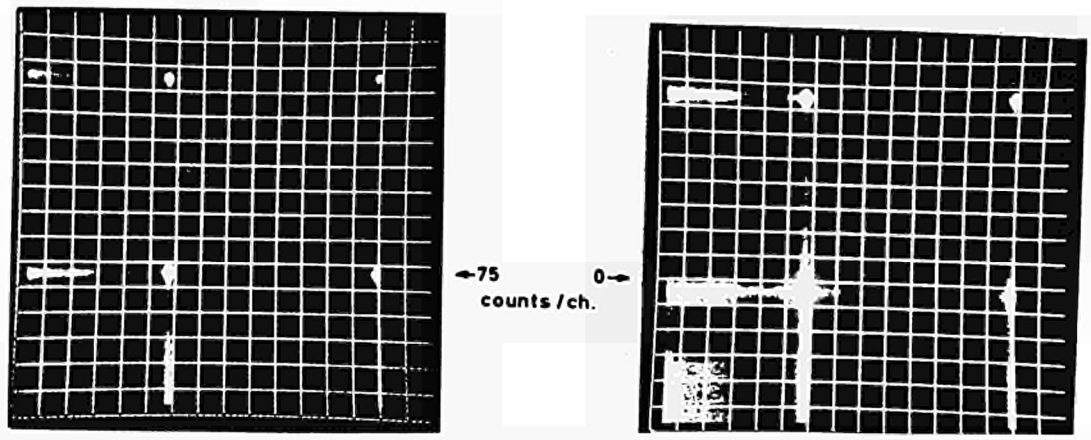

Fig. 12. Two-parameter spectrum of ^{60}Co gamma-gamma coincidences, displayed on a storage tube.

$$S_n = (n-1)\cdot M_{n-1} + P_n \qquad (6)$$

$$S_n = n\cdot M_n + Q_n \qquad (7)$$

Q_n, the remainder from this calculation, is made to be positive in all cases, and is entered into the count location before the next interval begins. No information has been lost by this process. The only change is that the large quantity S has been replaced by three smaller numbers, M, C and n.

The averaging algorithm for calculating a new average (mean) from the previous mean and a new count is explained in connection with Table 1 and Fig. 9. Table 1 shows a few examples for the validity of the relation

$$(n-1)\cdot M_{n-1} + P_n = n\cdot M_n + Q_n \ . \qquad (8)$$

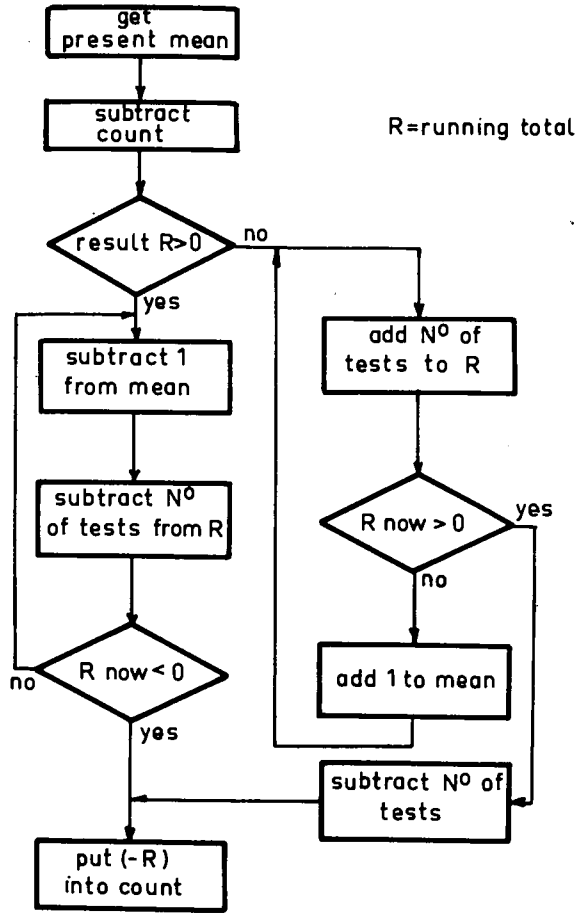

Fig. 9. Average algorithm for mean rate analysis.

Table 1

M_{n-1}	P_n	n	$(n-1)M_{n-1}+P_n$ (Total)	M_n	Q_n	$n\cdot M_n+Q_n$
104	112	5	416+112=528	105	3	525+3=528
104	106	5	416+106=522	104	2	520+2=522
104	104	5	416+104=520	104	0	520+0=520
104	101	5	416+101=517	103	2	515+2=517
104	93	5	416+ 93=509	101	4	505+4=509

The average programme is entered when the end of an interval is reached. At this point n intervals have been completed. The rate measurement stored is M_{n-1}, the count $P_n = Q_{n-1}+C_n$. To test if the mean rate has been maintained, the contents of the two locations are compared, i.e. $M_{n-1}-P_n$. If the rate is larger, then the previous estimate was too high and must be reduced to avoid a negative remainder. If the rate is smaller than the observed count, the rate is low. In this case the rate value is increased if M can be increased by an integral amount still leaving a positive remainder, i.e. when $P_n - M_{n-1} - n$.

Figure 8d, e, f shows the course of measurement of the 1024 channel ^{60}Co spectrum. Figure 8d shows this spectrum after 1 interval, Fig. 8e after 3, and Fig. 8f after 820 intervals. It is seen that the display improves in precision as the experiment progresses but maintains the amplitude constant. It is possible to compare in Fig. 8 the differences in display between the normal and mean rate analysis as the experiment progresses.

5. MULTIPARAMETER ANALYZERS

The situation is radically new when one considers the number of channels necessary for measuring the probability density function in more than one parameter. In a multiparameter experiment the "event" or "descriptor" is made up of more than one component. Thus a number of discrete digitization may have to be recorded as a single entity. They may represent combinations of energy, time-of-flight and specific ionization (dE/dx) information, for example.

A typical two-parameter situation may be represented by two energy measurements. The first two-parameter ana-

lyzer, providing 64x64=4096 channels and using a magnetic drum for storage, was built by Chase[37] in 1959.

Commercial analyzer systems have become available with large memories of up to 20.000 channels. Recently computers have been widely used as multiparameter analyzers of different kind. It is obvious, however, that without some special technique the analysis is limited to a few thousand direct accumulating channels, dictated by the size of the fast computer memory.

6. ANALOG MEMORY ANALYZERS

Digital storage is the accepted manner of dealing with digital information in probability distribution measurements. Its use in pulse analysis has been stimulated by the rapid development of digital storage techniques using magnetic cores. Yet it could be questioned if under certain circumstances the use of the simpler analog storage technique could be justified.

A somewhat related instrumentation field where both techniques are used competitively in commercial instruments is the signal retrieval of repetitive signals buried in noise. In certain instruments the digital technique involving the digitalization of the measured quantity is followed by the less costly analog storage technique. Such an analog memory can be composed, for example, of a bunch of capacitors, one for each analyzer channel.

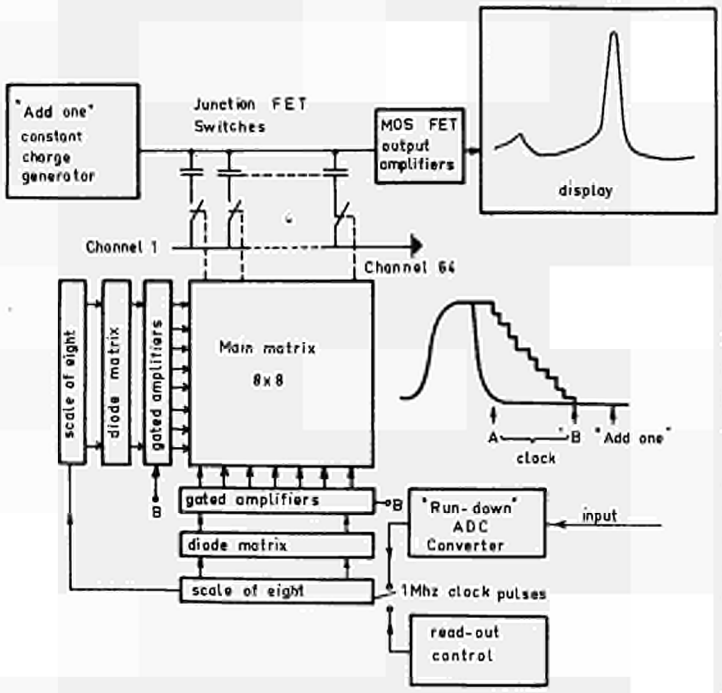

Fig. 10. Analog memory analyzer, using a bunch of capacitors.

Figure 10 shows a block diagram of an analog memory analyzer, Westman, Petrusson, Tove[38].

Channel addressing is performed in a conventional manner using an amplitude to time conversion unit. The address pulses are fed to two series connected scales of eight. The address information is taken from these registers via the decoding diode matrices to the main matrix. The gated amplifiers isolate the matrix during the address counting places. At the end of this procedure the proper channel switch is closed.

The storage of the pulse numbers is performed according to the "analog" principle. Each pulse causes a small constant charge to be added to the channel capacitor, a short time after addressing is completed. Read-out is performed by closing sequentially all channels and using a CRT or an XY recorder as a display unit.

An analog system has limitations such as finite storage time, stringent requirements on equality and stability of capacitor values (in order to avoid the inequality between the channels) the existence of "noise" voltages introduced by switching transients, and a limited number of permissible read-out processes before the distortion of a spectrum results.

However, these drawbacks may be significantly reduced in many cases, because of advances in the component field, and then analog systems become interesting due to their simplicity and higher speed. Figure 10 shows also a spectrum measured by means of the described analog memory system with a resolution of 64 channels and a maximum count of 10^5 pulses per channel.

Analog memories with capacitors are usable only for systems with a moderate number of channels. For larger systems there is another analog memory in the form of a display storage tube, having a viewing screen with storage and integration properties, Stüber[39].

The block diagram of a two-parameter storage tube analyzer is shown in Fig. 11a. The operation will be as follows: For each incoming nuclear event a constant charge increment has to be

placed at the proper spot on the storage screen. For two-parameter events it is convenient to attach the address part of one parameter to the horizontal (x) direction and the address part of the other parameter to the vertical (y) direction. The x and y address parts are accepted by registers with e.g. 10 bits each and converted by digital-to-analog converters into x and y deflection voltages. When the deflection field has been settled, the electron beam is pulsed on for a short time to deposit a charge measurement on the storage screen.

The charge picture storage tube has a fluorescent screen and the picture looks like that of an oscilloscope tube. The internal structure of such a tube is outlined in Fig. 11b. The whole viewing screen of the tube can be brought to fluorescnence by a stream of slow electrons, which penetrates into a fine mesh backing electrode, coated by a thin film dielectric surface. The flooding electrons can be controlled by the potential on the storage surface. If this potential is made sufficiently negative the flooding electrons cannot reach the viewing screen. If positive charges are now deposited on the storage surface, the mesh will become permeable to the flooding electrons at the charged places, and a luminous projection of the charge distribution will be produced on the viewing screen. A desired charge pattern can be written onto the storage surface by means of a high-energy electron beam from the writing gun. This beam deposits positive charges onto the storage surface as the secondary electron emission factor is greater than unity. The integration capability of the tube is given by the fact that each spot on the storage surface acts as a little capacitor.

Figure 12 shows the ^{60}Co gamma-gamma coincidence spectrum displayed on the storage tube. By changing the bias voltage of the backing electrode, it is possible to shift the cut-off point of the storage surface, so that only the highest peaks of the stored "charge mountains" become visible.

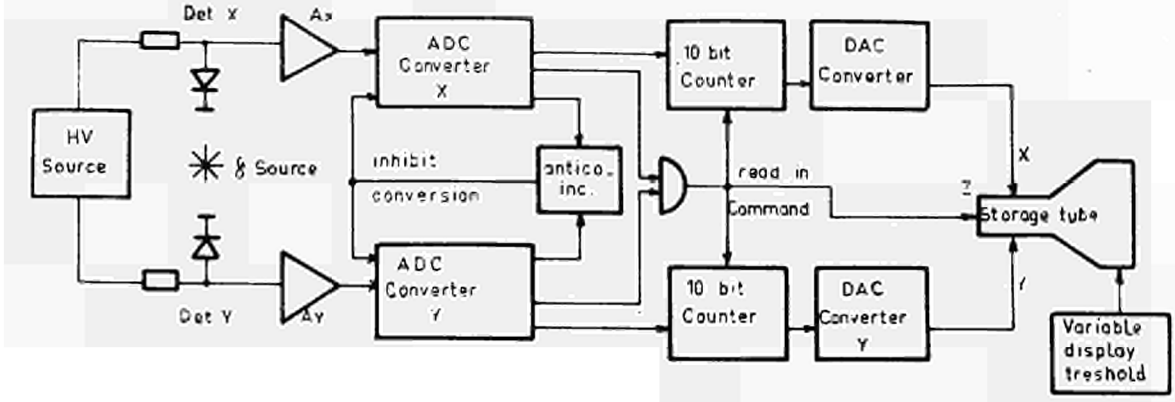

b)

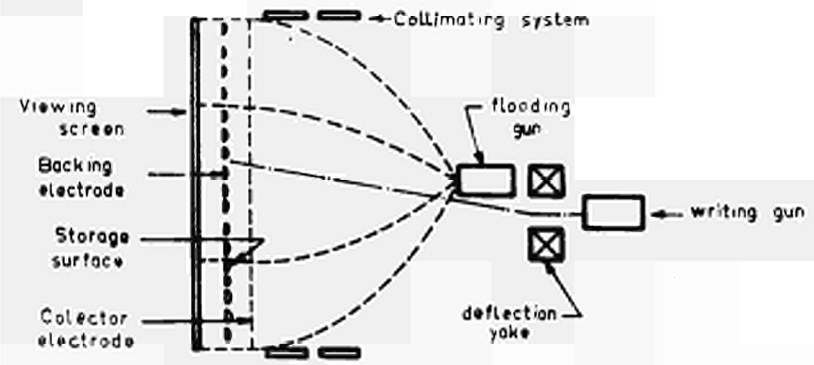

Fig. 11. Storage tube analyzer. (a) Two-parameter experiment, block diagram. (b) Basic storage tube structure.

Spectra with more than 100.000 channels can be displayed on such a system. This system is applicable in situations where it is not of primary importance to measure the number of counts per channel with great accuracy.

7. ASSOCIATIVE ANALYZERS

In a multichannel analyzer the input signal describing an external event is expressed as a digital number which we call the "descriptor". In a conventional analyzer the descriptor defines the location in the memory at which the "count" (number of occurrences of descriptor) is stored. The principle of connection of a physical field of descriptors to memory locations in classical analyzers is shown in Fig. 13a.

With increasing resolution of nuclear radiation detectors and analog-to-digital converters the full range of descriptors may be very large. In certain nuclear physics and biology experiments, particularly those involving coincident spectra, although the possible range of descriptors is very large, the number of different descriptors which actually occur during experiment is much smaller. A few such two-dimensional spectra, displayed in a map form are shown in Fig. 19. Such spectra in a 1000x1000 resolution have a range of 10^6 possible descriptors, while only thousands of those actually occur in experiments. If one uses a conventional analyzer for the measurement of such spectra, one must provide a large memory (10^6 channels), of which only a small percentage of locations would be useful, and all other locations would be empty.

An alternative technique is to allow locations only to those descriptors which actually occur in the experiment. Since the correspondence between the location and the descriptor is lost, it is necessary to store the descriptor as well as the associated count. Hence the system must be content addressable or associative. The principle of connections of the physical field of descriptors to memory locations in associative analyzers is shown in Fig. 13b. The numbers show the sequence of arrival of the first descriptors of different kind from the experiment. The first descriptor will take the first available locations of the memory, the next different descriptor the second location etc.

When a new datum comes to the associative analyzer input it must be

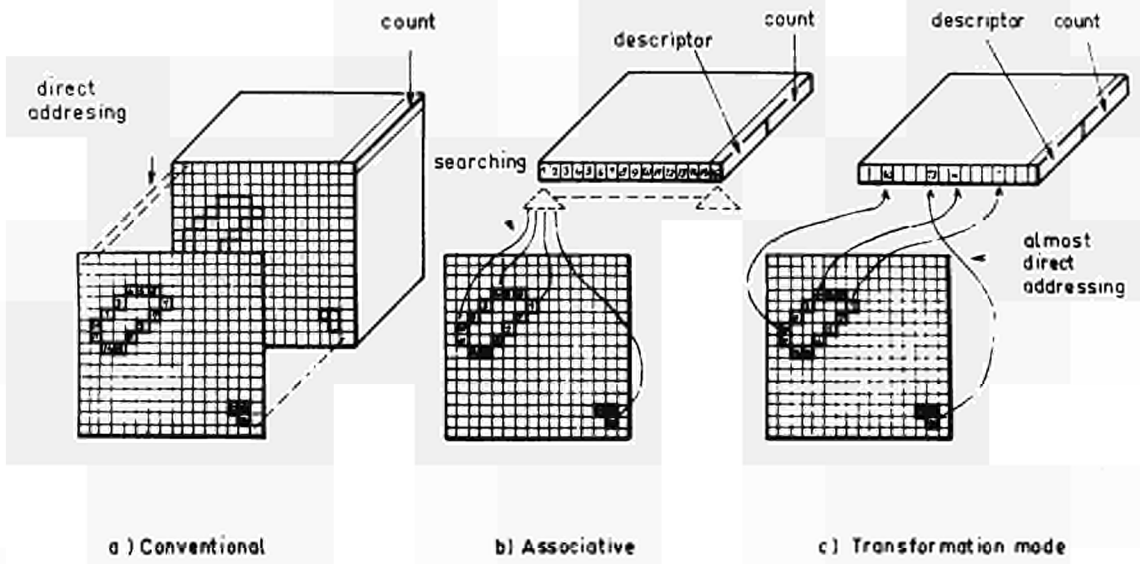

Fig. 13. Different principles of direct accumulating megachannel analyzers: (a) conventional analyzer, (b) associative analyzer, (c) transformation mode analyzer.

sorted into its channel on a list, hence some searching will be required to locate a descriptor. An obvious routine for searching the list is to compare the descriptor for a new event with the descriptor in each location, until a match is found. If the list is of length r, the average number of comparisons will be c = r/2 (for r = 4096, c = 2048 comparisons). A marked reduction in access time may be achieved by using a tree search algorithm, as was actually done in the first associative analyzer[41].

This procedure requires repeated comparisons of pairs of descriptors. Each comparison yields one of the following three answers: (1) they match, (2) the first is greater, or (3) the second is greater. According to the answer the comparison is either finished or proceeds on to the left or right branch of a "tree", Fig. 14. If there are r descriptors on the tree, the average number of comparisons is reduced from r/2 to approximately $\log_2 r$ (for $r = 2^{12} = 4096$, $c = \log_2 r = 12$ comparisons). Figure 15 shows the high resolution spectra, measured directly on-line with associative analyzer, Souček [41,42]. a,b,c presents a map display of 3x256x256 spectrum, using particle identification for grouping (cyclotron experiment). (d) 256x256 ^{207}Bi gamma-gamma spectrum, isometric display.

8. MOST ACTIVE ZONE ENCODER FOR MULTI-PARAMETER ANALYSIS

Associative mode analyzers ask for a descriptor to be stored in the memory as well as for an associated count. Hence about 50% of the memory would be occupied by descriptors. The situation has been improved by introduction of "zone selection". Here are the basic principles of zone selection, as proposed by Hooton[43].

In many experiments information occurs in groups or clusters of channels. The descriptor field is divided arbitrarily into a number of zones of equal size. Each of them is a potential digital window. If data occur in any channel within a particular zone the location of the zone in the field is held in an associative memory. Hence for each zone it is necessary to store only one "zone descriptor". A group of storage locations is assigned for counts for different channels inside the zone. For example, if the zone is of size 4x4 = 16 channels, it is necessary to provide one space for storing the descriptor of the zone, and 16 spaces for counts, which can be addressed inside a zone using 2 least significant descriptor digits. Hence in total it is necessary 1+16 = 17 spaces and the fraction

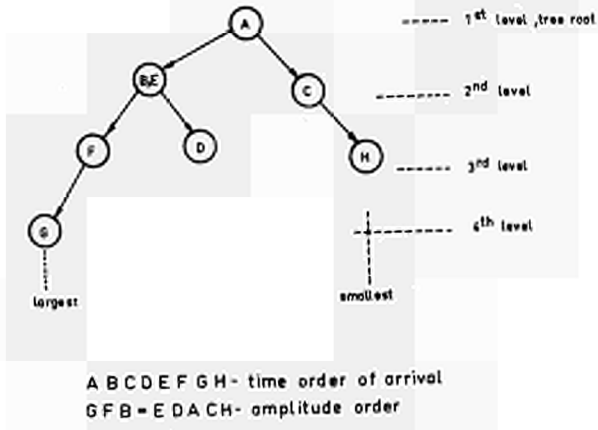

Fig. 14. Tree search algorithm used in programmed associative analyzer.

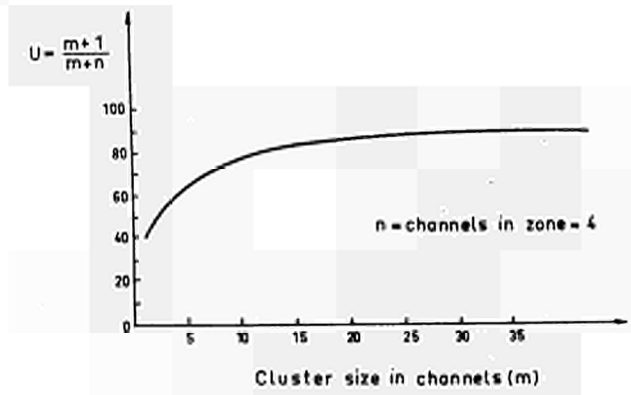

Fig. 16. Mean memory utilization in zone selection, as a function of cluster size.

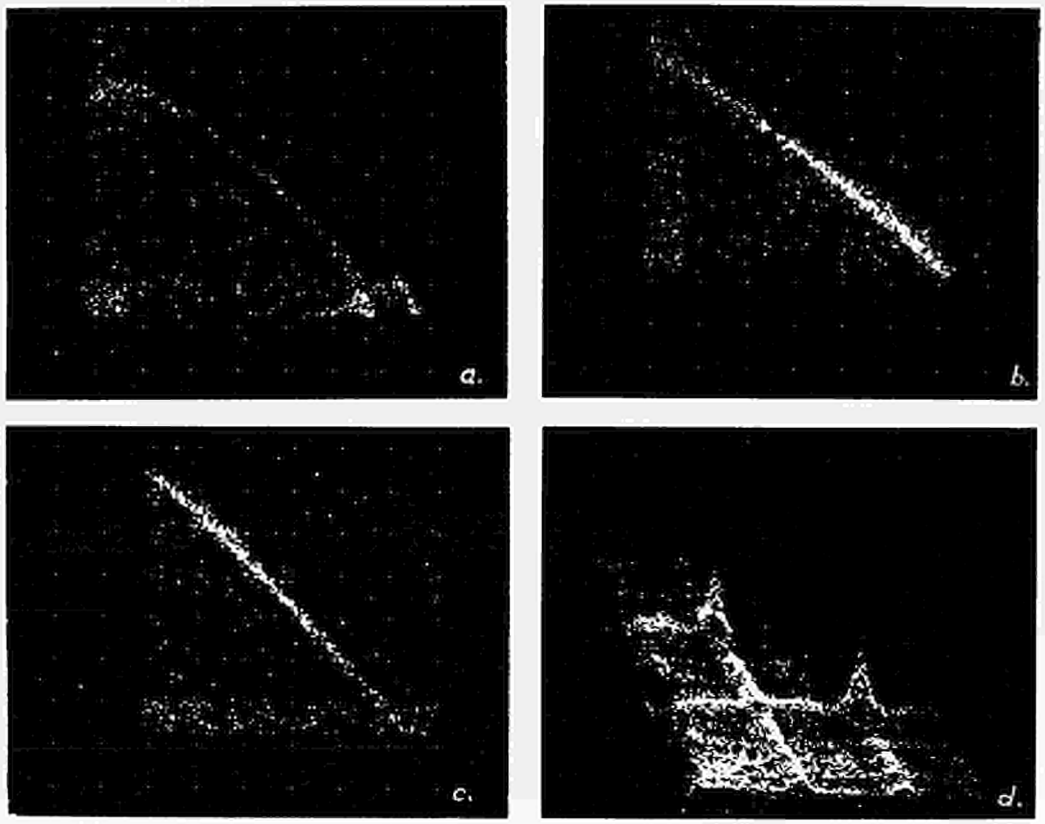

Fig. 15

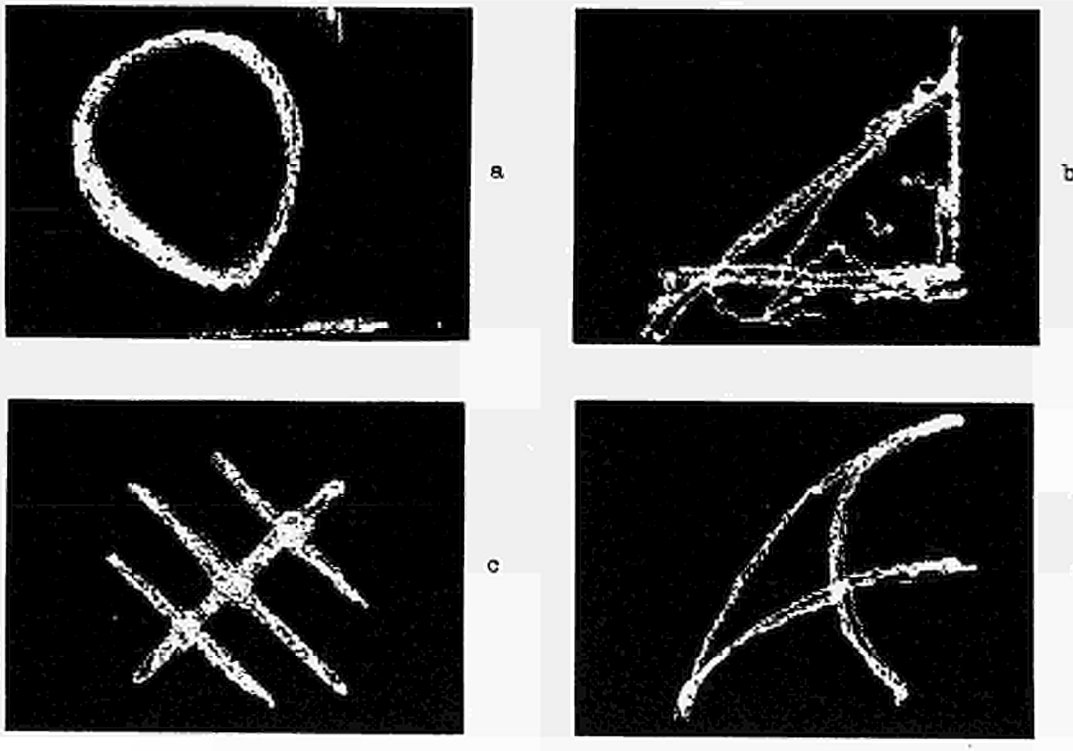

Fig. 19

of the memory containing the counts would be $u_1 = 16/17 = 94\%$. In the associative mode without zones it would be necessary to have 16 spaces for descriptors and 16 for counts, giving $u_2 = 16/32 = 50\%$.

Of course, the high efficiency u_1 would be achieved only if the clusters of the spectrum were much larger than the size of the zones.

It can be easily shown that the mean utilization of the memory is approximately

$$u = \frac{m + 1}{m + n} \qquad (9)$$

where m is the number of channels in a cluster, and n the number in a zone. It is supposed that the cluster and the zone can be in any relative position, and eq. (9) gives an average. Eq. (9) is shown in Fig. 16.

A hardware zone selection analyzer was built by Best, Hickman, Hooton and Prior[44] using sophisticated technique of the transfluxor associative memory. At the same time Best[45] designed a computer - software zone selection analyzer. Figure 17 represents a part of a 256x256 channel spectrum measured by this system. One can notice that the spectrum is composed of zones, of 4x4 channels each.

9. TRANSFORMATION MODE ANALYZERS

Associative and zone/associative analyzers are limited by increased dead time, since a comparison must be made between each input descriptor and the memory content to find the appropriate channel location. To overcome this limitation, Hooton[46], Rosenblum[47], Souček[48] and Spinrad[5] suggested to look for a procedure of randomizing type. The problem is similar to the file address problem by key-to-address transformation. The characteristic of nuclear spectroscopy is that is does not assume an a priori knowledge of the key set (spectrum or descriptor set) and asks for a procedure suitable for high speed on-line application.

Souček, Bonačić and Čuljat[49] investigated different randomizing transformations, and found that the most suitable for nuclear spectroscopy is the transformation based on the division of polynomials. The transformation can be realized as a part of a computer data taking interrupt routine, or as a hardware box between an analog-to-digital converter and a computer.

By passing through a transformation box, each descriptor produces a pseudo-

Fig. 17. Map display of a two-dimensional spectra, measured with zone selection computer associative analyzer.

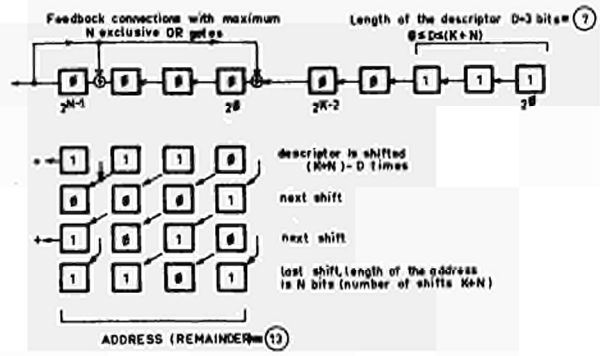

Fig. 18. Generation of a pseudo-random address, through the division of polynomials.

random address into which it is stored, Fig. 13c. It would be ideal if any distribution of descriptors (spectral shape) would produce a uniform distribution of addresses throughout the memory. For practical spectra there is, however, the possibility of two or more descriptors being transformed to the same address. Because of that, the transformation is used only to generate the address on the list at which to start searching. This method makes almost direct addressing possible, as in conventional analyzers, and high utilization of the memory space as in associative systems.

Figure 18 shows the principle of transformation through division of polynomials.

The descriptor D is left shifted through the shift register having feedback through exclusive or gates. The descriptor and the feedback configuration present polynomials. When the least significant descriptor bit reaches the top of a shift register, the operation of "polynomial division" is finished and the shift register will contain the remainder. In a given example, the descriptor presents decimal 7, and produces the remainder decimal 13. Experimentations with different spectra and different feedbacks show that the remainder might be used as a descriptor address on the list.

The randomizing feature of such transformations is shown in Table 2. The descriptors 0-1024 (in 32x32 XY matrix) are fed through the transformation box, with the feedback over 5 stages of the register, producing addresses 0-31. For exsmple, the descriptor X=08, Y=0 produces address 3, descriptor X=21, Y=2 produces address 16 etc. It is obvious that the produced addresses are pseudorandomly distributed over the field. Over this pattern one can draw maps of twodimensional nuclear spectra of arbitrary shapes, and see that all addresses are produced with almost equal probability.

The transformation mode analyzer is

TABLE 2

Experiment with 1024 descriptors (32×32 field), using division by the polynomial $T(x)=x^5+x^4+0+x^2+x+1$ which can produce addresses 0-31. Pattern of all possible addresses.

00	01	02	03	04	05	06	07	08	09	10	11	12	13	14	15	16	17	18	19	20	21	22	23	24	25	26	27	28	29	30	31
0|R	7	14	9	28	27|R	18	21	3	4	13	10	31	24	17	22	6	1	8	15	26	29	20	19	5	2	11	12	25	30	23	16
27|	28	21	18	7	0|	9	14	24	31	22	17	4	3	10	13	29	26	19	20	1	6	15	8	30	25	16	23	12	5	12	11
13	10	3	4	17	22	31	24	14	9	0	7	18	21	28	27	11	12	5	2	23	16	25	30	8	15	6	1	20	19	26	29
22	17	24	31	10	13	4	3	21	18	27	28	9	14	7	0	16	23	30	25	12	11	2	5	19	20	29	26	15	8	1	6
26	29	20	19	6	1	8	15	25	30	23	16	5	2	11	12	28	27	18	21	0	7	14	9	31	24	17	22	3	4	13	10
1	6	15	8	29	26	19	20	2	5	12	11	30	25	16	23	7	0	9	14	27	28	21	18	4	3	10	13	24	31	22	17
23	16	25	30	11	12	5	2	20	19	26	29	8	15	6	1	17	22	31	24	13	10	3	4	18	21	28	27	14	9	0	7
12	11	2	5	16	23	30	25	15	8	1	6	19	20	29	26	10	13	4	3	22	17	24	31	9	14	7	0	21	18	27	28
15	8	1	6	19	20	29	26	12	11	2	5	16	23	30	25	9	14	7	0	21	18	27	28	10	13	4	3	22	17	24	31
20	19	26	29	8	15	6	1	23	16	25	30	11	12	5	2	18	21	28	27	14	9	0	7	17	22	31	24	13	10	3	4
2	5	12	11	30	25	16	23	1	6	15	8	29	26	19	20	4	3	10	13	24	31	22	17	7	0	9	14	27	28	21	18
25	30	23	16	5	2	11	12	26	29	20	19	6	1	8	15	31	24	17	22	3	4	13	10	28	27	18	21	0	7	14	9
21	18	27|R	28	9	14	7	0|R	22	17	24	31	10	13	4	3	19	20	29	26	15	8	1	6	16	23	30	25	12	11	2	5
14	9	0|R	7	18	21	28	27|R	13	10	3	4	17	22	31	26	8	15	6	1	20	19	26	29	11	12	5	2	23	16	25	30
24	31	22	17	4	3	10	13	27|R	28	21	18	7	0	9	14	30	25	16	23	2	5	12	11	29	26	19	20	1	6	15	8
3	4	13	10	31	24	17	22	0|R	7	14	9	23	27	18	21	5	2	11	12	25	30	23	16	6	1	8	15	26	29	20	19
30	25	16	23	2	5	12	11	29	26	19	20	1	6	15	8	24	31	22	17	4	3	10	13	27	28	21	18	7	0	9	14
5	2	11	12	25	30	23	16	6	1	8	15	26	29	20	19	3	4	13	10	31	24	17	22	0	7	14	9	28	27	18	21
19	20	29	26	15	8	1	6	16	23	33	25	12	11	2	5	21	18	27	28	9	14	7	10	22	17	24	31	10	13	4	3
8	15	6	1	20	19	26	29	11	12	5	2	23	16	25	30	14	9	0	7	18	21	28	27	13	10	3	4	17	22	31	24
4	3	10	13	24	31	22	17	7	0	9	14	27	28	21	18	2	5	12	11	30	25	16	23	1	6	15	8	29	26	19	20
31	24	17	22	3	4	13	10	28	27	18	21	0	7	14	9	25	30	23	16	5	2	11	12	26	29	20	19	6	1	8	15
9	14	7	0|R	21	18	27|R	28	10	13	4	3	22	17	24	31	15	8	1	6	19	20	29	26	12	11	2	5	16	23	30	25
18	21	28	27|R	14	9	0|R	7	17	22	31	24	13	10	3	4	20	19	26	29	8	15	6	1	23	16	25	30	11	12	5	2
17	22	31	24	13	10	3	4	18	21	28	27	14	9	0	7	23	16	25	30	11	12	5	2	20	19	26	29	8	15	6	1
10	13	4	3	22	17	24	31	9	14	7	0	21	18	27	28	12	11	2	5	16	23	30	25	15	8	1	6	19	20	29	26
28	27|R	18	21	0|R	7	14	9	31	24	17	22	3	4	13	10	26	29	20	19	6	1	8	15	25	30	23	16	5	2	11	12
7	0|R	9	14	27|R	28	21	18	4	3	10	13	24	31	22	17	1	6	15	8	29	26	19	20	2	5	12	11	30	25	16	23
11	12	5	2	23	16	25	30	8	15	6	1	20	19	26	29	13	10	3	4	17	22	31	24	14	9	0	7	18	21	28	27
16	23	30	25	12	11	2	5	19	20	29	26	15	8	1	6	22	17	24	31	10	13	4	3	21	18	27	28	9	14	7	0
6	1	8	15	26	29	20	19	5	2	11	12	25	30	23	16	0	7	14	9	28	27	18	21	3	4	13	10	31	24	17	22
29	26	19	20	1	6	15	8	30	25	16	23	2	5	12	11	27	28	21	18	7	0	9	14	24	31	22	17	4	3	10	13

specially suitable for spectra such as in Fig. 19. Those spectra are simulated by a CRT-light pen-PDP-8 system, according to the known results of the following experiments:

a) D+P — P+P+N 21.1 MeV, 34°, -34°
b) Van de Graaff experiment: $^{6}Li+^{3}He$ — — P+alpha+alpha, 3 MeV, 37.5°, -37.5°
c) Biological spectra, Jahns line phantom
d) Two parameter spectrum $^{3}He(^{3}He,2p)^{4}He$

Each of those spectra contains 1024 descriptors in the 128x128 field. The descriptors have been fed through the programmed transformation box in the SDS 930 computer, always producing practically uniform distribution of 1024 different addresses.

Figure 20 shows the number of lost descriptors L(s), which have not found an available place, and the average number of comparisons, as a function of the maximum available number of comparisons, for one of the spectra from Fig. 19, but for 2048 descriptors. In practice, the number of locations in the memory will be at least for a few percent larger than the number of descriptors in a physical field, giving results better than those in Fig. 20.

The block diagram of the described transformation system, designed by Souček, Bonačić and Culjat[50,51] is shown in Fig. 21.

10. WINDOW PRESELECTION

In a two- (or more) parameter experiment, every event is characterized by two parameters, X and Y. The experimental matrix XY might be as big as 4096x256 channels. To store the event in the whole matrix during the experiment requires an expensive data acquisition system. A cheaper solution is to put constraints on one parameter, say X, and to record Y as a function of these constraints. This is realized by setting windows on the spectrum of one parameter. Window preselections have been designed in different laboratories[52-56].

A simplified block diagram of a 16 window discriminator, Spilling, Gruppelaar and Van den Berg[56] is shown in Fig. 22. The main features are the matrix board and the two 12-bit adder, one adder for the lower threshold and one for the upper. They are on one side connected to the 12-bit lines from the X-address unit. The other side of the adders is connected to 24 horizontal rails on the matrix board, 12 rails per adder set. A four-bit scaler is, via a decoding matrix, connected to 16 vertical rails on the matrix board, one rail per window. To obtain the window settings, the vertical and horizontal rails are connected with diode pins in the binary code in such a way that the

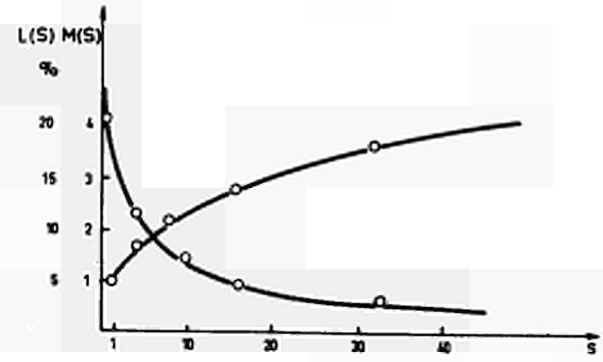

Fig. 20. Average number of comparisons M(s) and percentage of lost descriptors L(s), as a function of maximum permitted number of comparison S.

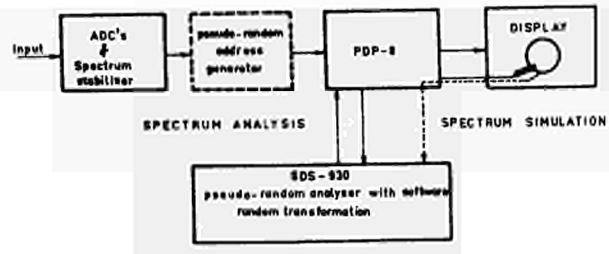

Fig. 21. Computer system for pseudo-random transformation of nuclear data.

combinations on each vertical rail define a lower and an upper threshold. The horizontal rails keep the corresponding side of the adders in "1" states. When the four-bit scaler is counting, one after the other of the 16 vertical rails are energized via the decoding matrix, and successively all lower and upper thresholds are compared with the binary information on the X bit lines. The adders sum the binary information on both sides in the standard way. The adders are wired in such a way that if an X event has arrived in one of the selected windows, the output (carry) from the lower-threshold adder and no output from the other will result, producing an "accept" pulse. At this moment bits from the ADC and from the scaler are transferred to the memory. Scaler bits determine the window address. In particular instruments, the following number of subgroups or windows can be manually selected: 16 of 256, 8 of 512, 4 of 1024 or 2 of 2048 channels.

If one has selected 16 subgroups, then the first eight bits of the Y ADC (256 channels) and four bits of the scaler (16 subgroups) are connected to the memory block (4096 words).

Gamma-gamma coincidence measurements have been performed on the reaction $^{44}Ca(n,gamma)^{45}Ca$ with a 6.5 cm^3 Ge(Li) detector and a 12.7x12.7 cm NaI detector, and some of the results are shown in Fig. 23 (4 windows of 1024 channels each).

The main advantage of the window selection technique is its simplicity. The main disadvantage is a need to make preexperiment in order to be able to set the window limits. The data out of the windows are lost.

11. EVENT RECORDING ANALYZERS

All the systems outlined above belong to the class of direct accumulating analyzers. They form the probability density function during the experiment,

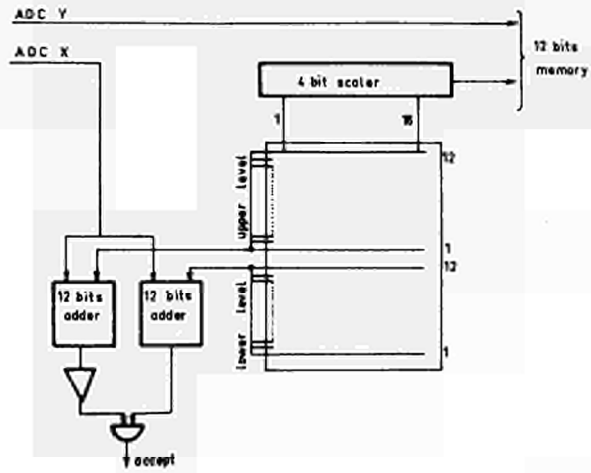

Fig. 22. Block scheme of the 16-window digital discriminator.

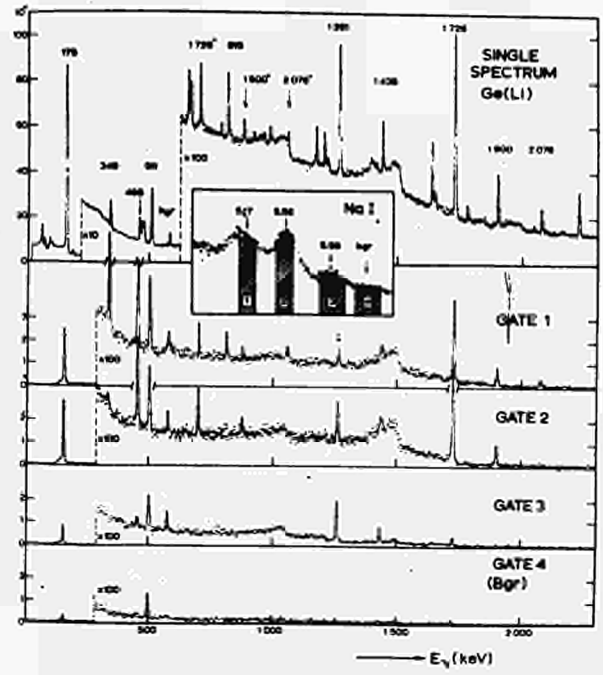

Fig. 23. Spectra coincident with four windows in the NaI channel, each in 1024 channels. The window settings are shown in the insert. A Ge(Li) single spectrum is shown in the upper part.

as data are coming. Direct accumulating systems are highly preferable by the experimenters, owing to many advantages, the most important being the contact with the experiment.

However, there are situations in which all possible multiparameter combinations are needed. The simplest procedure used to meet this requirement is to record the addresses (descriptors) on an inexpensive bulk storage medium in the sequence of their arrival. Paper tape and magnetic tape are most frequently used.

At the completion of the experimental run, the tapes are read for sorting through a digital computer. Multiple passages of the tape are usually necessary. Each pass is used to sort on a different subset ("software window selection") of the total number of channels. The main advantage of the event recording technique is its low cost in comparison with that of directly accumulating analyzers. Its chief liability is an unavoidable loss of contact with the course of experiment, because the spectra are not available until after the experiment is over. To diminish this limitation, a modest accumulating analyzer is frequently put on the data stream to monitor the course of the experiment. There is a number of event--recording systems described (e.g. [57], [58], [60]).

12. SPECTRUM STABILIZATION

During pulse height analysis of pulses from radiation detectors some errors appear caused by the measuring instrument itself. One of the most significant errors is the spectrum unstability, which is very important when the analysis lasts long, for instance from a few hours to a few days. The spectrum unstability is due to the preamplifier and amplifier drift, and to the ADC zero and gain drift. The measuring errors exhibit in the fact that the same energy does not correspond to the same channel.

There are several different methods for spectrum stabilization. A direct method corrects the errors mentioned as they are generated. Most often the feedback control is used.

Hardware or software solutions make difference between indirect methods. A feature common to these methods is the correction of digitalized information. Digital on-line stabilization is an example of hardware solution. The basic principle is the comparison of the spectrum measured with the known (calibrated) spectrum or with the referent signal[59].

A software off-line stabilization method[60] will be briefly described. The spectrum measured is sorted in the memory during one definite time interval. Afterwards a calibration pulse with constant amplitude from the pulse generator is registered onto the magnetic tape. The measured spectrum is also registered. After the second interval the calibration pulse and a new part of the measured spectrum are stored onto the magnetic tape.

Data taking is stopped after a sufficient number of intervals. The computer accumulates the spectra measured in separate intervals into one integral spectrum. Due to the system unstability the calibration pulse has not generated the same address number. By correcting the measured spectrum the computer snifts the spectrum as much as the calibrated pulse was shifted but in the opposite sense. The same occurs with every part of the spectrum from the magnetic tape. After correction, parts of the spectrum are accumulated together.

Figure 24 shows the same integral

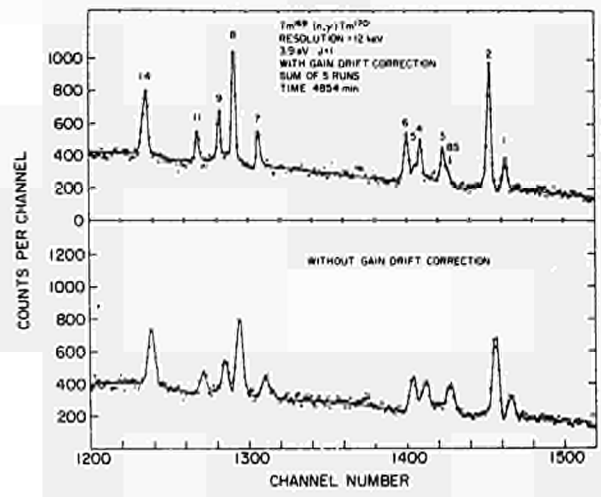

Fig. 24. Thullium spectrum stabilization. The whole spectrum without correction (lower figure); the spectrum with correction (upper figure).

spectrum with (upper) and without (lower) correction. The area under the spectrum is the same in both cases, but the peaks are wider and lower in the uncorrected spectrum.

13. TRENDS IN ANALYZING SYSTEMS

Some of the major steps in the development of analyzing systems are shown in Table 3. The tendency is to increase the number of channels and the speed of operation. It is interesting to notice that practically all major steps in the development have been obtained through adaptation of the techniques which existed in some form in other fields, notably in computer technology. Due to the severe requirements in spectrometry, adaptations have usually been quite sophisticated. It is probable that there are additional techniques, waiting to be noticed by analyzer designers, and adopted for spectrometry application.

The future analyzer systems will tend to be more complex, more rapid, with more channels. A number of investigators have already described experiments which require three, four or more

Table 3

Year	Introduced in analyzers	Number of direct accumulating channels	Feature	Designers
1950	Amplitude to time conversion	-	-	Wilkinson[15]
1951	Delay line memory	128	slow	Hutchinson & Scarrot[16]
1955	Electrostatic memory	-	-	Higinbotham[17]
1955/56	Core memory	256	fast	Byington & Johnstone[18] Schumann & Mc Mahon[19]
1959	Magnetic drum, two parameters	4096	slow	Chase[37]
1962/63	Computer-software systems	$nx10^3$	moderate	number of systems[20-33]
1963	Sliding scale converter	-	fast	Cottini, Gatti & Svelto[9]
1965	Software associative memory	$nx10^5$	moderate	Souček & Spinrad[5,41,42]
1966	Hardware associative memory and zone selection	$nx10^5$	fast	Hooton, Best, Hickman and Prior[43,44,45]
1968	Weighting converter with additional test	-	fast	Hrisoho[10]
1968	Pseudo-random transformation	$nx10^6$	fast adaptive	Souček, Bonačić & Culjat[49,50,51]

parameter analysis, with megachannel resolution.

Owing to the rapid development of integrated circuitry, one can predict combinations of analog and digital data processing techniques, at higher level. Only to give an example, such a combination can be: preselection of a number of interesting regions from large spectra, using analog window amplifiers, followed by the digital pseudo-random transformation analyzer.

It is probably reasonable to predict further increase in the use of small computers in complex experimental systems. They will make their imprint most markedly in real-time data reduction, feedback control and multi-experiment time-sharing.

References

1. Chase R.L., Nuclear Pulse Spectrometry (Mc Graw-Hill, New York 1961)
2. Korn G.A., Random-Process Simulation and Measurements (Mc Graw-Hill, New York 1966)
3. Bendat J.S., Piersol A.G., Measurement and Analysis of Random Data (John Wiley and Sons, New York 1966)
4. Bendat J.S., Interpretation and Application of Statistical Analysis for Random Physical Phenomena, IRE Transac. on Bio-medical Electronics, January 1962, 31-43.
5. Souček B., Spinrad R.J., Megachannel Analyzers, IEEE Trans. on Nucl. Sci., NS 13, No 1, 183-191, 1966.
6. Spinrad R.J., Data Systems for Multiparameter Analysis, in Annual Review of Nuclear Science, Vol. 14, 1964.
7. Chase R.L., Proc. Conf. Utilization Multiparameter Analyzers, Nucl. Phys. Grossinger, N.Y., 1962, CU(PNPL)-227, 79-82.
8. Bonitz M., Nucl. Instr. Methods 22, 238-252 (1963).
9. Cottini C., Gatti E. and Svelto V., Nucl. Instr. Methods (letter), 24, 241-242 (1963).
10. Hrisoho A., Proc. Internat. Conf. on Nucl. El., Versailles, 1968.
11. Moody N., Electron. Eng., 24, 289 (1952).
12. Cottini C., Gatti E., and Gianelli G., Nuovo Cimento 4, 156 (1956); Cottini C. and Gatti E., Nuovo Cimento 4, 1550 (1956).
13. Lefevre H. and Russel J., Rev. Sci. Instr., 30, 159-166 (1959).
14. Chase R.L., and Higinbotham W.A., Rev. Sci. Instr. 28, 448-451 (1957).
15. Wilkinson D., Proc. Cambridge Phil. Soc. 46, Pt. 3, 508 (1950).
16. Hutchinson G., and Scarrot G., Phil. Mag., 42, 792 (1951).
17. Higinbotham W.A., Proc. Internat. Conf. Peaceful Uses At. Energy, Geneva 1955, 4, 53-61.
18. Byington P.W., and Johnstone C.W., A 100-Channel Pulse Height Analyzer Using Magnetic Core Storage, IRE Conv. Record 10, 204-210 (March 1955).
19. Schumann R.W., and McMahon J.P., Rev. Sci. Instr. 27 (9), 675-685 (1956).
20. Bromley D.A., Goodman C.D., and O'Kelley G.D., Proc. Conf. Utilization Multiparameter Analyzers Nucl. Phys., Grossinger, N.Y., 1962 CU(PNPL)-227, 35-38.
21. Deinert R.H., and Koerts L.A., Nuclear Electronics, II, 197-204 (Internat. Atomic Energy Agency, Vienna 1962).
22. Kenney R.W., Nucl. Instr. Methods 20, 342-344 (1963).
23. Kirsten F.A., and Mack D.A., Nuclear Electronics, II, 127-141 (Internat. Atomic Energy Agency, Vienna 1962).
24. Nakamura M., and Simonof G.S., Proc. Conf. Instr. Tech. Nucl. Pulse Analysis, Monterey, Calif., 1963.
25. Collinge B., and Marciano F., Nucl. Instr. Methods 16, 145-152 (1962).
26. Groom D.E., and Marshall J.H., Rev. Sci. Instr. 33 (11), 1249-1255 (1962).
27. Matalina L.A., Chubarev S.I., and Tishechkina A.S., Nuclear Electronics, II, 121-125 (Intern. Atomic Energy Agency, Vienna 1962).
28. Spinrad R.J., Nucleonics 21 (12), 46-49 (1963).

29. Spinrad R.J., Transac. IEEE PT, Group Nucl. Sci., 11 (3) (1964).

30. Brun J.C., Verroust G., and Victor C., J. Phys. Radium Phys. Appl. 23, 129A-133A (1962).

31. Norbeck A., Proc. Conf. Utilization Multiparameter Analyzers Nucl. Phys, Grossinger, N.Y., 1962, CU(PNPL)-227, 56-58.

32. Kane J.V., and Spinrad R.J., Proc. Conf. Utilization Multiparameter Analyzers Nucl. Phys., Grossinger N.Y., 1962, CU(PNPL)-227, 149-154; and Nucl. Instr. Methods 25, 141-148 (1963).

33. Krüger G., and Dimmler G., Proc. Internat. Symp. Nucl. Electronics, Paris 1963.

34. Souček B., Bonačić V., Culjat K., Proc. IV Yugoslav Internat. Data Processing Symposium, Ljubljana 1968.

35. Hooton I.N., Best G.C., Nuclear Instr. Methods 56, 284 (1967).

36. Best G.C., Hooton I.N., AERE Report R 5425, Harwell, England 1967.

37. Chase R.L., IRE Natl. Conv. Record, Pt. 9, 196-201 (1959).

38. Westman A., Petrusson E., Tove P.A., Proc. Int. Conf. on Nucl. Electronics, Versailles 1968.

39. Stüber W., Proc. Int. Conf. on Nucl. Electronics, Versailles 1968.

40. Widley P.T., Computer Journal 3, 84 (1960).

41. Souček B., Rev. Sci. Instr. 36, 750-753, June 1965.

42. Souček B., Nucl. Instr. Methods 36, 181-191, 1965.

43. Hooton I.N., IEEE Trans. on Nucl. Sci., NS 1, No 3, 553, 1966.

44. Best G.C., Hickman S.A., Hooton I. N., Prior G.M., IEEE Trans. on Nucl. Sci., NS 13, No 3, 559, 1966.

45. Best G.C., IEEE Trans. on Nucl. Sci., NS 13, No 3, 566, 1966.

46. Hooton I.N., Proc. EANC Conf., Karlsruhe 1964.

47. Rosenblum M., Brookhaven Natl. Lab., private communication 1966.

48. Souček B., IEEE Trans. on Nucl. Sc., NS 13, No 3, 571, 1966.

49. Souček B., Bonačić V., Culjat K., Radnić I., Internat. Conf. on Nucl. Electronics, Versailles 1968.

50. Souček B., Bonačić V., Culjat K., Nucl. Instr. Methods 66, No 2 (1968) 202.

51. Bonačić V., Souček B., Culjat K., Nucl. Instr. Methods 66, No 2 (1968) 213.

52. Durand P., Giraud P., Proc. Intern. Symp. Nuclear Electronics, Paris 1963, p. 643.

53. Thenard J., Victor G., Nucl. Instr. Methods 26 (1964) 45.

54. Poole M.A., Brookhaven Natl. Lab., Informal Report IH-363, 4-21-65.

55. Colling F., and Stüber W., Nucl. Instr. Methods 64 (1968) 52.

56. Spilling P., Gruppelaar H., Van den Berg P.C., Proc. Intern. Conf. on Nuclear Electronics, Versailles 1968.

57. Proc. EANDS Conf., Karlsruhe 1964.

58. Proc. Intern. Conf. Nuclear Electronics, Versailles 1968.

59. Gere E.A., Miller G.L., IEEE Trans. on Nucl. Sci., NS 13, June 1966, p. 508.

60. Bhat M.R., Borrill B.R., Chrien R.E., Rankowitz S., Souček B., Wasson O.A., Nucl. Instr. Methods, 53, 108-122, 1967.

DISCUSSION

Gedcke : - Would you please comment on the merit of using a "most active zone encoder" as compared to using a small on-line computer with a large memory disc file ?

Soucek : - The "most active zone encoder" is definitely faster and enables direct accumulation analysis. The second is slower due to the transfers of data between core buffers and drum, but has larger storage capacity. I believe that one can obtain the best performance by combining three techniques: drum backing store ; zone encoding, and pseudo-random transformation.

PERFORMANCE TESTS FOR GE(LI) SPECTROMETERS

H.Meyer, H. Verelst

Central Bureau for Nuclear Measurements
EURATOM, Geel, Belgium

Summary

Test equipment for the simulation of experiment conditions was developed to simplify the design and to standardize the test of high precision instrumentation for spectrometers in the future.
For linearity, stability and resolution tests an electronic precision pulse generator has been developed which allows an almost perfect simulation of detector signals and a measurement accuracy, better than 0.01%.
A random generator for the simulation of Compton continua is described which has been applied together with the precision pulser for high rate performance tests of a spectrometer. In such a way experiment conditions were simulated without the need of detectors and radiation sources.
Suitable detector tests are also desirable to reach an optimum overall response of a spectrometer.
For comparison, high rate measurements of a spectrometer, designed earlier and equipped with additional fast circuits to reduce pile-up effects, has been performed up to input rates of 3.10^5 cts/sec; ^{60}Co γ-rays detected with a planar detector and the simulated spectrum of the 1.33 MeV line were applied for that purpose.

Introduction

The high precision of the order of 0.01% achievable with Ge(Li)-spectrometers for the measurement of γ-spectra has involved strong demands with respect to equipment for the test of the electronic instrumentation and the detectors. Optimum performance of a system is possible only by choosing the best compromise for the influencing parameters, which is dependent on given experiment conditions; the features of applied detectors have to be taken into account also.
For the test of the electronic instrumentation involved it is desirable to use instead of detector and radiation electronic equipment for simulation purposes. Such a simulation allows defined and reproducible test conditions and therefore comparable results. A sufficient test of complex equipment without the need for detector systems and radiation sources can be reached.

Precision pulse generators are applied to simulate monoenergetic peaks in a spectrum and to test the electronic contribution to the energy resolution of a spectrometer, but also to measure its linearity and stability. Mostly generators with mercury switches are used for such purposes up to now. Equipment with electronic switches has been designed also[1,2], but the performance is limited with respect to the realizable pulse shapes and(or) the accuracy achieved.
Electronic pulsers have the advantage that a greater long term reliability, higher pulse rates and an external control can be achieved. For the measurement of differential non-linearities the possibility of random pulse distances might be an advantage.

The last mentioned feature is less important for the simulation of monoenergetic peaks from γ-spectra detected by Ge(Li)-detectors having always low rates.
High rate effects are introduced mainly by the Compton background which is responsible for a spectrum degradation by pile-up effects due to the random occurrence of signals. The small relative full energy and escape peak efficiency of Ge(Li) detectors in connection with the high energy resolution obtainable are the reasons for the dominant influence of pile-up effects on the overall performance of a Ge(Li) spectrometer.
Equipment for the simulation of experiment conditions will be incomplete, therefore, if a Compton continuum simulator is not available to test the high rate performance of spectrometers.
The combined use of a precision pulser and a Compton continuum simulator generating randomly spaced signals and a suitable spectrum shape will allow a nearly complete simulation of a γ-spectrum from a Ge(Li) detector. The full energy efficiency of a detector can be simulated by the adjustment of pulse rate relations.

For comparison, a Ge(Li) spectrometer of earlier design[3,4], but equipped with additional circuitry for pile-up inspection, has been tested with γ-rays of ^{60}Co and with a simulated spectrum for the 1.33 MeV line. The measurements are demonstrating the features of the simulation method.

Detector tests

In addition to the electronic noise contribution of detectors due to their leakage current and capacitance - easily measurable with standard methods - the charge collection

time and its spread can have a strong influence on the overall performance of a spectrometer. Field irregularities due to insufficient compensation, for instance, caused by a precipitation of lithium in the detector volume, or edge effects and trapping effects can be the reason for a performance much worse than expected for a normal behaviour determined by the effective detector thickness and the limited carrier velocity. The minimum measuring times for complete charge collection are of great importance, especially at high event rates where short pulses are desired to have small pile-up effects. Too short measuring times (pulse shaping parameters) introduce charge losses and charge loss fluctuations degrading the resolution of mono-energetic peaks especially at higher energies of γ-rays.

Simple test equipment has been proposed for the measurement of the charge collection time spread [5, 6] (see also, Fig. 1), but as it can be seen also from measurements performed on detectors out of our own production (Fig. 2), only rough results can be obtained. The time spread for the collection of the last fraction of charge determining the necessary measuring times for a small degradation of resolution is not detectable.

We have applied therefore in addition high resolution measurements at various γ-ray energies and pulse shaping time constants to determine the minimum acceptable measuring time for which the fictive Fanofactor derivable from the measurements will not increase with the energy of γ-rays [4].

Precision Pulse Generator

General

With good Ge(Li) detectors a resolution (FWHM), better 0.05% can be obtained in the 10 MeV region; an accuracy in the energy determination, better 0.01% is possible if the stability and linearity of the conversion gain determined by the associated electronic instrumentation will admit such feature of a spectrometer.
Test equipment, simulating detector and radiation should be adapted in performance.
To measure a Fanofactor for detector tests of the order of 0.1 with an accuracy of $\pm$ 10% the stability of a spectrometer and therefore also of a test pulser should not be worse than $\pm$ 0.005%.

The precision pulser to be described, which fulfills the required demands, has been designed originally for the application as reference signal source of a servostabilized Ge(Li) spectrometer[3]. For that purpose a double pulse generator which is synchronizable by control signals from the A.D.C. was desired to perform bias and gain stabilization. The possibility of a continuous signal amplitude adjustment should allow full flexibility in the choice of the upper and lower level of an analysis region - a region is determined by analog control levels and the reference signals must correspond to fixed channel numbers within the region.

In addition to a sufficient stability of signal amplitude a pure exponential pulse shape with great decay time constant was of interest to allow a simple RC circuit as coupling network to the preamplifier input for a perfect simulation of detector signals (by pole-zero cancellation), but also to obtain only a small increase of noise level.

Principles of circuit layout

A known circuit arrangement[2] consisting of a controlling dc reference voltage and two electronic switches has been chosen for the realized pulse generator type (Fig. 3): The closure of the primary switch charges a condenser 'C' in some microseconds to the given reference potential. Thereafter, the primary switch is opened and the secondary switch closed generating a signal with fast rising edge and a slow exponential decay (τ = RC) by discharge of 'C' via a resistive load 'R', the input resistance of an output attenuator adapting the dynamic range of the pulser to the desired energy range of a spectrometer.
The switches, emittercoupled transistor pairs, will guarantee, if suitably driven, negligible offset voltages and small 'on' resistances, very stable vs. temperature and load variations.
For a multiple pulser generating different pulse amplitudes simply more than one controlling dc voltage and primary chopper to charge 'C' in suitably chosen time distances are needed.
For differential nonlinearity tests a reference voltage level varying linearly with time can be taken (f.i., a triangular wave shape, generated as shown in Fig. 3).

The known chopper configurations use mostly transformers to drive the switch; their frequency response limits the application, especially, if signals with pure exponential decay and a great decay time are desired. By isolating the driving circuitry and its biasing elements from the system ground (pat. appl.) a time interval limitation with respect to the states of a switch has been avoided.
For the realized pulse generators bistables were used to drive the switches. Special transformers with very low coupling capacity were applied to introduce the control signals for the bistables and to transfer their biasing power via a dc-converter. Optoelectronic coupling for the control signals and the biasing energy or an isolated battery for biasing purposes would also be possible solutions to avoid the appearance of the control signals at the pulser output and a frequency dependent leakage path for the controlled signals via the switch control circuits to the system ground.

Performance

The performance of the realized pulse generators depends strongly on that of the controlling dc voltage, the circuitry of which consists of a temperature controlled reference diode fed by stable buffer supplies, a high precision potentiometer (1 Kohm) and a selected operational amplifier as voltage follower.
With respect to the stability of pulse amplitude against ambient temperature fluctuations, the influence of the 'on' resistance of the secondary chopper (R on $\approx$ 1.5 ohms) has to be taken into account also but is of minor importance due to its great stability and because of the sufficiently high input resistance of the output attenuators (1 Kohm). The attenuators themselves are arranged in separate screened boxes; high precision resistors assure a small contribution to a residual instability of pulse amplitude.

A small nonlinearity of pulse amplitude vs. the setting of the precision potentiometer is reached first of all by the choice of a suitable potentiometer but also by the selection of a voltage follower with small bias current and high common mode rejection ratio (selected type, LM 201, CMR > 10^5 up to 10 Volts).
A third factor which influences the nonlinearity of the 'dc' signal is given by a small dependence of the chopper 'on' resistance on the signal current - about 0.001% in our case for signals up to 10V into 1Kohm load.
The pulse risetime which has been obtained by the choice of suitable chopper transistors is 5 nsec for small pulses and will increase to 15 nsec for 10V pulse amplitude. This risetime variation introduces a nonlinearity which is dependent on the final pulse shaping in a spectrometer. For RC shaping and small time constants, τ, this nonlinearity effect will become dominant (τ = 1 μseç, nonlinearity $\approx$ 0.01%).

The 'dc' nonlinearity was tested by short-circuiting the primary chopper and loading the secondary chopper in its 'on' state with its nominal load by the attenuator (Fig. 5B). The overall stability of the dc voltage vs. temperature has been measured under the same conditions. The obtained temperature coefficient was of the order of 1 ppm/°C. An overall linearity test of a spectrometer by the application of the test pulse generator and the well-known γ-ray energies of ^{56}Co has been performed (Fig. 4) which can be taken also as a measure of the pulser performance. The results demonstrate that the overall nonlinearity of the pulse generator should be well within $\pm$ 0.01%.
For the measurement of the short and long term stability of the pulse amplitude the pulser was connected directly to a servostabilized ADC calibrated to an equivalent resolution of 40 000 channels (Fig. 5A). In reality, a comparison between two pulse generators of the same type is performed, the reference pulser of the ADC and the test pulser. The difference in the peak widths of the two pulsers - after subtraction of the regulation step width of the servostabilizer - will therefore determine only approximately the fluctuations of the test pulser amplitude. For the short term fluctuations mainly a residual background introduced by the dc converter of the chopper is responsible - the derivated peak width from pulser signals [FWHM] is 0.0040%. The long term fluctuations and a peak shift are mostly due to a residual instability of the precision potentiometer and of the output attenuator - after 30 hours a peak width [FWHM] of 0.0049% instead of 0.0040% was received; the peak shifted by 0.2 channels, i.e. about 5 ppm. The variations of the ambient temperature during the measuring period were of the order of 2°C.

Generation of rectangular pulses

The pulser can be applied for the generation of stable rectangular pulses if a resistive load is connected directly to the primary chopper. A minimum pulse width of 2 μsec, a rise time (10% to 90%) of 15 nsec max. and a decay time constant of about 1.2 μsec was obtained.

Simulation of γ spectra for high rate performance tests of Ge(Li) spectrometers

General considerations

Due to the low efficiency and high resolution of Ge(Li) detectors a considerable degradation of spectra occur already at low event rates for the full energy and double escape peaks. Practically all pile-up effects are introduced by the Compton background.

The high rate performance of Ge(Li) spectrometers has been tested up to now only with the help of Ge(Li) detectors and suitable γ-ray sources [4, 7, 8] or by the simulation of monoenergetic peaks with random pulse generators [9].
The first method has the disadvantage of limited flexibility and universality; results are dependent on the applied detectors. A comparison of the performances of different spectrometers is not easily obtainable due to the lack of comparable and defined test conditions. One should also not forget that not always and everywhere suitable detectors and sources are available for the designers and producers of instrumentation.
The second method does not really simulate experiment conditions because signals caused by events from monoenergetic peaks will be piled up by each other only with small probability due to their low differential rate.
We have therefore tried to simulate spectra in a more realistic way by generating an idealised Compton continuum of random signals and applying the precision test pulser described before for the simulation of a monoenergetic peak (Fig. 6). The chosen spectrum shape for the simulation of the Compton continuum (Fig. 7) has the additional advantage that the qualitative and quantitative degradation of a spectrum by pile-up effects can be easily detected, but also can be

calculated to analyse differences between performances expected and measured. For a simplified case, i.e., assuming rectangular signal shape, an ideal stretcher at the input of the ADC and only the existence of double pulse pile-up, the deformation of the idealised spectrum has been calculated as demonstrated (Fig. 7).

Continuum pulser, circuit principle and features.

For the generation of the continuum with rectangular spectrum shape a fast time height converter has been applied as the main element (Fig. 8).
Random short pulses are generated with a suitably biased zener diode to start the converter while a high frequency pulse train from a repetitive pulse generator at the stop input of the converter will stop the conversion with that pulse which is the first after the arrival of a random start pulse. The result is a spectrum of signals having an exponential decay, the maximum amplitude of which is proportional to the equal distance of the pulses from the repetitive generator. That distance is also the deadtime of the continuum pulser and should be small therefore to assure a sufficient simulation of detector signals up to high rates. It is obvious that also the maximum pulse rise time will be equal to that dead time or what is the same, to the analysis range of the time-height converter; 100 nsec had been chosen as suitable upper limit, which is also in agreement with typical risetime fluctuations of detector pulses.
Also spectral parts of a continuum can be generated for test purposes by using a delayed start pulse to stop a conversion or by opening the stop input with a delayed start pulse as is shown in Fig. 8.
The fact that the risetimes of the output pulses are proportional to their amplitude means, that detector signals cannot be simulated perfectly; but this will be of small importance with respect to the generated continuum.

The output pulses from the continuum pulser are fed into the preamplifier input of the system to be tested in the same way as described for the precision pulser: an attenuator and a coupling network to cancel the exponential decay and to calibrate the induced charge will simulate the shape and energy range of detector signals.
A maximum rate of more than 3.10^5 cts/sec can be generated; the signals have a decay time constant of 50 μsec. Equivalent Compton edges up to 10 MeV for charging capacitors down to 0.5 pF can be simulated.

The monoenergetic peak

The signals from the precision pulser for the simulation of the monoenergetic peak may be generated in equal and repetitive time intervals. Their frequency can be adjusted in such a way that always the desired peak efficiency is simulated correctly. A certain disadvantage is the constant signal risetime.
To simulate the risetime fluctuations of detector signals belonging to a monoenergetic peak one could apply also another solution for a peak simulation instead of the precision pulser. A time-height converter could be used for which the conversion current is controlled by a random digital word generator with a digital-to-analog converter at its output. That random signal determining the digital word would also start the time-height converter; the constant output pulse amplitude could be adjusted by an accurate threshold device stopping the conversion.
Signals having random risetimes are time distances but constant amplitude would be available in such a way; but the signals will rise only linearly with time, a sufficient peak stability might be a problem, too.

High rate tests of a Ge(Li) spectrometer with ^{60}Co γ-rays and a simulated spectrum

An existing Ge(Li) spectrometer [3] (Fig. 9), already equipped with pile-up inspection circuitry being an integral part of the pulse-height converter has been improved by the application of equipment for an external fast pile-up inspection.
The original circuitry inspects the signals to be analysed first, by opening the linear input gate of the converter only if the signal level is below the noise level (rising edge inspection).
Secondly, the time distance between the 'zero' cross-over of a signal arriving after gate opening and its peak detection is inspected. This shape inspection against pile-up on the trailing edge of a signal to be analysed is not very efficient, especially for small pile-up signals.
Therefore, a fast signal path has been introduced which will interrupt or disable a conversion always in such cases for which the distance of a pile-up signal from one accepted for analysis is smaller than the risetime of the signals at the analysis input of the converter. Pile-up signals down to about 4 KeV equivalent will cause a rejection (for smaller Ge(Li) detectors, 10 pF capacitance) if they follow or precede signals accepted for analysis at a distance greater 450 nsec. The low level limitation is first of all due to the worse signal-to-noise ratio in the fast signal path.

The high rate tests performed with ^{60}Co γ-rays and demonstrated for the peak at 1.33 MeV (Figs. 10, 11) show the mentioned low level limitation clearly; the peak width [FWHM] is not very much improved by the fast

inspection circuitry; the peak-to-background ratio starts to be improved already at about 4 keV above the peak-location (Fig. 11B) - 4 keV is the noise level in the fast signal path to which the zero level threshold of the fast inspection has been adjusted.

For comparison, the experimental conditions of the measurements with ^{60}Co γ-rays - with respect to the energy, 1,33 MeV - were simulated with the before mentioned continuum simulator and precision pulser. (Fig. 12, 13). It was assumed that the full Compton background is introduced by the 1.33 MeV line of the source.
The performance of the detector which has been used for the measurements with radiation (0.4% partial full energy peak efficiency; detector capacitance 10 pF) as taken into account for the tests.
Fig. 12 demonstrates already the improvement obtained by the fast pulse distance inspection. The background reduction preferably on the high energy edge of the peak should be noted.

The high resolution measurements (Fig. 13) show better results than the same tests performed with the detector and ^{60}Co γ-rays (Fig. 11). This is mainly due to the differences in the overall spectrum shapes.

The improvement of the spectrometer by the fast pulse distance inspection - preferably a better rejection of pile-up by the low energy Compton background - can be demonstrated in the best way by the application of lower and higher energy spectral regions out of an equivalent Compton continuum for high rate tests (Fig. 14): the pile-up by low level signals of high rate is rejected only to a large extent with the help of the fast inspection circuitry.

Conclusions

It is hoped that the performed studies will contribute to define the measuring conditions for the test of high precision spectrometers with Ge(Li)-detectors by the application of adapted test equipment and methods. A sufficient definition of measuring methods must be seen as a preliminary condition for the comparison of high precision instrumentation of different origin especially. Future work in this respect should lead to more detailed rules for the specification of the features of equipment.

Acknowledgements

The contributions of L. Hubbeling with respect to his inventive and developmental works for the precision pulse generator is acknowledged gratefully. The measurements and developmental works of P. Klopf, H. Schipke and W. Heinz should also be very much appreciated.

Literature

1) M. G. STRAUSS, L. L. SIFTER, F. R. LENK F. R. LENKSZUS, R. BRENNER, IEEE Trans. Nucl. Sci. NS-15, N° 3(1968), 518

2) Berkeley Nucleonics Comp., Oregon, USA, Prec. Pulser, Mod. PB2

3) P. KLOPF, H. MEYER, H. VERELST, Int. Symp. on Nucl. Electronics, Versailles, France (1968)

4) H. MEYER, H. VERELST, Int. Symp. on Nucl. Electronics, Versailles, France (1968)

5) M. G. STRAUSS, R. N. LARSEN, L. L. SIFTER, IEEE Trans. Nucl. Sci. NS-13, N° 3 (1966), 265

6) E. SAKAI, T. A. McMATH, Nucl. Instr. & Meth. 64 (1968), 132

7) M. G. STRAUSS, I. S. SHERMAN, R. BRENNER, S. J. RUDNICK, R. N. LARSEN, H. M. MANN, R. S. I. 38 (1967), 725

8) F. S. GOULDING, D. A. LANDIS, R. H. PEHL, Gatlinburg Conf. on Semicond. Det. and assoc. Circ., May 1967 (UCRL-17560)

9) C. W. WILLIAMS, IEEE-Trans. Nucl. Sci. NS-15, N° 1 (1968) 297

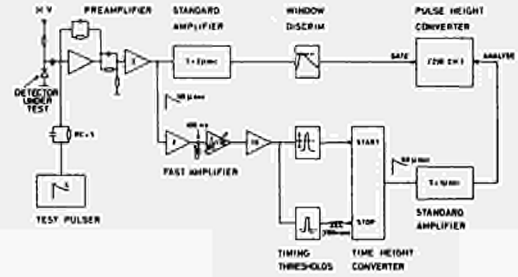

FIG.1 MEASUREMENT OF CHARGE COLLECTION TIME SPREAD, TEST EQUIPMENT

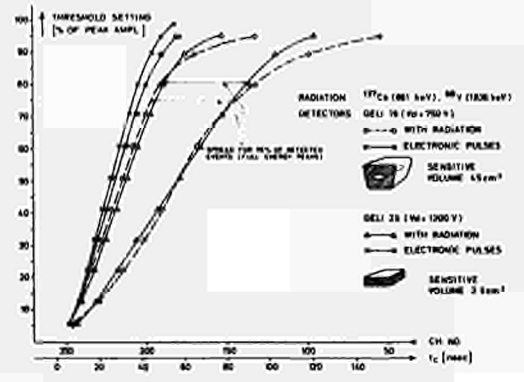

FIG.2 CHARGE COLLECTION TIME SPREAD OF GELI DETECTORS.

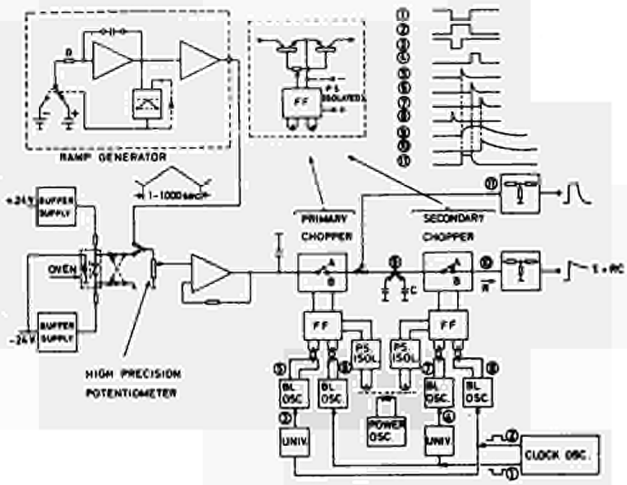

FIG. 3 PRECISION PULSE GENERATOR

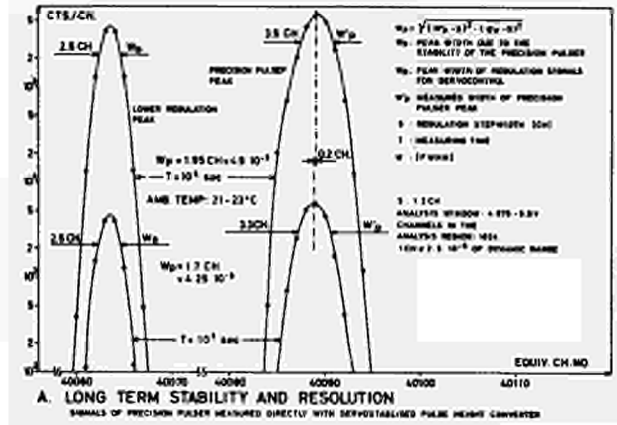

A. LONG TERM STABILITY AND RESOLUTION

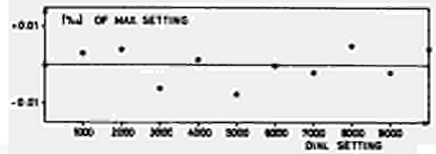

B NONLINEARITY OF D.C. SIGNAL

FIG.5 PRECISION PULSER PERFORMANCE

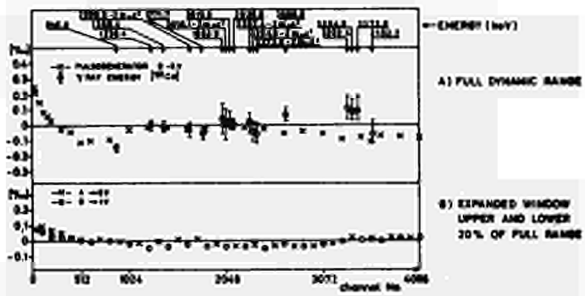

FIG.4 INTEGRAL NONLINEARITY OF A SPECTROMETER MEASUREMENT WITH PRECISION PULSER AND DERIVATION FROM A γ SPECTRUM (^{55}Co)

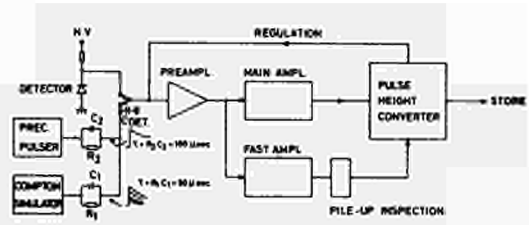

FIG.6 SIMULATION OF EXPERIMENT CONDITIONS, CIRCUIT DIAGRAM

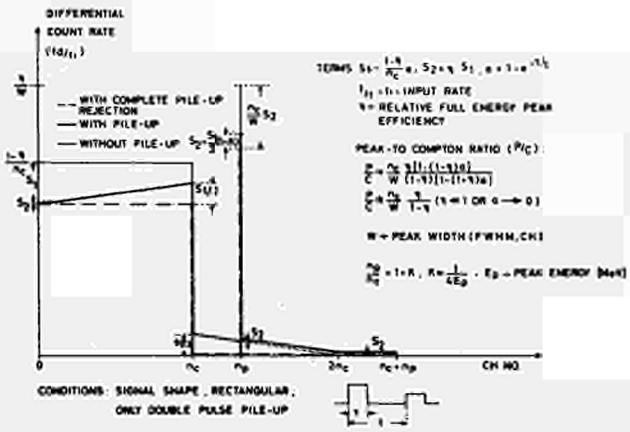

FIG.7 SIMULATED γ SPECTRUM, INFLUENCE OF PILE-UP (SIMPLIFIED)

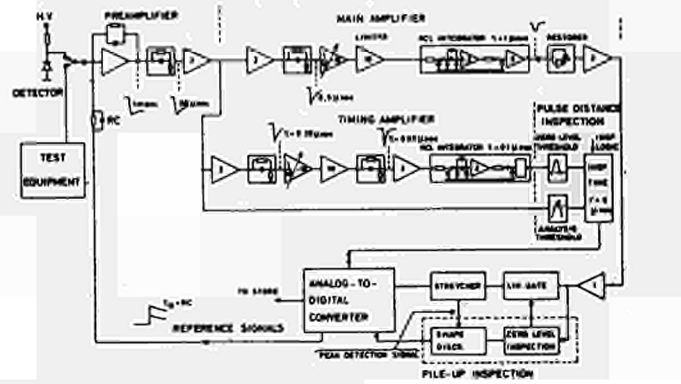

FIG.9 PULSE HEIGHT SPECTROMETER

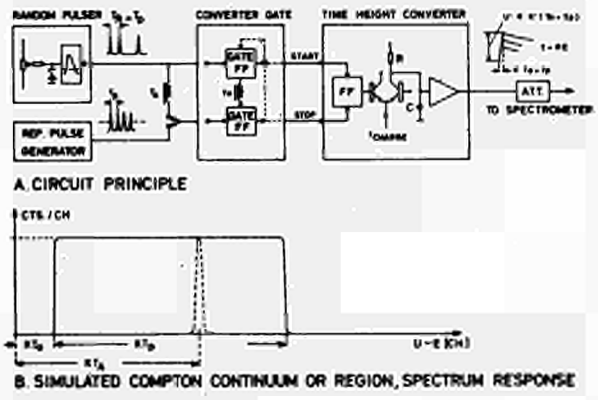

FIG.8 CONTINUUM PULSER

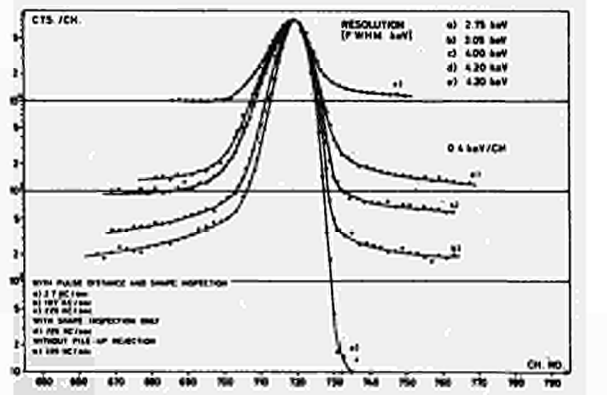

FIG.10 SPECTRAL PERFORMANCE AT DIFFERENT INPUT RATES [^{60}Co, 1.33 MeV]
DETECTOR: GELI 26 h (2.5 cm², PLANAR), PULSE SHAPING: 1 μsec RCL FILTER

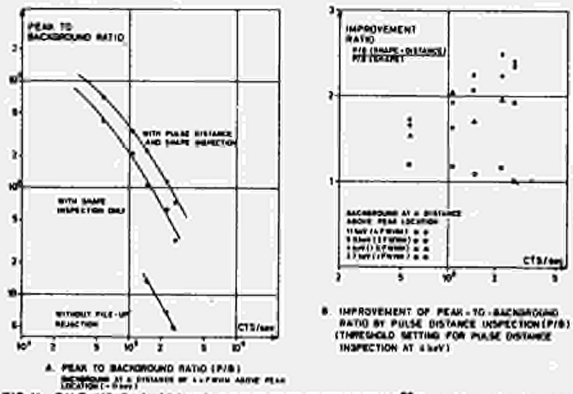

A. PEAK TO BACKGROUND RATIO (P/B)

B. IMPROVEMENT OF PEAK - TO - BACKGROUND RATIO BY PULSE DISTANCE INSPECTION (P/B) (THRESHOLD SETTING FOR PULSE DISTANCE INSPECTION AT 4 keV)

FIG. 11 PILE-UP BACKGROUND ABOVE THE PHOTOPEAK (^{60}Co, 1.33 MeV) V S. INPUT RATE

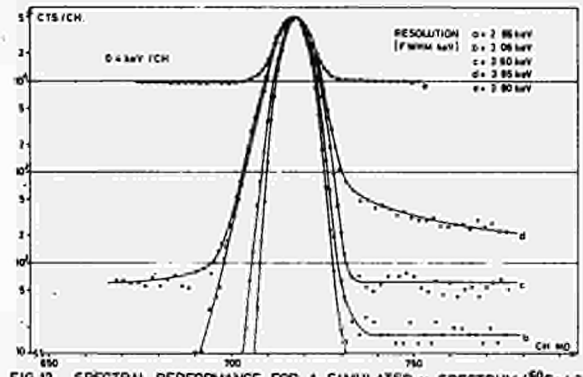

FIG. 13 SPECTRAL PERFORMANCE FOR A SIMULATED γ SPECTRUM (^{60}Co 1.33 MeV) AT DIFFERENT INPUT RATES

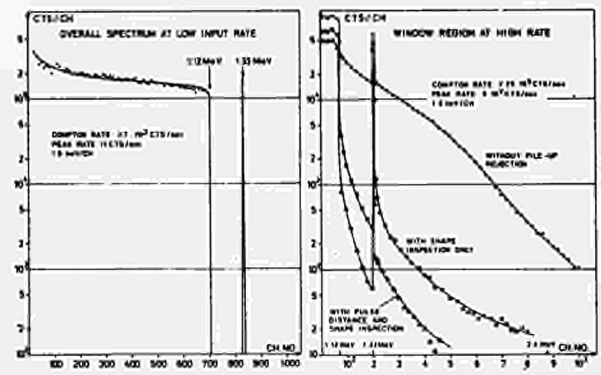

FIG. 12 SIMULATION OF A γ SPECTRUM FROM A GELI DETECTOR FOR SPECTROMETER TESTS AT HIGH RATES

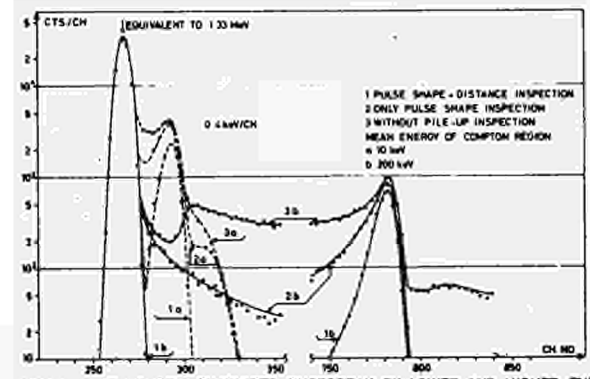

FIG. 14 PILE-UP OF A SIMULATED PHOTOPEAK BY LOWER AND HIGHER ENERGY SPECTRAL REGIONS OUT OF THE COMPTON CONTINUUM (SIMULATED)

FAST ADC FOR PULSE HEIGHT ANALYSIS

R. Kurz
Tennelec, Inc.
Oak Ridge, Tennessee, U.S.A.

Abstract

A unique 11-bit analog-to-digital converter based on a series-parallel technique is described. The short encoding time of 3 μsec (independent of channel number) makes multiplexing of several independent or dependent channels possible. Measured integral nonlinearity over all channels is less than 0.005% and differential linearity is in the order of 0.15%. Stretchers (peak or area), ADC, and multiplexer are designed as NIM modules. TTL integrated circuits are used for digital operations. Computer linking is convenient, or the ADC can be operated equally well with any memory unit.

Introduction

The high resolution capability of nuclear semiconductor detectors made it necessary to use pulse-height analyzers with as many as 8000 channels[1]. With this many channels, ADC conversion time and stability become major problems. In linear pulse processing, improved techniques such as "pole-zero cancellation"[2], baseline restoration[3], and time variant filters[4] have made possible substantial improvements in performance at high count rates. The acquisition rate of data in many spectral measurements is limited by the resolving time of the ADC. In this paper a new ADC is described having excellent stability and a resolving time of 3 μsec for 2048 channels. The technique can be extended to 8192 channels with only slightly longer resolving time.

The ADC most commonly used in pulse-height analysis is the Wilkinson type[5]. Conversion time of the Wilkinson ADC of a given number of channels depends on the maximum clock rate which can be used. High clock rates still present major problems, even at the present state of the electronic art. The maximum conversion time for a 4000 channel, 100 MHz converter is longer than 40 μsec. Some effort has been made to reduce the conversion time of a Wilkinson ADC by developing a "coarse-fine" circuit in which the ramp first varies rapidly and then slowly for the final comparison. The clock pulses are fed to different stages of the scaler according to the rate of the ramp[6]. Use of a "chronotron" type time analyzer rather than a gated clock also has advantages[7] at the expense of complexity.

The most commonly used method for fast conversion of analog signals is that of successive approximation. The first step in this technique is to compare the input with a reference signal from a digital-to-analog converter (DAC) which biases off the input signal by exactly 1/2 of the rated dynamic range. If the difference between the input signal and the DAC signal exceeds zero as detected by a comparator, a "1" is stored in an address register and an additional 1/4th is subtracted from the input signal by the second step in the DAC. If the input signal is below the 1/2 level, a "0" is stored in the address register and the initial 1/2 level is replaced by a 1/4th level from the DAC. This process is repeated a total of 12 times for decoding into 4096 channels, each time halving the DAC levels involved.

While the differential linearity of the successive approximation technique is not sufficient for pulse height spectroscopy, this difficulty can be overcome by using a sliding-scale technique[8] which essentially averages over channel-width variations. The successive-approximation technique requires one step per bit to convert any number. The steps are done in sequence. The total conversion time is at least as large as the number of bits multiplied by the comparator decision time. The comparator decision time depends on the accuracy required. With a 4000 channel ADC having a dynamic range of 8V (2 mV channel width), the comparator must settle to 0.2 mV in order that the comparator contribution to channel width fluctuations be not more than 10%. A 12-bit state-of-the-art ADC requires decision times of 2 μsec, making the conversion time equal to 24 μsec.

The preceding review was covered in much greater detail by Robinson, et al.[1] and the reader is referred to that paper for additional information.

Series-Parallel ADCs

The subject of this paper is an ADC* using a series-parallel technique[9] which was developed to reduce conversion time without sacrificing linearity or stability. High speed is obtained by using relatively slow comparator circuits to generate several bits in parallel rather than high speed circuits in series. These comparators, which are few in number, are used several times, each time subtracting a portion of the input signal and successively amplifying and encoding the residue.

In consideration of the increased use of computers for pulse height analysis, the ADC to be described here was designed with that trend in mind; the descriptions to follow are oriented towards such use.

63-Channel ADC

A block diagram illustrating the basic principles of operation is shown in Fig. 1. First the blocks will be described, then the sequence of operations.

The blocks are (1) an operational amplifier A in which the gain can be switched from A_1 to A_2 to A_3 by

* Patent applied for.

switch S3; (2) a bias network with switchable bias levels B1 and B2; (3) a 3-level encoder containing comparators (discriminators) biased at levels L, 2L, and 3L. This encoder has two output lines Q1 and Q2 which indicate in a binary code the four possible states of the encoder according to the table shown below it; (4) three registers which when operated by set pulses lock the output lines into the same states as the input lines. Once set, these lines remain fixed until a reset pulse occurs at the very end of the operating sequence, regardless of a change in state of the input lines; (5) two DACs in which switches S4 through S7 are closed when the Q lines controlling them are in the 1 state and opened when in the 0 state. Referred to the input of amplifier A, DAC 1 can furnish 4 bias levels which subtract from the input signal v_1 in the amounts of 0, L/A_1, $2L/A_1$, or $3L/A_1$ volts. Similarly, DAC 2 biases off the input signal v_1 in the amounts of 0, L/A_2, $2L/A_2$, or $3L/A_2$ volts. Referred to the output of the amplifier, the synchronization of S3 with the DAC switches is such that v_2 is biased off in the amounts of 0, L, 2L, or 3L volts regardless of whether DAC 1 or DAC 2 is being used; (6) a set of digital multipliers and (7) a digital adder. The multipliers weight the channel number placed in the adder according to the settings of S3 and the registers.

The system shown in Fig. 1 can exist in a maximum of 64 possible states to yield 63 channels of information. To get this many states, the encoder, which can exist in only 4 states, must be used 3 times. In each of the 2 successive steps after the 1st, its sensitivity must be increased 4 times by switching amplifier gains. Simultaneously, the DACs must be switched in such a way that only the residue from the preceding step is amplified and applied to the encoder.

To get specific, we assign numbers to the various quantities and trace the sequence of operations with the aid of Figs. 1 and 2.

For this example, ignore the presence of the input bias lines from B1 and B2.

Let $A_1 = 1$, $A_2 = 4$, and $A_3 = 16$
$L = 16$, $2L = 32$, and $3L = 48$.

(These parameters were chosen to make 1V = 1 channel for ease of explanation.)

In the DACs, switches S4 and S5 control bias voltages of 16 and 32 volts respectively, and S6 and S7 control levels of 4 and 8 volts respectively. The multiplier connected to REG. 1 gives its digit output a weighting factor of 16, and the one connected to REG. 2, a factor of 4.

Referring to the timing diagram in Fig. 2, the input voltage v_1 must be constant throughout the time sequence. Assume a level of 38.5 volts. At t_o, S3 is in the A_1 position and the amplifier has unity gain. The $2L = 32$ volt level of the encoder will be exceeded and the Q2 and Q1 lines set to 1 and 0, respectively. At the end of Step 1, REG. 1 is set, 32 counts are stored in the adder, S5 is closed, and a 32-volt increment is subtracted from v_1, leaving a residue of 6.5V.

During Step 2, the amplifier gain is 4X and v_2 becomes $4 \times 6.5 = 26$V. This signal is large enough to exceed the L = 16 volt level of the encoder, setting the Q2 and Q1 lines to 0 and 1, respectively. At the end of Step 2, REG. 2 is set, 4 counts are put in the adder, S6 is closed, and a 4-volt increment is subtracted from the previous residue of 6.5V, leaving a new residue of 2.5V.

During Step 3, the amplifier gain is 16X and v_2 becomes $16 \times 2.5 = 40$V. This signal sets the $2L = 32$ volt level of the encoder, and when the set pulse occurs, adds 2 more counts to the adder for a total of $32 + 4 + 2 = 38$ counts. Thus, the adder indicates that the 38.5-volt input fell into the 38th channel.

The channel number of this system can be expressed by Eq. 1, a generalization of which is given in the appendix.

$$N = N_1 + N_2 + N_3 \tag{1}$$

$$\begin{aligned} N_1 = {} & 48H[v_1-48] + \\ & 32H[v_1-32]H[48-v_1] + \\ & 16H[v_1-16]H[32-v_1] \end{aligned}$$

$$\begin{aligned} N_2 = {} & 12H[4(v_1-N_1)-48] + \\ & 8H[4(v_1-N_1)-32]H[48-4(v_1-N_1)] \\ & 4H[4(v_1-N_1)-16]H[32-4(v_1-N_1)] \end{aligned}$$

$$\begin{aligned} N_3 = {} & 3H[16(v_1-N_1-N_2)-48] + \\ & 2H[16(v_1-N_1-N_2)-32]H[48-16(v_1-N_1-N_2)] \\ & H[16(v_1-N_1-N_2)-16]H[32-16(v_1-N_1-N_2)] \end{aligned}$$

where

N_1, N_2, N_3 = counts registered during the 1st, 2nd, and 3rd steps of the encoding, respectively

v_1 = input signal in volts

Heaviside operator $H[x] = 0$ if x is negative
$= 1$ if x is positive

In each of the N_1, N_2, and N_3 terms of Eq. 1, at most one line can be different from zero.

The residues at the input to the encoder at the starts of the 2nd and 3rd steps are, respectively

$$\begin{aligned} \text{Res. } 1 &= 4(v_1-N_1) \\ \text{Res. } 2 &= 16(v_1-N_1-N_2) \end{aligned} \tag{2}$$

The system described above exhibits high speed, but as in the conventional successive-approximation techniques, the comparators must settle to a fraction of a channel width in order to keep their contribution to the

channel-width fluctuations small. Furthermore, the differential linearity depends on the accuracy of the gain steps in the amplifier shown in Fig. 1. These shortcomings can be substantially overcome by introducing redundancy to the encoding process.

35-Channel ADC with Redundancy

In the 63-channel ADC described in the last section, let

$$A_1 = 1,\ A_2 = 3,\ \text{and}\ A_3 = 9$$
$$L = 9,\ 2L = 18,\ \text{and}\ 3L = 27.$$

In the DACs, let switches S4 and S5 control bias voltages of 9 and 18 volts respectively, and S6 and S7 control levels of 3 and 6 volts respectively. With this arrangement, the system capability is reduced from 63 one-volt channels to 35 one-volt channels, but the desired redundancy is obtained. The new arrangement is described by Eq. 3. The level diagram is shown in Fig. 4.

$$N = N_1 + N_2 + N_3 \tag{3}$$

$$N_1 = 27H[v_1-27] + 18H[v_1-18]H[27-v_1] + 9H[v_1-9]H[18-v_1]$$

$$N_2 = 9H[3(v_1-N_1)-27] + 6H[3(v_1-N_1)-18]H[27-3(v_1-N_1)] + 3H[3(v_1-N_1)-9]H[18-3(v_1-N_1)]$$

$$N_3 = 3H[9(v_1-N_1-N_2)-27] + 2H[9(v_1-N_1-N_2)-18]H[27-9(v_1-N_1-N_2)] H[9(v_1-N_1-N_2)-9]H[18-9(v_1-N_1-N_2)]$$

where the symbols have the same meanings as before.

The residues at the encoder input are

$$\text{Res. } 1 = 3(v_1-N_1) \tag{4}$$
$$\text{Res. } 2 = 9(v_1-N_1-N_2).$$

The redundancy exists in that there is more than one way in which a channel number may be obtained. For example, channel 18 can be obtained in three ways:

$N_1 = 18$	$N_1 = 9$	$N_1 = 9$
$N_2 = 0$	$N_2 = 9$	$N_2 = 6$
$N_3 = \underline{0}$	$N_3 = \underline{0}$	$N_3 = \underline{3}$
18	18	18

To test the effectiveness of this redundancy, suppose we have a pulse of 18.5V and there are no errors in the system. From Eq. 3, the channel count is obtained in the following way:

$N_1 = 18$, Res. $1 = 3(18.5-18) = 1.5$
$N_2 = 0$, Res. $2 = 9(18.5-18-0) = 4.5$
$N_3 = \underline{0}$
18.

Now suppose that the 18-V level was high and the amplifier gain was low, preventing the 18-V level from being exceeded at the first step of encoding:

$N_1 = 9$, Res. $1 = 2.9(18.5-9) = 27.5$
$N_2 = 9$, Res. $2 = 8.7(18.5-9-9) = 4.4$
$N_3 = \underline{0}$
18.

Thus, the same count is obtained, but in a different way.

For the 35-channel system described here, the amplifier should be able to accommodate a 36-volt output signal. The output requirement is greatest when the input signal is just lower than the maximum permissible value, namely: (36-δ) volts, where δ is a vanishingly small quantity:

$N_1 = 27$, Res. $1 = 3(36-\delta-27) = 27-\delta$
$N_2 = 6$, Res. $2 = 9(36-\delta-27-6) = 27-\delta$
$N_3 = \underline{2}$
35

Thus, during the first step, the amplifier output reaches 36-δ volts, but during succeeding steps, the residues do not exceed 27-δ volts.

We now examine in greater detail the effects of component errors beginning with the comparators.

Over most of the range of pulse inputs, the same comparator level is not involved in more than 1 step of the encoding, but to best examine the effect of errors, it is desirable to choose a channel number in which the same level is involved 3 times; Channel 13 = 9 + 3 + 1 meets this condition.

Let the 9V level be high by 1V, and scan the input signal from 12V to 14V in order to compute the widths of the 12th and 13th channels. A sample computation follows:

$v_1 = 12 + \delta$ $\quad N_1 = 9$, Res. $1 = 3(12+\delta-9) = 9+\delta$
$L_1 = 9+1 = 10$ $\quad N_2 = 0$, Res. $2 = 9(12+\delta-9-0) = 27+\delta$
$N_3 = \underline{3}$
12

We see that a signal barely exceeding 12V produces a residue at the beginning of the 3rd step barely large enough to exceed the 3L = 27 level. No error is incurred at this channel edge.

To find the transition point between the 12th and 13th channel, we know that $N_2 = 3$ and $N_3 = 1$. Thus, using the equation for Res. 2, we can set it equal to the comparator level of 10V:

$$\text{Res. } 2 = 10 = A_3(v_1 - N_1 - N_2)$$
$$= 9(v_1 - 9 - 3)$$
$$\text{from which} \quad v_1 = 13\tfrac{1}{9}\text{V}.$$

There is no error at the transition between channels 13 and 14.

The conclusions to be drawn from the preceding example are: (1) channel 12 extends from 12V to 13-1/9V and channel 13 from 13-1/9V to 14V, (2) the channel-width error of 1/9V is exactly equal to the error in comparator level divided by the maximum gain of the input amplifier. This latter result is in sharp contrast to what would have been obtained in the non-redundant system: If we had assumed that the 16-V level was actually at 17V, we would have found that input signals between 15 and 17 volts would all fall into channel 15, and input signals between 17 and 18 volts would fall into channel 17 -- channel 16 would be missing. The 1-V error in the comparator level would be carried through the sequence unchanged and would account for the 1-channel error at the end.

In the preceding example we examined the effect of a comparator level being too high by 1V. We now examine what happens if it is too low by 1V, i.e., $L_1 = 8$V.

Let

$v_1 = 7 + \delta$ $\quad N_1 = 9$, $\quad \text{Res. } 1 = 3(7+\delta-9) = -6 + \delta$

$L_1 = 9 - 1 = 7$ $\quad N_2 = 0$, $\quad \text{Res. } 2 = 9(9+\delta-9) = -18 + \delta$

$N_3 = \underline{0}$

9

Evidently, a signal which should have fallen into channel 7 fell into channel 8. We can easily show that channel 6 extends from 6V to 7V, that channel 8 does not exist, and that channel 9 extends from 7V to 9V. The reason for this error is that any situation which leads to a negative residue at any step of the encoding sequence will be magnified during all succeeding steps without hope of correction. This would be a serious shortcoming if there were no means of avoiding it, but there is such a means:

During each but the last step of the process, bias the input signal or the comparators by an amount which is the sum of two factors: (1) one-half the difference between the number of comparator bits and the ratio of gain change between that step and the next one, and (2) the sum of all biases applied during later steps. A general formula for an optimum bias referred to the amplifier input is given in Appendix 2. The biases appropriate to the 35-channel encoder are given below.

$$B2 = \frac{A_1}{A_3}\frac{L}{2}\left(k + 1 - \frac{A_3}{A_1}\right)$$
$$= \frac{1}{9}\ \frac{9}{2}(3 + 1 - 3)$$
$$= 0.5\text{V}$$
$$B1 = 0.5\text{V} + \frac{1}{3}\frac{9}{2}(3 + 1 - 3)$$
$$= 2\text{V}$$

where B2 is the bias applied during the second step of the encoding sequence by S2 in Fig. 1, and B1 is the bias applied during the first step by S1.

If we include the biases given above in Eq. 3, we get:

$$N = N_1 + N_2 + N_3 \tag{5}$$
$$N_1 = 27H[(v_1 - 2) - 27] +$$
$$\text{etc.},$$

or:

$$N_1 = 27H[v_1 - 29] +$$
$$18H[v_1 - 20]H[29 - v_1] +$$
$$9H[v_1 - 11]H[20 - v_1]$$

$$N_2 = 9H[3(v_1 - N_1) - 28.5] +$$
$$6H[3(v_1 - N_1) - 19.5]H[28.5 - (v_1 - N_1)] +$$
$$3H[3(v_1 - N_1) - 10.5]H[19.5 - (v_1 - N_1)]$$

$$N_3 = 3H[9(v_1 - N_1 - N_2) - 27] +$$
$$2H[9(v_1 - N_1 - N_2) - 18]H[27 - (v_1 - N_1 - N_2)] +$$
$$1H[9(v_1 - N_1 - N_2) - 9]H[18 - (v_1 - N_1 - N_2)]$$

and

$$\text{Res. } 1 = 3(v_1 - 0.5 - N_1)$$
$$\text{Res. } 2 = 9(v_1 - N_1 - N_2)$$

If we use Eq. 5 to rework the preceding example but with $L_1 = 9\text{V} \pm 1\text{V}$, it will be found that if $L_1 = 9\text{V} + 1\text{V}$, channel 12 is too large by 1/9th volt and that if $L_1 = 9\text{V} - 1\text{V}$, it is too small by 1/9th volt. Thus, the biasing technique allows the comparator levels to be low as well as high.

It is stated without proof that the error made in the recorded channel width is $A_1 \Delta L / A_3$, where A_1/A_3 is the ratio of 3rd-step gain to 1st-step gain and ΔL is the error in the pertinent comparator level, provided that $\Delta L \leqslant A_3 B_2 / A_1$ where B2 is the bias referred to the input. Within this limitation, errors generated during the first 2 steps of encoding are corrected during the 3rd step. If the comparator level is in error by more than $A_3 B_2 / A_1$ but less than $A_3 B_1 / A_1$, not all of the error generated during the 2nd step is corrected in the 3rd.

So far, we have concentrated on the effects of errors in comparator level. Using Eq. 5, a similar analysis could be carried out for errors in amplification. It would be found that larger errors could be tolerated during earlier steps of encoding than during later steps, and that the absolute error in a channel width would be proportional to the fraction of amplifier dynamic range being used.

With regard to the DACs, it seems that there is no technique for reducing the effect of errors which may arise there. For this reason, it is desirable to keep to a minimum the number of DACs used. For a given large number of channels, this is accomplished by optimizing the number of steps of encoding, the change in amplification between steps, and the number of bits in the comparators.

11-Bit ADC

We now turn our attention to the implementation of a 2048-channel ADC. Because of the short resolving time achieved (3 μsec), multiplexing several inputs is very practical. It was decided at this point that the best compromise between flexibility and cost would be obtained by packaging the ADC proper in one No. 4 AEC NIM module, and all other circuits such as stretchers, routing boxes, channel-select switches, a computer interface, etc., into different modules. One exception to this concept is made because it proved easy to implement: dual parameter capability with the necessary routing logic is built in.

To achieve the necessary differential linearity, the Gatti sliding-scale technique[8] is used (we will refer to it as "averaging") and it is built into the ADC.

The block diagram of Fig. 1 and the timing diagram of Fig. 2 are still applicable, but portions of Fig. 1 are expanded in Figs. 5, 6, and 7. Extensive use is made of standard TTL integrated circuits which have output voltage levels of +0.4V for a logical 0 and +2.5 for a logical 1. The system is now described in detail.

Gain switching is done in 3 steps: X1, X12, and X144. A 15-level (4-bit) parallel encoder is used which can exist in 16 possible states. The encoder and amplifiers constitute an ADC with a capacity of (16 X 144)-1 = 2303 channels. Of these, 128 are used for averaging, leaving 2175. It was decided to limit the number of usable channels to 2048 by using the 11th bit as an overflow signal which is connected to the clock generator; internal logic prevents an input signal from being stored. The linear dynamic range is ~4V to give channel widths of ~2mV.

The amplifier system is made up of 3 separate operational amplifiers, each having a 1%-settling time of less than 0.1 μsec. The arrangement is shown in Fig. 5.

The input operational amplifier A_a is chopper stabilized, has a tempco of 0.5μV/°C, and an open-loop gain of 10^8. The 2nd and 3rd amplifiers, A_b and A_c respectively, have tempcos of 5μV/°C and open-loop gains of 300,000.

The first group containing A_a has 3 inputs, one of which is used with the built-in averager. The others may be used as current inputs or, if external resistors are added in series, as voltage inputs. If 950-ohm resistors are used externally, an input signal of 4V at either input will produce an output signal of 4V, which is the rated operating level for this ADC. For purposes of discussion, assume R1 and R2 to be 1k each.

Gain switching is accomplished by driving the diode bridge D1-D4 into or out of conduction. With the diodes conducting, R4 and R5 are in parallel to give a resistance of 1k and a gain of unity to the first stage (the 1k resistor is trimmed to compensate for the diode resistances and component errors, but as stated earlier, some error can be tolerated in the first 2 steps of encoding). With the diodes open, only R5 is in the feedback circuit and the gain jumps to 12. The output of DAC 1 is connected to the summing junction Σ1. The prebias to prevent negative residues is furnished through R6. A positive signal at B1 diverts the bias current away from Σ1.

The second stage A_b is an inverter for the convenience of using switching signals and DAC signals of the same polarity in both input and output stages.

The third stage A_c is similar to the first in all respects.

During a normal encoding sequence the amplifiers are never overloaded (which is one of the features contributing to the speed of this system), but an excessively large input signal will cause overload. To prevent long recovery times or, in extreme cases, damage, a limiter circuit like the one shown in the figure is connected between Σ and v_o in both input and output stages. For positive-going output signals (negative residue), the upper diodes conduct and reduce the gain to 0.5 or less. For negative-going output signals, the lower diodes conduct when the 5V level is exceeded and again reduce the gain to 0.5 or less.

Two 4-bit DACs are used. The DAC currents are 0.25mA, 0.5mA, 1mA, and 2mA. A typical current generating stage is shown in Fig. 7. The DAC current equals V_{REF}/R and is regulated by an operational amplifier with a dual FET input stage. The reference voltage V_{REF} is 10V, and the resistors are accurate to ±0.01% with a tempco of 1 ppM/°C. The output stages use FETs instead of bipolar transistors to prevent diversion of current to their inputs. A cascode circuit is used to avoid voltage swing at the drain of Q1, thereby reducing the gain-bandwidth requirement of amplifier A_1. A positive pulse at the DAC control diverts the current into the control

circuit, and a negative pulse allows all of it to flow into Σ.

Only DAC 1 is a high-precision unit; DAC 2 is much less accurate because it controls the lower-weight bits in the encoding process.

The 15 comparators shown in the lower left corner of Fig. 5 are contained in eight μA 711 integrated circuits. Each comparator has a separate bias control connected to a highly stable 4V reference supply. The spacing between levels is 0.25V.

Since 15 separate comparators do not in themselves produce a binary output, a coding circuit is required. The encoding is done in two steps: first, to Gray code, then Gray to binary. The reason for this is to avoid the possibility of encoding errors which may arise from the transients of several binary stages being switched simultaneously. In the Gray code converter, only one stage at a time can switch between transitions, and the use of a register between the two code converters allows the Gray to binary encoder to settle before its output information is transferred to Registers 1 and 2.

The clock generator in Fig. 7 consists of a series of J-K flip-flops connected as univibrators to control clock pulse widths and spacings. The clock must be started externally by a pulse into START A or START B. For multiplex or dual parameter operation, both START inputs are used (this will be covered later in greater detail). The timing sequence for the control of the various operations was covered in the description of the 63-channel ADC, and the timing diagram in Fig. 2 applies to this system as well.

The averager consists of a 7-bit scaler which controls a 7-bit DAC. Each time a buffer store command occurs, a digital number between 1 and 128 is subtracted from the channel address register and a proportional linear signal is added to the input plifier. The number subtracted from the address register does not advance in a monotonic sequence from step to step, but changes in pseudorandom fashion. This is accomplished by cross-connecting the lines between scaler and DAC as shown in Fig. 8. The reason for doing this is to avoid beat patterns in channel widths which otherwise could occur when a constant-frequency pulser is used for spectrum stabilization or for testing.

Multiplexing

The multiplexing of two input signals will now be discussed. Coincidence or dual parameter measurements are a special case of multiplexing and will be discussed at the same time. To flag the computer that a coincidence has occurred, a separate coincidence circuit which receives its information from an early part of the amplifier chain must be used. This coincidence circuit must produce a signal which is applied to the COINCIDENCE input in Fig. 7.

In coincidence measurements, both inputs are generated simultaneously. Since the ADC can process only one signal at a time, logic circuitry not included in the ADC must be provided to ensure this sequential processing. It was felt that this circuitry is best included in the stretchers which precede the ADC. Furthermore, it is desirable to make the logic in the stretchers self contained, i.e., to avoid the use of command lines from the ADC to the stretchers, if possible.

We now digress to describe the stretchers which were designed for use with this ADC.

The salient front panel terminals and the interconnections are shown in Fig. 9.

Each stretcher contains a voltage-to-current converter and an output linear gate. By operating in the current mode, gating is simplified, and all outputs may be connected together without the need for additional circuitry. In multiplex operation, each gate is normally closed. An internal strobe, timed to start after the stretching process is complete, opens the gate for 3 μsec. A START signal is generated in coincidence with the start of the strobe signal unless an INHIBIT signal is present. If it is, the STROBE OUTPUT, LINEAR OUTPUT, and START OUTPUT signals are suppressed until the INHIBIT signal disappears, after which a normal, 3-μsec pulse is generated.

The cross-connection between STROBE or BUSY terminals and the INHIBIT terminals ensures that only the outputs from one stretcher at a time are presented to the ADC. In each stretcher, the storage capacitor is discharged and the BUSY signal terminated by the termination of the internal STROBE pulse. Thus, if signals appear simultaneously in both channels, one stretcher capacitor must remain charged for 3 μsec and the other for at least 6 μsec. Since there is no feedback from the ADC to the stretchers, normal stretcher operation occurs whether or not the signals are accepted by the ADC.

When the outputs of more than two stretchers are multiplexed into the ADC, a routing box must be used to select outputs one at a time and to generate flags for routing to particular regions of the memory.

With the foregoing in mind, we now return to a description of the operating conditions for coincidence measurements.

In such a measurement, it is frequently desirable to route the coincident pulses to a particular region of the memory. To do this, we require that the START B pulse be generated before the START A pulse and that it have a particular time relationship to the COINCIDENCE pulse applied to the ADC. These requirements are covered below.

In the stretcher, the BUSY OUTPUT pulse is generated by a low-level discriminator connected to the LINEAR INPUT. As a result, the BUSY OUTPUT pulse always

starts before the STROBE OUTPUT pulse. By cross-connecting the BUSY OUTPUT of stretcher B to the INHIBIT INPUT of stretcher A, we ensure the condition described in the preceding paragraph.

At the start of the clock pulse train in the ADC, a pair of latches recognize and store the fact that CHANNEL B and COINCIDENT pulses occurred. At the end of the clock train, a STORE command transmits this information to a second pair of latches (which are part of the BUFFER REGISTER) where it is held while the computer processes it. This information tells the computer which memory regions to use when the CHANNEL B and COINCIDENCE pulse are present. For the first set of latches to lock on the COINCIDENCE and CHANNEL B pulses, the CLOCK 1 pulse must be present at the same time as the CHANNEL B pulse. Since the CLOCK 1 pulse is generated ~1 μsec after START A or START B, whichever occurs first -- START B in this instance -- it is necessary that the START B pulse be at least 1 μsec wide. The COINCIDENCE PULSE may start at any time, but it may not end sooner than the end of the START B pulse or later than the end of the encoding time.

For non-coincidence pulses occurring in channel B, a CHANNEL B flag will occur but not a COINCIDENCE flag. By computer programming, this condition can be used to store channel B pulses in a memory region different from channel A or coincidence pulses.

The capability of storing information in different memory regions can be extended by adding sets of latches (the output latches would be part of the BUFFER REGISTER) to the system as indicated by the CHANNEL J path in Fig. 7. Each additional path must be activated by a START pulse which is OR-gated into the CLOCK GENERATOR and which also is applied to the input latch of the additional path. It should be noted that by computer programming, each additional path can be coded as a binary number. Thus, 3 paths allow selection of 8 memory regions.

We now consider another facet of the interaction between the computer and the ADC.

In many cases, the ADC will furnish data to the computer which, for one or more reasons, cannot process it at the instant of appearance. The implementation for coping with this situation is described below.

After the encoding process is complete, a CLOCK BUFFER signal from the CLOCK GENERATOR locks the digitized input signal into the BUFFER REGISTER and sets a toggle in the CLOCK GENERATOR which will not allow another STORE command or CLOCK BUFFER signal to be generated until the toggle is reset. The STORE command notifies the computer that there is information in the BUFFER REGISTER. If a 2nd input signal enters the ADC, it will be encoded, but unless the computer clears the BUFFER REGISTER and furnishes a READY signal to reset the toggle mentioned above, a gate in the CLOCK GENERATOR will be closed, blocking a new START signal and preventing the encoding of a 3rd input signal. If the COMPUTER READY pulse appears any time before a 3rd START signal occurs, the encoded 2nd pulse is locked into the BUFFER REGISTER by a new CLOCK BUFFER signal and the encoding continues. Input pulses which occur while the ADC is storing 2 encoded signals will be lost.

The START A and START B circuits respond only to leading edges of start signals. Thus, even if a signal is present at the input terminal of the ADC, if the START gate was closed at the instant the START signal appeared, the linear signal will not be encoded. This feature prevents errors from occurring because the encoding process was begun after the start of an input signal but too late to complete the encoding before the end of the input signal.

Tests and Performance

In Fig. 10 is shown an oscillogram of the input signal to the multilevel comparators obtained with a pulse generator connected to the input of the ADC. The 3 steps of encoding are clearly shown. The 1st and 2nd steps last for ~0.75 μsec each and the 3rd step, ~1.2 μsec. Total encoding time is 2.7 μsec. The spacing between comparator levels in this instance is 0.265V. Thus, the 1st step has a weight of 3.45/0.265 X 144 = 13 X 144 = 1872 channels, the 2nd step a weight of 2.38/0.265 X 12 = 9 X 12 = 108 channels, and the 3rd step a weight of 1.08/0.265 = 4 channels. The sum of these factors adds up to 1984 channels.

In Fig. 11, the input pulse height was swept back and forth through the dynamic range of the ADC while looking at the signal to the comparators. The effects of pre-bias and overlap are shown in this photo as blank areas above and below the spectra during the 2nd and 3rd steps of encoding. The reason for the blanks is as follows:

There are 15 comparators and therefore 15 encoding levels. As the input signal is increased slowly from zero, the encoding levels during the 3rd step are sequentially exceeded. When the input signal gets large enough to exceed the sum of the pre-bias existing during the first step of encoding (which has a weight of ~2 encoding levels) plus 12 additional encoding levels, the 1st level of the 2nd step is exceeded, subtracting a weight of 12 levels from the 3rd step. Since this transition occurred when the input signal level was between the 14th and 15th channel, the subtraction of 12 channels from the 3rd step causes the next cycle of increase to begin between the 2nd and 3rd levels of Step 3. Thereafter, continued increase of input signal amplitude causes the voltage at the input to the comparators to cycle between the 2nd and 14th+ levels during the 3rd step of encoding.

A similar situation exists for the 2nd step of encoding, but during this step, the pre-bias applicable at this stage in the encoding process determines the lowest level during

the cycling process.

The height of the blank spaces below the pulse height continua during the 2nd and 3rd encoding steps varies according to the particular settings of the pre-bias controls.

In Fig. 12 a display of channel profiles is shown. The averager was connected during the measurement and resulted in a slight broadening of the profiles. As shown, the top 3% of the profile occupies ~85% of the channel width. The display was obtained as follows:

Additional logic circuits were assembled to select one channel address from the output of the ADC. This channel was connected to a multichannel analyzer (MCA) operating in the multiscaler mode. Then a sweeping pulser was connected to the input of the ADC and slowly scanned across the channel of interest. While the ADC was being scanned, the channel address of the MCA was advanced at fixed time intervals of ~0.1 sec. After the profile was mapped, a photograph was taken, the next higher channel was selected, the scanning repeated, and a second exposure made on the same photograph. The process was repeated 5 times to obtain Fig. 12.

A count rate test was performed by dc-coupling a pulser into the ADC. At 300,000 Hz, the measured shift was ~0.3 channels.

A temperature test was performed. The measured bias shift from 20°C to 40°C was 0.5mV, corresponding to ~0.25 channel in a 4-volt dynamic range, or ~6 ppM/°C.

Nonlinearity was measured with a 17-bit computer-controlled pulse generator[10] at the National Reactor Testing Station, and it was found that the integral nonlinearity was ~0.005% over all channels.

In an overnight run at substantially constant temperature, peak-to-peak fluctuations in zero and scale factor (gain) were 0.2 channels and 0.002%, respectively.

Figure 13 is a recording of counts vs channel number using a sliding pulser as the signal source. The results of 2 runs were superimposed to show that the fluctuations from channel to channel were predominantly statistical. The 2 solid lines labelled $\sigma_{rel} = 1.1\%$ refer to the standard deviation associated with an accumulation of 8500 counts from a random source. In this instance, source statistics exceeded ADC statistics by a considerable margin.

In a comparative test between this ADC and a well known, high quality 1600 channel Wilkinson type, the new ADC showed ~30% less fluctuation from channel to channel.

All of the preceding tests were made without stretchers and, therefore, are measures of the ADC performance alone. It is apparent from the results obtained that in a meaningful operational test, the system performance will be limited by the performance of the stretchers.

Acknowledgments

The writer wishes to acknowledge the earlier work of A. M. R. Ferrari whose fast ADC, while quite different from the one described in this paper, set the stage for the present one. Also, to simplify the explanation of this ADC, Mr. Ferrari wrote the equation which describes its operation (Eq. 1 in the text). The writer also wishes to thank Drexel Lamb for constructing and making many of the tests on the experimental model, W. R. Burrus and W. A. Gibson of Tennecomp, Inc. for their comments and suggestions, Paul Aebersold of Tennecomp for his programming help in computer-testing the ADC, Russell Heath and his group at the National Reactor Testing Station for their help in testing the linearity and stability of the ADC, and Edward Fairstein for his encouragement and consultation during this project.

References

1. L. B. Robinson, F. Gin and F. S. Goulding, "A High-Speed 4096-Channel Analogue-Digital Converter for Pulse Height Analysis," Nucl. Instr. and Methods 62, 237 (1968).

2. L. B. Robinson, "Reduction of Baseline Shift in Pulse Amplitude Measurements," Rev. Sci. Instr. 32, 1057 (1961).

3. C. H. Nowlin and J. L. Blankenship, "Elimination of Undesirable Undershoot in the Operation and Testing of Nuclear Pulse Amplifiers," Rev. Sci. Instr. 36, 1830 (1965).

4. V. Radeka, "Optimum Signal-Processing for Pulse-Amplitude Spectrometry in the Presence of High-Rate Effects and Noise," BNL Report No. 12325, Brookhaven National Lab., Upton, New York.

5. D. H. Wilkinson, "A Stable Ninety-nine Channel Pulse Amplitude Analyser for Slow Counting," Proc. Cambr. Phil. Soc. 46, 508 (1950).

6. I. De Lotto, P. F. Manfredi, P. Maranesi, F. Vaghi and R. Vecchio, "A Fast Pulse Amplitude-to-Time Converter for an Equivalent Clock Rate of Some GHz," Nucl. Instr. and Methods 65, 228 (1968).

7. Rupert Patzelt, "Prinzip eines schnellen ADC hoher Auflosung," to be published in Acta Physica Austriaca.

8. C. Cottini, E. Gatti and V. Svelto, "A New Method for Analog to Digital Conversion," Nucl. Instr. and Methods 24, 241 (1963).

9. Digital Equipment Corporation, Logic Handbook, (1968).

10. W. W. Black, "A Precision, Computer-Controlled Pulse Generator and its Application," Nucl. Instr. and Methods 53, 249 (1967).

Appendix 1

Definitions

An analog-to-digital converter (ADC) of the type being considered here contains a number of equally spaced digitizing levels. If there are N levels above zero, then between these levels there are N equally spaced channels above zero plus an overflow channel. In this paper, beginning with the baseline, we number the channels 0, 1, 2, · · · . Thus, an N-level ADC contains N-1 equally spaced channels which have non-zero numbers associated with them, plus an overflow region.

An N-level encoder can exist in N + 1 possible states.

Parallel-Series ADC

If encoding is done in several discrete steps with a multilevel comparator, the total number of channels produced, not counting the 0th channel but including the overflow channel is

$$N = \frac{A_m}{A_1}(k+1) - 1$$

where

A_m = amplifier gain during the mth step of encoding.

A_1 = amplifier gain during the 1st step of encoding.

k = number of encoding levels above the baseline which the comparators have.

The total number of channels N is made up of subgroups $N_1, N_2 \cdots N_m$ which are quantized during each step of the encoding process. For any given input signal,

$$N = N_1 + N_2 + \cdots + N_m = \sum_1^m N_i .$$

$$N_1 = \frac{A_m}{A_1} k\, H[A_1 v_1 - L_k] +$$

$$\frac{A_m}{A_1}(k-1) H[A_1 v_1 - L_{k-1}] H[L_k - A_1 v_1] +$$

$$\vdots \qquad \vdots \qquad \vdots$$

$$\frac{A_m}{A_1} H[A_1 v_1 - L_1] H[L_2 - A_1 v_1] .$$

$$N_2 = \frac{A_{m-1}}{A_1} k\, H[A_2(v_1 - N_1 L_1) - L_k] +$$

$$\frac{A_{m-1}}{A_1}(k-1) H[A_2(v_1 - N_1 L_1) - L_{k-1}] H[L_k - A_2(v_1 - N_1 L_1)] +$$

$$\vdots \qquad \vdots \qquad \vdots$$

$$\frac{A_{m-1}}{A_1} H[A_2(v_1 - N_1 L_1) - L_1] H[L_2 - A_2(v_1 - N_1 L_1)] .$$

$$N_i = \frac{A_{m-j+1}}{A_1} k\, H[A_i(v_1 - L_1 \sum_1^{j-1} N_n) - L_k] +$$

(continued)

$$\frac{A_{m-j+1}}{A_1}(k-1)H[A_j(v_1-L_1\sum_1^{j-1}N_n)-L_{k-1}]H[L_k-A_j(v_1-L_1\sum_1^{j-1}N_n)]+$$
$$\vdots \qquad\qquad \vdots \qquad\qquad \vdots$$
$$\frac{A_{m-j+1}}{A_1}H[A_j(v_1-L_1\sum_1^{j-1}N_n)-L_1]H[L_2-A_j(v_1-L_1\sum_1^{j-1}N_n)].$$

where

N = total number of channels recorded in a complete encoding cycle,

N_j = number of channels recorded at the jth step of encoding,

N_n = number of channels recorded during an earlier step of encoding,

m = number of steps in the encoding, therefore the number of different gain steps used during encoding,

A_j = amplifier gain at the jth step in the encoding where j can vary from 1 to m,

v_1 = input voltage to the ADC. This signal remains constant during a complete encoding cycle,

L_1 = threshold voltage of the lowest-level comparator,

k = number of encoding levels associated with the comparators,

L_k = topmost comparator level,

H = Heaviside operator: $H[X] = 0$ if X is negative, $H[X] = 1$ if X is positive.

In the above formula, if the $(k-1)$th term in N_j is examined:

$$\frac{A_{m-j+1}}{A_1}(k-1)H[A_j(v_1-L_1\sum_1^{j-1}N_n)-L_{k-1}]H[L_k-A_j(v_1\sum_1^{j-1}N_n)]$$

it will be seen that this term will be positive if and only if the residue at the beginning of the jth step exceeded the $(k-1)$th threshold level but not the kth level. If this term is positive, the residue will be:

$$A_j(v_1-L_1\sum_1^{j-1}N_n)-L_{k-1}.$$

The term $L_1\sum_1^{j-1}N_n$ is the number of channels recorded during all preceding steps of encoding, but not including the jth step.

The factor A_{m-j+1}/A_1 is the weighting factor by which the count must be multiplied before it is added to the address register at the end of the jth step.

Numerical examples of the preceding are given in the main body of the text as part of the descriptions of the 63-channel and 35-channel ADCs.

Appendix 2

Within a particular range of error in the comparator levels or amplifier gain, negative residues will not occur if redundancy and pre-bias are introduced into the system. Redundancy is obtained if the gain ratio between encoding steps, A_j/A_{j-1}, is less than the number of encoding states, $k+1$. The number of overlapping channels between steps which result from this redundancy is $(k+1)-A_m/A_{m-1}$; multiplying by L_1 gives the overlap in volts, measured at the input to the comparators. The optimum bias applied to the input of the amplifier (not at the comparators) at the $(m-1)$th step is that amount which splits the overlap in half:

$$B_{m-1}=\frac{L_1}{2}\frac{A_1}{A_m}(k+1-\frac{A_m}{A_{m-1}})\text{ volts.}$$

For the $(m-2)$nd step, the pre-bias is

$$B_{m-2}=B_{m-1}+\frac{L_1}{2}\frac{A_1}{A_{m-1}}(k+1-\frac{A_{m-1}}{A_{m-2}})\text{ volts.}$$

At the jth step,

$$B_j = \sum_{i=1}^{m-2} B_{i+1} + \frac{L_1}{2} \sum_{i=1}^{j-1} \frac{A_1}{A_{i+1}} \left(k + 1 - \frac{A_{i+1}}{A_i}\right).$$

The bias may be included in the general formula given in App. 1 by substituting $(v_1 - B_j)$ for v_1, wherever it appears; the subscript j must correspond with the particular step of encoding in which the substitution is made.

A numerical example of the preceding is given in the main body of the text as part of the description of the 35-channel ADC. A diagram illustrating the relationship of bias to comparator levels is given in Fig. 3.

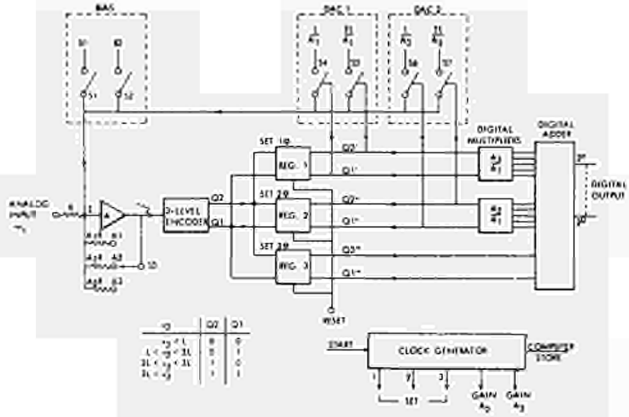

Fig. 1 - Block diagram of a parallel-series analog-to-digital converter.

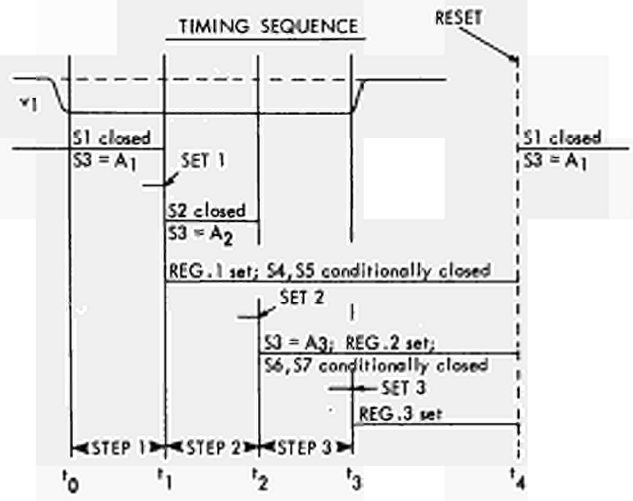

Fig. 2 - Timing diagram for a parallel-series ADC.

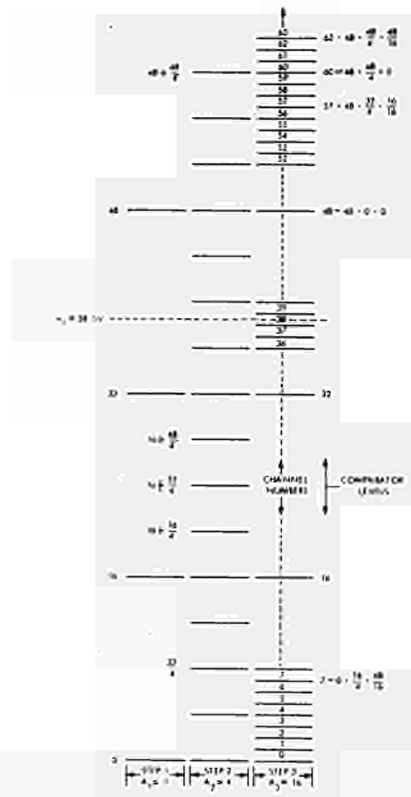

Fig. 3 - Voltage levels referred to the input during the three steps of encoding in a 63-channel parallel-series ADC.

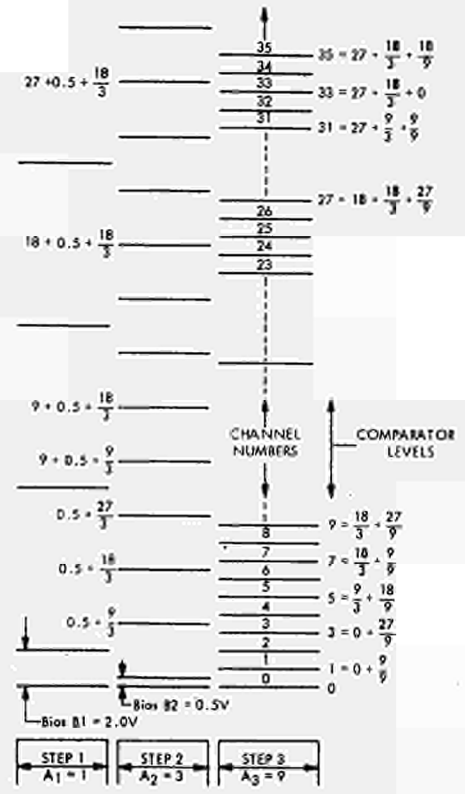

Fig. 4 - Voltage levels referred to the input in a 35-channel ADC showing pre-bias during the first and second steps of encoding.

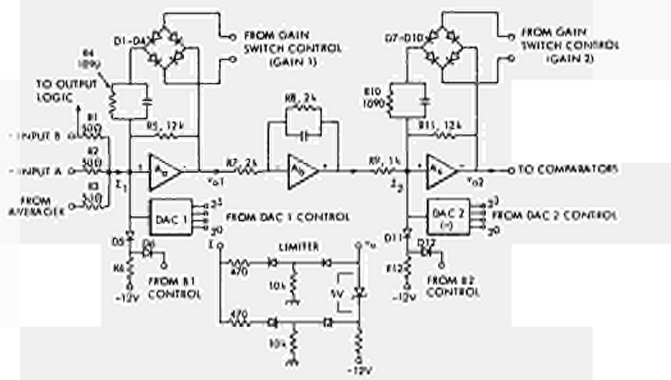

Fig. 5 - Block diagram of switched amplifiers in 11-bit ADC.

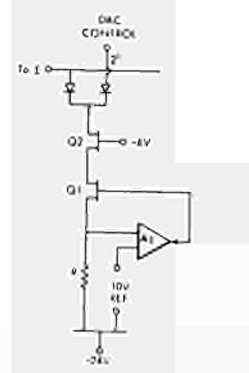

Fig. 6 - One current branch of the DAC in the 11-bit ADC.

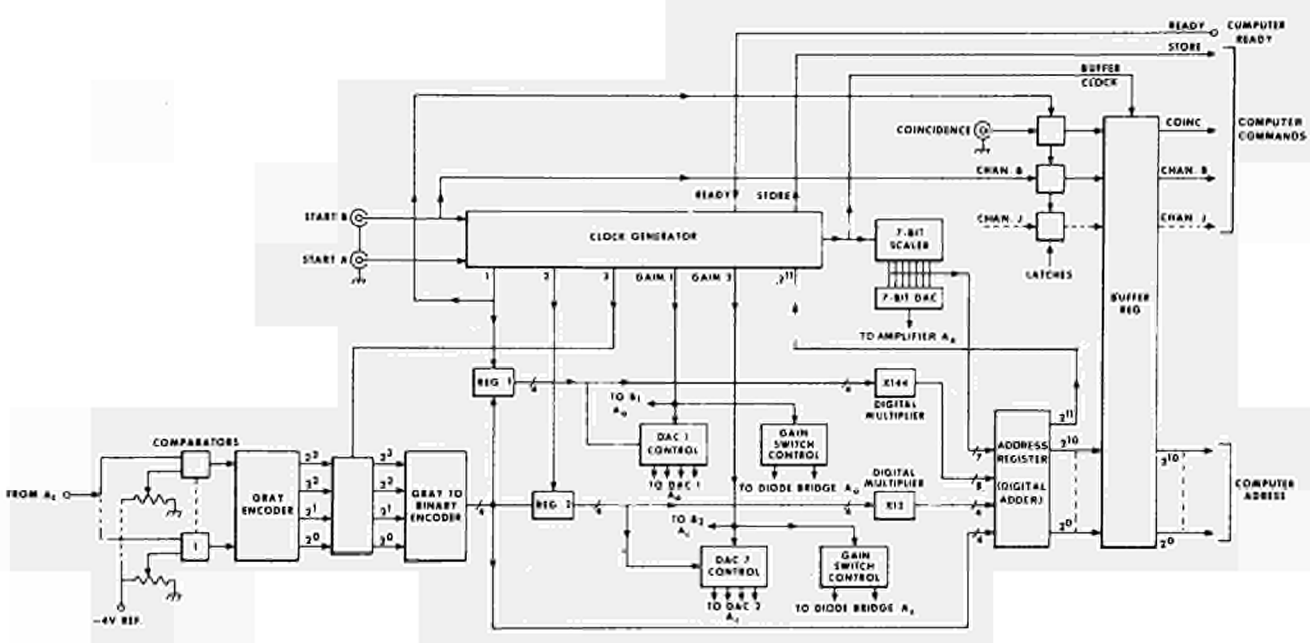

Fig. 7 - Digital blocks of a 2048 channel ADC.

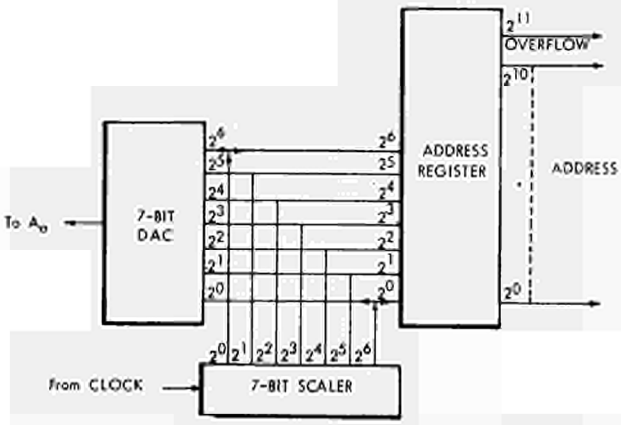

Fig. 8 - Averager logic. Note that the 2^0 line of the scaler is connected to the 2^6 lines of the DAC and ADDRESS REGISTER.

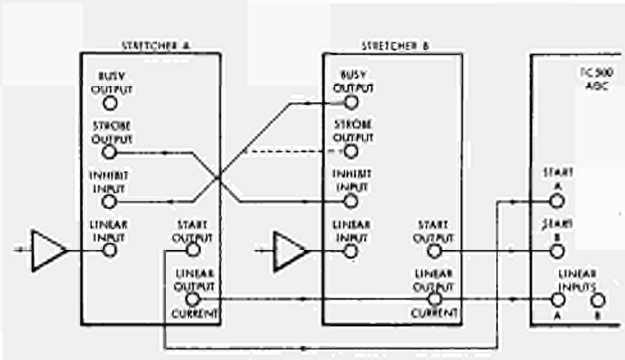

Fig. 9 - Interconnections between stretchers and the ADC for dual parameter (coincident) operation. The cross-connections between the stretcher INHIBIT INPUT and BUSY or STROBE OUTPUT ensures that the two START OUTPUTs will not occur simultaneously.

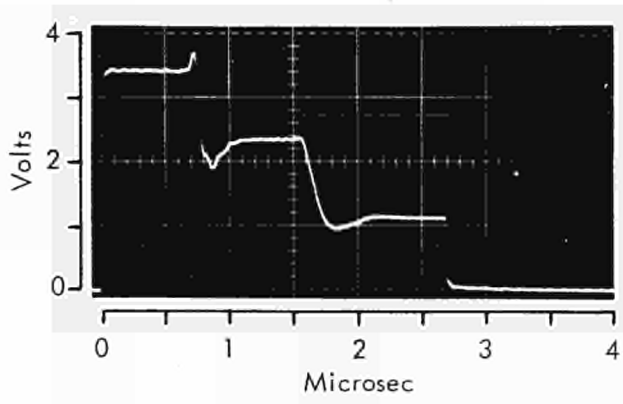

Fig. 10 - Input signal to comparators corresponding to channel No. 1984 showing the three steps of encoding.

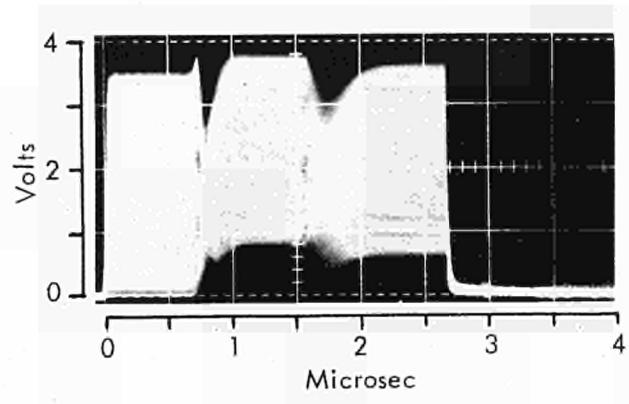

Fig. 11 - Input signal to comparators when ADC input pulses are swept in amplitude from 0 to 3.5. V (0 to channel No.1984).

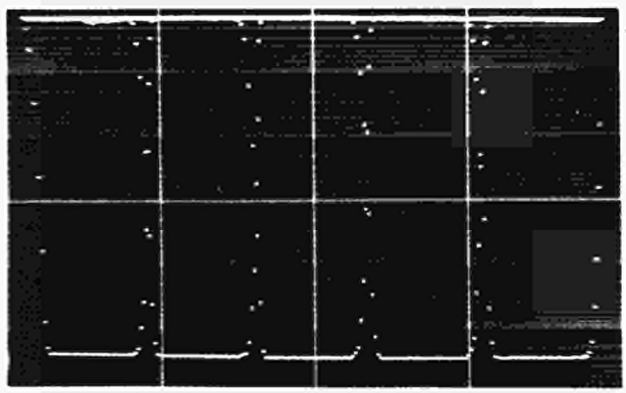

Fig. 12 - Channel profiles for five contiguous channels.

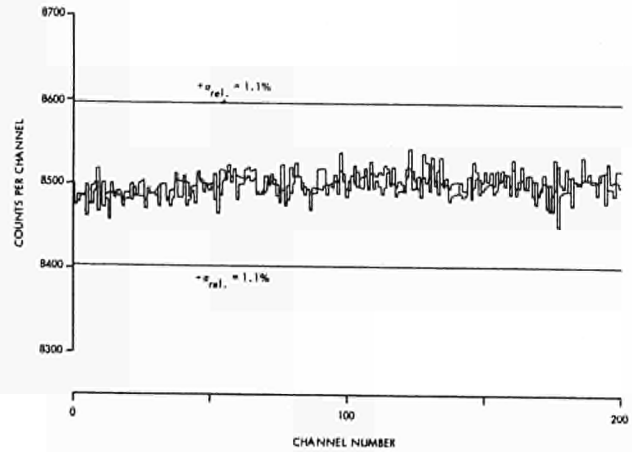

Fig. 13 - Counts vs channel No. using a sliding pulser as a signal source. Two runs are superimposed to show that the fluctuations are mainly statistical. The lines labelled $\sigma_{rel} = 1.1\ \%$ refer to the standard deviation of 8500 counts from a random source.

ANALYSIS OF NONLINEAR FEEDBACK LOOPS IN PULSE STRETCHERS*

I. Alleva[1], I. De Lotto[2], P.F. Manfredi[3], P. Maranesi[3]

1. CISE Laboratories - Segrate (Milano) - Italy
2. CNR and University of Bologna - Italy
3. CESNEF - Polytechnic School of Milano - Italy

SUMMARY

The behaviour of a stretcher is analyzed here, taking into account the effects of the main nonlinearities in the feedback loop. The dependence of the parameters of the active devices on their working point has been carefully examined.

The COLDAC II computer program has been used for simulating the different circuit diagrams; the results are compared with the experimental outcome.

1 - Introduction

Two previous papers[1,2] have been devoted to the analysis of the various blocks a feedback stretcher consists of . A circuit classification was suggested, according to the working mode of the different arrangements , upon which a two time-constants linear theory was based, with the aim of theoretically foreseeing the actual behaviour of a peak stretcher.

Although the theoretical conclusions of the quoted papers were found to agree with the real features of these circuits and to explain some of their practical limitations, a closer view of the problem is believed to be desirable for a number of reasons.

The linear theory of papers [1,2], indeed, has been found very accurate in determining the values of circuit parameters which ensured that the closed-loop poles of the stretcher were real. This is in connection with the feature, common to some stretcher circuit diagrams, according to which the lower is the difference between input signal and stored voltage, the more critical is the feedback loop as far as a monotonic response is concerned. In this case, a theoretical small-signal analysis which allows to determine the response of the stretcher in the region near its standing working point, gives information about the behaviour of the circuit during the final part of the stretching operation.

*Work partially supported by CNR contracts N. 115.2550.05003 and N. 115.2550.03303

The linear approach to the problem is considered in this paper as the first step to be tempted, and it appears here analyzed in more deep detail, and supported by a careful knowledge of the dependence of the small signal parameters of the active devices on their working point. The limitations of the linear analysis, however, are easily understood. As a matter of fact, peak stretchers are usually designed for a very wide input range (of the order of 1000:1), so that the parameters of some active device in the feedback loop are subject to large variations.

So, the linear theory fails in evaluating , for instance, the dependence of the linearity inaccuracies on the input amplitude, throughout the useful range of the stretcher. In a feedback stretcher in which the closed-loop poles are real, regardless of the actual dynamic working point, nonlinearity is due, for input signals of finite width, to the dependence of the risetime of the stored voltage on the input amplitude. In a feedback stretcher, which exhibits complex closed--loop poles in a certain range of values of its circuit parameters, the peak amplitude of the stored voltage could be nonlinearly related to the input amplitude even if the input signal is very long. In the second case, for signals of finite width, combination of both sources of error is to be expected. Obviously, only a nonlinear analysis of the circuit can thoroughly explain the two quoted behaviours and suggest which working condition to choose. The case of anywhere real closed-loop poles is often preferable because it does not introduce any low-level inaccuracy provided that the input signal is long enough. The condition of real poles, however, is usually in conflict with the requirement of a high charging speed, so that in some fast stretchers it is convenient to not respect it strictly. The practical consequence of complex closed-loop poles is that the voltage stored in correspondence of an input step of amplitude V_i^o can be higher than V_i^o . The difference between the stored voltage and V_i^o , as we will show later increases with V_i^o up to a certain value, determined by the features of the feedback loop, beyond which it turns out to be almost constant. So, except for a first region of the output amplitude range,

a good linearity can be obtained, the condition of complex poles resulting merely in a fixed step added to the stored voltage. The closed-loop response of the stretcher, in the case of complex poles appears to be monotonic across the storage capacitorowing to the unidirectional current behaviour of the charging device. So, the first maximum of the actual oscillating voltage across the storage capacitor is stretched. Consequently, this oscillation cannot be completely characterized by experimental observations, as its frequency and damping ratio cannot be measured. Moreover, the amplitude of this oscillation is strongly dependent on the nonlinear characteristics of the involved devices, so that the linear model fails as soon as the input amplitude in higher than a few millivolts. On the other hand it is very difficult to test experimentally the linear model on the actual circuit, owing to the errors introduced by both noise and inaccuracies of measuring equipments at very small values of the stored voltage.

We have therefore preferred, for a careful analysis at any level of input signal, to use COLDAC II, a computer program for the time analysis of lumped non linear, time-dependent networks. In this paper a stretcher is briefly characterized on the base of the inaccuracies which affect its behaviour: amplitude-dependent risetime and overswing in the stored voltage.

Sources of these inaccuracies are acknowledged to be variations in the working point of both comparison amplifier and unidirectional-output amplifier.

The analysis of the nonlinear circuit is based upon a circuit model suitable for COLDAC II program; the dependence of the parameters of the active elements involved in the feedback loop of the stretcher is introduced as a result of careful experimental measurements.

Then the linear model is used for a theoretical prediction through zeros-poles analysis of the behaviour of the circuit in a region near its standing working point.

Finally the results of the computer nonlinear analysis are presented, for some circuit diagrams which already appeared, toghether with the corresponding experimental tests in the quoted references [1) 2)]

The computer results agree with the experimental outcome, and better clarify the intrinsic behaviour of a stretcher.

2 - Simple approach to stretching operation

Fig. 1 shows the simplified block diagram of a feedback peak stretcher.

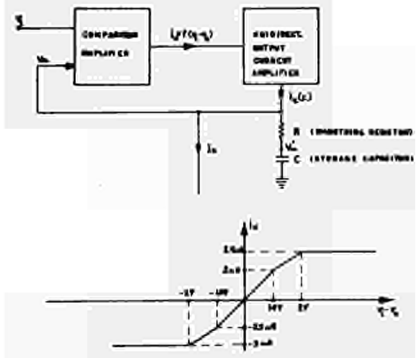

Fig. 1 - Simplified block diagram of a feedback peak stretcher

The $i_u = f(v_i - v_u)$ characteristic of the comparison amplifier is intended to suit the actual behaviour of a long-tailed pair using field-effect transistors [1,2]. The unidirectional-output current amplifier delivers in its standing state a very low current ($I_o \simeq 1\ \mu A$) as suggested by holding-time considerations.

The comparison amplifier and particularly the unidirectional-output current amplifier introduce in the feedback path open-loop zeros and poles which change their position continuosly during the charging time.

This is mainly due to the large variations in the working point of the output stage of the charging amplifier.

Moreover the nonlinear characteristic of the open loop $\frac{dic}{d(v_i - v_u)}$ d.c. transfer function, due to the saturated behaviour of the gain of the comparison amplifier and to the nonlinearity in the d.c. current gain of the charging amplifier, would introduce an amplitude-dependent shape of the output pulse even if the open-loop poles were constant.

Being the open-loop poles not constant, moreover, it is impossible to design a linear phase-lead network for a good compromise between the requirements of monotonic closed-loop response and high charging speed throughout the amplitude range of the stretcher. Usually in peak stretchers a phase-lead correction is introduced using a resistor in series to the storage capacitor, as shown in fig. 1.

This resistor adds a zero in the open-loop transfer function of the system, and this zero can often prevent the stretcher from exhibiting any overswing on the stored voltage. This resistor, however, introduces

an integrating time constant on the storage capacitor, thus affecting the actual charging speed which is determined by the risetime of the voltage across C. In the following we will intend with the term "monotonic response" of the stretcher any behaviour in which the voltage across the storage capacitor does not exhibit zero slope at a finite time.

Complex closed-loop poles can give rise either to zero slope in the output signal at a finite time or not.

In the first case, the voltage stored in correspondence of an input step of amplitude V_i^o goes beyond V_i^o as the first peak of the oscillating waveform is stretched. This situation is quite often present in actual stretchers. The problem is to analyze the features of this overswing, in order to reach a compromise between the maximum amplitude of the overswing which can be tolerated and the charging speed. So, the choice of R is the very heart of this discussion, as any increase in its value, while reducing the amplitude of the overswing, worsens the speed features of the stretcher.

In section 4 the small-signal linear model of the stretcher is analyzed, for a closer look at its behaviour in the neighborhood of its standing working point, that is both in correspondence of very small input amplitudes ($\sim$ 1 mV) and at very low values of the difference $v_i - v_u$.

3 - Transistor model and experimental evaluation of its parameters

The previous discussion showed that for a careful analysis of a stretcher, a rather sophisticated large-signal equivalent circuit of the transistor is required.

To clarify some amplitude-dependent effects which occur in actual stretchers, this model must account for the variations with collector current I_c and collector-to-base voltage V_{CB} of the following small-signal parameters of the transistor: common emitter d.c. current gain β , cutoff frequency f_β for the common-emitter current gain and obviously common emitter input impedance.

A generalisation of Ebers and Moll model has been chosen, as it is particularly suitable for a general purpose simulation program of electronic circuits through a digital computer and allows a simple fitting of transistor nonlinearities on the base of the corresponding experimental diagrams.

Fig. 2 shows the circuit diagram of the assumed model. This model implies the transistor be represented by a lumped element circuit described at a bypole level and obviously it has all the limits of this kind of approximation. We must point out, however, that the main purpose of this model was that of describing the dependence on the working point of both β and f_β Effects related to the actual distributed nature of the transistor are not involved in the model of fig. 2,

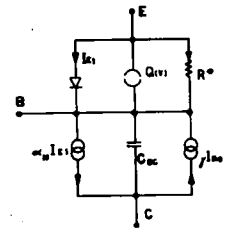

Fig. 2 - transistor equivalent circuit

nonetheless their importance in predicting the behaviour of practical stretchers seems to be lower than the importance of lumped integrating time constants around the loop.

Looking at the model of fig. 2, the charge Q is dependent on the emitter-to-base voltage and it is the sum of the charge stored in the emitter-base junction and of the diffusion charge.

The diode accounts for the nonlinear d.c. characteristic of emitter-base junction.

Two current-controlled current sources are shown in fig. 2. The first one, the characteristic parameter of which is α_N represents in the usual way the current gain of the transistor, while the second one which is controlled by the current through R^* and the parameter of which is γ , accounts for the dependence of the small signal current gain β on the working point.

Both α_N and γ are constant as this feature speeds up appreciably the analysis in the computer simulation program.

The small signal current gain β is related to the model parameters by the relationship:

$$\beta = \frac{\alpha_N \cdot \frac{dI_E}{dV_{EB}} - \gamma \frac{dI_{R^*}}{dV_{EB}}}{(1-\alpha_N)\frac{dI_E}{dV_{EB}} + \gamma \frac{dI_{R^*}}{dV_{EB}}} \qquad (1)$$

where $I_{R^*} = I_{R^*}(V_{EB})$ is the nonlinear characteristic of resistor R^* . The values of $\frac{d I_{R^*}}{dV_{EB}}$ are so low with respect to $\frac{dI_E}{dV_{EB}}$ so that the presence of R^* in parallel to the base-emitter diode affects the dynamic impedance seen at the base only to a negligible extent.

The model of fig. 2 needs, to fit the actual transistor, the knowledge of the following parameters and relationships:

$$\alpha_N\ ,\ \gamma\ ,\ C_{CB}\ ,\ Q = Q(V_{EB})\ ,\ I_E = I_E(V_{EB})\ ,\ I_{R^*} = I_{R^*}(V_{EB})$$

As the common emitter cutoff frequency f_β is related to the parameters of the model by the equation

$$\frac{1}{2\pi f_\beta} \simeq \frac{\beta}{\alpha_N \dfrac{dI_E}{dV_{EB}}} \cdot \frac{dQ}{dV_{EB}} \qquad (2)$$

the fitting of the actual transistor on the base of the given model occurs as follows.

As a first step α_N, β, f_β, C_{CB} and d.c. characteristic of the transistor under test are measured or deduced from the data sheets supplied by the manufacturer.

Therefore from eq. (1) and (2) both $\frac{dI_{R^*}}{dV_{EB}}$ and $\frac{dQ}{dV_{EB}}$ are deduced as functions of V_{EB}. Both $Q = Q(V_{EB})$ and $I_R^* = I_R^*(V_{EB})$ are evaluated integrating the differential relationships $\frac{dI_{R^*}}{dV_{EB}}$ and $\frac{dQ}{dV_{EB}}$ with zero initial conditions.

We would like to point out that, according to the given model, the base cutoff frequency of the transistor must be measured preventing the base-collector capacitance from interfering with the emitter capacitance.

This has been obtained introducing the transistor under test in a suitable feedback arrangement which allowed f_β to be measured also in correspondance of collector currents of few microamperes.

In specifying the dependence of transistor parameters on the working point we have looked at the average characteristics of some S.G.S. PNP specimens (2N2894, BFX48, 2N4034 and 2N4035) which had been extensively used in the development of peak stretchers in our laboratory.

The manufacture's data sheets have been used for deducing the values of the parameters in the range 1÷100 mA of collector currents, while these curves have been completed by suitable measurements in the low-current range (1 μA÷1 mA).

Fig. 3 gives the dependence on the working point which has been introduced in the computer simulation for the following parameters: f_β, β, I_E, Q.

Observe that the equivalent circuit of the transistor here introduced with the nonlinear parameters experimentally measured can take into account, often with good approximation, most of the phenomena which occur in the actual transistor both at low and high injection levels, obviously with the limitations related with the particular topology of the circuit.

Finally we would like to point out that the dependence of C_{BC}, β and f_β on V_{CB} has been at the present neglected in the model of fig. 3, for it was experimentally acknowledged that it affects the behaviour of a stretcher to a lower extent than the dependence of both β and f_β on I_c usually does.

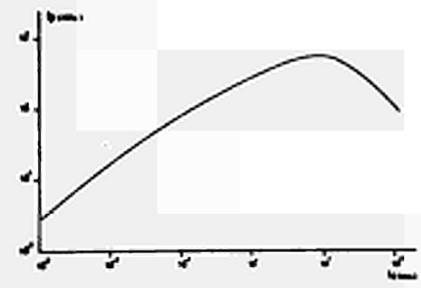

a

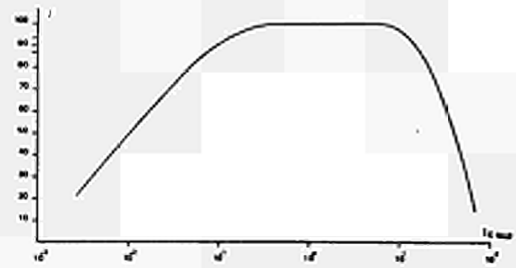

b

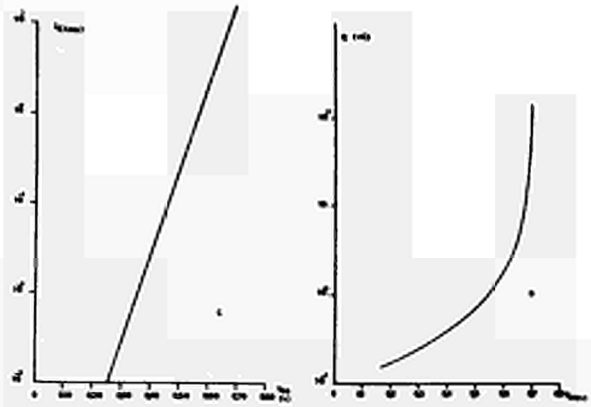

c d

Fig. 3: a) Cutoff frequency f_β versus collector current I_c

b) Small-signal d.c. current gain β versus collector current I_c

c) $I_E = I_E(V_{EB})$ static dependence

d) $Q = Q(V_{EB})$ characteristic

4 - The linear model of a stretcher

Fig. 4 shows a simple stretcher diagram using a grounded -emitter transistor as unidirectional-output amplifier.

In the same figure the equivalent circuit of the stretcher is also drawn , and the transistor model of fig. 2is introduced.

The comparison amplifier is represented, from an equivalent point of view, by a current source which is controlled by the current flowing through the non linear resistor R_C. The values of R_C are very high ($R_C > 10^{10}\,\Omega$) so that the storage capacitor is discharged through this path to a negligible extent.

The values of the parameter K are correspondingly high , so that the nonlinear characteristic $i_u = f(v_i - v_u)$ of fig. 1 is accounted for.

The linear model of the stretcher is based upon a linearisation of the parameters of both comparison amplifier and charging transistor around the standing working point which corresponds to $I_o = 1\,\mu A$.

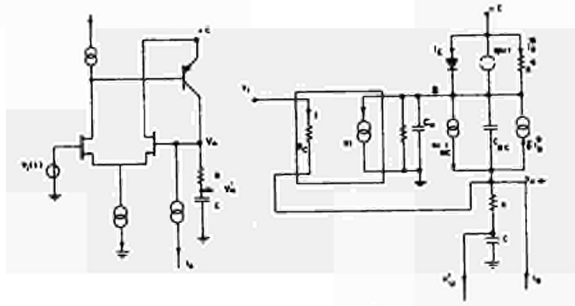

Fig. 4 Stretcher diagram using a grounded-emitter transistor as charging amplifier and corresponding equivalent circuit.

The effects of base spreading resistance as well as of both emitter and collector bulk resistance are neglected as they, in fact, do not appreciably modify the behaviour of the circuit. In this way the output capacitance C_o of the comparison amplifier appears in parallel to the differential $\frac{dQ}{dV_{EB}}$ capacitance which accounts for the internal cutoff frequency of the transistor, this being a particular feature of the stretcher which belongs to the type-I as defined in the quoted references [1,2].

The circuit of fig. 4 has two open-loop zeros, the values of which are:

$$z_1 = -\frac{1}{RC} \qquad z_2 = \frac{\beta}{R_B C_{BC}}$$

where R_B is the dynamic resistance of the transistor, which appears looking into its base.

It has, moreover, three main open-loop poles, the values of which are:

$$p_1 = 0$$

$$p_2 \simeq -\frac{C + C_{BC}(1+\beta)}{R_B C_T C_{BC} + RCC_{BC}(1+\beta) + CR_B(C_T + C_{BC})}$$

$$p_3 \simeq \frac{1}{p_2} \cdot \frac{C + C_{BC}(1+\beta)}{RR_B CC_{BC} C_T}$$

where C_T is the sum of the output capacitance C_o of the comparison amplifier and of the total emitter capacitance of the transistor, $\frac{dQ}{dV_{EB}}$.

Owing to the low collector current in the transistor, R_B is very high ($\sim 10^6\,\Omega$) while $\frac{dQ}{dV_{EB}}$ in this working condition practically coincides with the junction transition capcitance, which is of the order of 1 pF, so that the "equivalent" value of f_β is strongly affected by C_o.

When the collector current of the transistor increases, the effect of C_o becomes less and less important because it is masked by the presence of the junction diffusion capacitance which is roughly proportional to I_c. The value of the storage capacitor C was assumed equal to 500 pF.

The given expressions of z_1, z_2 and of p_1, p_2, p_3 require a number of comments.

1) With the actual values of components' parameters which are introduced in a stretcher, in which the charging transistor is moderately fast,
$|p_3| \gg z_2 \gg |p_2|$
p_2 occuring at an angular frequency of the order of some 10^5 rad/s when the transistor works at collector currents as low as 1 μA.

2) The C_{BC} capacitance correlates the values of z_1, p_2 and p_3, so that the circuit designer is not completely free in the choice of the compensating zero z_1.

3) Any increase in the value of the smoothing resistor R has the effect of shifting p_3, p_2 and z_1 toward the origin of the complex plane. While p_3 and z_1 are strongly dependent on R, R affects p_2 to a lower extent.

4) The real-positive zero z_2, owing to the low value of β and to the high value of R_B which correspond to the 1 μA working point, occurs at a rather low angular frequency, of the order of some 10^7 rad/s.

Interesting conclusions can be deduced from the analysis of the closed-loop poles for different values of the smoothing resistor R.

For very low values of R, there is a real negative

pole far from the origin which has no practical importance, and two complex poles with positive real part. For these two complex poles the build-up ratio is rather low, so that the practical consequence on the stored voltage is an added overwing . Increasing R the stretcher complex poles shift to a condition of negative real part which for certain values of R gives rise to a monotonic behaviour of the stored voltage in the sense defined in section 2. Further increase of R causes the closed-loop poles to shift again in the positive half-plane and a switching mode could occur. All these considerations were well known from the laboratory development of peak stretchers and have been throughly confirmed by the nonlinear analysis on the computer.

Fig. 5 shows the root loci plotted for the stretcher of fig. 4 where the value 4pF has been assumed for C_a and C_{BC}, all the other values of circuit parameters being deduced by the linearization of the nonlinear characteristics given in fig. 1 and 3.

These loci have been obtained with the aid of Brancaleone computer program[3].

The previous linear analysis, although limited in predicting the behaviour of the stretcher shows that the drawbacks of the stretcher of fig. 4 are due both to the collector-to-base capacitance C_{BC}, which coupled with the high value of R_B gives rise to a low-frequency real positive zero and to the reduced cutoff frequency of the grounded-emitter transistor which works at low standing current.

The cascode arrangement of the unidirectional output amplifier of fig. 6, where the upper transistor work at a standing current of 2 mA and the lower one at 1 μA has the advantage with respect to the circuit of fig. 4 of no interference between the compensating zero due to R and the values of the open-loop poles.

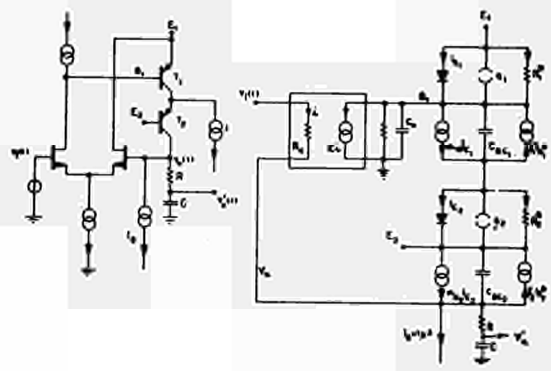

Fig. 6 Stretcher using a cascode arrangement as charging amplifier and corresponding equivalent circuit

The circuit of fig. 6 has the following open-loop zeros:

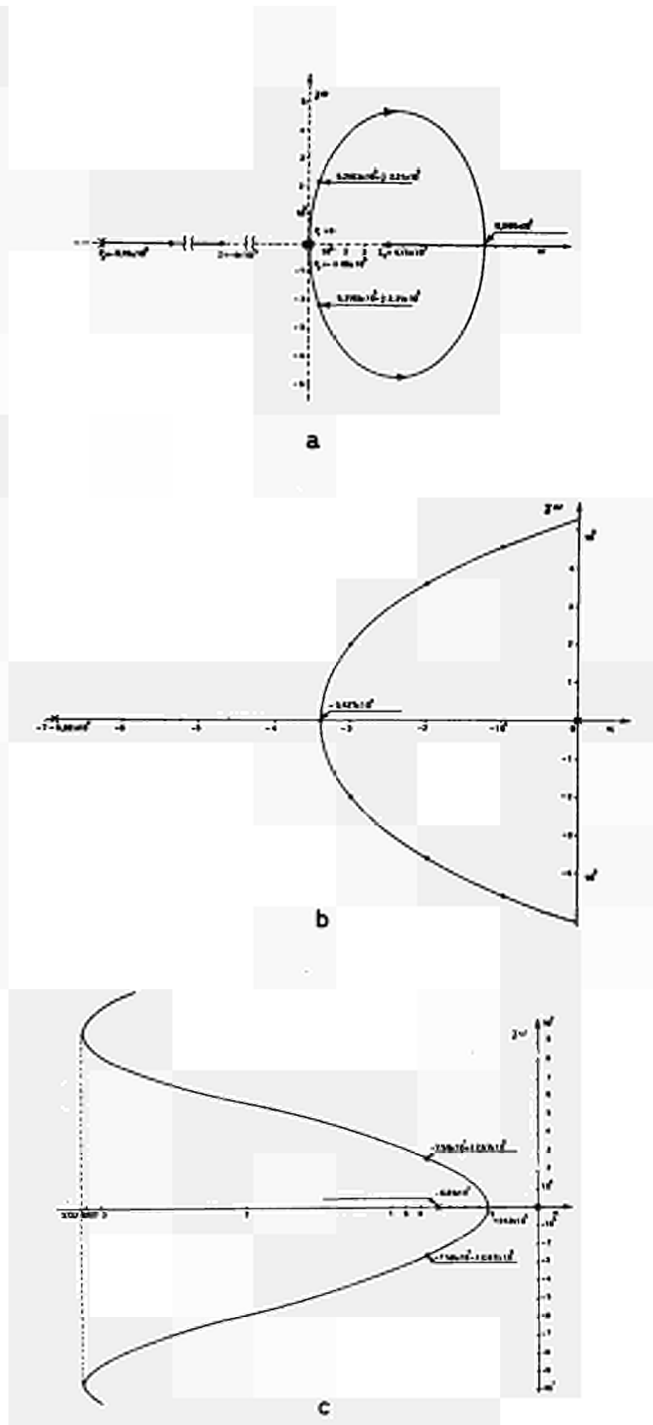

Fig. 5 Root loci for the stretcher of fig. 4

a) R = 50 Ω.

b) Same locus as a) but with expanded scale near the origin

c) R = 500 Ω

$$z_1 = -\frac{1}{RC} \qquad z_2 = \frac{\beta_1}{R_{B1} C_{BC_1}}$$

and the following open-loop poles:

$$p_1 = 0$$

$$p_2 \cong -\frac{1}{C_{BC,1}(1+\beta_1)R_{E2} + R_{B1}(C_{T1}+C_{BC1}) + C_2 R_{E2}}$$

$$p_3 \cong \frac{1}{p_2} \cdot \frac{1}{R_{B1} R_{E2} [C_{BC1} C_{T1} + C_2 C_{T1} + C_2 C_{BC1}]}$$

where the index 1 refers to the upper (high current) transistor and the index 2 to the lower one. C_2 and R_{E2} are respectively the total emitter capacitance $\frac{dQ_2}{dV_{EB,2}}$ and the dynamic d.c. resistance $\frac{dI_{E_2}}{dV_{EB,2}}$ of the lower transistor.

As now β_1 and R_{B1} refer to the high-current transistor, the real positive zero z_2 occurs at a higher angular frequency than in the previous case, which improves the closed-loop behaviour of the stretcher.

Again $|p_3| \gg |p_2|$, but p_2 now appears to be strongly affected by the Miller-amplified $C_{BC,1}$ capacitance. Depending on the value of $C_{BC,1}$ the pole p_2 can also occur at a lower frequency than in the previous case. So to eliminate this troublesome effect, the charging amplifier of fig. 7 is preferable, thanks to the high current cascode arrangement which drives the final low current grounded-base stage.

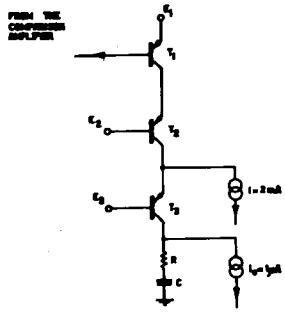

Fig. 7 Charging amplifier using three transistors

5 - Main features of COLDAC II analysis program[4,5]

This program has been developed for the time analysis through a digital computer of electrical circuits employing lumped components, both linear and nonlinear, active or passive, time-dependent and time independent. All the elements of the circuit must be described at a bypole level.

The program consists of three steps: input of data, analysis, output of results. The input of data has been studied for an efficient man-machine communication. Very simple rules for describing the circuits and an exhaustive error diagnosis make the system of easy use also for designers who are not experienced in programming.

Nonlinear and time-dependent devices are intended to by described by tables of numbers representing, for instance, the result of suitable measurements.

The analysis proceeds along the line indicated in a previous paper [4]; it takes advantage from Kron's method of interconnecting solutions and updating the solution matrix, from Kathzenelson's technique for solving nonlinear algebraic systems and it uses a variable-step integration subroutine.

A suitable data structure has been designed which is a compromise between a list structure and a matrix structure.

The program turns out to be very efficient and of general validity; it is believed to be competitive with those available at the present on modern digital computers.

The output plots the time diagrams and prints the values of the variables which are specified in the input instructions.

The program is implemented in FORTRAN IV on both IBM 7040 and UNIVAC 1108 of the Polytechnic School of Milan.

6 - Discussion of the results of the nonlinear analysis

The behaviour of the stretcher of fig. 4 has been analyzed through COLDAC II computer program, assuming as a first step a low value of both C_o and C_{BC} capacitances (2pF).

Fig. 8 shows the overswing in the stored voltage $v'_u(t)$ as afunction of the amplitude V_i^o of the input step for different values of the smoothing resistor R. As it appears from fig. 8 the amplitude of the overswing increases as R is reduced as it may be predicted by the linear theory.

It is more important, however, to observe that this overswing is practically constant as soon as the input amplitude V_i^o exceeds about 10 mV for $R > 100\,\Omega$. Note that a constant overswing does not affect differential and integral linearity. The input amplitude above which the overswing can be considered almost constant decreases when R is increased. For

values of R higher than about 1 KΩ no overswing exists and the accuracy of the stretcher in correspondence to an input rectangular pulse is only determined by its width .

We must point out, once more, however, that the absence of any overswing does not necessarily imply that the closed-loop poles are real.

The hypothesis of an internal oscillation which coupled with the unidirectional characteristic in the output current of the charging transistor gives rise to the observed overswing, has been tested assuming in the simulation program a transistor, ideally simmetric with respect to the base-emitter voltage.

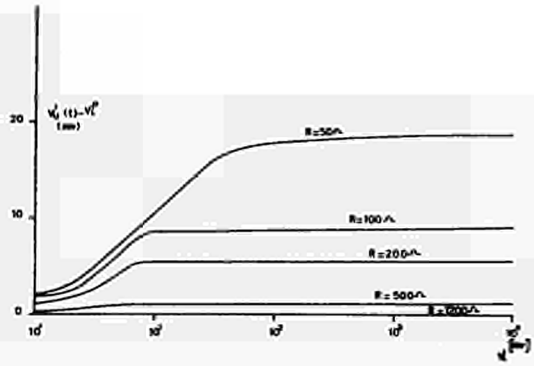

Fig. 8 Overswing amplitude $v_u^1 - V_i^o$ as a function of V_i^o with R as parameter

The almost linear damped oscillation which has been observed in this case across the storage capacitor has thoroughly confirmed the basic assumptions.

The period of this oscillation was of the order of 1.5 μs for R = 200 Ω . The knowledge of this period is important because it gives a however rough idea about the sensitivity of the overswing amplitude to the risetime of the input pulse.

Fig. 9 shows the same variable $v_u^1(t) - V_i^o$ of fig. 8 as a function of R for different values of V_i^o.

Fig. 10 shows the dependence on the input amplitude V_i^o of the time interval T elapsing between the leading edge of the input step and the time at which 90% of the stored voltage is reached.

This time T accounts for both the delay-time and the true risetime. The given curves are not suitable , indeed , for deducing with high precision the accuracy of the stretcher with input pulses of finite width, as these curves do not take into account the final part of the leading edge of the stored voltage, where the circuit is far more slow. They have only the aim of clarifying the dependence of the charging speed on R and on the amplitude of the input pulse.

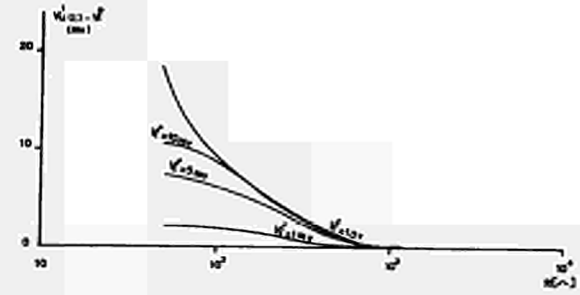

Fig. 9 Overswing amplitude $v_u^1 - V_i^o$ as a function of R with V_i^o as a parameter

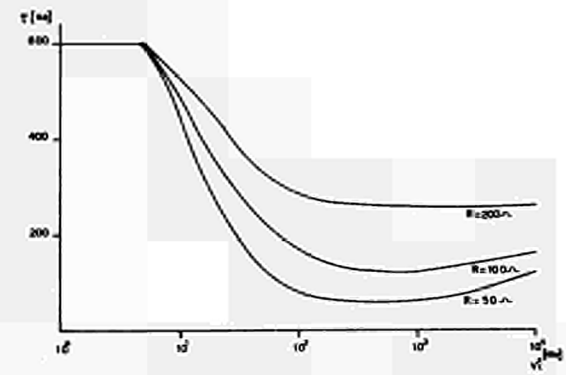

Fig. 10 Time interval T against V_i^o with R as a parameter

As fig. 10 shows, T is very high for small input pulses ($V_i^o < 10$ mV) because the working point of the charging transistor is in the low-current region. The strong dependence of T on V_i^o is due to the fact that with such small values of R, the stretching speed is mainly determined by the features of the feedback loop, and only to a negligible extent by the output time constant RC.

T increases with V_i^o in the final part of the diagram, owing to the saturated behaviour of the comparison amplifier at these voltage levels, and to the assumed dependence of f_β on I_c.

The given results confirm the previous theoretical predictions of the linear model according to which a high charging speed requires a working mode corresponding to low values of R and therefore

with an overswin g present in the stored voltage which limits the low-level accuracy.

We would like to point out, moreover, that the given figures agree well with the actual behaviour of stretchers using one charging transistor.

For better clarifying the intrinsic speed limitations of the stretcher of fig. 4 when a high accuracy for small input signals is required, a further analysis has been done.

A circuit with C_o and C_{BC} of 4 pF each and a smoothing resistor $R^o = 1,5$ K which ensures that no overswing appears, has been considered. To evidence the actual accuracy for rectangular input pulses, the time T' elapsing from the leading edge of the input pulse to the 99% of the stored voltage has been deduced.

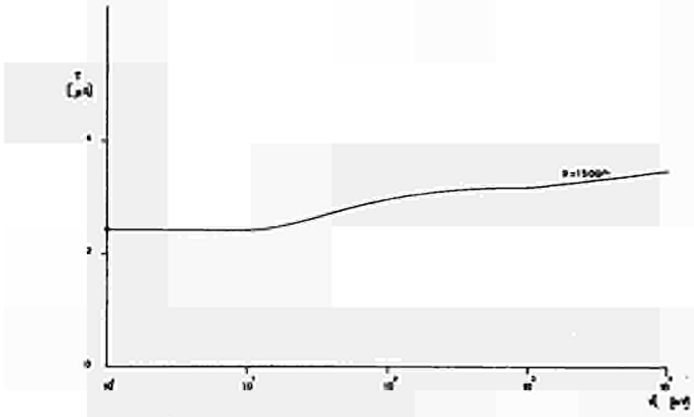

Fig. 11 Time T' against V_i^o

The statement given by the linear theory, according to which a charging amplifier using a simple cascode arrangement (fig. 6) does not improve appreciably the risetime when the values of C_{BC} are rather high, has been tested. As a matter of fact, the risetime is strongly limited, as previously pointed out by the dominant pole accounting for the Miller amplification of the collector-to-base capacitance of the high current transistor of the cascode.

In the stretcher using a 4pF-output capacitance comparison amplifier and a 4 pF C_{BC} charging transistor, a second transistor has been added, similar to the already existing, thus realizing the cascode arrangement. The value of R for no overswing has been found to be of the order of 1.2 K, which results in an improvement in the risetime with respect to the values given in fig. 11 of about 20%.

The stretcher using the charging amplifier of fig. 7 has been tested. Fig. 12 shows the time interval T' against V_i^o for the value R = 100Ω of the smoothing resistor which practically ensures the absence of any overswing in the stored voltage. The improvement for what both risetime value and risetime dependence on V_i^o are concerned is evident if fig. 12 is compared with fig. 10

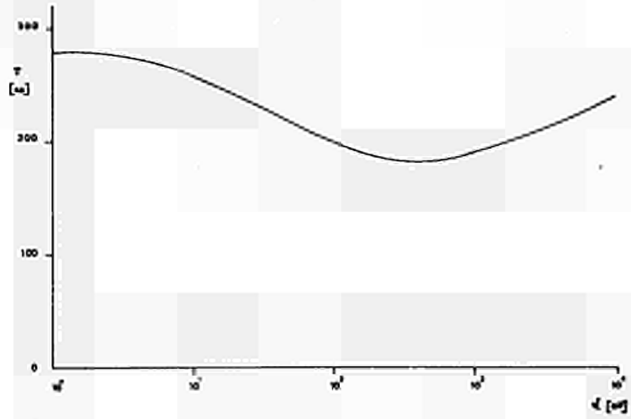

Fig. 12 Time T' against V_i^o for R = 100Ω in the case of a two grounded base transistor charging amplifier

The analysis made on the computer, therefore, confirms the experimental results of papers 1,2) according to which a current-driven unidirectional-output amplifier, even if the three transistor arrangement is used, is not suitable for stretching short input pulses (shorter than 100 ns).

The arrangement of fig. 13 using an emitter feedback in the charging transistor which works at a high current level and a low current diode in series with its collector had been found experimentally to be more suitable for pulse widths in the range of some 10 ns.

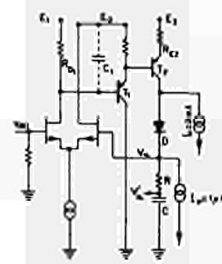

Fig. 13 Fast stretching arrangement

To improve the yet available experimental knowledge mainly for what the conflict between overswing and charging speed is concerned, computer analysis has been used. The storage capacitor has been lowered to 250 pF, while the transistors' and comparison amplifier characteristics were the same

as before. It has been found that also in correspondence of a smoothing resistor as low as 25 Ω no appreciable overswing has been detected. Fig. 14 shows the dependence of the total delay + risetime T' measured up 99% of the final value on the output amplitude.

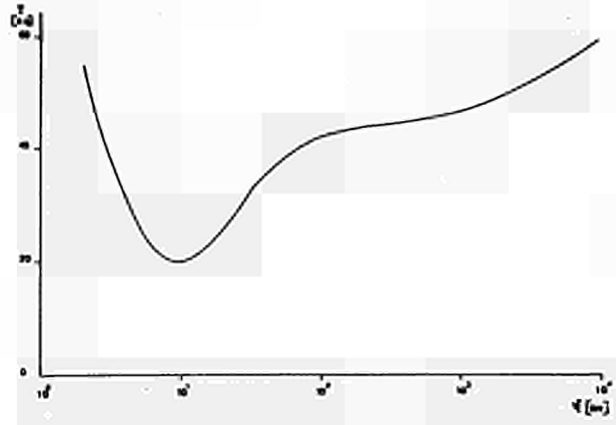

Fig. 14 T' versus V_i^o dependence for the stretcher of fig. 13

As fig. 14 well clarifies, stretching times of the order of 50 ns are compatible with a high accuracy on a 1000:1 amplitude range.

Acknowledgements

The authors would like to thank Prof. E. Gatti for the critical discussions and Mr. G. Perna for his support during the use of COLDAC II program.

Bibliography

1) P.F. Manfredi, P. Casoli: "On the design of pulse-peak stretchers" IEEE Trans. on Nuclear Science, NS-16, Feb. 1969, 392

2) P.F. Manfredi, P. Casoli: "Accuracy and charging speed in peak stretchers" to be published on Energia Nucleare

3) A. Alessandrini, A. Berruti, G. Massimello:"Brancaleone , a digital code for root loci determination" Report CISE-R219 - 1966

4) I. Alleva, I. De Lotto, A. Ghirardi, G. Valle: "Un sistema grafico per l'analisi circuitale" Alta Frequenza 37 (1968) 41

5) I. Alleva, I. De Lotto, P. Perna: "Coldac II, a general purpose network analyzer" To be published on Alta Frequenza .

DISCUSSION

Patzelt : - Do you think that this method is superior to the use of 2 similar stretcher--circuits in cascade, the first with a low value of the storage capacitor, to obtain a fast rise time ?

Manfredi : - In fact, the fast stretcher I showed before is intended as the first stage of a cascade connection of two stretchers, the second one being designed according to the actual holding-time requirements. As you may see, the storage capacitor of the fast stretcher has been lowered to 250 pF, thanks to the consideration you just mentioned, because in the first stage of the stretching chain we mainly worry about charging speed.

Miller : - I notice that your charging circuits employ charging from transistor collectors. Have you also analyzed the properties of circuits employing charging from transistor emitters ?

Manfredi : - Charging from a transistor collector is preferred, in fact it is more suitable for the particular configuration of the comparison amplifier we were looking at. For this reason, circuits employing charging from a transistor emitter have not received attention in our analysis.
I acknowledge that they could present some attractive features, provided that they are introduced in a proper feedback loop, i.e. a feedback-loop of the virtual-ground-comparator type. As these feedback loops are suitable, in fact, for pulse widths in the 1 μs range, they have been neglected in our analysis, which is mainly devoted to fast stretchers.

Koeman : - Since there is such a non-linear behavior in pulse stretchers, it is useless to speak about 10-90% rise time. I believe there must be specified how much time a stretcher circuit needs to reach the input pulse level within a certain accuracy - say 1:4000. There is no direct correspondence between the latter definition and the rise time 10-90%.

Manfredi : - I agree with you. The total (delay + rise) time measured from the leading edge of the input pulse up to the instant at which the voltage across the storage capacitor reaches a fixed fraction of its final value cannot be put in immediate correspondence to the figures which actually define the stretching accuracy. This point is also stated in Ref. 1,2. As a matter of fact, the curves given in Fig. 10 have the purpose of describing the behaviour of the circuit rather than of giving an accurate figure about its accuracy. However, the curves of Figs. 11, 12, 14 which refer to the monotonic working mode of the stretcher are more meaningful. For them the total (delay + rise) time has been defined assuming as reference level 99% of the final voltage

across the storage capacitor. For a given input amplitude, in this case, this time represents the width of a rectangular pulse beyond which the absolute accuracy of the stretcher, according to the definition given in Ref. 1, 2, is better than 1%.

Koeman : - With respect to thermal stability owing to the high available charging current, the FET's of the comparison amplifier have a large bias current ; they have for this reason generally a high temperature coefficient in the gate-to-source voltage. It may be difficult to maintain thermal stability if both devices are not thermally coupled strongly, even when dissipation is switched off during the time that no input signal is present or during processing.

Manfredi : - In reply to this question - a complete analysis is given in Ref. 2.

AN ANALOGUE-TO-DIGITAL CONVERTER EMPLOYING RECYCLED SUCCESSIVE APPROXIMATIONS

K. Kandiah, A. Stirling, D.L. Trotman,
Electronics & Applied Physics Division, Atomic Energy Research Establishment,
Harwell, Berkshire, England.

Abstract

The successive approximation technique is faster than most other methods of analogue-to-digital conversion. The main drawback is that it normally uses a multiplicity of high precision components. This paper describes a method in which the signal is recycled through the same conversion stage by using sample and hold circuits.

1. Introduction

Improved radiation detectors and low noise amplifiers continue to make greater demands on the accuracy and speed of analogue-to-digital converters (ADC's). Conversion using a linear ramp and a clock has the merits of simplicity and good differential linearity for clock frequencies up to about 100 MHz[1]. For modern nuclear spectrometers 8192 channels are sometimes required and the ramp converter is then rather slow. Converters using successive approximations are generally fast but most of them require a large number of high precision components[2]. The converter described here uses the successive approximation technique but the number of high precision components is kept to a minimum by recycling the signal through one conversion circuit. High accuracy can therefore be achieved with readily available components and with simple initial adjustments. The converter, in its present standard form, is limited in speed to about 26 μS for 13 bit conversion but arrangements for increasing the speed and accuracy are discussed at the end of the paper.

Pulse peak stretchers have traditionally been part of the ADC in nuclear spectrometers. Methods of improved signal processing, particularly for high counting rate conditions, have dictated a change in this practice. We have found it desirable to combine pulse amplification and signal processing in one unit which then feeds a flat topped signal with the necessary command for conversion to the ADC. This paper does not describe the signal processing unit.

2. The Method

All successive approximation methods use standard weights and a balance detector. In one of the usual methods for binary coding, a series of weights decreasing by factors of 2 are used, one for each bit in the conversion. In an alternative method the signal remaining after subtracting the standard weight, is amplified by a factor 2 and is tested again for the next significant digit. This process is then repeated n times for a conversion to an n+1 bit code. This latter method lends itself to recycling the signal through the same measuring circuits as in the converter described here.

The block diagram of the basic elements of the new converter is shown in fig. 1. The "follow and hold" circuits A and B are not essential for the coding process and their purpose will be discussed later when considering differential linearity. Let us first consider the case in which the signal, in the range 0 to -6V, is applied to that input of the "gated OR" which is normally fed from the output of "follow and hold" B. The purpose of the "gated OR" is to transfer the signal level into the measuring circuit at the start of the conversion and then provide a path for recycling the signal during conversion. It is therefore equivalent to a two-way switch. The coding for each consecutive bit is carried out under the control of "sample" pulses fed alternately to the "sample and hold C" and "sample and hold D" which have exactly unity gain. The number of bits in the code is one greater than the number of pairs of these "sample" pulses.

Let us now consider the conversion process in detail from the instant the input signal is transferred through the "gated OR" into the measuring circuit. The level discriminator has a threshold of -3 V. If the signal is more negative than -3 V a "1" is fed by the discriminator to the digit output point and to the weight generator which in turn feeds a fixed level of +3 V into the summing unit. If the signal level is more positive than -3 V the digit output is a "0" and the output of the weight generator is 0 V. This is the coding process for the most significant bit.

The conversion for the later bits takes place at the end of each cycle which consists of two parts. In the first part a "sample" pulse is applied to "sample and hold C" whose output appears at the other input of the summing unit, immediately after the "sample" pulse. The summing unit adds the output of the weight generator and the signal at the output of the "sample and hold C". Thus for a signal voltage of E the output of the summing unit, hereafter called the remainder, is (E+3) when the previous bit is a "1" and E when it is a "0". The second part of the cycle consists of a "sample" pulse applied to "sample and hold D" which presents the remainder, through the "gated OR", to the measuring circuit in order to determine the next bit.

In an ideal situation it is desirable to have high speed, good integral and differential linearity and stability. The accuracy is determined by

(i) zero stability, linearity and gain stability of the sample and hold circuits, the X2 amplifier and the summing circuit,

(ii) the threshold stability of the level discriminator,

(iii) the stability of the weight generator.

The speed is limited by the slowest of any of the units. The functions of summing and amplification by a factor 2 are obtained in the "sample and

hold C" circuit which differs from "sample and hold D" only in the addition of two high precision resistors. It will be shown later that these sample and hold circuits have extremely high gain at low frequencies so that the only error they contribute is due to their limited speed. Similarly the accuracy of the level discriminator and the weight generator become limiting factors only at high clock rates.

3. The Sample and Hold Circuit

The basic circuit is shown in fig. 2. It uses a long-tailed pair of matched transistors J_1 and J_2 to compare the input and output levels and feed an error correcting current through the common base amplifier J_3 to the holding capacitor C. The voltage on this capacitor is fed to the output through a buffer stage with a gain of approximately 1 using an FET input. The circuit is in the "sample" or "follow" mode when the gate inputs are disconnected from the emitters of J_3 and J_4. It behaves like a fed-back amplifier with a closed loop gain of exactly 1 at low frequencies because of the large open loop gain ($>10^5$). The loop is unconditionally stable when the capacitor C is large enough. If the currents through J_3 and J_4 are suddenly switched to zero by the gate inputs, the output voltage will remain steady at the value that existed at the input just before this switching, apart from a small droop due to the difference between the collector leakage currents of J_3 and J_4.

For signal steps of the order of millivolts the response of the system on "follow" is that due to a time constant of 100C/I where I is the sum of the emitter currents in the long tailed pair in mA. Since the values of C and I are typically 1 nF and 4 mA the system response to small signals has a time constant of about 25 nS. For larger signals the time constant increases and ultimately the rate of change of output is limited by the maximum current I/2 available to charge the capacitor. Taking the above values for C and I this gives a slew rate of 2V/μS. Since the full scale signal level is 6 V this will require "sample" pulses of not less than 3.1 μS for a 12 bit conversion dictating a minimum clock period of 6.2 μS.

The slew rate is improved by means of complementary emitter followers which increase the current available to charge or discharge the capacitor when large error signals are present. The complete circuit incorporating this feature, the X2 amplification and the subtraction of the "weight" is shown in fig. 3. TR1, TR8 and TR9 have the same functions as J_1, J_2, J_3 and J_4 of fig. 2. The error current from the collector of TR8 flows through R_{15} which then develops the necessary voltage to drive the complentary emitter followers TR6 and TR7. The resistor R_{14} in series with the holding capacitor C_1 ensures a monotonic response and D_2 is a protection diode. TR5, TR4 and TR3 form the buffer stage between the capacitor and the output, giving very high input impedance and low output impedance. R_5 and R_6 provide the gain of 2 to the output and also present the correct impedance of 100Ω to the negative "weight" current of 30 mA which is fed into the junction of these resistors. In order that the switching of these "weight" currents does not overload the buffer amplifier the junction of the resistors R_7 and R_8 is fed with the "complement" of this current by the weight generator. TR2 provides constant emitter current for the long-tailed pair TR1. TR10 and TR11 are used to switch the circuit to the "hold" condition by means of a positive voltage applied to the base of TR10. During the "hold" condition the current in TR2 is also cut off through D_3 in order to eliminate differential heating in TR1.

The circuit will depart from a simple or ideal behaviour for a number of reasons and adjustments to compensate for the important errors are provided. The offset voltage in TR1 will introduce a zero error and this is corrected by adjusting the current in one collector by means of RV1. Another cause of zero error is that due to the difference in the times at which TR8 and TR9 are cut off when going to "hold". This can be due to differences in current gain or cut off frequency of TR10 and TR11 and due to stray capacitance from the emitters of these transistors to various points of the circuit. This switching error causes a step in the output voltage when going to hold and causes differential non-linearity in the channels whose boundaries are determined by the more significant bits. This switching error is compensated by means of the small capacitor C_2. Without these two adjustments there will be channel widths which have more than ± 50% error on a conversion to 10 bits. With the compensations suitably adjusted these errors are tolerable up to 14 bits.

There are other second order effects which affect speed and accuracy in combination. The most serious, in most of the models of the equipment already made, is that due to charge absorption in the material of the insulating board which is used to construct the unit. This shows itself as a partial loss of charge from C_1 when the circuit is put into the "hold" condition immediately after a step signal is applied to it. With C_1 at 1 nF the loss of charge is about 0.02% with a time constant of between 2 and 5 μS. Since the sample and hold circuits are in the "hold" condition alternately for slightly longer than half the clock period this error becomes appreciable for clock periods of 2 μS or greater. The use of a larger capacitor for C_1 will reduce this effect but the time taken to charge the capacitor to full scale is also increased in proportion so that the clock period will have to be increased. A larger capacitor leads to a larger error due to increased differential heating of TR1 during the charging of the capacitor.

In the "follow" condition the output voltage is equal to twice the input voltage within the tolerance of the resistors R_5 and R_6 which have a relative accuracy of much better than 0.01%. When a step input is applied the output voltage comes within 1 mV of the correct value in about 0.35 μS and within 0.2 mV of the correct value in about 0.5 μS as observed with a good oscilloscope. These times determine the shortest "sample" pulses that can be used in appropriate cases.

4. The Level Discriminator and Subtractor

It has been stated that the weight consists of 30 mA fed into 100Ω. The discriminator should therefore have a threshold of exactly -3 V. It

was convenient to generate a reference voltage of -5 V and obtain the correct threshold for the discriminator by an attenuator as shown in the circuit of fig. 4. The input is applied through a series resistor of 1 k to one base of the matched pair TR1 while the reference of -3 V is applied to the other base. The error is amplified and appears at the emitter of TR4 with a gain of 1000 at low frequency.

In order to reduce differential heating in TR1 it was felt desirable to apply feedback in order to maintain constant power dissipation in these transistors. This feedback is applied through D_1 and D_2 in parallel so that the emitter voltage of TR4 rapidly changes by about 0.72 V when the input signal crosses threshold. The rate of change of output is limited by C_1 which is required to maintain closed loop stability. The time taken to obtain the full output voltage change when the input exceeds the threshold by only 1 mV is almost 1 μS. This is the factor which limits the speed of the present converter to 2 μS clock periods for 13 bit conversion. We have not found a standard discriminator or comparator which combines the necessary speed and freedom from thermal effects but a new design is now being tested.

The output of the discriminator is used to control the current flow from an accurately defined current source of -30 mA into the "subtract" and "complement" inputs in fig. 3. When a "1" is present at the output of the discriminator a current of -30 mA is fed into "subtract" and 0 mA into "comp". When a "0" is present the situation is reversed. The presence of the current for a "1" will subtract -3 V from the output of the sample and hold circuit of fig. 3. It should be noted that the resistors (R_5, R_6 in fig. 3) used to obtain amplification by an exact factor of 2 are also the resistors used to generate the subtract "weight" when an accurately defined current is fed into them. The only high precision resistors required are therefore R_5, R_6 and the resistor which converts a reference voltage to a current for the "weight".

The low frequency stability of the discriminator threshold and subtract currents are determined by the usual transistor parameters such as current gain and stability of emitter base voltage difference of matched pairs of transistors. Using well chosen standard transistors these effects together will not be greater than 10 p.p.m./°C. The limited switching speeds of these circuits may introduce errors at high speeds due to variations in clock periods etc., which are determined by standard integrated circuits, and these may well amount to another 10 p.p.m./°C at clock periods of about 1.5 μS.

5. Differential Linearity

The main disadvantage of successive approximations is the possibility of large errors in channel width at or near the channels bounded by the more significant bits in the converted code. These may arise in the present unit due to the following factors:-

(a) relative error between the discriminator threshold and the "weight" i.e. error in obtaining the remainder,

(b) error in the amplification of X2 and the non-linearity of the "sample and hold" circuits,

(c) errors in the voltage transferred from one "sample and hold" circuit to the next during the recycling process.

The discriminator threshold and the subtract current are each set up with a high resolution multiturn potentiometer whose sensitivity of adjustment is approximately 30 p.p.m. in the standard converter. This may lead to about 25% channel width error at the most significant bit boundary for 13 bit conversion. The stability of these settings is such that the change of channel width will be less than a further 5% under normal laboratory conditions.

The non-linearity in the "sample and hold" circuits when using long clock periods is too small to be measured. The X2 amplification depends on the relative value of R_5 and R_6 (fig. 3) and these can be guaranteed to 50 p.p.m. with standard components and about 10 p.p.m. with special selection. It is seen that this could lead to a channel width error as much as 40% in 13 bits with standard resistors and 8% with special selection. We have not found it necessary to use specially selected components or adjustments for normal applications.

The error in the voltage transferred from one "sample and hold" to the next has been found to be the main cause of differential non-linearity. As mentioned earlier charge absorption in the dielectric of the board on which the ADC is made leads to a loss of voltage on the holding capacitor after going to "hold" and results in about 100% channel width error on 13 bits i.e. there is one channel whose width is double the average and another which is zero. By mounting the components which are directly connected to the holding capacitor on good insulators this effect can be eliminated. This leaves smaller errors due to differential heating in TR1 (fig. 3) which contribute about 20% channel width error on 13 bits using a 2 μS period for recycling.

In order to reduce the actual channel width error, which lies between ± 40% for 13 bit conversions in all the units made so far, to somewhat less than 1% a simple method is used which relies on the addition of a random voltage to the base-line. Each measurement then consists of conversion of the base-line voltage just before the pulse arrives and a second conversion of the total voltage of the pulse with the added base-line voltage and taking the difference between the two digital codes. This method differs from that originally proposed by Gatti[3] in that no digital to analogue conversions are involved and the same ADC is used to obtain the two codes. The main attraction of this method is its inherent simplicity and the absence of any further high

precision components. The purpose of "sample and hold A" and "sample and hold B" in fig. 1 is now apparent. "Sample and hold B" is switched to hold just before the pulse and this voltage is converted into the appropriate code. At a suitable time, in the meanwhile, when the input pulse has a flat portion "sample and hold A" is switched to hold. When the first conversion is complete the second voltage is inserted through "sample and hold B" into the system in order to obtain the second code.

This method of improving the differential linearity has many of the problems associated with any form of the sliding scale method. It is necessary to choose the range of the random base-line voltage and its rate of change to match the known non-linearity of the basic converter. In our converter the base-line is moved by a constant small step after each pulse and when the amplitude of this staircase reaches a predetermined value the direction of the staircase is reversed and this goes on until the voltage reaches zero when it is reversed again. In effect a sawtooth voltage of constant peak-to-peak value is added to the base-line. It can be shown that this method always increases the measured line width of any spectrum by a small amount. This effect can be reduced if the conversion for each of the two voltages is carried out to say two bits more than the desired code and the two least significant bits are ignored after the subtraction of the codes. Thus the actual conversions are to 15 bits but only the more significant 13 bits are finally used.

It is evident that the simplicity of this method is obtained only at the cost of a large increase in dead time after each input pulse. By using the conventional sliding scale method with an auxiliary register and DAC the dead time of the converter will be about 26 μS for 13 bits. However since we convert to 15 bits twice, the total dead time will be about 60 μS. Since this still permits a reasonably high count rate capability, taking into account the facility for queing of signals provided by the sample and hold feature, the system is satisfactory for most applications.

6. The Digital Logic and Control

The basic control system for the converter consists of a two-phase clock. A shift register is used to store the code since it appears in serial form. The method of improving differential non-linearity discussed above requires an adder. In the present converter the adder is required to operate on a serial number in which the most significant digit appears first. We use the method proposed by Cooke-Yarborough[4] which has an essential simplicity when using custom designed binary circuits. Since we use standard TTL integrated circuits the simplicity is lost and a penalty in speed owing to propagation delays in the circuits is also paid. However it is sufficient for clock periods down to 1.5 μS.

Since it is essential to strobe the level discriminator at a suitable time and to provide gating facilities for the serial adder it is necessary to use a four-phase clock. Having built a fairly sophisticated digital system for these purposes it is a relatively simple matter to introduce additional digital control of the output code. Thus digital back-bias is achieved by inserting this number into the adder just before conversion. Additional digital processing built into the converter includes the ability to select any channel for the stabilisation of gain as determined by a spectral line or artificial pulse and similar arrangements for zero stabilisation. All these numbers can be strobed into the converter at the beginning of the conversion and can be changed from event to event if necessary so that the converter can serve multiple signal processing units. Further details of the logic and the digital processing system will be described elsewhere.

7. Overall Performance

All measuring systems are limited in performance at least by the inherent noise. A simple method of measuring the noise is to increase the number of bits in the conversion and look at the line width of an input level which is free of noise. When using 15 bits the system will count most of the time only in one channel indicating a peak-to-peak noise of less than 180 μV referred to the input. By looking with an oscilloscope at the analogue voltage on one of the sample and hold circuits during such a conversion it can be seen that about half of this is due to ripple at the mains supply frequency.

The temperature affects the calibration of the instrument to a limited extent. The zero changes by about 20 μV/°C and full scale by less than 20 p.p.m./°C. The temperature rise of the bulk of the equipment is only 15°C above ambient and therefore permits the use of standard low price components. The time constant of this temperature rise has two components - one of a few minutes and another of about one hour. When switching on from cold the time for the zero and full scale code to settle down, as measured by noting the automatic zero and gain stabilising voltages, are summarised in Table I.

Table I

Settling Time for Full Scale and Zero When Switching on from Cold with Constant Ambient Temperature

Time	1 min.	5 min.	10 min.	15 min.	>1 hour
Zero error (μV)	900	200	<100	<100	<100
Error at full scale (p.p.m.)	400	150	80	60	<20

Both full scale and zero are relatively unaffected by pulse rate but some units have shown a change of nearly 40 p.p.m. at full scale for a change of rate from 500 Hz to 10 kHz.

The differential non-linearity will be much less than 1% provided the test procedure does not contain unfortunate relationships between any two

of the numbers such as pulse rate, number of pulses for each scan of the base-line randomising voltage, and the sweep rate of the test pulse amplitude. A sensitive method of detecting irregularities is to use the method devised in this laboratory for measuring the noise performance of complete head amplifier-spectrometer systems. Test pulses of two fixed amplitudes with equal frequency at each amplitude are analysed by the system. If the amplitudes are sufficiently near to each other the spectrum will have two peaks with a valley above zero counts. If the ratio of the counts in the peaks and in the valley are measured the noise can be related to the known pulse separation by the calibration in fig. 5 assuming gaussian distribution. It is seen that small changes of the order of 1% in noise level give measurable changes in the peak/valley ratio. Irregularities in channel width show up as marked asymmetry of this double humped spectrum.

8. Discussion

It is now possible to consider the merits and disadvantages of the new converter. It has already been noted that by using a method of reducing non-linearity which involves two additional bits and two complete conversions per event the dead time is not much less than the fastest ramp type converter that can be made. It should however be noted that the absolute accuracy of our converter is much better than any reported so far and the range of signals can be extended down to zero.

The real merit lies in the small number of high precision components and the simplicity of the setting up procedure. Neglecting the components in normal power supplies, which are not critical in any case, the setting up of the reference voltages for the level discriminator and the subtract generator requires two sets of high stability but not high precision resistors and two high resolution potentiometers in order to take up the voltage tolerance of the zener diodes. These two controls can be set up with a digital voltmeter as a monitor.

Three high precision high stability resistors determine the X2 amplification and the weight and these have such a small initial tolerance that no adjustment is required. The temperature coefficient of these components is such that they are not limiting factors in the performance.

The only other adjustments are those mentioned in connection with the "sample and hold" circuits. There are four preset adjustments which require a sensitive oscilloscope for monitoring and which can be set up in a few minutes.

A common property of all successive approximation methods is that, for a given accuracy and stability, the magnitude of the weight and the minimum coding time for any bit depends on the number of bits to follow in the conversion. It has been our target to maintain channel width errors, before correction, to less than 25% and the maximum drift in a working day to a small fraction of a channel. Considerable relaxation of this target is tolerable in most practical situations. Under these conditions we have achieved conversion times of 8 μS for 11 bits, 12 μS for 13 bits and 18 μS for 15 bits but we have not found it necessary to offer these speeds in the standard instrument. When charge absorption in the dielectric is eliminated and with an improved discriminator we expect to be able to maintain the high speed and accuracy. It is our opinion that further improvement in speed will require the use of other techniques.

References

1. Gere, E.A. and Miller, G.L. I.E.E.E. Trans. Nucl. Sci. NS-13, No. 3, p.508, June 1966.

2. Robinson, L.B., Gin, F. and Goulding, F.S. Nucl. Instr. and Meth. 43, p.237, July 1968.

3. Cottini, C., Gatti, E. and Svelto, V. Nucl. Instr. and Meth. 24, p.241, 1963.

4. Cooke-Yarborough, E.H. Electronic Letters, I.E.E. Vol. 3, No. 2, p.77, February 1967.

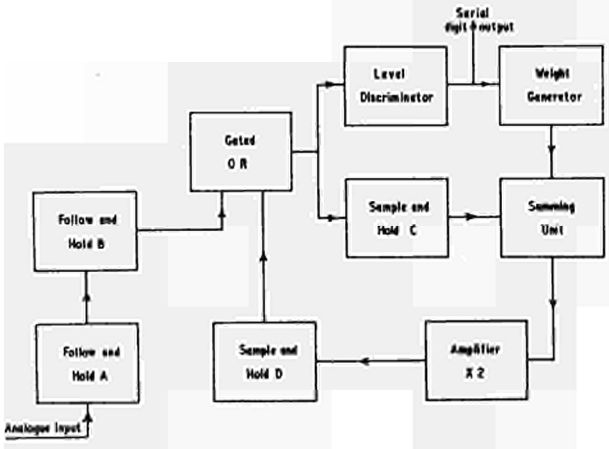

Fig. 1 - Block diagram of analogue to digital converter.

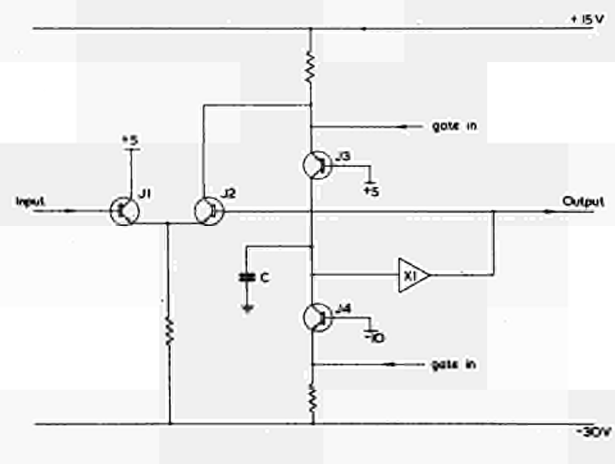

Fig. 2 - Sample and hold circuit.

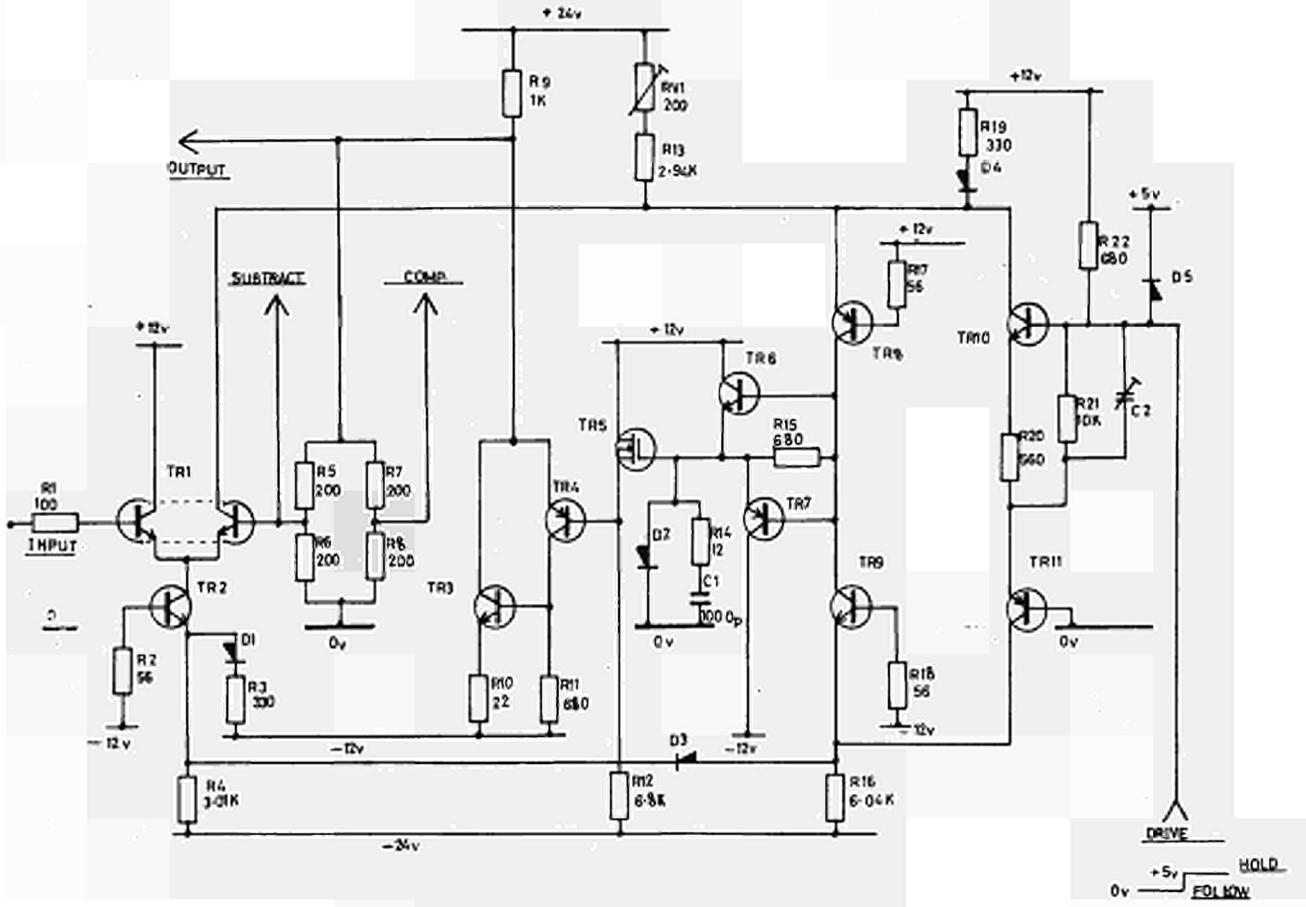

Fig. 3 - Sample & hold, amplifier (X2) & Subtractor.

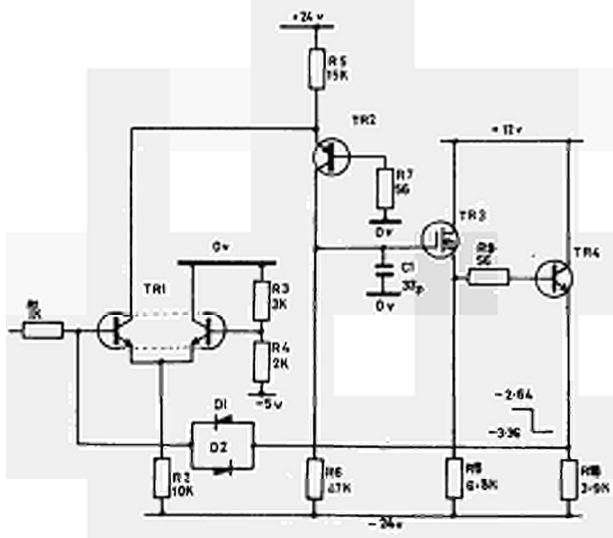

Fig. 4 - Discriminator

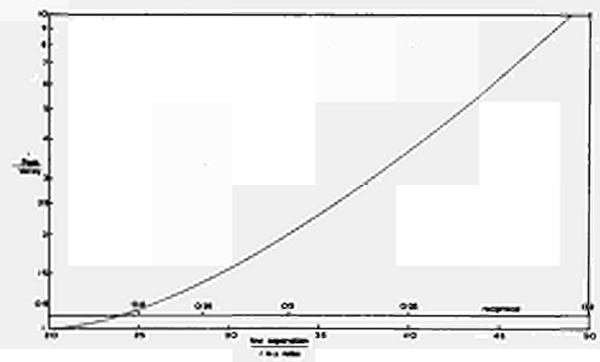

Fig. 5 - Peak/Valley Ratio of Spectrum with Two Superimposed Gaussians of Equal Intensity.

A NORMALIZING ADC FOR USE WITH POSITION SENSITIVE DETECTORS

G.L. Miller

Bell Telephone Laboratories, Incorporated
Murray Hill, New Jersey

and

A. Senator

Rutgers, The State University
New Brunswick, New Jersey

Summary

Position-sensitive detectors based on the principle of resistive charge division require a normalizing operation in order to extract the position information. In the present case this operation is carried out within a special ADC, whose inputs are the detector output signals and whose output is the normalized digital position information. The conversion is carried out by using a ramp ADC in which the position signal defines the peak voltage on a stretcher capacitor, while the total charge signal defines the rundown current.

The entire system, from the preamplifier inputs to the digital output, is servo-stabilized. This is achieved by periodically injecting reference pulses of fixed and known amplitude ratios into the preamplifier inputs. These reference signals correspond to two fixed positions on the detector, and the servo stabilizer demands that these positions correspond to two preassigned channel numbers.

Electrical tests indicate a precision of ~ .1% for a 2 to 1 range of total signal charge, while tests with 12 MeV deuterons (using an 80 cm long proportional counter) give a FWHM position resolution of ~ .2%

Introduction

The principle of position sensing by the use of resistive charge division is well known and has been employed in numbers of instances[1-6]. For high-resolution applications it has proved necessary to provide a dividing or normalizing operation in order to extract the position information, and this has been performed by a variety of analog techniques.

This situation has recently been modified, at least in principle, by the increasing use of on-line digital computers, enabling the required division to be performed numerically inside the machine. Two factors militate against this, however, namely that two high-resolution ADC's are required (to avoid quantizing errors), and that most small computers are not delivered with a high-speed divide capability. A programmed multiplication or division, on the other hand, commonly takes of the order of a millisecond, implying a corresponding reduction in the system counting rate. Bearing in mind that high-resolution applications (~ .1% or better) also require some form of servo stabilization, it is clear that the maximum counting rate would be still further reduced if the appropriate corrections were to be made arithmetically on an event by event basis.

The boundary conditions for the present development were therefore to attempt to provide a simple servo-stabilized system with a position resolution of ~ .1% and an operating speed at least an order of magnitude greater than that provided by an on-line programmed division. The detector for which the ADC was built is an 80 cm long gas proportional counter mounted in the focal plane of a magnetic spectrograph at the Rutgers University Nuclear Physics Laboratory, (to be reported in detail elsewhere[7]). However, the system is thought to be applicable to a wide range of position-sensitive detectors based on resistive charge division.

The electrical connections to the detector and preamplifiers are shown in fig. 1, where x is a normalized position co-ordinate ranging from 0 to 1, and Q_T is the total signal charge. After suitable shaping and amplification it is the xQ_T and Q_T signal that must be divided, one by the other, to provide the position information.

The Rundown Unit

An examination of the division schemes reported in the literature to date indicates that quite good performance has been achieved by dividers of the $t = Q/i$ type[6,8,9]. None of these has so far been stabilized, however, and all involve a height-to-time-to-height process to provide an output amplitude to be digitized by an external ADC. The latter then performs a height-to-time conversion of its own to provide an overall process of height-to-time-to-height-to time.

For this reason it was decided to investigate the relatively simple scheme shown schematically in fig. 2 in which the $t = Q/i$ process is involved

only once, in a ramp ADC, to provide the normalizing and digitizing functions simultaneously. Here the stretcher capacitors C_1 and C_2 are charged to the peak of the xQ_T and Q_T signals via the (amplified) diodes D_1 and D_2. (All buffer amplifiers, switches, etc., have been omitted from the diagram for clarity.) At a suitable time after the peak of the Q_T signal, a current proportional to Q_T, and defined by the voltage on C_2 divided by R, is used to provide a linear discharge of C_1. The rundown time of C_1 is then a direct measure of the position x.

The mode of operation of the circuit that provides the rundown current can be clarified with the help of fig. 3. In fig. 3(a) is shown a conventional negative feedback circuit in which all the input signal current flows through β from the amplifier output. Figure 3(b) shows a similar situation except that the current required to balance I_{IN} is now provided by a voltage-controlled (i.e. high input impedance) device labelled G_m. The essential difference between fig. 3(a) and fig. 3(b) is that, in the latter case, the current required to balance I_{IN} flows from an external source rather than from the amplifier output. For this reason 3(b) has been dubbed a "negative feedby" circuit[11]. (It is worth noting in passing that a wide range of current-current transfer functions can be realized in this way by using the modification shown in fig. 3(c)).

This scheme can be used to provide high quality controlled current generators except for the unavoidable initial charging transient of the G_m element itself. This is unimportant in the present application, however, since the rundown current is only steered into C_1 after the feedby loop has settled.

The operation of the xQ_T loop is shown schematially in greater detail in fig. 4. Quiescently the gate and feedby current generators are off while the dump generator is on. The dump current is carried by D_1 and A_1, and the entire loop is operating in its linear range. As a pulse enters the Q_T stretcher (similar to that shown in fig. 4 but inverted), it trips a low-level discriminator which rapidly turns off both the Q_T and xQ_T dump generators during the rise of the pulse. After the peak of the pulse has passed, D_1 turns off and D_2 turns on, which information (from the Q_T channel) is used to turn on both the Q_T and xQ_T gate current generators and simultaneously to start the rundown. An appropriate time after the end of rundown (signalled by the computer) the gate and feedby generators are turned off and the dump generators turned back on, rapidly resetting the system to its initial quiescent state. Examination of this scheme of ADC operation reveals that it is independent of the time constants of the input signals and also simplifies a number of other problems since it does not require an external linear gate.

The A_1 loop is conventional, employing a grounded emitter stage, operating with a dynamic load, which drives an emitter follower to charge the stretcher capacitor. The unity gain loop A_2 provides constant power operation of its input FET in a simple way. This feature is important in avoiding thermal transient effects, and the scheme employed is shown in fig. 5. Here the FET source-drain voltage is bootstrapped, and constant, while the source-drain current is also substantially constant because it is primarily the current through R_1, which itself operates at constant voltage.

These loops, which have been found to be exceptionally stable and well behaved, employ 1500 pf stretcher capacitors, can be charged to 8V in $\sim .5\ \mu s$, and exhibit overall charge and rundown nonlinearities of less than .1%. The droop on the Q_T stretcher during the maximum holding time of $\sim 130\ \mu s$ is less than .01%.

The rundown unit is constructed on a single card and is mounted in a single width NIM module.

The Servo Pulse Generator

Servo stabilization of the entire system is carried out by injecting reference pulses into the preamplifier inputs at the rate of ~ 100 per second. The reference pulse generator is mounted close to the preamplifiers, and is shown schematically in fig. 6. Quiescently switch S_3 is closed while S_1 and S_2 are open. As S_3 is opened either S_1 or S_2 is closed, which thereby steers the current I_S from R_4 into one of the two taps on R_1, R_2, R_3. In this way reference pulses of opposite polarity are generated simultaneously and injected into the two preamplifier inputs.

The values of R_1, R_2, R_3 are chosen so that the the two xQ_T pulse amplitides are in the ratio 1 to 8. In this way the system is led to believe that "particles" enter alternately at positions $x = 1/8$ and $x = 1$, thereby providing servo reference peaks in the position spectrom at channels 128 and 1024.

It is noteworthy that the absolute magnitude of the reference pulses are unimportant, it is only their ratio that must be held constant. This factor is used to advantage by providing an intentional slow sweep on the reference pulse amplitudes. The mean value of the amplitude is set to correspond roughly to the particles of interest (since the gas detector corresponds to dE/dx) while the sweep amplitude is set to span an appropriate range of signal amplitudes. In this way the amplitude independence of the division process can be continuously monitored while data are being accumulated.

The Digital System

The time gate signal from the rundown unit controls a clock oscillator which drives a ten bit address scaler as shown in fig. 7. The use of a simple clamped oscillator is not usually considered good practice in high quality converters because their frequency tends to "chirp" as they equilibrate after turn-on, resulting in serious ADC nonlinearities. In view of their appealing simplicity, however, it was considered worthwhile to see if this performance defect could be

removed. Working on the assumption that the chirp was probably of thermal origin, the oscillator of fig. 8 was investigated. Here Q_1 and Q_2 form an emitter-coupled multivibrator, while the saturating switch Q_3 provides the clamping action. It is clear that the average power dissipated by Q_1 and Q_2 is the same whether the loop is oscillating or clamped. The long-tail pair Q_4, Q_5 comprises an output buffer amplifier, and simultaneously provides for a non cycle-slicing oscillator turn-off. This feature follows from the fact that the input to D_1 is held low while the loop is oscillating, keeping Q_3 off, while when the gate input goes high Q_3 does not turn on unless, or until, Q_4 does so. It is of course important to choose VZ_1 slightly greater than VZ_2 to ensure proper clamping action. In addition to the non-slicing feature the loop always starts oscillating in the same phase. This follows from the fact that the emitter of Q_3 is released first as the transistor comes out of saturation, while the collector of Q_3 is momentarily pulled negative by the collector-base charge storage action. The use of this form of synchronously clamped constant-power oscillator results in measured nonlinearities of $< .1\%$ in the converter performance.

In addition to the foregoing properties, the oscillator is frequency-controlled to provide stabilization of peak location along the position-sensitive dimension of the counter. This feature is conveniently provided by the use of diodes D_2 and D_3, together with the controlling current source. Increasing control current decreases the voltage excursions across R_3 and R_4, thereby raising the oscillator frequency in a linear manner. The mean clock frequency is ~ 8 MHz, while the frequency control range is of the order of $\pm 10\%$. (This relatively low clock frequency was chosen to simplify and economize in the design of the digital system which uses slow, low-cost, microcircuits throughout. It is not, however, in any way fundamental to the system operation.)

Returning to figs. 2 and 7 it can be seen that the servo-stabilizing action closely parallels that of a previously reported system[10]. Servo pulse control signals are sent to the reference pulse generator, while just prior to this the rundown unit and digital system have been cleared and set to zero in readiness to accept the servo information. Following conversion, bit 7 or 10 is interrogated (depending on whether it was an $x = 1/8$ or $x = 1$ servo event), and one of two holding integrators is approximately incremented or decremented. (These integrators are simply 1 μf capacitors connected to FET source followers which provide the servo output directly.) The integrator outputs are used to control the clock frequency ($x = 1$ events), or the end of rundown level ($x = 1/8$ events). Servo events also set a tag bit in the output word sent to the computer, allowing servo peaks to be stored in, and displayed from, a separate region of the memory.

The digital unit consists of two cards and is built in a double-width NIM module. This module is also provided with two front-panel meters indicating the state of the servo integrators.

Performance

Using electrical pulses to simulate detector signals the ADC position linearity has been shown to be .1%. In the same tests the position address itself was found to shift by $\sim .1\%$ for a 2 to 1 range of total signal charge amplitude Q_T.

Using 12 MeV deuterons incident on an 80 cm long gas proportional counter at 45°, a position linewidth of 1.6 mm FWHM was obtained while accepting a 2 to 1 range of Q_T signal amplitudes. This corresponds to a position resolution of .2% for the length of the detector.

Acknowledgements

It is a pleasure to acknowledge the contribution of M. Allen, E. Bretz, and C. Olah, of the Rutgers University Nuclear Physics Laboratory in the construction and testing of the system, and to thank the Laboratory Director, Prof. G. Temmer, for his constant interest and support.

References

1. E. Norbeck and R.C. Carlson, Nat.Acad.of Sci. Pub. NRC 1184 (1963) 42

2. E.J. Ludwig, W.M. Gibson, and J.S. Hood, IEEE Trans.on Nucl.Sci. NS-12 (1965) 247

3. E.J. Ludwig, RSI 36 (1965) 1175

4. G. Kalbitzer, R. Bader, W. Melzer, and W. Stumpfi, Nucl.Instr.Meth. 54 (1967) 323

5. G. Kalbitzer and W. Melzer, Nucl.Instr. Meth. 56 (1967) 301

6. R.B. Owen and M.L. Awcock, IEEE Trans.on Nucl.Sci. NS-15 (1968) 290

7. J. Fischer, G.L. Miller, N. Williams. A. Senator, and R. Stensgaard. To be published

8. M. Tsukuda, Nucl.Instr.Meth. 25 (1964) 265

9. P.K. Patwardhan and V.S. Indurkar, IEEE Trans.on Nucl.Sci. NS-15 (1967) 323

10. E.A. Gere and G.L. Miller, IEEE Trans.on Nucl.Sci. NS-13 (1966) 508

11. E.A. Gere, H.P. Lie, and G.L. Miller, IEEE Trans.on Nucl.Sci. NS-14 (1967) 161

DISCUSSION

Maeder : - Have you considered using an exponential discharge to measure the ratio of two signals ? If one signal is discharged exponentially from its peak value using an RC circuit, the time it takes to fall to the value of the other signal is a measure of the logarithm of the pulse ratio.

Miller : - *The system you propose has been used and is in the published literature. It suffers from the drawback that it needs almost as much hardware as that required to provide a true quotient, while providing an output that is not the direct quantity of interest.*

Elad : - *Could you comment on the relative speeds of feedback and feedby ?*

Miller : - *Feedby is inherently slower than feedback in that it takes time for the transconductance element to charge and equilibrate. Until this time is over the output signal does not bear a well defined relation to the input signal. The basic difference between the circuits, however, is not in speed of response but rather that feedby yields a current -current transfer function, while feedback provides a current-voltage relationship.*

Abend : - *What is the maximum counting rate of the system ?*

Miller : - *The maximum counting rate of the system is set by the choice of rundown current and clock frequency. For the present applications, to a position-sensitive proportional counter, the average conversion time is ≈60 μsec. This time was not set by any basic electronic limitations, but rather by economic considerations and questions connected with the physics of gas counters.*

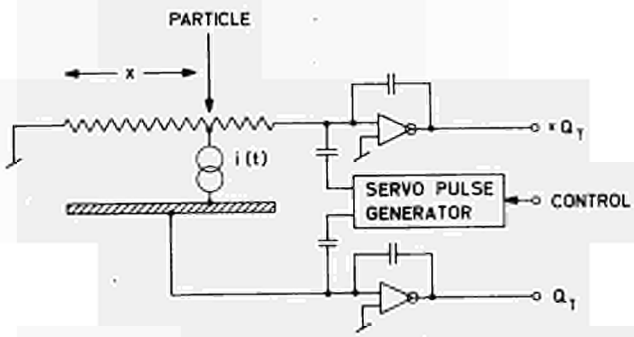

1 Diagram showing the position-sensitive detector with its associated preamplifiers and reference pulse generator.

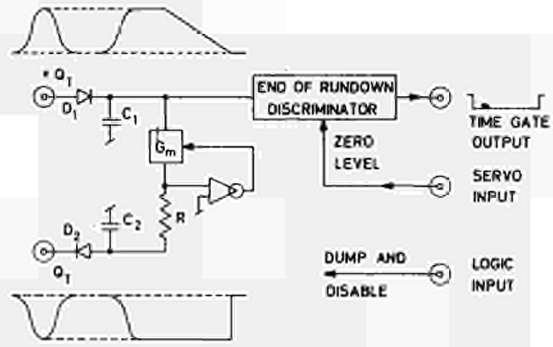

2 Basic scheme used in the rundown unit.

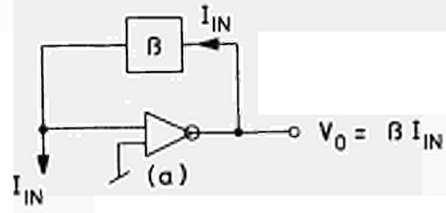

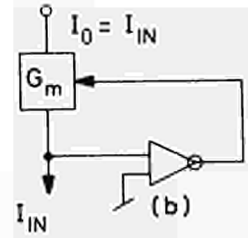

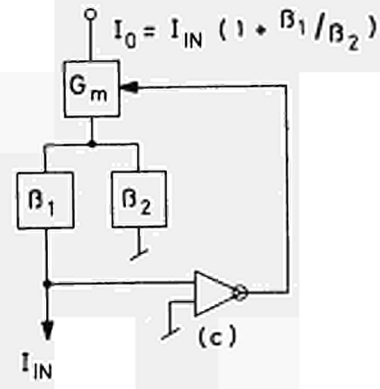

3 The feedby principle is shown in (b) and (c) and is contrasted with negative feedback as shown in (a).

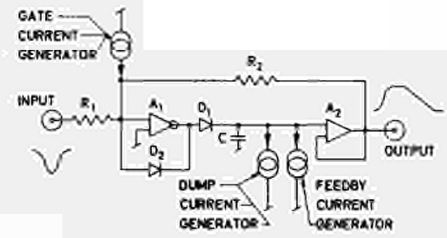

4 Block diagram of the xQ_T rundown unit.

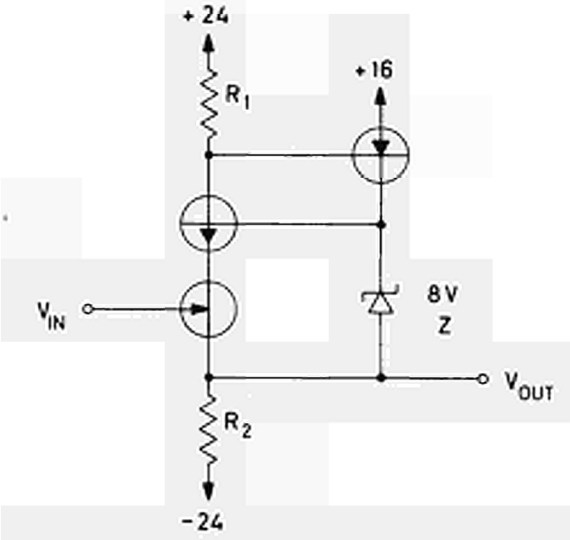

5 High impedance unity gain followers using constant power input elements.

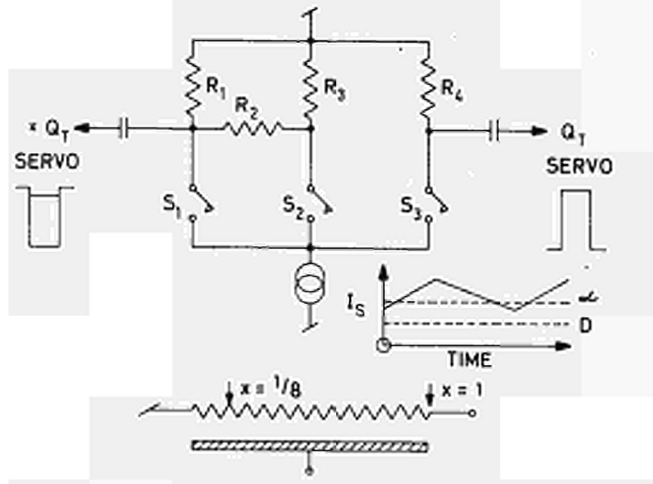

6 Basic scheme used in the servo pulse generator.

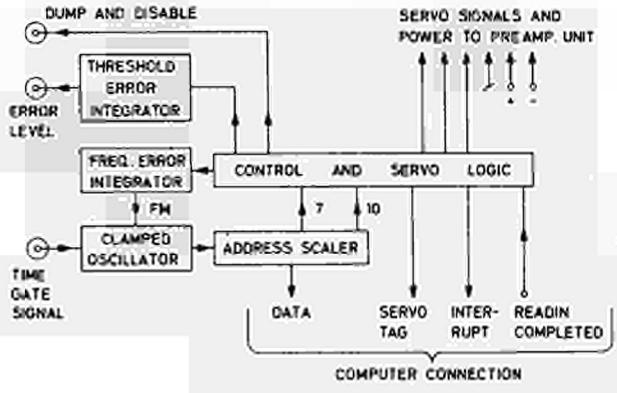

7 Block diagram of the digital system.

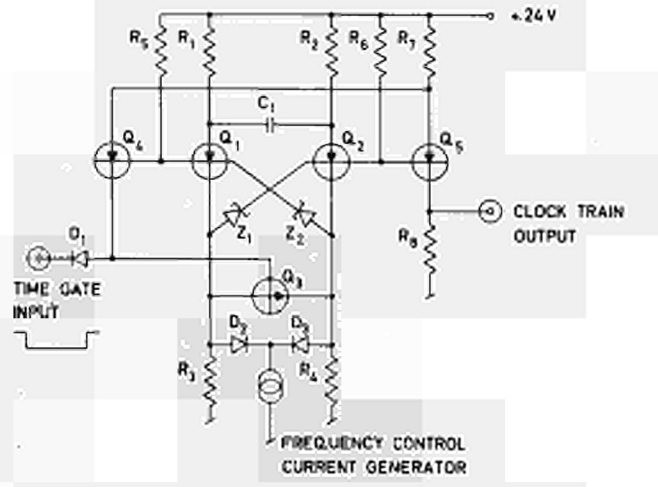

8 Schematic of the synchronously clamped clock oscillator.

DIRECT DIGITALIZATION OF THE QUOTIENT OF TWO PULSE HEIGHTS *

W.M. Carpay and S.S. Klein

Technische Hogeschool Eindhoven

The Netherlands

ABSTRACT

A fast quotient digitalization circuit (QDC) for use with position-sensitive detectors is described. The larger pulse is used as reference in a nonsynchronous successive approximation ADC.
A speed of more than 5 bits/μs and 7-bit-accuracy over a range of 0,5-5 V for the larger pulse may be obtained. The use of stretched pulses is not necessary if the pulse shapes are similar.

1. Introduction

Commercially available position sensitive semiconductor junction detectors[1] allow determination of the location x at which a particle hits the detector with an inaccuracy of $< 1\%$. The position signal is to be obtained as the quotient of two pulses, one (E) representing the energy deposited in the detector and the other one (E_x) a location dependent fraction of it. The fraction f (x) is approximately equal to x, expressed in units of the detector length l. When the energy is a known function (or even one of several discrete functions) of x, it is not always necessary to perform the division. When, however, a spectrum of E values may impinge at any part of the detector, some means must be devised to determine the quotient as accurate as possible. An apparatus constructed for this purpose should meet the following requirements:

1. The ratio must be obtained in digital representation;
2. The inaccuracy of the ratio should be better than 0.01 over the entire range;
3. These conditions should be met over a dynamic range of at least 1 : 5 for the energy.

Furthermore, if the output is to be used for gating and/or subrouting purposes,

4. the results should be obtained within at most 10μs, if possible within 1μs.

* This investigation is partly supported by the "Nederlandse Organisatie voor Zuiver Wetenschappelijk Onderzoek" (Z.W.O.) through the "Stichting voor Fundamenteel Onderzoek der Materie" (F.O.M.).

2. Possible methods to obtain the quotient of two pulse heights in digital form.

The determination of a quotient may be done, in principle, in 3 ways: a) Analog to Digital Conversion of both signals and digital division, b) Analog division and Analog to Digital Coversion, and c) Direct comparison of both signals in an Analog to Digital Converter with the E-pulse used as reference voltage. We first compare these methods.

Method a) generates three quantization errors. When the acceptable energy values range from αE_{max} to E_{max}, the accuracy of αE_{max} is critical. For a determination of x with 7-bit accuracy, the sum of the quotient truncation error and twice the quantization error in E should be less than 2^{-8}. Therefore E should be determined to better than 2^{-9}, or (for $\alpha = 2^{-3}$) E_{max} to better than 2^{-12}. This means that even for 7 bit accuracy in this case two 11 bit ADC's and a digital computer are necessary (It is assumed improbable that all errors would be maximal at the same time. If this assumption is not correct, then 12 bit conversion is necessary). The time necessary for the conversion is therefore about 10μs even with advanced ADC's, and the division of two 12 bit numbers will take at least 10μs even with a fast computer.

Method b) and c) both have the advantage to avoid an accumulation of quantization errors: the only quantization error occurs in the determination of the quotient. Method b), however, causes an accumulation of three function-generating errors, because the logarithms of the pulse heights are generated and subtracted and the result is exponentiated. A logarithm circuit accurate to 1% has been published.[2] Assuming subtraction to be perfect, we still remain with twice that inaccuracy, plus the inaccuracy of exponentiation. It is clear that the result is at best accurate to 2%. An analog ratio circuit with a 1% accuracy was announced[3] but never appeared in print. In method c) the use of a pulse-wise variable reference voltage seems unusual. Once the problems arising from this complication are solved, however, it probably is the only one to possibly combine speed and accuracy in the way desired.

3. More detailed considerations concerning the ADC method for determining the ratio of two pulse heights.

Once the decision has been taken to revert to the third method, the type of ADC

must be chosen. It was hoped at first that a commercially available ADC might be used, but we did not discover an ADC in which short pulses could be used as reference.

A ramp type pulse reference ADC has been described by Patwardhan and Indurkar[4]. Their circuit has a 2% accuracy for a minimum ratio of 0,2 and 1-10 Volt dynamic range. It takes 20 μs for a full conversion. The circuit does not, therefore, suffice the conditions (2) and (4). To suffice the accuracy condition, it is advisable that the number of analog operations on the pulse other than amplification be restricted to a minimum. The operations necessary in a pulse-reference ramp-type ADC are: stretching of both pulses and voltage-to-current conversion. In a successive approximation ADC the latter operation may be replaced by a division in a ladder network. Furthermore, using a successive approximation ADC with a switched ladder network and comparator for each bit, it is possible to work with pulse shapes that have to be accurately similar only. This requirement is generally fulfilled by the common pulse shaping circuits, after collection in the detector has ended. It should, therefore, be possible to work without stretching circuits or to use a much simplified switched time constant integrator. As a bonus this type of ADC also makes nonsynchronous and therefore very fast operation possible. The complexity of the circuit caused by the additional comparators and networks is compensated for to a certain extent by the absence of clocking circuitry. Therefore we decided to construct an asynchronous pulse reference successive approximation digitizer, which is described below.

4. Quotient Digitalization Circuit.

Block diagram. The block diagram is given in fig.1. Let us suppose that all comparators have low output. As soon as a pulse appears on both inputs the comparators C_n start to compare E_x with $2^{-n}E$. Depending on whether the output of C_1 is high or low, L_2 either switches to $\frac{1}{4}E$ or remains at $\frac{1}{4}E$. Simultaneously, the other ladder networks do or do not change output. In the former case, therefore, E_x is now compared to $(0,5 + 2^{-n})E$. Now C_2 reaches its final state and actuates the $\frac{1}{8}E$ switches in $L_3 \ldots L_7$, etc. etc. until the last comparator reaches its stationary state. As only one of the comparators has to make a critical decision, the duration of the approximation cycle is generally determined by the switching time. We succeeded in getting this time down to about 50 ns. The worst case critical decision time is, however, 200 ns. Therefore it is clear that the asynchronous operation gives an important improvement in speed. Note, moreover, that the circuit may start to look for its end state as soon as the pulses appear and is (for 1 μs rise time pulses) near the decisive state when the pulse is at its top. Therefore, for RC-shaped pulses, a stretcher is not absolutely necessary.

Ladder network. The switched ladder network is shown in fig.2. Resistors were selected with an accuracy of 1‰ from a stock of 1% metal film resistors. The switched resistors were chosen 200 Ω low to compensate for the FET resistance in its conducting state. Networks so constructed are identical and linear to 1‰ without further care. The differential linearity is better than 3% except at halfway point where it is near 10%. With easy corrections the differential linearity is improved to 1%. As the overall attenuation is slightly altered by this operation and 1‰ accuracy and 10% differential linearity are sufficient for our aims it was not applied. It is probably advantageous to use selected FETS and more accurate resistors in the significant bits. A further possibility is to choose the last pair of resistors after measuring the impedance of the network at the preceding node. The temperature coefficient of the ladder network was smaller than 10^{-3}%/°C.

Switching. The ladder network switches are actuated by a Schmitt trigger (fig.3) switching between the cutoff points of the n-channel and p-channel FETS. The capacitive feedthrough of the switching pulses is not negligible but of short duration. It is nevertheless, an important limit to the switching speed. It is attenuated in the ladder network, but to diminish its effect diodes are added to ground and a "dirty" E line. (In view of large transients the concept of "clean" and "dirty" lines was also applied to ground and supply lines). It was tried to compensate the feedthrough pulses, but as the compensating pulses have slightly different shapes the net result of these attempts was a diminishing of the amplitude of the feedthrough at the cost of prolongation of the disturbance on the millivolt level. The overall effect was that the worst case decision time deteriorated when compensation was applied. In the present circuit, therefore, no compensation was applied. It is hoped that such effects may be diminished using suitable MOS-FET's.

Accuracy. The accuracy of the circuit is determined at the upper limit of the E input voltage range by the accuracy of the switching network, which is mainly a problem of selecting resistors. In the present circuit, a 7-bit accuracy with 10% differential linearity was realized. At the lower limit of the E range, DC shifts of impedance transformers and comparators are the main problem. Even mV shifts can cause a very large inaccuracy when the E pulse is of the order of 250 mV. Some DC shifts will cancel partly, e.g. the temperature shifts of the impedance transformers feeding both inputs of a comparator. For other shifts, the cancellation is incomplete (the DC shift of the "master" E source, for instance, is attenuated more or less in the ladder network, while the DC shift of the "master" E_x source is present in full strength at each comparator.) Therefore, extensive work was done on the impedance transformers, with the result shown in fig.4. This circuit has a 20 ns risetime, an input impedance of 1 MΩ (inclusive the resistor) parallel to 3 pf, an output impedance of 4 Ω (which is ample for feeding all networks in parallel), it does not oscillate on capacitive loading and has anoutput level

shift of 0.28 mV/°C. Taking the specified accuracy of the μA 710 into account, the QDC now has a total inaccuracy of better than 3 mV/°C, which is sufficient to allow analysis of 300 mV E pulses with 1% accuracy. Adding 2 mV for the stretcher circuits (when used) would give 1% accuracy from 500 mV. (Note that stretcher circuits also introduce their own contribution to the differential error[5], which is of the order of 0,5%)

Range. The maximum value of the E pulse in the present circuit is about 4500 mV, but might be increased to 9 V by a suitable shift in the supply voltages for the comparators. The dynamic range therefore is at least 1 : 9 and could be increased up to 1 : 30.

5. Use with or without stretchers.

It was already indicated that the QDC is able to reach a decision in approximately the rise time of a common spectroscopy pulse. As stretchers in general are liable to introduce level shifts and thresholds, which are an important source of error in the determination of quotients, it is important to consider the gain expected from stretcherless operation.

The ratio of two pulses with approximately equal RC/CR time constant determined shapes is constant to within a fraction β for a time $\pm\sqrt{\beta}\tau$ around the peak. Whenever the combined threshold effects are a larger fraction of the smallest accepted pulse height than $\{(I+\Delta\tau)/\tau\}^2$, in which I is the sampling time jitter, $\Delta\tau$ the pulse shape uncertainty and τ the RC time, stretcherless operation is advantageous. To quote an example, the rise time jitter of commercial position sensitive detectors is about from 50 - 100 ns; this causes a minor (<0,25%) effect on the pulse shape if RC ≈2μs. The RC shaping time constants in commercial amplifiers are accurate to about 5%. Without any precautions, therefore, ½% accuracy is obtained, if the QDC output is strobed within 200 ns from the mean of both shaping time constants. A better accuracy is obtained easily when the time constants are trimmed. It seems that the advantage gets larger when higher accuracy is required, if only the conversion is ready before the pulse top. Other pulse shapes may be less advantageous. The time constants for a delay line clipped, RC integrated pulse should be equal to the same accuracy as the final result, for instance. (Note that this pulse shape is also a notorious one for accurate stretching!)

Unhappily, the time constants for optimal signal-to-noise ratio are not equal for the E& E_x signals from position sensitive detectors. It will be advantageous to use gated integration[6] together with suitable delay line differentiation for the pulse shaping. This is a very suitable method because it is easy to integrate over a time sufficient for the operation of the QDC with a droop difference between the integrator outputs of less than 10^{-2}%.

6. Conclusion.

The instrument described above opens interesting possibilities for accurate and fast determination of the quotients of pulse heights. The possibility to dispense with stretcher circuits is a useful side result. The application of the circuit will be primarily in cases where counting rates are too high to allow on-line computer handling of the output data of position-sensitive devices or, where no computer is available, to provide position subrouting of multichannel-analyzer recorded spectra.

REFERENCES.

1) e.g. from Nuclear Diodes, P.O. Box 135, Prairie View, Illinois 60069.
2) A. Harmanci, H. Guillon, V. Goursky, Colloque international sur l'electronique nucleaire, Paris, 1968, communication 102.
3) J. Quidort, Colloque international sur l'electronique nucleaire, Paris, 1968 - Programme scientifique, p.41.
4) P.K. Patwardhan and V.S. Indurkar, IEEE Trans. NS-15 nr.1, 323 (1968).
5) P. Casoli and P.F. Manfredi, IEEE Trans. NS-16, nr.1, 392 (1969).
6) W.W. Goldsworthy, IEEE Trans. NS-14 nr.1, 70 (1967).

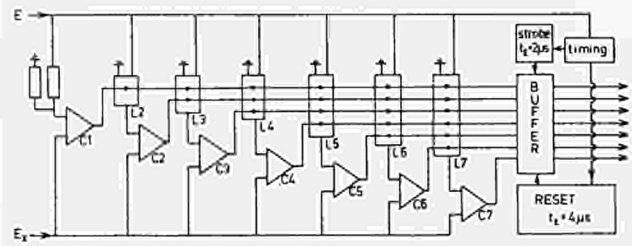

Fig. 1 - Block diagram of the QDC
C1...C7 Comparators ; L2...L7 Switched ladder networks with output $(2m+1)2^{-n}E$. m is the binary number generated by the preceding comparators ; n is the order of the next approximation.

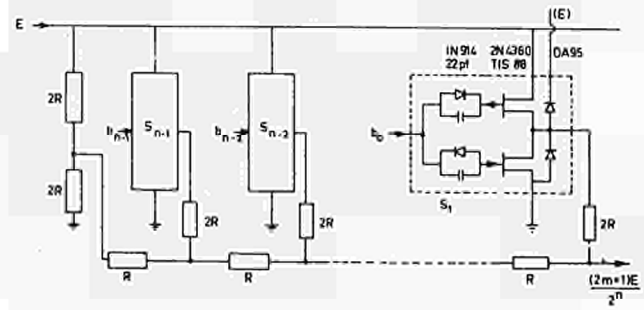

Fig. 2 - Switched ladder network, b_n-1 is the output of C_n.

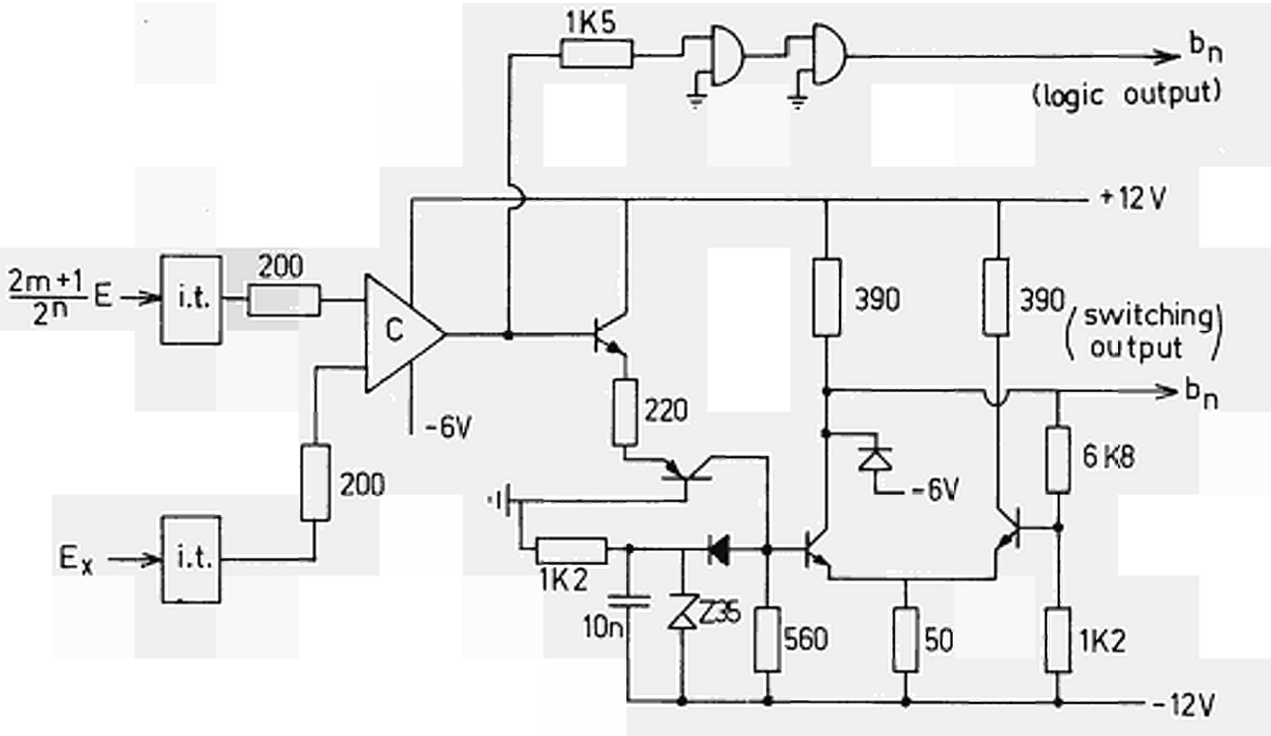

Fig. 3 - Comparator and Associated Circuitry
i.t. Impedance transformer ; C µA710 Comparator ; Transistors : 2N4124, 2N4126 ; Diodes 1N914

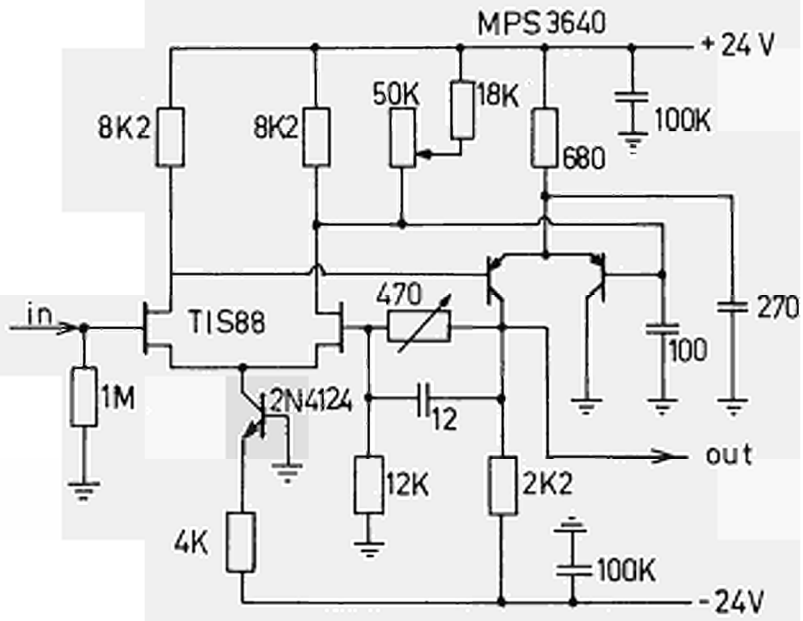

Fig. 4 - Impedance transformer with small DC shift.

AN ANALOG SPECTRUM STABILIZER

Thomas Friese

Hahn-Meitner-Institut für Kernforschung Berlin, Sektor Elektronik

Summary

An analog spectrum stabilizer with digital memory for the error signal is described. A peak or slope of the spectrum is used as reference. External gain drift will be totally compensated by controlling the gain of an amplifier, whose feedback loop partly consists of FETs, working as VCRs.

Introduction

In complex experiments, where pulse height datas of more than one detector, especially photomultipliers, are processed, a stabilization of each pulse height spectrum is useful. For this purpose a simple stabilizer has been built, which uses a peak or a slope, e.g. Compton edges, as a reference and compensates a gain drift of more than $\pm$ 10%.

Peak and Slope as Reference

As reference for spectrum stabilization normally a peak is used, which will be splitted into two halves by three thresholds (Fig. 1). If the pulse rates in the two halves are not equal, an error signal will control the gain until the difference of the up-rate and the down-rate becomes zero. Sometimes a spectrum may be superposed by another spectrum or background, which has a flat slope in the region of the reference peak. Then the up$^+$-rate may become higher than the down$^+$-rate thus producing an error signal causing a spectrum shift. Instead of a peak a slope of a spectrum can be used as a reference. It will be divided into three parts by four thresholds the width of the medium part being twice of the width of the lower and the upper part. When the gain decreases, the rate in the medium part will decrease more than the sum of the rates in the side parts. So the difference of the up- and down-rates can be used for producing an error signal in the same manner as a peak does. An advantage of using a slope, however, is the fact, that the difference of the up*- and down*-rates will not be influenced by a background, as Fig. 1 shows.

Instrument Block Diagram

The principle of the analog spectrum stabilizer is similar to that of digital stabilizers involved in some ADCs of multichannel analyzers, The reference peak or slope will be selected by a highly stable biased amplifier and the following comparators (μA710). A peak, a valley, a positive or negative slope can be chosen as a reference. The discriminator logic drives a 10 bit up/down binary counter. When the pulse height of the reference drifts to a smaller value, the up-rate becomes higher than the down-rate, by which the output voltage of the DAC is decreased. This results in an increase of the gain of the controlled amplifier thus compensating the drift of the reference totally. This control loop has an integral characteristic. A warning is given when the contents of the counter is more than $\pm$ 90% of the control range. This regulation principle requires a gain control without any delay. For convenient reference finding an unblanking signal is available.

Gain Conrolled Amplifier

The amplifier should accomplish the following requirements: DC-coupling, low zero drift, output $\pm$ 10V, gain variation $\sim\pm$ 10%, gain setting without delay. FETs used as voltage controlled resistors (VCR) have a tolerable unlinearity only at low U_{DS}. Therefore a serial-parallel control circuit was chosen (Fig. 3). The FETs T_1 and T_2 are controlled sequentially thus keeping U_{DS} always low. With decreasing gain the additional capacitive feedback becomes more effective keeping the risetime nearly constant within the control range. The gain as a function of control voltage is nearly uncritical because of the integral characteristic of the control loop. A simple set-up for checking and measuring the differential nonlinearity is chown in Fig. 4. For other purpose, where the gain must be proportional to the control voltage, selected pairs of VCRs may be used as shown in Fig. 5 and 6, or in similar circuits. The principle is, that one VCR is controlled proportional to the control voltage by feedback and the second one is controlled in parallel to the first one. The circuit Fig. 6 has the advantage, that the linearization network [1] R_2, R_2 can be used without any feedthrough of the control voltage to the output.

Automatic Peak Finder

Fig. 7 shows an automatic peak finder with extended gain control range. Because the steps within the control range must be small and a stable 13 bit DAC is expensive, the fine control range uses 10 bit and the range is extended by a 3 bit counter with DAC, whose steps are smaller than the 10 bit step of the fine control, thus guaranteeing overlapping ranges. To start the automatic peak finding, all counters and the flipflop are resetted and the gain has its lowest

value. A pulse generator with a frequency of about 1/10 of the peak rate feeds the 10 bit divider and the 10 bit up/down counter, so that the gain increases. If the stabilizer does not lock on a peak, the 961-carry of the up/down counter switches the 3 bit up/down counter to the next higher number and resets the 10 bit divider and the 10 bit up/down counter. According to the diagram in Fig. 7 the gain increases until the 10 bit up/down counter locks on the reference. Then the carry of the 10 bit divider sets the flipflop, which stops the automatic searching process by switching off the pulse generator. Now the 10 bit up/down counter runs to its final value. A large gain drift will switch the coarse gain to the next higher or lower step and starts again a normal searching process.

References

[1] Thomas B. Martin: "Circuit Application of the field effect transistors". Semicond. Prod. March 62, page 30..36

DISCUSSION

Acerboni : - How much is the resolution of the spectrometer affected by the stabilizer ?
Friese : - Of course there is some influence on the resolution, but it is much less than the drift of a photomultiplier.
Stanchi : - Do you assume that the slope of the background in the region of interest is linear ?
Friese : - To a first approximation, it is linear, so that the stabilizing point is largely independent of background changes.
Gatti : - I would like to suggest calling your new method of stabilization "inflection point stabilization" rather than "slope stabilization". The fact that the method is independent of an added constant slope is, in fact, its principal advantage.
Friese :- Yes, this may be a better description of the method. I thank You for this comment.

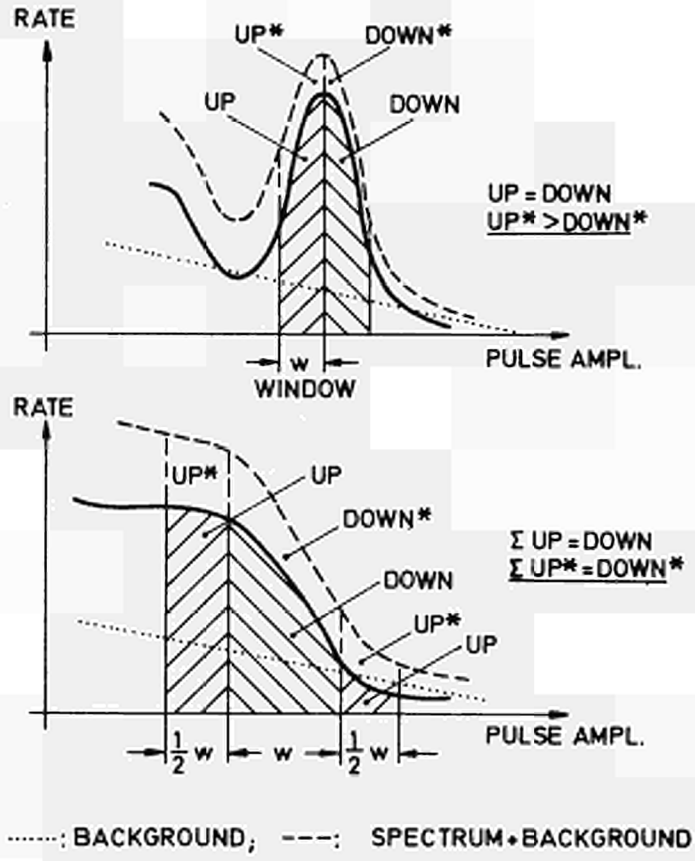

Fig. 1 - Peak and slope influenced by background.

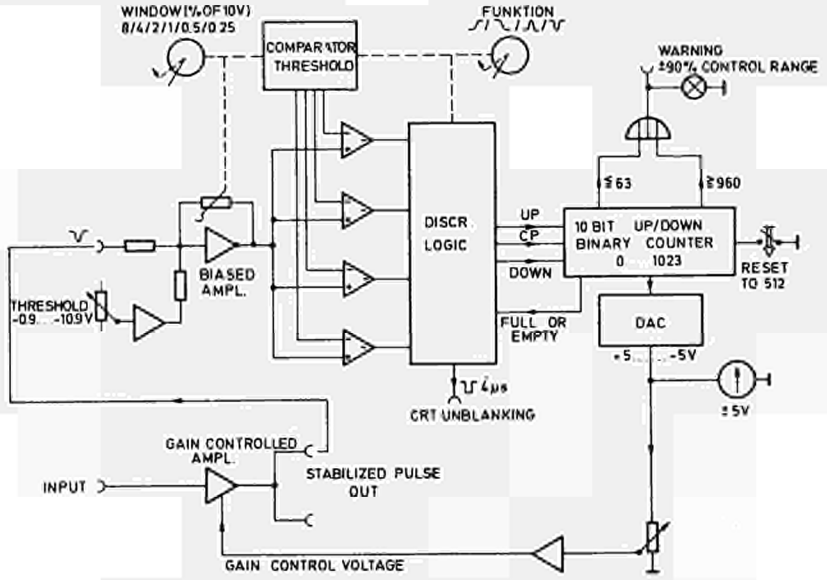

Fig. 2 - Block diagram of the analog spectrum stabilizer.

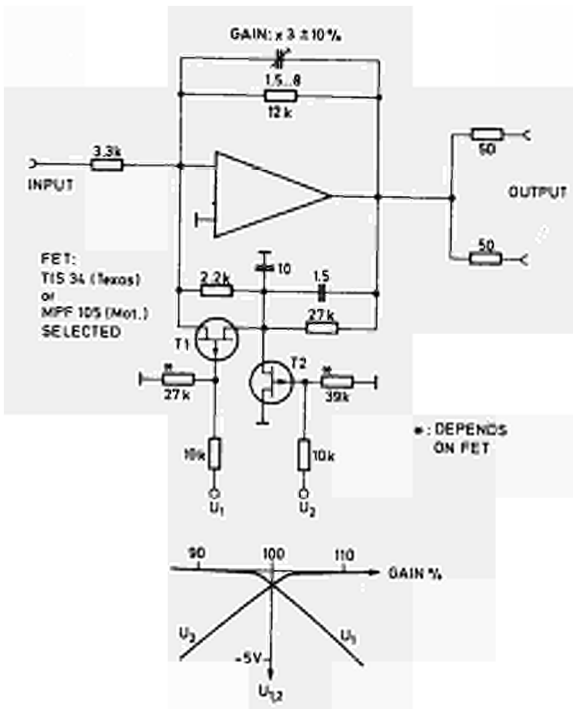

Fig. 3 - Gain controlled amplifier.

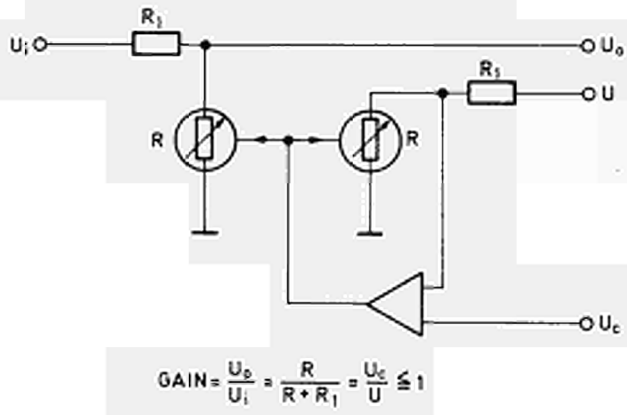

$$GAIN = \frac{U_o}{U_i} = \frac{R}{R+R_1} = \frac{U_c}{U} \leqq 1$$

Fig. 5 - Voltage controlled attenuator.

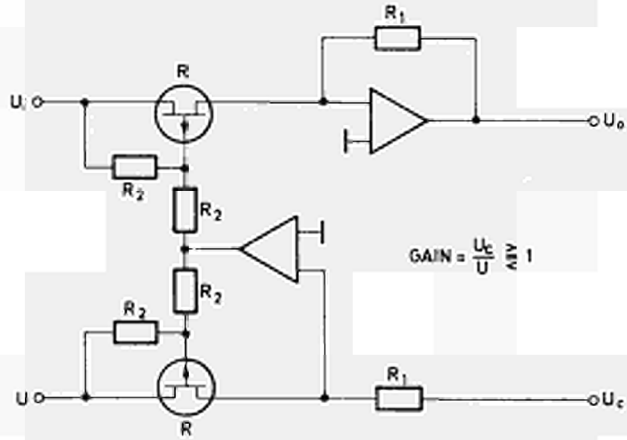

Fig. 6 - Gain controlled amplifier, using FETs with linearization network.

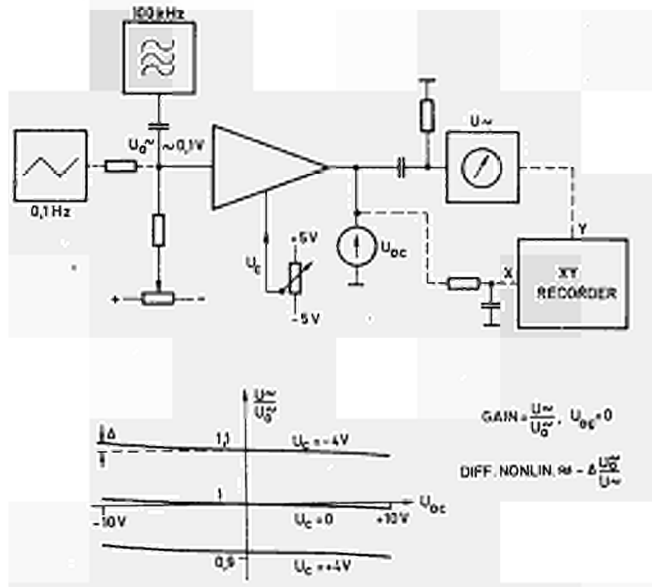

Fig. 4 - Test of differential nonlinearity (Δ enlarged for better understanding).

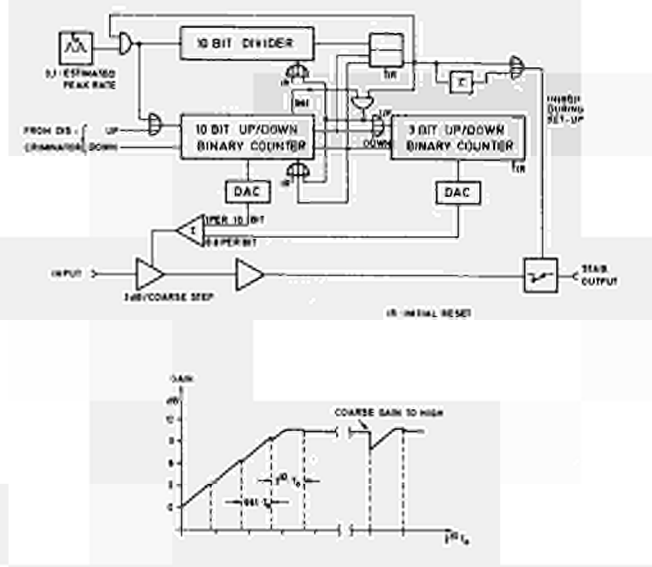

Fig. 7 - Automatic peak-finder and range extension.

A DATA-HANDLING SYSTEM FOR LARGE-SCALE SPACE RADIATION EXPERIMENTS

J. B. Reagan, R. D. Reed*, J. C. Bakke and J. D. Matthews
Physical Sciences Laboratory
Lockheed Palo Alto Research Laboratory
Palo Alto, California 94304, U.S.A.

Summary

A satellite data-handling system which controls, collects, identifies and transmits scientific data on Polar Cap Absorption (PCA) events and on auroral particle fluxes has been designed. The system controls the transmision and earth-reflected reception of signals from a multi-frequency ionospheric sounder on board the satellite. In addition, the system collects low and high energy particle radiation data in both digital and analog form from the twenty spectrometers and detectors which comprise the experimental payload. Appropriate identification data such as synchronization patterns and time information are provided in the resulting serial, pulse-code-modulated output to telemetry and ground-based digital computers. A description of the satellite data-handling system, the experimental payload and the telemetry system is presented.

Introduction

While the processing of data from nuclear physics experiments in the laboratory has required increasingly complex electronics, the handling and processing of data from large-scale space radiation experiments has required similar increases in complexity but with the added constraints of the spacecraft. One of the greatest difficulties encountered by the scientist in the space radiation field is that of obtaining data-handling systems which are compatible with both the requirements of the experiments and the spacecraft telemetry. In almost every situation, the sophistication and accuracy of an experiment will be determined by the type of data-handling system used. Unfortunately in many cases, experimenters must adapt their experimental requirements to existing general purpose data-handling and telemetry systems which were not designed for specific scientific experiments. In an effort to optimize the scientific output of a large experimental payload for the investigation of Polar Cap Absorption (PCA) and auroral events, a digital-data-handling-system (DDHS) has been designed by the scientists and engineers of our laboratory. This on-board system controls, collects, identifies, calibrates and transmits all of the pertinent data from twenty scientific experiments for subsequent automatic data reduction by ground-based digital computers.

Experimental Payload

The experimental payload consists of eighteen detectors and spectrometers for the measurement of low and high energy particle radiation precipitating in the polar regions during Polar Cap Absorption (PCA) and auroral events. In addition, the payload contains an earth-reflecting ionospheric sounder, a tri-axis magnetometer, and an in-flight calibration system. The instruments are broadly divided between those having digital data outputs and those having analog data outputs, as shown in Figure 1. The three high-energy particle spectrometers for the measurement of protons (HEPS), protons and alpha particles (HEAPS), and electrons (HEES) and the five high-energy angular distribution instruments (HE/ADI) are digital in nature. The low-energy particle instruments consisting of three multiple-particle analyzers (MPA), a crossed-field analyzer (CFA), three total-energy detectors (TED, TEP) and three angular distribution instruments (ADI) have analog data outputs. These analog outputs, along with the tri-axis magnetometer outputs, are digitized to 0.4 percent accuracy on board the satellite and subsequently handled as digital data. The analog receiver information from the earth-reflecting ionospheric sounder is handled in a special manner to be discussed in a later section. A brief description of each of the different classes of instrumentation and their relationship with the digital-data-handling-system (DDHS) follows.

High-Energy Instruments

The primary particle flux input to the polar regions during PCA events consists of moderate-to-high-energy protons, electrons and alpha particles. The flux and spectrum of each of these particle types are measured with high-sensitivity, high-resolution spectrometers similar to those used successfully in previous satellite flights[1,2] and employing both solid-state and scintillation detectors. The high-energy proton spectrometer (HEPS) and the high-energy proton-alpha spectrometer (HEAPS) utilize totally-depeleted, surface-barrier, solid-state detectors in a telescope arrangement. The detector configuration is surrounded by a combination of a plastic-scintillator

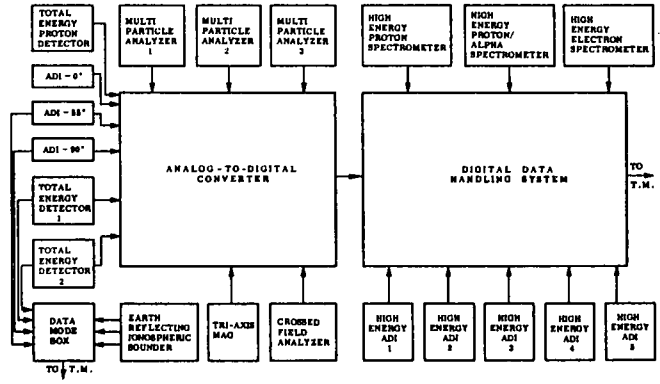

FIG. 1. Block diagram showing the instruments employed in the PCA experiment payload and their relationship with the digital-data-handling-system.

*Current address: Martin Marietta Corporation
Denver Division

anticoincidence ring and shielding material to eliminate particles not entering through the detector aperture. A logic network under the control of the DDHS establishes the conditions required for analysis of pulses from the respective detectors. The two solid-state detectors in the telescope arrangement are operated both in coincidence and anticoincidence during the four time-shared modes of operation that are programmed by the DDHS. The four modes of operation are selected to emphasize four different energy and particle regions. In particular, energy regions where the flux intensity is expected to be low are given special emphasis to obtain statistically significant data within the limited sampling possible with existing telemetry systems. Each energy region is analyzed exclusively for a period of 250 milliseconds out of every second. In this manner, a complete analysis of protons and alpha particles is obtained each second.

Those signals from each detector which satisfy the logic requirements in each mode of operation are analyzed by two multichannel analyzers of the successive approximation type. The analyzers, which were designed by our group, are operated in a dual-parameter fashion, i.e., the pulse-height information from both detectors corresponding to a single particle event are analyzed and read out to the data-handling system simultaneously. Each analyzer possesses a 256-channel resolution and requires 10 microseconds per analysis. Channel addresses are read directly to the DDHS as 8-bit binary words at a periodic rate of 250 addresses per second. This latter rate therefore provides a representative sampling of the input spectrum and is dictated by the overall bandwidth limitations of the telemetry system and not by limitations within the analyzers. The absolute input counting rate from each detector is obtained by scaling with two 16-bit binary accumulators those input counts which satisfy the logic requirements. Each accumulator is read out to telemetry as two 8-bit words once per mode of operation under the control of the DDHS. The accumulators are cleared after each readout and then opened to count for the duration of the next time mode. The combination of accumulator capacity and the readout rate of four times per second allow a maximum input rate of 2.63×10^5 counts per second to be properly scaled. The dead time associated with the scaling operation is approximately 1 microsecond and is established by the various coincidence and anticoincidence resolving times. The time-base accuracy of this process is determined by the master clock in the DDHS which is designed to have an accuracy and stability better than $\pm 3 \times 10^{-7}$ over the complete environmental conditions encountered on a typical satellite. The high-energy electron spectrometer (HEES) consists of a large plastic scintillation detector viewed by a photomultiplier and surrounded by at least 3.4 gm/cm^2 of shielding. Pulses from the photomultiplier are periodically analyzed by a 256-channel pulse-height analyzer while the absolute rate is obtained from an accumulator in a manner similar to the readout of the proton spectrometers.

To obtain a measure of the angular distribution of the incident protons and alpha particles in a PCA event, five instruments (HE/ADI) are located at various orientations with respect to the zenith. These instruments are all identical and utilize thin solid-state detectors biased at two distinct thresholds to identify and separate moderate energy ($\sim$ 1 MeV) protons and alpha particles on the basis of their energy loss in traversing the detector. Each detector is surrounded by sufficient shielding material to minimize the background from penetrating particles. Pulses within the two differential energy bins are accumulated in separate 16-bit binary counters which are read and reset eight times per second by the DDHS.

Low-Energy Instruments

The low-energy particle input to the polar and auroral zones will be measured with a combination of channel multiplier and total-energy detectors. Several instruments employing channel multiplier sensors in conjunction with magnetic and electrostatic energy analysis similar to those used successfully on previous satellite flights[3,4] will provide high resolution spectral data on precipitating protons, electrons and alpha particles. The channel multipliers will be operated in the saturated-pulse mode, and the pulse rates above a predetermined threshold will be measured with logarithmic count-ratemeters. Approximately five decades of count-rate information will be covered in each ratemeter with a corresponding 0-5 VDC output. Each multiple-particle analyzer (MPA) is in essence a spectrometer consisting of nine channel multiplier detectors with magnetic analysis to establish differential energy analysis on both protons and electrons and with thin foils to establish higher-energy integral thresholds.

Scintillator-photomultiplier combinations[5,6] will measure the total energy flux of each of three angles and at two energy levels to provide a measure of the angular distribution of the incoming particles. The two energy levels will be established by electrostatic grids located in front of the scintillator. A repeller grid will be programmed between two potentials under control of the DDHS. Particles which exceed the repeller threshold will be accelerated by a second grid and deposit their energy in the plastic scintillator. In addition, three other scintillation detectors will be used to measure the total energy of protons (TEP) and electrons (TED) above thresholds determined by aluminum depositions on the scintillator surfaces. The photomultipliers will be operated in a constant-anode-current mode where the high voltage across the tube decreases with increasing light intensity from the scintillator in approximately an exponential fashion. In this manner, over five decades of light intensity corresponding to an equivalent particle flux can be measured by converting the potential across the tube to a 0-5 VDC analog output which is then digitized to a 0.4 percent accuracy for subsequent handling.

Earth-Reflecting Ionospheric Sounder

The DDHS also controls the transmission of a pulsed, multi-frequency, earth-reflecting ionospheric sounder (ERIS) operating in the vicinity of 20, 30, 33 and 60 MHz. The reflected signals from the earth's surface after transmission through the D-region of the ionosphere are processed on board the satellite. The intensity of the reflected signals provide a measure of the absorption of electromagnetic radiation in the D-region of the ionosphere during PCA events. This absorption data will be correlated with the particle energy input to this region as measured with the large complement of low and high energy particle detectors and spectrometers just described.

The sounder will be operated on a pulsed basis with a transmission pulse time of approximately 1 ms at a rate of 10 pulses per second, i.e., at a duty cycle of 1 percent. Power outputs of 100 watts at each frequency will be transmitted. The signal at 60 MHz is expected to suffer the least attenuation in its round trip path through the D-region. The return signal at 60 MHz will therefore be used as a trigger and, in some cases, as a monitor of the reflected power. Increased attenuation is expected in the return signals at the lower frequencies when the satellite traverses an enhanced ionization region. The received signals will be amplified and applied directly to constant-bandwidth voltage-controlled oscillators. These oscillators will convert the analog signals to frequency information for transmission to the ground. In this manner, the full details of the return signals will be continuously available. Multiple reflections from other ionization layers in the ionosphere and from background sources beyond the Fresnel zone illuminated by the transmitted signal can be analyzed with greater precision as the entire signal is continuously presented. Control of the transmission time and duty cycle and time identification will be performed by the master time base of the digital-data-handling-system.

Magnetometer and Data Switch

A tri-axis magnetometer is included to establish the orientation of the detectors in the geomagnetic field. A data mode box is also included to allow the broadband frequency capabilities of the constant-bandwidth VCO system to be shared upon command between the ERIS and four of the low-energy instruments from which high-time resolution data is desired. The data mode box is essentially a four-pole, double-throw electronic switch utilizing junction-type field-effect transistors as the switching elements.

In-Flight Calibration System

An in-flight automatic calibration system is employed to monitor the performance of all sensors and electronics in the payload. The quality and accuracy of the data from the payload is only good to the extent that both sensor and electronics performance can be continuously monitored in flight. In an effort to reduce the overall uncertainties in gain and energy thresholds and in electronic calibration curves to less than a few percent, a calibration of all sensors and electronics in the payload is performed periodically in flight.

All particle sensors are equipped with low-intensity radioactive sources. In the case of the high-energy spectrometers, these sources usually contain monoenergetic lines which can be pulse-height analyzed to measure gain shifts as small as one percent. In the low-energy channeltron instruments, radioactive sources are used in conjunction with a programmed four-level integral discriminator[4] to monitor the gain and to establish the counting efficiency of the channel multiplier detectors. The programming of these integral discriminators is performed automatically by the DDHS a short while after application of power to the instruments. Appropriate low-energy beta sources such as tritium are used with the total energy detectors. In the case of the TED and TEP detectors, the total energy deposited by the source in the scinitllator is used as a monitor of the performance. In the case of the variable-energy detectors (ADI's), a two-step analysis of the source is achieved as a variable electrostatic threshold is programmed through its two levels by the DDHS.

To monitor the detailed response of the photomultiplier sensors used in the total-energy instruments over the entire dynamic energy range of interest, a programmable light source is included in each detector. These light sources are ruggedized, gallium-phosphide, light-emitting diodes* which are sequentially programmed through four-distinct constant-current levels under the control of the DDHS. Approximately three decades of light intensity are obtained in this manner and this range is sufficient to monitor the shape of the response curve.

Calibration of the logarithmic ratemeters and of the binary accumulators over their entire dynamic range is also performed in flight by the DDHS. The master time-base frequency and three other lower frequencies obtained by counting down the fundamental frequency are applied sequentially to all counting electronics during the calibration period. With such a stable and accurate time base the ultimate overall accuracy in the data will be limited to the telemetry accuracy of 0.4 percent.

Digital-Data-Handling-System

The fundamentals of the digital-data-handling system (DDHS) are shown in Figure 2.

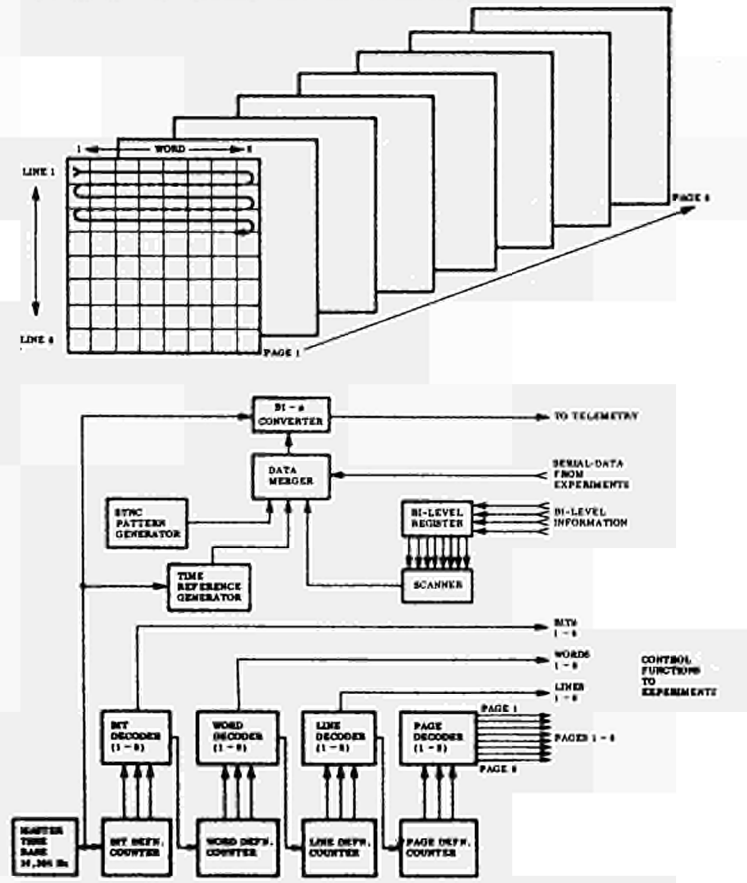

FIG. 2. Fundamentals of the Digital-Data-Handling-System.

* Available from Electro-Nuclear Laboratories, Inc., Menlo Park, California (Type 484)

The main time base of the system is established by a highly stable ($\pm 3 \times 10^{-7}$ stability) clock operating at a frequency of 16,384 Hz. The time-division multiplexed format has been arranged such that a frame of data contains 512 words with each word consisting of 8 bits. The data is presented to the telemetry at a rate of four frames per second. The basic 8-bit word has been chosen as the building block of the system. A digital word therefore contains one of the following: binary information on an analog channel which has been digitized to a resolution of one part in 256; a pulse-height analyzer channel address describing a channel between 0 and 256; one-half of a 16-bit accumulator; or eight discrete bi-level monitors.

After a careful review of the time multiplexing requirements of the 80 signal outputs which emanate from the twenty instruments in the payload, a word, line and page format was chosen for the presentation of the data. As shown in Figure 2, a line consists of 8 words and contains a combination of the different types of data described. A page consists of 8 lines of data or 64 words. Finally, the 512-word frame contains 8 pages of data. The time multiplex commences on word 1, line 1, and proceeds in the manner described by the arrow in the figure. By evaluating the overall data requirements prior to designing the DDHS, it became evident that many data channels were repeated several times throughout the frame. A tremendous reduction in the number of gates required to define the 512 words and 4096 unique sequential functions was realized by the judicious placement of these data channels in the page format. A corresponding reduction in the complexity and power requirement has thus also been realized. Such optimization of a system can only be realized as a result of an intimate association between the experimenter and the data-handling designers. Indeed, maximum utilization is achieved when both individuals are involved in both phases of the design effort.

The master-time base is scaled-down and decoded by the bit, word, line and page definition decoders shown in Figure 2. Signetics type DTL and TTL integrated circuits are used throughout to generate these functions. Each function is made available to the various experiments in the payload. For example, if an 8-bit channel address is to be read out in equal periodic intervals at 256 times per second it might be located in word 1, lines 1 through 8, and on pages 1 through 8 of the above format. That particular channel address register would therefore receive the control function corresponding to these locations only.

The master time base is also utilized as a time reference generator to provide a unique time code to each frame of data. This function is essential when data are to be tape recorded on the satellite for subsequent playback to the ground. The time code can be correlated with re time over a tracking station so that the ephem is associated with the stored information can be determined. The time-reference generator consists of a 24-bit counter which is read out as three words. The counter is updated once per frame of data and therefore the counter will recycle every 45 days.

A sync pattern is also generated which makes the resultant serial, digital data compatible with automatic ground-based processing equipment and computers. The sync pattern generator consists of four words, i.e., 32 bits, into which a unique combination of 1's and 0's have been stored to identify the beginning of a new frame of data. A bi-level register and scanner is also provided which presents eight discrete, on-off monitors to the telemetry.

The data merger shown in Figure 2 receives the data from the experiments, the sync pattern, the time-reference code, and the bi-level monitor data and controls the flow of all of this information in a prescribed serial manner to the telemetry. The non-return-to-zero (NRZ) output of the merge unit is then converted to bi-phase digital data such that a transition from one to zero or vice versa will always occur during each bit period even if the data has zero value. The resulting waveform is more cyclic and compatible with direct recording on tape recorders than the original NRZ data where transitions might not occur for extended periods of time within a frame.

Telemetry System

The interface of the DDHS with the satellite telemetry system is shown in Figure 3.

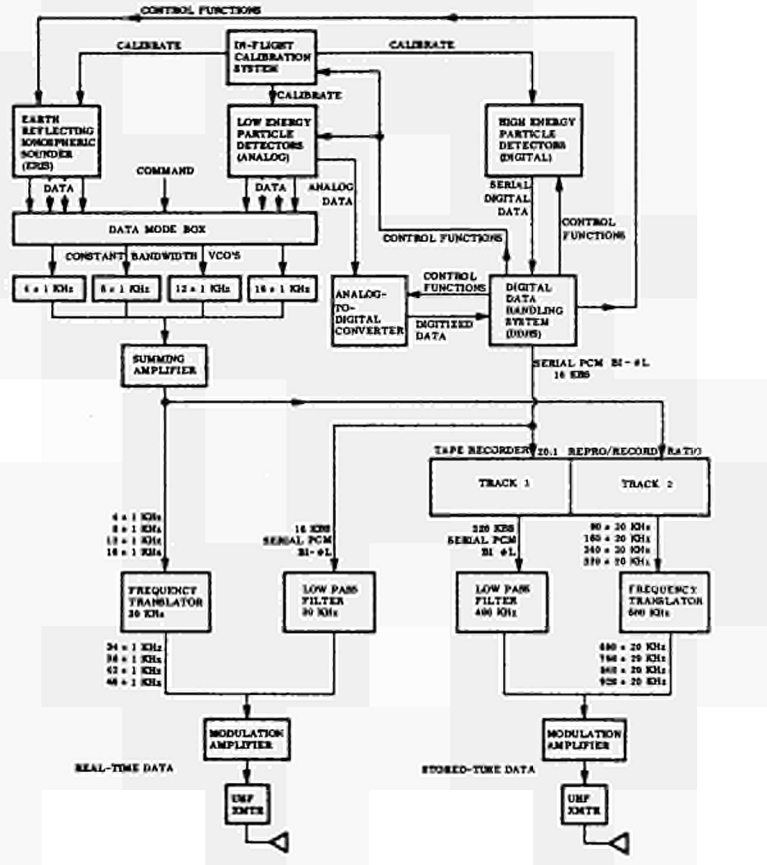

FIG. 3. The Complete Satellite System for the Measurement of PCA Events Including the Telemetry Link to the Ground.

This figure also shows the relationships between the DDHS and the three major types of experiments. The high-energy particle detectors supply their digital data directly to the DDHS when the proper control functions are received from the latter. The low-energy particle detectors provide their outputs to the DDHS through the analog-to-digital converter shown. Four analog instruments requiring high data sampling are also read out through the data mode box. This data mode box allows either the ERIS data or four other items of data to be read out into moderately wideband voltage-controlled-oscillators (CBW-VCO). These VCO's convert the analog data to frequency information which can be more easily and faithfully handled and transmitted to the ground. The output frequencies of four VCO's are summed in an amplifier to form a frequency composite suitable for recording.

The serial, bi-phase digital data from the DDHS and the frequency-modulated (FM) data from the data mode box are applied to two tracks of a commercially available satellite tape recorder. With the on-board tape recorder, data can be obtained over regions of geophysical interest such as the southern polar region, where tracking stations are not readily available. The recorded data is then played back at a later time over a tracking station at a 20:1 reproduce-to-record ratio. The initial data frequencies are therefore increased by this factor such that the reproduced information must be transmitted over a UHF data link.

The output of the two tape recorder tracks are first merged into a frequency composite prior to modulating the transmitter. The serial PCM data from the DDHS, which is now at a bit rate of 320 KBS, is passed through a low-pass filter to remove the frequency components above 400 KHz from the data. The FM composite from the remaining track is applied to a frequency translator operating at 600 KHz. This translator heterodynes each of the VCO frequencies and allows the sum frequencies to pass through while filtering out the difference frequencies and all frequency components below 600 KHz. The two frequency composites are then summed to form an overall modulating signal between DC and 980 KHz for the UHF transmitter. The two tracks of data are also read out over an additional telemetry link during the tape recorder playback operation to assure continuous data coverage.

Conclusions

A satellite digital-data-handling-system has been designed which controls, collects, identifies and transmits scientific data on PCA and auroral particle events from 20 instruments having 80 signal outputs. The resultant data are directly compatible with automatic, ground-based processing equipment and computers. In handling and controlling such a large volume of complex data, several techniques have been employed which should prove valuable to experimenters in the nuclear physics laboratory. Since nuclear experiments, particularly those associated with large accelerators, are becoming increasingly complex and involving large numbers of sensors, digital and analog multiplexing techniques such as those employed in this satellite system will become more widely accepted in the near future. Utilization of a common time base, with appropriate decoding, whether it be computer or hardware generated, for the control, identification, performance monitoring, calibration and readout of laboratory sensors and instruments will also become more widely used. Finally, data merger units which can gather the information from many sources into a small number of inputs compatible with small scale and large scale digital computers will most certainly be desirable items in future laboratory experiments. It is hoped that some of the features presented in this system will prove useful in designing such future systems.

Acknowledgments

The authors wish to acknowledge the many valuable suggestions and continued support which Dr. R. G. Johnson has provided during the design of this system. We also wish to acknowledge the valuable assistance of Dr. W. L. Imhof and R. D. Sharp of this laboratory.

The support of the Defense Atomic Support Agency through the Office of Naval Research [Contract NOnr 3398(00)] and the Lockheed Independent Research Program are greatly appreciated.

References

1. Rowland, J. H., J. C. Bakke, W. L. Imhof and R. V. Smith, "Instrumentation for Space Radiation Measurements," IEEE Trans. Nuc. Sci. NS-10, 178-182, 1963.

2. Reagan, J. B., J. C. Bakke, W. L. Imhof and R. V. Smith, "Multichannel Spectrometer for the Measurement of Trapped Particles," IEEE Trans. Nuc. Sci. NS-12, 83-88, 1965.

3. Shea, M. F., G. B. Shook, J. B. Reagan, L. F. Smith and T. C. Sanders, "Channel Multiplier Instrumentation for the Measurement of Low-Energy Auroral Particles," IEEE Trans. Nuc. Sci. NS-14, 96-99, 1967.

4. Reed, R. D., E. G. Shelley, J. C. Bakke, T. C. Sanders and J. D. McDaniel, "A Low-Energy Channel-Multiplier Spectrometer for ATS-E," IEEE Trans. Nuc. Sci. NS-16, 359-370, 1969.

5. Reagan, J. B., D. L. Carr, J. D. McDaniel and L. F. Smith, "Satellite Instrumentation for the Measurement of Auroral Phenomena," IEEE Trans. Nuc. Sci. NS-11, 441-446, 1964.

6. Reagan, J. B., D. L. Carr, J. D. McDaniel and T. C. Sanders, "Low-Energy Electron and Proton Satellite Instrumentation for Auroral Studies," IEEE Trans. Nuc. Sci. NS-14, 49-55, 1967.

REAGAN 4.1.

DISCUSSION

Boucke : - Question n.1 : do you use FET IC's in your system ? Question n.2 : what type of light emitting diodes are you using and what is the power consumption of the 256 channel analyzer ?

Reagan : - We are using the Signetics series DTL and TTL integrated circuits but not FET type. In answer to your second question : the type of light emitting diodes which is currently being used is the gallium phosphide diode type 484 provided by the Electro-Nuclear Laboratories. In answer to your last question the 256-channel analyzer we are commonly using consumes approx. 1 Watt at 28 V dc. This unit has no memory at all. The technique is to feed the channel analyzer directly to the telemetry and therefore the capacity obtained is limited to 256 samples per second.

COMPENSATION OF PULSE DETERIORATION IN MINIATURE CABLES BY MEANS OF SWITCHING TRANSISTORS

by D. Maeder and G. Vuilleumier,
Laboratoire de Physique Nucléaire Expérimentale
de l'Université de Genève

Summary

Delay boxes for standard fast-logic pulses (2 ns FWHM) should have > 400 MHz bandwidth. Amplitude loss and pulse widening data will be given for a 100 ns delay produced by different types of coaxial lines. In order to use a transistor for loss compensation, a special correction network adapted to the $\sqrt{f}$ attenuation characteristic is required. The theory of a suitable correction circuit is given, with numerical results for various RC combinations, up to 3 poles. Experimental tests show that the overall response function can be corrected within a fraction of a dB over a 300 MHz bandwidth. Application to variable-delay boxes is discussed. A slight circuit modification allows the use of the compensating transistor as the switching element for remote delay control.

1. Introduction.

Pulses with ns rise and fall times are currently manipulated in nuclear instrumentation. For example, the CLR/A[1] series of fast logic modules developed at the University of Geneva has the following performance characteristics :

1) Standard unit load is 75 Ohms to ground, externally applied at the end of an input chain (max. 3 in cascade).

2) Input level specifications apply to a "slow regime" (each state has a minimum duration of 5 ns).

logical 0 ⟶ $0\ (^{+0,5}_{-0,2})$ Volts

logical 1 ⟶ $-0,7\ (^{+0,2}_{-0,5})$ Volts

3) The "fast regime" is defined at any input by standard pulses of 0,7 Volts peak amplitude and 2 ns FWHM.

4) Any output (or $\overline{\text{output}}$) can drive : two parallel load units (37,5 Ω) in the slow regime; one load unit in the fast regime.

Operation into one 50 Ohms load is always possible, at the expense of some signal deterioration.

When signals are passed through logic gates, switching elements regenerate fast pulses to their standard shape. On the other hand, transmission through passive networks (such as delay lines) results in amplitude loss and/or spread of pulse width.

In a linear circuit having a well defined HF cutoff characteristic (3 dB at f_c), the rise time spread of a sharp wavefront can easily be evaluated from well-known approximate rules, which also permit a simple estimate of the deterioration of a short pulse. For example, ≤0,8 dB amplitude loss and 2,0 ⟶ 2,1 ns spread requires an f_c of linear transmission networks ≳ 400 MHz, while tolerating a 3 dB loss and spread from 2,0 ⟶ 2,7 ns would allow $f_c \gtrsim 180$ MHz. In coaxial cables, distorsion is more complex[2], but an order of $f_{3dB} \sim 200...400$ MHz is indicative of requirements for low-loss transmission of the fast standard pulse. This rules out the use of miniature cable for lengths > 20 ns (see table 1).

The present paper has a two-fold purpose :

1) Is there a possibility of loss compensation by transistors?

2) Can the same transistors be used as switches for remote control of delay boxes (to replace costly and slow coaxial relays) ?

2. Properties of coaxial lines.

The transmission of signals through a coaxial line is fully determined by its characteristic impedance Z_o

$$Z_o = \sqrt{\frac{R+j\omega L}{G+j\omega C}}$$

R,L: series resistance and inductance.
G,C: parallel conductance and capacitance.

and by its propagation constant $\gamma = \alpha + j\beta$

$$\gamma = \alpha + j\beta = \sqrt{(R+j\omega L)(G+j\omega C)}$$

α being its attenuation constant and β its phase constant.

With usual dielectrics, G may generally be neglected.

The attenuation factor α is essentially due to the DC resistance of the

cable, increased proportionally to the square root of the frequency by the skin effect. For sufficiently high frequency, the skin depth is supposed to be small compared with the radius of curvature; then the series resistance is :

$$R = \frac{\sqrt{\mu w}}{\sqrt{2} \cdot \pi \cdot d \cdot \sqrt{\sigma}}$$

where μ is the magnetic permeability
w is the angular frequency
d is the diameter of the innerconductor
σ is the conductivity.

Assuming $\mu = \mu_0$, only the two last parameters can be varied to decrease the skin effect losses at a given frequency. Any physical correction should increase one or both of them.

Table 1 gives the characteristics of some 75Ω coaxial cables.

TYPE	OVERALL Ø (mm.)	DC RESISTANCE (Ω/100 ns)	TRANSMISSION LOSS (dB/100 ns) at f=(MHz)			
			0	100	200	400
RG164/U	22	0.06	0.006	0.65	0.76	1.3
RG 11/U	10	0.4	0.04	I.25	1.75	2.5
RG 59/U	6	4	0.4	2.5	3.5	5
G 02223*	2.25	25	2.5	6	8	11

Table 1.

*G 02223 is a miniature coaxial cable manufactured by SUHNER (HERISAU, SWITZERLAND).

The transition between the DC and the $\sqrt{f}$ attenuation is given by Terman[3] for a solid round wire and for a conducting cylinder. The second assumption is useful for miniature cables where the inner conductor is often made of copper-plated steel.

Table 2 shows the mesured deterioration of standard CLR/A pulses after passing through a 100 ns section of different cables.

TYPE	AMPLITUDE (% of input)	FWHM (ns)
RG 11/U	80 %	2.0
RG 59/U	70 %	2.1
G 02223	50 %	2.2

Table 2.

We have tried a very large cable (Flexwell HF 35/103, 103 mm Ø, 100 ns length) and noticed that higher transmission modes than the fundamental TEM may be excited, giving rise to a dispersion. Our measurements gave a fall of the group-velocity of about 4 % between 2 and 3 GHz and 6 % between 3 and 4 GHz.

On the other hand, preliminary tests of the pulse response of a superconducting miniature coaxial cable (diameter = 3,5 mm) are encouraging.

For most applications, especially delay boxes for nuclear instrumentation, an electronic correction would be preferable. For example, a switching transistor capable of a 11 dB gain at 400 MHz would allow the use of the G 02223 miniature cable in lengths up to 100 ns and up to that frequency.

3. Limits of loss compensation using transistors.

Supposing the DC current gain β of a transistor is affected by only one time constant at high frequencies, it will start to decrease from a characteristic frequency f_β with 6 dB/octave and reach the unit value at a frequency called f_t. This assumption is justified to determine the slope for some octave only from f_β ; around the extrapolated f_t, the behaviour of the current gain is more complex; one way to study this point for any given transistor has been published by the authors[4].

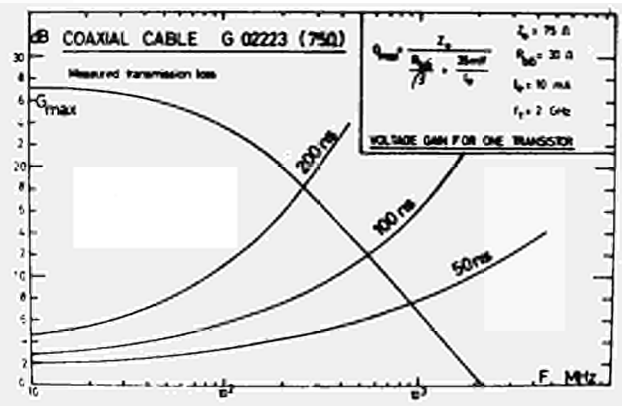

Fig. I: Transmission loss of miniature coaxial cable compared with maximum voltage gain of a single transistor amplifier with infinite DC current gain and f_t = 2 GHz.

In fig. 1, the intersection of G_{max} and the considered loss curve gives the upper frequency limit (f_{lim}) to which it is theoretically possible to provide a flat bandwidth. For a real circuit, this frequency will be the frequency of maximum gain of the amplifier and the -3 dB frequency for the response of the overall system.

4. Theory of correction circuit.

To compensate the skin effect losses, an amplifier should have a gain that increases as $\sqrt{f}$; the configuration of such an amplifier is given by fig. 2.

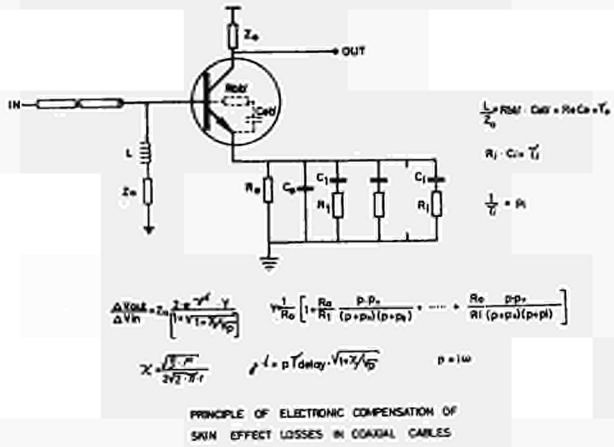

Fig. 2.: Principle of the electronic compensation of skin effect losses.

In fig. 2, R_0 and C_0 are provided to compensate for the 6 dB/octave decrease of the current gain up to f_{lim}. Therefore, R_0C_0 is set equal to $1/2\pi f_{lim}$, while R_iC_i ($i \geq 1$) are to be evaluated for optimum compensation at $f < f_{lim}$.

In the formula for the voltage gain, in fig. 2, the term $2/(1+\sqrt{1 + \chi/\sqrt{p'}})$ is assumed to be ~ 1.

Furthermore, we consider the exponential $e^{-j\beta\ell}$ as a pure delay. In the remaining factor Y, the complex contribution of each R·C is multiplied by the real quotient R_0/R_i, acting as a weight.

To calculate the correction elements, we adopted the following experimental and computing procedures :

a) measurement of the cable response in time domain and digitalisation of the obtained curves.

b) Computer transformation to frequency domain.

c) Spacing of the p_i is chosen such that $p_{i-1}/p_i \geq 2$. E.g., $p_{i-1}/p_i \sim 10$ is sufficient to correct the response within 1 dB in a frequence range where the required correction is 3 dB/octave. p_1 is arbitrarily chosen near $2\pi f_{lim}$; a large (p_{i-1}/p_i) ratio facilitates the subsequent calculations but will leave correspondingly larger wiggles in the final response curve.

d) Response calculations begin with the weights of all poles ($i \geq 1$) set equal to zero. Through successive approximations starting with p_1, individual weights are adjusted by trial and error.

5. Results.

Fig. 3 shows the correction obtained with p_0 and one pole p_1 whose weight was =1.78.

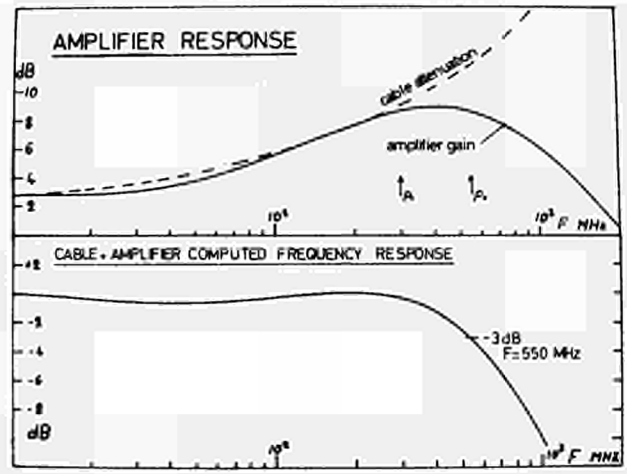

Fig. 3.: One-pole correction for $\sqrt{f}$ response.

Fig. 4 shows the experimental result for $p_0 \approx p_1 \approx 600$ MHz, $p_2 \approx 100$ MHz. The weights are 0,5 for p_1 and 0,2 for p_2, which is much less than in the first example, because of the additivity of the terms forming Y.

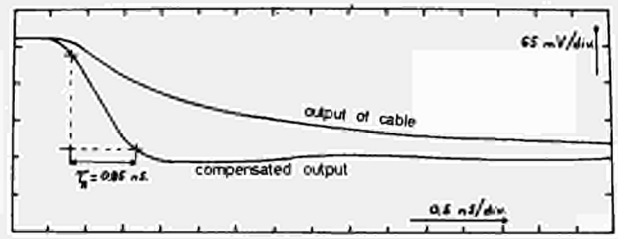

COMPENSATION OF SKIN EFFECT LOSSES IN COAXIAL CABLES

Experimental result with computed elements for 100 ns miniature cable 002223

3 time constants; transistor 2N 3960

Fig. 4.: Step response of a compensated amplifier.

We made computations for 5,7 and 10 poles, but found that the mesured response was not much better than in fig. 4.; parasitical elements introduced by the wiring obliged us to use adjustable components and to deviate considerably from computed optimum values.

6. Delay boxes for nuclear instrumentation[6].

The following characteristics would appear desirable for a modular delay box:

a) CLR/A compatible.

b) Delay range : T_o to T_o + 127,5 ns, with $T_o \leq 10$ ns.

c) Delay control : manual and/or automatic in eight binary steps.

d) Circuitry compatible with CAMAC system (see accompanying paper by D. Maeder)[5].

The conventional solution for such performance is to use high quality cable with coaxial relays for delay control.

The compensating amplifier provides an attractive solution allowing the construction of a small (2/24 CAMAC units) delay box. To this end, we had to transform the described correction circuit to a form which is suitable for electrical control of the delay length.

Control of 8 bits is achieved in a series of 4 complementary sections, built with NPN (k odd) and PNP (k even) transistors, where k (= 1, 2, 3, 4) is the number of the section. Each section is controlled by 2 bits as shown by fig. 5, with unit steps given by $\Delta T_k = 2^{(2k-3)}$ ns.

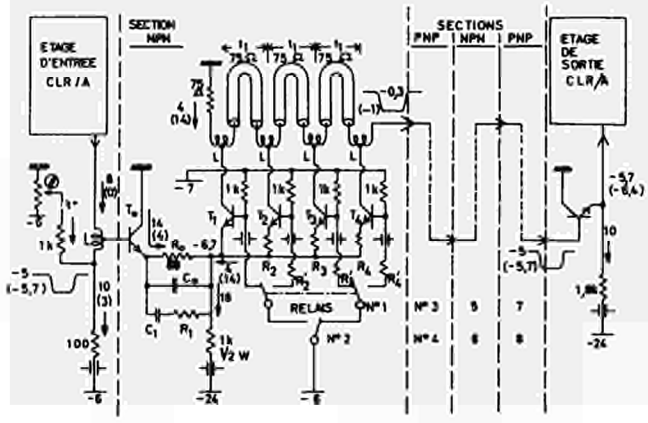

Fig. 5.: Principle of standard CLR/A 127,5 ns delay box.

In each section, the electronic switching circuit can insert 0,1,2 or 3 delay units; notice that relay contacts of fig. 5 max be replaced by switching transistors, controlled by logic gates of the CAMAC system.

In the first two prototypes, there is only one $\sqrt{f}$ correction, adjusted to the longest delay length of that section. Resistors R_2, R_3, R_4, together with parasitic input capacitances of transistors, reduce DC and HF gain sufficiently for shorter delays. The mesured overshoot on the output for zero delay is less than 5 %. Some practical problems still remain unsolved for the series construction of such delay lines : groups of five similar HF switching transistors are to be selected if we don't want to adjust the corrections to each transistor.

References.

1) D. Maeder : Proc. of the Monterey Conference 1963 on Instr. Techn. in Nucl. Pulse Analysis, Paper 1. Nat. Acad. of Sc. Series Rep. Nr. 40, p. 325; Bulletin A.S.E. 55 (1964) 361; Nucl. Instr. and Methods 31 (1964) 349-352.

2) R.L. Wigington and N.S. Nahman : Transient Analysis of Coaxial Cables Considering Skin Effect; Proc. IRE, Feb. 1957.

3) F.E. Terman Radio Engineers Handbook, p. 35 f.f. Mc Graw-Hill Book Comp. Inc., N.Y. 1943.

4) D. Maeder and G. Vuilleumier : Simulateur analogique de transistor, Helvetica Physica Acta 40, 4, (1967).

5) D. Maeder : Digital High-Voltage Supply for Automatic Testing and Regulation of Photomultiplier Gain, Ispra Nuclear Electronics Symposium, May 1969.

6) D. Maeder and Mme Sabev : Système de circuits logiques avec affichage et commande en vue d'une télécommande par ordinateur; Colloque Int. sur l'Electronique Nucléaire, Versailles, sept. 1968, p.57

Acknowledgements.

The authors whish to acknowledge Mme Sabev, M. Chevalley and M. Schindler for their collaboration and the Swiss National Research Foundation for financial support.

DISCUSSION

Righini : Could you please specify which is the delay range of the unit and the minimum step increase ?

Vuilleumier : Minimum overall delay of the circuit shown in Fig. 5 is $T_o \approx 9$ ns. Depending on relay positions, additional delays are inserted in 0,5 ns steps up to 127.5 ns maximum.

Zajde : - I have two questions : what is the amplitude linearity of your active loss compensation system ? Second question is : can this system be used with a small signal ?

Vuilleumier :- Within the range corresponding to $\pm$ 0,5 V on a 75 Ohm load, gain is quite linear for the low frequency components, up to at least 200 MHz. Near f_{lim}, feedback is no longer effective to assure very good linearity, in fact, ultimate rise-times may differ by ~ 10% for positive-and negative - going wavefronts. If logic signals of 0.80 V or more were applied directly to the correction circuit, its nonlinearity will become marked, but this is sufficient for logic applications.

Arbel : - In a production model, do you have to adjust the compensating network individually for each transistor ?

Vuilleumier : - The practical problem remains to match groups of 5 transistors, if we don't want to adjust the corrections for each transistor. In each section of Fig. 5, the best and the poorest transistors of the group should be placed at the ends of the cable strings.

Stanchi : - Did you try to utilize your system also for analog signals ? If yes, as I know that Dr. Maeder presented a sampling for single events with recirculating loop, did you try to utilize this system for the sampling ?
In this case how many recirculations without serious deterioration and what is the circulating time for running a loop ?

Vuilleumier : - We precisely did not make the iteration and it hasn't been applied to that problem but it may be in a few weeks because I am working on that project and we have made a computer program for these corrections for our single event sampling analyzer. We can feedback something like 30 circulations and the rise-time will be something like 2 ns but we hope that it will be a little better with the computed elements.

Stanchi : - And the time of the circulation what is it ?

Vuilleumier : - It's 100 ns, but of course we don't use for that miniature coaxial cables. I must say that a big coaxial cable was intended for analogical memory and it hasn't given the expected results.

DEADTIME CORRECTIONS IN A TWO-PARAMETER SYSTEM CONTAINING FOUR DETECTORS

Gudmar Grosshög
Department of Reactor Physics
Chalmers University of Technology
Gothenburg, Sweden

Summary

A study of the deadtime correction in a complicated counting system is performed. It is shown how the transfer of information can be divided into extrinsic and intrinsic transfer. The intrinsic transfer depends on the total information flow from all detectors and has been treated with an experimental method, which is compared to a numerical model. The extrinsic transfer depends on the information flow in each detector line. It is shown that this effect can be studied through pile-up.

Introduction

As a counting equipment grows in complexity, the problem of doing an exact correction for the pulse losses will be more and more difficult [1-6]. One has therefore reasons to keep the correction as low as possible by having short conversion times and using a buffer memory before the often slow memory block. The consequence of this is, however, that the losses will depend not only on the intensities but also on the time and amplitude distribution of the stored pulses. Although it is difficult, it is quite possible to correct for these effects, since all information about them is contained in the measured distributions. There are, however, other effects that we know nothing about. They arise from those parts of the pulse spectrum, which are rejected in different places of the equipment by analog or digital data reduction. So we are forced into some method by which we can measure at least the main part of the correction.

The system

The purpose of the system is to measure the time and amplitude distribution from four detectors simultaneously. The capacity of the memory block is 1024 channels, which can be arbitrarily subgrouped in binary steps for the three parameters: number of detectors, amplitude channels and time channels. The method is applicable to different combinations of these parameters. Results are given for the subgrouping 4 detectors, 32 amplitude intervals and 8 time intervals. The division in amplitude is linear but in time it is logarithmic [7, 8].

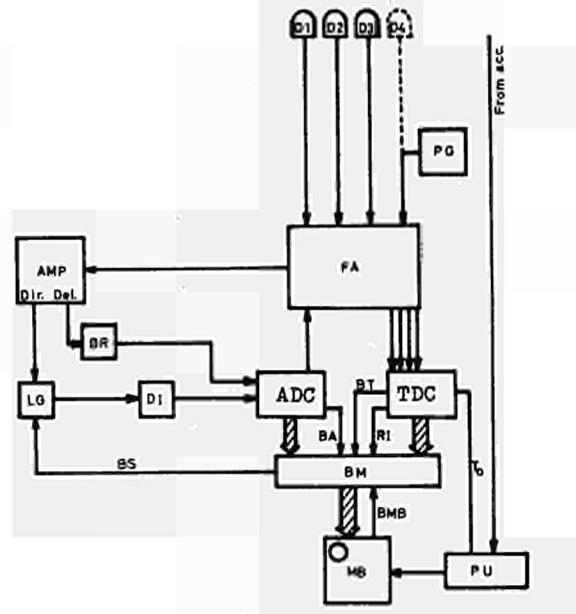

Fig. 1. Principles of the equipment.

The principles of the system are sketched in figure 1. A repetitive start pulse (T_0) passes a programming unit, which controls the measuring time. It is switched on manually and off either by the condition that it has reached a preset number of measuring cycles or by the condition that there is an overflow in any of the channels in the memory block.

The pulses from the detectors (Dn) are amplified and added by an summing amplifier in the amplifier unit (FA). The signal from the addition circuit is fed into an amplifier (AMP) with two outputs, one direct and one delayed. The delayed output is over a base line restorer (BR) connected to the direct current input of the analog-to-digital converter (ADC). If the system is not busy, the pulse from the direct output passes a linear gate (LG) and activates a discriminator (DI), which triggers the ADC and the logic circuits in FA. From these a signal in the actual detector line starts the time-to-digital converter (TDC).

From now on the conversion proceeds in both ADC and TDC. The conversion time is fixed to 4 microseconds in TDC but depends on the amplitude in ADC. The result of the conversion is loaded into the buffer memory (BM), where it is kept until both the conversions are ready and the memory block (MB) has completed a possible preceding storing cycle. TDC gives the time information in a linear scale. A conversion to the logarithmic time scale[7] is realized during the transfer of the information to the memory block.

The system busy signal (BS) to the linear gate is evaluated in the buffer memory from the signals BA, BT, RI and BMB. It signals busy if ADC or TDC or the buffer memory is engaged or if the time is outside the actual time interval. The overall deadtime of the system depending on the amplitude, the time channel width and the intensity. The minimum deadtime for a stored pulse is about 8 microseconds.

Deadtime losses

A schematic picture of the equipment from the view of deadtime losses is given in figure 2. In the block marked " system " we have collected all parts that have the same influence on the deadtime for all of the detectors.

In order to give the system information about which of the detectors that is responsible for the actual signal, all amplifiers are followed by a one bit memory (monostables marked MS1 to MS4 in the figure). One of the first actions taken by the system after the arrival of the pulse is to read this information. As every monostable is controlled directly by its own detector, this part of the equipment will have a deadtime that depends on the pulse rate of the detector in question.

So we see that two different types of deadtime appear in the system. The first depends on the pulse rate in each detector line, the second depends on the summed pulse rate and the pulse amplitude distribution from all detector lines. We will in the continuation use the attributes extrinsic and intrinsic for these effects.

We can now write

$$P_i(a,t) = G_i(R_i) \cdot H\left(\sum_{i=1}^{4} R_i\right) \cdot R_i(a,t) \qquad (1)$$

where

P_i = stored number of pulses for detector i
R_i = incoming number of pulses for detector i
H = intrinsic transfer function
G_i = extrinsic transfer function for detector line i
t = time
a = amplitude

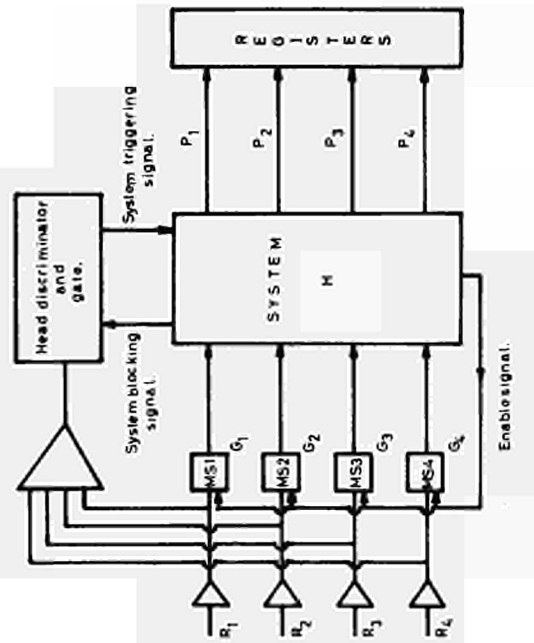

Fig. 2. Working principle for deadtime considerations.

In this equation we have assumed that the intrinsic and extrinsic transfer functions are independent of each other. Owing to the effects of overlapping this is generally not true. The equation is, however, a good approximation if, for a given i, any of the functions is not far from 1.

Intrinsic transfer.

Experimental method

Suppose that we have a known distribution of well separated pulses in one detector line i.g. 4. In that case $G_4 = 1$ and

$$P_4(a,t) = H \cdot R_4(a,t) \qquad (2)$$

from which

$$H(t) = \frac{\int_{a_l}^{a_u} P_4(a,t)\,da}{\int_{a_l}^{a_u} R_4(a,t)\,da} \qquad (3)$$

where a_l and a_u are the amplitude limits.

The transfer function given by this method contains the effects of all the detector lines but the test line. This depends on the fact that the test pulses are well separated and not Poisson distributed. We use this method in order to have G_4 equal to one and because the test pulses can in this case easily be generated by an ordinary pulse generator. With a constant pulse rate of 72 pulses per second in the test channel the influence of this is approximately one per mille.

So, we can measure the intrinsic transfer function simply by exchanging the detector in one detector line with a pulse generator. The numerator of equation 3 is then recorded in the analyser and the denominator can be counted in a scaler gated by a signal, which gives information about the time of interest.

Error analysis

The statistical errors of the method depends primarly on the variations of the recorded number of counts from the test line. In order to investigate this variation a series of runs was made with $H(t) \equiv 0$ and the number of input pulses going from 15 to $65 \cdot 10^6$. It was found that the standard deviation varied in the some way as that of a Poisson distribution. In 75 % of the runs the difference was less than 3 %. As an example the distribution of the channel contents for one run with $5.8 \cdot 10^6$ pulses is given in figure 3.

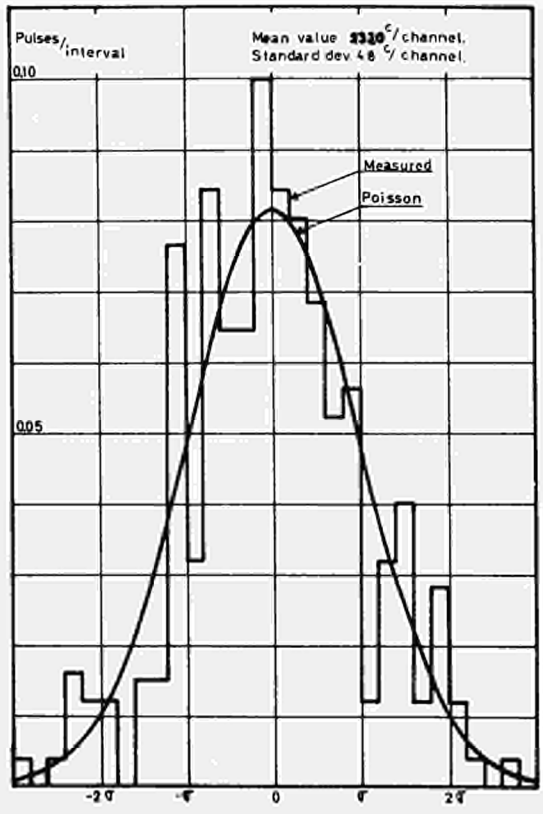

Fig. 3. Probability density function of the test line.

Numerical model

The method has been checked with a rather simple numerical model. This model uses the fact that if the channel width is small, the effects from the amplitude converter will predominate. We assume also that the transfer time between the buffer register and the memory block is zero. The deadtime can now be separated into two parts. The first is the sum of all constant waiting times (t_w), the second is proportional to the converting time and therefore also to the amplitude. The relation between the deadtime calculated in number of channels after the arrival of the pulse (k) and the amplitude (a) can then be written

$$k = t_w + c \cdot a \qquad (a \geq 0) \tag{4}$$

where c is a proportionality constant that depends on the settings of the amplitude converter. The inversion of this equation is

$$a(k) = \frac{k - t_w}{c} \qquad (k \geq t_w)$$
$$a(k) = 0 \qquad (k < t_w) \tag{5}$$

The probability that a channel j is closed is then

$$S(j) = \sum_{i=1}^{j-1} \sum_{k=j-i}^{\infty} p(a(k), i) \qquad (j>1) \tag{6}$$
$$S(j) = 0 \qquad (j=1)$$

p (a, i) is the probability of a pulse in the linear time channel i and amplitude channel a. It can be calculated approximately from the stored distribution P (a, i) as

$$p(a,i) = \frac{P(a,i)}{N} \qquad (a, i \text{ inside the measured range})$$
$$p(a,i) = 0 \qquad (\text{elsewhere}) \tag{7}$$

where N is the number of repetitions. It is assumed that the system is open in the beginning of each cycle and that all pulses above the discriminator level are stored. The intrinsic transfer function is finally

$$H(i) = 1 - S(i) \tag{8}$$

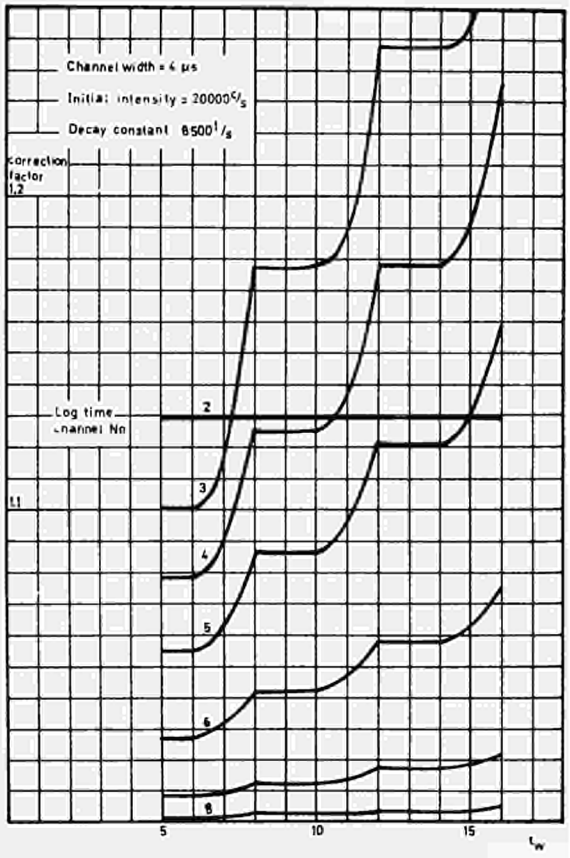

Fig. 4. Calculated correction factor as a function of the deadtime t_w.

The result of a calculation with this method is shown in figure 4. The distributions are taken from an ordinary experiment with eight logarithmic time channels and 32 amplitude channels. The calculation is made in a linear time scale but the result is transferred back to the logarithmic scale. Time channel number one is zero, as the system always is considered to the open at that time, number two is constant because t_w is larger than the channel width. The other curves show plateaus and transients. With 32 amplitude channels the deadtime variation is 1.6 microseconds, which gives transients in the channel limits that last over a period of 3.2 microseconds. The shapes of the transients are determined by the amplitude distribution.

We have also compared the model to the correction factor obtained from measurements using the above method. The result is shown in figure 5. The input to the experiment is a neutron and gamma field, where the neutrons give a dominant peak decreasing with a decay constant of approximately 8500 1/s. The difference between the runs is that they have different starting times, which gives the different initial intensities noted in the figure. The relative accuracy of the experimental points is also indicated in the figure.

From the figure we conclude that there is satisfactory agreement between the model and the experiment in the intermediate part, but there are deviations both in the beginning and the end part of the curves. We shall, however, keep in mind that all common effects are included in the experimental values. In the beginning there are transients, which have not been accounted for in the model. The effects in the end part may depend on uncertainties in the gating signal to the scaler needed for the denominator in equation 3. The correction is, however, low and second orders corrections may also come into the picture.

The result of this investigation is that a check of the experimental method has been obtained. The rather simple model gives correct results in the main part of the experiment but not in the limits. The model is also expensive by consuming rather long computing time. It is therefore not attractive to expand the model by putting more routines into the computer program.

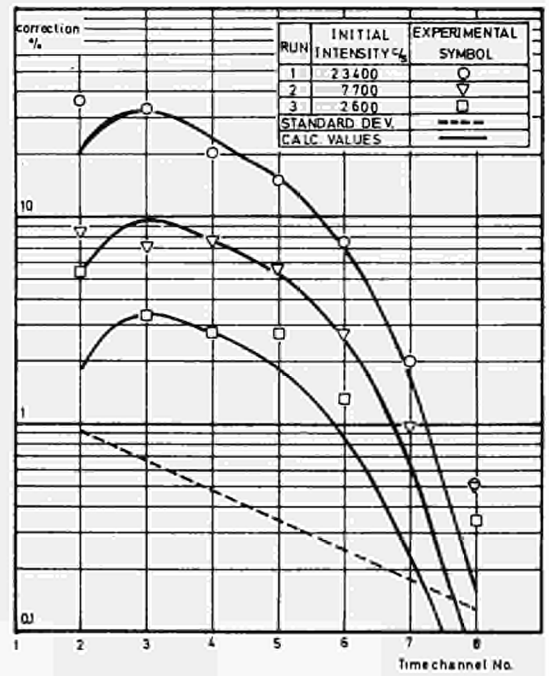

Fig. 5. Comparison between measured and calculated values of the intrinsic deadtime correction.

Extrinsic transfer

In the detector lines we have to take two effects into account. Firstly, there is the effect of pile-up in the amplifier chain, secondly, the monostables have a time period during which they can not be reactivated. So, the system we have to study here is two serial connected blocks If the deadtimes of these are t_1 and t_2, we can state the following about the resulting deadtime t_m.

a. If $t_1 \geq t_2$ then $t_m = t_1$

b. If $t_1 < t_2$ then $t_1 + t_2 > t_m > t_2$
(t_m depends on intensity)

c. If $t_1 << t_2$ then $t_m \approx t_2$

From these statements it is clear that it is favourable to have the largest deadtime in the beginning of the chain. This presupposes that all irrelevant information can be sorted out at this early stage, which often is not possible. One is therefore left with a compromise and must try to sort out as much irrelevant information as possible to the lowest price in deadtime.

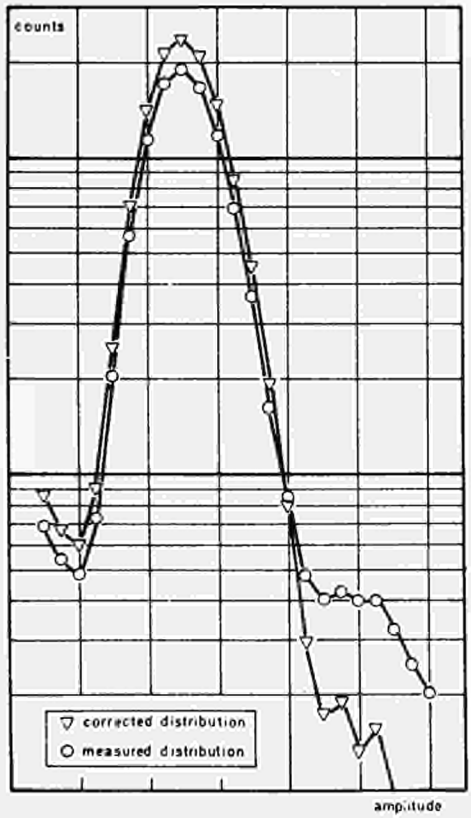

Fig. 6. Comparison between a measured and a corrected amplitude distribution.

In our case the deadtime of the monostables is of the same order as that of the pile-up effects. As the pile-up effects are reflected on the amplitude distributions, we will use them to study the extrinsic deadtime effects.

Pile-up is a coincidence in the analog parts of the system between two different pulses. The result is an analog addition between the two pulses, which gives a pulse with strange shape[9]. If we can assume that the resulting pulse has a definite length (τ) we can write

$$p_m(a)\,da = p(a)\,da + \tau\,(I_1 - I_2)\,da$$

$$I_1 = \int_0^\infty \int_0^\infty g(a_1, a_2, a)\, p(a_1)\, p(a_2)\, da_1\, da_2 \qquad (9)$$

$$I_2 = p(a) \int_0^\infty p(a)\, da$$

where

$p_m(a)$ = the measured distribution in counts per second and amplitude interval.

$p(a)$ = the corrected distribution

$g(a_1, a_2, a)$ = the probability that a pulse with the amplitude a_1 and a pulse with the amplitude a_2 is stored as a pulse with the amplitude a.

The function g depends on the pulse shape and on how the ADC treats strange pulse shapes. As a simple model we assume that the undisturbed pulse has a rectangular shape with amplitude a and length $\tau/2$. Then we can write

$$g(a_1, a_2, a) = \delta(a - ea_1 - ea_2) \qquad (10)$$

where δ is the Kronecker delta function and e is a parameter to be determined.

Equation 9 can easily be solved by iteration, starting with $p_m(a)$ as the first approximation for $p(a)$. For ordinary values of the pulse rate the iteration converges in few steps.

Errors in the parameters e and τ give distortions in the resulting amplitude distribution. The parameters can therefore be determined by trial and error with the condition that the distortions shall be out. In our case we have found $e = 0.9$ and $\tau = 3$ microseconds.

Another problem is the low part of the amplitude distribution, which is not measured. In order to take this into account we have to extrapolate the distributions down to zero.

It should be pointed out that pile-up caused by pulses from different detector lines is sorted out by a coincidence circuit. The result of this operation is a blocking of the whole system. Therefore, the deadtime caused will be contained in the intrinsic deadtime.

As an example the amplitude distribution before and after correction is given in figure 6. The intrinsic correction is 20 % and the local intensity is 40, 000 counts per second.

Acknowledgements

The author is grateful to professor N.G. Sjöstrand and the members of his institution for help and valuable discussions during this work. Particularly I want to thank Gunnar Rönnberg for his work with the computer programs.
The work has been supported by the Swedish Atomic Research Council.

References

1. F.Rau und G.H. Wolf, Nucl. Instr. and Meth. 27 (1963) 321.
2. Kerstin Löw, Nucl.Instr. and Meth. 26 (1964) 216.
3. H. Seufert, Nucl. Instr. and Meth. 44 (1966) 335.
4. P. Paatero and K.Eskola, Nucl. Instr. and Meth. 44 (1966) 357.
5. C.E.Cohn, Nucl. Instr. and Meth. 41 (1966) 338.
6. J.Harms, Nucl.Instr. and Meth. 53 (1967) 192.
7. G.Grosshög, CTH-RF-10 (1967) (internal report).
8. G.Grosshög, CTH-RF-16 (1968) (internal report).
9. A.M.R. Ferrari and E.Fairstein, Nucl. Instr. and Meth. 63 (1968) 218.

A DATA-COLLECTING SYSTEM FOR PULSE RADIOLYSIS EXPERIMENTS

by

K.E. Neisig and S.O. Nielsen

Danish Atomic Energy Commission
Research Establishment Risö

Summary

The study of chemical reactions resulting from electron irradiation has been carried out by means of an advanced optical channel that measures the light transmission through a reaction cell containing the irradiated sample.

This paper describes the electronic instrumentation for these experiments and especially the digital equipment that collects all measurements and experimental parameters.

1. Introduction

Pulse radiolysis can be monitored by measuring the time variation in transmission of monochromatic light through the sample after irradiation with microsecond electron pulses. This variation reflects physical and chemical reactions e.g. between free radicals and various exited states, and is of considerable interest, because much important information, such as absolute rate constants and absorption spectra may be derived from it.

Pulse radiolysis experiments have been carried out at the 10 Mev linear accelerator at Risø over the last few years[1]. A description[2] of the monitoring instrumentation that collects analog data with time constant 80 nsec on polaroid films will appear shortly. It is, however, convenient for understanding the following discription of the data collecting system to take a brief look at the essential parts in the experimental set-up at the linac.

2. Experimental Set-Up

The chemical sample to be investigated is placed in the reaction cell as seen in fig. 1. Via an optical system a light beam from a Xe lamp is transmitted through the cell that is made of Suprasil quartz. The optical channel consists of a system of quartz lenses, mirrors and a monochromator and is terminated in a photomultiplier.

The normal current to the Xe-lamp is approx. 27 A, but in a pulsed mode the lamp may accept a current boost of approx. 150 A for something like 600 μsec, thus increasing the light intensity 25-30 times during the measurement. Two spherical mirrors are placed one on either side of the reaction cell, allowing the light beam to sweep 4-20 times through the cell.

When an electron pulse is released from the accelerator and penetrates the sample in the reaction cell, the light transmission through the sample is changed due to radiation induced light absorption. By means of the photomultiplier this change in light transmission is recorded with the equipment following next, which has hitherto been oscilloscopes equipped with polaroid cameras.

Conversion of the results to digital form suitable for computer calculations was, however, a troublesome and time-consuming process. As seen in fig. 1 three traces may be derived through RC-filters with different time constants matched to the individual choises of sweep rates. Basically these signals, e_1, e_2 and e_3, are fed to the inputs of the digital system. Other signals, e_4, e_5, e_6 and e_7, are derived from a secondary emission chamber which detects the direction and total charge of the pulsed electron beam. It is essentially a circular metal foil disc split into four quadrants. The current from each quadrant is integrated separately by a charge-sensitive amplifier.

3. Basic Requirements of the Data Collecting System

In fig. 2 are shown oscilloscope traces, which may be taken as representative and from which some basic requirements to be met by the data collecting system can be derived. One large division on the ordinate corresponds to 10% transmission through the sample in the reaction cell. One large horizontal division is 2 μsec related to the upper trace. The oscillation at the starting 100% transmission level is noise pick-up in the channel. Because of the strong Cerenkov radiation during the electron pulse that would overload the vertical amplifiers in the oscilloscopes, it is necessary to clamp the input signal to the oscilloscopes to an arbitrary level visible on the oscilloscope screens

during the pulse. The clamp action stops 0,2 μsec after the Cerenkov light has died away. The remainder of the trace in fig. 2 is the proper radiolytic absorption transient. The lower trace is the same transient as that shown above, but recorded with 20 μsec per division. Traces of several seconds length are also sometimes required.

The optical transmission is recorded in its entirety as a function of time using an analog-to-digital converter. The sampling frequency, fs, must be selected as at least twice the highest frequency component to be recognized. Higher frequencies, e.g. due to noise, must be cut off by filtering circuits that allow only the signal to pass in the frequency range 0-½ fs. Because of the drop of high frequency components in the signal it seems advantageous to let also fs decrease with time. Basically, this requires a corresponding shift in the filter cut-off in order to avoid frequency-folding in the range from 0-½ fs.

Based on these considerations it was found convenient to split the complete radiolytic absorption transient into three distinct sections called K_1, K_2 and K_3 corresponding to the signals e_1, e_2 and e_3 each section having preselected, but constant sampling frequencies. The first section K_1 is characterized by the maximum frequency content of the signal. Therefore a relatively high sampling frequency in K_1 is required. The trace as observed in K_2 differs from that in K_1 only in that a higher degree of filtering may be tolerated without distortion of the information. Transfer from K_1 to K_2 may result in some DC offset, which is tolerated because it is possible to normalize the characteristic by a short transitional sampling interval during the subsequent off-line data handling. In the third section, K_3, only small changes in the information occur; consequently a relatively low sampling rate, which allows insertion of the four values e_4, e_5, e_6 and e_7 between consecutive samplings, is employed.

4. Description of the Data-Collecting System

Fig. 4 shows a block diagram of the essential parts in the digital system. To the left is shown the eight-channel analog multiplexer, which, as mentioned, accepts three absorption traces and four signals from the secondary emission chamber and a separating marker signal announcing that these signals follow. The output from the multiplexer is handled in the fast A/D converter capable of making a complete 8-bit conversion in 125 nsec.

The digital information is temporarily stored in the fast shift register, which acts as a buffer (80 words) and accepts the initial steep slope of the transient in K_1 and, in accordance with a preselected sampling programme, transfers this information to a slower ferrite core memory. The programme mentioned involves a choice of sampling intervals: T_1, T_2 and T_3, from the master clock. Further the number of samplings: N_1, N_2 and N_3, is selected from the counters BCD_1, 2, and 3, corresponding to trace sections K_1, K_2 and K_3 respectively. The counters BCD K_2 and BCD K_3 provide the transitional sampling interval between K_1, K_2 and K_2, K_3. As earlier mentioned, the signals from the four charge-sensitive amplifiers e_4, e_5, e_6 and e_7 represent the dose delivered by the electron-beam. Once digitized, they are recorded after a constant time interval determined by the counter BCD_6, and the four values are inserted between consecutive samplings in section K_3.

5. System Details

Essential parts of the digital system are built of integrated logic circuits of the TTL family as is the case with the high-speed buffer. It consists of eight rows of serial-in, serial-out 8-bit shift-register packages, ten in each row, and is thus capable of storing and transferring 80 8-bit words at a clock rate of about 15 MHz. The combination of high-speed buffer and ferrite core memory was found to be the more economical solution compared with that of using a high-speed film memory, even though it was necessary to add auxiliary circuits, e.g. the BCD_5 counter used to transfer the last 80 words in the measurement to the core memory before the read-out cycle was initiated.

Another device composed of integrated circuits is the master clock that covers seven syncronous decades. It is possible to select sampling intervals according to the pattern $n \cdot 10^{-q}$ sec, with n = 1, 2, 5 and q = 0, 1, 2, ...7.

Among units built with discrete components is the eight-channel analog multiplexer. It consists of eight linear gates that may be switched sequentially to the output stage.

In fig. 5 is shown a single gate of the multiplexer. The switching time obtained is 20 ns max.

6. Information Read-Out

When a measurement has been carried out, the discrete values from the absorption transient together with the charge condition of the quadrant detector are stored in the ferrite core memory in purely binary form. The selected sampling intervals T_1, T_2 and T_3 and the number of samplings N_1, N_2 and N_3 are stored in coding circuits and BCD counters respectively. In fig. 6 the information sources mentioned are shown connected to the read-out bus. By means of the

units word-to-symbol, symbol-to-bit this information is transferred to the teleprinter, which stores it on punched paper tape and in table form.

Acknowledgements

We thank Mr. K.B. Hansen for valuable discussions during the planning phase of the digital system described, Mr. Th. Hviid for development of the input amplifiers and the linear gates, and Mr. J.N. Petrov for his work with the binary-to-BCD converter.

For aid in the laboratory with the I.C. composition and the system layout we want to thank Mr. V. Thøfner, Mr. Sv. Nielsen and Mr. K. Davids.

References

1) S.O. Nielsen, P. Pagsberg, J. Rabani, H. Christensen and G. Nilsson. "Pulse Radiolytic Determination of Ultraviolet Absorption of Hydrogen Atoms in Aqueous Solution". Chem. Commun. 1523, (1968)

2) H.C. Christensen, G. Nilsson, P. Pagsberg and S.O. Nielsen. "Pulse Radiolysis Apparatus for Monitoring at 2000 Å". Rev. Sci. Instr. in press.

3) S.I. Taimuty and B.S. Deaver, Jr. "Transmission Current Monitor for High Energy Electron Beams". Rev. Sci. Instr. 32, 1098, (1961)

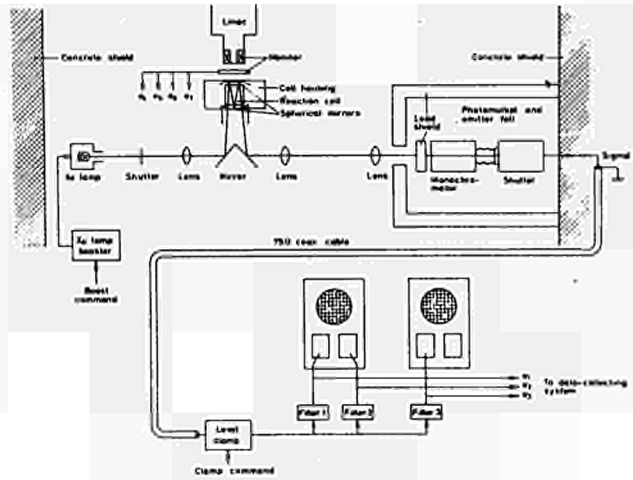

Fig. 1 - Experimental set-up.

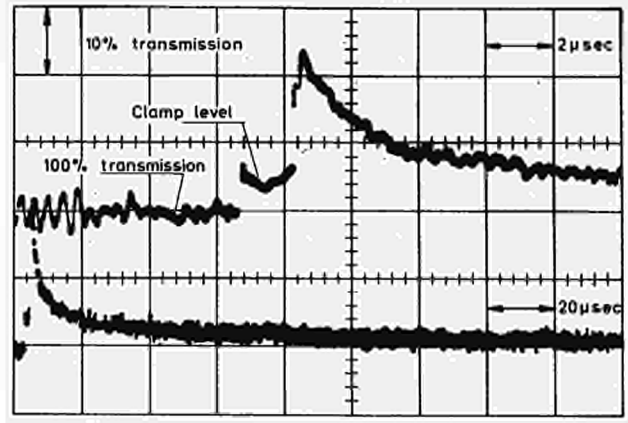

Fig. 2 - Radiolytic optical absorption transients.

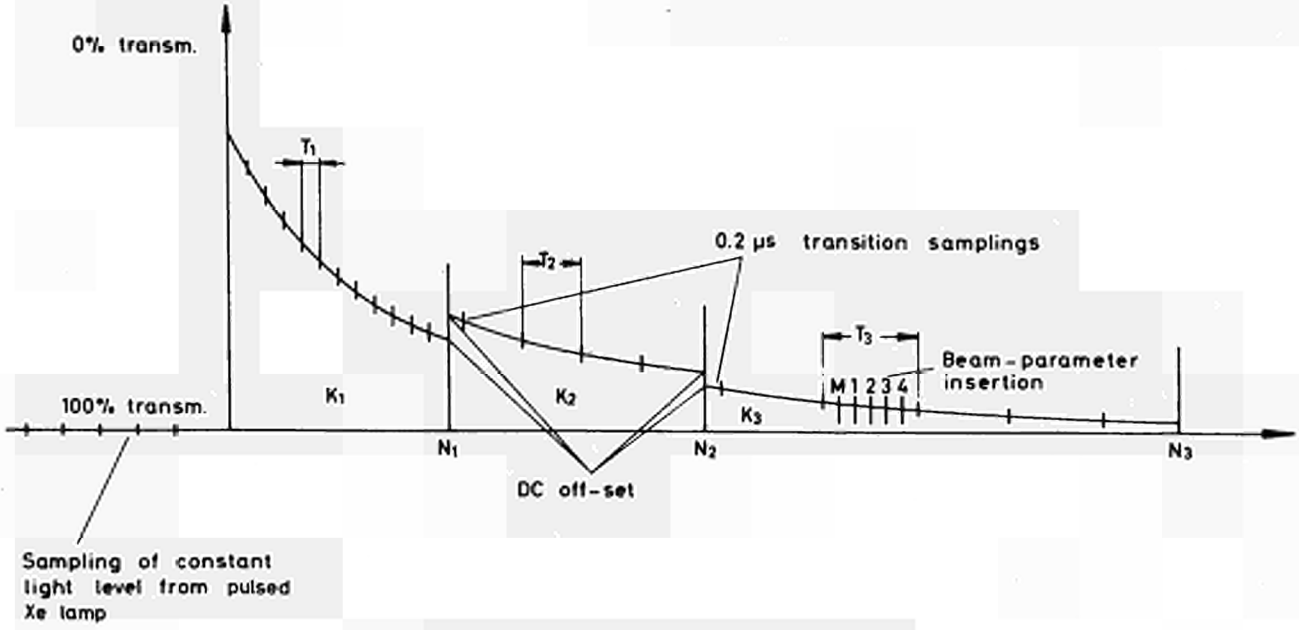

Fig. 3 - Idealized absorption transient.

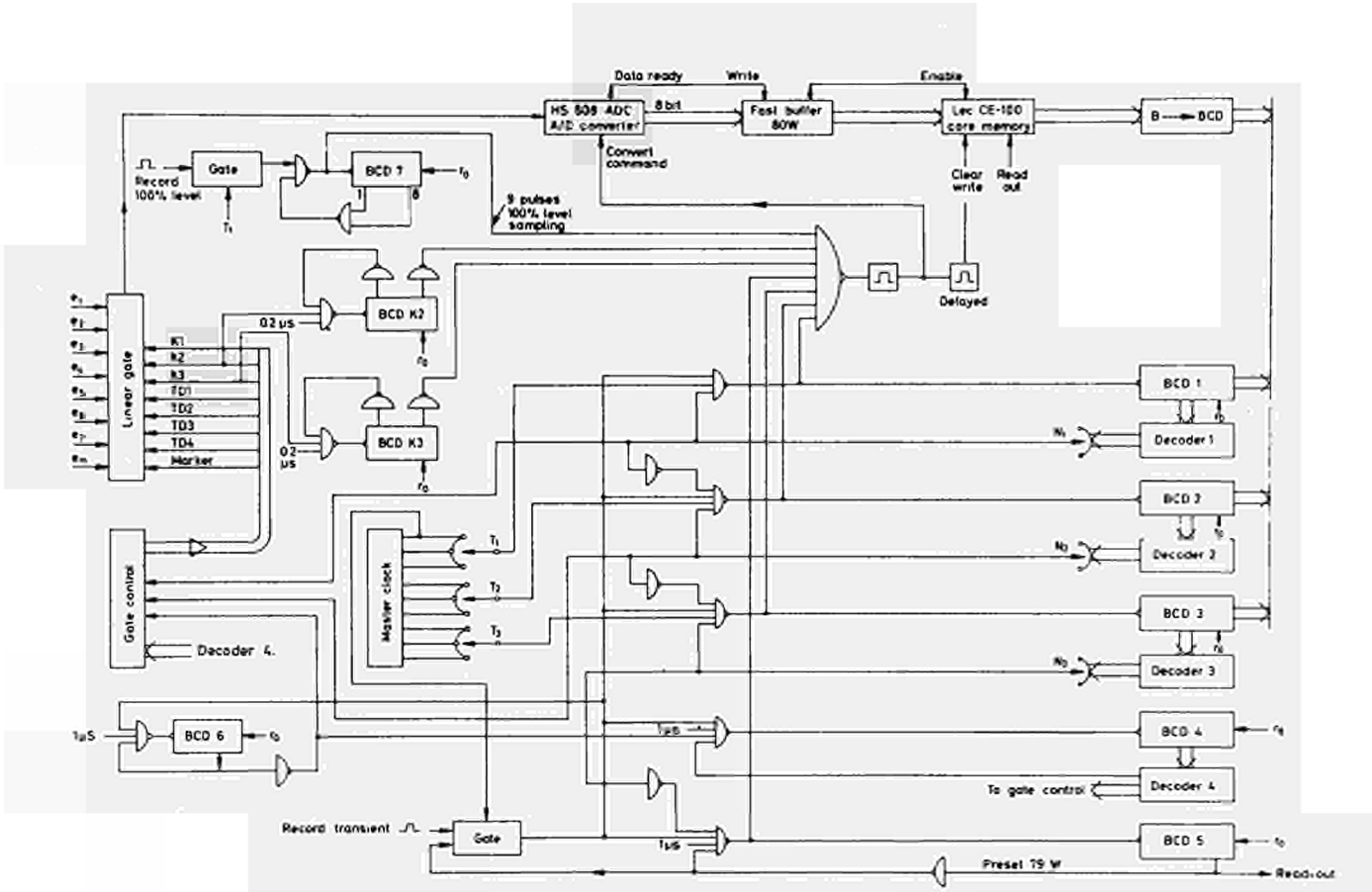

Fig. 4 - Data-collecting system.

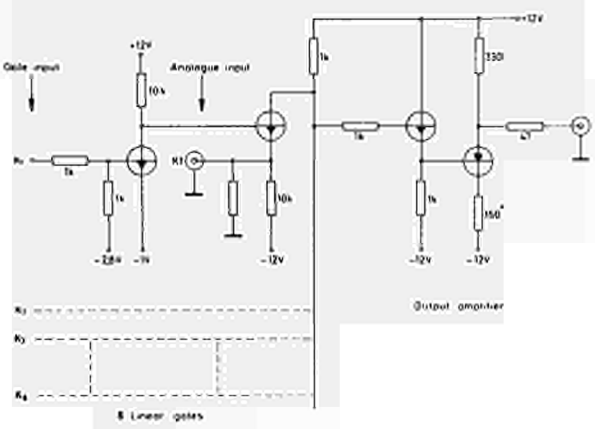

Fig. 5 - Schematic of the linear gates.

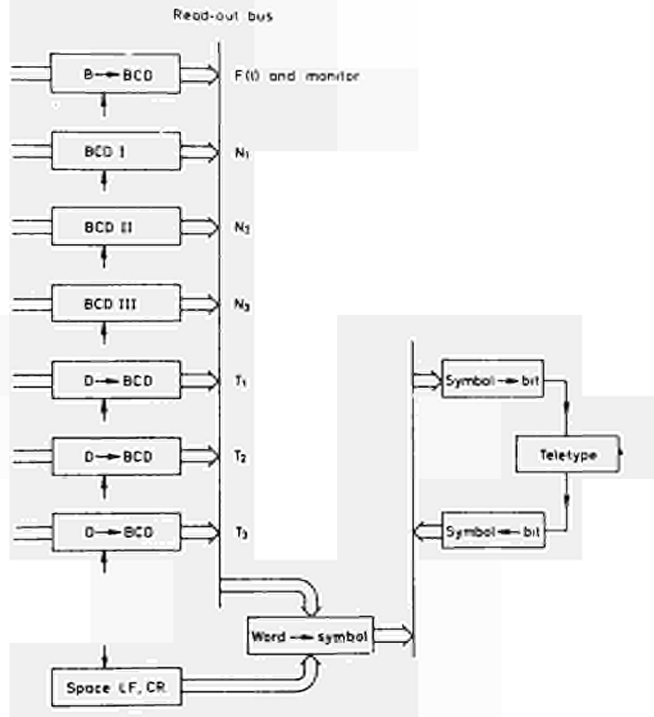

Fig. 6 - Read-out.

WIRE PROPORTIONAL COUNTER ARRAYS WITH FAST DIGITAL ARITHMETIC FOR DECISION MAKING *

L. J. Koester, R. M. Brown, U. Koetz, T. Clark, S. Segler, and R. Taylor

Department of Physics, University of Illinois, Urbana, Illinois

SUMMARY

Multiwire gas proportional counters have been tested with a finely collimated beam of 1 GeV/c particles. In each case, the distance from wires to wall was 1/4 inch, and 0.002 inch stainless steel wires were used. Wire spacings of 1/8 inch and 1/16 inch were compared. With a 90% argon, 10% methane filling at one atmosphere, the operating voltage was 3.0 Kv for 1/8 inch and 4.7 Kv for 1/16 inch spacing. Efficiencies greater than 99% were achieved, and little difference in timing was observed between the two geometries. A mixture of 90% Ne, 10% He bubbling through heptane at 0°C required 1.95 Kv for 1.16 inch spacing but did not improve the time jitter. Running alternate wires at negative voltage also did not improve the jitter.

These counters have been used to trigger spark chambers. A new scheme of fast arithmetic is in preparation for making decisions.

MOTIVATION

In a proposed experiment on elastic scattering of mesons by complex nuclei, some of the scattering angles of interest are as small as 5 milliradians. With an incident beam 5 cm in diameter, many of the scattered particles remain in the area of the beam. Three hodoscope planes with elements 1-3 mm in size are needed to determine whether or not a beam particle traversed the target undeflected. Otherwise it would be necessary to pulse the spark chambers for each incident particle and to wait about 10^{-3} sec for them to recover before the next event.

Among other properties, the hodoscopes should present a minimum of scattering mass to the beam, should be capable of 3 mm spatial resolution, and should deliver signals to trigger spark chambers less than 1 microsecond after the particle traversal. Finally, their recovery time should be short enough to permit a reasonably intense beam. Probably these specifications can be met with scintillation counters, but the multiwire gas proportional counter arrays seem very promising and economical relative to phototubes.

The second part of the problem is to make the logical decision whether the particle trajectory was straight or not. For one dimension. if three planes each containing N elements are used, the number of possible straight line combinations requires N^2 three-input coincidence circuits. If, instead, a binary position coordinate is assigned to each element, the complexity of the logic is roughly proportional to $\log_2 N$. If the planes are equally spaced along the beam direction, and the particle intersects these planes at positions X_1, X_2, and X_3, then for a straight line, $X_1 + X_3 = 2 X_2$. This test can be made with a single addition and shift in less than 100 nanoseconds with integrated circuits.

MULTIWIRE PROPORTIONAL COUNTERS

Construction

Charpak[1] and Fischer[2] have described the construction of counters similar to ours. The chambers are made of epoxy fiberglass or lucite with 0.002 inch diameter stainless steel wires and thin conducting walls. The wires are spaced 1/8 or 1/16 inch apart over a 2 inch square active area. The distance from the wires to either wall is 1/4 inch. An interesting observation (well known to gas counter experts) is that aluminum walls are light sensitive. Thin aluminum foils coated with aquadag, however, provide a good wall of lower mass than a wire grid. Copper foil on mylar is also satisfactory from a functional viewpoint.

The simplest gas to use is 90% argon - 10% methane flowing continuously at a very low rate. The regular spark chamber Ne-He mixture must be mixed with heptane or pentane. The percentage mixture critically affects the operating voltage. The best procedure is to prepare the mixture in a previously evacuated tank at high pressure. Very reproducible results may be obtained by bubbling the gas through liquid heptane or pentane at 0°C if the liquid is contained in a washing bottle immersed in ice water. It is important that the gas flow slowly and make very fine bubbles as it passes through the fritted glass plug.

A charge sensitive preamplifier designed by C. J. Rush[3] was chosen for its speed, low noise, and simplicity. Its gain was approximately 3.5×10^{12} V/coul when driving a 50 Ω line. Since output signals of 0.2 V amplitude were obtained for minimum ionizing particles, the gas multiplication in the counter was of order 10^4. Four printed circuit boards containing four preamplifiers each were mounted close to the wire chamber inside an aluminum shielding box. Signals from the individual wire preamps were brought out in a bundle of RG 174/u cables to the logic panel.

Testing with 1 GeV/c Particles

In order to measure the counter efficiency, delay time, and time jitter, a 1 GeV/c test beam was prepared at the Argonne Zero Gradient Synchrotron. This beam was defined geometrically by two plastic scintillators 1/32 inch high and 1 cm wide placed 12 inches apart along the beam axis, followed by a third scintillator 1 inch high and 1/8 inch wide, a threshold gas Cherenkov counter, and another scintillator 1 inch square. The aluminum box containing the counter was mounted

on a milling machine platform between the first two scintillators. The wires were horizontal, and the box had thin foil windows to transmit the particles. The counter could be moved with a precision of 0.001 inch to scan the ribbon beam vertically across the wires, or horizontally along the wires.

For this test run, the logic panel contained a discriminator for the output of each wire preamp. The (dual) discriminators were Motorola MC 1035 integrated circuits connected as one-shots followed by a single transistor level shifter. The following logic circuitry was the regular NIM standard type available at Argonne.

The first test was concerned with the counting efficiency as a function of position. Signals from three adjacent wires were gated by a coincidence output from the scintillators and scaled concurrently. Coincidences of two adjacent wires were also recorded. Figure 1 shows the result for a counter with 1/8 inch spacing and argon-methane gas.

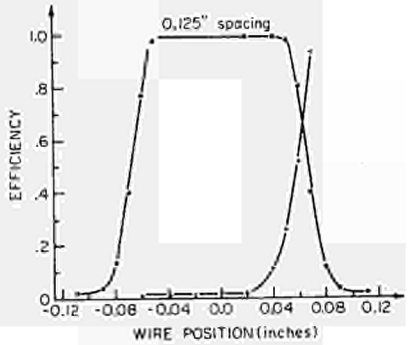

Figure 1. Counting efficiency for 1/8 inch wire spacing. A beam of 1 GeV/c particles 1/32 inch high was scanned across the wires. The dots and crosses refer to two adjacent wires. Argon-methane at 3.0 Kv.

Greater than 99% efficiency is achieved at 3000 V applied voltage. The counter efficiency is also 99% between the wires if one includes non-coincident signals from the two adjacent wires.

Since the efficiency depends somewhat on the gate width, a time-to-amplitude converter and multichannel pulse height analyzer were used to observe the distribution of delay times from one wire. Figure 2 shows the distribution obtained when the beam was centered on the wire as described above.

An artificial delay was inserted in the stop signal from the wire so that it would never precede the phototube signal. The peak of the distributions corresponds to a delay of 33 ns at the input to the preamplifier. A 230 ns wide gate from the scintillators included 99% of the wire signals.

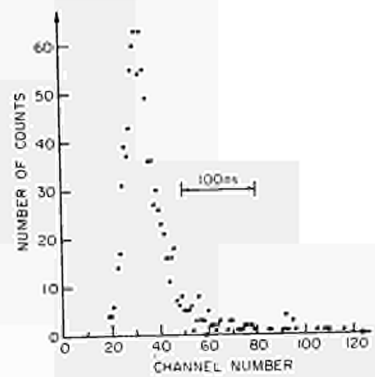

Figure 2. Distribution of time delays with the beam centered on the wire (position zero in Figure 1). The peak corresponds to a delay of 33 ns from the particle arrival until the input signal at the preamplifier reaches discrimination level.

Figure 3 is the time distribution obtained with the beam centered halfway between wires.

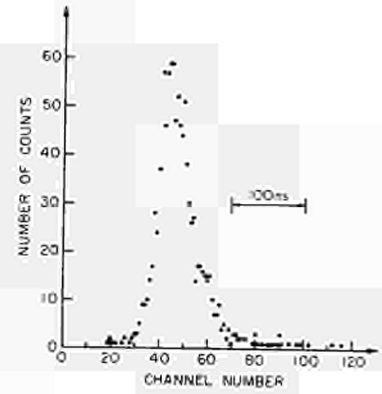

Figure 3. Same as Figure 2, except that the beam is centered midway between wires. The peak is about 30 ns later than in Figure 2.

Here the stop signal results from either of the two wires, whichever comes first. A shift of some 30 ns in the most probable delay is noted.

The distribution of pulse heights from the counter wire is of interest in connection with timing and particle identification. For

this purpose, the threshold Cherenkov counter signal could be used to select pions and lighter particles or protons. The distributions for light and heavy particles are shown in Figures 4 and 5 respectively.

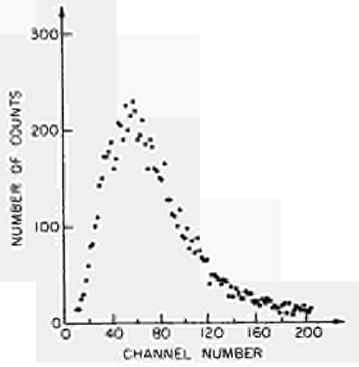

Figure 4. Pulse height distribution for particles with $\beta > 0.99$. Wire spacing 1/8 inch, argon-methane filling at 2.7 Kv. Beam centered on wire.

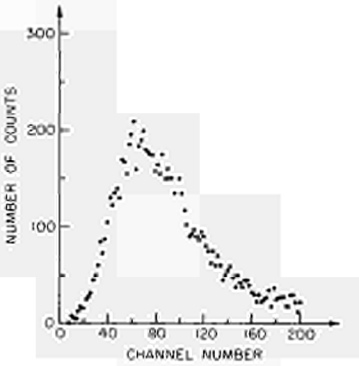

Figure 5. Pulse height distribution for particles with $\beta < 0.99$ (mainly 1 GeV/c protons). Same conditions as Figure 4.

The peak positions are very roughly proportional to the ionization density. The widths are in agreement with Charpak's measurements[1], but not with those of a Landau calculation[4]. The instrumental resolution is indicated by the spectrum of Fe^{55} (with lines at 3.0 and 5.9 KeV) shown in Figure 6.

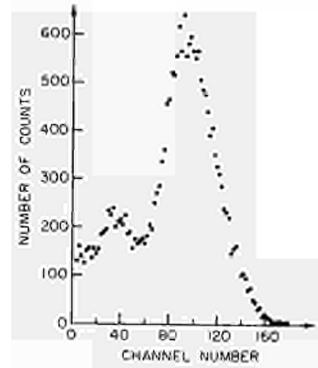

Figure 6. Pulse height distribution for Fe^{55} source poorly collimated with lines at 3.0 and 5.9 Kev. Calibration different from Figures 4 and 5.

Unfortunately, this source was not well collimated, so some ionization was shared by two or more wires. The energy calibration if Figure 6 is different from that in Figures 4 and 5.

One might expect smaller time delays from a multiwire array with 1/16 inch spacing because the applied voltage is 4.9 Kv instead of 3.0 Kv for the same gain, and the average drift velocity should be higher. The distance from wires to either wall was 1/4 inch as before. Figure 7 is a plot of the efficiency as a function of position.

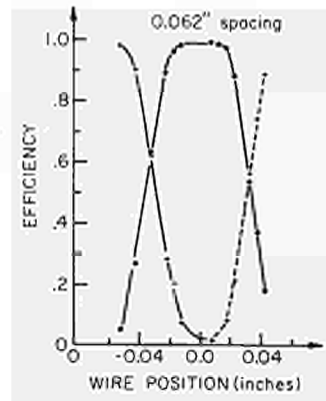

Figure 7. Efficiency for 1/16 inch wire spacing. Argon-methane filling at 4.7 Kv. Same method as in Figure 1.

The time delay distributions were not very different from those of Figures 2 and 3.

To see if the speed was limited by the argon-methane gas mixture, we tried neon-helium with heptane at 0°C at an applied voltage of 1.95 Kv. No improvement in timing was attained.

The final test involved the application of a negative voltage to alternate wires. If this negative voltage is too small, the efficiency falls drastically in the neighborhood of the negative wire. With argon-methane in the counter with 1/16 inch spacing, half of the wires were held at ground potential by the preamplifiers as usual. The alternate wires were run at -1400 V while the walls were at -2800 V. Between 99 and 100% efficiency was reached everywhere, but the peak of the time distribution occurred about 22 ns later than in Figure 2. It seems that there is no particular advantage in running alternate wires at negative potential.

Wire spark chambers (sparkostrictive) were set up downstream from the proportional counters, and the latter were used successfully as part of coincidence logic to trigger the spark chambers. Two proportional counter chambers with their wires orthogonal were placed in coincidence with no difficulty.

Fast Arithmetic

The binary encoding scheme mentioned above was not completed in time for the test run. It employs TTL integrated circuit logic as indicated in Figure 8.. The signal from the preamplifier is standardized by a sense amplifier to produce a timporary logical 1. The latch holds this 1 if it is present at the strobe time determined by fast scintillators. The latches provide a buffer for later transfer to computer memory. A simple arrangement of AND gates resolves cases in which two adjacent wires register. The encoder forms a binary number corresponding to each wire, and the adding and shifting determines whether the track was straight or deflected as indicated above. The decision can be made in time to trigger spark chambers. This technique is applicable to a broad class of experiments and looks promising.

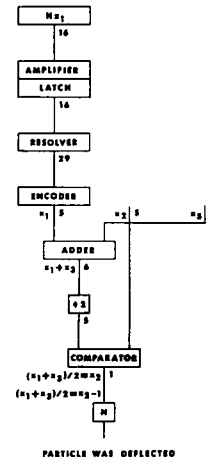

Figure 8. Fast arithmetic logic for one plane of 16 wires. The numbers indicate number of line - one per wire or binary bit. If the trajectory is straight, the spark chambers are inhibited.

References

1. G. Charpak et al, Nucl. Instr. Methods 62, 262 (1968).

2. J. Fischer, BNL 12804

3. C. J. Rush, Electronics Division, Argonne National Laboratory, Argonne, Illinois.

4. L. D. Landau, J. Phys. U.S.S.R. 8, 201 (1944).

*Work supported in part by the Atomic Energy Commission

DISCUSSION

Booz : - I want to ask you : 1) what gas pressure you are using. 2) the distance of the wires is rather low and I think therefore that the profile of the different wires was influenced by the track structure of the fast protons to a large extent.

Koester : 1) One atmosphere. I should also mention that the distance from wires to wall was 6 mm. 2) Yes. The response from adjacent wires is partly due to delta rays.

Maeder : - Is not there any dip in the sensitivity curves for the arrangement of alternate wires ?

Koester : - No, because there is a very large electric field between the wires in that case and so even though you entered the beam directly on the dead wire with the negative voltage on it, the electrons are accelerated to the adjacent wires which are sensitive so that if you make the profile again you have 100 % efficiency everywhere in the chamber.

Maeder : - You showed the principle of data processing for the data coming from a number of such wire planes. Have you considered any encoding system of showers of particles?

Koester : - Not very seriously, that's an interesting problem.

Maeder : - Then, I may add that for this problem threshold logic offers very promising solutions for treating the general case.

NUCLEONIC APPLICATIONS OF E^2CL MONOLITHIC INTEGRATED CIRCUITS

Z.H. Cho
Institute of Physics
University of Stockholm
Sweden

SUMMARY

Applications of a new generation of the E^2CL monolithic integrated circuits, whose propagation delay and rise time are only of the order of 1 - 2 ns, are described. The inherent high speed operation facilitates simple solutions for the construction of a nanosecond coincidence circuit and more complicated logic circuits. Advantages as well as some disadvantages of the E^2CL IC, in particular for the application to nuclear pulse circuitry, are discussed. Solutions for problems, especially in connection with the low output current and mismatching of the output impedance, are described. As application examples, a quadruple coincidence and mixer circuit, an E^2CL-TD binary, and a time to pulse-width conversion circuit are presented. For picosecond applications, e.g. the application to a TPHC etc. the time jitter of the E^2CL IC has also been investigated and the results are reported.

INTRODUCTION

Most present day integrated circuits are not fast enough to match the speed of available fast switching transistors, for instance Motorola 2N3960 and 2N4261. However, their potential feasibility of high speed switching and the rapid development brought the nucleonic application to our attention. The recently announced Mullard FKH 111 series[1] is a good example and has been adapted in our laboratory, especially in application to a time to pulse height converter and a coincidence circuit[2]. Measured values of the propagation delay and rise times of the E^2CL IC are less than 2 ns. These figures are comparable to the best UF switching transistors available. In particular for fast nuclear electronics applications, the E^2CL IC may be considered superior to transistors and existing DTL or TTL IC in the following respects:

1) The output voltage swing satiesfies most of the requirements of the nucleonic modules.

2) Logic functions of considerably high speed can be obtained because of the absence of the Miller effect in the input gate transistors.

3) Input-output logic levels match with other discret high speed semiconductor components, such as transistors, tunnel diodes and back diodes.

4) Balanced construction, which is virtually independent from the input gate couplings, provides well balanced complementary output pulses.

5) Ground based reference voltage and catching diode facilitate easy interstage couplings.

On the other hand, low output current and fixed 75 ohms output resistances make the circuit (E^2CL) somewhat inconvenient. These problems have been solved partially by using transistors and diodes.

DESCRIPTIONS OF THE E^2CL IC AND OUTPUT INTERFACES

The E^2CL monolithic integrated circuit is basically a current steered nonsaturating logic with an input capacitance of around 2 pf, and rise and fall times of less than 2 ns. Output logic swing of E^2CL is approximately equal to base emitter voltage drop of silicon transistor i.e., V_{BE}, thus the noise margin is around 250 mv. A simplified circuit diagram of the 1/2 E^2CL is shown in fig. 1. The E^2CL works with negative logic, i.e. OV voltage for logical "O" and - 0,7 for logical "1". Fig. 2 shows three basic operations (a) NAND or AND (b) negative OR with two additional 1/2 E^2CL as an inverter and (c) ac coupled positive OR or NOR arrangements respectively. The output current of the E^2CL is 10 ma, and thus a 75 ohms output resistor provides - 750 mv, logical "1". This low output current is the major disadvantage for the nucleonic application, since

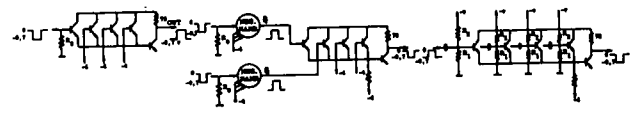

Fig. 1 Simplified schematic diagram of the E^2CL IC (FKH 111A).

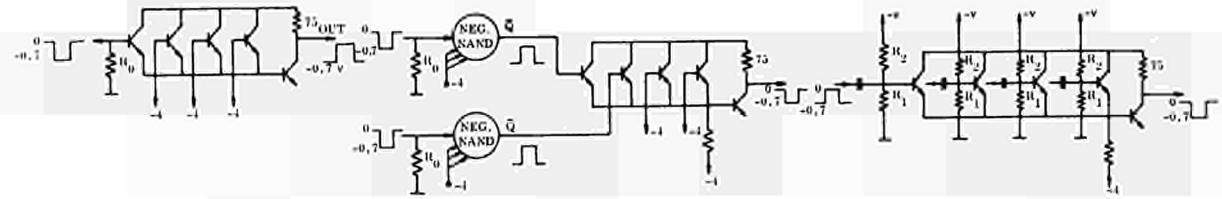

(a) (b) (c)

Fig. 2 Basic coupling schemes: a) NAND (or AND) mode, b) negative OR (or NOR) mode with two NAND mode inverters, c) AC coupled NOR (or OR) mode.

most of the nucleonic modules are 50 ohms terminated and consequently provide only - 500 mv. For this reason short dc coupling is recommended whenever possible. Long distance coupling with coaxial cable will require additional considerations.

In the following simple solutions to this problem, using transistors and diodes, are presented. Fig. 3 (a) shows a simple emitter follower with one transistor, where R_B has been chosen for maximum speed [3]. Fig. 3 (b) shows a dc coupled voltage follower circuit where a diode is coupled to compensate the emitter base voltage drop V_{BE} of the transistor so that the output voltage at the anode of diode D_1 follows the base voltage of the transistor T_2. Fig. 3 (c) shows output pulses from the emitter follower circuit with different transistors and direct output from the E^2CL. Output pulse shapes and dc levels of the voltage follower circuit of (b) are shown in fig. 3 (d).

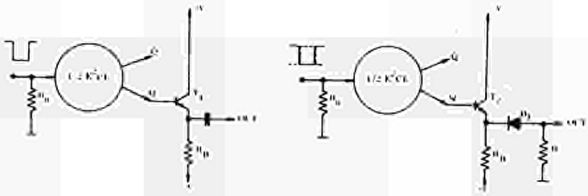

(a) (b)

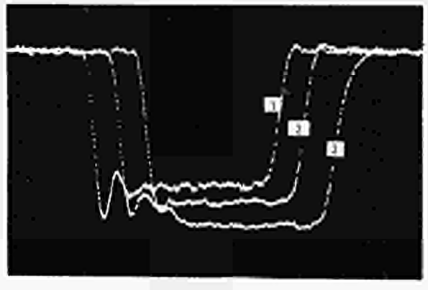

(c)

Fig. 3 Output interfaces and their pulses:
a) conventional emitter follower,
b) voltage follower,
c) output pulses (1) with direct, and (2) and (3) from emitter follower circuits with 2N3960, and with 2N964 respectively.

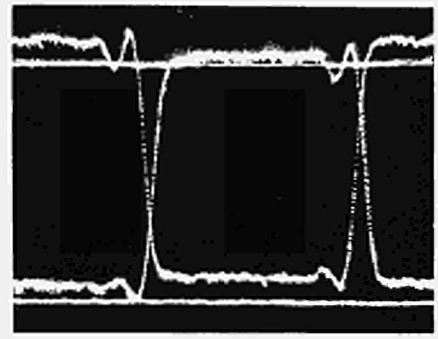

(d)

Fig. 3 d) Output pulses from the voltage follower circuit of b) and its dc levels. (Horz. 5 ns/cm, Vert. 100 mv/cm).

Somewhat reduced output voltage caused by differences between V_{BE} of the transistor and the diode forward voltage drop was acceptable in all the logic operations. As has been indicated by Crowther et al [1], each additional loading degrads the rise time of the output pulse by an order of RC, i.e. the output resistance times the input capacitance. In the FKH series is 75 ohms and C is 2 - 3 pf, thus there results a rise time degradation of 150 ps, or more, for each additional loading.

APPLICATION EXAMPLES AND DESCRIPTIONS OF THE CIRCUITS

The following circuits were construced and their performances tested:

1) Quadruple coincidence and mixer circuit [4]
2) E^2CL-TD binary
3) E^2CL-TD time to pulse-width conversion circuit.

The length of the wirering between the E^2CL ICs, was always kept short, i.e. 2 cm or less when emitter followers or voltage followers were not used.

a) Quadruple coincidence and mixer circuit (fig. 4).

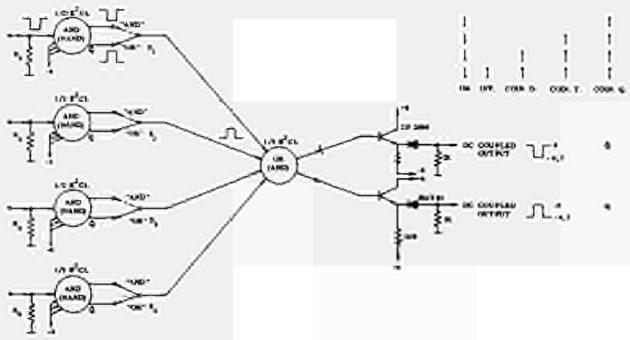

Fig. 4 Quadruple coincidence and logical mixer circuit with E^2CL ICs. Depending on the S_1, S_2, S_3, and S_4 switches, the following functions can be implemented: inverter, double, triple, and quadruple coincidences as well as logical mixing.

This unit was originally constructed as a part of a double coincidence selector circuit for a multiple input time to pulse-height converter[5]. With this simple unit, double, triple and quadruple coincidence operations, as well as quadruple logical mixing, are possible. Outputs are split to two complemantary pulses and the voltage follower circuits are added for external coupling (especially for dc coupling).

b) E^2CL-TD binary circuit

The E^2CL was found to be very useful in combination with a tunnel diode. In this way the tunnel diode was well isolated and stable operation was achieved. For the E^2CL and tunnel diode combined application, the following points may be important: 1) available currents for set and reset, 2) switching load line for tunnel diode bistable operation and output resistance of the E^2CLs, 3) output voltage level of tunnel diode and input logic level requirement of the E^2CL, 4) switching time jitter associated with shot and thermal noises of the tunnel diode[6]. Considering the forgoing points, a E^2CL-TD binary circuit is arranged as is shown in fig. 5 (a). Load line construction of this circuit is shown in fig. 5 (b), where the currents available for set and reset are also indicated. Equivalent circuits for the set and reset transients are shown in fig. 5 (c). From the equivalent circuits the load line is determined by

$$(R_1 + R_{1S}) \;//\; (R_2 + R_{2S}) = R_L$$

where R_{1S} and R_{2S} are the output resistances of the E^2CLs. In the steady state the total current I_o is $I_k + I_2$ where I_k and I_2 are given by

$$I_K = \frac{12V}{R_k} \quad \text{and} \quad I_2 = \frac{V_2}{R_2 + R_{2S}}, \quad \text{respectively.}$$

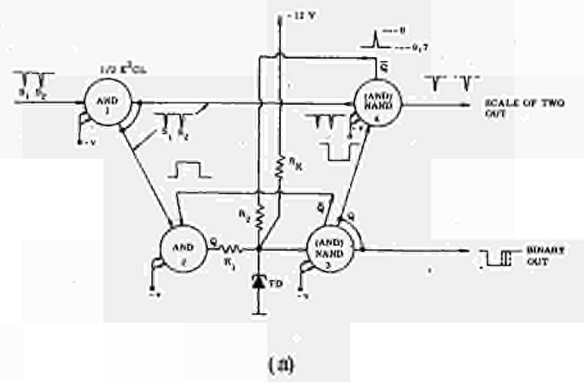

(a)

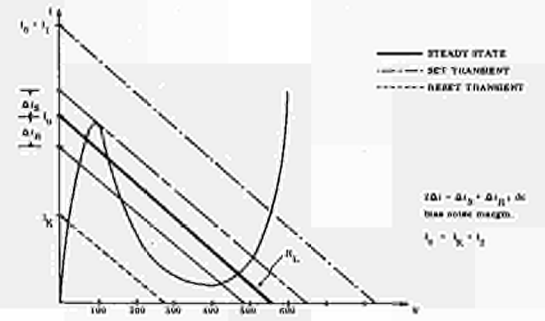

(b)

Fig. 5 The E^2CL-TD binary: a) circuit diagram an pulse waveforms at the various points, b) biasing of tunnel diode, where the available trigger currents and dc bias noise margins (Δi_S and Δi_R) are indicated

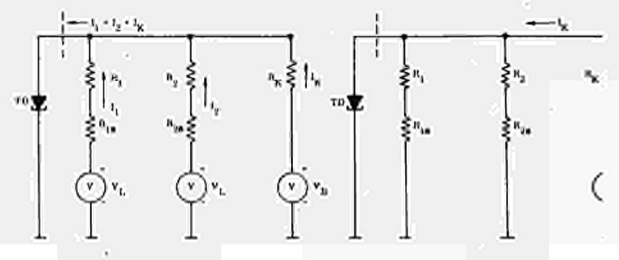

(c)

Fig. 5 c) Equivalent circuits for the set and reset transients.

With optimum load line, i.e. 52 ohms, with TD 253. (10mA) the bias supply voltage margin was better th 125 mv. In the E^2CL-TD binary circuit shown in fig 5 (a), the tunnel diode TD 253A is placed between th AND 2 and NAND 3. In this circuit, the delay times of each 1/2 E^2CL have been effectively utilized, thu the first pulse S_1, with the TD at low voltage state, allows pulse S_1 to pass AND 2, but not NAND 4. Th negative pulse S_1 which passed AND 2 sets the TD t the high voltage state and the outputs (complementar from NAND 3 are fed to AND 2 and NAND 4 thus inh bits pulse S_2 at AND 2 and opens the NAND 4 gate fo

the S_2 pulse. Pulse S_2 which passed NAND 4 is fed back to the TD via R_2 and resets the TD to low voltage state and so on. The delay time associated with NOR 2 and NAND 3 effectively blocks the pulse S_1 at NAND 4. AND 2 is not only blocking the pulse S_2 but also delaying the pulse S_1 at the TD, thus the delay times of AND 2 and NAND 4 cancel each other at the TD, and the circuit becomes independent from the other AND or OR E^2CLs. It thus permits high frequency operation. In this circuit the maximum operation frequency is, in first order, limited by the speed of the E^2CL. Thus an operation frequency of 250 MHz is expected. Fig. 6 shows experimentally observed binary operations of the circuit at 140 MHz. Advantages

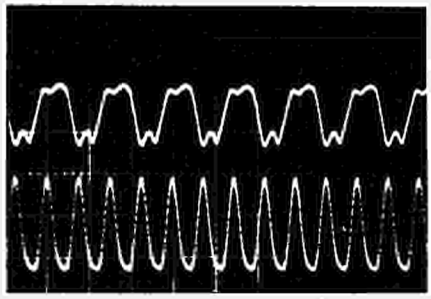

Fig. 6 Output waveforms of the E^2CL-TD binary circuit shown in fig. 5 (a). Binary operation at 140 MHz. (Horz. 10ns/div., Vert. 100 mv/div.)

of the circuit are: 1) No inductance is involved, thus operation is independent from the input pulse shapes and speeds. This is in contrast with the high frequency binary circuit using tunnel diodes [7], where inductance limits high, as well as, lower frequency operation. 2) From the binary circuit two outputs are avaiable, i.e. scale of two from NAND 4 and the binary output from NAND 3. 3) High stability is achieved and operation was reliable from dc up to 140 MHz and minimum pulse resolving time was 4 - 5 ns.

c) E^2CL-TD time to pulse-width conversion circuit.

A time to pulse-width conversion circuit is derived from the E^2CL-TD binary circuit. In this circuit a reset pulse generator was added for the selection of a pair of pulses within the time range of interest. The circuit is similar to the one described earlier [2] and is shown in fig. 7. Even with a single random pulse, the circuit resets itself automatically and gives an output pulse with a fixed pulse-width where the width is determined by the delay line DL1. The negative output pulse from NAND 7 is differentiated by C_1 and R_3. The differentiated negative pulse is passed when a negative pulse from NAND 3 exists at NAND 8. The timing diagram of the operation is shown in fig. 8. This type of time to pulse-width conversion circuit is the basic core of the time to pulse-height converter (TPHC) [8, 9]. A TPHC constructed with similar circuit in combination with the constant current generator shows good performance [2]. A unique feature of this method is that the t-w conversion is obtained from one

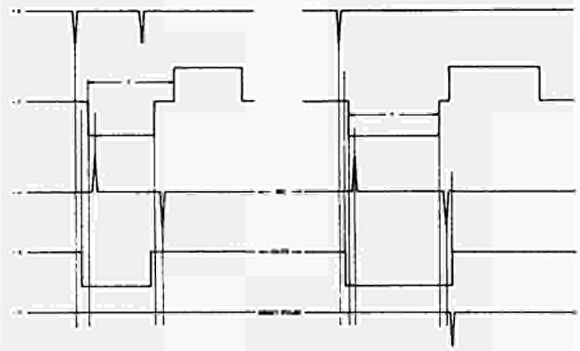

Fig. 8 Timing diagram of the reset pulse generator in the time to pulse-width conversion circuit.

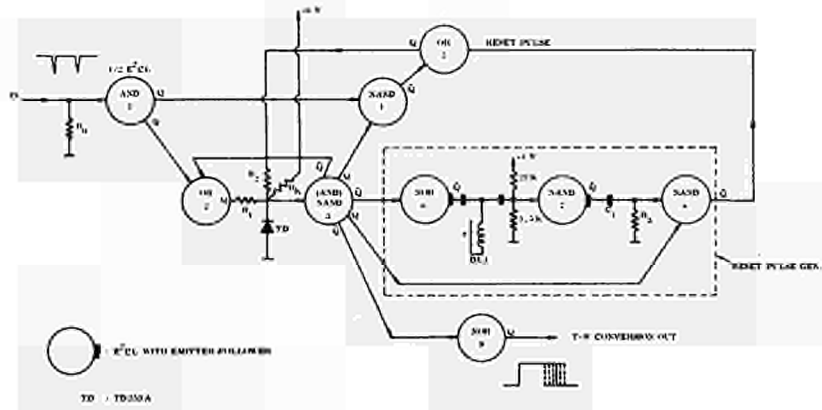

Fig. 7 Schematic diagram of the time to pulse-width conversion circuit. The conversion outputs are obtained from NAND 3 or NOR 9.

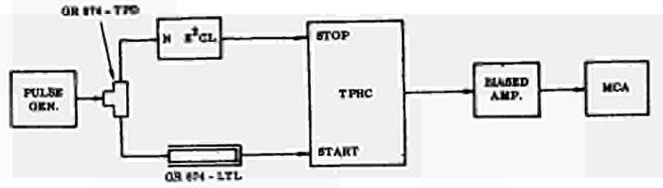

(a)

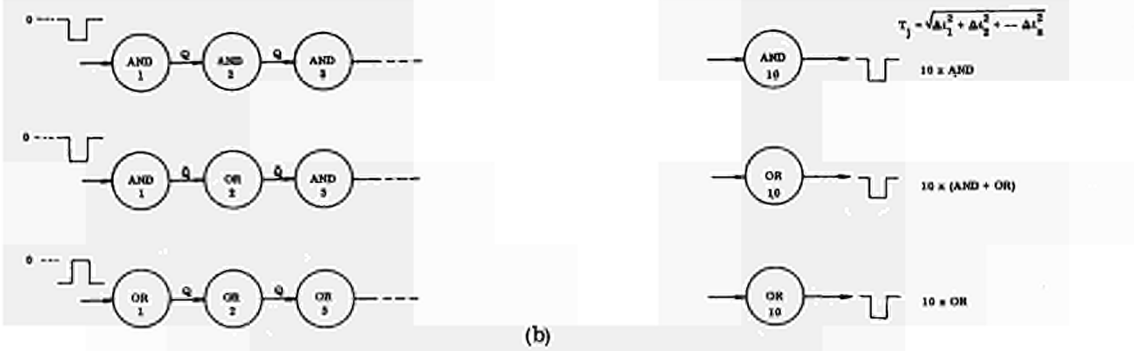

(b)

Fig. 9 Time jitter measuring arrangements, a) block diagram, b) three different modes of the couplings.

input channel. This method offers increased efficiency as compared with the ordinary start-stop or overlap types and is capable to handle random pulses such as the pulses from a radiation detector.

TIME JITTER OF THE E^2CL and E^2CL-TD CIRCUITS

Investigations of switching time jitter of the E^2CL and the E^2CL-TD hybride circuit have been made briefly. The time jitter contribution of the individual E^2CL unit may become important when the E^2CLs are used in an application such as a time to pulse-height converter, where the time resolution is only of the order of 10 ps or less. It is common that these types (E^2CL) of fast switching circuits have triggering time jitter, in association to the various noises. First, the time jitter of the E^2CL alone was measured, and then the combined circuit with a tunnel diode was studied. The picosecond time jitter can be measured by use of either a TPHC or a sampling oscilloscope. In both instruments the inherent electronic time jitter is of the order of 10 ps. The oscilloscope method, however, is not well suited for quantitative measurement. With the method using a time to pulse-height converter, a spectrum broadening of a few picoseconds could be detected. The simple time jitter measuring arrangement used here is shown in fig. 9 (a) and (b). In this arrangement, the time jitter of the test circuit T_j may be obtained from

$$T_j = \sqrt{t^2(j) - t^2(0)}$$

where t (j) and t (0) are the FWHM of the observed time jitter with test units inserted and the inherent time jitter of the TPHC, respectively. To observe appreciable time jitter, a number of units were cascaded as is shown in fig. 9 (b).

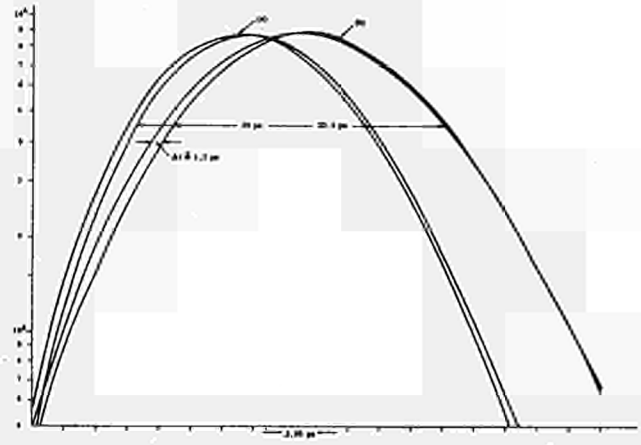

Fig.10 Time jitter measurements. Curve (a) is the direct measurement with delay line and (b) is with ten FKH 111 AND modes. In both, the repeated measurement errors were 1.2 ps. Broadening of the overall time resolution curves with 10 x FKH 111 (curve b) were 5 ps. (Each channel corresponds to 3.95 ps.)

The observed time jitter in this case is

$$t(j) = \sqrt{t^2(0) + T^2_j}$$

where $T^2_j = \Delta t^2_1 + \Delta t^2_2 + \ldots + \Delta t^2_n =$

$\sum_{j=1}^{n} \Delta t_j^2$ or $n\overline{\Delta t}^2$

From this one could derive the mean jitter of a unit $\overline{\Delta t}$

$$\overline{\Delta t} = \sqrt{\frac{t^2(j) - t^2(0)}{n}}$$

As seen from fig. 9 (b), three different types of couplings were made, AND-AND, AND-OR mixture, and OR-OR, and the measured results of the three different modes were nearly the same. A typical measurement is shown in fig. 10. From this one may calculate the mean time jitter of one unit $\overline{\Delta t}$ = 6 ps. In this measurement, the error was about 1 ps. The observed average time jitter of 6 ps is quite acceptable in most applications. The obtained figure may be considered somewhat large when we consider that the time spectrum with ten stages of the FKH 111 was in a thermally unstable, drifting state and since some other measurements with thermally stabilized conditions show an appreciably reduced time jitter spectrum. Therefore one may conclude that switching time jitter of the E^2CL may be considered negligible in most cases.

The time jitter associated with the E^2CL-TD binary and t-w conversion circuits is worth investigating, since the tunnel diode is coupled between the E^2CL and is triggered by the pulses of definite rise time and amplitude. A number of time jitter investigations were reported on tunnel diodes 6.9). An expression which may be applicable to our problem is given by[6]:

$$\sigma_T = \frac{A\,(e\,I_{eq} + 2\,KT/R_L)^{\frac{1}{2}}\,B^{1/6}}{\alpha^{5/6}\,C^{1/3}}$$

where A = 0.65, α is the slope of the input pulse, B is one half of the curvature at the diode's peak, C is the capacitance of the tunnel diode. For the E^2CL α and R_L are fixed the values being 2,5 ma/ns and 52 ohms, respectively, with a 10 ma tunnel diode. In this case, the contributions of thermal noise is much less than that of the shot noise. The calculated result with a 10 ma tunnel diode shows σ_T of 1 ps. In the time to pulse-width conversion application, the switching time jitter of the reverse direction adds linearly to the forward switching time jitter σ_T. The reverse switching time jitter σ_{TR} is not well known. However, it is expected to be lower than σ_T if one assumes that shot and thermal noises predominate. The relevant experimental verification of this result could not be made at present.

CONCLUSION

The usefulness of the E^2CL IC was investigated as an initial phase of the application of the new generation of E^2CL or ECL integrated circuits in the field of fast nucleonic circuitry. It can be concluded that the E^2CL is a useful component which can perform a large number of basic nucleonic operations such as coincidence, logical mixing and anti-coincidence etc. The several application examples indicate greatly simplified systems, with a minimum of circuit complexity and cost. Somewhat detailed, but not rigorous, investigations of the time jitter also show promising results in the application to a picosecond precision timing circuitry such as the TPHC. It is also suggested that the E^2CL might be exploited in a more flexible and useful way in combination with other discret semiconductor components such as tunnel diodes. The techniques reported in this paper can be applied to other series of the fast integrated circuits such as the Motorola MECL[11] and RCA ECCSL[12] which will be available soon.

ACKNOWLEDGEMENT

The author would like to thank Dr T.R. Gerholm for his kind support and excellent working conditions offered to me. The author is also indepted to Dr. B Åström at the Research Institute of Atomic Physics for a careful reading of the manuscript and for several valuable comments.

This work is supported in part by the Swedish Atomic Research Council.

References

1) G.O. Crowther, G.C. Deli, C.F. Hill, E.E. Lawrance, M.A. Malek and A.R. Rao, Mullard Technical Communications, Vol. 9 No 87 (1967)

2) Z.H. Cho and N. v. Gersdorff, Nucl. Inst. & Meth. (To be published)

3) The Semiconductor Handbook, Motorola, 2nd Edition 8-235 (1966)

4) S.P. Asija, IEEE Spectrum, Vol. 5 (No 12) 77 (1968)

5) T.R. Gerholm et al, to be published

6) D.E. Nelsen, MIT, RLE, Tech. Rept. 456 (1967)

7) W.F. Chow, IRE Trans. on Electronic Computers, Vol. EC-9, 295 (1960)

8) F.A. Johnson, Nucl. Inst. & Meth., Vol. 59 237 (1968)

9) A. Ogata, S.J. Tao and J.H. Green, Nucl. Inst. & Meth. Vol. 60 141 (1968)

10) A. Barna, Standford Linear Accelerator Center, Standford Univ., Standford Calif. SLAC, Rept. 52 (1965)

11) M.R. Byrd, W.H. Julitz, P.M. Lee and C.D. Philips, Electronics, Vol. 41 No 21 (1968)

12) R.L. Sanguini, RCA Technical Presentation (1968)

DISCUSSION

Koester : - This is just a comment. You mentioned that you could not test your binary at 250 MHz for lack of a 250 MHz oscillator. We often make a train of pulses from a single mercury switch pulse by passive splitting through transmission lines.

Maeder : - On one of your slides we saw indication of a 75 Ohm load. Does this mean that you are working with 75 Ohm cables.
Cho : - No, we are using 50 Ohm cables matched by emitter followers.
Stanchi : - Can you give some details on the instrumentation used for obtaining your resolution in the range of tens of pico seconds ?
Cho : - Such a small time jitter can be detected by observing the broadening of the jitter time spectrum which is superimposed with inherent electronic time resolution of the TPHC.
Vuilleumier : - Did you compare the performance of your circuits with commercial MECLIII, which has flip flops that count at 300 MHz clock frequency, and are available since summer 1968 ?
Cho : - We have been awared that MECL III's are capable to operate as you have mentioned, but at the local, MECLIII were not available until now. If we use MECLIII gate circuit, I believe, we can operate with the method I have described, toggle switching frequency of 500 MHz.

MULTIPARAMETER ANALYSIS AND RECORDING SYSTEM (MARS) FOR ISOTOPES IDENTIFICATION OF TRANSURANIUM ELEMENTS

B. V. Fefilov, L.P. Chelnokov
Joint Institute for Nuclear Research, Dubna, USSR

Multiparameter analyzer for experiments on search and identification of alpha-radioactive isotopes of far transuranium elements produced by bombarding targets with heavy ion-beams on the 310-cm cyclotron of JINR is described. The analyzer was intended for data acquisition and accumulation by five parameters: an energy and a half-life of the original nucleus, an energy and a half-life of a daughter nucleus and the number of a detector. Moreover, the analyzer has special control units for performing an experiment. There are four alpha-spectrometers with semiconductor detectors, stabilization system and a common ADC on 2000 channels.

Experimental

In experiments on search for alpha-radioactive isotopes of transuranium elements with the heavy ion accelerator the method of the original nucleus identification by alpha-radioactive daughter nucleus formed at their alpha-decay and the definition of the genetic bond between them is applied. At the bombardment of ^{243}Am with ^{22}Ne ions short-lived isotopes of element 105 are synthesized and alpha-radioactive isotopes of element 103 with known properties are produced after its alpha-decay [1,2].

The experimental setup included a high-speed nucleus collector with a selected time exposition in front of the corresponding pair of detectors(it used four semiconductor detectors for higher efficiency). In the case of an alpha-partiticle appearance in the selected energy region (for the original nucleus) its energy(E_1) and time $T_1 = t + t_o$, where t_o is a summarized time of the nuclear transfer from the target to the collector with the help of a gas streem and the collector transporation to the detector are recorded.

The appearance of original α-particle is a control signal for stopping the collector pneumatic movement for the time equal approximately to three half-lives of the expected daughter nuclei. At the appearance of an α-particle E_2 and T_2, counted from the moment T_1, are recorded. After the exposition the cycle is repeated.

Analyzer

The multiparameter analysis and recording system(MARS) (Fig.1) consists of four α-spectrometers with semiconductor detectors with own normally closed linear gates before the common analogue-to-digital convertor(ADC) on 2000 channels, stabilization units operating with two calibrated pulses from the common precision pulse generator, time-analysis units and control-units for an analyzer, experimental setup and pulsed operation of a cyclotron, recording units for a teletype or an integrated external memory(ferrite cores or magnetic tape). Thus the analyzer realized five-parameters analysis: detector number(event identification), an energy and a half-life of the original and daughter nucleus alpha-radioactive isotopes.

Using normally closed linear gates excludes a noise summation of spectrometer amplifiers on the input of a common ADC and therefore a high resolution is attained.

The detector number register has an apparatus surplus(4 bits instead of 2bits) for the control reliability. This register determines the values of a linear discharge capacitance slope in the ADC depending on a stabilized alpha-spectrometer. The stabilization of the thresholds and conversion slopes(gain) (Fig.2) is performed successively as the target was bombarded with an ion beam, recording logic being blocked(the accelerator operates on a pulsed mode with 100-200 Hz). Thus the operation does not take useful time for experimental data recording.

The system notices events as a clutter if there is the pulse coincidence in any two amplifiers and does not record them.

The basic logic unit in the system is the "code comparator" performing algebraical function determination of the difference sigh between two codes written in the positional number system(Fig.3). One code is mounted by switches setup, another is changed from various analyzer registers. The code comparators(CC)are used for the selection of energy regions (analogues of "digital windows")E_1 andE_2, collector exposition time and time intervals for the timer units, for the choice of 2x4 stabilization points of the thresholds and conversion slopes of the four amplifier-conversion systems in accordance with the energy equivalents of calibrated pulses in each alpha-spectrometer. Thus there is a possibility of combining the energy scales of all the alpha-spectrometers.The identical energy scales are necessary for comparatibility of E_1 and E_2 digital windows and are very convenient for spectrum processing. The code comparators operate with potential codes and

do not require special instructions for its function.

The analyzer is performed on the diode-transistor logic elements with potential coupling. There is a priority logic for the first event pulse and a store of the second one with the help of a buffer register in the case of using a teletype, a reliable protection system against signal errors and random malfunctions, running check of the experimental setup, of the cyclotron and the dead time indication system etc.

Conclusion

Using four spectrometry amplifiers and a cross blocked logic against coincidence pulses, external blocking from the accelerator upper-shown analysis and recording system(MARS) is characterized by a very low background and clutters. The experiments therefore were performed with reaction cross-section below $10^{-34}cm^2$ that is it ensured a long-time operation without malfunctions.

The application of the stabilization system by two calibrated pulses with a common ADC and the code comparators has essentially reduced an amount of details and units and has given a good control adaptability in a wide range.

References

1. G.N. Flerov, Contributions Intern. Conference on Nuclear Structure,Tokyo, 1967.
2. G.N. Flerov et al. Experiments on Search for Alpha-radioactive Isotopes of Element 105, Preprint JINR,P7-3808, Dubna,1968.

Figure symbols

D -Semiconductor detector
PA - Preamplifier
> -Linear amplifier
F -Fotodiode
PPG -Precision pulse generator
Det. Num. Reg. -Detector number register
LG -Linear gate
Σ -Summator
ADC -Analogue-to-digital converter
Stab.Sys. -Stabilization system
A.Reg. -Auxilary register
Att. -Attenuator
Syn. -Synchronizator
CC -Code comparator
EF -Emitter follower

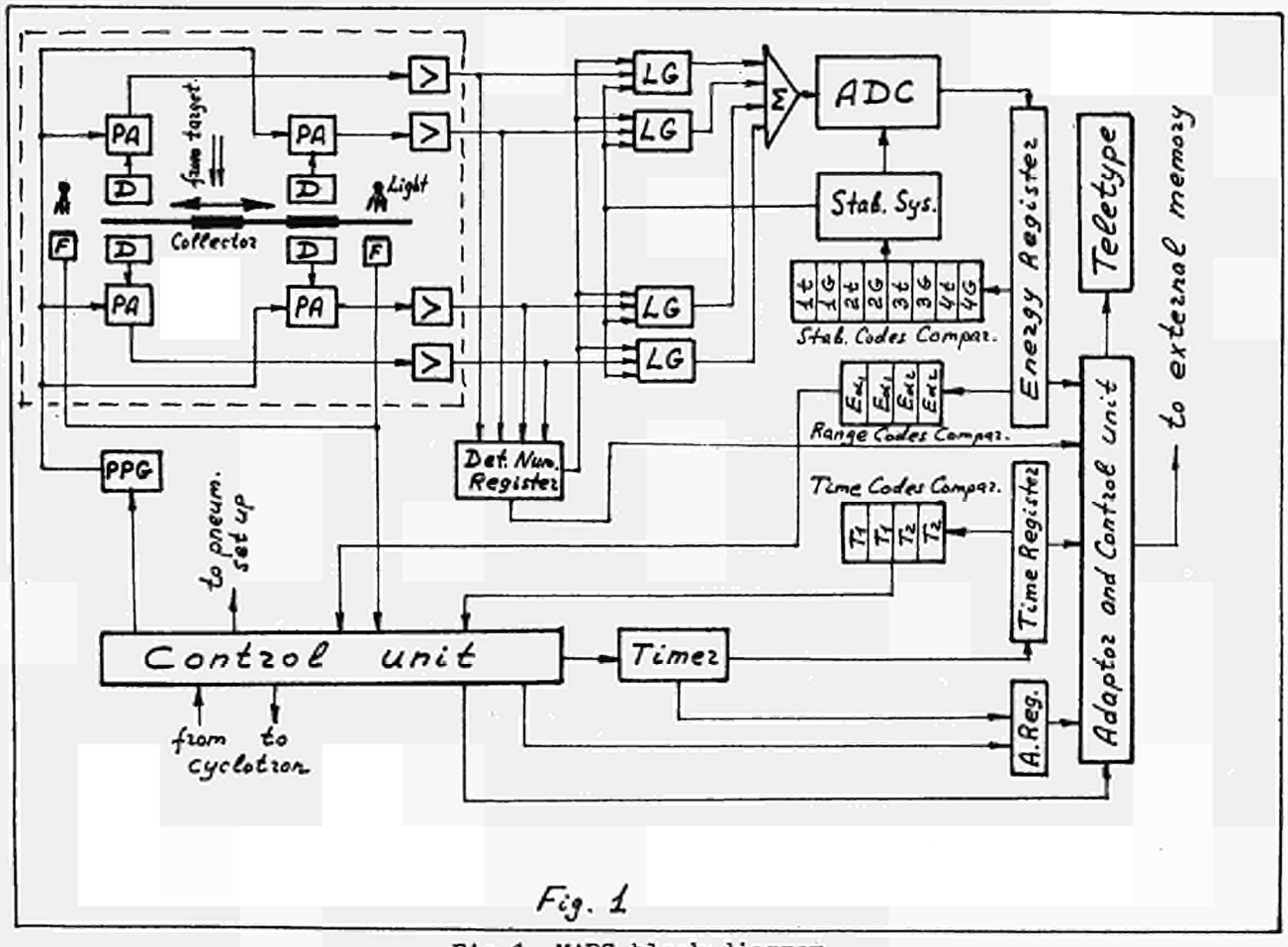

Fig. 1

Fig.1 MARS block-diagram

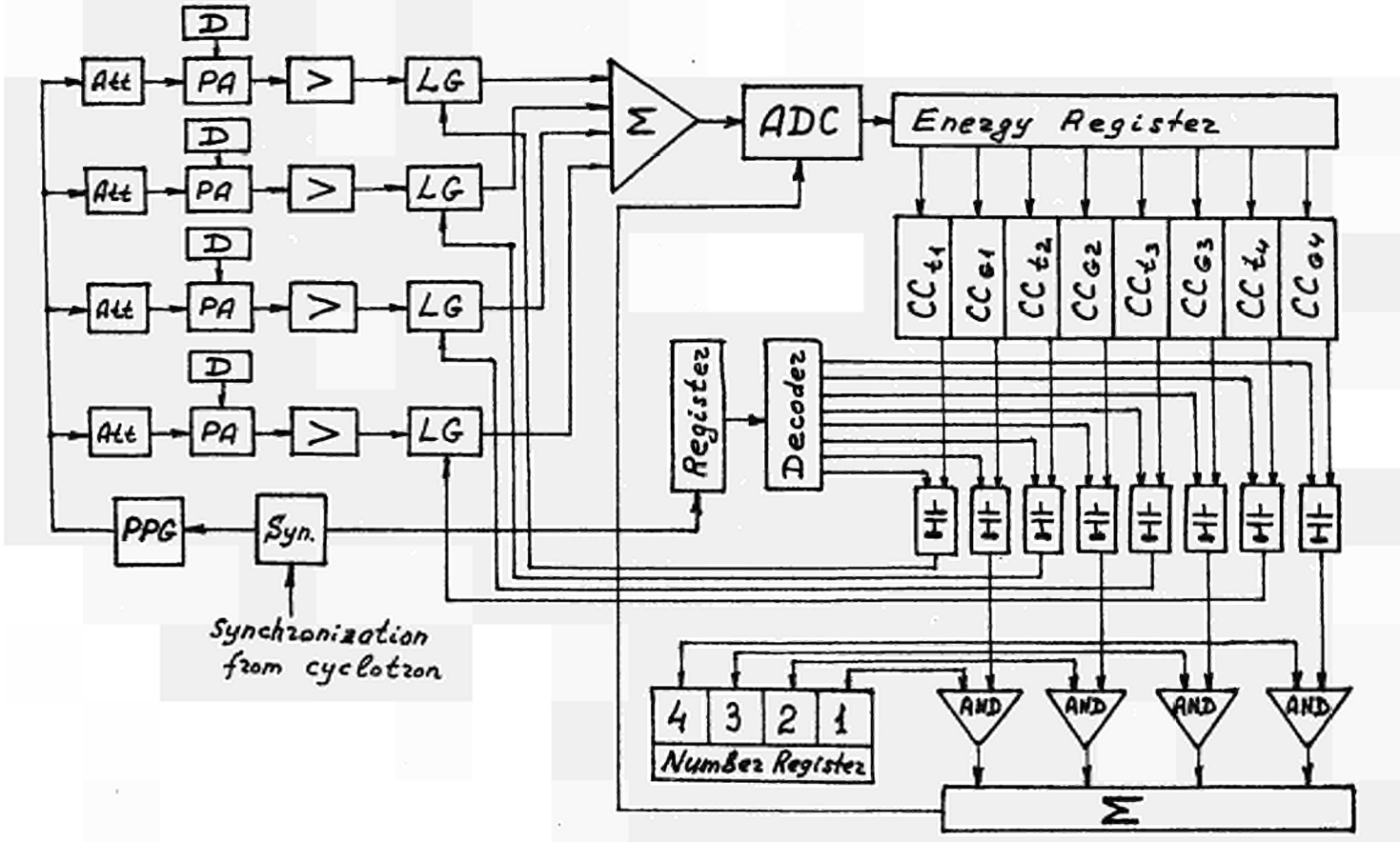

Fig.2 Stabilization system

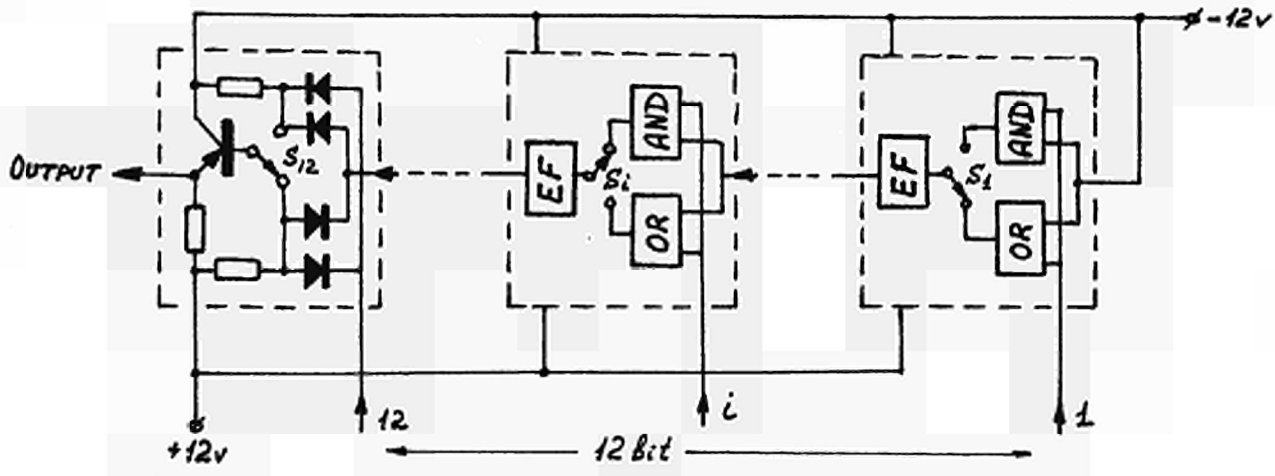

Fig.3 Code comparator

J.R. Kosorok

Battelle Memorial Institute, Richland
Washington, USA

A PROGRAMMED CONTROL and INSTRUMENTATION SYSTEM FOR A NUCLEAR REACTOR

A small control computer has been interfaced with a nuclear reactor instrumentation and control system. The test reactor's electric heating system, rated at 384 kW, can heat it to 1000°C. Its graphite moderator is blanketed with pressurized nitrogen to inhibit oxidation. The digital computer directly controls the nitrogen and heating systems, and provides operational aids for the reactor personnel. The central processor has 8K words of core storage and utilizes 3 magnetic tapes for bulk storage. In addition to the digital control hardware for over 100 analog and 190 digital inputs, two unique features are a three color, alpha-numeric, display and two six decade analog-to-digital converter channels.

Eleven closed loops were controlled with a digital simulation of a proportional-plus-integral controller, which was modified to provide several notable features: (1) aids in controller adjustment, (2) transducer signal conditioning, and (3) compensation for process nonlinearities. Other features of the control system reduce operator errors during start-up and operation of the nitrogen and heat systems.

The complete programmed system is composed of a highly integrated set of executive control, input/output and functional routines which perform the above mentioned control and assist the operator during nuclear operations.

DIGITAL HIGH-VOLTAGE SUPPLY FOR AUTOMATIC TESTING AND REGULATION OF PHOTOMULTIPLIER GAIN

by D. Maeder,
Laboratoire de Physique Nucléaire Expérimentale
de l'Université de Genève

Summary.

The main contituents of an automatic testing and regulating system are recalled. Automatic control is required for logic modules, delay boxes, attenuators, and phototube voltage supplies. Rather than depending on automatic monitoring of manually adjusted voltages, a direct digital setting of nominal voltages should be attempted.

The original prototype, adjustable from 0....2555 V in 5 V-steps, was built as a self-contained module, with complete manual and electronic control circuits. A more recent version, oriented towards CAMAC control of a large number of identical channels, requires a separate control panel for manual operation; on the other hand, its compactness allows 16 channels to be housed in one crate. Circuit diagrams and performance data are presented.

1. Introduction.

The necessity of frequent checking of individual phototube channels in complex detector systems (such as beam telescopes, anticoincidence shields, hodoscopes, etc.) has led us to the development of a test system using a fast light-emitting diode mounted close to each photocathode. By suitable programming of the light flashes in the different channels (single or coincident, with adjustable timing and/or amplitude), various kinds of particles having well-defined energies can be simulated. Precise relative timing is obtained from standard fast logic modules such as the CLR/A system[1]; a complete test pulse logic includes gates that permit light flashes to be produced only during experimental deadtimes (e.g., intervals between accelerator burst; readout time of spark chambers; etc.). Thus, periodic testing and readjusting can go on even during an experiment, provided that the data acquisition system has enough capacity to analyse "experimental" and "artificial" events separately, and that timing and gain adjustments are accessible to automatic control.

Fairly large test pulses are required for triggering the XP21 light flash diodes, even when these are mounted close to the photomultiplier cathode. Typically, a 40 V pulse of 3 ns FWHM, will release some 3000 photoelectrons in a 56 AVP tube. In order to vary such pulses in a predictable manner (and to avoid, e.g., multiple flashes due to cable reflections), we found it necessary to use low-loss delay boxes (75 Ω) and to match the 20 Ω dynamic impedance of the XP21 diodes by a miniature 2:1 ferrite core transformer mounted just outside the light guide[2]. Remote control of test pulse transmission through attenuators and delay boxes clearly requires mechanical contacts satisfying special geometrical conditions (coaxial, or subminiature).

On the other hand, no attenuators are needed for adjusting phototube outputs. Varying the high voltage supplies provides an apparently simple solution, which does not involve coaxial elements. However, when this common practice is to be extended to computer-controlled experiments, new problems arise, which will be discussed in the present paper.

2. Basic System Considerations.

Commercial H.V. supplies for phototubes usually have a manual control system which provides the necessary stability and resolution (typically 10^{-3}) for one output. When an experiment involves many phototubes, individual H.V. supplies would appear desirable; in practice, however, economic considerations often impose a compromise such as the use of a common, well-regulated H.V. unit for a whole group of phototubes. Individual adjustments are still possible by inserting a variable resistor into each phototube supply lead. Loss of direct calibration and increased source impedance are well-known drawbacks of this method, whose users depend on relatively inaccurate voltmeter readings rather than on control settings (although the latter would normally offer better resolution).

In search for a more satisfactory solution, some experimenters suggested a centralized, high-precision measuring station (a DVM) that would be connected to each H.V. channel in turn . The results would either be printed out, or

transmitted to a computer programmed to request manual corrections where necessary. Automatic execution of corrections by means of voltage dropping resistors appears impractical : neither a set of relay contacts operating at high potential, nor a servo motor acting on an insulated potentiometer shaft would seem to offer an economic solution. A further difficulty with this system is the slowness of DVM operation which adds another delay to the unavoidble time constants in the regulation loop.

We think that digitally controlled individual H.V. supplies are the correct answer to these problems. Experimenters will no longer insist on monitoring the phototube voltages by a slow measuring instrument if they can rely on self-checking circuits that produce an alarm signal whenever the actual voltage deviates (say, by 1°/oo) from the digital setting. Such a system requires a small digital memory ($\leq$ 10 bits) associated with each H.V. channel, which may be adressed for monitoring ("read") or adjusting ("write") by a computer at random times. If successive "write" commands are spaced at least by the settling time of the H.V. generator, feedback stability problems are eliminated from the computer programing task, and the response function will depend only on the feedback loop within the H.V. unit itself.

3. A Single-Channel H.V. supply.

In developing a prototype along these lines in 1968, we followed the general idea that new instruments should not only be adapted to computer control, but must allow manual operation as well, both locally and/or remotely controlled. Furthermore, the local digital memories should conserve their contents in case of power failure or general shutdown; therefore, we used magnetic latch relays that could be flipped by pushing a button either on the H.V. unit itself, or on a remote synoptic control panel[2]. When the CAMAC system was announced, we modified the relay control circuits in such a manner that an inverted strobe pulse could flip the relays as well.

The prototype delivers a voltage adjustable in 5 V-steps from 0...-2555 V into 3 MΩ ; it occupies one quarter of a standard crate width. A brief description was included in ref.[2].

4. Design considerations for Multichannel H.V. Supplies.

The single channel prototype was considered too bulky and too expensive to be used in large quantities. Compactness could be gained mainly by abandoning the magnetic latch relays, since a protected memory function might eventually be archieved by other means (such as magnetic cores) and might be centralized in a separate CAMAC module. The remaining circuitry was reexamined for further simplifications, until a complete H.V. channel (without manual controls) was compressed to 1/16 of a crate width. In order to conserve the possibility of manual control, one set of push-buttons and indicator lamps per crate is sufficient. To make best use of the available space, we suggest to house 16 H.V. channels in a special crate, whose front panel carries all the necessary push-buttons, lamps and relays for manual control of any selected channel (Fig. 1), including "enable/disable" of channel output (keeping the digital setting in memory while the output is cut off). The 16 channels are identified by the 16 subadresses of a CAMAC module to which the crate is connected via a 50 pole cable.

Alarm signals ("overload", indicating too low an output voltage) are displayed individually on the front panel for every channel concerned. In CAMAC terms, the logic sum of these signals is a source of "LAM".

5. Electrical Circuits.

A complete channel is contained on two printed-circuit cards, whose schematics are shown in Fig. 2 and 3.

5.1. Digital control section (Fig. 2, left)

It should be noted that one additional control circuit (common for all channels) is required for subadress decoding, L*-mixing and gating, etc.

5.2. Digital-to-Analog converter (Fig. 2, center).

The number of bits was reduced from 9 (relay prototype) to 8 (TTL-controlled version) in order to limit the number of I.C.'s. The reference voltage was increased to +12 V so that voltage drops in the switching transistors would be less significant.

The saturating transistor configuration used for the 4 most significant bits has voltage drops on the order of 10 mV ($\pm$ 5 mV), and assures a constant driving-point impedance of 40 kΩ for the input to the differential amplifier, balanced by R_x.

5.3. Variable duty-cycle oscillator (Fig.2, right).

Without the resistor R_y, T_{5+6} would oscillate symmetrically (δ = 50 %) and

attain its maximum frequency of about 140 kHz, when the differential amplifier T_{1+2} is balanced ($\Delta U_{12} \approx 0$). A few mV unbalance in either direction would change the duty cycle towards $\delta \to 0\%$ resp. 100% and reduce the frequency considerably. R_y was chosen such that a positive value of U_x cannot increase δ beyond 70%.

5.4. Overload monitor (Fig. 2, extreme right).

At low duty cycle, T_8 is mostly conducting, keeping the 5 V Zener diode nonconducting. R_z was chosen to bring the Zener diode into conduction when $\delta \gtrsim 50\%$.

5.5. High voltage block (Fig. 3.)

During "on" periods, $T_{4,5}$ are saturated, so that the voltage drop across the primary of the H.V. transformer is about 28 V. Primary current increases at a rate of 0.6 A/μ sec. At 50% duty cycle, the "on" period lasts for 3.5μ s, so that peak current is about 2A, and average current becomes $\frac{1}{2}$.2A. δ =0.5A, equal to the limit set by protection circuits in the 30 V supply leads to individual channels.

5.6. Overall Performance.

Normally, the duty cycle remains below 30% even when the external load is reduced from its nominal 3 MΩ value to 2 MΩ at full voltage. The circuit will stand short circuits, but will be damaged by operation without a feedback resistor to the point U_x, since the voltage may then rise to over 3000 V. At nominal load and with properly adjusted feedback, output voltages coincide with digital settings within ± 3 V.

6. Acknowledgements.

It is a pleasure to thank Mme Sabev and M. Vittet for their collaboration, and to the Swiss National Research Foundation for financial support.

References.

1) References are given in paper 4.2 (D. Maeder and G. Vuilleumier).

2) D. Maeder and Mme Sabev, Colloque International sur l'Electronique Nucléaire, Versailles, sept. 1968, p. 57-1.

Figures.

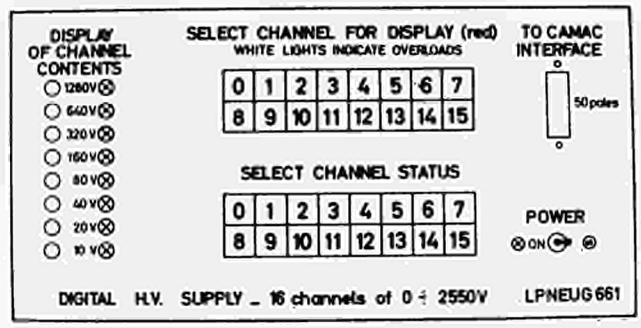

Fig. 1. Front panel of a digital 16-channel H.V. unit.

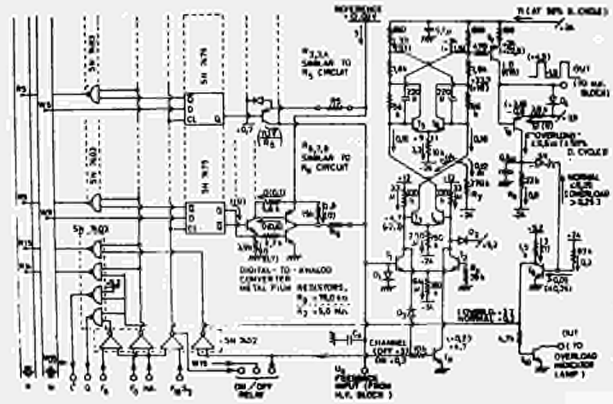

Fig. 2. Control circuit for a H.V. channel.

All diodes are type 1N3062
All PNP transistors = MPS3702
All NPN transistors = MPS6531
except T_{1+2} = BCY55 (matched pair)

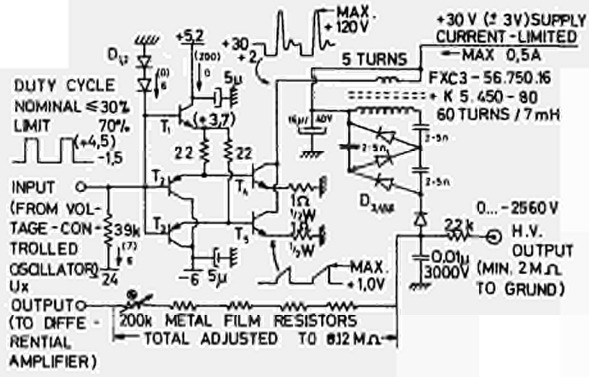

Fig. 3. High voltage block.

Transistors : $T_{1,4,5}$ = BFY56
$T_{2,3}$ = MPS6534

Diodes : $D_{1,2}$ = 1N3062
$D_{3,4,5,6}$ = SEM30

A COMPUTERIZED DATA ACQUISITION SYSTEM FOR HIGH EVENT RATES FROM MANY SOURCES*

D. G. Dimmler
Brookhaven National Laboratory
Upton, New York

Summary

Semiconductor banks with many individual counters can impose very high data rates on a computerized data acquisition system even with modest individual detector rates. The purpose of this paper is to discuss some results of a design study made for a data acquisition and control system used in an X-ray diffractometer. The system collects, processes, and records up to 385,000 events per second, detected from several semiconductor banks with 128 counters each. An integrated diode matrix, a derandomizer and an external memory arrangement will be described. Also, some system software considerations will be mentioned.

Introduction

Semiconductor detector banks with many individual counters are being used more and more frequently in nuclear instrumentation. This can impose very high data rates on a computerized data acquisition system even with modest individual detector rates.

High data rates from many individual sources typically introduce two problems in a computerized data acquisition system using a small general purpose computer:

1. The usual scanner for the input data multiplexing becomes too slow.

2. The available small scale computers do not have independent memory banks, so that the usual cycle stealing scheme for data input tends to slow down or completely lock out the central processor unit.

Also, a small dedicated computer system usually does not have the peripherals necessary for convenient program preparation.

The following paper discusses some results of a design study for a computerized data acquisition and control system used in an X-ray diffractometer. The objective was to find an inexpensive and straightforward solution for the above-mentioned problems.

The proposed system collects, totalizes, processes, and records data from semiconductor detector banks with 128 individual counters each. It is designed for two detector banks with expandability to any practical number. Input data at a peak rate of 385,000 randomly occurring events per second over all detectors can be collected. A dead time loss of less than 1% is guaranteed at a rate of 100,000 events per second. The system should be placed in operation during the summer of 1969.

General Description

Figure 1 sketches the total proposed system. One line per detector is connected to the input of the multiplexor (1), which converts an event pulse to a binary number describing the detector address (2). A fast derandomizing buffer holds the address temporarily (2). The increment processor reads, via a dual access controller, the contents of the location addressed by the incoming event, increments this number by one, and writes the result back. In parallel to this activity, the computer system, a Varian 620i positions the stepping motors of the mechanical gear assembly on which the detector banks are mounted, processes and records on magnetic tape the previously detected data, and determines the next position of the detector assembly. Also, display requests are satisfied.

This report concentrates on the data collection path and on the outline of the software. A more detailed description of the system will be given elsewhere.[1]

*This work was performed under the auspices of the U.S. Atomic Energy Commission

Multiplexor and Decoder

A fast diode matrix is used for multiplexing and decoding instead of the usual scanning method, which is inherently too slow. Recently available integrated diode matrix chips[2] have made diode matrices feasible for a large number of inputs. As compared to discrete diodes, they allow higher packing density, a simple and more economical mechanical design, and better control of the stray capacitances. Any individual diode in a chip can be disconnected by destroying a fuse contained in the chip with a capacitor discharge so that any desired matrix format may be constructed. Since individual diode recovery times are 10 nsec, the 30 nsec conversion time obtained is determined to a large extent by the stray and diode capacity. In order to assure high speed and easy expandability, the matrix is segmented. One segment consists of a 32 x 6 matrix using 4 chips, with the necessary supporting logic (Fig. 2). The timing is shown in Fig. 3.

The input gates are normally open. From a pulse arriving at any of the 32 input lines in Fig. 2, the matrix produces a five-bit binary number (2), which is fed into a transient register. A gate pulse, produced simultaneously with the binary number starts a timing chain. After 30 nsec the gate to the multiplexor will be closed and the derandomizer gates opened (4) if no other transient register was filled with information. In this same path the additional bits for the segment address are added. Finally, the transient register will be cleared (5) and all input gates opened again by removing the gate break pulse (3). The total elapsed time from the leading edge of the event pulse to the reopening of the gate is 100 nsec. Texas Instruments 74HN integrated circuits with typical propagation delays of less than 15 nsec are used. Each segment is an independent unit. Addition of segments will not impose additional delays. The system is currently developed for two detector banks with a total of eight segments. Provision is made for the extension of the segment address currently consisting of 3 bits, if more segments are added.

Overlapping Pulses

A second event pulse occurring in the matrix segment before the gate break pulse (3) has arrived, will be superimposed (logical OR) in the transient register, and will result in an erroneous binary number (pulse 6 in Fig. 3). The probability that a second pulse arrives in the 30 nsec before the gate break pulse arrives at a peak rate of 25,000 events per second per segment is 25×10^3 events per second times 30×10^{-9} seconds per time interval, and equals 7.5×10^{-4}.

Simultaneous events occurring in different matrix segments will be rejected. It is highly probable that the background generated from other sources is high enough to render this error insignificant. In case this prediction does not hold true, a hybrid logic circuit using a current summing technique has been designed, which detects the condition "more than one out of 32".

Condition 7 in Fig. 2 shows a pulse which has already arrived and is just in the process of dropping at the time the gate break pulse is being removed. This may cause erroneous input due to different delay times in the various paths through the matrix. Therefore, provision is made that the gate break (3) will only be released if no new gate pulse (2) is active.

Derandomizing Buffer

In order to meet the dead time requirement, a derandomizing buffer unit is used between the matrix and the computer unit. The derandomizer is organized according to Fig. 4. The input and the output address vectors are completely independent, so that during output from the buffer to the computer no additional dead time is being introduced into the input. The unit has a detection logic for the buffer empty condition, in which case the output process will stop. The buffer filled condition is detected if the input vector after increment has the same value as the output vector. Additional input will be rejected. This overflow condition should occur very seldom.

The cumulative probability that x or more events arrive in a time interval equal to the number of derandomizer stages times the interval required to output one event into the computer is[3,4]

$$P_o = \sum_{x = x'}^{X = \infty} \frac{e^{-m} m^x}{x!}$$

where:

m = average input rate unit time $\frac{\overline{N_i}}{\overline{N_o}} N_r$

$\overline{N_i}$ = average input rate per second

$\overline{N_o}$ = average output rate per second

N_r = number of derandomizer stages

$x' = N_r + 1$

The computer takes 2.6 μsec to take one event from the buffer. With an average input rate of 100,000 events per second the probability that 8 stages are filled up becomes $m = 10^5$ events/second $\times$ 2.6 $\times$ 10^{-6} sec/output of one event $\times$ 8 stages, or 2.08 and the resultant probability[3] of the buffer being full is 3 $\times$ 10^{-4}.

Data Input to the Computer

The addresses in the derandomizer will be used to increment corresponding memory locations in an array of n words in core memory, where n is the total number of detectors. Input and totalization of an event can be realized in three different ways in a small computer.

1) Each event generates an interrupt. The interrupt program analyzes the data. The maximum data rate is determined by the length of the interrupt program. 25-30 μsec/event is an average for the currently available small computers, so that a rate of about 40,000 events per second would load the central processor to 100%

2) The data are transferred into a buffer area in core memory via a data channel, while an analyzer program loop processes the events from another buffer area, which has been filled before in a "ping'pong" scheme. The rate depends on the length of the program loop, which is somewhat shorter than the interrupt program in method 1, because less overhead is involved. A typical execution time is 15 - 20 μsec.

3) External logic, which has access to the address lines of the core memory, performs a read from a core location, increments and writes in the core location. In this scheme the total process takes only one or two memory cycles, which is about 1 - 3 μsec in present small computers. Because of the high input rate required, method 3 has been chosen.

Dual Access Controller and External Memory

Independent memory banks are usually not available in small scale computers. In order to achieve a high input rate without locking out the central processor unit, a dual access memory scheme has been used.*[5] A 16-bit/4096-word core memory[6] with a full cycle time of 1 μsec is connected (Fig. 5) as an external memory via a dual access controller to the increment processor of the data collection interface. Either the CPU or the increment buffer can have access to the memory. In case of a simultaneous request, the increment processor has priority. The software in the computer will be arranged so that very little access is necessary from the CPU to this memory portion, so that the CPU will not be slowed down by the data collection.

Figure 6 shows a flow diagram of the increment process. If an address is available in the derandomizer, a base address is added and a read cycle is requested. The request may be delayed

*This device was developed and is marketed by Varian Data Machines for the 620i computer taking BNL's specifications into consideration.

by a maximum of 1.5 µsec due to a CPU access. After the request is honored, the controller will be switched to burst mode, locking out further CPU access. The lock out is released when no addresses are waiting in the derandomizing buffer. A watchdog timer in the increment processor makes sure that after 50 µsec the lockout is released for at least one CPU memory cycle. The complete read-increment-write cycle takes 2.6 µsec. Two modes are available to handle an overflow. Mode one is shown in Fig. 6. If the processor increments from all ones to all zeros, an overflow base address is added to the address, and an additional read-increment-write cycle is executed. For each detector bank of 128 counters, an overflow array of 128 words has to be assigned in the core memory. In method 2 the address is replaced by a fixed memory location address and an additional cycle is executed. In this case only one more location is necessary, which indicates the total number of overflows within a given measurement. Method 2 saves memory space, but can be used only if relatively few overflows occur within a measurement. The two modes are manually selectable.

Software Considerations

The experimenters who will use this system in the future expressed a strong desire to have a flexible tool in their hands. The concept of measuring single crystal X-ray intensities simultaneously by many individual counters is new in crystallography. Optimizations, expansions and changes of the initial methods are expected. A complete and unchangeable set of specifications for the measuring sequence and the controls would therefore be undesirable at this time. The system must be able to grow with new, even unexpected, demands. The possibility of change is a main objective in the design of the software system.

If an experimenter prepares an experiment, he will write several application programs, here called tasks, which describe a measuring sequence, provide the on-line data processing desired, and take care of the formatting of the input and output data. The software operating system coordinates and services the tasks, handles control messages from the teletypewriter, executes all interactions with peripheral devices and the experimental apparatus, and provides error actions.

In a typical use of the system, the experimenter goes through the following phases:

1. Preparation of tasks
2. Debugging of tasks
3. Execution of the experiment
4. Analysis of the data obtained.

Convenient program preparation (phase 1) requires fast peripheral devices, such as a line printer, and extensive file handling capabilities. Analysis (phase 4) of the data obtained requires, in addition, high computational power. These are typical resources available in a large scale computer. Therefore, in both these phases the laboratory computer center (2 x CDC 6600, CDC 924) will be used. An assembler written in FORTRAN has been designed for use on the CDC 6600, which produces object code from the Varian 620i DAS assembler language. Object programs and data files are exchanged between the center and the Varian 620i via magnetic tape or paper tape.

Debugging of the tasks (phase 2) will be done either off-line on the 620i, using company supplied debugging software, or on-line under the operating system described for phase 3. Debugging may take valuable time from the system. We are considering, therefore, plans to design at a later time a simulator for the 620i on the CDC 6600. It is of course understood that such a simulator would be useful mainly to catch errors in on-line data processing routines. On-line interactions would apparently always be debugged by a test run of the real experimental apparatus.

Operating System

The tasks being executed in the system interact very frequently with the apparatus setup, the input/output devices, and the teletypewriter. All these devices are slow as compared to the central processor, and the task has to wait for the completion of an interaction. A single user multi-programming operating system is being designed which permits the experimenter to make use of the waiting periods.

Many tasks may be processed simultaneously. Figure 7 shows the basic flow of control in the system. A task consists of one main program, private subprograms, and links to library programs in a common pool. A task is executed strictly sequentially. Any interaction with peripheral devices is initiated only within the task via a library program in the common pool. The operating system takes care of the execution and termination of the interaction. The user inserts a YIELD instruction at a point where the task cannot proceed without waiting for the termination of an interaction.

With this mechanism, many tasks are serviced simultaneously according to a priority list. As shown in Fig. 7, at each clock increment (the clock is set to 1 second), a monitor loop is entered which searches through a list of tasks in process, beginning from task 1, which has the highest priority. If an active task is found, the task is entered or reentered and execution proceeds until one of the following three actions occur:

1) A YIELD instruction has been executed (voluntary YIELD)

2) A task attempts to select a device which is already busy (involuntary YIELD)

3) The next clock increment arrives (involuntary YIELD).

In all three cases the current program counter is preserved and the task is turned inactive. In cases 1 and 2 control returns to the monitor loop, which searches for the next lower priority task which is active. In case 3, control goes to the start of the loop which searches for the highest priority task which is active. The common library program pool is not reentrant. If control is in a library program at a time a clock increment occurs, the increment will be skipped.

The monitor loop skips an inactive task. If all interactions requested by a task are terminated, the task is returned to the active condition by the system. The next time the loop control comes around, the process will proceed up to the next YIELD.

The operating system includes a linking loader as part of a load task. Therefore, any task can be loaded on-line in parallel with other activities.

Acknowledgements

Many people have contributed ideas and effort for this paper. In particular, I would like to thank M. A. Kelley, who is writing the software operating system. I also wish to thank V. Radeka for valuable discussions. W. Michaelson has done a considerable amount of the detailed engineering design.

References

1. R. Thomas, et al., A Parallel Data Acquisition System for Simultaneous Measurement of Single Crystal X-ray Intensities (to be published)

2. Radiation Inc., Microelectronics Div., Melbourne, Florida

3. Beyer, Handbook of Probability and Statistics, p. 180-186. The Chemical Rubber Co., Cleveland Ohio (1966)

4. W. C. Hamilton, Statistics in Physical Science, p. 12, Ronald Press Cie, New York, N.Y. (1964)

5. Varian Data Machines, Irvine, Cal.

6. Versastore III Core Memory System, Varian Data Machines, Irvine, Cal.

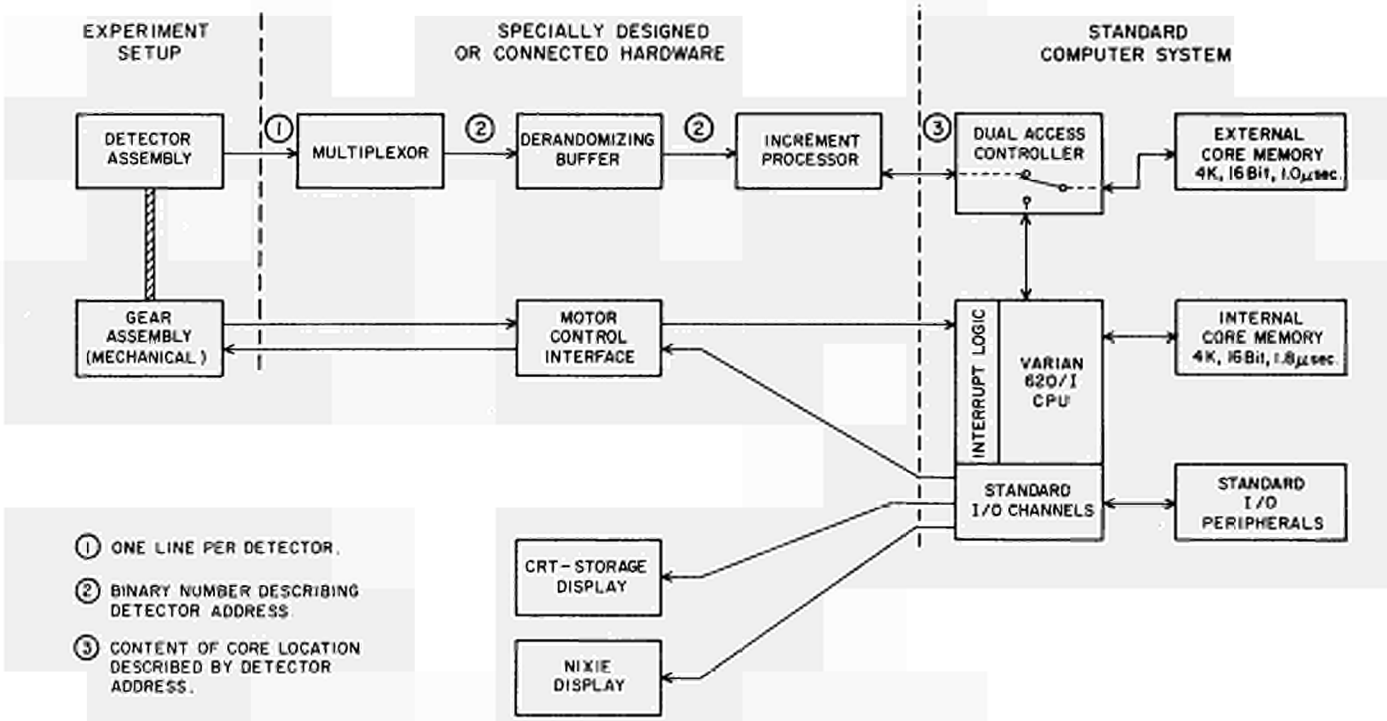

Fig. 1 - AESOP multidetector diffractometer data Acquisition and control system.

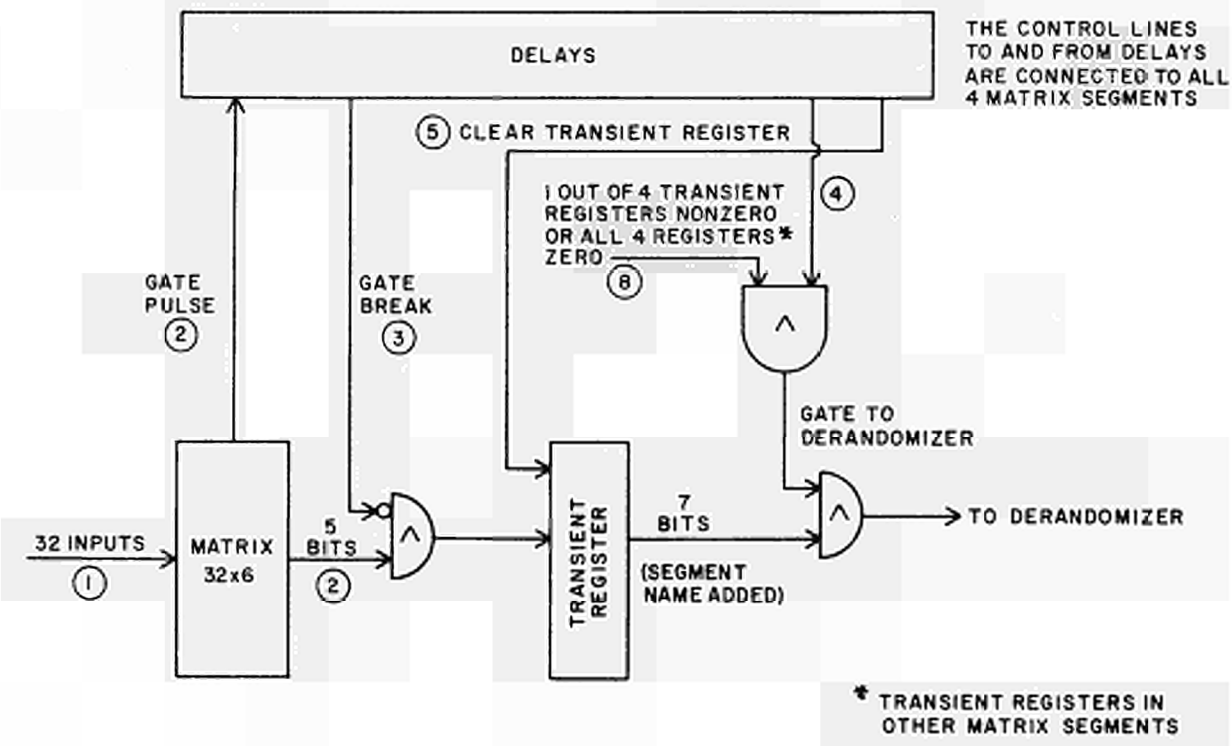

Fig. 2 - Block diagram of a matrix segment.

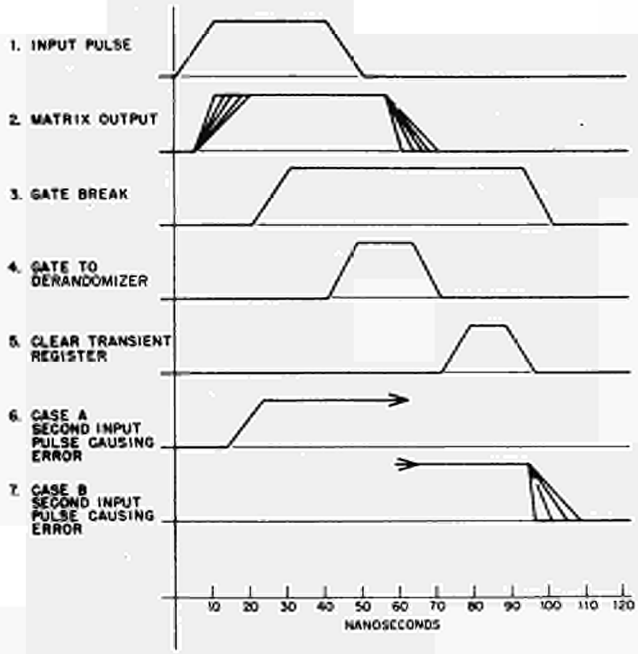

Fig. 3 - Timing of the matrix.

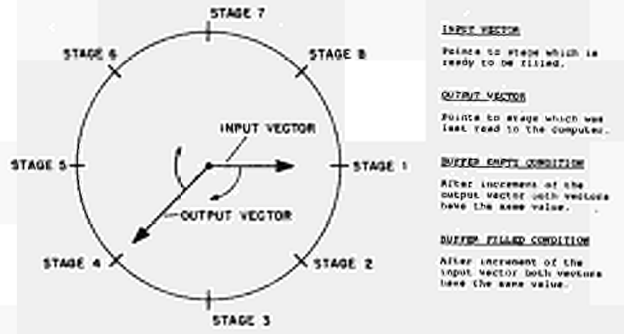

Fig. 4 - Organization of the derandomizing buffer.

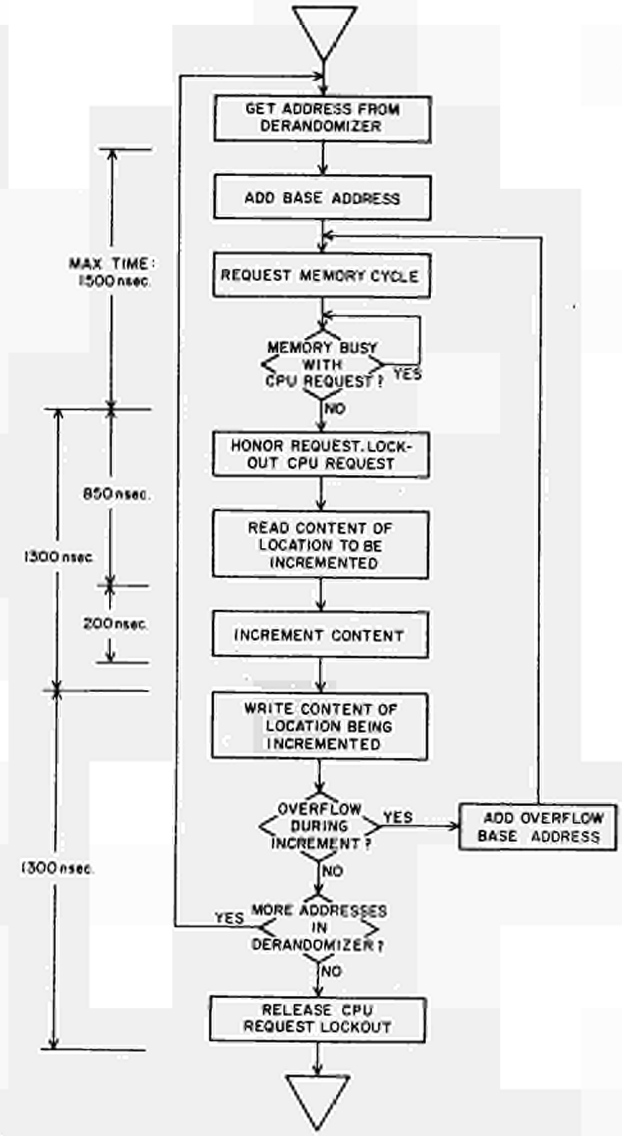

Fig. 6 - Flow diagram and timing of the increment process.

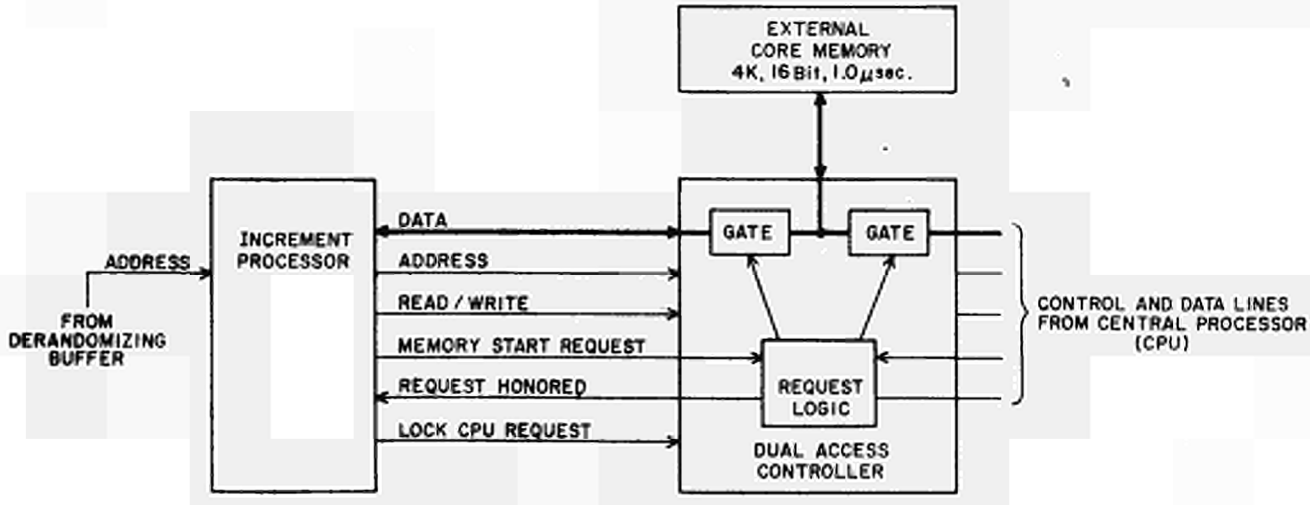

Fig. 5 - Dual access controller and external memory connected with increment processor.

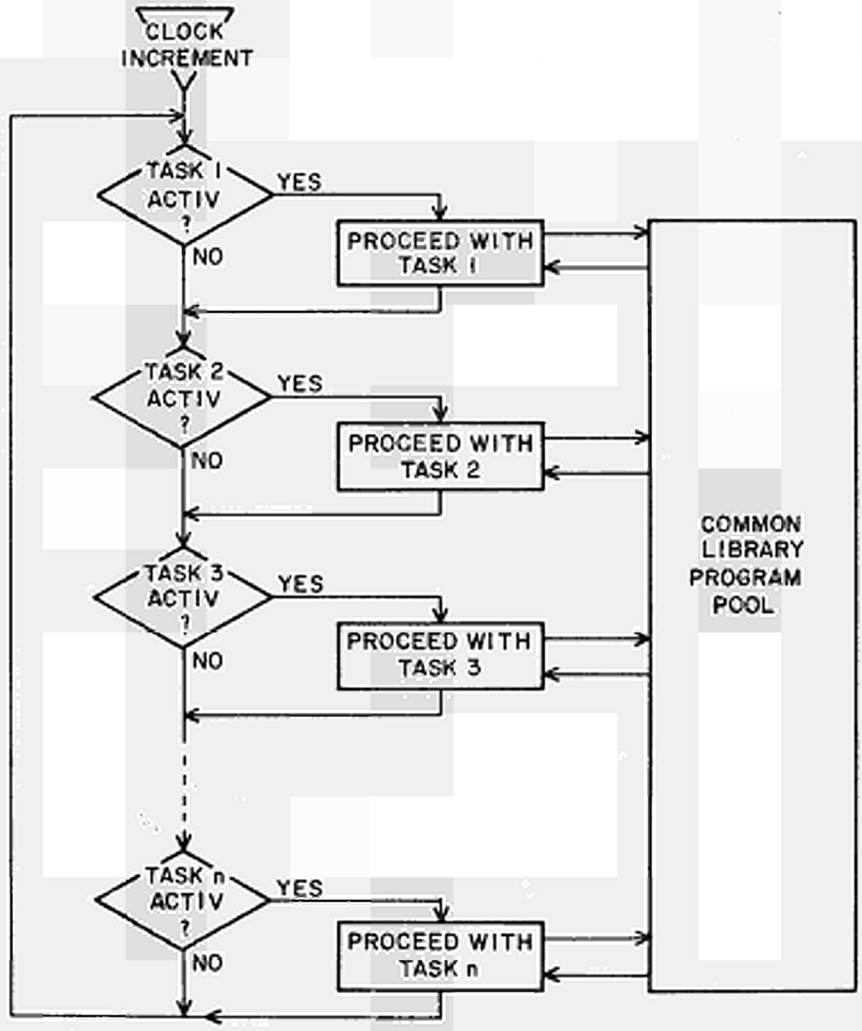

Fig. 7 - Flow of control in the operating system.

COMPUTER SYSTEM FOR ON-LINE NEUTRONIC NOISE ANALYSIS AND CALCULATION OF NUCLEAR REACTOR PARAMETERS

M. Čarapić*, Ph.D., D. Velašević, M.Sc., S. Stanković, B.Sc.
Boris Kidrič Institute of Nuclear Sciences
Beograd - Yugoslavia

Summary

The system design is based on the theoretical and experimental work known as variance to the mean method[1,2,3]. The paper describes the variance to the mean method in on-line computer application. The interface hardware and basic ideas of programming and conceptual advantages over the existing systems are discussed.

Introduction

The variance to the mean method of noise analysis for zero power reactor unperturbed assemblies is based on the fact that the evolution of the neutron chains and the detection and generation of neutrons are stochastic processes.

In Fig. 1 the equivalent single-detector experiment correlation system is presented.

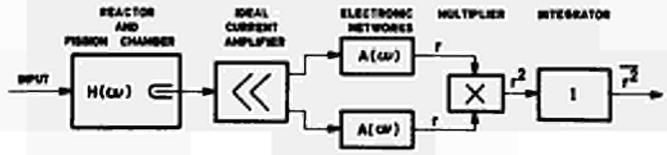

FIG. 1.

releases two synchronized responses

F - fission rate
W - detector sensitivity
l - prompt neutron life time
ν_2 - nuclear parameter
k^2 - effective multiplication constant.
α - prompt neutron decay constant.

For the short time approximation of the point reactor model

$$H(\omega)=\frac{1}{\alpha+i\omega} \qquad (2)$$

The electronic network in this experiment is a gate, or switch closed in the measuring time interval T. Consequently, its transfer function is

where
H (ω) - transfer function of the reactor and chamber
A (ω) - transfer function of the electronic network
r - pulse rate.

The variance of the pulse rate is found to be[1]

$$\overline{r^2}-\bar{r}^2=F\frac{W^2}{l}\left(\frac{\nu_2 k^2}{l}+2k\right)\int\left|\frac{d\omega}{2\pi}A(\omega)H(\omega)\right|^2+\pi_{12} \qquad (1)$$

π_{12} - additional term due to the fact that each registered reaction

$$A(\omega)=\frac{1-e^{-i\omega T}}{i\omega T}$$

Having in mind that $\pi_{12}=\frac{WF}{T}$, (3)
all expressions mentioned above could be inserted into the equation (1), which finally gives

$$\overline{r^2}-\bar{r}^2=F\frac{W^2}{l}\left(\frac{\nu_2 k^2}{\alpha l}+2k\right)\frac{e^{-\alpha T}-1+\alpha T}{\alpha^2 T^2}+\frac{WF}{T} \qquad (4)$$

In the actual experiment the number of counts in the interval (t-T, T) is n. Therefore,

$$r(t)=\frac{n(t-T,t)}{T} \qquad (5)$$

---

*The author has partially performed the work at Brookhaven National Laboratory, U.S.A.

so that the variance to the mean of the number of counts n in one interval T is

$$\frac{\overline{n^2}(T)-\overline{n}^2(T)}{\overline{n}(T)}=1+\frac{W}{1-K_p}\left[\frac{\chi_2 K^2}{1-K_p}+2K\right]\left(1-\frac{1-e^{-\alpha T}}{\alpha T}\right) \tag{6}$$

where $k_p = 1-\alpha_1$.

The expression on the left-hand side in the above equation is the variance divided by mean value which is equal to unity for Poisson distribution. Thus, the second term on the right-hand side of this equation is the discrepancy from Poisson law which is the function of reactor parameters and the measuring time interval T.

Experimental Arrangement

The variance to the mean of the number of counts in the preset time interval T_i can be determined from the probability distributions

$$\overline{n}(T_i) = \sum_{n=1}^{\infty} p_n(T_i)\, n(T_i) \tag{7}$$

$$\overline{n^2}(T_i) = \sum_{n=1}^{\infty} p_n(T_i)\, n^2(T_i) \tag{8}$$

where $p_n(T_i)$ is the probability of the occurence of n pulses in the time interval T_i.

Consequently, the problem of the variance to the mean measurement is reduced to the measurement of the probabilities $p_n(T_i)$. Once having the probability distribution $p_n(T_i)$ for each time interval T_i, the computer can calculate the experimental variance to the mean and using the fitting procedure determine the reactor parameters. In order to find out the probability $p_n(T_i)$, the following system conception was proposed (Fig. 2).

The pulses from the fission chamber are fed within the interval T_i to the event counter. Time intervals T_i are generated by the computer program and preset the timer. At the end of the time interval T_i the interrupt is initiated and the content of the event counter is read into the computer.

For each time interval T_i there is a table of K_i locations in the memory space. If the number of counts in some time interval T_i is n, the content $R_n(T_i)$ of the corresponding n-th location is incremented by one.

In this way, the probability $p_n(T_i)$ is defined as

$$p_n(T_i) = \frac{R_n(T_i)}{\sum_{n=1}^{K_i} R_n(T_i)} \tag{9}$$

The time intervals T_i are generated in a cycling way to avoid any correlation.

It is obvious in this experimental arrangement that the required interface hardware is very simplified compared with other ones consisting of 128 scalers[2] besides the other units. On the other hand, there is a flexibility of assigning a variable number of the memory locations K_i for each table.

Statistical Methods for On-Line Data Handling

After an estimate that enough data have been collected for a good

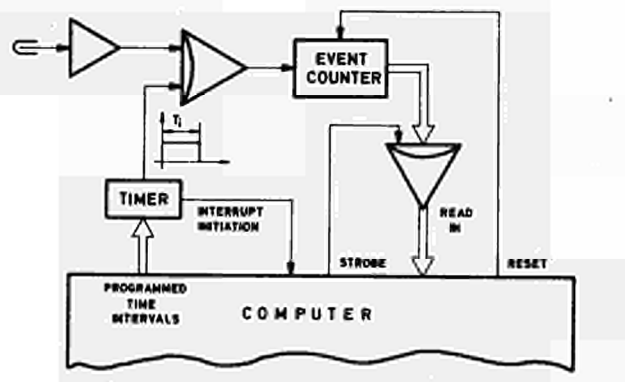

FIG. 2

statistical accuracy, the computer calculates the experimental function

$$Z_i=\frac{\overline{n^2(T_i)}-\overline{n}^2(T_i)}{\overline{n}(T_i)}=\frac{\sum_{n=1}^{K_i}\frac{n^2(T_i)R_n(T_i)}{\sum_{n=1}^{K_i}R_n(T_i)}-\left[\sum_{n=1}^{K_i}\frac{n(T_i)R_n(T_i)}{\sum_{n=1}^{K_i}R_n(T_i)}\right]^2}{\sum_{n=1}^{K_i}\frac{n(T_i)R_n(T_i)}{\sum_{n=1}^{K_i}R_n(T_i)}} \tag{10}$$

Referring to the Eq. 6, one obtaines

$$y_i=Z_i-1=a\left(1-\frac{1-e^{-bx_i}}{bx_i}\right) \tag{11}$$

where

$$a=\frac{W}{1-K_p}\left[\frac{\chi_2 K^2}{1-K_p}+2K\right]$$
$$b=\alpha$$
$$x_i=T_i$$

The exact fitting of the experimental and the theoretical functions is not possible and adequate.

The least squares method is usually used in such a kind of experiments, and it will be shown how it could be applied in an on-line computer experiment for a solution of particular problem where the memory space is critical*.

The parameters a and b appear nonlinearly in Eq. 11. For the solution of such a problem the Gauss method[4] is applied. If the values of the two parameters are expected to be $a=a_o$ and $b=b_o$, these values are to be used as the first guess. If Eq. 11 is expanded in a truncated Taylor's series about the point (a_o, b_o), and having in mind that this is a function in two dimensional parameter spaces, the following sum of squares is to be minimized.

$$\sum_{i=1}^{N}\left(Dy_{i,o}-\left[\frac{\partial y_i(a,b)}{\partial a}\right]_{\substack{a=a_o\\b=b_o}}\cdot\Delta a-\left[\frac{\partial y_i(a,b)}{\partial b}\right]_{\substack{a=a_o\\b=b_o}}\cdot\Delta b\right)^2=\min \tag{12}$$

where

$$Dy_{i,o}=y_i-a_o\left(1-\frac{1-e^{-b_o x_i}}{b_o x_i}\right). \tag{13}$$

$$\left[\frac{\partial y_i(a,b)}{\partial a}\right]_{\substack{a=a_o\\b=b_o}}=1-\frac{1-e^{-b_o x_i}}{b_o x_i} \tag{14}$$

$$\left[\frac{\partial y_i(a,b)}{\partial b}\right]_{\substack{a=a_o\\b=b_o}}=a_o\frac{1-e^{-b_o x_i}(b_o x_i+1)}{b_o^2 x_i} \tag{15}$$

N is the total number of time intervals T_t, $\Delta a=a-a_o$, and $\Delta b=b-b_o$.

In this way, the nonlinerar problem is reduced to the liner one, and the normal equations written in matrix form become

$$X\cdot A=Y \tag{16}$$

where

$$X=\begin{bmatrix}\sum_{i=1}^{N}\left[\frac{\partial y_i(a,b)}{\partial a}\right]^2_{\substack{a=a_o\\b=b_o}} & \sum_{i=1}^{N}\left[\frac{\partial y_i(a,b)}{\partial a}\cdot\frac{\partial y_i(a,b)}{\partial b}\right]_{\substack{a=a_o\\b=b_o}}\\ \sum_{i=1}^{N}\left[\frac{\partial y_i(a,b)}{\partial b}\cdot\frac{\partial y_i(a,b)}{\partial a}\right]_{\substack{a=a_o\\b=b_o}} & \sum_{i=1}^{N}\left[\frac{\partial y_i(a,b)}{\partial b}\right]^2_{\substack{a=a_o\\b=b_o}}\end{bmatrix} \tag{17}$$

$$A=\begin{bmatrix}\Delta a\\ \Delta b\end{bmatrix} \tag{18}$$

$$Y=\begin{bmatrix}\sum_{i=1}^{N}\left[\frac{\partial y_i(a,b)}{\partial a}\right]_{\substack{a=a_o\\b=b}}Dy_{i,o}\\ \sum_{i=1}^{N}\left[\frac{\partial y_i(a,b)}{\partial b}\right]_{\substack{a=a_o\\b=b_o}}Dy_{i,o}\end{bmatrix} \tag{19}$$

The matrix equation (16) ($A=X^{-1}Y$) is solved, and the new values of the parameters are evaluated

$$a_o+\Delta a \quad \text{and} \quad b_o+\Delta b$$

Now, the test for the convergence is performed, i.e.,

$$\frac{\Delta a}{a_o+\Delta a}\leqslant\varepsilon_a \qquad \frac{\Delta b}{b_o+\Delta b}\leqslant\varepsilon_b \tag{20}$$

The iteration procedure, namely the reevaluation of the parameters continues until above conditions are met. If the convergence criteria are satisfied, this does not mean that the experiment should be finished. There is no indication on statistical accuracy.

In other arrangement, the experiment has been set up so that data were collected on a specially designed hardware and all calculations were done in an off-line computer. In that case, the experimenter was not able to control the

---

* The general solution has been given by R.H. Moor and R.K. Zeigler, Los Alamos Report, LA-2367/1960.

duration of the experiment. He had no criteria for the good statistics in the course of the experiment and was forced to fetch data repeating in that way the measurement and calculations several times.

In our experimental arrangement several criteria were introduced. The on-line computer tests these criteria and if anyone is not satisfied it automatically continues the data collection and calculation program. As soon as all conditions are met, the computer stops the experiment and types out the relevant data.

As already mentioned, the conditions (20) are to be treated as one criterion. There are another pure statistical criteria defining the quality of the experiment. First of all, the value of the minimized sum of squares is of interest

$$M^2 = \sum_{i=1}^{N} \left[y_i - a\left(1 - \frac{1-e^{-bx_i}}{bx_i}\right)\right]^2 \qquad (21)$$

where a and b are the final values in the iteration procedure.

Furthermore, it is necessary to know the error of the parameters a and b. The computer tests the variances

$$\sigma_a^2 = C_a \frac{M^2}{N-2} \qquad (22)$$

$$\sigma_b^2 = C_b \frac{M^2}{N-2} \qquad (23)$$

and correlation coefficient

$$r_{(a,b)} = \frac{\mathrm{cov}(a,b)}{\sqrt{\sigma_a \cdot \sigma_b}} \qquad (24)$$

where

$$\mathrm{cov}(a,b) = C_{ab} \frac{M^2}{N-2} \qquad (25)$$

C_a , C_b - main diagonal elements of the matrix X^{-1}

$C_{ab}=C_{ba}$ - the remaining element of the same matrix.

All of these criteria are preset and could be changed during the experiment, which is the matter of the experienced experimenter. This is another advantage of the proposed method.

Programming Procedure

Basically, there are two programs in the system. One of them, written in the machine language, is concerned with the data collection and the other one, written in FORTRAN, with the calculation.

Both programs have the linkage to ensure real-time operations. The flow-diagram is shown in Fig. 3.

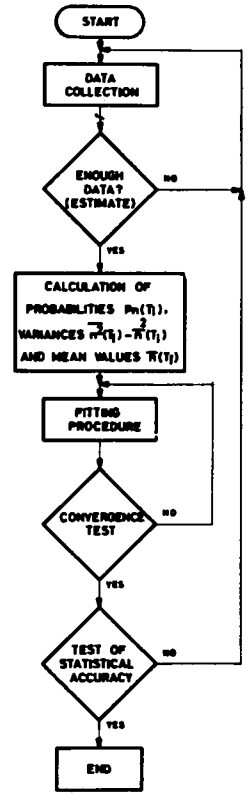

FIG. 3

In the data collection program there are N tables corresponding to n chosen time intervals Ti. Each table contains K_i memory locations, where Ki is variable depending on the time interval length. In this way, the required memory size is greatly reduced.

The other part of the program is written in FORTRAN and the linkage with the machine language data collection program is made to ensure real-time operations.

If N=50 and max K_i=128 are accepted, 8k memory locations are sufficient for the whole program to be executed.

Interface Hardware

Referring to Fig. 2, the current pulses from the fission chamber having the collection time of 20 nsec., are applied to a wide band amplifier at a distance of 500 feet, as shown in Fig. 4.

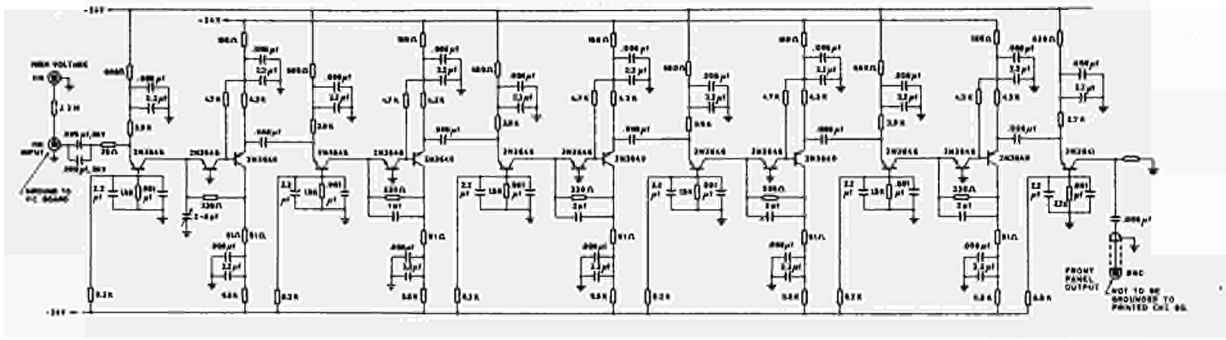

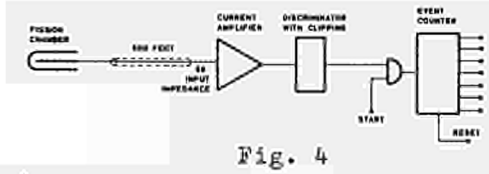

Fig. 4

This is a modified version of Rush's amplifier[5]. The rise time of the amplifier is 4 nsec, gain of 5000, input impedance of 50 ohms, and the equivalent input noise of 0.1 μA. After clipping and discrimination the pulses are counted by a seven bit binary counter and the results sent to the computer.

The timer is preset with the successive programmed time intervals Ti, gates the event counter to start counting. At the end of the measuring time interval, the interrupt is initiated. In the interrupt subroutine the data are strobbed into the computer.

All micrologic circuitry is designed by standard interface cards of the SDS T-series.

Conclusion

The application of the on-line computer for real-time operation in the described experiment offers a great deal of advantages.

First of all, the program itself could easily be changed to correspond to the particular experiment conditions, from the operator console.

The duration of the experiment is greatly reduced by the on-line examination of statistical accuracy. Namely, the experiment stops as soon as the statistical criteria are met.

The hardware is considerably simplified and it consists of very common units. Only the amplifier and the fission chamber are to be carefully designed. The computer may be placed far away from the nuclear reactor and used for other purposes.

Acknowledgement

Gratefully acknowledged are the stimulating and helpful discussions with W. Higinbotham, R. Chase, R. Spinrad, and C. Sastre from the Brookhaven National Laboratory, U.S.A.

References

1. Borgwaldt, H. and Stegemann, D., A Common Theory for Neutronic Noise Analysis Experiments in Nuclear Reactors, Nukleonik 7, 1965.

2. Bayer et al., Techniques for Zero Power Assemblies, ANL-7320.

3. Pal, L., Statističeskaja teorija cepnih reakcii v jadernih reaktorah, Acta Phys. Hung., Tom XIV, Fasc. 4.

4. Trotter, H.F., Gauss Work (1802-1826) on the Theory of Least Squares, An English translation, AEC-TR-3049 (1957).

5. Rush, C., New Technique for Designing Fast Rise Transistor Pulse Amplifier, The Review of Scientific Instruments, Feb. 1964.

DISCUSSION

Keddar : I would like to know first of all which parameters are measured. If the method is applied to the zero power reactor what is the accuracy ?

Carapic : - This work has partially been performed in Brookhaven National Laboratory on plutonium essentially but partially this work continued in Belgrade on zero power reactor. As far as accuracy of the estimation of the parameters is concerned we found the same result as in the previous experiments. This is only an improvement in the decreasing time for performing the experiment.

A COMPUTER ON LINE IN ACTIVATION MEASUREMENTS

L. Arcipiani, U. Farinelli, A. Gibello
C.N.E.N., C.S.N. Casaccia, Roma
Laboratorio Fisica e Calcolo Reattori

Summary

The problems involved in large scale automation of experimental laboratories are briefly discussed. The possibility of automating experiments of different types by means of a central computer working in time-sharing is being investigated at Casaccia. To gain experience in this respect, the equipment for activation measurements of the Reactor Physics Laboratory has been connected to an IBM 360/30 computer. The time sequence of the experiments is controlled by the computer, and the processing of data is carried out in real time. Hardware, software and operating procedures are briefly reviewed in the paper. The need to keep a high degree of flexibility is stressed.

1. Introduction

Automation is generally introduced to decrease the need of manpower and to increase the efficiency of well-established and fully standardized processes. The automation of the operations carried out in a research laboratory involves non-conventional problems, since no fixed routine can be assumed for the measurements, and a very high degree of flexibility is required. The purpose of automation, in such a case, is first of all to improve the understanding by the experimenter of what is happening at all times in his measuring equipment, to identify immediately any malfunctioning, to assist the operator in taking, or to take directly, actions to maximize the acquisition or to avoid the loss of useful information, to store in a consistent form data to be used for subsequent processing, and to supply from time to time a general view of the outcomes of the experiment as compared to expectations, thus enabling the experimenter to take a quick decision on the further course of actions.

With such a view in mind, it is difficult to assess whether, or to what extent, a certain research activity should be automated; the problem being not so much in finding a correct solution to meet certain specifications, as in drawing these specifications, in establishing the amount of flexibility necessary to meet actual needs, without unduly limiting possibilities or introducing unrealistic complications, and in deciding what is the most concise and effective presentation of the information to the experimenter.

A pilot programme was started at C.N.E.N. Casaccia to investigate what amount of automation it would be convenient to introduce in the various experimental areas, and what type of general philosophy should be followed. Two main lines are possible: to supply each experiment or group of homogeneous experiments with a local process computer having a configuration adequate to meet all on-line computation requirements (further off-line processing can follow, via manual transfer of punched or magnetic tapes); or to limit the local equipment to the necessities of high-speed accumulation and/or reduction of data (e.g. a set of scalers, a multichannel analyzer, a process computer with no peripheral equipment) and to connect in real time all such local equipments to a central computer of sufficient capacity, working in multiprogramming, which controls the operation of the data collecting local installations, supplies the necessary processing facility for large amounts of data or complex computing programmes, and sends back the appropriate information. In this second scheme it seems realistic to assume that feedbacks requiring a delay time of, say, less than 0.1 sec. are taken care of by the local equipment, while slower actions may be handed over to the central computer.

Since experience on the first scheme is already available at Casaccia (several process computers of various complexity are in operation in connection with experiments of different type) it was decided to carry out some pilot tests on the second type of automation. If this line will prove to be the most valuable, it will be necessary to replace the present computer with a larger one, having a memory capacity and operating system adequate for handling data from a large number of experiments.

The selection of the first experiment to be automated by the use of a central computer was based on the consideration that the experience thus gained should be as meaningful as possible. Therefore, the experiment should be one requiring a high degree of flexibility and should provide the opportunity for the direct control of the equipment by the computer. The laboratory of activation measurements was selected as presenting these characteristics, and also because it involved a relatively slow flow of data but a somewhat complex real-time processing, thus making a link with the central computer relatively more attractive than the use of a local process computer.

A second experience, consisting in the connection between a local process computer and the central computer, has just started and will not be reported here.

2. Measurements to be automated

The measurements carried out in the laboratory to be automated consist in the determination of the activities of samples irradiated in nuclear

reactors and critical facilities to study neutron flux distributions and spectra. The equipment consists in 4 general purpose counting systems; a different type of measurement can be performed at a given time by each of the systems (samples with different half-lives or radiation characteristics, flux scanning, cadmium ratio or spectralindex measurements etc.). Each counting system,(CS)as shown in Fig. 1,consists of an automatio sample changer,(SC) 2 independent counting chains (each including radiation detector, amplifier, integral or window discriminator and scaler), and a third scaler which can be used as a timer for both chains, or for other purposes (e.g. coincidence counting). A digital clock, common to all systems, can be read "on flight" by means of a buffer.

With referenoe to Fig. 1, the sample changer operates as follows. Samples to be measured (S1,S2,...) are loaded in magazine (1), while a reference sample,(monitor M)is put in position (4).The samples are sequentially taken to the counting position (2) and counted alternatively with the monitor in a predetermined sequenoe (for instance: S1, M, S2, M, S3, M... or S1, S2, S3, M, S4, S5, S6, M... etc.). Measured samples are discharged into magazine (3). In measurements like cadmium ratio or spectral index determination, the sample ohanger can be used to count alternatively two fixed samples (S1,S2,S1,S2,S1,...). The sample changer is operated by sending electrical pulses to its control unit, whioh in turn provides a signal when the operation of changing a sample is completed.

Measurements on a system generally involve a number of samples ranging from 2 to 50; typical counting times range from 15 to 200 sec. The change of a sample takes about ten sec. Pulses accumulated on the counting scalers during a measurement vary from 0 to about 10^6. Counting a set of samples constitutes a cycle. Suoh cycles are repeated several times on each set of samples in order to be able to check the statistical consistency of the data. Short term stability of the electronics is checked by the periodic insertion of the monitor and by comparing the counts on the two chains. In order to make these checks, it is generally necessary to correct for background, dead-time losses and radioactive decay. From the point of view of data acquisition, eaoh system typically supplies two-three data of up to 20 bits every 20-200 sec; a measuring cycle (e.g. 30 samples plus monitor) may last two hours; a run (consisting of a certain number of cycles) seldom lasts more than 10-15 hours.

What has been described is applicable to the majority of the measurements carried out in the laboratory; in order to detail specifications for the automation, an effort was made to group all these measurements in a few homogeneous groups as concerns data acquisition, types of checks to be performed and corrections to be applied.

Occasional measurements that do not fall into this scheme should be manageable by minor changes in the software.

With non-automated operation, raw data are punched on paper tape and printed at the end of each measurement; the "feeling" of the operator alone guarantees that the experiment is proceeding correctly. At the end of a run, the punched tape is taken to the computer for processing: the evidence of incorrect performance of the equipment (for instance from the statistical analysis of the data) or of unexpected results that need confirmation may come too late to re-measure the samples (e.g. in the case of not too long half-lives).

Specifications for the automation require the computer to perform a preliminary check on the data after each measurement prior to changing the sample; to decide whether to change the sample or to repeat the measurement; to make a more complex consistency check at the end of each cycle; to give pertinent information to the experimenter at each step, so that he can take over the control or check the equipment if necessary; to store the data and to make the final analysis at the end of a run.

3. The computer

The computer used in this connection is an IBM 360 model 30. Its configuration includes a 64 K bytes memory (1 byte = 8 bits), 2 disk units and 3 magnetic tape units, a card reader/puncher, a printer, a paper tape reader, and a data adapter unit (2701) for teleprocessing connections. A third disk unit, a second printer and a plotter are now being added to this configuration. The computer is currently used both for local scientific computation and as a teleprocessing terminal for a microwave link with the larger computers at C.N.E.N. Computing Centre in Bologna. Some non-numerical data processing is also carried out.

The computer works under control of the DOS operating system.

4. Hardware of the connection and operating modes

The computer is linked with the experimental equipment via an IBM-1070 terminal and a special unit acting as a multiplexer for the counting chains (Chain Multiplexer: C.M.). Two basic modes of operation are possible; they differ mostly as for the role of the computer in the actuation and timing of the counting systems. They are schematically represented in Fig. 2, where the dotted lines correspond to functions of Mode 1 only. In Mode 1 measurements in each counting system are terminated by the corresponding timer (preset counting operation is also possible). The system than "calls" the computer to be read, operated upon and restarted. In Mode 2 the computer itself terminates the measurements, using its internal clock. The following description

applies to Mode 1; Mode 2 will be briefly discussed at the end of this Section.
When beginning a run of measurements with one or more systems, the experimenter sends to the computer by means of a digital selector unit (called D.I. = Decimal Input) all the data necessary to identify the system(s), the type of measurement, the monitoring programmes to be applied, and other information required for the control and processing of the experiment. The first measurement is then initiated manually.
Counts from the chains are accumulated on Laben Mod. PFS 136 scalers: these are 6-decades, 30 MHz micrologic based scalers without visual display, with an internally selected address for identification. When the prefixed time is reached, the timer stops itself and the scalers, and a signal is sent to the Chain Multiplexer.
The Chain Multiplexer (C.M.) is a unit expecially developed by Laben to convoy data and controls to and from a number of scalers (up to 64). On receiving the signal from a counting system, the C.M. reads on flight the general clock, then scans the scalers, looking for those in stand-by conditions. It reads the first scaler, transferring its content on a buffer, and sends to the 1070 unit a Process Alert (P.A.) signal to indicate that there are data ready to be sent to the computer.
The 1070 identifies the origin of the P.A. and when the computer requests it, transfers from the C.M. buffer to the 360 the address and the content of the first scaler. This procedure is repeated as long as there are scalers to be read: each time the computer receives a data, it sends back an acknowledgement signal, which cancels the data on the C.M. buffer and leaves it ready to read the next scaler. Data are sent character by character from the C.M. to the 1070 which is located close to the experimental equipment; the 1070 serializes the data bit by bit, to send them to the 360 computer through about 50 m of telephone cable. The connection to the computer is by means of the 2701 Data Adapter Unit. The transmission includes parity checks (VRC & LRC).
As soon as the data from a system are received, the computer executes the required processing and supplies the results to the experimenter by typing them on the 1053 unit (always through the 1070) together with other useful information contemplated by the control programmes. If the checks on the data have been positive, the computer operates the change of the sample, by sending the appropriate address to the 1070, which is directly connected to each of the sample changers. When the new sample is in the counting position, the sample changer sends a signal to the P.A. bus, which is identified by the 1070; upon reception of this signal, the 360 sends orders of "reset" and "start" to the scalers of the counting system involved. These orders are actuated by sending to the C.M., through the 1070, appropriate messages including the address of the system to which they are directed. The channelling of these orders to the scalers is performed by the C.M.
The description outlined above refers to operation Mode 1; Mode 2 shares with the first the data transfer operation, the data checks, the actuation of the sample changers and of the scalers. In the second mode the counting times requested are defined by the experimenter before starting measurements on the D.I. and are sent to the computer. The internal timer of the 360 stops the scalers accordingly.
The present connection makes use of 40 points (20 input and 20 output points) of the 1070 system as compared to 60 available on the present configuration and 300 possible. This allows an easy expansion of the installation to control other systems or other single counting chains.
The C.M. allows the visual display of one scaler at a time by panel selection.
In order to allow the continuation of the experiments even if the computer is out of operation the C.M. can be directly connected to a printer and to a paper tape puncher, so that automatic (non-automated) operation is possible.

5. Description of the software

Two types of programmes have been written for the link:

1) a programme called "LINK CONTROL PROGRAMME" (L.C.P.);
2) a set of programmes written in FORTRAN language for on-line intermediate and off-line final data processing.

The L.C.P. supervises the whole on-line processing. It includes a set of subprogrammes for collecting data, for translating and editing messages between 360 and 1070, for printing intermediate results on the 1053, for sending orders to 1070 (such as actuation of a S.C., reset and start of scalers etc.).
The L.C.P. is written in Assembler and BTAM languages (Basic Telecommunication Access Method). The latter consists of a set of macro-instructions which control transmission and reception of messages on the telecommunication line and enable the L.C.P. to use the Supervisor facilities.
The L.C.P. is based on the two operations of "polling" and "addressing". The "polling" operation is used by the computer to interrogate the 1070 terminal and enable it to transfer data, when the 1070 is put in alert status by a Process Alert signal. "Addressing" is the operation by which the computer addresses messages to the 1070 terminal. "Polling" and "addressing" operations are performed by the instructions READ and WRITE. In both cases some control characters are required to perform the requested operation, such as the polling character (o), the addressing character (9), or the address of the 1070

terminal (Q). Data are exchanged between the terminal and the computer in the form of blocks of characters; the beginning and end of each block is marked by control characters inserted and recognized by the hardware.
Once initiated, the data transfer to or from the computer storage proceeds automatically until the end of the block. In the meantime the normal work of the computer can continue.
Blocks may consist of up to 281 characters. Thus, since the speed of transmission of the 1070 is 66.7 characters/sec the transfer of a block of data takes a few seconds.
The general structure of the L.C.P. is represented in the flow-chart of Fig. 3, for operation Mode 1. The L.C.P.:
- controls the polling of the terminal
- carries out some preliminary analysis on the data received from the terminal
- sends to the terminal the results of the analysis and appropriate orders
- accumulates data and/or results on a disk
- recognizes error conditions and takes consequent actions and writes alarm messages for the experimenter.
- calls the appropriate programme for the on-line processing at the end of each measurement cycle.

As specified in the former section the experimenter manually starts the measurements after introducing the initial information by means of the D.I. The L.C.P. then starts sending periodically a "polling" signal to the 1070 terminal in order to investigate whether any counting system is ready to transfer data.
After receiving the polling signal, the terminal may transmit either a negative response (indicating that there are no data to be transmitted: Process Alert is off) or a block of characters representing the address and content of a scaler.
After a negative answer, the L.C.P. will wait τ seconds before sending another polling signal, letting the central processing unit of 360 to perform other works in the meantime. In the case of a positive answer, the computer will send to the terminal an acknowledgement signal which initiates another data transfer.
A special case occurs when one or more C.S. stop while another C.S. is transferring data or, later, while these data are being analyzed. To account for this possibility, the L.C.P. repeats the polling routine before analyzing the data from a C.S., and interrupts periodically (every τ' sec.) the analysis to perform a polling routine.
The further data acquired during these operations are stored in a waiting queue and later analyzed in the same order in which they have been acquired.
Once the analysis of the data from one of the C.S. has been completed, and the measurements are checked as good, the L.C.P. operates the corresponding sample changer.
During the polling routine, if the L.C.P. recognizes a P.A. indicating that an operation of changing a sample is terminated, it sends the reset and start signals to the corresponding counting system.
The procedure just described refers to the operation Mode 1. Mode 2 is conceptually simpler, since the computer itself stops the C.S., by clocking the duration of the measurement on its internal timer.

6. Data analysis and error handling

As mentioned, the L.C.P. performs a preliminary analysis on the data before starting a new measurement. This analysis aims to identifying possible large inconsistencies, caused, for example, by equipment malfunctioning. This analysis can be based upon the ratio of the counts in the two chains of the same C.S., or upon a statistical analysis when the same sample is measured several times, or upon a comparison with prefixed values.
At the end of a cycle of measurements, one of a set of programmes ("Cycle Process Phase") is transferred from disk into the fast memory of the computer, for a more detailed analysis of the measurements and for an intermediate processing. The type of preliminary analysis and the programme for the "Cycle Process Phase" are both selected at the beginning of each run.
The L.C.P. phase and the "Cycle Process Phase" are organized into an overlay structure. Data are called from disk and results are sent either to the 1053 typewriter or to a disk.
At the end of the run, data accumulated on disk can be further processed off-line.
The "Cycle Process Phase" and the final processing programmes are written in FORTRAN language and may be very different according to the particular problem being investigated.

One of the problems, which arises with links, lies in deciding how error conditions should be handled. A compromise is necessary between a very comprehensive error handling and a reasonably simple and possibly short link control programme. When working in multiprogramming, it is desirable that the L.C.P. should not be such as to reduce unduly the memory available for the other work of the computer.
However we have tried to inform the experimenter on the nature of the error and to override the error whenever possible.
Errors may have three origins: malfunctioning of the measuring equipment, failure in the connection hardware and human mistakes.
Substancial errors of the first type are detected by the L.C.P.; less relevant errors (like a slow drift of a chain) are detected by the Cycle Process Phase, which can perform a more detailed analysis of the data, since the overlay structure allows more memory space to be used for this purpose.
If the check of the data performed by the L.C.P. at the end of each measurement is positive, the sample is changed and the cycle continues; if

it is negative, an error message is sent to the experimenter, and the measurement is repeated on the same sample (i.e., a reset-start order is sent to the C.S. without operating the S.C.). This procedure is repeated for a number of times; if the error persists, the experimenter is warned by a "trouble message", and the C.S. is put out of operation. The experimenter has the possibility, after checking the equipment, to re-start the system and to re-enter into the L.C.P. routine.

Most errors of the second type are detected by the input/output routines of the Supervisor, which set indicators for examination by the L.C.P.

If the L.C.P. receives an acknowledgement indicating error, it re-transmits the data up to three times. If recovery is not possible the programme is discontinued and cannot be resumed without operator action.

As for errors of the third type only operational experience will demostrate how fool-proof the system is.

7. Computer organization

As mentioned in Section 3, the computer works under supervision of the D.O.S. operating system. The four parts into which the computer memory can be subdivided when working in multiprogramming, have in our case the following destinations: a part for the Supervisor programme, a "background area" used by the problem programme currently being executed in the course of the batch processing (the "background job"), the foreground-two area for the teleprocessing with Bologna and the foreground-one area for the programmes needed for the link (L.C.P. and Cycle Process Phase). The highest priority is thus assigned to the link.

In allocating memory space, consideration was given to the necessity of maximizing the area available for background jobs; however, about 20 K bytes had to be assigned permanently to the Link Control Programme. The Supervisor and the programme for the teleprocessing with Bologna take about 10 K bytes each, so that the background area is actually reduced to 20 K bytes. Larger background problems can be processed in the hours in which the teleprocessing is not operating. Anyway large programmes are generally run at Bologna via teleprocessing, and this policy will be enhanced in the future by the use of an improved radio-bridge link. However, it is clear that the extension of the real-time processing would require a larger computer at Casaccia.

8. Conclusions

It is too early to draw any final conclusion from this experiment; the software is still undergoing continuous changes to make it more respondent to the needs of the experimenter, and no reliable comparison was as yet possible between pre-and post-automation operation of the equipment.

However, some preliminary conclusions are that no major difficulties are involved in the hardware, while problems are present in the software and in computer organization. The reduction of the different types of measurements to a few standard patterns, at least in the case of activation measurements, although somewhat distressing at first, eventually proved to be possible without losing flexibility. Sophisticated on-line control programmes can be envisaged and usefully applied, provided the computer capacity is adequate.

9. Acknowledgements

A major contribution in writing and debugging the software is due to V. Angelini; checking of the hardware and initial operation tests were performed by D. Antonini and R. Scafè.

LABEN S.p.A. met in a most cooperative spirit the unusual requirements posed by this problem; I.B.M. of Italy supplied assistance, especially as concerns operating systems and languages.

DISCUSSION

Lidofsky : - You said 64 K : you mean K bytes or K words ?

Farinelli : - K bytes

Lidofsky : - The second thing is that you said that apparently the line that you may take in the future is to go with bigger system. Is your problem that you don't have enough memory for your program or that you have problems with time-sharing on the programming system ?

Farinelli : - Both. The memory area now devoted to real time processing is only 20 K, and can accomodate only one type of data reduction ; we think that about 256 K would be needed for large scale automation of experiments at Casaccia. The Disk Operating System is not flexible enough to deal with many-level multiprogramming.

Bisby : - I think you have discussed a semi-automatic system since I presume that the software defined the control programme of the sample-changers and this could only be changed for example, the time of a counting period, by manual presetting of the timer register ?

Farinelli : - Preset operation is possible if the number of counts is selected manually by the experimenter.

Vuilleumier : - What is the capacity of your microwave link to Bologna and do you see in it a way to extend a small computer to a large machine ?

Farinelli : - The present capacity of the microwave link with Bologna is between 2000 and 4000 bits/sec., there are plans to extend it to 20.000 in the next future.
We have considered the possibility of using this link (or an extended one) to process in real time at Bologna data from experiments at Casaccia, but we have decided this was not realistic.

Bossel : - I have another question for this micro wave length that this link has just a speed of 2000 to 4000 b/s, we have a link between two computers at Zurich which is 40.000 b/s and this goes over fast telephones lines, so I thought that with micro wave link you could go up.

Farinelli : - Of course you could, in principle there is no limitation. We just don't think we need it.

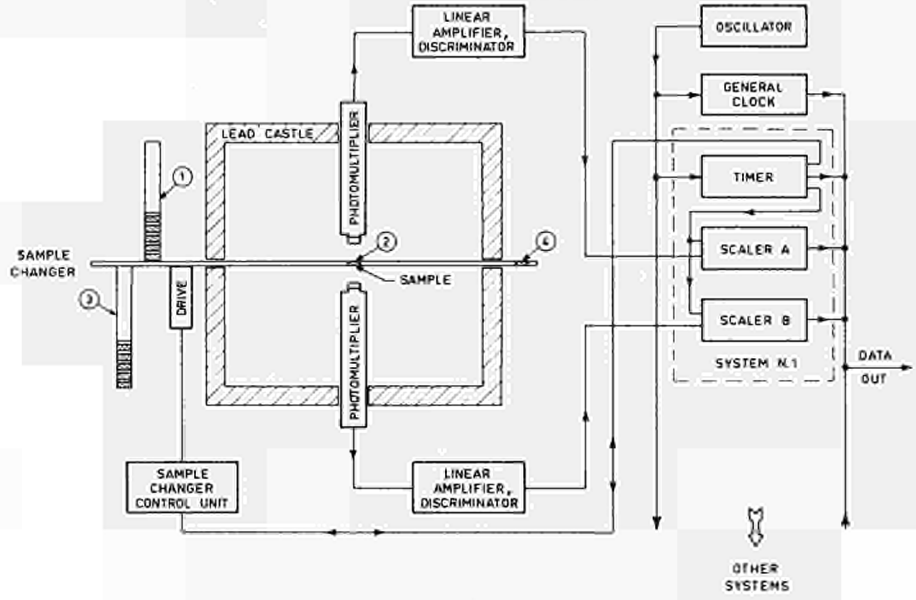

Fig. 1 - Typical counting system.

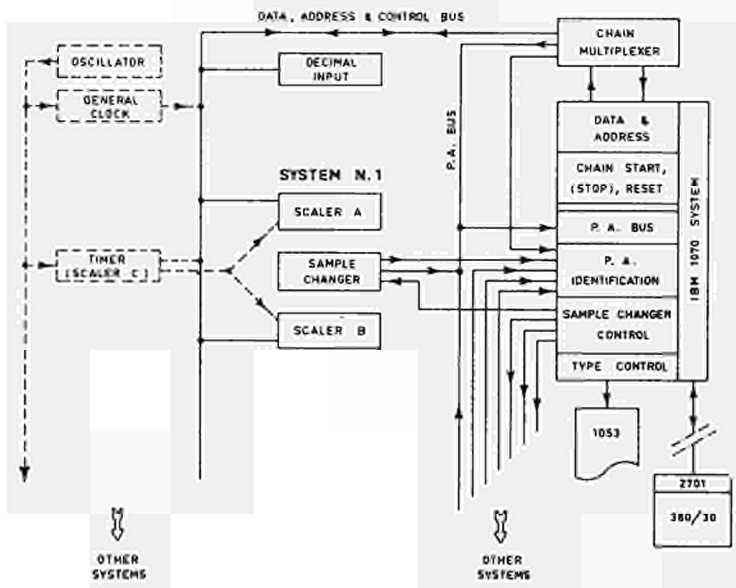

Fig. 2 - Block diagram of the hardware.

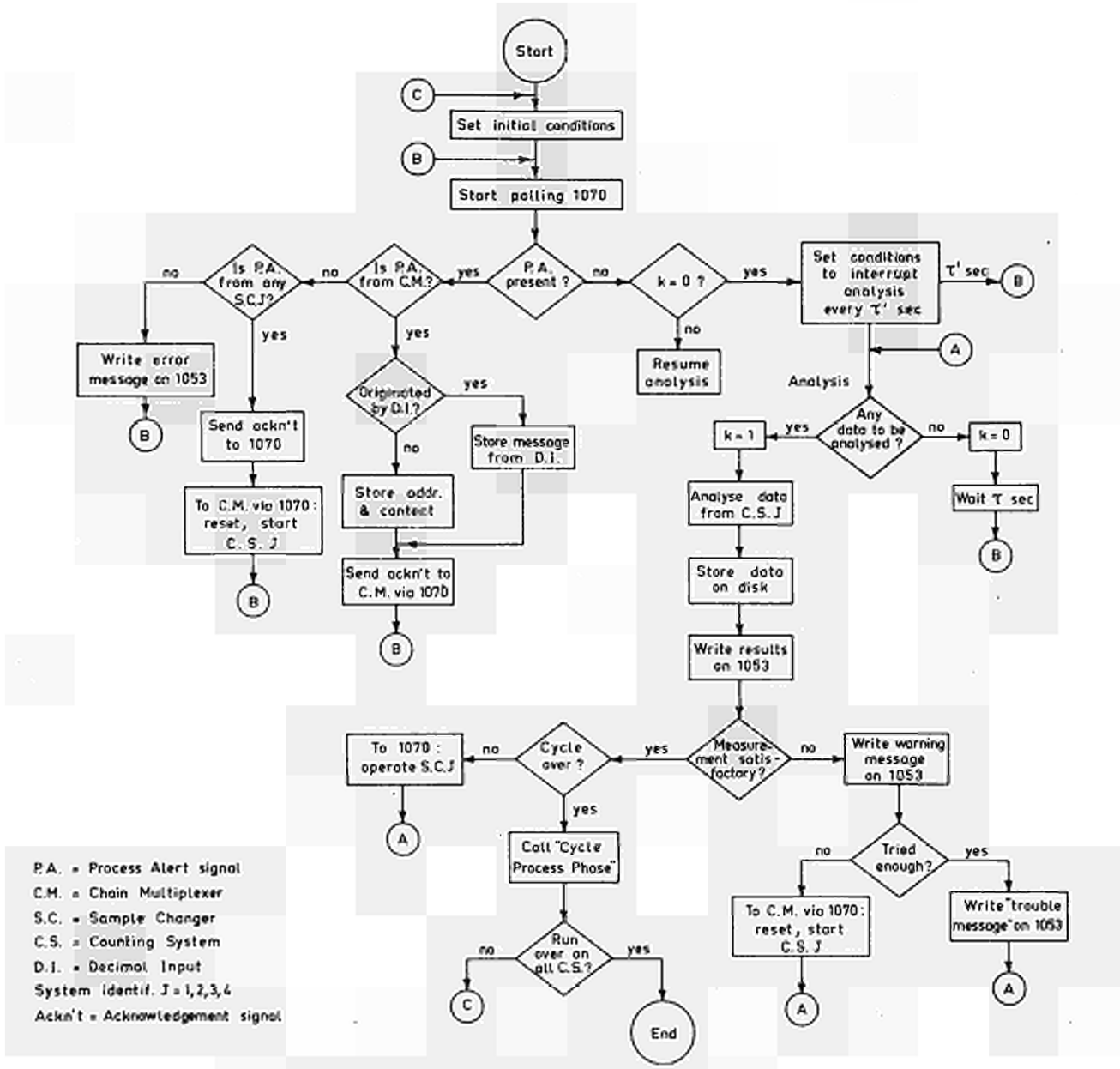

Fig. 3 - General flow chart of the Mode 1 "Link Control Programme".

USE OF A COMPUTER ON-LINE IN EXPERIMENTS AT THE FAST CRITICAL ASSEMBLY SNEAK[++)]

by

P.L. van Velze[+)] and H. Walze

Institut für Angewandte Reaktorphysik
Kernforschungszentrum Karlsruhe, Germany

Summary

A DDP 124 computer with a data acquisition system is used for on-line data processing and control of nuclear reactor experiments at the fast critical assembly SNEAK.

Some of the applications are described. It is shown that by using an on-line computer experiments at the reactor can be performed with a considerably improved efficiency.

1. Introduction

In the fast zero power reactor SNEAK the neutron physics of large fast reactor cores with uranium and plutonium fuel can be investigated. A specific core is mocked up in SNEAK only during a relatively short period in which all experiments have to be carried out. Because it is very time consuming to repeat certain experiments later, it is important to have the possibility of immediate judgement about the successfullness of the experiments. Besides it is possible to improve the quality of the experiments in this way.

In order to achieve optimum data processing and experiment control, a digital computer for use on-line is installed. The selected system is a DDP 124. It has a 24-bit word and a 16-K core memory with 1.75 µs cycle time. The central processor has a fixed wired floating point arithmetic. An IBM compatible magnetic tape unit and a digital plotter belong to the periphery.

2. The On-Line System

For the acquisition of data from external sources like digital position indicators or digitized outputs of ionization chambers five 24-bit registers have been built. Each register consists of six 4-bit modules. Each module can be used either as binary counter or as parallel buffer. The modules are normally controlled by a quarz-stabilized programmable timer.

The interface system consists of five 24-bit data channels, 16 command lines and 10 sense lines. The command lines serve for altering the status of experimental equipment, e.g. switching an amplifier or starting a motor. The sense lines can be used for checking the equipment or environmental conditions of the experiment.

The data transfer is accomplished by the interrupt technique: when a register connected to a data channel is ready for transfer, the timer generates an interrupt request and the register provides a jump address. The request forces the central processor to halt its current operations and to perform a jump in to the data transfer subroutine specified by the jump address. The data are stored in a storage field to which the interrupted main program has access.

During or after on-line data processing the measured raw data are stored on magnetic tape. Therefore off-line reevaluation of an experiment can be done at a later time if there is any doubt about the correctness of the real time data processing.

3. Reactivity Measurements

In many experiments a real time reactivity determination is wanted. The computer code KINEMAT, based upon the inverse kinetic equations calculates the reactivity as a function of time from the time behaviour of the neutron flux. The neutron flux is measured with a linear channel, consisting of an ionization chamber, µµA-amplifier and a voltage-to-frequency converter. The output pulses, of which thefrequency is proportional to the neutron flux, are counted in a register during a time interval controlled by the timer. Experiments in which KINEMAT is used, are control rod calibrations, measurements of temperature reactivity coefficients and material worth experiments.

Control rods are calibrated by moving them stepwise through the core. The neutron flux and rod position data are continually fed into the computer. The KINEMAT code calculates the mean value of reactivity and the statistical accuracy for each single step. If the accuracy has reached a preset limit the computer gives a command to

---

[+)] EURATOM-Delegate

[++)] Work performed within the association in the field of fast reactors between the European Atomic Energy Community and Gesellschaft für Kernforschung mbH., Karlsruhe

the moving mechanism of the rod for the next step. Immediately after completion of the calibration procedure the plotter draws the rod calibration curve. This curve is fitted through the measured reactivity vs. position points (see attached figure).

For measurement of temperature reactivity coefficients a fissile material sample in the reactor is periodically heated and cooled with a gas flow. The temperature variations in the sample and in the surrounding reactor are measured with thermo-couples. A switching network controlled by the timer connects the thermo-couples with a voltage-to-frequency converter, of which the output is fed into a register together with the digitized neutron flux signal. The computer program determines whether the demanded accuracy is reached.

In the case of material worth experiments a drawer which is loaded with fuel and the material sample is oscillated in the reactor core by a traverse mechanism. Drawer position and neutron flux data are input for the KINEMAT program. As soon as the statistical accuracy of the measurement has reached a preset limit, the computer initiates an automatic sample change.

During all of the described experiments a continuous reactivity plot can be drawn. With this real time display an immediate decision on the continuation of an experiment is possible.

4. Spectrum Measurements

Another application of the computer is the determination of the neutron energy distribution in SNEAK with sets of foils that are irradiated in the reactor. The difference in intensity of selected γ-activities induced in various foils is used to determine the neutron energy distribution in the reactor. The γ-spectrum of the foils is measured by a detector system connected to a pulse height analyser in a counting room. Foil changing is done by a fully numerically controlled changing mechanism. For each neutron spectrum measurement very many different foils are irradiated. The large amount of data obtained with the pulse height analyser makes on line processing useful.

After each measurement the content of the analyser memory is transferred into a terminal in the counting room, which is connected to one of the registers in the computer room.

The content of one channel of the analyser makes just a 24-bit word. After temporary storage of a pulse height spectrum in the core memory of the computer, the data are stored on magnetic tape for later evaluation.

In conclusion it can be said that on-line data processing is the only method by which optimum use of the reactor for experiments is possible.

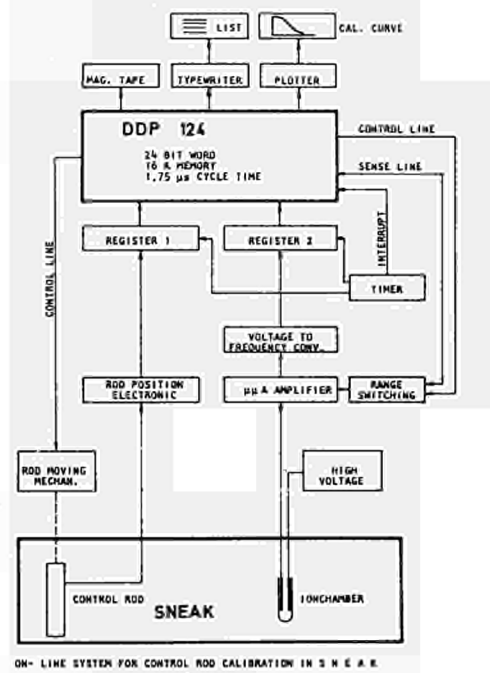

ON- LINE SYSTEM FOR CONTROL ROD CALIBRATION IN S N E A K

DISCUSSION

Hugues : - I would like to know what safety aspects you have considered by using the on line control for your reactor.

Walze : - As I expected the question I should stress that we don't use the computer for operating reactor and for any function of safety. We only use a computer for experimental purposes.

N U D I A C :
DATA ACQUISITION AND PROCESSING SYSTEM APPLIED TO PHYSICS EXPERIMENTS AND TO NUCLEAR MEASUREMENTS

J. MOISSET (Soc. INTERTECHNIQUE - France)

M. BARTHELEMY (Speaker)
Commissariat à l'Energie Atomique
Centre d'Etudes Nucléaires de Saclay
B.P. n° 2 - F - 91 - Gif-sur-Yvette
(France)

Abstract

The system presented here was designed to perform the functions involved in the acquisition, processing, display and filing of experimental data, particularly in the field of nuclear spectrometry. It is set up around a central computer unit with 8,000 words of 18 bits and having as special peipheral equipment a display unit and a disc memory. A direct-access multi-channel acquisition coupler gives simultaneous handling facilities for several acquisition channels in different modes (e.g. amplitude analysis, multi-scale mode and multi-sampling).

The obtained data are processed by external patch programs with a high processing speed which utilise the microprogramming possibilities of the central unit. The system is programmed by a simplified original and interpretative-type language (PHITROL) geared to spectrum processing.

This system was designed and developed by the INTERTECHNIQUE company in collaboration with the CEA.

Introduction

The NUDIAC system was designed to perform the functions of acquisition, processing, display and filing of experimental data, particularly in the field of nuclear spectrometry.

The basic intentions of the system were as follows :
Development, with a low-capacity (8,000 words) computer unit, of a system geared to spectrum processing and having high-performance acquisition characteristics as regards acquisition rate and input simultaneity,
Conditions enabling a permanent dialogue to be carried on between the user and the system by means of a sophisticated display unit.
To make available to the physicist a simple, easily assimilable language for the constitution and processing of spectra, and suited to the complete real-time section (acquisition, clocks, display),
Equipment of the system with a library affording as direct access as possible for filing spectra and previously formed instruction sequences.

We shall lay particular emphasis in this paper on the points which make this system an original one, namely :
The acquisition technique, which uses a particular design at the primary-event processing stage,
The display technique,
The PHITROL original real-time language.

I - System set-up

(fig. 1 gives a diagrammatic representation of the basic system set-up)

The system is based on a central computer unit equipped with 8,192-18 bit machine words (basic cycle 1.8 µs - 4 working registers ; memory which can be extended to 16,384 words).
The following are connected to the two-way input-output bus line :
An acquisition coupler, which serves to concentrate information and provides an interface between the coders or the external devices and the processing unit on the other. This coupler also fulfils "channel clock" functions.
"External patched operator" modules (OPCE), designed to increase the system's possibilities during elementary data processing in the acquisition phase,
A fixed-head disc memory with 131,000 words,
A display unit with associated cathodic indicators providing a visual presentation of texts and spectra. Either one or two indicators may be associated with this unit,
A display console affording quick actuation of the various functions (scales, display zone, reticule displacement, mode selection),
An ASR 33 input/output teleprinter, used for controlling the input system, and for printing out tables or output messages,
An IBM compatible magnetic tape unit, 7- or 9-track, used for recording elementary events, mainly for multi-parameter experiments. This unit can also be used as a spectrum library extension,
A slow coupler.

II - Main functions of system

II.1 - Acquisition function

This is the phase in which account is taken, either in real-time or deferred time, of information precoded in digital form. Acquisition can be performed in real time from the acquisition coupler or in deferred time, for instance, from a prerecorded magnetic tape. We shall confine ourselves to describing the real-time mode of acquisition.

II.1.1 - Real-time acquisition. This is performed by a 4-channel fast coupler which multiplexes and marks the channels, input format 16 bits + 2 marking bits. Each channel has a special order of priorities and can also operate in independent mode or correlated mode with one or more other channels.

When information is available at coder* level, there is an automatic transfer of the data by the "direct access to memory" method in a 128-word storage zone called "input zone". The coupler itself manages the arrangement by a "queueing" mode in the input zone.

When the input zone is saturated, the acquisition function automatically switches over to a second zone of exactly the same length, and a changeover interrupt signal is emitted.

The first zone is then used by the central unit simultaneously with the acquisition function in the second zone. This makes it possible to eliminate the random character of the moments of appearance of the events and ensures continuous acquisition to the extent that the average input rate is lower than the average rate of utilisation of events in the associated zone.

It is important to emphasise that the real-time data input mode is the same whatever the mode of operation of the coupler channels is ; only the mode of utilisation of the input zone will vary with the modes of operation.

II.1.2 - Possible channel-operation modes. We list below several possible modes of acquisition, although this list is not exhaustive :

Amplitude analysis,

Time analysis,

Multi-parameter amplitude or time analysis,

Multi-scale mode analysis,

Multi-sampling mode analysis.

It should be noted that it is possible simultaneously to manage several channels working on different modes.

II.1.3 - Input zone utilisation. This is triggered off by the program in response to a zone changeover interrupt signal. It consists of making several consecutive runs over the input zone, with a specific mode of utilisation for each run.

The number of runs depends on the number of modes of utilisation required and also on the number of channels working.

Example : (Channel 1 = amplitude analysis,
(Channel 2 = multi-scale,

With this example we should have :

(1) an initial run with operating mode M1 processing, for the channel 1 events, the ranking address and "+ 1" at the processed address, and for the channel 2 events, rejecting these events,

(2) a second run with operating mode M2 transferring data into a storage zone in the case of channel 2 events, and for channel 1 rejecting such events.

This mode of operating in successive runs thus permits either conditioning, which we have just demonstrated, or utilisation of the same data several times, e.g. building up a control spectrum and ranking non-integrated data on magnetic tape.

Since the input zone is utilised in such a way that there is interlacing with the acquisition function, in order to obtain a high acquisition rate, this utilisation time must be kept down to a minimum.

In order to achieve this aim, we have designed an "external patched operators" device (OPCE) making use of the microprogramming possibilities offered by the processing unit (access to the various functions and internal registers). These operators are in fact highly optimised patched subroutines, which can be used by the program in the same way as a registered program. Triggered by the computer program, an external patched program is carried out in sequence, from a ring counter synchronised with the 450-ns computer clock. The patched program sequence can be interrupted at specific moments in order to afford direct access to the memory, which in particular comes into action upon each new acquisition request ; it can also be interrupted by computer program interrupts.

Each input zone utilisation mode Mj is set up by an OPCE patched operator, which considerably reduces the central unit occupation time. By way of example, the operator which performs the "add one to memory function" with translation of the origin address, channel-number test and overflow test, takes 4.05 µs for the selected channel and 1.8 µs for the rejected channels.

II.2 - Display function

The display unit is for presenting spectra which have been built up or are in the course of acquisition, and is also used to present texts, axes and points.

Spectrum presentation can be performed in mono or bitrace linear mode or (and) in mono or bitrace biparametric mode.

Two markers shifted from a console enable to point out characteristic points of the curves

or surfaces presented.

The display unit consists of :
A coupler,
One or two cathodic indicators with their deflection and brilliance amplifiers (8 x 10 inches),
A photosensitive pencil device.

The coupler receives from the central processor the information to be displayed, as well as the control words for its interpretation. It transmits the analogue deflection and brilliance signals to the cathodic indicators.

The display coupler was designed to relieve the computer to the greatest possible extent of the repetitive tasks involved in the processing of an image. In particular, it performs by patch control the framing, the sensitivity control operations, axis generation, character generation, and the incrementing of the channel address during the building-up of spectra. The display coupler determines the co-ordinates of a point from the information (18-bit words) transmitted by the computer. A computer word can represent a "control word" or an "argument word". A "control word" determines for the argument words which follow it :
The operating mode or operation code,
The brilliance level,
The sensitivities on the axes (in vertical feed 64 to 256, 000 counts, in horizontal feed 32 to 512 channels.

II.2.1 - Image build-up. An image is built up point by point in a 512 x 512 point base grid. The sum of the control words and the argument words defining an image constitute the "display list". This list is made up of several word blocks.

II.2.2 - Image output. The output of the various blocks forming an image is performed in the "direct access to memory" mode under the control of an automatic transfer address unit, i.e. without any action on the part of the program except for the triggering of this control unit.

II.2.3 - Image timing. An image oscillator generates an interrupt every 55 ms which triggers the output of a new image.

II.2.4 - Image modification. Through the operation of external controls on a console the image can be modified (mono or bitrace operation, change of vertical sensitivity, shift of reticule, magnifier mode, plane or isometric projection, change of zone displayed, etc.).

None of the console controls acts directly on the display unit. At the end of each image, the state of the console is read by the computer and the "display list" modified accordingly before the output of a new image.

II.2.5 - Photosensitive pencil. A connected photosensitive pencil can be used to designate a point or used in "writing mode".

III - Programming

For operation of the NUDIAC system, we had to define, on the one hand, a simplified language suitable for spectrometry experiments and, on the other hand, a system of operation for managing this language.

The basic intentions were :

a. As regards the language proper, to define :
   A simple language which can be directly assimilated by the physicist and is geared to the building-up and processing of spectra (table),
   A language suited to the complete real-time section (clocks, acquisition, display).

b. As regards the operating system :
   Capability of performing a processing operation on one or more spectra on the basis of the above-mentioned language simultaneously with the acquisition operation,
   System controllable either in step-by-step operation (conversational) or in sequential operation (sequential execution of a series of instructions),
   Reduction of the service operations which have to be performed by the operator to a minimum, making intensive use of the disc memory and the display unit.

III.1 - Language.

The description which follows has been deliberately simplified but it does afford an idea of the possibilities offered by the language.

PHITROL is a real-time language working entirely with unsigned integers in Version 1 and floating-point numbers in Version 2.

III.1.1 - Operands. The operands may be of two types :
   Scalars in variable or constant form,
   Vectors.

a) Scalars. The variables consist of a group of one to three alphanumerical characters, the first of which is always a letter.
   E.g. : A, AB 1, A 50.
   Declaration of variables is implicit.
   There are a certain number of permanently declared variables. These are :
   The clocks : HCO,
   HC (cycle clock) and HV (channel clock),
   The processing indicators : IC (overflow indicator),
   The markers linked to the display unit : RT_1, RT_2.

b) Vectors. Series of scalars (table), identified by means of the name of a variable preceded by the sign (:).
   E.g. : : VEC.
   A vector is declared as shown by the following instruction example :
   STA (: V 1, 512).
   Vector : V 1, stable, 512 components.

II.1.2 - Operations on scalars. The four elementary arithmetical operations are available.

The number of arithmetical operators for a line is limited to one.

III.1.3 - Operations on vectors. Similar operations are performed on the vector components, namely the sum, the difference, the product and the quotient of the homologous components of the argument vectors.

III.1.4 - Functions. These are generally written in the following form :
Variable = function code (argument, . . argument),
Vector = function code (argument, . . argument).

The arguments may be variables, numerical and literal constants, or vectors.

The function code consists of one to three alphanumerical characters, the first of which is always a letter.

The main functions scheduled in PHITROL are :

Vector smoothing,
Vector reduction,
Finding of maximum,
Calculation of area between two limits,
Abscissa at mid-height.

III.1.5 - Jump instructions. Two jump instructions are available :

Unconditional jump,
Conditional jump.

E.g. : BRI (A 1) - BRC (IC 1, A 1),
A 1 is the label for the jump line,
IC 1 is the tested variable.

III.1.6 - Input/output instructions. These permit the input and output of data during the program by means of the teleprinter key or the tape reader/puncher.

III.1.7 - Real-time instructions. These instructions define the parameters necessary for acquisition on each channel.

The arguments shown between parentheses denote the symbolic name assigned to this acquisition function, the numbers of the channels concerned, and the starting and stopping conditions.
E.g. : DEF (AC 1, 1, S, A, 0) - MOD (M 1, 1, : V 1) - DEP (AC 1, 2, A 1).

III.2 - Language utilisation system (SEL)

SEL is a set of program with the aid of which the NUDIAC system can be operated with the PHITROL programming language.

The language is made up of instructions, a series of instructions forming a sequence.

With SEL a maximum of five sequences can be defined.

The total number of instructions for all five sequences must be less than 500.

The five sequences together constitute a program.

One or more sequences may be idle.

SEL enables the following operations to be carried out :

III.2.1 - Editing. This means the preparation and modification of one or more sequences by means of the teleprinter key, the punched tape and (or) the sequence library.

After a program has been prepared, it can be modified by making use of the facilities afforded by the editor unit for insertion or elimination.

The state of the editing zone may be shown on the display unit (display of five lines either side of the current line) or on the teleprinter (printing of n lines from the current line).

III.2.2 - Filing in library. The programs and the spectra are filed in a library.

Two card-indexes show the names and locations of each of the programs or spectra in the library.

III.2.3 - Interpretation/execution. Every program in the editing zone which has previously been verified may be interpreted/executed.

Execution of a sequence consists, for each instruction, of :
Interpreting it,
Identifying the arguments contained in this instruction and locating them (fast memory or disc memory),
Finding the corresponding module in the disc memory and loading it into the fast memory,
Triggering the execution of this module.

In the case of vector arguments, if the available space in the fast memory is insufficient, the interpreter then proceeds to segment the spectra.

Simultaneously with the interpretation and execution, acquisition is carried out on a "master" mode by direct access for the input of the elementary data and by interrupt mode in the case of operation of the input zone.

The appearance of an acquisition or clock interrupt may necessitate suspension of execution of one sequence in favour of another of higher priority.

When execution of the higher-priority sequence has been completed, that of the broken-off sequence is resumed.

The five sequences have priorities on a decreasing scale from 0 to 4.

All three operations described above are performed from a zone in the auxiliary memory called the editing zone.

SEL is managed from the teleprinter by means of meta-instructions.

There are two possible modes of operation, namely :
Step-by-step operation :

Each instruction issued is interpreted and then executed immediately if deemed significant.

There is no storage of this instruction ; once it has been executed, the system awaits the next instruction.

Sequential operation :

This consists of executing, in its entirety, a program consisting of one or more sequences.

This execution phase assumes that the instruction has previously passed through and editing phase.

III. 2. 4 - "SEL" organization. The system "SEL" consists of :

A supervisor, which performs the following operations :

management of the real-time equipment,

analysis of the messages issued by the operator by means of the teleprinter (meta-instructions),

calling up and linking up with the master programs.

Master programs. There are four of these :

the editor unit, operating entirely in the editing zone (disc memory),

the verifier, also operating in the editing zone and permitting analysis of the syntax of the various instructions prior to execution,

the librarian unit, which is responsible for management of the library and its card-indexes,

the interpreter, which is responsible for execution of the various instructions and management of the arguments.

IV - Technological construction

The entire system consists, as regards the real-time equipment, of two five-unit racks, prepatched from the outset in ordre to receive all the available options.

The logic employed is based on DTL-type integrated circuits, except the OPCE part, for which it was necessary to use TTL circuits.

This system was designed and developed by the INTERTECHNIQUE company in co-operation with the CEA.

* Erratum : read "digital converter" instead of "coder" in the text.

DISCUSSION

De Lotto : - I would like to know if this language is compiled or interpreted.

Barthelemy : - The language is not compiled ; it is interpreted by instructions. Each macro-instruction PHITROL is interpreted and then executed. The modules of program concerned are called by the interpreter under the control of supervisor, from the disc memory to the fast memory before execution.

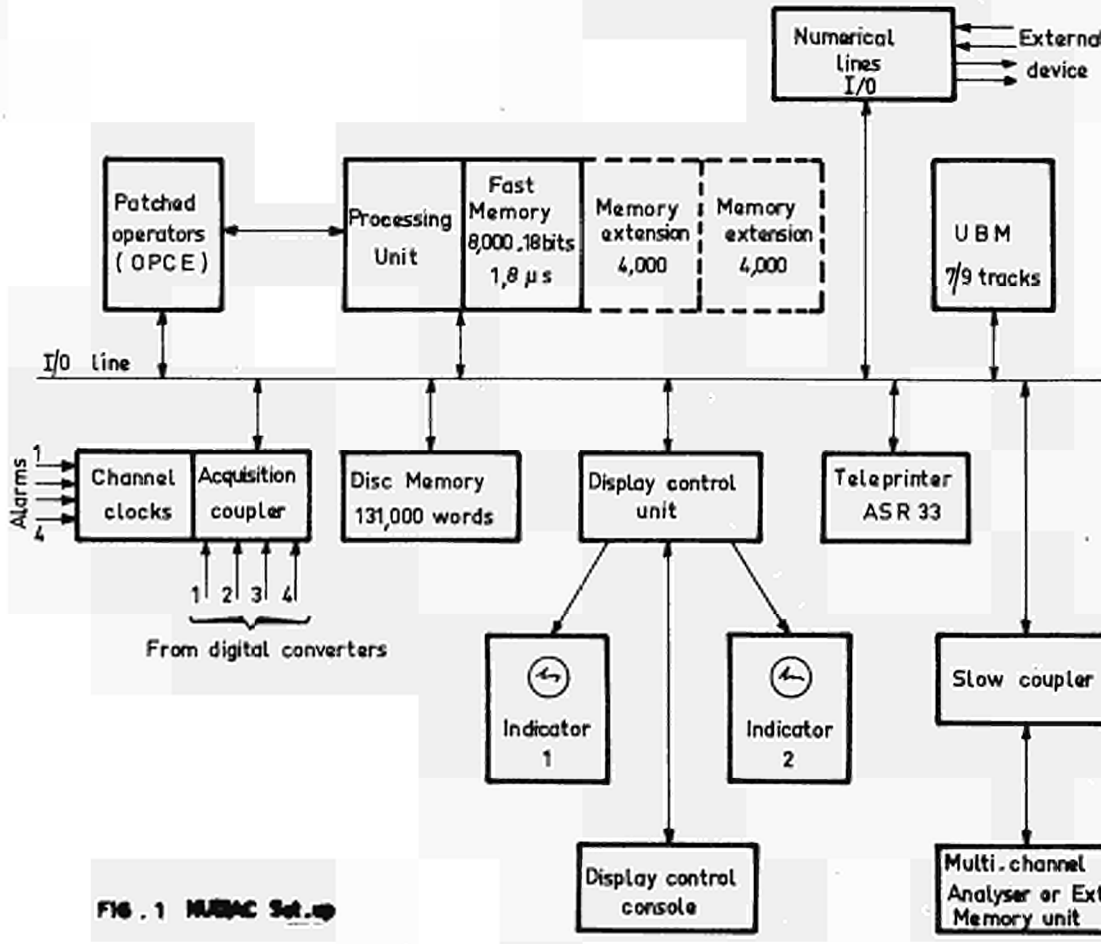

FIG. 1 MUSAC Set-up

AN ON-LINE DATA HANDLING SYSTEM FOR PHYSICS EXPERIMENTS AT THE SWISS FEDERAL INSTITUTE FOR REACTOR RESEARCH

J.-B. Bossel, W. Hälg
Eidg. Institut für Reaktorforschung, Würenlingen
Switzerland

Summary

An on-line data registration and reduction system with a computer CDC 8090 serves primarly neutron scattering experiments. The instruments connected to the computer system for this purpose are a time-of-flight spectrometer and a multiaxis spectrometer. Beside this, the system also registers data for the study of heat transfer in a Natrium Loop, and processes 247 temperatures of the Reactor Diorit. All connections between the computer and its peripherals use telephone cable, each line consisting of a twisted pair of conductors terminated on 75 Ohms, the longest connection being for the time 300 m long. An appreciation on the reliability of this system is also presented.

1. Introduction

The system we shall present in this paper was devised to serve many experiments. Up to now the following ones have been connected to the computer:

- 2 time-of-flight spectrometers for slow neutrons
- a data collecting system for temperature correlation experiments on a liquid Sodium Loop
- the registretion of 247 temperatures on the reactor Diorit[1].

In addition to this, the system is also able to offer many services to other experimentators whose experiments are not directly connected to the computer, as for example:

- the output from multiaxis neutron spectrometers may be read from paper tape and viewed on the system display
- the same display has been used for visualising and photographing calculated reactor flux distributions. These distributions were prepared on magnetic tape by a large computer.
- the programs for the multiaxis spectrometer are also computed off-line and written on magnetic tapes, which are played back on our system and tranemitted on paper tape.

All these jobs are accomplished in time-sharing, while the data from the connected experiments are handled on-line.

2. Survey of the system

2.1 The central system

When we use the expression central system, we mean the computer itself with all the peripherals

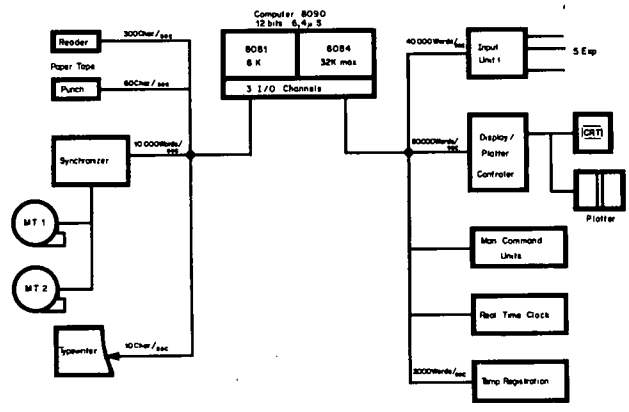

Figure 1 : The Data Registration System

which are common to all experimenta. The display unit, which could be located near the computer as well as near every experiment is not part of the central system. The latter comprises the following items:

Computer of the type CDC 8090[2]

core memory	8k 12-bit words
cycle time	6,4 microseconds
I/O channels	2 (1 is buffered)
I/O speed	70,000 and 60,000 words/s max.
mean instruction time	15 microseconds
interrupt lines	4 (2 are external)

External memory CDC 8084

core memory	3 times 8k 12 bit words
I/O channel	1 buffered, with repetitive mode
I/O speed	100,000 words/s max.

can be shared by a second computer

To the computer belong the usual peripherals such as Paper-Tape Reader and Punch, a Typewriter and a Synchronizer for up to 8 Magnetic Tape Units, with the following characteristics:

Magnetic Tape CDC 601

number	2
tape speed	35 ips
density	200/556 bpi IBM compatible
I/O speed	10,000 words/s at 556 bpi

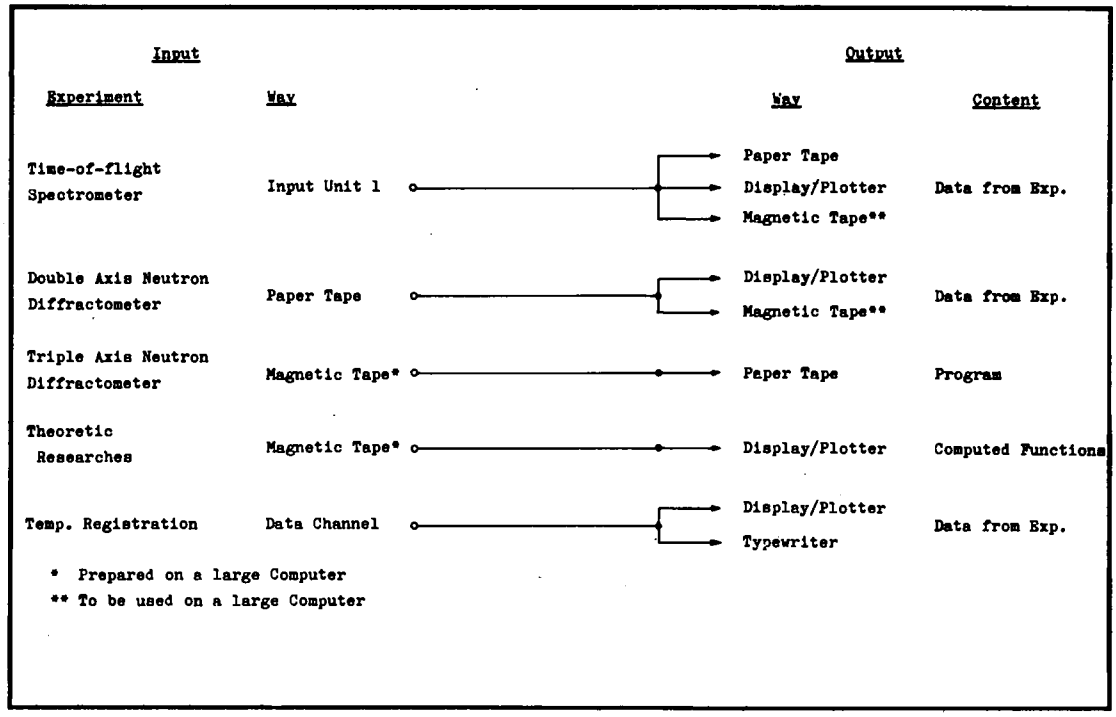

Figure 2 : I/O Commands through the Manual Command Units

Derandomizer

memory capacity	8 words 24 bits
access time	1 microsecond max. for the entrance with highest priority
experiment connections	5 (24 bits), with different priority levels

is connected to a computer I/O channel

Real Time Clock

time	month, day, hour, minute
stability	better $0.5\ 10^{-6}$ or 1 s/month
time base	1 Mhz Querz

a battery provides independence from the main for about 10 hours

2.2 The peripherals belonging to the experiments

Manual Command Units

they are connected to an I/O channel and allow a code of 15 bits to be transmitted to the computer by a manual interrupt.

Display Unit

capacity	4096 points
resolution	256 points for X,Z coord. 64 lines for Y coordinate
representation	1 line, Y lines and isometric
refresh rate	20 frames/s at 4096 points/frame
CRT	RM 503 and HP 4100

is connected to the external buffer channel because of the availability of the automatic repetitive mode

Point Plotter

speed	6 points/sec maximum
Plotter	Mosley

is connected to the Display Unit, from which it can copy the images

Time-of-Flight Unit

comprises actually two separate units with the following characteristics:

detector channels (per unit)	15
channel width	2 to 16 microseconds
start delay	up to 256 ms, in 1 microsecond increments
dead time	3 microseconds including the transmission to the derandomizer

Low-Level Multiplexer[1]

speed	50,000 commutations/s
common mode signal	200 V max.
offset	$\pm$ 40 microvolts at 20°C $\pm$200 microvolts at 40°C

is connected to a differential amplifier, an A/D Converter and a control unit which transmits the information on the computer I/O channel at 2,000 points/s (limited by the bandwidth of the amplifier).

Multipurpose Unit

allows the transmission of 24-bit information to the derandomizer. This information may be built up of

5 different sources (up to 12 bits each), for example A/D Converter, scaler, multiswitches etc. This unit is used for measurements on a Sodium Loop for temperature correlation experiments.

Interrupt Unit (in construction)

increases the interrupt capacity of the central system to 60 priority levels on each external interrupt line. Each line may be enabled or disabled by the program. This unit is connected to an I/O channel and gives to the computer on request the number of the interrupt line which has been set.

Interface Unit (in construction)

is connected to a computer I/O channel and allows the transfer of 24-bit informations in two directions, from and to the experiments. It is the central unit of a subsystem consisting of a Read-Out Unit, a preselecting Unit and an Angle Positionning Unit, subsystem which will be used to control a multiaxis spectrometer.

Relative Units to the Real-Time Clock
(in construction)

Will be used to preselect absolute and relative time intervals for the control of experiments.

Memory Unit (in construction)

core memory	4k 12-bit words
cycle time	6.4 microseconds
I/O channel	1, buffered with repetitive mode
I/O speed	100,000 words/s

will replace the function of the external buffer channel for driving the display, and will thus free this channel for other I/O tasks. It will be connected to a computer I/O channel.

3. A general evaluation of the system, its mode of operation and suggestions for increasing its effectiveness

The system described in this paper may be judged from two points of view:

a) The availability should be as high as possible

b) The flexibility of the system should be high, its services as good as possible, and there should be a fast access to the information which has been gathered.

3.1 The run time of the main elements of the system

Computer Run Time	about 13,000 hours (the On Time will be larger)
Magnetic Tapes: run time	about 660 hours
Derandomizer: run time	about 11,500 hours
Manual Command Units: run time (two units)	about 20,000 hours

3.2 Breakdowns

Major breakdowns

During this time, we have had 9 major breakdowns of the system, i.e. the computer was blocked and unable to collect data. The causes of breakdown were:

1 diode

4 driver transistors of a core memory

2 other transistors

2 no reason found

Minor breakdowns

We define as minor breakdown a defect which allows the system to continue work with reduced capacity until it is repaired. The causes here were:

3 transistors

3 electro-mechanical devices

3.3 The availability of the system

The availability is defined as the ratio

$$\frac{\text{run-time - down time}}{\text{run time}} \cdot 100.$$

If we consider the major breakdowns only (9) and set a down time of 15 hours/breakdown, giving an idle time of 135 hours and therefore an availability of 99 %. We have not considered in the above calculation that there have been other causes preventing operation of the system such as power failures and error of manipulation. Both kinds of failure do not cause large down times so that we can assume 100 hours for about 20 failuras as a first approximation. This gives an availability of 98.2 %.

3.4 Maintenance

Maintenance is performed by ourselves for the chief reason that the system has to work around the clock over periods of up to 7 weeks. Preventive maintenance is carried out on the electromechanical devices only when the experiments do not run. We have also received support from the manufacturer of the computer who repairs the prints which need special elements.

3.5 A user's point of view

3.5.1 The peripherals

Actually, we do not find that the availability is the most important point to be considered. The quality of services the computer offers are most important, and depend very much on the peripherals, especially on the devices responsible for the output of information. The experimenter will want to have fast access to his information, and to receive it in digestible way.

The display plays an important rôle in the I/O devices and its presence was one of the conditions the experimenters wanted to be met when we proposed

to replace our multichannel analyser by a small computer.

The magnetic tapes have been found to be an extremely valuable tool for all I/O operations in connection with a large machine.

Paper tape is still the most used medium for short outputs which may be tabulated on an off-line typewriter.

The on-line typewriter is only used for registering all commands, the status of the system, and the alarms.

3.5.2 The central computer

The most limiting factor in our system is the internal speed of the computer. The cycle time of 6.4 microseconds allows an average I/O speed of 50,000 informations/s (A single information contains a word of 24 bits transmitted to the derandomizer), but we have calculated that the processing time for an information from the time-of-flight spectrometer amounts to 560 microseconds, including 120 microseconds for input operations. This gives us an intrinsic limitation of the information rate of 1780 information/s, which could be raised to more than 10,000 if the computer had a cycle time of 1 microsecond. We think that an optimalization of the programs could only give a speeding up factor of 50 %.

Neither the 12-bit word length, nor the absence of an arithmetic unit has been felt as a constraint on the operation.

3.6 A better system, how?

3.6.1 Software

If we had to indicate which instructions we would like to find in our repertoire to increase the processing speed, we would suggest:

- shift instructions with a number of shifts corresponding to the whole word length
- search instructions to the first zero or non-zero bit from right or left in a word
  instructions to set or reset any bit in a word to zero or one
  instructions for byte manipulation

The implementation of these operations would certainly not be possible on a machine with less than 16 bits per word.

3.6.2 Hardware

We have already remarked that a faster cycle time would increase the throughput of the computer. Since the number of interrupt lines was too low we increased it to 120.

We would find a line-printer and a display/plotter system with alphanumeric capability very useful, but we find that we do not need them as long as there is access to a large computer system with a short turn-around time.

4. Comments on the security factors of the computer

4.1 Parity control in core memory

The chief advantage of a parity control here is that an error brings the computer to a stop, thus preventing the error to propagate. If the error is due to a transient, there will be no delay in restarting the system.

4.2 Memory protection

This kind of protection should be advantageous in a system with frequent changes and additions to the programs, allowing the debugged routines to be guarded against faults caused by these new programs. This protection could also be used to distinguish between instructions and constants, so that an attempt by the computer to interpret the latter as an instruction would cause the program to stop.

We believe that the memory protection feature would be more important to a system like ours than the parity control.

4.3 Automatic restart after a power failure (dead start)

Such a feature could not only bring advantages to a data registration system. We think of the restart of magnetic tapes, for example, which has to be done manually, and of other peripherals which possibly could not be put again into service automatically.

The best protection is still to have a power source with enough safety. One should also consider the problem of what happens when a peripheral is switched off erroneously, in which case our system still hangs up.

5. The transmission of information over long distances

If we wanted to connect all the possible sources of information in the Institute to our data handling system, the longest data line would be about 500 m. We already have a 300 m connection with an experiment: the measurements on a Sodium Loop are transmitted to the derandomizer and then written on magnetic tapes, because the treatment of this information can only be made on a powerful computer.

For the realization of these connections, we have adapted the technique used on the computer I/O channels to make them suitable for longer distances. As we already use normal telephone cable with twisted pairs of conductors, we drive them symmetrically with their characteristic impedance and terminate them accordingly. This gives us a transmission line with the following characteristics:

impedance	75 ohms
capacity	100 pF/m
ohmic resistance	10 ohms/m
delay	.56 microsecond/100 m

signal at the termination	- 6 V

The crosstalk over a distance of 300 m gives a small peak of 1.2 V after 0.4 µS on a pair terminated on 75 ohms when 18 pairs are driven by signals of - 6 V.

A point that may be changed concerns the impulse height at the termination of the line. We have chosen 6 V because we thus could terminate our cables with 1/2 watt resistors, and we found it to be a big reduction from the 18 volts (but unterminated) we have been accostumed to for a long time. But we could certainly reduce this voltage by a factor of two or more.

6. The programmation

As a rule for such systems, the programmation has been done in machine language with the help of an assembler for the first programs which have been used. For further additions and changes we have directly translated our instructions into machine language. The reasons why we no longer use the assembler are:

- it was not possible to make changes without reassembling the whole program
- we do not have a card input but have to use paper tape for the symbolic version, so that it is not easy to make changes and corrections.
- The assembler would have taken up too much core space to remain permanently in the computer.

7. The monitor for the system (Fig. 3)

Our monitor for the system is only a short program of 270 words. It is divided in five sections, each section corresponding to a peripheral which can work in time-sharing. These sections are:

magnetic tape job

paper tape job

typewriter job

manual commands

sorting information (derandomizer f.ex.)

The computer runs through these sections in a closed loop, and checks if anything is to be done. A job slice is of variable length, depending on which peripheral is used:

magnetic tape I/O	about 25 ms for one record
paper tape, typewriter	50 microseconds for one character
preparation of an output line	5 to 20 ms
sorting 128 information (derandomizer)	about 70 ms

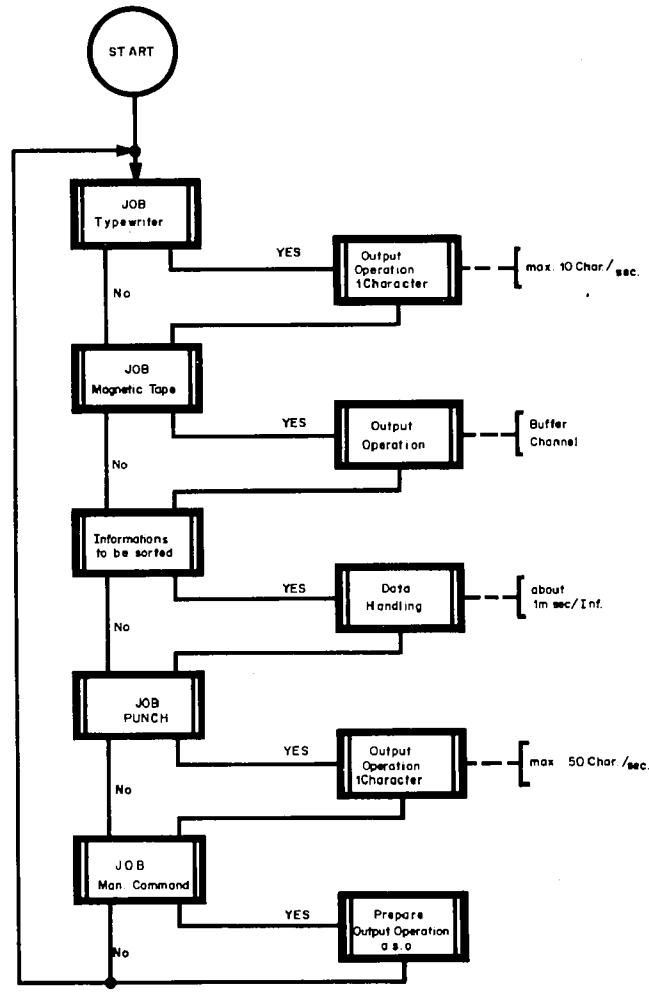

Monitor

Figure 3 : Main Program: Flow Chart

There may be up to 3 peripherals working simultaneously, i.e. as much as I/O channels. But there may also be more than one peripheral working on the same channel in time-multiplexing, as long as the overall capacity of transfer is not attained.

Conclusions

We have presented a data handling system which has been implemented at the Institute of Reactor Research in Wurenlingen. This system is working in an on-line and time-sharing mode and serves several physics and engineering experiments, as well as other users. We have tried to make the system as flexible as possible, looking for a rapid access to the information. Many peripherals have been developed and built at our Institute, and the computer itself shows a run time of 13,000 hours. We have in mind to extend the capability of our system by adding a mass-storage device, specially useful in conjunction with the multiaxis spectrometer we shall soon connect directly to the computer, and/or a second computer which could share the extended memory.

References

1. The On-Line Temperature Control System at the Swiss Reactor DIORIT
   J.B. Bossel, W. Hälg, H. Ryser
   Paper presented at the OECD Seminar on the Application of On-Line Computers to Nuclear Reactors, Sandefjord, Norway, 2nd-6th September 1968

2. Control Data® 8090 Computer System
   Reference Manual
   Pub. No. 60091500

DISCUSSION

Vuilleumier : - Do you check the parity for your transmission of data and how many pulses do you have for any transmission of data ?

Bossel : - We don't have a parity control for the transmission of our data but we check the format of the incoming words : for instance we have 24 bits for each component which comes from our time-of-flight spectrometer. We use in fact four bits for experiment number, 10 bits for channel number and another four bits for detector number. This makes 18 bits. We have other six bits and we make a kind of control on them. We've experienced many kind of errors from the time-of-flight spectrometer but we never catched an error of transmission.

A CAMAC MULTI-USER SYSTEM

G.C.Best and I.N.Hooton
Atomic Energy Research Establishment,
Harwell, England.

A data collection system for multi-user access to a small computer is being implemented using CAMAC hardware. The system is described, and some of the general principles involved in the software for such systems are discussed.

The CAMAC System

The principle of the CAMAC system of modular instrumentation is that electronic units may be connected via a standard dataway to any computer for which an interfacing 'controller' exists. As the range of controllers and available units increases it should be possible to connect virtually any type of data collecting process to any computer with a minimum of difficulty. This is obviously an attractive concept, and one likely to find widespread use in laboratory computer systems and elsewhere. The ability to alter the hardware configuration at will makes it particularly attractive for multi-application and multi-user systems. However, it should be realised that the availability of CAMAC does not of itself reduce the complexity of any given system. Simplification of the hardware is achieved by shifting some system problems, such as parameter variation, from the hardware into the software. Thus the full potential of the modular system will be realised only if suitable software can be devised to control it without imposing undesirable constraints on the hardware, or demands on the computer. This paper describes the implementation of a specific system using CAMAC, and discusses some of the general problems encountered.

The Multi-User Requirement

The system described is to be used by Analytical Sciences Division at Harwell, primarily for routine analysis work. Its basic object is to provide a common computer facility to serve a number of independent users, working in adjacent laboratories. The system is to be implemented using a Honeywell DDP-516 computer with 8K of store, and magnetic tape backing. In general on-line computation is not required, data being collected on magnetic tape for subsequent processing on a larger machine. The bulk of the experiments involve multi-channel or multi-scaler operations, but there are automatic plate scanners and the possibility of other types of input in the near future.

The MUSTARD System

The system is known as MUSTARD, Multi-User System to Acquire Real-time Data. Up to 8 users share the computer, subject to core limitations. It will be convenient to describe the system as the user sees it, before discussing organisation.

The users may not be experts in computer use and for this reason system entry is by a dialogue technique to ensure complete and correct information. Before using the system, each user must specify his requirements at the central teletype. All commands to the system are selected by typing a single character at the teletype.

Each class of experiment requires a certain group of CAMAC units, which have already been placed in the user's CAMAC crate. Such a group is described as a 'set'. The user types in the physical position of his units in the CAMAC crate, in a prescribed order according to unit function, the order being specific to the operation required. Once the 'set' is defined it is ascribed a set number, which is held permanently, so that set redefinition is necessary only for change of experiment, or change in physical arrangement.

The user now defines his requirement of core store. If sufficient store is available he is allocated an 'array', to be linked with the 'set', and is asked for an identifying title for the experiment, and a user code. These are used to tag collected data for subsequent identification.

Once store and hardware are defined the user has the choice of several alternative commands. These give entry to question and answer routines for various types of experiments, system routines which provide information about system status, or control routines which enable the user to print out data, use a display, or read or write magnetic tape. Selecting an experiment command allows the user to define the parameters of his particular experiment. Once the complete definition has been entered the experiment can be run, either from the central console or at the experiment. Each experimental 'station' is provided with a manual switch register which allows local control of the starting and stopping of data taking, and of parameter changes etc.

Experimental Operation

When the experiment is started, by enabling those units specified in the particular 'set', data will normally be transferred into the computer by autonomous transfer via the controller into one of a number of data buffers. Buffer overflow automatically calls a program interrupt, and the controller retains the number of the autonomous channel which has overflowed. The program enables an alternative buffer and allows data taking to continue.

Other units such as live-time clocks, or local manual registers, may call directly for program interrupt. Both autonomous and program interrupts are channelled through an interrupt

sorter which calls the controller. Each input to this unit has an associated code which can be preset to provide the necessary data about the transfer. In the autonomous case the interrupt sorter provides a complete definition of the transfer, giving the unit address, function and sub-address codes for the autonomous operation, and the autonomous channel number. In the case of a program interrupt, only the unit position is given. At the end of the experiment the accumulated data can be dumped onto magnetic tape for future processing and is automatically labelled with the user's identity, date, experiment title, and serial number.

Program Structure

The MUSTARD program consists of two sections, a work loop in which background tasks can be performed, and the interrupt structure which is the main section of the program and deals with all the processes involved, since essentially all operations are entered as interrupts. At present the work loop is little more than a wait loop, though it may prove possible to insert some background computation if time and core space permit.

The structure of the interrupt sequence is shown in Figure 1. Possible sources of interrupt are tested in sequence, with groups of interrupts tested together where possible. The teletype has the highest priority as the overall command element and is tested first. If the test proves affirmative, indicating a command interrupt, the individual command can be identified by the character entered, and the program sequence directed to the appropriate response routine. Data buffer overflow is tested next in order of priority. The controller is interrogated to determine whether a buffer has overflowed, and if so which one. Direct program interrupts from the CAMAC system can be tested at the controller. If this type of interrupt is identified then the position number of the calling unit is read directly. The number is then looked up, in a table formed during the initial defining sequence, to determine what type of unit (e.g., clock, switch register, etc.) has called for interrupt, which array it relates to, and what action is to be taken. Since normally the action required by such an interrupt is relatively small the overall time in the interrupt sequence is not excessive. The group test method minimises the time to identify an interrupt. In the case of control operations where long question and answer sequences are involved, a general 'command' flag is used. This allows other interrupts to be serviced during a command interrupt, with control being returned into the command program at the completion of each sequence, instead of into the work loop.

Conclusion

The system described is in an early state of development though it seems likely that reasonable data rates will be achieved and that a substantial proportion of memory will be available for data. However, at this stage some general remarks may be made.

It is an advantage if the general software approach can be standardised at least to some extent, so that each system is not an entirely new problem to be attacked ab initio. The program structure adopted here provides a general framework which could be applied to a range of problems. Within the framework the program sequences to execute particular functions are almost without exception short and simple. Moreover, the introduction of additional operations requires no change in the program structure, only the addition of more function sequences at appropriate entry points, which already exist.

System programs for small computers will normally be generated in machine code. A program of small routines may be largely recoded for alternative machine languages without much difficulty or effort. Moreover the simple program blocks are themselves fairly easy to follow, an important point where users are inexpert and system documentation important.

It is obvious that the benefits of CAMAC depend upon the ability of the system control software to avoid imposing restrictions not inherent in the hardware. To achieve this the hardware, particularly of controllers and interrupt sorters must be arranged with the software problems very much in mind. If this can be done it should be possible to produce extremely versatile systems, rapidly and easily.

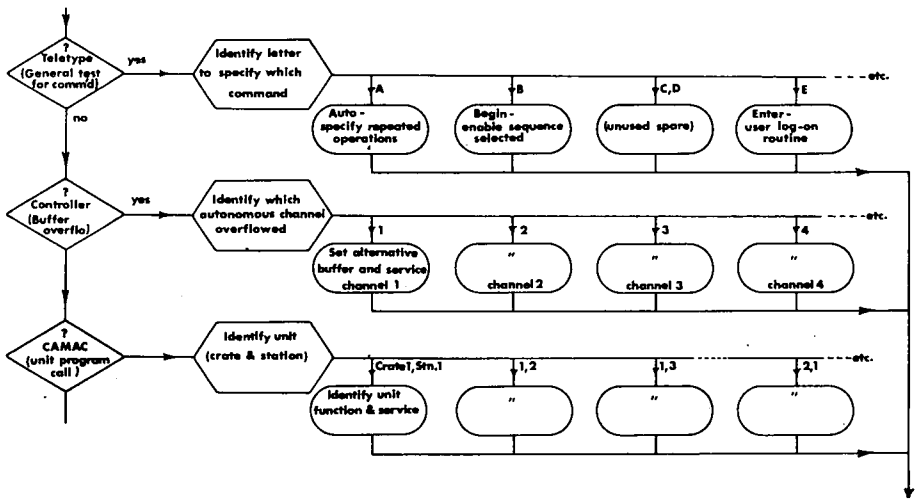

Fig. 1 - MUSTARD Interrupt Organization

ON THE "ESTER" SYSTEM FOR SIMULTANEOUS RUNNING OF SEVERAL ON-LINE MULTIPARAMETRIC EXPERIMENTS

J. ZEN, A. MUSER, J.D.MICHAUD and F. SCHEIBLING
Centre de Recherches Nucléaires, STRASBOURG, France

ABSTRACT

An on-line data acquisition and processing system using an IBM 1800 computer is described. This system allows several independent research teams to use simultaneously the computer for real time data acquisition and processing on a multilevel priority time sharing basis.

INTRODUCTION

The ESTER (Entrée-Sortie en Temps réel) system at Strasbourg is built around an IBM 1800 computer, which has a core memory of 32K 16-bit words and a large number of input/output terminals (digital I/O registers, external interrupt registers, nuclear data entry channel, typewriters, printer, card reader, plotter and a 1.5 million word disk storage unit). The system is designed to handle the data issuing from independent experiments running on 4 Van de Graaff accelerators (2, 3,4 and 6 MeV), and has been operational as a 16K channel multiparametric analyser since September of 1967 for the 6 MeV accelerator.[1]

Major evolutions with respect to the initial installation have been achieved in both software and hardware components. They are the development of on-line data analysis, the increase of multiparametric data acquisition capacity up to millions of channels, the performance of batch processing jobs (assembly, compilation, etc.) during experiments, the connection to a 4096 channel analyser for the 4 MeV accelerator[2] and the development of a permanent monitoring display unit. This paper describes the present state of features provided by the system to support simultaneously a number of various independent tasks. Figure 1 shows the general installation of different components of the whole system. Those on the left side of the figure are mounted together constituing an experiment console called "ESTER", which is situated in the near of measurement equipments.

MULTILEVEL OPERATING SYSTEM

The ESTER installation is operated under an IBM supplied process control operating system (TSX)[3] which is slightly modified to become more powerful to handle external interrupts and allows multiple users to provide various independent tasks simultaneously. The modified version operating system is a 5 hierarchical task level programming system which takes about 4K words of the core storage. Tasks are assigned to one of the levels according to their urgence and CPU service time needed. Time-consuming tasks are assigned to the lowest priority level. Various tasks are listed below in their priority order (highest level first).

1. Initiation and stopping of data acquisition, data input buffer management, set up of lower level task schedules and test points. These first level task routines are resident in the core at all times. They may be called to run at any time by external interrupts, buffer full interrupts or internal timers. These interrupts are not necessarily on a same hardware level. But as the response and service times required are so short (generally some milliseconds maximum), these interrupt routines may be considered to belong to one unique logical priority level.

2. Spectra transfer programs. These programs perform transfer of spectrum data either from a multichannel analyser or from the computer core memory to the disk storage and conversely. Spectra stored on the disk are catalogued by numeric symbols to facilitate inter-task communication. The CPU time (order of seconds) and memory storage resources needed in this case are more important than in case 1. The programs on this level are therefore stored on the disk in core-image format and the desired program is loaded in the core for execution when it is requested through the external interrupt facility.

3. Spectra display routines, analysis program task scheduler. These routines respond to interrupts of lower priorities than those already mentioned. They are controlled from the function keyboard and operate in the same manner as the second level tasks. Display routines run continuously for 100 seconds. One can repeat a request for another 100 seconds display if desired and the display may be stopped at any moment by modifying the status of a test point. The task scheduler is responsible for recording various data analysis requests to be entered in the 4th level job sequence table with information (1 to 10 arguments) necessary for the corresponding analysis program.

4. Spectrum analysis and output. Analysis programs may be general purpose calculations on a spectrum or simply output of the spectrum to some output device. The requested spectrum analysis tasks are processed in an order according to their software assigned order, or on first request first served basis as a stack job monitor from the card reader. Special sophisticated analyses may be requested provided that the program has been compiled and loaded on the disk before.

5. Batch processing jobs. Any job on this level is initiated with control cards and is executed as time is available. The batch processing job may consist of assembling, compiling and debugging new programs, modifying or building new disk resident core image programs (tasks), as well as executing time consuming tasks such as plotting a spectrum.

A common overlay storage area of 8K words is allocated to the various tasks of the last 4

levels. When, during the execution of such a task, a higher level disk resident task is called, the current level program is immediately suspended and saved, leaving the core area for the execution of the requested task. Three 8K word save areas are provided on the disk (for the levels: 3, 4 and 5).

A core resident "common" area of 16K words is shared among the data acquisition programs and the other tasks. This area is in priority used as "storage area" for the spectra formation in real time, but may also be used by all other programs as "working area". The memory organization is shown in figure 2.

DATA ACQUISITION

The data acquisition system that we have developed serves general purpose multiparameter analysis with a great flexibility. Three methods are generally used for data acquisition: totalization in multichannel analyser, collection on magnetic tape and direct storing in the computer memory.

If the number of bits necessary to define an event is smaller or equal to 12 bits (4096 channels) we use the classical multichannel analysers. When there is enough statistics, the contents of the memory is transferred to the computer for processing. However, if one needs frequent calculation on the spectrum during its formation, it is preferable to introduce directly the data from the ADCs to the computer.

If the number of bits necessary to define an event is greater than 12 bits, we also introduce directly the data into the computer. We don't have a system to collect the data on a magnetic tape without using a computer.

For our computer we distinguish three different functions for data acquisition:

- Transfer of spectrum from a multichannel analyser,

- Direct entry into the computer of the event data and recording on an auxiliary memory (disk),

- Direct entry into the computer of the event data and formation of spectra in the core memory.

The events occurring randomly in time, all direct acquisition of the data must be under channel control, freeing the central processing unit for other tasks. The channel commands directly the storage of the data into the core memory on a cycle stealing mode basis.

In the classical operation, the channel commands the storage of the words corresponding to an event into a data table of the core memory. When the data table becomes full, the central processing unit is interrupted for processing the contents of the table and the next incoming data are stored in a second table. When the processing of the first table is finished, the processing unit continues the interrupted task. The time for processing such a table must be short in comparison with that used to fill a table. So, only preliminary processing of the incoming data can be done such as storing them on an auxiliary memory or forming spectra in the core memory.

We have written a program which sorts the data, switching one part to the "memory storage area" for spectrum formation and the other part to a disk for later processing.

If the sorting doesn't involve complicated operations, it is possible to do it with electronic circuits and to store the sorted data with another channel. This permits a much higher input rate than the method, where only one channel is used. Our computer is equipped with the Nuclear Data Acquisition channel which performs the Add One To Storage of function[4]. We use this channel to reach directly to the memory "storage area" for spectrum formation. To perform the AOTS the channel needs 2.75 /usec.

Data sorting

Many sorting operations are easy to do with electronic circuits. For example, if we analyse a spectrum of 1024 x 64 channels, we choose the two more significant bits of a parameter and switch to the NDA channel all data which it contains for analysing an interesting part of the spectrum in real time.

Another example: If we analyse a 128 x 128 channel spectrum with the NDA channel, we can switch to the classical input channel the data which correspond to the fortuitous coincidences.

As the third example we mention an interesting experimental method. If we analyse a biparametric spectrum XY, it is important to analyse simultaneously the two single spectra X and Y. As the rate of the single events is generally very high and as the spectra do not need too much core memory, it is logical to switch these data to the NDA channel. We have developed a unit for the simultaneous analysis of the two types of spectra (coincidence and singles) with the same ADCs[5]. This unit may be used with the multichannel analyser BM 96 - Intertechnique or with the 1800 computer.

Synchroniser

The "synchroniser" is a unit in which the incoming data are switched to the two different input channels. This unit also controls the time sequence of the different signals needed for the channel operation when the incoming data come randomly in time. A "synchro" signal is needed to request a cycle steal operation on the channel, which then reads a word. When this is done, a "ready" signal is delivered by the 1800 channel. So a next transfer of a word cannot be done before this signal is present and if eventually a new word is ready to be transferred by an ADC, a dead time increase occurs for the experiment. The control of all these signals is done by the "synchroniser".

Four different modes of data acquisition are possible with the "synchroniser":

1. The NDA channel is used alone. This mode is analogous to that used in a multichannel analyser with the difference that when the count in a given core location is incremented from $(7FFF)$ to $(8000)_{16}$ an interrupt occurs and this word is processed under program control which is chosen at the beginning of the experiment.

As for the multichannel analyser we use: ADCs, timer coder and/or reference parameter indicators (detector number, beam charge, etc.). A pinboard is employed to define the length of the parameters X, Y ... etc. A 4-way multiplexer permits the use of 4 different ADCs with a "first come first served" priority.

2. The classical input channel is used alone. In this case an event can be defined with more than one word. We use a maximum of 4 input registers. The different words are transferred in sequence of the computer. A "synchro" signal is used for each word. The "synchroniser" controls and delivers the signals.

3. Both channels are used for direct data acquisition. The "synchroniser" needs a "mode" signal coming from the data sorter unit. This signal permits it to create the "synchro" signal for one or the other channel.

4. Transfer of a spectrum from a multichannel analyser. A special transfer interface was developed to coordinate in this mode the "synchroniser" with the multichannel analyser. If the transfer mode is requested, the direct acquisition mode using the classical channel is interrupted. As it is not possible with the 1800 to know under program control the word count of the interrupted table, we have built an external word count register, which is read when the interrupt occurs.

As the length of the multichannel analyser words are of 20 bits, two words per channel are transferred to the computer. The transfer program transcodes the data from the BCD code into natural binary code and writes the data sector by sector on the disk.

The transfer interface controls the timing of the different signals necessary for the different elementary operations: channel advance for the multichannel analyser, synchro and ready signals for the computer channels. The timing depends on the memory cycle of the multichannel analyser, the transcoding time of the processing unit and the writing time on the disk. The total operation lasts several seconds.

VISUALIZATION

Two systems of visualization are in service now. We called them "hardware-software visualization" and "hardware visualization"[6]. For these systems we use a display unit Intertechnique RG 96. This unit has been modified in order to permit the display of a monoparametric spectrum of 4096 channels. Fig. 3 shows an isometric display of a spectrum stored in the computer memory.

"Hardware-software visualization"

We developed a unit containing all the control circuits and connections between the RG 96 and the IBM 1800 computer.

Connection circuits. (Fig. 4) An oscillator synchronizes the computer channel on which the digital output is connected. After that the channel sends a signal "ready" which is used to increment an address register connected to the "address" input of the RG 96.

The digital output register gives 16-bits words. The bit 0 clears the address register when it is on the "1" level. This bit is on the "1" level for the first word of each image. A switch called "count full scale" selects 8 bits from the bit 1 to bit 15. This 8 bit word is supplied to an D/A converter connected to the analog input of the RG 96.

On the RG 96 there are thumbwheel switches for the X and Y displacements of the reticule. When the X-Y parameters of this visualized channel coincide with the values read on the thumbwheel switches, a signal occurs. If the "numeric" pushbutton is pressed on the AD 260 unit, this signal stops the oscillator and an external interrupt is given to the computer. Then, the computer reads the binary content of the last channel and supplies this, converted in BCD code, to a numeric display unit using "Nixie" tubes.

Commands. The AD 291 unit has some switches connected to digital inputs of the computer. These switches permit the operator to choose the visualization parameters.

The configuration of the stored spectrum is defined by two rotary switches "XMEM" and "YMEM". A series of pushbuttons "Origine" indicate the position of the spectrum in the storage area of the computer memory. The configuration of that part of the spectrum which has to be visualized is defined by two rotary switches "XDISP" and "YDISP". The position of the XdispYdisp area in the XmemYmem area is defined by two thumbwheel switches "X1" and "Y1" (Fig. 5).

Programs. These programs permit:

1. Visualization of a spectrum of 16K or 8K by integration on X,Y or X and Y, and reduction of the number of points to 4K.

2. Visualization of a monoparametric spectrum having a maximum of 4096 channels.

3. Visualization of any area, up to 4096 channels maximum, contained in the storage area of the computer memory.

4. Simultaneous visualization of two parts of a spectrum, each of them less than 2048 channels. The two parts are superposed on the screen of the display unit, the first being more intense.

5. Visualization of a spectrum stored on the computer disk, without transferring it into the storage area, with integration or not, according to the dimensions of the spectrum.

To execute some of these programs, it is required to press a pushbutton of a unit "program request" AD 260. The "numeric" pushbutton for the numeric display of the content of a channel is also on this unit. When we press this button, an external interrupt occurs in the computer. Pulse outputs of the computer are used to turn the lights of the lighted pushbuttons on and off. These lights indicate to the operator the execution of the required programs.

This system presents some important advantages with regard to a visualization using only an oscilloscope. Indeed, in this case, the computer must give the X-Y address and the content C of each channel. Then one is rapidly limited by the time necessary for the computer channel which works by cycle stealing.

With the "hardware-software" visualization, it is necessary to transmit only the content of each channel. These words are stored in an output table written by the "visu" program. This table being chained on itself, the images are transmitted without interruption. If we perform data acquisition and visualization simultaneously, the table is periodically modified.

We can also use the visualization simultaneously with a data processing program, but the place in core necessary for the visualization program limits the dimension of the processing program to about 3K words. To remove this limitation, we have developed the "hardware visualization" which permits the display of the storage area during data acquisition without the visualization program in core.

"Hardware visualization"

This unit permits three modes of visualization.

The first one operates in this way: When an event occurs, it is analyzed and A/D converters give a word to the 1800 made by the X-Y parameters of the event. This word is transmitted simultaneously to the "hardware visualization" which transmits it to the RG 96. Then we see on the CRT a point on the screen the coordinates of which correspond to the X-Y parameters of the event. We only need for that a flip-flop register which memorizes the parameters of an event until the next event.

This mode of visualization is especially used in biparametric analysis and allows one to see the areas where the events are the most frequent.

The second mode is a little more complex. When an event occurs, the descriptor is memorized in the flip-flop register and, simultaneously transmitted to the "1800" which adds 1 to the corresponding word of the memory. At the end of this operation, the computer transmits a signal "transfer accept". When the "hardware visu" receives this signal, it sends another signal to the "channel write out" of the 1800. This device reads the address on the register and transmits the contents of the incremented word to the"hardware visu". This is possible on the 1800 because a hardware device permits one to write, to read and to add one to a word of the momory without using the central unit. The content of the word is then transmitted to the A/D converter in the visualization unit AD 291 which is used for the "hardware-software visu". This second mode is especially used in monoparametric analysis.

We are developing a third mode. It operates in the same way as the second mode but the address of the point is furnished by a register in which an oscillator adds one periodically. The NDA channel is simultaneously used for the acquisition and the visualization. The two operations are independent, but the circuitry gives the priority to the acquisition.

These three modes of visualization "100% hardware" show the interest of a direct memory access device for a computer used for data acquisitions in nuclear physics. With this system, we have more free space in the core. The output tables and the program preparing these tables and the program preparing these are no longer necessary. We also save the time formerly necessary for the central unit to rewrite the tables during the acquisition.

ANALYSIS PROGRAMS

Real time I/O subroutines

Most of real time I/O subroutines are written in re-entrant coding. They may be called by analysis programs or used for other tasks. The followings are examples of some FORTRAN calling sequence:

```
CALL NIXIE (N)
CALL LCONF (I,J,K,L)
CALL VISU (IBUF,N)
```

Subroutine NIXIE allows to display a number N on "Nixie" tubes. For following the evolution of a task andcommunicating rapidly some simple results, this subroutine is very useful. Subroutine LCONF allows to read a group pf 4 numbers indicated on decimal data entry switches. Subroutine VISU may be used to display N points of a data array IBUF (e.g. theoretical spectrum).

The use of keyboard typewriter as means of communication between experimenters and the computer has revealed that the typewriter was too slow for the frequently used tasks. Also an alpha-numeric character generating program has been written. The scope used is the same as that used for the spectrum display and it is easy to formulate messages. For example, to display the message shown in figure 6, one only needs to call the subroutine TEXTI written as follows:

```
      SUBROUTINE TEXTI
    1 FORMAT ('DONNEE C = ...')
      CALL SCOPE (1)
      RETURN
      END
```

Real-time program library

The real time program library consists of general purpose FORTRAN programs already compiled and edited in core-image form, so that they can be executed immediately upon request through a pushbutton causing an interrupt and a thumbwheel referencing the program by a number. These programs are always stored on the disk and the selected one is then brought to the computer memory.

Generally, a program needs some data (e.g. definition of spectra, constants or other parameters). They can be given in two ways; first on a data panel defining eight variable values through various kinds of buttons, the meaning of each of them in the actual program is specified to the user by a message in the CRT. Second, data can be given through the typewriter in a conversational mode. In both cases, the user needs to know only the number of the program which performs what he wants. After calling it everything is explained to him. The results of programs are either a new spectrum which appears by itself on the CRT or some numbers written on the typewriter.

Often, during an experiment, the user wants to repeat after each run the same sequence of operations on the new spectrum, for instance: make some transformation on the spectrum, sum

the counts in regions, print or plot all or part of the spectrum... It would be cumbersome to have to call separately each program, each time with the same data. To avoid that he can at any time define a new real-time program defining this sequence with fixed data. For now this has to be done by punching some CALL cards, compiling and editing, which takes a few minutes, but in the near future this will be done without compilation, the sequence of called subroutines with their arguments being stored on the disk. These subroutines are the same as those called by the above programs after the data entry has been completed.

CONCLUSIONS

The whole system described above is still in evolution. Its principal benefits are presently: 1. Simplicity and high rate possibility in data acquisition mode. All the important functions are commanded by specific switches as in a classical multichannel analyser. The high rate of data acquisition is due to the use of 2 input channels and electronic data sorting devices. 2. CPU time and memory space gain owing to the hardware circuits we have developed for the visualization system. 3. Easiness to perform spectrum analysis with the programs which are written in conversational mode and always available from the disk library. 4. Ability to write quickly special programs making use of a large number of real time subroutines.

The next steps of development will be: 1. the installation of an experiment console at the 2 MeV accelerator, 2. the adjunction of a larger scope with a light pen, (this will facilitate the simultaneous using of the system by multiple users.) and 3. automatic connection between Ester and an IBM 360-40 computer. The hardware connection was installed by IBM at the beginning of 1968. The 1800 TSX programming system has been modified to support the 360 connection channel. But as the 360-40 works in batch processing mode, it cannot respond to the real time request without having a large fixed partition reserved exclusively for the connection. A dynamic memory allocating system on the 360 is under development and partially tested. It is expected to become operational shortly.

REFERENCES

1. Muser, A., Zen, J., Michaud, J.D., and Scheibling, F. "Utilisation d'un ensemble IBM 1800-360/40 pour l'acquisition et le traitement des données en temps réel", Coll. Internat. El. Nucl. Versailles, France, 1968.
2. Zen, J., Muser, A., Michaud, J.D., "Acquisition et traitement de données par le système ESTER/IBM 1800", Coll. Sté. Franç. Phys. Strasbourg, France, 1968
3. IBM 1800 Time-Sharing Executive System Concepts and Techniques. Form C26-3703 IBM Systems Reference Library.
4. Clark, N.R., and Gillette, W.L. Jr., "Nuclear Data Acquisition Adaptation for IBM 1800 Data Acquisition and Control System", Form L26-2049, International Business Machines Corporation, Special Systems Development, San Jose, California, U.S.A.
5. Muser, A., Zen, J., Michaud, J.D., and Scheibling, F., "Analyse Simultanée des événements corrélés XY et des évènements simples X et Y par échantillonnage", Nucl. Inst. and Meth. 63, 263, (1968).
6. Muser, A., Zen, J., and Michaud, J.D., "Visualisation et sortie de spectres enregistrés dans un IBM 1800, Coll. Sté. Franç. Phys. Strasbourg, France, 1968.

DISCUSSION

Bisby : - So far no authors has mentioned how much does it cost to handle automatic hardware and there is a great deal of hardware involved. I wonder if you also could give some indication of the effective cost of this hardware in relation, if you like, to the computer cost.

Scheibling : - I'm sorry, it is difficult to answer such a question. Anyway it is much less expensive than the computer itself.

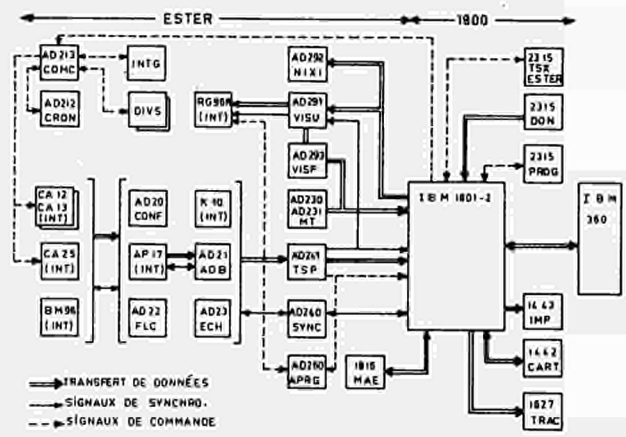

Fig. 1 - ESTER SYSTEM CONFIGURATION (CA12-13-25= ADCs, BM96 = 4096 channels analyser, AD20-21-22-23-AP17-K10=Data sorters, MT = Memory buffer, TSP = Spectrum transfer unit, SYNC = Synchroniser, APRG = Program request unit, AD291-292-293-RG96 = Visualization units, AD212-213 = Dead-time measurement units, INTG= Current integrator).

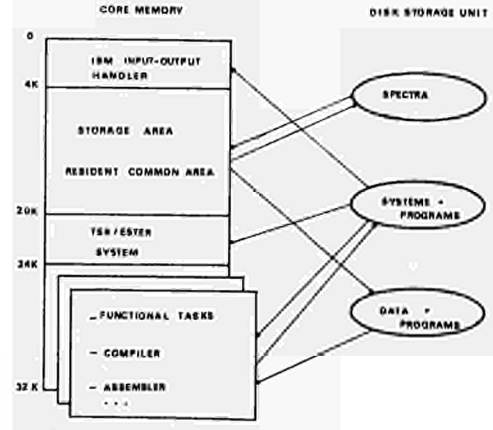

Fig. 2 - Memory storage organisation.

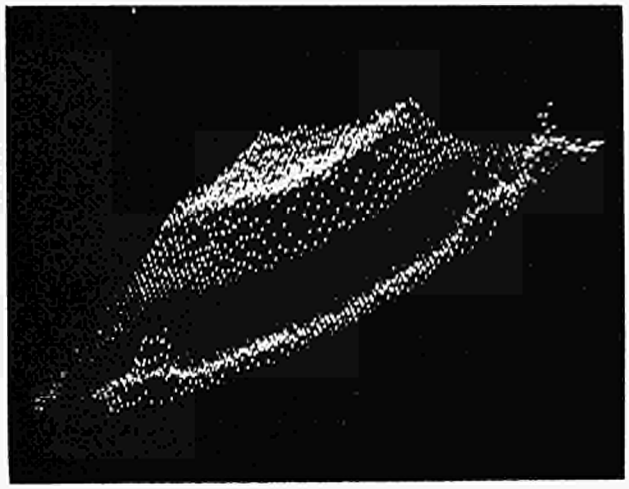

Fig. 3 - Isometric display of a three-body cinematics spectrum.

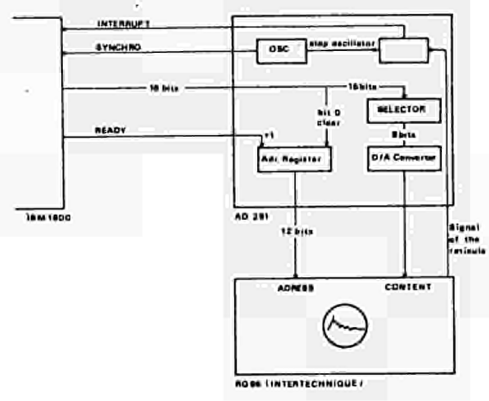

Fig. 4 - Block diagram of the "Hardware-Software" visualisation.

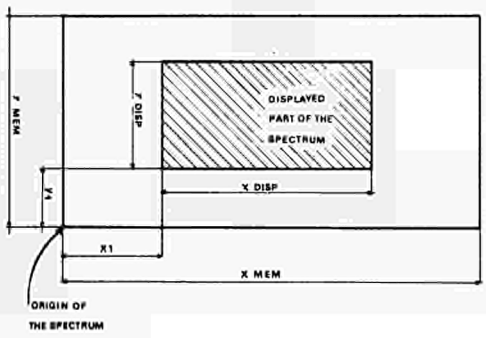

Fig. 5 - Choice of the display area.

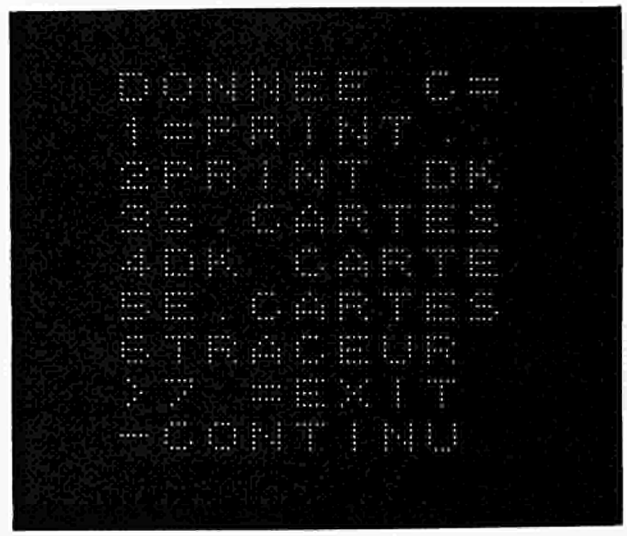

Fig. 6 - Example of a message displayed on the scope.

DATA ACQUISITION AND REDUCTION IN ACTIVATION ANALYSIS BY ON LINE COMPUTER

G. Di Cola - Scientific Data Processing Center
F. Girardi and G. Guzzi - Activation Analysis Laboratory
A. Termanini - Electronic Instrumentation Section

Joint Nuclear Research Center, Ispra (Varese), Italy

Abstract

The direct connection between an activation analysis laboratory and an IBM 360/65 computer is presented. The system is designed to automatically process data from gamma spectrometers in a minimal time. Control analyses needing a fast answer can thus be performed with an increased overall productivity of the equipment.

Introduction

Processing of gamma spectrometric data by means of electronic computers has been carried out at the Activation Analysis Laboratory in Ispra since 1962.

Gamma ray spectra were processed batchwise with delay times of the order of one day. Although this delay is acceptable for much routine work, some applications, such as analyses for nuclear reactor control, require faster answers. Furthermore, if the delay time could be kept within one minute or two, it is believed that by minimizing useless countings, the overall productivity of the counting equipment could be increased considerably.

Direct coupling of electronic computer and analytical units can be considered a promising way of conceiving analytical chemistry techniques. Therefore, a project has been designed to set up an experimental teleprocessing link via coaxial cable, between the laboratory and the Scientific Data Processing Center (CETIS) where an IBM 360/65 is in operation. The personnel of the Activation Analysis Laboratory, of the Electronic Instrumentation Section and of CETIS are cooperating on the realisation of this project which can be considered as a first step towards a more complete teleprocessing network.

The experience gained through the operation of this system will be extended to other applications in the field of nuclear measurements and analytical techniques.

Counting Equipment

The question arose as to whether the installations already available could be used to advantage. This equipment consists of two LABEN A 51 multichannel analysers connected with Teletype High Speed Tape Punchers by means of LABEN control units model UC 151 and CU 1. In order to guarantee the operation of the installations in the conventional mode and to limit the cost of the on line connection, modifications have been conceived to maintain the existing units and to utilize as much as possible their characteristics.

In this way the setting up of new electronic equipment has been limited only to the essential parts.

The content of each channel of the analyser is serialized by the puncher control unit and in our particular case, is also converted into BCD 1 2 4 8 code; besides the tape punchers control the read-out of the analyser memory in a synchronous mode. This reading mode also enables the use of an external trigger as a synchronism generator. Higher reading speed, only limited by the electrical characteristics of the analysers, can be then reached if not forbidden by slow recording systems.

A modification in this sense has been made on the two different puncher control units connected with the analysers, which can be easily switched from the conventional read-out system to another system inhibiting the punchers and sending the memory content to an external reader. It has been also necessary to provide the analysers with some external operating signals to control the read-out memory cycle.
With these minor modifications the analysers are able to transmit the memory content outside the conventional read-out system.

Two pneumatic sample changers are included in the installation for sending irradiated samples to the gamma-ray detectors. The whole system can work automatically without operator control as it is already frequently done.

Digital Input Device

Since it is necessary to process in different ways the data coming from the analysers, in order to pick-up from the computer the desired program, it has been thought to add to the existing units a Digital Input Device (DID) controlled by the operator in the Activation Analysis Laboratory.

To meet this requirement, ten-positions manually programmable switches are available in a single unit. This has been a cheap way to realize a console capable of transmitting instructions to the computer. In our particular case the switches are divided in two groups of 12, each group related to a multichannel analyser.

By means of these switches the operator can send to the computer information related to the flow pattern of the program needed for each analyser and indicate the number of channels utilized and pre-established on the spectrometer.

The data of the DID are stored in a parallel mode and serialized during the read-out in

order to be coherent with the output of the analysers. In the same unit an electronic clock is built-in. Once the initial time is obtained by manual resetting of the clock, it starts to count seconds until the beginning of the measurement on one of the two analysers. At that moment, without stopping the accumulation of the time, its content (i.e. the starting of the measurement) is transferred to a buffer from which it will be picked-up when the memory of the corresponding analyser is unloaded.

The clock is provided only with one buffer as the alternate working of the analysers is foreseen.

Telecommunication System

In the counting room of the Laboratory shown schematically in Figure 1 an IBM 1070 Process Telecommunication Terminal capable of monitoring, supervising and controlling a large number of instruments, has been installed. It is composed of an IBM 1071 Control Unit and of an IBM 1072 Multiplexer. On the basis of the specifications of these units, connections among the data sources and the IBM 1070 System are realized in a colloquial way by means of an Interface Unit which executes the instructions of the IBM 1070 and provides for their correct execution from the above-mentioned laboratory instruments.

Obviously the Interface also provides for the modification of signal levels in order to allow their collection and their transmission to the IBM 1070 Terminal. A block diagram of the equipment is given in Figure 2.

The IBM 1072 Multiplexer disposes of 50 addressing points grouped in modules of 10. The first module has been reserved for digital input purposes and three operative addresses chosen for the control of the equipment, have been realized as follows:

Address	000	DIGITAL INPUT DEVICE (DID)
Address	001	ANALYSER I with CLOCK and UC 151 CONTROL UNIT (A I)
Address	002	ANALYSER II with CLOCK and CU 1 CONTROL UNIT (A II)

The second one reserved for output purposes is directly utilised for the IBM 1053 Unit which prints the result obtained from the data processing done by the central computer, at a rate of 13 characters per second. Other modules are free for other uses.

Interface signals and addresses are responsible for the correct unloading of the data source buffers. The software of the system needs the definition of a peripherical station which could be composed of a console, and eventually of readers, printers and analog devices.

In the present configuration two different stations are identified by:

Station 1	DID address 000	
	A I address 001	
	PRINTER IBM 1053	address 010
Station 2	DID address 000	
	AII address 002	
	PRINTER IBM 1053	address 010

An application program is associated with each station which, when working, are interrogated at a prefixed rate.

From a memory unloading point of view, the data sources can be divided into two groups. The first one, composed of the DID, is always ready to transmit its content if interrogated; whereas the second group, composed of the clock and alternatively of the Analyser I or of the Analyser II, must completely accumulate the data in its memory before being unloaded. It is evident that if the reading request of the analyser's buffer is formulated during the counting, the request is delayed until the successive cycle of interrogation.

The reading speed of the sources, 134.5 characters per second, is established by the IBM 1070 System. At this rate the data source's buffers are unloaded.

As stated above, the DID buffer is composed of 25 digits to which one "end of data" character defining the end of a complete set of information, has been added. The buffer pools of the operative system of the IBM 360/65, for organisation reasons, require that each set of information be divided in blocks of about 900 characters. If the information contained in the analyser is less than 900 character (128 channels) one end character as for DID is added; on the contrary for longer memory contents (256 or 512 channels) the Interface controls the subdivision in blocks of 900 characters. Each block terminates with an "end of block" character. Successive blocks are immediately transmitted upon central computer's request. The clock memory content is always associated with the first block of information.

The communication facility between the Activation Analysis Laboratory and the Central Computer is a coaxial cable 750 m in length supplied with symmetrical end adapters (MODEM) which modulate and demodulate the pulse coded signals.

To allow future developments on the transmission speed, MODEM have been designed to reach a maximum frequency of 120 K bytes per second. The peculiar features of this facility are: the capability of distinguishing the logical zero from the no working condition, and the possibility of operating in a full duplex mode keeping the same transmission speed simultaneously in the two different directions. A service telephone works on the same line.

Operation of the System

The whole system operates as follows:

i) At the beginning of the working day stations are opened by the central computer. The operator in the laboratory switches the equipment to transmission mode and records gamma-ray spectra in the usual way. While the radioactive specimen is being counted, the operator sends to the computer, through the DID, a set of digits by which he refers to a certain experimental set up and gives instructions on the kind of calculations to be performed.
ii) A the end of the counting period the analysers switch to a ready position and await the interrogation from the computer which will be presumably done each minute.
iii) At that moment the content of the clock's buffer and that of the analyser memory will be transmitted; 12 - 30 seconds are required for a complete spectrum read-out (256 or 512 channels).
iv) The treatment of the data starts immediately. The computational time for the complete processing of one spectrum is limited to 1 - 2 seconds.
v) Once the results have been obtained they are immediately transferred back to the laboratory. The essential information required to evaluate the results, including a few necessary control data, are condensed in a few typewritten lines.

At the end of the transmission the analysers automatically reset for another counting sequence.

System Programs

The personnel of IBM in collaboration with those of CETIS have produced a system supporting automatic and non automatic stations. It runs under an operating system working in a multiprogramming environment. In this environment the IBM 1070 is considered as an automatic terminal which is scanned at prefixed rates by the control program. As soon as new data are available, the control is given to the processing programs.

The control program dynamically loads the processing program related to a station and takes it in core as long as it is active, releasing it then immediately after.

At the main computer side, an IBM 2701 Unit controls the data flow between the IBM 1070 Terminal and the central core. Eventual transmission errors are sensed to the control program which retries a few times the input-output operation.

The computing program is written in Fortran IV language where the input-output statements have been substituted by special subroutines of the system. It is not permanently resident in the computer store and is executed in a partition of the IBM 360/65 memory under the control of the HASP/MFT operating system. The program is divided into independent segments, each designating its own successor, and occupies less than 10 K bytes of the central core. A few data are made accessible to all the segments by being stored in a common data area, while the bulk of them (as spectra, libraries, etc.) are accessible on data sets.

The transfer of the control from one segment to the next is obtained by a subroutine of the system to which the name of the next segment must be supplied. Other special subroutines have been realised for BCD to integer conversion, integer or floating to BCD conversion, character expansion, etc.

The main features of the computer program are:
- collection of gamma ray spectra on data sets,
- smoothing of spectra,
- search for photopeaks,
- computation of areas and errors,
- calibration of the spectrometers,
- neutron flux evaluation,
- qualitative and quantitative analyses of gamma spectra.

The program is capable, when required, of correlating data obtained from different spectra (calibration of spectrometers, decay calculations, comparative analyses) and performing the up-dating of libraries and tables.

The flow of the program can be followed in Figure 3. It will be realised in four steps, three of which are already working.

Acknowledgements

Without the support and assistance of the IBM staff composed by E. Brugnoli, S. Provinciali and L. Chiesa, and of J. Pire of CETIS, the operating system would have not be realised in a so short a time.

The highest praise goes to S. Gecchelin of CETIS for his partecipation in the computational program setting-up.

Discussions and criticisms of W. Becker of the Electronic Instrumentation Section are also acknowledged.

DISCUSSION

Lidofsky : - Do you do spectrum fitting to get peak areas ?
Guzzi : - The search of the gamma peaks is performed by a simple program using Covell method. The overlapping of peaks is not considered for the moment.

Lidofsky : - Does the FORTRAN operating system reside in your 10 K byte requirements?
Guzzi : - The FORTRAN operating system of the teleprocessing link resides, I think, in the partition of IBM 360/65 memory available for us.

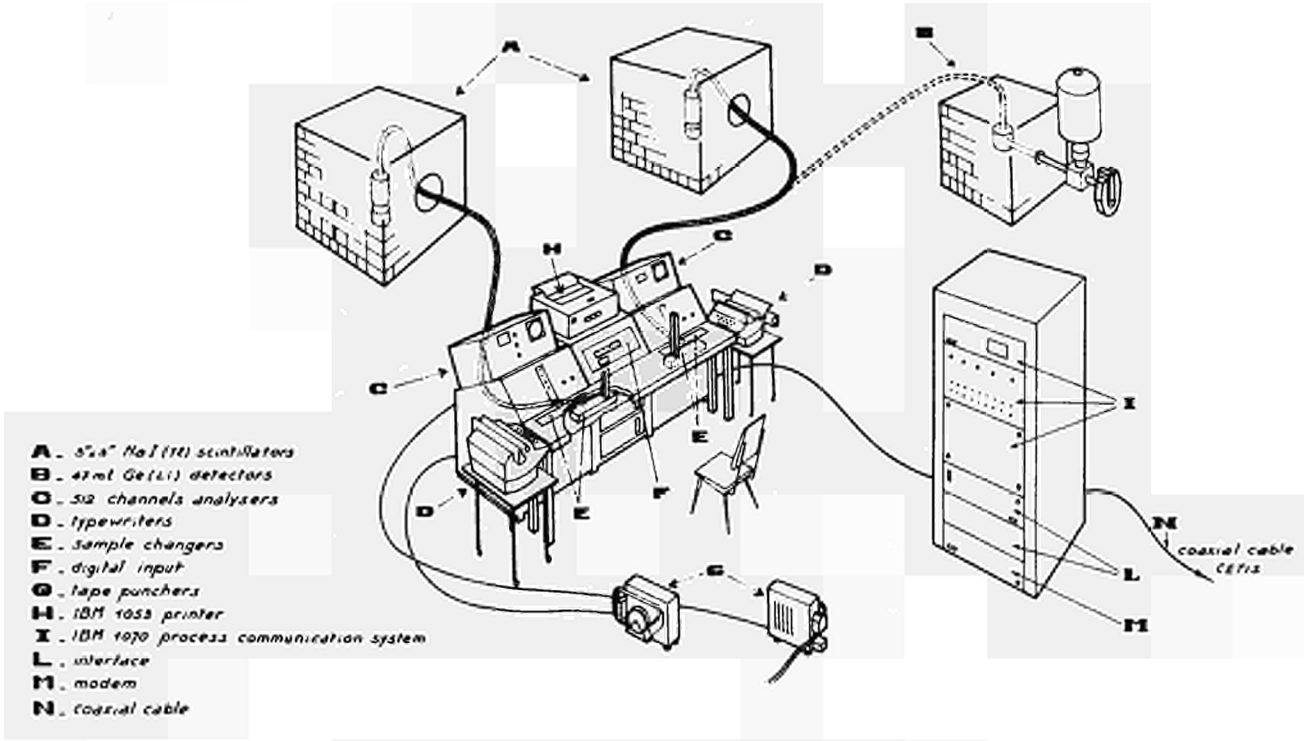

Figure 1 Schematic view of the Activation Analysis Laboratory counting room

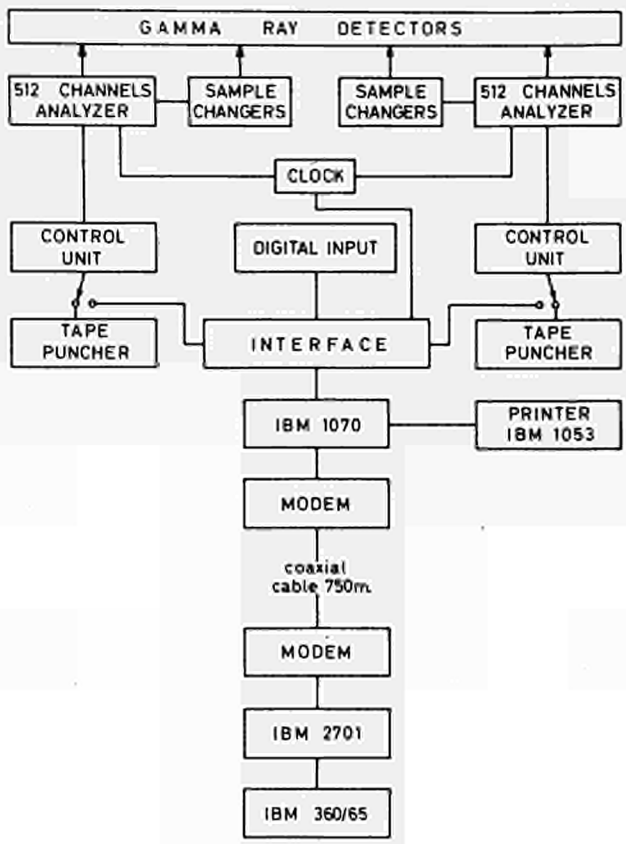

Figure 2 Block diagram of the teleprocessing system hardware

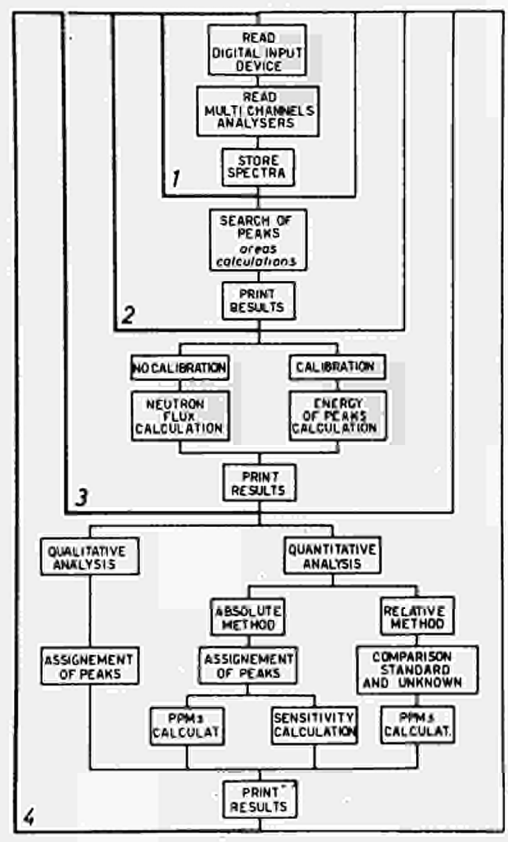

Figure 3 Flow pattern of the computing program

DATA HANDLING SYSTEM FOR ACTIVATION ANALYSIS BY MEANS OF A SMALL PROCESS COMPUTER

by

Palle Christensen and E. Mose Christiansen

Danish AEC Research Establishment Risö, Electronics Dept.

Summary

A central data handling system for three pulse-height analysers already in use in activation analysis is described. PHA data are transferred to an incremental magnetic tape recorder via a PDP8 I with a 32k disk. An oscilloscope is used for spectrum display and as an aid in peak calculations. System commands are given from a Teletype.

Introduction

In activation analysis γ-spectroscopic methods are used for the determination of the contents of selected chemical elements. A known quantity of a sample and a standard reference are irradiated with thermal neutrons. The element is identified by the energy of a characteristic peak; the concentration of the element is determined from the peak area.

Increasing amounts of data from three activation-analysis facilities make the long turn-around times for batch processing on a remote IBM 7090 unacceptable.

This problem may be greatly reduced in two ways at the same time:

(1) by spectrum calculations in the laboratory (simple problems) and

(2) by making data outputs on IBM 7090 compatible magnetic tapes ready for processing (complex problems).

After the introduction of Ge detectors and a 50 MHz 4096 channel ADC another problem has come up, namely that of removing data fast enough from three analysers as often used in the analysis of short-lived isotopes, where successive measurements are made.

Data dump from the analysers to a magnetic tape recorder gives high-speed data removal; a cheap incremental tape recorder may be used for all three analysers if it is buffered with a small computer. This computer may then also be used for formating of magnetic tape and for laboratory spectrum calculations if an xy display is available.

Equipment

Three Nuclear-Data pulse-height analysers are situated in different laboratories. They will be connected to a PDP8 I[1] with coaxial cables of up to 45 m length. The PDP8 I has 4096 words of 12 bits and a memory cycle time of 1.5 μsec. The computer has an extended arithmetic unit, a 32k disk, built-in buffer registers, and D/A converters for an xy display, and a 3 Teletype option, so that Teletype machines may be placed at the analyser laboratories. An 11" oscilloscope, Hewlett Packard 1300A, is used for display. An incremental magnetic tape recorder with seven tracks and a speed of 600 char/sec is also connected to the computer. A high-speed paper tape reader and a puncher are available, too.

A block diagram of the system is shown in fig. 1.

All the interface is made from standard DEC Flip-Chips[2]. The interface between computer and analysers may be of special interest. Diagrams are shown in figures 3 and 4.

Data Handling

Data transfer from the analysers to the computer is under programmed control and is performed with blocks of 128 computer words. When 128 words have been transferred to the computer, they are stored at the disk. When all channels are at the disk they are sent to the tape recorder via the computer.

If the data were to be transferred directly to the magnetic tape, a very fast and expensive tape recorder would have to be used because the data from the analysers have to be removed in a few seconds. The data transfer from the analysers to the disk is fast enough. Therefore we can use an inexpensive and slow incremental recorder. The disk is necessary in the system for other purposes, for instance storage of 4096 channels, each of 20 bits, in connection with spectrum calculations. This amount of data cannot be contained in the PDP8 I memory.

Data transfer from an analyser to the computer is requested by a Teletype command on a "first come, first served" basis. After the transfer command a number is typed for identification; this number follows the spectrum and is used when the spectrum has to be refound either in this system or at the IBM 7090. If not all channels are used, that is also specified. A data transfer request from analysers to computer stops other activities in the computer during transfer.

Data from the 4096 channel analyser are in 20-bit parallel binary code and are transferred by 10 bits at a time; before storage at the disk, the binary information is converted into the BCD code.

Data from the 1024 and 512 channel analysers consist of six 4-bit digits (BCD). They are transferred by 4 bits at a time and stored as BCD information.

Fig. 2 is an illustration of the data transport times in the system.

The transfer times for the full analyser memories are given in the following table.

Transfer times	4096 Chan	1024 Chan	512 Chan
Analyser to disk	2.5 sec +)	0.6 sec	0.3 sec
Disk to tape	43 sec	11 sec	5.4 sec

It is possible to bring the full memories of all three analysers to the tape in about 1 minute.

+) An ND 3300 magnetic tape control can handle 4096 channels in 1 sec.

Display and Spectrum Analysis

Automatic spectrum evaluation is only possible on large computers, but the combination of a small computer, a versatile data display and a skilled operator may give excellent results in a very short time.

The display is programmed, and 32 to 512 channels may be displayed with 9-bit precision (in either linear or logarithmic scale). In our first programme version all transport of data and scaling in connection with the display is ordered from a Teletype, but a light pen will later be available; this will make many of the operations easier.

Two movable vertical markers are displayed superimposed on the spectrum; the markers are placed by Teletype orders; after a move of a marker, its new position is printed on the Teletype. We are planning to put the intensity calibration into the markers as dark spots.

The basic calculation of the energy and intensity of a spectrum line consists in finding the peak centre location, computing the area of the peak and subtracting the background.

Before the operator chooses the upper and the lower limit, the section of the spectrum to be examined is smoothed as described by Savitzky and Golay[3]. This smoothing will remove the statistical scattering to such an extent as to make it easy to choose the limits of the peak; furthermore smoothing is necessary for the approximated numerical methods used in the peak calculations.

For peaks with a half width of five channels a 5-point third-order smoothing gives acceptable results[4].

The smoothed spectrum is now displayed (fig. 5.). For peak-area computation the operator places the low-energy marker at the minimum on the low-energy side of the peak. The high-energy marker is placed where an imagined tangent would touch the high-energy part of the peak. On a Teletype command the area is computed by integrating the counts between the markers.

The background is defined as the trapezoid under the intersection points between markers and spectrum. This area is computed in the same operation as mentioned above and subtracted from the whole area.

For symmetrical peaks the peak position is determined as the abscissa to the mean of a horizontal line intersecting the peak top. This line is fixed in the following way: The six peak points with the highest intensity are chosen in such a way that the lowest point is at the low-energy side of the peak. The horizontal line must intersect this point.

This operation is performed by placing the left display marker in the above-mentioned point and giving a Teletype command.

Programming and Commands

The software consists of an interrupt programme and subroutines for the peripherals.

The calculation programmes have a modular form, being built from subroutines. The subroutines are called by Teletype commands by typing a single character.

Programming is carried out in MACRO 8. In many of the computations the FLOATING POINT software package is used. A new input routine has been written as most of our data do not come from a Teletype. Conversion from fixed to floating format is carried out by using the extended arithmetic unit in the PDP8 I.

Conclusion

The system is not yet in use. The computer and most of the peripherals are being assembled in 19" racks together with the interface. Several of the display and calculation programmes have been written and are being tested on another PDP8 installation.

In the future we shall be interested in the investigation of other methods of peak calculation. This may take the form of fitting Gauss curves to the peaks; the peak may be displayed together with a superimposed Gauss curve; by means of Teletype or light-pen orders the constants of the Gaussian are adjusted to the "best fit" as controlled by visual inspection.

In the peak limit decision the low-energy part may be approximated to a second-order polynomium[5]. The upper limit may be chosen as the point of the Gaussion where a tangent from the minimum in the low-energy valley hits the curve.

Furthermore we shall consider the "digital filter" unfolding technique[6].

Acknowledgements

The authors wish to thank K. Heydorn of the Isotope Laboratory, where the system will be used, for his helpful advice concerning the system- and programme planning. We also thank C. Fog of the Electronics Department for designing the interface of the magnetic tape recorder and the analysers.

References

1) Small Computer Handbook (Digital Equipment Corporation, Maynard, Massachusetts, 1967).

2) Logic Handbook, Digital Equipment Corporation, Maynard, Massachusetts, (1967).

3) Smoothing and Differentiation of Data by Simplified Least Squares Procedures. A. Savitzky and M.J.E. Golay, Analytical Chemistry 36, No. 8, 1627 (1964).

4) Mathematical Smoothing of Gamma Ray Spectra.
H. P. Youle, Nuclear Instruments and Methods 54, 61 (1967).

5) Gamma-Ray Spectra Analysed by Computer Programme Using the Peak Area Method.
S.C. Choy and R.A. Schmitt, Nature 205, 758 (1965).

6) A Digital Filter for Unfolding Pulse-Height Distributions.
M.H. Young and W.R. Burrus,
Nuclear Instruments and Methods 62,82 (1968).

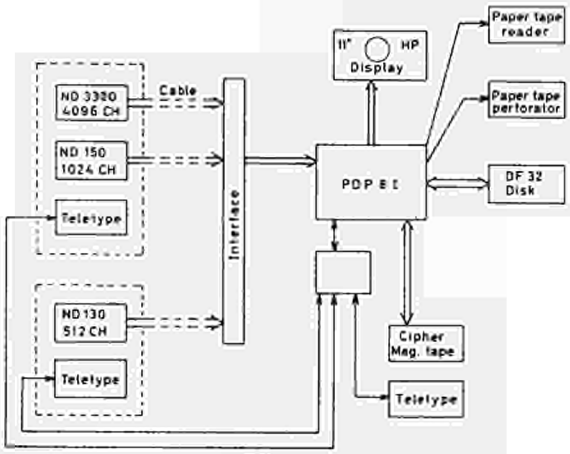

Fig. 1. PDP8 I system for activation analysis Block diagram.

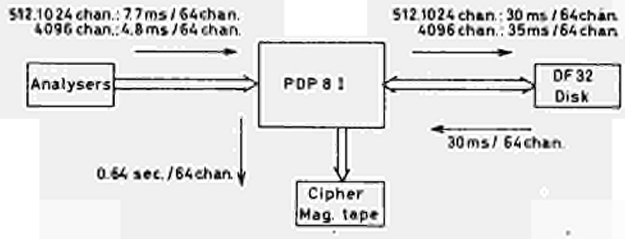

Fig. 2. Data transport times.

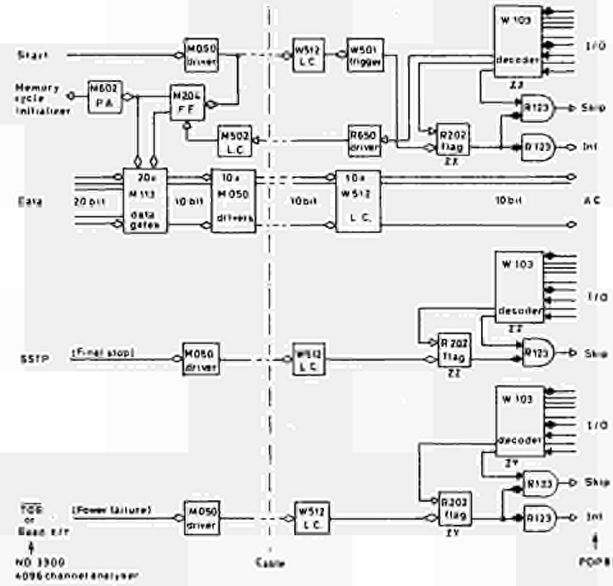

Fig. 3. Interface for 4096 channel analyser to PDP8 I connection.

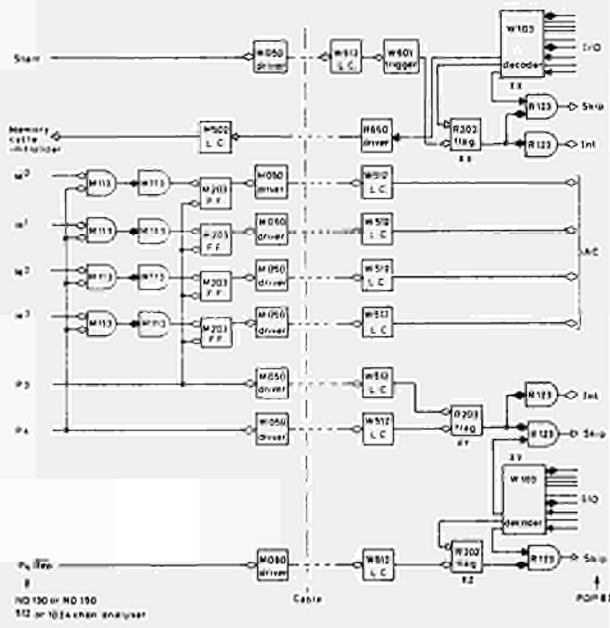

Fig. 4. Interface for 512 or 1024 channel analyser to PDP8 I connection.

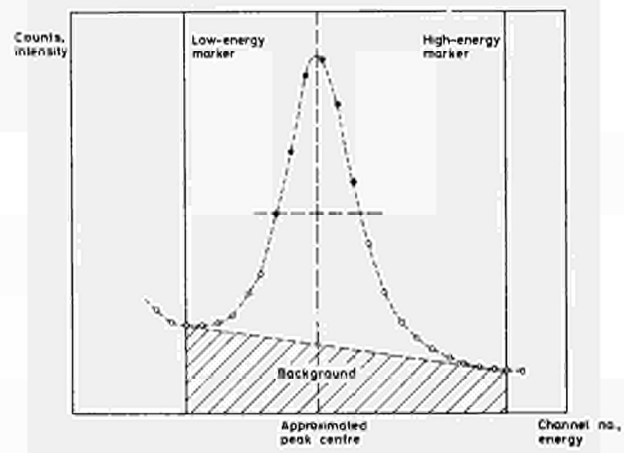

Fig. 5. Peak calculations.

A DISPLAY TERMINAL FOR ON-LINE NUCLEAR EXPERIMENTS

H. Klessmann and J. Zahn

Hahn-Meitner-Institut für Kernforschung Berlin

Berlin, Germany

Summary

The integration of on-line computers into experimental physics for nuclear data acquisition and data processing requires a display terminal which provides real time presentation of data in an immediately comprehensible format and which offers input means for dynamic interaction of the physicist with the experiment and the data analysis in progress. Design considerations and characteristics of an experimental display terminal are presented which we design particularly for on-line nuclear experiments. Data are displayed on a direct-view storage tube which eliminates the need for refreshing the information display and allows to have only a small display file in the computer memory if information is plotted as it is generated by computer program. Thus both computing time and computer storage capacity can be used more economically. A general command and data structure has been chosen for handling several different modes of display operation. By strictly modular design a very simple display having random point plot capability only can be extended to a more elaborate system with incremental or sequential point plot or with vector and character generation. In the simplest point plot mode any point may be addressed at random by one 24 bit word with 2 x 10 bits for x- and y position providing a 1024 x 1024 dot array. It takes 120 µs/dot for positioning and writing which corresponds to a maximum plotting rate of 8000 dots/s. For short deflections only the 5 least significant bits may be used which provides two points per 24 bit word and reduces plot time to 30µs/dot. Nuclear data like single and multiparameter spectra can be displayed in isometric and map representation with any format in x and y up to 128 x 128 channels (corresponding to about 16 000 dots displayed within 2 seconds). The information stored on the screen can be changed only by total erasure (0,5 seconds) and display of a new modified picture. This prevents real live display of an accumulating spectrum. Instead "snap-shots" of a growing spectrum are displayed at equal intervals which can be selected (e.g. 10 seconds). This method suggests that not the counts accumulated in each channel are displayed but the mean rate in counts per time interval by averaging at the end of each interval over all completed ones. This eliminates the need for changing the z-range of the display continuously because the accumulating spectrum will stay on the screen while improving its shape during the course of the experiment. Furthermore, only 10 bit data representing the calculated mean count rate is transferred to the display which eliminates the normal 20 bit data transfer from which 10 bits are selected at the terminal according to the required z-range. All display functions like mode switching, format, range logarithmic presentation etc. are controlled by means of function keys and command words via the computer. A cursor in write-through mode may be used instead of a light pen as a graphical input device to identify and mark particular points or areas of interest.

I. Introduction

The integration of computers for on-line data acquisition and analysis in experimental nuclear physics has been introduced since several years and is now becoming increasingly accepted practice. Although raising many new problems this trend is enhanced by several factors. It is a matter of progress that problems to be investigated in physical research become more complex - with more correlated parameters involved - and that smaller effects have to be measured with still higher accuracy. Because of the statistical distribution of events, generally, greater accuracy may be achieved by investigating a substantially increased number of events. These, in addition, are most often accompanied by a large amount of unwanted information. Therefore many accelerator and reactor experiments produce large quantities of data out of which meaningful information for the experimenting physicist may be extracted within reasonable time only by means of an on-line digital computer. Thus, four major functions have to be performed in advanced system as shown in Figure 1:

1. Acquisition and storage of data generated with statistical time distribution, often in large quantities and with high data rates. Sometimes data gathering of several experiments is performed simultaneously in a time-sharing mode.

2. Real-time reduction and analysis thereby employing the original computing ability for processing experimental raw data. Some of the more typical operations are classification of events, particle identification, peak integration, background subtraction, correction for dead time losses, normalisation of spectra and spectrum stripping, coordinate transformation and least square curve fitting. Either corrected data, reduced data or preliminary results of analysis

are obtained in order to extract a physical meaning out of the original experimental data.

3. Display of experimental data and analysis results. The presentation of information in real time, under various aspect and in an immediately comprehensible format provides a most effective assistence to the operating physicist for physical interpretation. The display of data permits to monitor the data collection, to recognize the instantaneous status of the experiment and to evaluate its progress.

Now the physicist is put into the position to make distinct decisions and to interact with the experimental equipment or/and the data processing in direct response to the information presented to him. By means of data input facilities he may change parameters or procedures thereby modifying the course of the experiment in order to get optimum results. Obviously, displaysin nuclear research are not just a matter of convenience to the user but a very powerful means for dynamic interaction of the physicist with the experiment in progress - via the computer. This indicates the fourth major function of on-line computers in nuclear experiments:

4. Real-time control of the experimental equipment and ultimately of the radiation facility. This feedback from the computer-under program control - into the experiment closes the loop of signal flow and really establishes the computer controlled experiment.

Now the computer may monitor the complete experiment configuration, set up initial conditions and parameters for different runs of an experiment and take appropriate action by a prepared routine if an interrupt indicates the demand for service. Many of the repetitive routine procedures commonly associated with experimental physics - calibrating, general test, drift checking - can be performed more often and with greater accuracy under program control. However, an experiment - per definitionem - cannot be subject to automation where human decisions are replaced by preprogrammed (computational) decisions. On the contrary, an advanced system allows effective interaction of the operator based upon decisions which have been made possible by intermediate results being immediately available and presented. Again the dominant importance of display in on-line nuclear experiments is emphasized. This outline of the general environment in which a nuclear display station is used seems necessary in order to understand the design considerations and specificic characteristics of our development.

II. Design Considerations

The characteristics of our experimental display station is determined by several aspects:

1. Data link. In nuclear data acquisition often rather small computers are employed in the vicinity of the experiment, either as an independent unit or as a satellite to a large computer. Normally the experimenter's display can be connected directly to the computer by parallel data link. Data transmission via telephone line by means of modem is of less importance. However, the display should be arranged to have a serial data input as an alternative whereby interfacing to different types of computers is simplified and data can be transmitted conveniently over small distances within a research installation (50 m to a maximum of about 2000 m) via simple twisted pair lines.

2. Display modes. If a display is linked to a small computer obviously low cost is of primary importance. This suggests a display with only random point plot capability. Then the display controller is most simple as it consists only of two digital-to-analog (D/A) converters and a digitally controlled unblank circuit. However by hardware implementation of other, additional display modes (like vector and character generation) both computing time and computer storage capacity can be used more economically. Therefore a strictly modular design is chosen, which allows a very simple display but also the extension to a more elaborate system. This, of course, needs a command and data structure which satisfies several different modes of display operation - all being compatible within the same programming system. By modular design the different requirements for display capability - as determined by application, ease of man-machine interaction or just users opinion - can be met easily. Needless to say that the implementation of all display modes is not the best choice.

3. Nuclear data monitoring. In nuclear experiments very often single or multiparameter spectra are accumulated in the computer memory. Then the experimental data flowing into the computer are arranged in a very orderly fashion as memory address is associated with the channel number and the content of each memory cell represents the number of events. Semiconductor detectors and pulse A/D-converters provide spectra with 4096 channels or even more, which may be an appreciable part of the computer core memory. To monitor the data collection an "Isometric/Map" display mode is very effective as the same memory block with the original data can be used directly for meaningful analog presentation appropriate to physical interpretation - without computation or use of an additional display file. Display in nuclear experiments often are used primarily for these monitoring purposes. With the advent of computer controlled experiments however a much more intimate man-machine communication on a conversational besis is needed, as the physicist manipulates the

experiment and its instumentation only via the computer. Therefore we feel that in on-line nuclear experiments more sophisticated display than just oscilloscopic monitors will be used. This aspect is part of our investigation of on-line computer display, their specifications and hardware - software trade offs.

4. Control of display functions. For dynamic interaction of the physicist with the experiment and the computer a keyboard with at least several function keys must be provided and provisions for light pen or cursor control should be foreseen. It is only consistent that all display functions like mode switching, format, range, logarithmic presentation etc. are controlled by means of function keys and command words via the computer. The obvious advantage is that execution of functions is determined by software rather than by specially dedicated hardware in the display.

5. Refresh type CRT display. One of the major design decisions concerns the use of a direct-view storage tube display as an alternative to the "refresh type" CRT. The conventional cathode-ray tube with short persistance phosphor (P 31) requires that the picture to be displayed without flicker must be repeated at least 30 times per second. At this rate flicker is already noticeable and often an even higher repetition rate e.g. 60 times per second is used in order to lower eye fatigue. On the other hand, mediumpersistance phosphor have only short life and are susceptible to burn in.

The time for plotting a picture is determined by

- the rate of data transmission via the computer-to-display communication link
- the settling time of the electron beam (including time performance of the D/A-converters and deflection amplifiers) and the dot writing time (point brightening)
- the amount of information to be displayed in a picture, i.e. the length of the display memory bank.

Writing a dot on a conventional CRT requires about 5 µs unblanking time, as longer brightening pulse width do not produce noticeable increase in spot intensity while pulses shorter than this introduces noticeable dimming (time-modulation of brightness). With an electrostatic deflection tube and fast D/A-converters (settling time < 2 µs) a plotting time of 8 µs per (random) point can be obtained. Thus, with the refresh time of 33 ms exact 4096 points can be plotted without appreciable flicker. This is just enough for presentation of a 4 K single or multiparameter spectrum in a 4 x 1024 channel or a 64 x 64 channel format. But no additional information (axis, range etc.) can be display. If all 4096 points possible were used for display of characters in a 5 x 7 matrix with an average of 20 brightened dots per character only about 200 characters can be displayed on the screen. (With electromagnetic deflection high-speed, high-cost deflection amplifiers must be employed even to obtain a plotrate of 30 µs/plot). We are certain that this performance is far from satisfactory for those applications which we anticipate in computer-controlled experiments - it may be sufficient if only monitoring is required.

A higher information density in refresh type CRT's can be obtained by replacing the simple dot generation for vector or character display by faster, more elaborate (and generally more expensive) system. For example, a stroke generator may form a character in 16 µs, which allows a maximum of 2000 characters to be displayed.

As displays in nuclear experiments generally are linked to a nearby computer the required data transfer rate of 125 kHz (8 µs/point) can be handled without serious problems either in parallel via twisted-pair cable or in serial via coaxial cable, preferably with bipolar pulses. Because the transmission link bandwidth does not impose serious restrictions it seems convenient to use the computer memory as a refresh buffer. This, of course, avoids the additional cost of a local refresh buffer memory in the display terminal, e.g. a magnetostrictive delay line as low-cost buffer with a storage capacity of up to 20 000 bit.

However, the fast repetition of data transfers to a conventional CRT-terminal for flicker-free display puts a heavy load on the computer both in terms of storage space and computer time:

- The complete display file containing the coded pattern of the picture must reside in the fast-access computer core memory.
- The computer must service the demands for output transfers with a repetition rate of 125 kHz, generally by cycle-stealing.

For small computers the repetitively regenerated display from the computer memory means an additional restriction to the per se limited capability and seems an uneconomic solution.

Further problems arise if several display terminals are required to operate from a computer simultaneously with different information on each. This is true especially in small systems having no computer dedicated to display organization and service. Because of the stringent timing for flickerfree presentation either the displays are serviced one after the other and consequently must share the total information transferred within 33 ms (e.g. 4 x 1024 points) or more elaborate schemes with interlacing of datatransfer and display between different units

combined with fast (not point plot) generators for vectors etc. must be employed.

6. Direct-view storage tube display.

The direct-view storage tube display used in our experimental terminals is a TEKTRONIX Type 611 Unit and offers several advantages:

- The image storage ability of the screen eliminates the need for refreshing the information display. Pictures with extreme high information density are presented absolut flickerfree without buffer memory and high-speed electronics.
- New data are written only once and may be transferred at random and at relatively low speed (in many other applications determined by the transmission link bandwith). Computer time for output transfers is reduced to an absolute minimum and moreover only a small display file in the computer memory is required if information is plotted as it is generated in the computer by program.
- The characteristics of the display unit (20 µs dot writing time and 3,5 µs/cm + 5 µs settling time) allows for small deflections a maximum plotting rate of 25 µs/dot. Thus 40 000 dots can be generated on the screen within a second compared, roughly, to the 4000 dot limit of flickerfree presentation with a refresh type CRT. Obviously, with a storage tube display simple point plot systems may be completely adequate for many application. Moreover, with a plotting rate of 25 µs/dot or slower the speed requirements on the electronics are quite modest.
- The display unit we use (Type 611 Mod. 162 C) has a horizontal axis of 21 cm and a vertical axis of 16 cm. The ratio of approximately 4/3 is reflected by the resolution specification for the two axis of 400 x 300 line pairs. Resolution is measured by using 400 x 300 stored dots - more closely spaced line pairs would exceed the 25% incremental storage limitation. Clearly, the screen resolution in terms of individual points is 800 x 600 dots.
- It is reasonable therefore to transmit 10 bits of position information for each axis which allows any point to be addressed in a 1024 x 1024 raster. This corresponds to an increment size of 0,2 mm (5 dots/mm). As the stored dot is about 0,25 mm (10 inch) in diameter, adjacent dots will overlap slightly and appear as a continous line. If dots are plotted every second increment they appear as individual dots.
- Storage tube display do not provide the possibilities of
  real live display,
  intensity modulation and
  light pen operation.
  All these features are used extensively in conventional display for nuclear experiments and therefore these limitation required some attention.

Real live display. Graphic or alphanumeric information written on the screen of a storage tube is stored and can be augmented by additional information any time. Changing part of the information stored requires total erasure of the screen and display of a new modified picture. Obviously this prevents real live display of a spectrum while accumulating. With the storage tube display the modified spectrum can be presented for example every 10 seconds (with 0,5 s erase time) or at even longer intervals. We are convinced that this is acceptable in most cases and it has the additional advantage of minimum loading of the computer. This method of presenting "snap-shots" of a growing spectrum at equal intervals suggests that not the counts accumulated in each channel are displayed but the mean rate in each channel. The experiment is divided into a sequence of equal intervals and the results are presented directly as counts per unit time interval independent of the number of intervals. At the end of the first interval the count collected in each channel gives an assessment of the rate. At the end of each subsequent interval a better assessment is made of the mean rate by averaging over all completed intervals[4]. This method is well known from signal averaging to improve the signal-to-noise ratio of repetitive waveforms and provides several advantages:

- The shape of the displayed spectrum in improved at regular intervals during the course of the experiment thereby showing increased precision but it is essential static in amplitude. This means that a spectrum while accumulating will stay on the display screen so that there is no need to change range continously in order to adjust range according to the growing spectrum.
- The display terminal receives only 10 bit data representing the calculated mean count rate. This eliminates the transfer of 20 bit data in isometric mode out of which 10 bits are selected at the terminal according to the required z-range.

Intensity modulation. Multiparameter nuclear data normally are displayed in an isometric or map (contour) pattern. These presentations become clearer and can be interpreted more easily if the dot intensification is proportional to the channel content (z-coordinate). The bistable character of the storage tube does not allow intensity modulation of stored information. The intensity modulation of an isometric display may be considered an operator's convenience; for map display two digital comparators are provided which control the unblanking circuit and thereby introduce contour lines for identification of the relief structure.

Light pen. The light pen is widely used as a graphical input device to identify and mark particular points or areas of interest or even to "write" by means of special programs. When pointed at the screen of refresh type CRT the light pen being a photosensitive device actually generates a pulse every time when the electron beam passes by. The content of the x- and y-position registers at that moment defines the location of the light pen and may be transferred to the computer. Obviously, this operation is not possible with static information stored on a storage tube screen having constant brightness. However the bistable characteristic of the storage tube allows the writing beam to produce a visible image at any point of the screen without storing this or disturbing previously stored information. This "write-through" is obtained if the electron beam hits the screen with an energy below image storage level which can be done either by reducing the beam intensity or by shortening the unblank pulse duration or by moving the beam with a high writing speed. As the Storage Display Unit Type 611 has a built in write-through circuit which moves the beam in a small cursor pattern, this cursor could be moved to any position on the screen by means of a "Mouse". This device contains two potentiometers mounted at right angles which control the x- and y-position of the cursor by moving the mouse on the table. The horizontal and vertical position are digitized by an analog-to-digital converter and are transmitted to the computer upon request of the operator. This input device is accepted as a very convenient equivalent to the light pen. In principal even with a storage tube display the operation of a light pen should be possible by generating a raster in write-through mode. But this is expected to work properly only as long as the light pen is not affected by light from previously stored information.

III. Display Modes and Data Format

The modular design chosen to meet different applications and requirements called for a general command and data structure to handle several different modes of display operation: 0) Random Point Plot (RAND), 1) Incremental Point Plot (INCR), 2) Sequential Point Plot (SEQU), 3) Isometric/Map Point Plot (ISO/MAP), 4) Comparator (COMP), 5) Vector (VECT), 6) Symbol or alphanumeric character (CHAR), 7) Information Erase (ERAS),

For economic and technical reasons it is not aspired or advised to implement all of these modes in a single display terminal; rather the choice for a limited combination and the flexibility to extend a very simple display to higher capability is a useful design feature. Furthermore, the general structure is not limited to storage tube displays but is applicable to conventional CRT-displays as well.

The experimental display operates a mode-control basis, as indicated in Fig. 2 showing the display-file word format for our 24 bit parallel data link. It is set into a particular mode by receipt of a unique code, and will stay in this mode until it receives a code placing it into a different mode. A "control word" is specified by a non-plotting 6 bit "control code" 111 010 = 72_8 which indicates that the next (second) character defines the mode how the succeeding "data words" should be interpreted. The third an fourth character may carry special information which at present are used only in (ISO/MAP)- and (COMP)-mode but generally are ignored.

"Data words" carrying binary information are identified by a logical zero in the first bit. This bit acts as a general escape bit into control mode. If the display controller detects the "control code" a new display mode is initiated. Datawords contain either 10 bit information for the x- and y-coordinate which allows to address any point of the display area or it contains only the 5 least significant bits (LSB) of the x- and y-position in which case the 5 most significant bits (MSB) remain unchanged. This often proves to be useful if a graphic picture is made up of many small elements, is is very economical as twice the information is transferred in one word and the shorter settling time allows a faster point plotting rate. The least significant 5 bits provide a maximum range of 31 increments in the 1024 x 1024 point arry which corresponds to a length of 6,2 mm. The second bit in each data word indicates whether the x- and y-registers are to be loaded with all 10 or only the 5 least significant bits. This allows to use both types of data as is convenient without mode switching.

Data words do not carry an intensify bit which indicates whether to unblank the beam or not in which case the specified position may be used just as a starting point for a new mode. It has proven that dot writing can be performed more simple automatically: the unblanking circuit is initiated after both coordinates (x and y) have been transferred and only if the next character is not the control code.

Random Point Plot (RAND)

In this mode the beam may be positioned in absolute coordinates to any location at random. It is either used to locate the start of a picture drawn in any other mode (INCR, SEQU, VECT or CHAR) or it is used simply to plot points. RAND is the most basic and can be implemented by a very simple display controller. It allows almost any complex picture to be displayed if sufficient storage capacity and sufficient time for plotting can be afforded because the complete picture pattern, point by point , must be generated by computer program and stored in the computer memory. Obviously, both computer time and storage capacity are utilized uneconomically. Every point is defined by one 24 bit word with 2 x 10 bits for x- and y-position so that any point

in a 1024 x 1024 array can be adressed. It takes 120 µs/dot for positioning and writing which corresponds to a maximum plotting rate of 8000 dots/s. For short deflections only the 5 LSB may be used which provides two points per 24 bit word and reduces plot time to 30 µs/dot. The position (0, 0) is in the lower left corner. Because the screen is rectangular actually 1024 points are addressable in the horizontal but only 768 points in the vertical direction.

Incremental Point Plot (INCR)

In this mode the beam can be moved only from one point to one of the 8 adjacent points by incrementing or decrementing the x- and/or y-position register. A single 24 bit word defines 4 points each being specified by a 6 bit character (+ x/-y/-x/+y/blank/unblank). As only adjacent points can be addressed it is useful that the point specified may be left blank or intensified under control of bit 5 or 6. The plot time is 30 us/dot which allows a maximum plotting rate of 33000 dots/s. Upon completion of incremental plotting an "End of Message" character (1 1 1 1 1 1) is given which is insignificant to the increment logic but stops the display and indicates that the next character will be the control code thereby providing the escape into the control mode.

This increment mode is introduced for three reasons:

- The hardware implementation is very simple and inexpensive
- The operation and data structure is identical to a mechanical digital plotter which for exemple allows 300 steps/s with 0, 1 mm increments (CALCOMP). The mechanical plotter has a much better resolution and linearity and cannot be substituted but ist seems very convenient to display data in the same fashion but at a very much faster rate of about 100 times.
- The incremental mode is well suited for the display of alphanumeric characters generated by program if only a short text must be added to an otherwise graphic picture and if the cost of a character generator is to be avoided. Characters can be generated in a 5 x 7 dot matrix; because an average of 24 dots must be stepped through and unblanked, the display of any character requires about six 24 bit words and 720 us/character.

Sequential Point Plot (SEQU)

In this mode horizontal (x-) position is incremented automatically - beginning at a start position defined by RAND-mode - while only the corresponding beam position in vertical (y-) direction is transferred from the computer. A 24 bit word contains the y-position of either 2 dots (10 bit each) or 4 dots (5 bit each). This mode is a combination of RAND and INCR and therefore requires only very little additional control logic.

Isometric/Map Point Plot (ISO/MAP)

This mode is used mainly for the display of nuclear data like single or multiparameter spectra which are or have been accumulated in a memory block in such an orderly fashion that the memory address corresponds with the channel number and the content of each memory cell represents the channel content or number of events accumulated. This mode allows to monitor incoming experimental data by using the same memory block as a display file without requiring any data conversion or additional storage space. Therefore 20 bit data (providing a maximum channel content of about 10^6) are transferred to the display where 10 successive bits may be selected (z-coordinate = channel content) to provide vertical deflection. With every data transfer the horizontal deflection (channel number) is incremented automatically.

The data may be displayed in various presentations as it is required by the operator and as it is most meaningful to him. Because all functions of the display are under computer control the format of data presentation is completely defined by the command word (see Fig. 2). The operator may change the format using several function keys whereby instructions are sent to the computer to alter the command word accordingly. The format is defined by

- z-range. 4 bits provide a selection of 11 different ranges: 0) $2^0 \ldots 2^9$ ... 10) $2^{10} \ldots 2^{19}$

  Range 0) selects the 10 least significant bits (with full scale deflection: 1024 events), while range 10) selects the 10 most significant bits (with full scale deflection: 1.048 576 events).
- vertical log: The vertical (z-axis) can be selected for logarithmic presentation.
- y/x-format. The x-format indicates the number of points per line while the y-format gives the number of lines to be displayed. The y/x-format is defined by 3 bits each in the following manner:

y	(lines)	x	(points/line)
0)	1	0)	1024
1)	2	1)	512
2)	4	2)	256
...			
6)	64	6)	16
7)	128	7)	8

  This allows any reasonable display format like 1 x 1024 (single spectrum)
  or 4 x 1024 (single spectrum subdivided)
  or 64 x 64 (multiparameter spectrum).
  A 128 x 128 channel presentation requires for example
  16 384 points to be displayed which can be

accomplished easily with a storage tube display.

- ISO/MAP-presentation. 2 bits select 4 different submodes which from a technical point of view are very similar although pictures many look rather different:

0) ISO 0^o
1) " 30^o
2) " 45^o
3) MAP

ISO 0^o is the normal way of presenting a single spectrum:
vertical: channel content z
horizontal: channel number

Several spectra may be presented one above the other as selected by a-format (lines). All spectra begin with x = 0 position (0^o shift).

in ISO 30^o and 45^o presentation several lines are presented one above the other as before, However, the x-coordinate starting position of each line is shifted to the right whereby the impression of a three-dimensional presentation is obtained.

In MAP-mode the beam is simply stepped through a point array as selected by y/x-format (using the x- and y-position registers) while the z-register content is compared with an upper and a lower level. A dot is unblanked if z-data are above the upper threshold or below the lower threshold. This provides a rough but clear impression of a relief as looked from atop. The height distribution becomes even more transparent if the comparator levels are changed. This may be done by loading data into the upper and lower level register using the comparator mode COMP of the command word.

Vector (VECT)

This mode provides a rapid method for generating straight lines between two points without specifying any point inbetween. After the beam has been positioned in RAND-mode to the starting point the display terminal receives a control word to enter VECT-mode so that the following data are interpreted as the end point of a vector drawn from the present beam position. The simplest method of interpolation is to incorporate low-pass filters for the x- and y-analog signals as indicated in the block diagram. This however has two minor drawbacks:

- Vector are drawn in constant time; the writing speed of long vectors can exceed the speed limit for storing the image. Hence the vector length must be limited.
- The method implies that the point of a vector is given in absolute coordinates (x, y). However, for programming it is more convenient to give only the coordinates ($\Delta x, \Delta y$) relative to the last beam position [2, 3].

This has the additional advantage that any graphic figure can be shifted to any location of the display screen just by altering the starting position (x_o, y_o) given in RAND-mode. A low-cost relative vector generator is investigated as a students diploma.

Symbol or character (CHAR)

This mode allows the display of alphanumeric text with a minimum of data transferred. A 6 bit code may be used to select a character so that 4 characters are transmitted by a 24 bit word. The 6 bit code provides 64 different characters out of which one non-printable character is used as a unique control character to indicate a control word and thereby providing exit from character mode into any other mode. In character mode all data are interpreted as a string of 6 bit characters. For our applications it is considered sufficient to have the following set of characters:

10 numerals	0 ... 9
26 capitel letters	A ... Z
18 Symbols	= ' ; . , : + - * / ( ) > < % + $?
10 control codes	

The control codes are used for these control functions:

0) Space
1) Line Feed
2) Carriage Return
3) Backspace
4) Backline
5) Double Size Characters
6) Normal Size Characters
7) Ignor (= No - Op)
8) End of Message (= Full Page)
9) Control Character

The normal/double size character feature (or normal/tilted) can be used the same way as black/red typing of a conventional typewriter. The writing of lower case letter would require another character generator which can be addressed by the submode bits of the mode control character.

The character generation[2, 3] is based on a 5 x 7-dot matrix through which the beam is stepped in a regular pattern. A character pattern read-only-memory unblanks at appropriate beam positions to generate the character as selected by the 6 bit character decoder. With a 5 x 7 dot matrix for character generation an average of 20 dots must be unblanked. Because only small beam deflections are involved as incremented through the pattern a plot time of 25 μs/dot or an average of 500 μs/character is obtained.

Information Erase (ERAS)

This mode is used to erase all information from the screen by initiating the erase control and at the same time to reset the x- and y-position registers to zero position (0, 0).

The erase time is 0,5 seconds.

IV. Circuit Description

The block diagram of the display terminal is given in Fig. 3 indicating these main sections:

- Interface for data display (computer output) and for operator instructions (computer input)
- Display controller
- Input devices (keyboard and mouse)
- Storage tube display unit (Tektronix Type 611)

The interface synchronizes the operation of the terminal and the display controller. For data display a timing circuit puts up a demand signal for data which are strobed into the input buffer upon arrival of a strobe signal. If the first 6 bit character is identified as the control code the second 6 bit character is transferred to the mode and submode control which decodes the mode and puts out commands to determine the sequence of data transfer from the input buffer to the registers of the display controller or the sequence of incrementing these registers. Fig. 3 indicates a 24 bit parallel link to the computer but clearly an interface for serial data output with an 8 bit input buffer (5 bit data + most/least significant data + data/control + parity) is an interface alternative already mentioned.

The display controller is designed in a modular way to meet different requirements by a combination of hardware and software capabilities. The random point plot generator provides the most basic and general display mode and is required for the implementation of any other display mode using modular mode generators. These are addressed by the interface mode control upon receipt of the corresponding mode selection character and data are transferred from the input buffer to the addressed generator via common (internal) 12 bit data bus - chosen to transfer either 10 bit or 2 x 6 bit data.

The fundamental point plot generator includes the 10 bit registers for x- and y-position, the x- and y-digital-to-analog converters and the unblank and erase control. The registers haveindependent input gates for the 5 most and least significant bits and can be incremented up and down for simple implementation of incremental and sequential plot mode. The 10 bit D/A-converters use a binary weighted ladder network with precision metal film resistors with the inputs switched either to ground potential or to a reference voltage of -10 V. The network output feeds an operational amplifier which supplies an analog output voltage of 0...1,5 V (1V is full screen deflection in x and y axis) and provides a maximum settling time of 2 µs (a much better performance than really is required).

Incremental as well as sequential plotting may be obtained by modular addition of rather simple control logic for interpretation of data. The increment generator receives 6 bit data with 4 bits specifying directly incrementing/decrementing the x/y-position registers and 2 bits unblanking or blanking. The timing is chosen 30 us/dot to be identical with the 5 bit random point mode. In sequential point plotting the x-position register is incremented automatically each time when data are transferred from the input buffer to the y-position register.

In isometric/map mode the selection of 10 bit data for z-presentation out of 20 bits in the input buffer is accomplished rather simple by serial transfer via the least significant bit bus line into the z-register and stopping this transfer after as many shifts as is specified by the 4 bit z-range information. This method avoids the complex gating array necessary for parallel selection. The y/x-format control specifies the counts (point/line) after which the x-position register is reset to zero and how often the corresponding x-overflow sets the y-register to a new position (number of lines). The often used logarithmic presentation of spectra is made available at very low cost by means of a simple logarithmic operational amplifier for the analog y-signal. Because this feature can be used also with sequential point plotting and in order to avoid another (z-) D/A-converter it is accepted that also line spacing in two-or four-spectra display is in logarithmic scale.

References

1. H. L. Gelernter, J. Birnbaum, M. Mikelsons, J. D. Russel, F. Cochrane, D. Groff, J. F. Schofield, D. A. Bromley, "An Advanced Computer-Based Nuclear Physics Data Acquisition System", Nuclear Instruments and Methods, 54 (1967), pp. 77 - 90.
2. R. Stotz, T. Cheek, "A Low-Cost Graphic Display for a Computer Time-Sharing Console", Technical Memorandum ESL-TM-316, July 1967, Electronic Systems Laboratory, Massachusetts Institute of Technology.
3. J. E. Ward, "Graphic Output Performance of the ARDS Terminal with the Tektronix Type 611 Storage Monitor", Projekt MAC Memorandum MAC-M-368, Electronic Systems Laboratory, Massachusetts Institute of Technology.
4. I. N. Hooton, G. C. Best, "Mean Rate Analysis of Multichannel Nuclear Data", Nuclear Instruments and Methods 56 (1967) pp. 284 - 288.

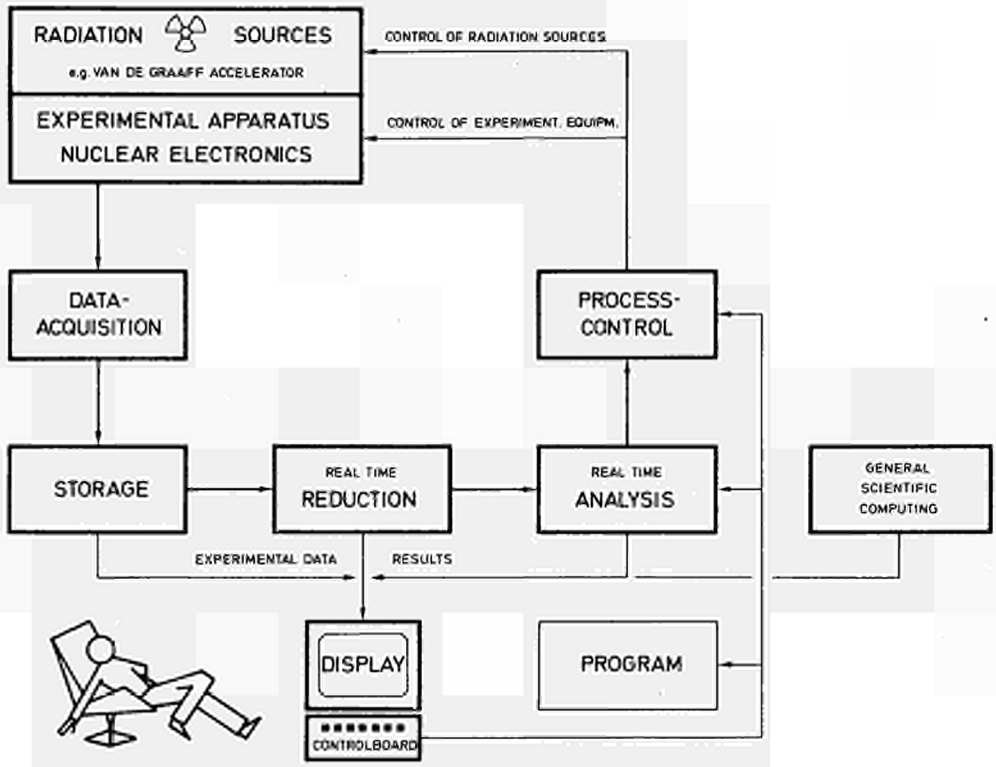

Fig. 1 - Functions of an on-line computer in low energy nuclear physics.

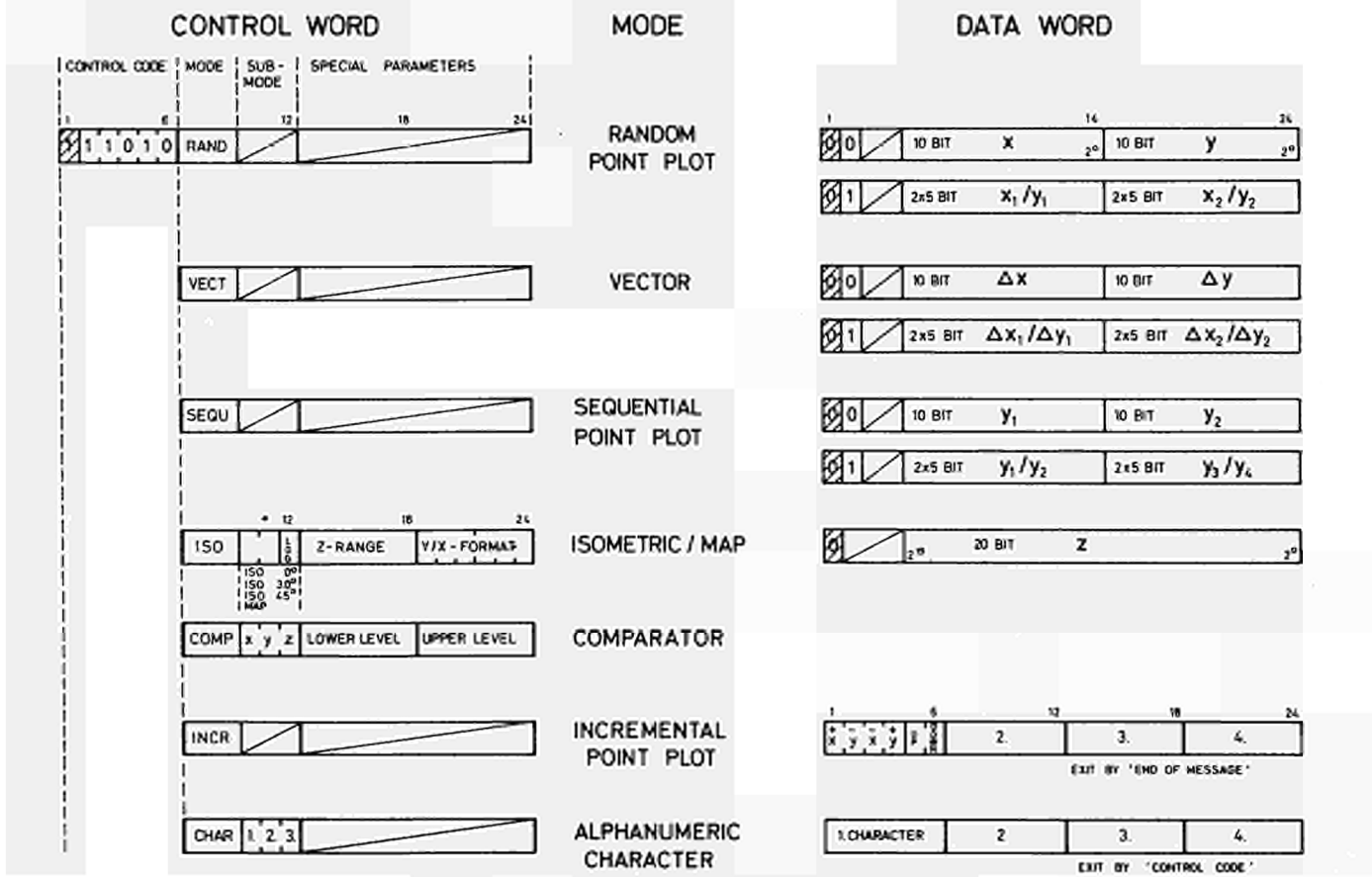

Fig. 2 Word formats in the display-file

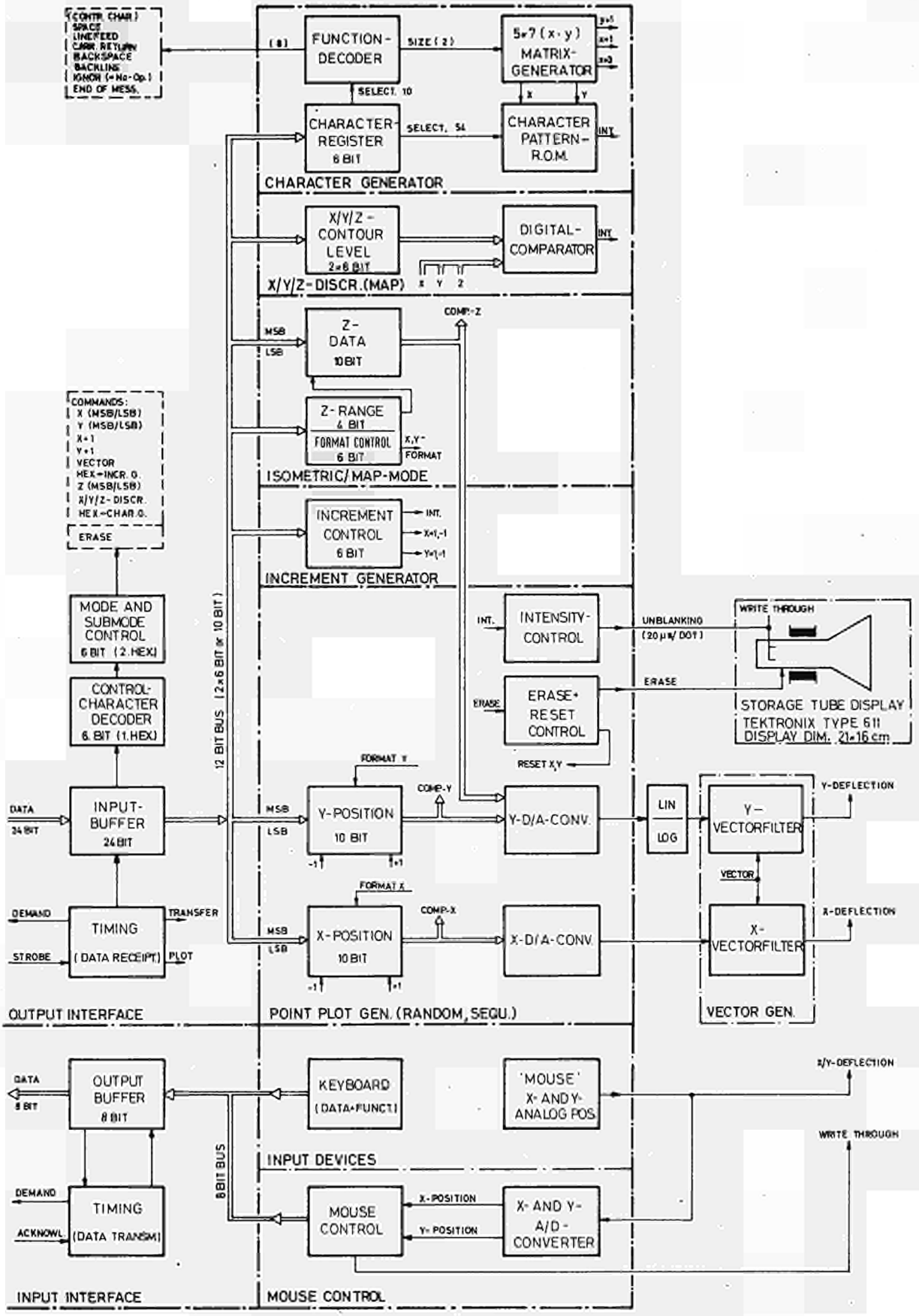

Fig. 3 Block diagram of the display terminal

COMPUTER CONTROLLED DATAWAY FOR NUCLEAR INFORMATIONS

J.F. Gilbert, J.J. Girod, J.L. Lecomte, M. Lesourne

Laboratoire d'Electronique et de Technologie de l'Informatique, C.E.A.-C.E.N.G. - Grenoble

At the Nuclear Research Center of Grenoble, a great number of block-memories such as computers, memory buffers of various sizes are used for different experiments in which the number of data to be stored is very important.

The experiments located at several kms are connected to the digital computing center by a data communication track managed by a CII 90.10 computer. This computer sends these informations to a 360.40 IBM computer.

The system is composed by a control unit and several terminal units connected by two coaxial cables or two telegraph pairs; in each of these units there is a modulator and a demodulator which realise the parallel-series or series-parallel transformation in high or low speed depending on the characteristics of the lines.

The maximum number of terminals is 15; each one can receive a maximum of 32 inputs or outputs of twelve bits. In the general case an experimenter uses 5 input-lines and 4 output-lines to connect a typewriter and several block memories. An input multiplexer device allows the collection of informations from one to 8 buffer-memories.

The data rate on the line in high speed mode (coaxial lines) is 1 M bauds for the "0" and 500 K bauds for the "1"; except for the control signals (word recognition bits, address bits, parity bits), the useful information transmission rate is 120 K bauds.

The intermediate computer CII 90.10 (memory of 8 K x 12 bits) scans the terminal units, receives the data when it detects a call, makes different controls on the transmission and sends these data to the IBM's auxiliary memories. To apply a process to the data the experimenter sends by the typewriter a call message and the needful features for this program. The results come back either onto the block memories displays or onto the typewriter or onto both of them.

Note:

Additional information can be found in the report LETI/MCTE/EG 525 of C.E.A.-C.E.N.G.

METHODS OF REDUCING THE NUMBER OF BINARY DIGITS REQUIRED TO CONVEY RANDOM COUNTING-RATE INFORMATION

by E. H. Cooke-Yarborough
Electronics & Applied Physics Division, A.E.R.E., Harwell, Berkshire, England

Summary

The digits resulting from counting random events can be encoded in ways which reduce the communication bandwidth required to transmit them to a remote point. A number of ways of doing this have already been reviewed; two further methods are now presented which appear to have significant advantages.

1. Introduction

Situations sometimes arise where it is necessary to count nuclear particles or photons, or other randomly-occurring events, at a remote location. At intervals the resultant count information is to be transmitted to some central point for recording and evaluation. Examples can occur in space research, in meteorology and in the routine monitoring of radioactivity in the area around a nuclear installation.

Often the transmitter power, and therefore the available bandwidth, is limited and it is desirable to avoid transmitting digits which carry little if any useful information. From this point of view, straight-forward binary counting of random events for a fixed time is inefficient. If, for example, the counting rate is near to the maximum which can be accepted, then the counting register is almost filled, and the less-significant half of the digits carries little information because of statistical uncertainties. If the counting rate is about the square root of the maximum which can be accepted, then the same applies to the least-significant quarter of the register digits, while the more-significant half of the register contains only 0's. Some methods of improving efficiency have been reviewed by Culhane and Nettleship[1]. Two further methods are described here which appear to have advantages over those already described.

The choice of the best method depends upon a number of factors, such as the range of counting rates which must be handled to a given accuracy, on whether or not the time available for counting is long enough to allow statistical uncertainties to be eliminated, etc. We shall consider the case where 8 bits are available for transmission and we aim to reduce the total errors to below 2% over a range of counting rates of 100:1 and below 1% over 10:1.

2. Quantizing Errors

It is important at the outset to distinguish between random errors due to the random occurrence of individual events and those due to the fact that we are performing a quantised measurement of an unknown counting rate. The latter error, which we call the quantizing error, will be present even if we know the pulses from our unknown source to be evenly spaced.

To consider this quantizing error it is convenient for the present to assume that our system is preceded by a prescaler with a very large scaling factor so that any randomness in the pulse source is effectively smoothed out. This arrangement also has the advantage that, provided the prescaler is set to 0 before counting commences, we know that a time just equal to the interval between pulses at the output of the prescaler will elapse before the first of these pulses occurs. The quantizing error which results from counting a number of these pulses within a given time is illustrated in Fig. 1. We see here two different pulse rates, both of which will register seven pulses within the counting time. The number of pulses which would truly represent the pulse rate lies anywhere between 7 and 8, and in the absence of other information, we can only assume that within these limits the probability distribution is rectangular. The mean square error is at a minimum if we take the number of pulses as most nearly representing the true pulse rate as $n + \frac{1}{2}$. There is a rectangular probability distribution of $\pm \frac{1}{2}$ about this value. The root mean square value of this error is $\frac{1}{2\sqrt{3}}$ or

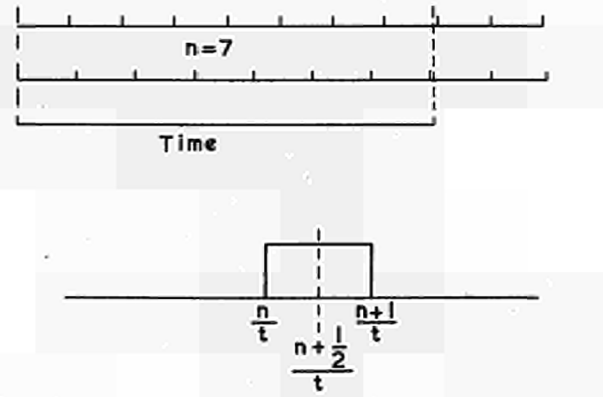

Fig. 1
Illustration of Quantizing Errors

0.288^{5}. Expressed as a fraction of the number of pulses it is $\frac{0.288}{n + \frac{1}{2}}$.

The quantising error of a scaler counting for a fixed time is thus inversely proportional to the number of pulses counted. The error for an 8-bit scaler is shown in Fig. 2. It will be

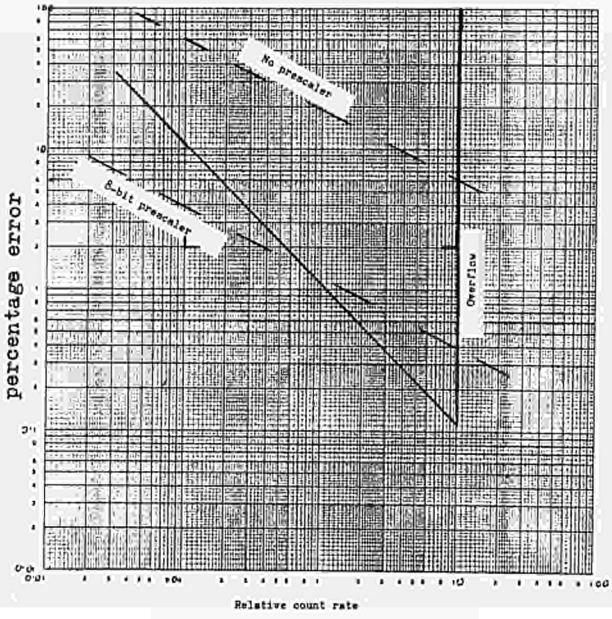

Fig. 2 Fixed Time Method

...

Solid line : Quantizing error
Broken line: Statistical error

seen that a prescaler is needed if statistical errors are not to predominate. Even if the prescaler is large enough to eliminate statistical uncertainties, this method is far from meeting our objective of an accuracy better than 2% over a 100:1 counting range. Moreover, the region where the highest accuracy is obtained is close to the overflow point, where the errors are, of course, large.

3. Fixed-Count Method

Another method often used is to measure the time L taken to register a fixed number of pulses N. Here, the counting period always ends on a count pulse, and in general this instant will lie between two time pulses. The relative counting rate is thus $N/(L + \frac{1}{2})$, and as before there is a rectangular probability distribution. In this case the quantising error is proportional to counting rate, as shown in Fig. 3. Apart from the fact that any statistical errors are now independent of counting rate, this method has disadvantages similar to the previous one, and again comes nowhere near meeting our objective.

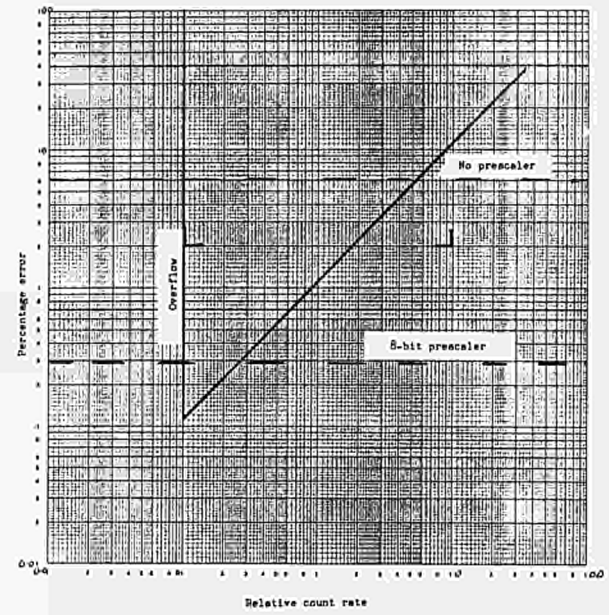

Fig. 3 Fixed Count Method

...

Solid line : Quantizing error
Broken line: Statistical error

4. Floating-Point Method

A better method[1] is to generate a number and exponent, again counting for a fixed time. Fig. 4 shows that this is superior to both of the previous methods, and, with an 8-bit prescaler, meets part of the objectives set out in the Introduction.

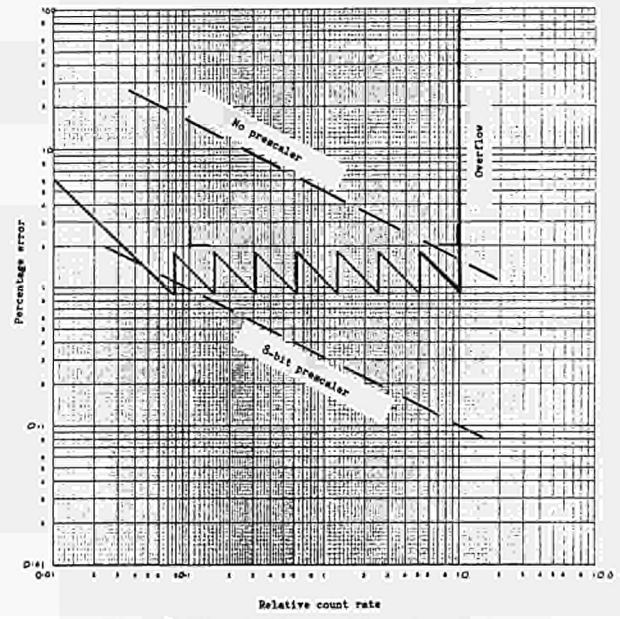

Fig. 4 Fixed Time: Floating Point
5 bits + 3 bits exponent

...

Solid line : Quantizing error
Broken line: Statistical error

It has two disadvantages; it overflows abruptly at the top of its range, and the logic system required to generate it is quite complex.

5. Square-Root Method

A computer programme has been described by Best[3] in which the number L appearing in a register is equal to the square root of the number of pulses counted, N. This is done by preceding the register with a tally, which is in effect a scaler which is set, after each carry into the register, to $-(2L + 1)$ so that its effective scaling factor is $(2L + 1)$ and rises as the count proceeds.[1] This is a special case of a programmed prescaler. To minimize the mean square quantizing error we take the total count N as $L^2 + L + \frac{1}{2}$. There is a rectangular error distribution about this value given by $\pm (L + \frac{1}{2})$, which to a good approximation lies between $\pm\sqrt{N}$. Thus the fractional r.m.s. quantizing error is $\pm 1/\sqrt{3N}$. This is plotted in Fig. 5.

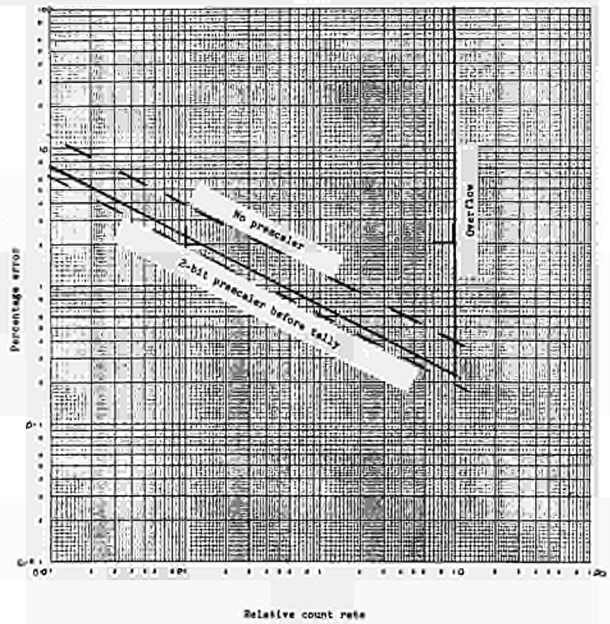

Fig. 5 Square-Root Counting for Fixed Time

...

Solid line: Quantizing error
Broken line: Statistical error

This method gives a substantially smaller quantizing error than the exponent method of Fig. 4 at the higher counting rates, and is quite easy to implement with hardware logic. In the present case the 8-bit register is preceded by a 9-bit tally scaler which accepts the input pulses. Each time this scaler generates a carry pulse, the contents L of the register are complemented into the 8 more significant digits of the tally scaler, whose least significant digit is simultaneously set to 1. Fig. 5 shows that if this tally scaler is preceded by a 2-bit prescaler, the r.m.s. statistical error is reduced to $1/\sqrt{4N}$ which is just less than the quantizing error at all counting rates. This arrangement almost meets our objectives.

6. Fixed Count or Time Method

All the methods described hitherto are subject to abrupt large errors when a register overflows. Overflow can be avoided if it is acceptable to cause the pulse counting time to be shortened automatically when the counting rate proves to be high.

A system which has been used in the U.S. space programme[1,2] is illustrated in Fig. 6.

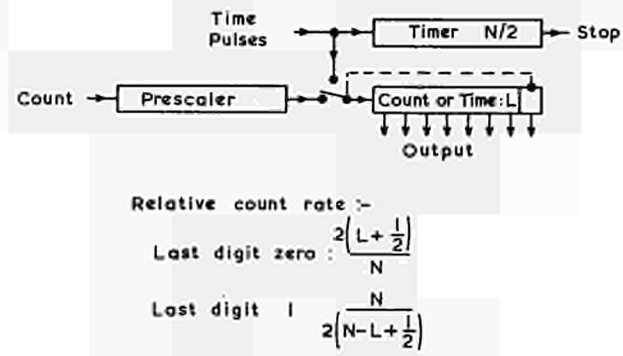

Fig. 6 Fixed Count or Time Method

This ingeniously combines the fixed time and fixed count methods. The scaler counts the output pulses from the prescaler in the normal way until there is a carry into the last digit position. At this point the input is switched from the prescaler to the time pulse source and time pulses are counted until the end of the counting period, determined by the timer. Thus, if the last digit is 0 the system operates as a fixed-time counting system in the normal way. If the last digit is a 1 then the register contains the number of time impulses which occurred after the carry into the last digit. Subtracting this number from the total number of timing pulses gives the time taken to count a fixed number of pulses, in this case 128. This yields the error curves shown in Fig. 7; as might be expected this is a combination of fixed time and fixed count curves, though the minimum error is greater by a factor 2, since the maximum number of count or time pulses counted is only 128. This method has the advantage of having no abrupt overflow and comes close to meeting our objectives.

7. Fixed Sum of Count Plus Time

The method just described can be improved by making use of a method described by the present author[4] in 1951. This method involved counting both time pulses and counts concurrently in the same register until a predetermined total was reached. The counting rate was deduced from the number of time pulses or counts which had occurred by the time the predetermined total was reached.

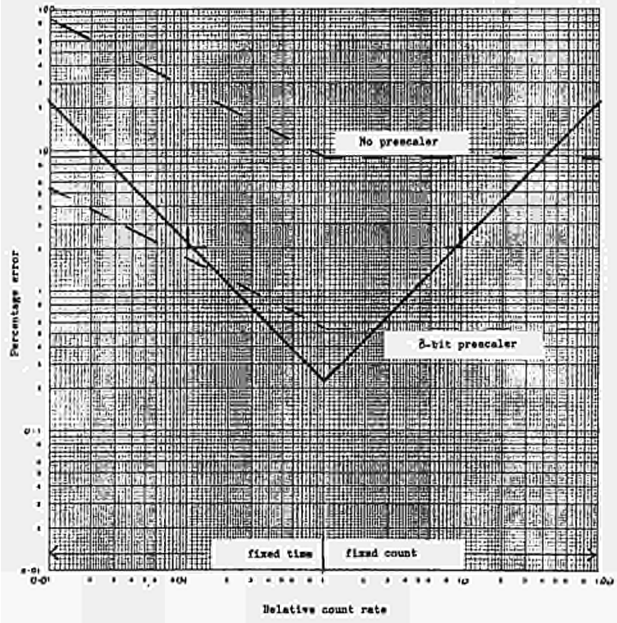

Fig. 7 Fixed Count or Time Method

• • •

Solid line: Quantizing error
Broken line: Statistical error

The method, illustrated in Fig. 8, can be applied by simple adaptation of the previous

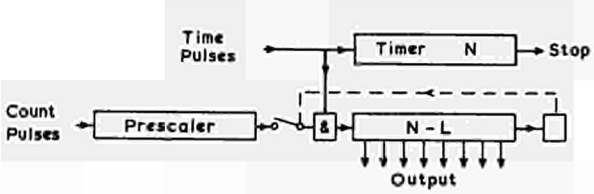

$$\text{Relative count rate} = \frac{N-L}{L}\left(1 + \frac{1}{2(N-L)} - \frac{1}{2(L+1)}\right)$$

Fig. 8 Fixed Sum of Count Plus Time

method (Fig. 6), the main difference being that instead of switching from input pulses to time pulses when the last digit goes to 1, both input pulses and time pulses are counted concurrently, until a carry from the last digit sets a bistable. This suppresses the input counts, leaving only time pulses to be counted for the remainder of the counting period. (There is no need to transmit the state of this bistable; there will always be enough time pulses to set it, even if no counts occur.)

At the end of the counting period the register will contain N - L, where L is the number of time pulses which had occurred when the total of time pulses plus counts was N. The nominal relative counting rate is (N - L)/L, but the quantizing errors are a little more difficult to determine. Input counting may terminate on either a time pulse or an input pulse. If it terminates on a time pulse, then there is a quantizing error of up to +1 in the numerator. If, however, the input counting ends on a count pulse, then there is an error of up to +1 in the denominator. The relative probabilities of these two kinds of error, and also the relative magnitudes, depend on the relative counting rate. The errors thus form two adjacent rectangular distributions. Calculations in the Appendix show that a slight modification to the Expression for the counting rate minimises the mean square value of these errors. This modification, which is significant only at high and low relative counting rates, is represented by the second and third terms in the brackets of the Expression in Fig. 8. The Expression for the resultant minimum error is calculated in the Appendix and the computed curve is given in Fig. 9. It will

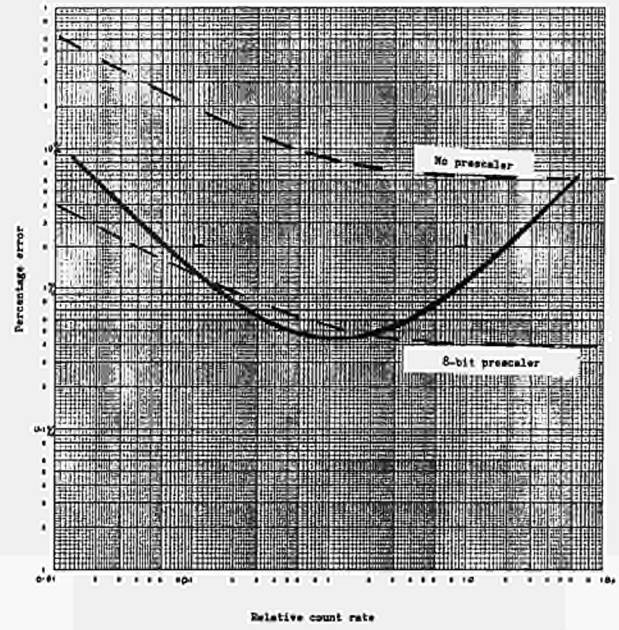

Fig. 9 Fixed Sum of Count Plus Time

• • •

Solid line : Quantizing error
Broken line: Statistical error

be seen that this method gives considerably lower quantizing errors at high and low counting rates than the method previously discussed, and that these errors are below 2% over the counting rate range of $2\frac{1}{2}$ decades and below 0.6% over one decade.

8. Conclusions

The present study has been confined to systems generating 8 bits of information. Within this limitation we can draw the following conclusions.

In situations where counting must proceed throughout a fixed counting period (for example, where the counts in several channels are to be compared and the source may be subject to fluctuation) the square root method has smaller errors than other methods described hitherto.

When the length of the pulse-counting period can be allowed to vary, and to differ between counting channels, and where the range of pulse rates to be counted covers more than a decade,

the fixed count + time method[4] has substantially lower errors than any other method which has been considered.

References

(1) J. L. CULHANE and R. NETTLESHIP; "Some methods for the compression of binary data in spacecraft experiments". I.E.E.E. Trans.Nuclear Science, Vol.NS 15, No.2, April 1968.

(2) J. B. ROGERSON; "The orbiting astronomical observatory". Space Science Reviews 2, pp. 621-652, 1963.

(3) G. C. BEST; "Square root display with a small computer". Nuc. Inst. & Methods, Vol.64 (1968), pp.171-172.

(4) E. H. COOKE-YARBOROUGH; "The counting of random pulses". J.Brit. I.R.E., Vol.11, No.9, Sept.1951, p.378.

(5) V. I. GOLDANSKII, A. V. KUTSENKO and M. I. PODGORETSKII; "Counting statistics of nuclear particles". Hindustan Publishing Corp., 1962, p.15.

APPENDIX

Calculation of Quantizing Errors for System Using Fixed Total of Count Plus Time

Total number of pulses counted = N.
Number of time pulses counted = L.
If counting is ended by a count pulse, relative counting rate lies between $\frac{N-L}{(L+1)}$ and $\frac{N-L}{L}$.
The probability of the count ending in this way is approximately $\frac{N-L}{N} = p$.
If counting is ended by a time pulse, relative counting rate lies between $\frac{N-L}{L}$ and $\frac{N-L+1}{L}$.
The probability of the count ending in this way is approximately $\frac{L}{N} = 1 - p$.
Suppose that the value of counting rate which gives least square error is $\frac{N-L}{L} - m$.
The width of the rectangular error distribution for count-terminated counting periods is $\frac{N-L}{L} - \frac{N-L}{(L+1)} = \frac{N-L}{L(L+1)} = b$.
The corresponding width for time-terminated counting periods is $\frac{N-L+1}{L} - \frac{N-L}{L} = \frac{1}{L} = c$
The mean square error is given by:-

$$p\int_{m-b}^{m}\frac{1}{b}x^2\,dx + (1-p)\int_{m}^{m+c}\frac{1}{c}y^2\,dy$$

$$= p\left[\frac{1}{3b}(m^3 - (m-b)^3)\right] + (1-p)\left[\frac{1}{3c}((m+c)^3 - m^3)\right]$$

$$= p\left[m^2 - bm + \frac{b^2}{3}\right] + (1-p)\left[m^2 + cm + \frac{c^2}{3}\right]$$

$$= m^2 + p(\tfrac{b^2}{3} - bm) + (1-p)(\tfrac{c^2}{3} + cm) \quad \ldots\ldots\ldots\ldots(1)$$

To find the value of m for least square uncertainty, differentiate this Expression with respect to m and equate to 0.

$$2m - pb + c - pc = 0$$

$$m = \frac{p(b+c) - c}{2} \quad \ldots\ldots\ldots\ldots\ldots\ldots\ldots\ldots(2)$$

Substitute(2)into(1)
Least square error

$$= \frac{p^2(b+c)^2}{4} - \frac{pc(b+c)}{2} + \frac{c^2}{4} + \frac{pc(b+c)}{2} - \frac{c^2}{2} + \frac{c^2}{3}$$

$$+ p\left[\frac{b^2}{3} - \frac{pb(b+c)}{2} + \frac{cb}{3} - \frac{c^2}{3} - \frac{pc(b+c)}{2} + \frac{c^2}{2}\right]$$

$$= \frac{p^2(b+c)^2}{4} + \frac{c^2}{12}$$

$$+ p\left[\frac{b^2}{3} - \frac{pb^2}{2} - \frac{pbc}{2} + \frac{bc}{2} - \frac{c^2}{3} - \frac{pbc}{2} - \frac{pc^2}{2} + \frac{c^2}{2}\right]$$

$$= \frac{p^2(b+c)^2}{4} + \frac{c^2}{12} - p^2\left[\frac{b^2}{2} + bc + \frac{c^2}{2}\right]$$

$$+ p\left[\frac{b^2}{3} + \frac{bc}{2} + \frac{c^2}{6}\right]$$

$$= p^2\left[\frac{b^2}{4} + \frac{bc}{2} + \frac{c^2}{4} - \frac{b^2}{2} - bc - \frac{c^2}{2}\right]$$

$$+ p\left[\frac{b^2}{3} + \frac{bc}{2} + \frac{c^2}{6}\right] + \frac{c^2}{12}$$

$$= \frac{c^2}{12} + p\left[\frac{b^2}{3} + \frac{bc}{2} + \frac{c^2}{6} - \frac{b^2}{4} - \frac{bc}{2} - \frac{c^2}{4}\right] \quad \ldots\ldots(3)$$

To obtain the least square error as a fraction of the square of the nominal counting rate, multiply Expression(3)by

$$\left(\frac{L}{N-L}\right)^2 = \frac{1}{(L+1)^2} \times \frac{1}{b^2}$$

The root mean square error is then

$$\frac{1}{L+1}\sqrt{\frac{c^2}{12b^2} + p\left[\frac{1}{3} + \frac{c}{2b} + \frac{c^2}{6b^2}\right] - p^2\left[\frac{1}{4} + \frac{c}{2b} + \frac{c^2}{4b^2}\right]} \quad \ldots\ldots(4)$$

now $\frac{c}{b} = \frac{L+1}{N-L}$ and $p = \frac{N-L}{N}$.

Substituting into the term in p^2 in Expression(4) yields:-

$$\frac{(N-L)^2}{N^2}\left[\frac{1}{4} + \frac{L+1}{2(N-L)} + \frac{(L+1)^2}{4(N-L)^2}\right]$$

$$= \frac{(N-L)^2}{N^2}\left[\frac{(N-L)^2 + 2(L+1)(N-L) + (L+1)^2}{4(N-L)^2}\right]$$

$$= \frac{(N-L)^2}{4N^2(N-L)^2}\,(N-L+L+1)^2.$$

For $N \gg 1$, this term $= \frac{1}{4}$.
Root mean square error (from Expression(4))

$$= \frac{1}{L+1}\sqrt{\frac{c^2}{6b^2}\left(\frac{1}{2} + p\right) + p\left(\frac{1}{3} + \frac{c}{2b}\right) - \frac{1}{4}}$$

$$= \frac{1}{L+1}\sqrt{\frac{(L+1)^2}{6(N-L)^2}\left(\frac{1}{2}+\frac{(N-L)}{N}\right)+\frac{N-L}{N}\left(\frac{1}{3}+\frac{(L+1)}{N-L}\right)-\frac{1}{4}} \quad \ldots\ldots\ldots\ldots\ldots\ldots\ldots\ldots\ldots\ldots\ldots\ldots (5)$$

From Expression(2)the counting rate, for least square error is taken as:-

$$\frac{N-L}{L} - \frac{p(b+c)-c}{2}$$

$$= \frac{N-L}{L} - \frac{N-L}{2N}\left(\frac{N-L}{L(L+1)}+\frac{1}{2}\right)+\frac{1}{2L} \quad .$$

$$= \frac{N-L}{L} - \frac{N-L}{2N}\left(\frac{N-L+L+1}{L(L+1)}\right)+\frac{1}{2L}$$

$$= \frac{N-L}{L} - \frac{(N-L)(N+1)}{2NL(L+1)}+\frac{1}{2L}$$

For $N >> 1$ this Expression approximates to:-

$$\frac{N-L}{L} - \frac{N-L}{2L(L+1)}+\frac{1}{2L}$$

$$= \frac{N-L}{L}\left(1+\frac{1}{2(N-L)}-\frac{1}{2(L+1)}\right) \quad \ldots\ldots\ldots (6)$$

In Fig. 9 the quantizing error derived from Expression(5)is plotted against the relative counting rate derived from Expression(6)for N = 256 and values of L from 5 to 251.

DISCUSSION

S.S. Klein: - Am I right in supposing that you need one extra bit for telling which kind of overflow occurred ?

Cooke-Yarborough: - There is no need to transmit the information that the register of Fig. 8 has overflowed, since it always overflows, due to the time pulses, even if there are no input pulses.

IMPROVEMENT OF SLIDING-SCALE ANALOG-TO-DIGITAL CONVERTERS THROUGH WEIGHTED AVERAGING(°)

E. Gatti — CISE Laboratories and Politecnico di Milano, Italy
P. F. Manfredi — CeSNEF Politecnico di Milano, Italy
V. Svelto — CISE Laboratories and Università dell'Aquila, Italy
P. Thieberger °° — Research Institute for Physics, Stockholm, Sweden and Tennelec Instrument Co., Oak Ridge, Tenn., USA

Abstract

Several figures of merit for characterizing an analog-to-digital converter are considered. It is shown that the sliding scale method of improving through averaging the performance of a converter can be made more effective by introducing variable statistical weights in the averaging procedure. It is found that a parabolic weighting function is the optimum for the differential linearity, if the channel boundaries are independently random distributed with equal variance. Moreover it is shown, through a computer simulation, that this weighting function is more convenient than a rectangular one to improve also a local differential linearity, while it is equivalent as far as correction of channel centroid errors is concerned. A triangular weighing function is found to be slightly worse than the parabolic one as far as overall differential linearity is concerned but somewhat better from the point of view of local behaviour.

Introduction

In a previous paper[1] the error introduced by a multichannel pulse height analyzer in the measurement of an amplitude probability-density function f(v) has been calculated adopting a linear approximation of f(v) in the neighbourhood of the examined channel.

Assuming that the first derivative of f(v) changes in a negligible way within one channel width, the following expression has been obtained for the difference ε_K between the number of counts stored in the K-th channel of the actual analyzer and the number of counts stored in the K-th channel of a suitably chosen reference instrument:

$$\varepsilon_K = f(KL+b)(L_K - L) + \left.\frac{df}{dv}\right|_{v=KL+b} \cdot L_K \cdot (x_K - KL - b) \qquad (1)$$

In eq. (1) L_K represents the channel width of the K-th channel and x_K its centroid position in the actual analyzer, while L and KL+b are the same parameters of the reference analyzer. The meaning of the introduced parameters is clarified in fig. 1, where a particular behaviour of both channel width L_K and centroid position x_K is plotted against the channel number k.

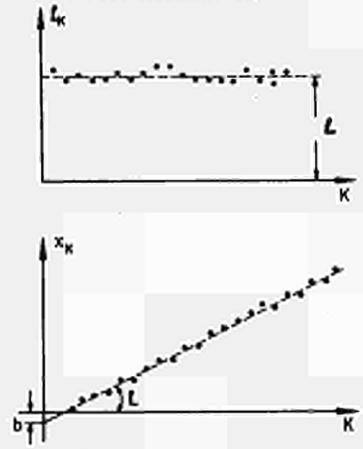

Fig. 1. Qualitative behaviour of channel width and centroid L_K and x_K versus channel number K, shown to define the reference values L and b.

The parameter L of the reference analyzer can be defined as the average value of L_K which corresponds to the value of L which minimizes the mean square error $\frac{1}{N}\sum_{1}^{N}{}_{K}(L_K - L)^2$.

b is the intersection on the vertical axis of the straight line with slope L which fits according to the criterion of least square-error the actual values of x_k.

Once L and b are defined, the ideal reference analyzer can be thought of as a system with constant channel width, equal to L, where b gives the value of the shift in the channel position of the reference analyzer for a best fitting of the instrument under test.

It should be noted that ε_K depends not only on the defined parameters, but also on the shape of the input spectrum f(v) and more precisely on the value of its relative slope. Therefore, the choice of L and b which minimizes the total mean square error $\frac{1}{N}\sum_{1}^{N}{}_{K}\varepsilon_K^2$ would require the knowledge of f(v). For this reason we have adopted a definition of L and b,

(°) Work partially supported by the Contract CISE-CNR N. 115. 1402. 01628
°° On leave of absence from Brookhaven National Laboratory, Upton, N. Y., USA.

independent of f(v), which minimizes the separate terms $\sum_{1}^{N}{}_{K} (L_K - L)^2$ and $\sum_{1}^{N}{}_{K} (x_K - kL - b)^2$ deduced from (1).

Moreover, it should be observed that the errors on the measurement of f(v) are also related to the functional dependence of both $L_K - L$ and $x_K - kL - b$ with K. As a matter of fact, if a limited number of channels is involved in the measurement of f(v), it is important that L_K be constant within the involved group even if its value is different from L. As a figure for evaluating this local behaviour, we can consider the difference between the channel widths of two contiguous channels, $L_K - L_{K-1}$.

The sliding-scale method through the averaging performed on M+1 continuous channels allows the lowering of both channel width and centroid-position inaccuracies, as thoroughly examined in[1].

The width of the generic channel K, after the averaging operation in which every channel i ($0 \leq i \leq M$) is involved with probability R(i) is given by:

$$L_{K,M} = \sum_{0}^{M}{}_{i} R(i)\, L_{K+i} \qquad (2)$$

In this equation, which in fact is intuitive, R(i) is a not yet defined weighting function. Previously this equation had been written for the case of R(i) independent of i (eq. 10 ref. [1]) and also in practical applications of the sliding scale method R(i) has so far always been a constant. It is our purpose to investigate the improvements of the sliding scale method which can be expected from a suitable choice of the function R(i).

Also the obtained correction of the centroid positions has to be considered. Indicating with Q_i the analog increment which is added to the input signal when the instrument is considered in the state i, and which allows the classification of the same input amplitude in different positions, (ideally $Q_i = i \cdot l$) we have:

$$x_{K,M} = \frac{1}{L_{K,M}} \cdot \sum_{0}^{M}{}_{i} R(i) \cdot L_{K+i} \cdot (x_{K+i} - Q_i) \qquad (3)$$

Criteria for choosing the weighting function

For an uncorrected analyzer with known statistical properties of the set of L_K, x_K, for a fixed number M+1 of channels on which the averaging is performed, and for Q_i with assigned statistical properties, the weight distribution function R(i) can be determined in a way such as to optimize the corrected instrument with respect to a desired feature.

It is obvious that a distribution R(i) which corresponds to a smooth change of weight with i will give rise to a more uniform local behaviour of both channel widths $L_{K,M}$ and centroid positions $x_{K,M}$ with respect to a distribution R(i) which varies more sharply with i. So from this viewpoint a distribution R(i) with a triangular profile, for example, is more suitable than a distribution with rectangular profile which changes abruptly from full weight to zero at the boundaries of the averaging range.

A first criterion for the choice of R(i) could be based on the minimization of the mean square channel-width error, that is, of the function:

$$\beta_M^2 = \frac{1}{N} \sum_{1}^{N}{}_{K} (L_{K,M} - L_M)^2 \qquad (4)$$

An alternative choice could be based on the minimization of the mean square centroid position error, that is, of the function:

$$\eta_M^2 = \frac{1}{N} \cdot \sum_{1}^{N}{}_{K} (x_K - kL_M - b_M)^2 \qquad (5)$$

Finally, R(i) could be chosen so as to optimize the mean square local channel width uniformity. This requires the optimization of the function:

$$\gamma_M^2 = \frac{1}{N} \sum_{2}^{N}{}_{K} (L_{K,M} - L_{K-1,M})^2 \qquad (6)$$

In some cases, it is useful to consider not only the mean square deviations defined by (4), (5) and (6), but also the corresponding maximum deviations which we can define as:

$$\beta_{M,\max} = (L_{K,M} - L_M)_{\max} \qquad (4')$$

$$\eta_{M,\max} = (x_K - kL_M - b_M)_{\max} \qquad (5')$$

$$\gamma_{M,\max} = (L_{K,M} - L_{K-1,M})_{\max} \qquad (6')$$

Whatever criterion is chosen to optimize the function R(i), the knowledge of the statistical properties of the uncorrected analyzer is required.

Results

As a first example the function R(i) which minimizes the mean square channel-width error (4) has been obtained in the appendix. The starting point was the assumed knowledge of the variances and covariances of the boundaries S_K which define the channel width according to:

$L_K = S_{K+1} - S_K$.

In the examined case (case A) the following expression is chosen for S_K:

$$S_K = K + \sigma_K$$

where σ_K's are considered independent, identically distributed random variables with zero mean value and variance independent of K.

We deal mainly with this case because it is normally the most important one, and because it offers the possibility of obtaining a simple mathematical form for the optimum R(i), which is given by the quadratic law:

$$R_{opt}(i) = \frac{6}{M^2+5M+6}\left(-\frac{i^2}{M+1} + i\frac{M}{M+1} + 1\right) \qquad (7)$$

$0 \leq i \leq M$

We must, nevertheless, point out, that the sliding-scale method is usually applied to converters of the successive approximation type, for which the channel width is not defined by two independent thresholds. However, as the comparison operations are always affected by the presence of switching transients and stochastic noise, uncorrelatad components in the boundaries of the channels are present; therefore the obtained results give useful indications also in this case.

We have also considered the case in which the channel boundaries are defined by binary weights, their errors being thought independent and characterized by a constant relative variance (case B). In this case the σ_K's are not independent, and their covariance $q_{K,r} = \overline{\sigma_K \cdot \sigma_r}$ are easily calculated. Under such circumstances the optimum function R(i) has not been explicitely deduced. Instead, the influence of these errors on an instrument which is optimized for type A errors has been calculated. The same procedure has been followed in a third case, in which the errors on the channel boundaries of a successive approximation converter with ideal binary weights are due to the leakage discharge of the storage capacitor in the input stretcher, as pointed out by Hrisoho[2] (case C).

The above mentioned cases A, B and C were simulated on a digital computer. Their behaviour was compared for three different distributions R(i):

$R(i) = \frac{1}{M+1}$ $\quad 0 \leq i \leq M$ (rectangular distribution) (8)

$R(i) = \frac{4}{M^2-1} i$ $\quad 0 \leq i \leq \frac{M}{2}$ $\quad$ M odd (9)

$R(i) = \frac{4}{M^2-1}(M-i)$ $\quad \frac{M}{2} < i \leq M$ (triangular distribution)

$R(i) = R_{opt}(i)$ (quadratic distribution given by (7)) (10)

For the three cases A, B and C the values of the thresholds S_K and the analog increments Q_i have been randomly drawn. Starting from these data for the uncorrected converter, which is assumed to have 256 channels, the distribution of both channel width and centroid position has been calculated as a function of $K (1 \leq K \leq 256)$ for the above quoted expression of R(i) and for the following values of M: 0, 15, 31, 63, 127, 255, the averaging being performed over M+1 channels. For each of these cases, the values of β_M and η_K as given by (4) and (5) were calculated.

In figs. 2A and 3A $\frac{\beta_M}{\beta_0}$ and $\frac{\eta_M^2}{\eta_0^2}$ are represented as functions of M for a multidiscriminator encoder (case A). They are both normalized to the corresponding values for the uncorrected converter. The three curves of each figure correspond to the three assumed distributions of R(i) as given by (8), (9) and (10). In this situation the quadratic law corresponds to the theoretical optimum for the channel width accuracy.

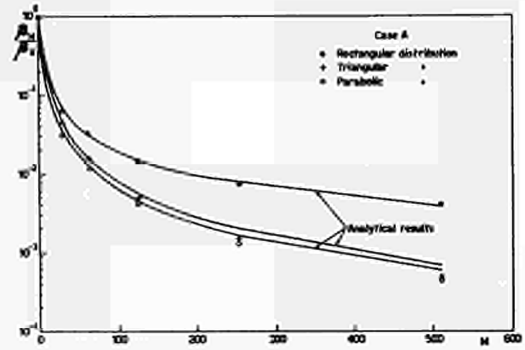

Fig. 2A. Channel width error β_M normalized to the value for the uncorrected converter β_0 as a function of M(M+1)is the number of channels over which the weighted average is performed) for a multidiscriminator converter (case A). The points are the results of a computer simulation with the three types of R(i) considered. The continuous curves represent the analytical results given in Table I.

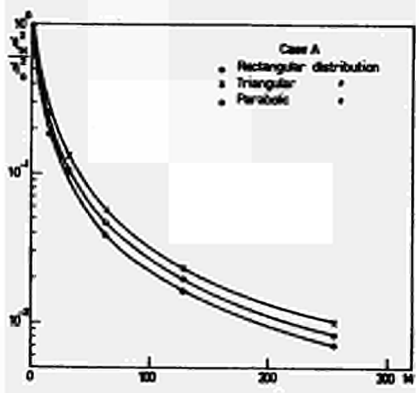

Fig. 3A. Normalized centroid squared error η_M^2/η_0^2 for the multidiscriminator converter (Case A) averaged with the three assumed distributions.

For each R(i), as it may be seen from the given plots, both channel width and centroid position inaccuracies decrease quickly as M is increased. The quadratic distribution, of course, gives the best result from the point of view of channel width uniformity; however, the behaviour of the triangular distribution is near the optimum one for high values of M.

In fig. 2A the continuous curve gives the analytic dependence of the channel width inaccuracy on M, while the points correspond to the result obtained from the simulation on the computer.

A good agreement has been obtained from the two different procedures, even if the points obtained through the computer simulation are related to one particular random drawing of the statistical parameters of the problem. In this case, also the analytical expression for (4) has been evaluated for the different distributions of R ; the results are collected in Table 1.

According to the results of fig. 3A, we see that the rectangular distribution gives the best performance from the point of view of the centroid position inaccuracy, although the correcting behaviour is not very different for the examined distributions. This fact suggests one when looking for optimum R(i) distributions, not to attach importance to the constraint due to eq. (5).

Figs. 2B and 3B show the same normalized errors β_M/β_0 and η_M^2/η_0^2 as in case A, for a successive approximation converter using binary weights (case B).

TABLE I

R(i)	Rect. Distr.	Triang. Distr. (M odd >1)	Parab. Distr.
$\frac{\beta_M^2}{\beta_0^2}$	$\frac{1}{(M+1)^2}$	$\frac{8}{(M+1)^2(M-1)}$	$\frac{6}{M+1}$ $\frac{1}{M^2+5M+6}$

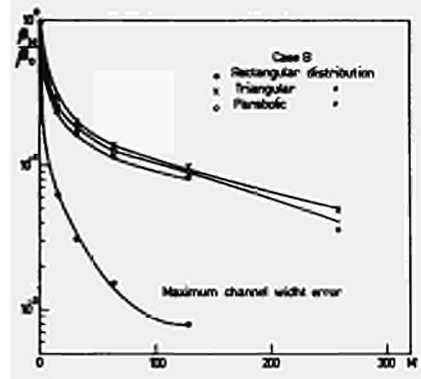

Fig. 2B. Normalized channel width for successive approximation converter (case B). The maximum relative error in channel widths has been also reported for R(i) rectangular.

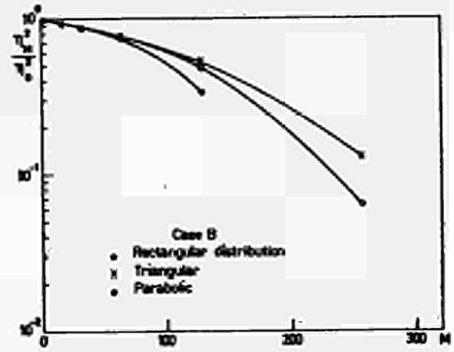

Fig. 3B. Normalized squared centroid error for case B.

The difference between the results corresponding to the three assumed distributions R(i) are rather small, a slight advantage being observed for the rectangular one. In this case, the point corresponding in the diagrams to the value M=255 has been omitted as, owing to the average performed over all the channels with equal weights, the errors drop to zero.

It should be realized that a definition of the quality of the converter based upon the parameters β_M and η_M^2, while certainly useful in case A, is not completely meaningful for converters of type B. To explain this point, let us examine the distribution of both channel width and centroid position inaccuracies, as functions of K for different values of M (fig. 4).

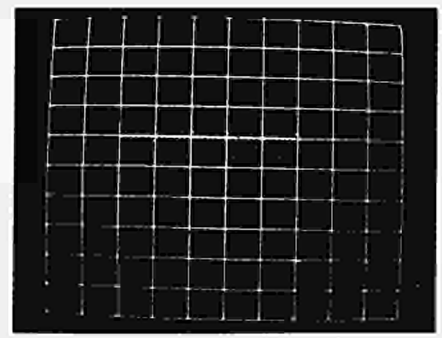

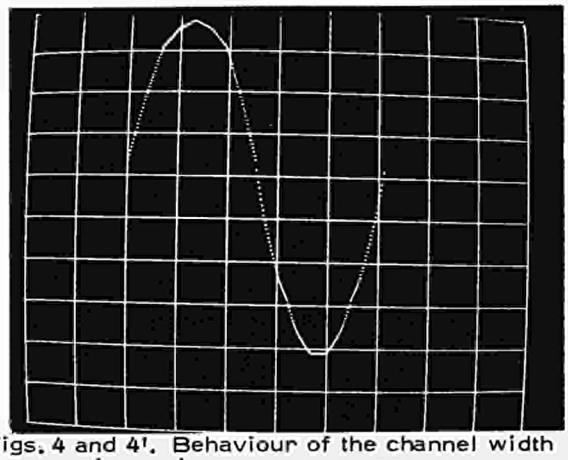

Figs. 4 and 4'. Behaviour of the channel width error $\frac{L_{K,M} - L_M}{L_M}$ for two different values of M(M=0, 127) for a successive approximation converter with R(i) parabolic. The vertical scale is different in the two pictures, being respectively $5.\,10^{-2}$ and $5.\,10^{-4}$ per division.

Tne uncorrected converter (M=0) shows a high channel width error restricted to a few channels; therefore, a parameter like β_0 which takes into account all the channels may be misleading. If we define the performance of the converter from the point of view of the channel width uniformity according to a different figure, for example, according to $\beta_{M,max}$ (eq. 4') a very sharp reduction of it is observed increasing M, as shown in fig. 2B.

The averaging effect on the converter not only reduces both channels width and centroid position inaccuracies, but also introduces a regularization in their dependence on K. For instance, the differences $L_{K,M} - L_M$ and $x_{K,M} - KL_M - b$ as obtained from the computer simulation, are plotted for two different values of M: M=0 and M=127 (figs. 4 and 4'; 5 and 5'). The errors depend on K in a more continuous way for M=127; this improves the local features of the converter, drastically reducing the value of γ_M^2 defined by eq. (6).

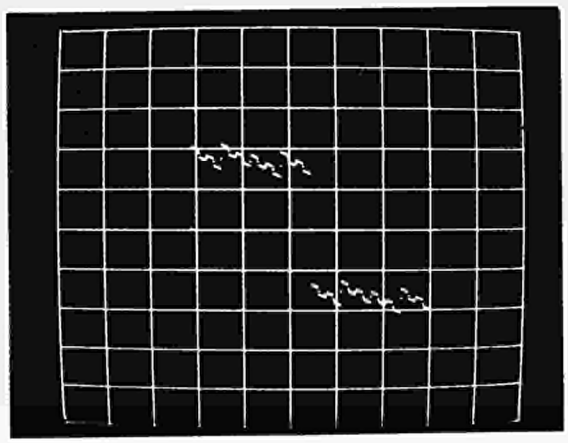

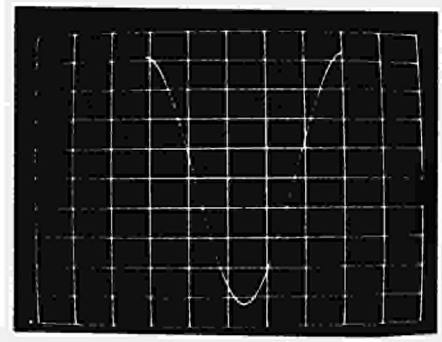

Figs. 5 and 5'. Behaviour of the centroid error $KL+b-x_K$ for the same channel threshold distribution and M values of fig. 4. Vertical axis $5.\,10^{-2}$ and $2.\,10^{-2}$ per division.

For the sake of simplicity, we don't show the curves similar to those of figs. 2 and 3 in the case of type C errors in the channel boundaries (errors due to the leakage discharge of the storage capacitor in a successive approximation converter with ideal binary weights); we have seen that these errors diminish, as M is increased, more quickly that in the case A of a multidiscriminator encoder.

For case A, the distribution R(i) which minimizes the error γ_M^2 given by (6) has been deduced. It has been found to be a fourth-order polynomial in the variable i. However, we do not develope this case, because, as is apparent from figs. 4' and 5', both a triangular or a quadratic R(i), thanks to their continuous behaviour, give good results as far as this parameter is concerned, while a rectangular distribution is definitely worse.

Another simple way of obtaining a quantitative indication of the relative merit of the functions R(i) with respect to local behaviour is to consider the quantity $\gamma_{M,max}$ (eq. 6'). Let us further assume that in the region over which averaging is performed, there is only one channel widly different from the others which are approximately equal. This is a situation characteristic of successive approximation converters (see, e.g., fig. 4). If the channel in question is the one which differs most from its neighbours, and if this difference is ΔL, then obviously we have for the uncorrected converter:

$$\gamma_{0,max} = \Delta L$$

As can easily be seen from (2) and (6') with the above assumptions the corresponding values after averaging will be:

$$\gamma_{M,max} = \gamma_{0,max} \left[R(i)-R(i-1)\right]_{max}$$

The correction factors $r = \left[R(i)-R(i-1)\right]_{max}$ obtained from (8), (9) and (7) are respectively:

$$r_1 = \frac{1}{M+1}$$ (rectangular distribution)

$$r_2 = \frac{4}{M^2-1}$$ (triangular distribution)

$$r_3 = \frac{6}{M^2+5M+6} \quad \frac{M-1}{M+1}$$ (quadratic distribution)

So for instance for M=127

$r_1 = 7.9 \times 10^{-3}$, $r_2 = 2.5 \times 10^{-4}$, $r_3 = 3.5 \times 10^{-4}$.

Conclusion

A real successive approximation converter will present all the previously examined kinds of errors. Taking into account both channel width and centroid-position inaccuracies as well as the regularity of their dependence on K, to which the local features of the converter are related, we conclude that a quadratic or a triangular shape of R(i) represent a better choice than a rectangular one if the averaging, as usually happens, does not involve all the channels. The quadratic function is somewhat better than the triangular one from the point of view of over-all differential linearity and channel centroid positions. The triangular distribution seems to be slightly superior as far as local behaviour is concerned and will often be easier to realize in practical applications.

Acknowledgement

One of us (P. Thieberger) gratefully acknowledges stimulating discussions with Angel Ferrari about the concept of weighted averaging and about the design of a converter with triangular distribution function.

Appendix

The width of the K channel, averaged over M+1 positions is given by:

$$L_{K,M} = \sum_{0}^{M}{}_i L_{K+i} R(i) = \sum_{0}^{M}{}_i R(i)\left[S_{K+i} - S_{K+i-1}\right] = 1 + \sum_{0}^{M}{}_i R(i)\left[\sigma_{K+i} - \sigma_{K+i-1}\right] \quad (1A)$$

where we have taken into account for the channel boundary $S_{K+i} = K + i + \sigma_{K+i}$ and for the normalisation condition $\sum_{0}^{M}{}_i R(i) = 1$

We define the mean square error in the channel widths as:

$$\beta_M^2 = \frac{1}{N}\sum_{1}^{N}{}_K \left(L_{K,M} - 1\right)^2 \quad (2A)$$

In expression (2A) we have approximated eq. (4) of the text by putting $L_M = 1$.

We must minimize (2A), taking into account (1A) and the normalization condition, with respect to R(i). If we consider σ_{K+i} as uncorrelated random variables with zero mean value and with constant variance, that is:

$$\overline{\sigma_l \cdot \sigma_r} = \beta_o^2 \delta_{lr}$$

being $\delta_{lr} = 1$ for $l = r$, $\delta_{lr} = 0$ for $l \neq r$ we obtain, after an ensemble average and few algebraic manipulations, the following difference equation for R(i):

$$2R(i) - R(i+1) - R(i-1) = K \quad (3A)$$

being K a constant given by the normalization condition. The normalization solution of (3A) is given by eq. (7) of the text.

References

1 E. Gatti, P. F. Manfredi and V. Svelto: "Some remarks about the sliding scale for analog to digital converters". Nuclear Electronics (Versailles, September 1968).

2. A. Hrisoho: " Etude théorique de la distributions des erreurs d'un convertisseur à composition de poids. Consequences pratiques. Conversion de precision. Conversion très rapide". Nuclear Electronics (Versailles, September 1968).

DISCUSSION

Chase : - Have you worked out some simple mechanism for realizing triangular or parabolic weighting distribution that are not much more complicated than that required for a linear weighting distributions ?

Svelto : - *Yes, we have thought of that : we have not realized everything but I think that it is possible, for instance, if you use a pseudo-random sequence generator to obtain the digital number to which associate the displacement of the analog scale, you can group very easily different digital numbers to which associate the same displacement according to a triangular or a parabolic law. It must be very simple to realize this way, so there must be some advantage and probably no much complexity.*

Battista : - *Have you tried any other kind of weighting functions like a staircase or a sine function ?*

Svelto : - *No, if I got the question, we tried only the three mentioned weighting functions : the parabolic one because it results to be the optimum for multidiscriminator type errors, the triangular as a good approximation to the parabolic one and the rectangular as the simplest.*

Battista : - *My question was because staircase function could be a good compromise between a triangular and a rectangular function.*

Svelto : - *I think that a staircase distribution has the disadvantage (as the rectangular distribution) to have discontinuities which reflect in a worsening of the smoothing properties which are peculiar of the continuous weighting functions.*

S. S. Klein : - *Have you thought of using a conversion from a suitable noise voltage, or something like, to determine the weight function after its conversion ? Maybe you would get a gaussian function from that way and this would generate an even better equalization than the parabola.*

Svelto : - *It can be a good suggestion.*

Gatti : - *We definitely know that the parabolic distribution is the best one under the hypothesis of independent equal standard errors in the channel boundaries as this result has been obtained by an optimization variational method.*

OPTIMUM STATISTICAL EQUALIZATION IN CONTROLLED ANALOG TO DIGITAL CONVERTERS

N. Abbattista, B. Marangelli, D. Marino, V.L. Plantamura

Istituto di Fisica, Bari, - Italy

As known, the statistical equalization of the channel width of the analog to digital converters enables to overcome the intrinsic limitations of such a system. In particular this method is strictly necessary for converters which work on the successive binary approximation technique, while, for Wilkinson converters, the equalization can be useful when it is also required a (statistical) reduction of the analysis time (1).

We remind that the equalization relates the width of a channel to the width weighted mean of a number of prefixed channels, whose weights may be either equal as in the "sliding scale" method (2) or not uniform as in "prediction" method (1). Considering the first method, a theoretical analysis has been carried out on the converter performance vs. the channel number on which the equalization is performed.

In this work the behaviour of a system with a second type equalization, as the weight law is varied, is being studied by simulation on a digital computer and experimentally by means of a particular successive binary approximation cyclic converter (3).

Briefly, in this converter the input signal is compared with a single level; the difference, if positive, is amplified by the factor two and compared again with the level, otherwise the signal itself is amplified by the factor two and compared again with the reference level. In every cycle, according to the difference sign, "0", or "1" bits are written in the output register; evidently the channel number of the converter is 2^N where N is the number of the cycles carried out.

The equalization is obtained realizing the conversion in two phases: in the first phase the converter runs for a certain number of cycles to give the most significant bits of the input signal conversion (prediction phase); in the second phase the same converter is used to operate the conversion of the difference between the input signal amplitude and the digital to analog conversion of the output register contents. The equalization is achieved setting (in the first phase) at random the less significant bits.

This type of converter allows, easily varying the bit number of the prediction, to obtain the required width weights law. Therefore a small on-line computer (like a PDP-8 computer) will be sufficient to optimize the equalization according to certain prefixed criteria, i.e.:

- to minimize the number of different channels which contribute to determine the width of a certain channel having established the number of channels on which one wants to make its average.
- to match the equalization to the particular signal spectrum while it is being stored, etc.

Finally, we think that the computer is necessary only in the present analysis phase, while a final set-up of the system might be a multichannel analyzer with a stored program.

REFERENCES

1) N. Abbattista, M. Coli, V.L. Plantamura, Nucl. Instr. Meth. 59 (1968) 163-166
2) C. Cottini, E. Gatti, V. Svelto, Nucl. Instr. Meth. 24 (1963) 241
3) N. Abbattista, M. Coli, V.L. Plantamura, Comunicazione 7B7,LII Congresso S.I.F., Bollettino S.I.F. 50 (1966) 43

STATISTICAL ERRORS OF DIRECT PULSE RATE RATIO MEASUREMENT

M. Konrad
Institute "Rudjer Bošković", Zagreb, Yugoslavia

Some digital and analog methods for direct rate ratio measurement of random pulses are considered and compared with respect to their figure of merit. It is shown that for completely random pulses the considered methods have the same figure of merit excluding the bistable method, whose figure of merit is smaller by a factor of 2. The analog method is given, whose realization is not so simple as that of the bistable method, but its figure of merit is the same as for other methods.

1. Introduction

The characteristics of some processes are directly related to the rate ratio of two random pulse sources. The rate ratio measurements can be used to determine changes in nuclear spectrometer systems, amplitude-to-digital converters etc. In most cases the rate ratios near 1 are of interest. Sometimes the origin of random pulses whose rate ratio is measured is the same source whose rate is time dependent. Then it is convenient to have a direct ratio reading independent of the absolute rate of the source.

The rate ratio is defined with

$$\bar{r} = \frac{\bar{n}_1}{\bar{n}_2} \tag{1.1}$$

where $\bar{n}_1$ is the average rate or source 1 and $\bar{n}_2$ of source 2. Since the processes are random, the measured rates n_1 and n_2 depart from their average values for Δn_1 and Δn_2. The measured rate ratio is then

$$r = \bar{r} + \Delta r = \frac{n_1}{n_2} = \frac{\bar{n}_1+\Delta n_1}{\bar{n}_2+\Delta n_2} =$$

$$= \bar{r}(1+\Delta' n_1)(1-\Delta' n_2+\Delta' n_2^2-\ldots) \tag{1.2}$$

where $\Delta' n_1 = \Delta n_1/\bar{n}_1$ and $\Delta' n_2 = \Delta n_2/\bar{n}_2$ are the relative rate measurement errors. The average value of the measured rate ratio (1.2) is not exactly equal to $\bar{r}$. If n_1 and n_2 are statistically independent it follows that the average value of the measured ratio is

$$(\bar{r}) = \bar{r}\left(1 + \left(\frac{\overline{\Delta' n_2^2}}{1+\Delta' n_2}\right)\right) \doteq \bar{r}(1+\overline{\Delta' n_2^2}) \tag{1.3}$$

Since the variance of the relative ratio error is

$$\overline{\Delta' r^2} = \frac{\overline{\Delta r^2}}{\bar{r}^2} = \overline{\Delta' n_1^2} + \overline{\Delta' n_2^2} \tag{1.4}$$

the difference will be negligible for a reasonable standard deviation $\sigma = (\Delta' r^2)^{1/2}$, so that $(\bar{r})$ can be replaced by $\bar{r}$.

The only information, concerning the rate of a random process are randomly occurring events. A rate measurement with a small expected error can be made only if the determination is made from a sufficiently large number of occurred events N_i, or what is equivalent, the measurement is performed over a sufficiently long time interval T. The measured rate is the ratio

$$n_i = \frac{N_i}{T} \tag{1.5}$$

The variance of the relative rate error is

$$\overline{\Delta' n_i^2} = \frac{k}{\bar{N}_i} = \frac{k}{\bar{n}_i \cdot T} \tag{1.6}$$

where k=1 for completely random occurring events (Poisson distribution) and k=1-p for events which can occurr only at clock times with a probability p (binomial distribution). The latter is the case when the primary source is a periodic pulse generator.

From (1.4) and (1.6) follows that the product of the relative error variance and the measurement time is a constant for a given system. Its reciprocal value

$$M = \frac{1}{\overline{\Delta' r^2} \cdot T} \tag{1.7}$$

can thus be used for comparison of different rate ratio measurement methods, and is their figure of merit. A higher figure of merit indicates that for the same measurement time the error variance is smaller, i.e. that the method is better. For analog methods whose response is exponential with time constant τ, the measurement time is taken somewhat arbitrarily to be equal to two time constant i.e.

$$M = \frac{1}{2\tau \cdot \overline{\Delta' r^2}} \qquad (1.8)$$

It is assumed in this paper that the relative error variance is small, i.e. that N_i are large numbers. The distribution of the random error can thus be considered to be approximately Gaussian, so than only the error variance has to be determined.

The rate ratio measurement methods can be divided into two groups: digital and analog. Either of these can be methods which give a rate independent error variance and methods which give a rate independent measurement time.

In the first case an increase of rate gives a decrease of the measurement time, and in the second case a decrease of the error variance.

2. Digital methods

The straightforward method for rate ratio determination is to count the number of pulses from source 1 and 2 over a fixed time interval T and to divide the number of counts. The result is

$$r = \frac{N_1}{N_2} = \bar{r} + \bar{r}(\Delta' n_1 - \Delta' n_2) \qquad (2.1)$$

If the pulses are completely random, $\Delta' n_1$ and $\Delta' n_2$ are statistically independent, so that the variance of the random error is

$$\overline{\Delta' r^2} = \frac{1}{\bar{T}} \left(\frac{1}{\bar{n}_1} + \frac{1}{\bar{n}_2}\right) \qquad (2.2)$$

The same result is also obtained if the pulses are derived from a common periodic primary source, and each of its pulses results either in a pulse of source 1 or source 2. $\Delta' n_1$ and $\Delta' n_2$ are then correlated so that $\Delta n_1 = -\Delta n_2$. The figure of merit is in both cases

$$M = \frac{\bar{n}_1 \cdot \bar{n}_2}{\bar{n}_1 + \bar{n}_2} \qquad (2.3)$$

This method is characterized by a decreasing random error with increasing rate.

A very convenient and simple direct ratio determination can be made by counting the number of pulses N_1 from source 1 over a time interval T, required to accumulate a given number of counts N_2 from source 2. N_2 can be chosen so that the division is performed only by a shift of the digits of N_1. The measured rate ratio is

$$r = \frac{N_1}{N_2} = \bar{r} + \frac{\Delta N_1}{N_2} \qquad (2.4)$$

Only N_1 is a random variable. The random error N_1 is due to two effects. The first is the statistical variation of N_1 due to the randomness of pulses from source 1. The second is due to the random variation of the measurement time T, i.e. due to the randomness of source 2. For completely random pulses the variance of the first component is $\bar{T} \cdot \bar{n}_1$ and of the second $\bar{n}_1^2 \cdot \bar{T}^2 / N_2$, where

$$\bar{T} = N_2 / \bar{n}_2 \qquad (2.5)$$

is the average measurement time. The variance of the relative error is thus

$$\overline{\Delta' r^2} = \frac{1}{N_2} \frac{(1+\bar{r})}{\bar{r}} \qquad (2.6)$$

The figure of merit is

$$M = (\bar{T} \cdot \overline{\Delta' r^2})^{-1} = \frac{\bar{n}_1 \cdot \bar{n}_2}{\bar{n}_1 + \bar{n}_2} \qquad (2.7)$$

The both considered methods have the same figure of merit and are thus equally good. However, in the latter case the variance of error is rate independent, while in the former case the measurement time is rate independent. The realization of an instrument based on the second method is much simpler, since it requires neither a timing device nor a unit for digital division.

3. Analog methods

A straightforward method for rate ratio determination which may be considered in a way as an analog version of the first described digital method, is shown in Figure 1. The two ratemeters are equal, i.e. have the same integration time constant τ and the same increment of the output voltage ΔE per pulse. The average normalized ratemeter output voltage is[1] (K is a normalization constant)

$$\bar{E}_i = \bar{n}_i = K \cdot \Delta E \cdot \tau \cdot \bar{n}_i \qquad (3.1)$$

For completely random pulses its variance is

$$\overline{(E_i - \bar{E}_i)^2} = \frac{\bar{n}_i}{2\tau} = \overline{\Delta n_i^2 \tau} \qquad (3.2)$$

Here i replaces the index 1 or 2. The out-

put voltage of ratemeter 1 is divided with the output voltage of ratemeter 2 in the analog division circuit, to given an output voltage

$$r = \frac{\bar{n}_1+\Delta n_{1\tau}}{\bar{n}_2+\Delta n_{2\tau}} = \bar{r}(1+\Delta n_{1\tau}-\Delta n_{2\tau}) \qquad (3.3)$$

with a variance of the relative error

$$\overline{\Delta' r^2} = \frac{1}{2\tau\,\bar{n}_1}(1+\bar{r}) = \frac{1}{2\tau}\left(\frac{1}{\bar{n}_1}+\frac{1}{\bar{n}_2}\right) \qquad (3.4)$$

The figure of merit is

$$M = \frac{1}{2\tau\cdot\overline{\Delta' r^2}} = \frac{\bar{n}_1}{1+\bar{r}} = \frac{\bar{n}_1\cdot\bar{n}_2}{\bar{n}_1+\bar{n}_2} \qquad (3.5)$$

A much simpler method of the rate ratio measurement is the bistable method[2,3,4] shown in Figure 2. The bistable is set into state 1 with pulses from source 1 and into state 0 with pulses from source 2. When in state 1, the bistable generates an output +1 and when in state 0 an output -1. The bistable output is averaged with a time constant in the network INT. The average time the bistable is in state 1 is the average time interval between a pulse from source 1 and source 2, which is $\bar{T}_1 = 1/\bar{n}_2$. Correspondingly, the average time the bistable is in state 0 is $\bar{T}_0 = 1/\bar{n}_1$. The average duration of the bistable cycle is

$$\bar{T}_B = \frac{1}{\bar{n}_1}+\frac{1}{\bar{n}_2} = \frac{1}{\bar{n}_c} \qquad (3.6)$$

$\bar{n}_c$ is the average number of bistable cycles per unit time. The average value of the bistable output E_B and of the output of the network INT, $\bar{E}$, is

$$\bar{E} = \bar{E}_B = \frac{\bar{T}_1-\bar{T}_0}{\bar{T}_1+\bar{T}_0} = \frac{\bar{r}-1}{\bar{r}+1} \qquad (3.7)$$

The actual average value of the bistable output taken over x bistable cycles is

$$\bar{E}_{BX} = \frac{(T_1)_x-(T_0)_x}{(T_1)_x+(T_0)_x} = \qquad (3.8)$$

$$= \frac{\overline{(T_1)_x}-\overline{(T_0)_x}+\Delta(T_1)_x-\Delta(T_0)_x}{\overline{(T_1)_x}+\overline{(T_0)_x}+\Delta(T_1)_x+\Delta(T_0)_x} = \bar{E}+\Delta E_{BX}$$

where $(T_1)_x$ is the actual time the bistable was in this period in state 1 and $(T_0)_x$ the actual time the bistable was in state 0. Neglecting higher order terms ($x \gg 1$) one obtains

$$\Delta E_{BX} = \frac{2r}{(r+1)^2}\left(\frac{\Delta(T_1)_x}{\overline{(T_1)_x}}-\frac{\Delta(T_0)_x}{\overline{(T_0)_x}}\right) \qquad (3.9)$$

This gives the relative ratio measurement error ($\Delta r_x = \Delta E_{BX}\cdot dr/d\bar{E}$)

$$\Delta' r_x = \frac{\Delta(T_1)_x}{\overline{(T_1)_x}}-\frac{\Delta(T_0)_x}{\overline{(T_0)_x}} \qquad (3.10)$$

and if all intervals T_1 and T_0 are statistically independent, its variance is

$$\overline{\Delta' r_x^2} = \frac{1}{x}\left(\frac{\overline{\Delta T_1^2}}{\bar{T}_1^2}+\frac{\overline{\Delta T_0^2}}{\bar{T}_0^2}\right) \qquad (3.11)$$

For completely random pulses $\overline{\Delta T_1^2} = \bar{T}_1^2$ and $\overline{\Delta T_0^2} = \bar{T}_0^2$. If all pulses are derived from a common periodic source, so that each pulse of the source results either in a pulse of source 1 or source 2, with probabilities p and 1-p respectively, then $\overline{\Delta T_1^2} = (1-p)\cdot\bar{T}_1^2$ and $\overline{\Delta T_0^2} = p\cdot\bar{T}_0^2$. The relative error variance is thus

$$\overline{\Delta' r_x^2} = \frac{2}{\bar{T}}\left(\frac{1}{\bar{n}_1}+\frac{1}{\bar{n}_2}\right) \qquad (3.12)$$

for the first case and

$$\overline{\Delta' r^2} = \frac{1}{\bar{T}}\left(\frac{1}{\bar{n}_1}+\frac{1}{\bar{n}_2}\right) \qquad (3.13)$$

for the second case. $\bar{T} = x\cdot\bar{T}_B$ is the average measurement time.

An averaging circuit with time constant τ has a weighting function

$$w(t,t_0) = \frac{1}{\tau}\exp\left(-\frac{t_0-t}{\tau}\right) \qquad (3.14)$$

If the errors for an adjacent time inverval are statistically independent and $\bar{n}_1 \gg \frac{1}{\tau} \ll \bar{n}_2$, the variance of the averaging circuit output is

$$\overline{\Delta' r^2} = \overline{\Delta' r^2(\bar{T}=1)}\cdot\int_{-\infty}^{t_0} w(t,t_0)^2\,dt \qquad (3.15)$$

where $\overline{\Delta' r^2(\bar{T}=1)}$ is the variance of the input quantity per unit time interval, i.e. for $\bar{T}=1$. For completely random pulses this gives

$$\overline{\Delta' r^2} = \frac{1}{\tau}\left(\frac{1}{\bar{n}_1}+\frac{1}{\bar{n}_2}\right) \qquad (3.16)$$

The figure of merit for completely random pulses is thus

$$M = \frac{1}{2}\,\frac{\bar{n}_1\cdot\bar{n}_2}{\bar{n}_1+\bar{n}_2} \qquad (3.17)$$

When all pulses are derived from a common periodic source and each pulse of the source results either in a pulse of source 1 or source 2 the figure of merit is

$$M = \frac{\bar{n}_1\cdot\bar{n}_2}{\bar{n}_1+\bar{n}_2} \qquad (3.18)$$

In the latter case the figure of merit is the same as for the two ratemeter method, eqn. (3.5), while for completely random pulses it is only one half of this value.

It can be seen that the simplicity of the bistable method compared with the two ratemeter method is paid by a decrease of the figure of merit for completely random pulses by a factor of 2. Both methods have a response time constant which is rate independent.

The differential integrator method with feedback is shown in Figure 3. The charges applied by the dosing circuits to the integrator condenser are influenced by the output voltage so that, proportionally to the output voltage E, the charge applied per pulse from source 1 is deminished, and that applied per pulse from source 2 is increased. The increments of the output voltage ΔE_+ per pulse on input 1, and ΔE_- per pulse on input 2 are

$$\begin{aligned}\Delta E_+ &= e(1-aE)\\ \Delta E_- &= -e(1+aE)\end{aligned} \qquad (3.19)$$

The average increase of the output voltage per unit time is thus

$$\left(\frac{\overline{dE}}{dt}\right) = \bar{n}_1\cdot e(1-aE) - \bar{n}_2\cdot e(1+aE) \qquad (3.20)$$

At the stationary state $\left(\frac{\overline{dE}}{dt}\right) = 0$. The average voltage is therefore

$$\bar{E} = \frac{1}{a}\,\frac{\bar{r}-1}{\bar{r}+1} \qquad (3.21)$$

The average speed with which for a departure $E-\bar{E} = \Delta E$ the voltage E approaches $\bar{E}$ is

$$\left(\frac{\overline{dE}}{dt}\right) = -e\cdot a(\bar{n}_1+\bar{n}_2)\cdot\Delta E \qquad (3.22)$$

It follows that $\overline{\Delta E}$ decreases to 0 exponentially, with the time constant

$$\tau = \frac{1}{e\cdot a(\bar{n}_1+\bar{n}_2)} \qquad (3.23)$$

which is the response time constant of the system to a small rate change.

The variance of the output voltage can be determined using the stationary condition, from which it follows that the probability of a transition of E through a level E_x in one direction, must be equal to the probability of the transition through this level in the opposite direction. The probability that the level E_x is crossed in the upward direction is that E is between $E_x-\Delta E_+$ and E_x, and that a pulse arrives from source 1. The probability that the same level is crossed in the downward direction is that E is between $E_x-\Delta E_-$ and E_x and a pulse arrives from source 2. This statement can be written in the form

$$\bar{n}_1\cdot\int_{E_x-\Delta E_+}^{E_x} P(E)\cdot dE = \bar{n}_2\cdot\int_{E_x}^{E_x-\Delta E_-} P(E)\cdot dE \qquad (3.24)$$

where P(E) is the probability density function of E. This integral equation can be solved approximately by substituting $P(E) \doteq P(E_x) + \frac{dP(E_x)}{dE}(E-E_x)$ and neglecting the second order terms. This gives the differential equation for the Gaussian distribution

$$\frac{dP(E)}{P(E)} = -\frac{2\cdot e\cdot a}{\Delta E_+^{\,2}\cdot\bar{r}}\,(E-\bar{E})\cdot dE \qquad (3.25)$$

with the variance

$$\overline{(E-\bar{E})^2} = \frac{\Delta E_+^{\,2}\cdot\bar{r}}{2e\cdot a} = \frac{e}{a}\,\frac{2\bar{r}}{(\bar{r}+1)^2} \qquad (3.26)$$

The variance of the relative error is thus

$$\overline{\Delta r^2} = \frac{e\cdot a}{2}\,\frac{(\bar{n}_1+\bar{n}_2)^2}{\bar{n}_1\cdot\bar{n}_2} \qquad (3.27)$$

and the figure of merit

$$M = \frac{\bar{n}_1\cdot\bar{n}_2}{\bar{n}_1+\bar{n}_2} \qquad (3.28)$$

The figure of merit is the same for the two ratemeter method, eqn. (3.5) and twice the figure of merit, eqn. (3.17) for the bistable method with random pulses.

Two simple realizations of charge dosing circuits including feedback are shown in Figure 4. Both circuits use diode pumps[5] driven by rectangular pulses which apply their charges to the integrator capacitor C. Figure 4a shows a particularly simple circuit. The change of the increments per pulse is directly performed by the condenser voltage which is the output voltage of the circuit. In the second circuit, Figure 4b, a part of the output voltage from the integrator is applied

to the upper ends of the charge dosing capacitors. If it is taken into account that circuit a) requires a high impedance isolation stage at the output, the circuit b) is not much more complex than circuit a).

Conclusions

All of the considered methods for the rate ratio determination with the exception of the bistable method have the same figure of merit. With respect to realization, there are great differences in complexity. The simplest digital realization enables the measurement system which gives a variable measurement time and a rate independent relative error variance. The simplest analog realization is the bistable method, which has a rate independent measurement time constant and a with rate decreasing relative error. However, if the maximum figure of merit is required, and the pulses are completely random, the simplest analog method is the differential integrator with feedback, where the time constant decreases with rate, and the relative error variance is rate independent.

References

1. R.D. Evans, The Atomic Nucleus, McGraw Hill Company Inc., New York 1955.
2. D.H. Wilkinson, J.Sci.Instr. 27 (1950) 36
3. K.W. Marlow, Nucl.Instr.Meth. 15 (1962) 188
4. J.L. Black, E. Valentine, Nucl.Instr. Meth. 31 (1964) 325
5. Cooke-Yarborough, Proc.Inst.Elec. Engrs. (London), 98 (1951) 191

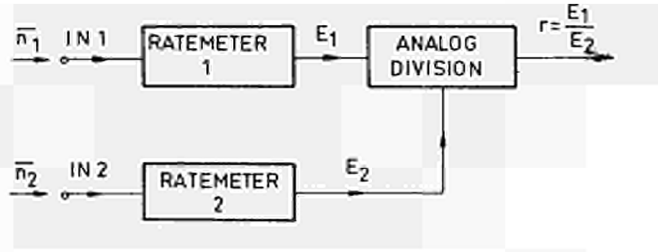

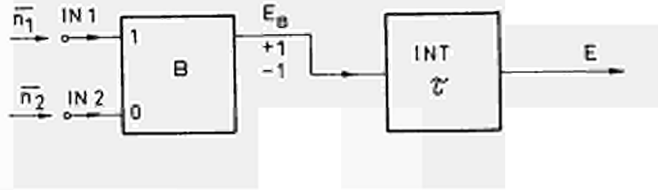

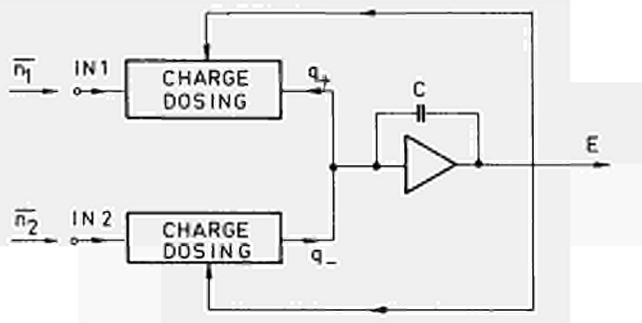

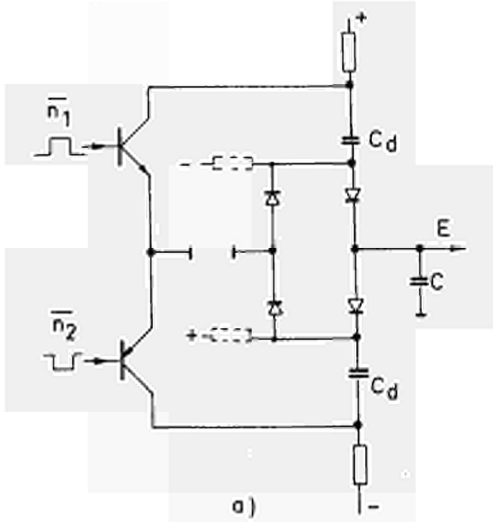

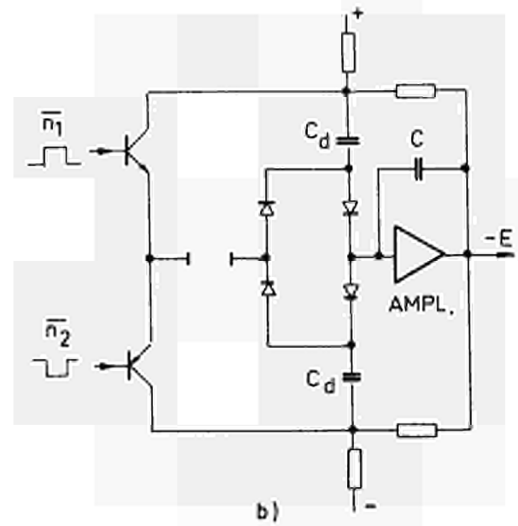

THE MEASUREMENT OF AUTOCORRELATION AND CROSSCORRELATION FUNCTIONS IN THE FAST DOMAIN AND ITS APPLICATIONS TO NUCLEAR ELECTRONICS

G. Amsel, R. Bosshard, R. Rausch, M. Sauce and C. Zajde,
Laboratoire de l'Accélérateur Linéaire, Ecole Normale Supérieure, 91 Orsay, France.

Summary

Auto and crosscorrelation functions of binary or gaussian processes were measured with subnanosecond precision using sampling and averaging techniques, yielding high speed automatic operation. For gaussian processes two methods are described based on conditional probabilities and sign correlation. Applications are shown to the characterisation of noise from pulse amplifiers and photomultipliers and of the dead time properties of fast randomly operated switching circuits.

Introduction

The study of random processes by correlation methods received increasing attention during the last years in various fields of physics and biology. The practical use of these methods in the fast time domain, i.e. below the microsecond region, was limited until now by technical problems. The applications of correlation analysis, both on theoretical and experimental level, to the study of the properties of noise in nuclear pulse amplifiers were described by the authors in ref. 1 and later in ref. 2 and 3. Such techniques have been subsequently used by Radeka[4]. More recently the authors showed[5] the usefulness of similar methods in the study of point processes generated for example by the dead time of fast discriminators fed by signals occuring according to a Poisson process. Thus the interest of correlation techniques was extended to more general stochastic phenomena than noise. In fact delayed coincidence measurements are in close relationship with crosscorrelation techniques, as shown in ref. 5.

The aim of this paper is to show how auto and crosscorrelation functions may be simply measured by conveniently operating a fast time averaging system comprising a sampling oscilloscope and a multichannel analyser. All the technical details of this system are given in ref. 3 and 6. This method is valid for the wide class of random processes considered below. Its extension to other processes would require a more sophisticated equipment and will not be considered here.

Some formula related to the autocorrelation of a random function X(t) may be recalled; in what follows the stationary case only will be considered. Then by definition, denoting the mean value $E[X(t)]$ by $\overline{X}$,

$$C(\tau)=E[X(t)X(t+\tau)] - \overline{X}^2 \qquad (1)$$

The basic properties of $C(\tau)$ which will be used here are : $C(-\tau)=C(\tau)$; $|C(\tau)| \leq C(0)=\sigma^2$, where σ is the standard deviation of X(t); X(t) is differentiable in the mean square if and only if $C(\tau)$ has derivatives of order up to two at the origin. Then $dC/d\tau=0$ for $\tau=0$. Details on the mathematics of correlation functions may be found in ref. 7.

If $Y(t)=X(t) * R(\tau)$, where $R(\tau)$ is the impulse response of a filter (two-port)

$$C_Y(\tau)=C_X(\tau) * R(\tau) * R(-\tau) \qquad (2)$$

On the other hand, if $Y(t)=X(t)-X(t-\Delta)$ is the result of clipping X(t) by a line of reflexion delay Δ, we have [1,2] :

$$C_Y(\tau)=2\,C_X(\tau)-C_X(\tau-\Delta)-C_X(\tau+\Delta) \qquad (3)$$

This relation is of basic importance in pulse amplifiers as will be illustrated.

Analogous definitions hold for crosscorrelations. Let us note only that if $Y(t)=X(t) * R(\tau)$

$$C_{XY}(\tau)=C_X(\tau) * R(\tau) \qquad (4)$$

and that

$$C_{YX}(\tau)=C_{XY}(-\tau) \qquad (5)$$

In what follows we shall chiefly consider autocorrelation; most of the results may be readily extended to crosscorrelations.

Binary functions

We shall consider here random functions which oscillate between two states A and B. To each state we associate a value, conveniently taken as 0 and 1 respectively. The resulting binary functions b(t) satisfy the basic relation

$$b^2(t)=b(t) \qquad (6)$$

and hence their moments $E[b^n(t)]$ are equal. We also have here the identity

$$E[b(t)] = Pr[b(t) = 1] \qquad (7)$$

We have therefore, X(t) being binary

$$\begin{aligned} E[X(t)X(t+\tau)] &= Pr[X(t)=1 \text{ and } X(t+\tau)=1] \\ &= Pr[X(t)=1]\,[Pr\ X(t+\tau)=1 / X(t)=1] \\ &= E[X(t)]\,E[X(t+\tau)/\ X(t)=1] \end{aligned}$$

Hence in the stationary case

$$C(\tau)=\overline{X}\,\Psi(\tau) - \overline{X}^2 \qquad (8)$$

where $\Psi(\tau)$ is the mean value of $X(t+\tau)$ knowing that $X(t)=1$,

$$\Psi(\tau) = E[X(t+\tau)/X(t)=1] \qquad (9)$$

$\Psi(\tau)$ may be readily measured by time averaging and $C(\tau)$ deduced, using (8). One has obviously

$$\Psi(0)=1 \quad \text{and} \quad \Psi(\infty)=\overline{X} \qquad (10)$$

Here $\overline{X}$ corresponds in fact to the "duty cycle", i.e. the mean time spent in the "state 1".

Fig. 1 shows the experimental set-up which allows to measure $\Psi(\tau)$. To the original averaging system [3,6] comprising the main oscilloscope, interface and pulse height analyser, an auxiliary sampling unit is added. Both oscilloscopes are triggered simultaneously at a fixed rate by a pulse generator at intervals much

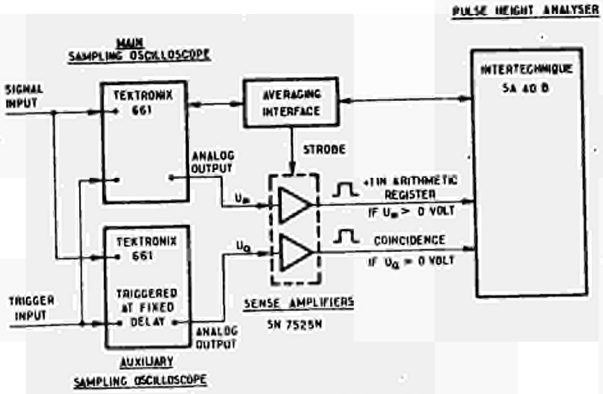

Fig. 1: Block diagram of the binary signal correlator.

longer than the correlation time of the process, typically at 1 to 10 KHz in the experiments shown here. The sampling delay τ_2 of the auxiliary unit is fixed and determines the origine of the delay scale .

The signal observed is considered in the "1 state" if it is found by the sampling units above a reference level, determined by the d.c. offset of the oscilloscopes and the bias of the sense amplifiers (set here to zero Volt).

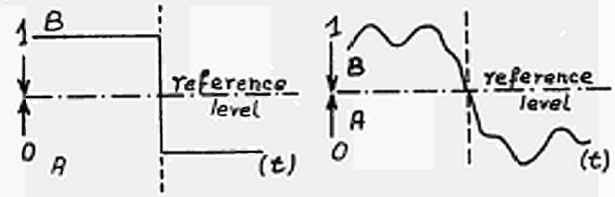

a) ideal case b) real case

For large enough and well defined binary signals the sense amplifiers may not be necessary. In any case the "smoothing" setting of the oscilloscope should be adjusted so as to obtain the correct value of the signal at the first sampling[6]. When the sense amplifiers are used the sensitivity of the system is determined by noise phenomena in the oscilloscope. It was observed that their effect is minimized when using the 50mV/cm scale. In these conditions the fluctuations of the analogue output are about 10 mVolt rms, the equivalent fluctuations of the reference level being around 1 mVolt rms. The minimum amplitude of the input binary function insuring correct operation is 5 to 10 mVolts.

The main unit automatically sweeps through the delays τ_1, a one to one correspondence between delays and channels of the analyser being maintained by the interface [6]. If the auxiliary unit finds the signal in the "0 state" and does not emit a "coincidence" pulse, the averaging system remains blocked. If it emits a "coincidence" pulse (which happens with probability $\overline{X}$) the result from the main sampling unit, operating at the delay τ_1 (0 or +1 according to the state of the signal), is stored and the channel address is incremented, inducing in turn an incrementation of τ_1. Hence the averaging process directly gives $\psi(\tau)$, with $\tau = \tau_1 - \tau_2$, signal speed being limited only by the sampling unit performance.

It should be noted that an easy generalisation of formula (8) and (9) shows that if two distinct binary functions are applied to the two oscilloscopes their crosscorrelation is measured with the same procedure.

Telegraph signals

Two state functions are encountered in binary data transmission and digital processing systems. We shall consider here as an example the so called telegraph signals. These are binary signals X(t), associated with a point process $\{t_i\}$ which change state at each t_i; they may be generated by applying pulses occuring at t_i to a scale of two. Obviously $\overline{X} = C = \psi(\infty) = 1/2$ and it is easy to show that the one sided derivative of $\psi(\tau)$ at the origin is

$$\frac{d\psi}{d\tau}(0) = \lambda \quad \text{for } \tau \lessgtr 0 \text{ or } \tau \gtrless 0 \qquad (11)$$

where λ is the density of the point process. Hence $\psi(\tau)$ and $C(\tau)$ have no derivative at the origin and X(t) is not a differentiable process. $\psi(\tau)$ has a characteristic cusp shaped appearance, the slope near the origin having a precise signification through (11), upon normalising the results by $\psi(0) = 1$.

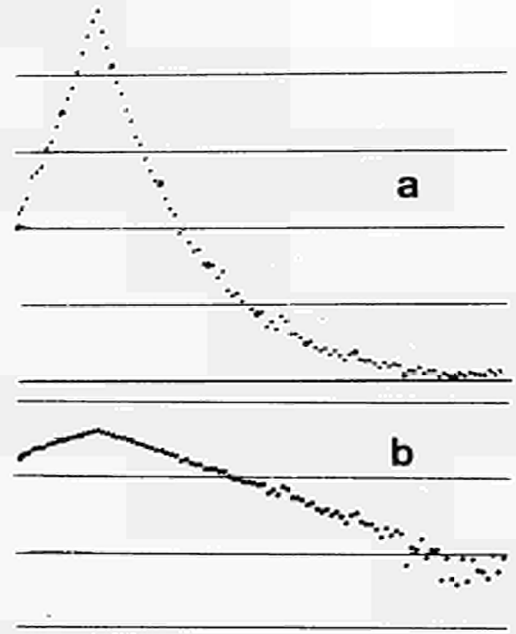

Fig. 2: $C(\tau)$ of a scale of two with poissonian input; 50 ns/chan. a) Linear plot. b) Logarithmic plot (3 decades full scale).

Fig. 2 shows the well known case of a scale of two with poissonian input, leading to

$$C(\tau) = \frac{1}{4} e^{-2\lambda|\tau|} \text{ or } \psi(\tau) = \frac{1}{2}\left[1 + e^{-2\lambda|\tau|}\right] \qquad (12)$$

Counting rate was 5.10^5 c/s; pulses from a fast, γ irradiated plastic scintillator followed by a fast discriminator were applied to a high speed d.c. connected scaler. Fig. 3 shows a typical result when the input to the scale of two

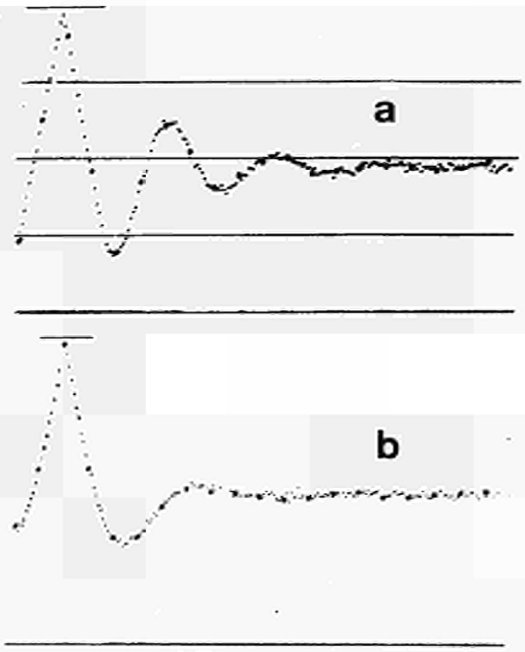

Fig. 3: $\psi(\tau)$ for a scale of two fed by a long dead time discriminator; 2.5 μs/10 chan. a) Fixed dead time. b) Random dead time.

is not poissonian. The pulses from the scintillator were applied here to a long dead time discriminator. In fig. 3a the dead time τ_0 is fixed, 15 μs : the oscillatory behaviour of $\psi(\tau)$ shows that the underlying dead time process tends towards periodicity at high input counting rates. In fig. 3b the dead time is random (the discriminator's triggering properties being here sensitive to the input pulse height spectrum) : the oscillations of $\psi(\tau)$ appear strongly damped.

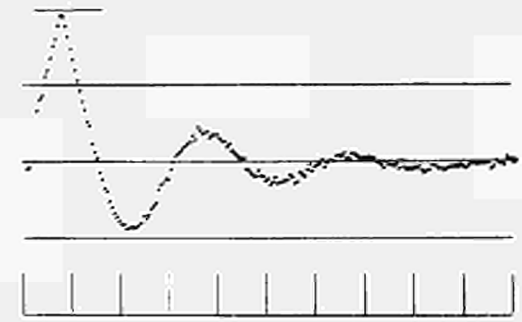

Fig. 4: $\psi(\tau)$ for a scale of 16; 0.5 μs/chan. (10 μs/div.), poissonian input.

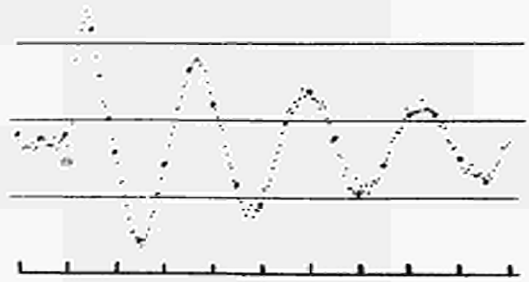

Fig. 5: $\psi(\tau)$ for a scale of 8; 10 μs/10 chan, fixed dead time input.

Fig. 4 shows $\psi(\tau)$ for the same input process as in fig. 2, but at the output of a scale of 16. Its comparison with fig. 3b is interesting as well as with fig. 5 in which the output of a scale of 8 was examined, the input being the same as in fig. 3a (the points in the first division should be discarded).

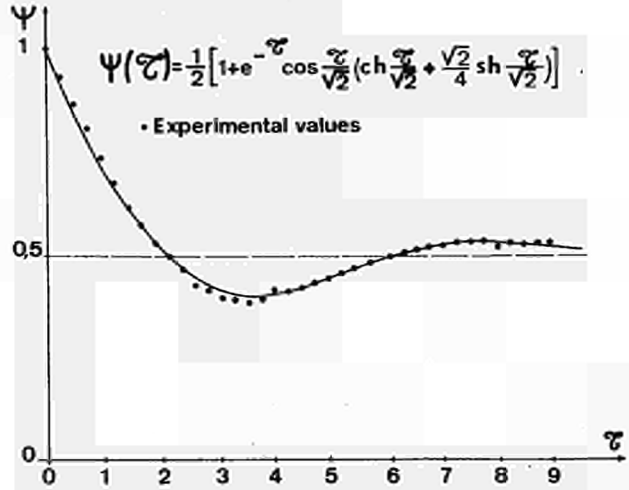

Fig. 6: Calculated and experimental values of $\psi(\tau)$ for a scale of 8 with poissonian input (time units : 2 μs = $\overline{L}_o$).

Fig. 6 shows a comparison between experiment and theoretical calculation for a scale of 8 with poissonian input, the same as for fig. 2. The derivation of the analytical expressions, like that of fig. 6, giving $\psi(\tau)$ for a large variety of cases will be given in a more detailed paper on this subject. τ is expressed in units equal to $\overline{L}_o = \lambda^{-1}$, the mean spacing of the input pulses.

Low duty cycle signals

When $X \ll 1$, the probability that the auxiliary oscilloscope finds X(t) in the "1 state" is small and the system works inefficiently. Let us consider the case when X(t) is generated by a point process $\{t_i\}$, each t_i being the origin of a short rectangular pulse of duration T, i.e. when X(t) comes from a discriminator. When T is very small, $\psi(\tau)$ is almost independent of T and reflects the statistical properties of the point process $\{t_i\}$ itself. The deeper mathematical signification of this remark and its experimental consequences were dealt with elsewhere [5]. We shall illustrate here this case only by an example pertaining to the study of the dead time properties of discriminators. To overcome the inefficient operation of the system the auxiliary oscilloscope is now disconnected and the main sampling unit is triggered at random by the input pulses themselves. The interface still maintains the correct delay-channel correspondence in these conditions [6]. For $0 < \tau < T_1 + 1$ is registered at each sampling; the time scale is chosen so that T corresponds to one channel, which contains hence a number equal to that of the sweeps. The high content

of the channel zero is representative of the theoretical aspect of the ideal $\Psi(\tau)$ associated with the $\{t_i\}$ in this case, which contains a δ component at the origin [5]. For $T < \tau < T_o$ there are no counts as, owing to dead time, no pulse can be present within T_o of a pulse which triggered the oscilloscope. For $\tau \gg T_o$ the continous branch of $\Psi(\tau)$ is registered; the shape of this branch depends on the ratio $\overline{L_o}/T_o$; its value corresponds at each delay τ to the probability to find an instant t_i in the vicinity of τ. For $\overline{L_o} \gg T_o$, $\Psi(\tau)$ is constant for $\tau \gg T_o$. This is illustrated

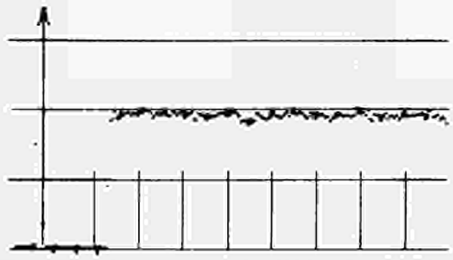

Fig. 7: Measurement of the dead time T_o of a discriminator by registering $\Psi(\tau)$ for $\overline{L_o} \gg T_o$; 10 ns/chan or 200 ns/div. The result is $T_o = 325$ ns.

in fig. 7, which clearly shows how precise the measurement of T_o may be, the discriminator working at random, in real conditions, in contrast with double pulse measurements using a pulse generator. Input counting rate was 14000 c/s, i.e. $\overline{L_o} = 71\,\mu s$, $\overline{L_o}/T_o \simeq 200$. Such measurements are in fact equivalent to delayed autocoincidence experiments, the delays being automatically swept through; the resolution is

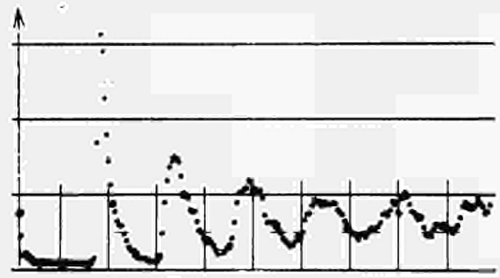

Fig. 8: $\Psi(\tau)$ measured for a dead time point process with $\overline{L_o}/T_o = 0.14$. 10 μs/div.

determined by T. Fig. 8 shows $\Psi(\tau)$ for a counting rate at the discriminator input of 457000 c/s and $T_o = 17\,\mu s$. $\Psi(\tau)$ has here a violently oscillatory behaviour, the successive peaks corresponding to instants t_i which are the first, second etc. following the instant which triggered the sampling unit. More experimental results and detailed analysis of this "conditional averaging" method may be found in ref. 5.

Gaussian functions

Correlation measurements in this case are simplified by the fact that the joint probability density of X(t) and X(t+τ) is completely determined by the correlation function $C(\tau)$. We shall assume $E[X(t)] = 0$, corresponding to the general case of noise from an a.c. coupled amplifier. Two methods will be shown here, allowing simple measurement of $C(\tau)$, based on elementary properties of gaussian random functions.

Conditional averaging

In this method the auxiliary oscilloscope is disconnected like in the preceeding case, the main sampling unit being triggered by the process under study itself, at a well defined triggering level x_o. On the other hand the analogue output is now digitized using the analyser's ADC like in classical time averaging, as described in ref. 3 and 6. It is well known [7] that in this case the conditional average is :

$$E[X(t+\tau) / X(t) = x_o] = x_o\, r(\tau) \qquad (13)$$

where $r(\tau) = C(\tau)/\sigma^2$ is the correlation coefficient of X(t). Experimental use of this relation was shown in ref. 1, 2 and 3. A specially designed Schmidt trigger with low hysteresis was used to insure triggering at x_o alternately on positive and negative slopes, so as to fulfill (13). The distorsion due to triggering on one slope only depends on the shape of $C(\tau)$ and will be dealt within a forthcoming paper. The results are conviniently normalised to $C(0) = 1$, σ being measured separately, using the sampling scope [3, 6]. x_o is chosen so as to give a reasonable counting rate, the mean spacing of the samplings being much larger than the correlation time. Results shown here were obtained at about 10^4 c/s. The convergence of the resulting average is very fast, as for $\tau = 0$, the sampled value, x_o, is well defined; as x_o/σ is usually around 4, the signal to noise ratio is good; finally multilevel coding is advantageous as compared with two level codings considered until now. In many cases, satisfactory results are obtained for fast noise within a matter of seconds.

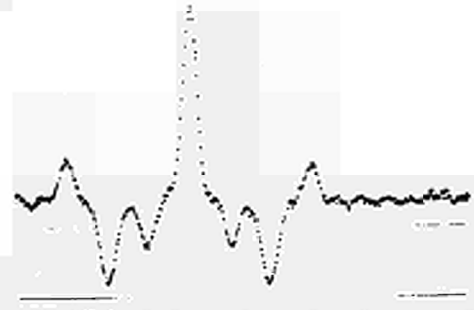

Fig. 9: $C(\tau)$ of the noise of a fast amplifier containing two unequal clipping lines; input short circuited. 1 ns/chan. Measurement by conditional averaging.

Fig. 9 shows a typical result corresponding to the noise of a 8 ns rise time amplifier [1] with short-circuited input, containing a 75 ns and a 35 ns clipping line. The lateral peaks may be explained by the repeated application of formula (3). Fig. 10 shows $C(\tau)$ for the fluctuations of the current from a 56 CVP photomultiplier,

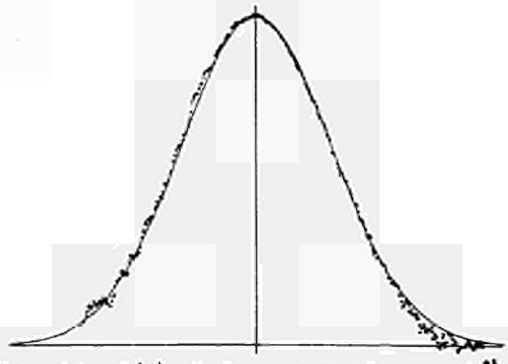

Fig. 10: $C(\tau)$ of the output of a continously illuminated 56 CVP photomultiplier. The curve is calculated from the average SER; FWHM = 3 ns.

which was continously illuminated (in practice 5 μs long light pulses were applied using a GaAs diode, to avoid destruction of the tube at high d.c. current). The mean current was about 10 times σ, insuring nearly gaussian behaviour. The calculated curve is the autoconvolution of the measured mean SER; the good agreement demonstrates the validity of the method in this not strictly gaussian case. As such measurements do not require the knowledge of the origin of the SER signals, like in time averaging, the corresponding problem does not show up here. It should be noted that the cathode-first dynode photoelectron transit time jitter has no influence on $C(\tau)$ and cannot be deduced from such measurements.

Crosscorrelation of two random functions X(t) and Y(t) may be obtained by triggering the oscilloscope with X(t) while averaging Y(t).

Sign correlation

Conditional averaging presents some disadvantages most difficult to overcome. For very fast phenomena the use of a trigger may have ill effects especially if the alternate slope method is used. On the other hand, if the two branches of $C(\tau)$ are to be registered, a delay should be inserted between the signal and the sampling unit input, so as to conveniently shift the origin of the delays. This was done in fig. 9 and 10, using an air cable. In the microsecond region such a procedure is impossible.

Principles. Another method in which these problems do not arise, but which converges more slowly, is sign correlation. In this technique, a binary function $\breve{X}(t)$ is introduced having the same zeros as X(t); this means that $\breve{X}(t)=1$ if $X(t)>0$ and $\breve{X}(t)=0$ if $X(t)\leq 0$. $\breve{X}(t)$ is a telegraph signal with mean value 1/2. It is easy to see that $\Psi(\tau)$ is directly measured for $\breve{X}(t)$ upon applying X(t) to the correlator of fig. 1, provided the reference level is set precisely to zero. The sign determination of X(t) is perturbed for small values of X(t) by the equivalent input noise of the sampling unit; the amplitude of X(t) should not be therefore too small, a typical acceptable value being 30 mVolt rms, or about 100 mVolt peak to peak. From well known relations applying to joint gaussian random variables we have:

$$\Psi(\tau) = \frac{1}{2} + \frac{\text{Arc sin } r(\tau)}{\pi} \qquad (14)$$

and inverting (14) we obtain

$$r(\tau) = -\cos \pi \Psi(\tau) \qquad (15)$$

Hence $r(\tau)$ may be readily deduced from the measured $\Psi(\tau)$ through (15). This formula leads to a nearly linear relation between $r(\tau)$ and $\Psi(\tau)$ for $|r(\tau)| \ll 1$, i.e. for $\Psi(\tau)$ near $1/2$ ($r(\tau)=0$ implying $\Psi(\tau)=1/2$). On the contrary for $|r(\tau)|$ near 1 the relationship is quadratic and in particular we have, differentiating (15) twice

$$\sqrt{-\ddot{r}(0)} = \pi \left| \frac{d\Psi}{d\tau}(0) \right| \qquad (16)$$

where the one sided derivative of $\Psi(\tau)$ is written. We may notice that (16) shows, recalling (11), that $\frac{1}{\pi}\sqrt{-\ddot{r}(0)}$ is the expected number of zeros of X(t) per second, a classical result. Moreover, from the point of view of the zero statistics of X(t) the measurement of $\Psi(\tau)$ yields more directly significant results than that of $C(\tau)$. In fact, as we shall see, $\Psi(\tau)$ represents a magnified image of $r(\tau)$ near $\tau=0$ and contains in this vicinity far more precise results than would give a direct measurement of $r(\tau)$.

Results. In what follows we shall take $\sigma=1$ and write $C(\tau)$ for $r(\tau)$. Fig. 11 shows a typical $\Psi(\tau)$ measured for the noise from an ORTEC 109 A charge sensitive preamplifier, with open input. The noise was filtered by an ORTEC 410 main amplifier. The comparison with the calculated $C(\tau)$ illustrates the effect of the transformation (15), in particular the cusp shaped appearance of $\Psi(\tau)$. The magnifying effect near $\tau=0$ (i.e. $r(\tau)\simeq 1$) is further illustrated by fig. 12 in which $\Psi(\tau)$ should be compared to the measured $C(\tau)$ (by conditional averaging) and to the calculated $C(\tau)$ (from $\Psi(\tau)$ by 15). The noise originated here from the fast amplifier used for fig. 9, containing now no clipping, and with 50 pF at its input. Fig. 12 shows how very

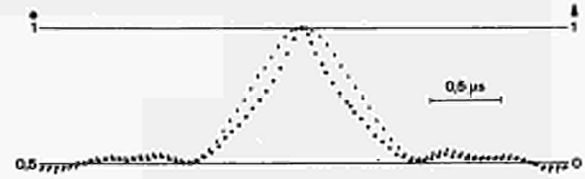

Fig. 11: Measured $\Psi(\tau)$ (●) and corresponding calculated $C(\tau)$ (▲) for the noise of a charge sensitive low noise amplifier. Input open; one 0.8 μs delay line; 0.5 μs integration.

small fast noise components may be measured with high precision in presence of slow components, when using sign correlation. Fig. 13 shows correlation functions for the same noise as in fig. 9, the fast amplifier containing here only one clipping line. Fig. 13a fully illustrates formula (3). Fig. 13b shows that the general shape of $C(\tau)$ is preserved by sign correlation; the relative amplitude of the lateral peaks goes over from 1/2 to 1/3.

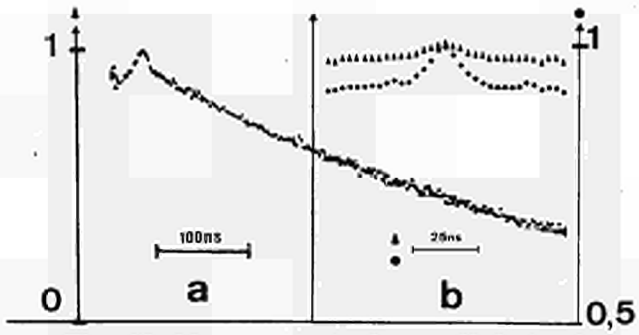

Fig. 12: Measurement of a small fast noise component showing the advantage of sign correlation upon real correlation in this case. a) measured $C(\tau)$; b) $\psi(\tau)$(●) and calculated $C(\tau)$(▲).

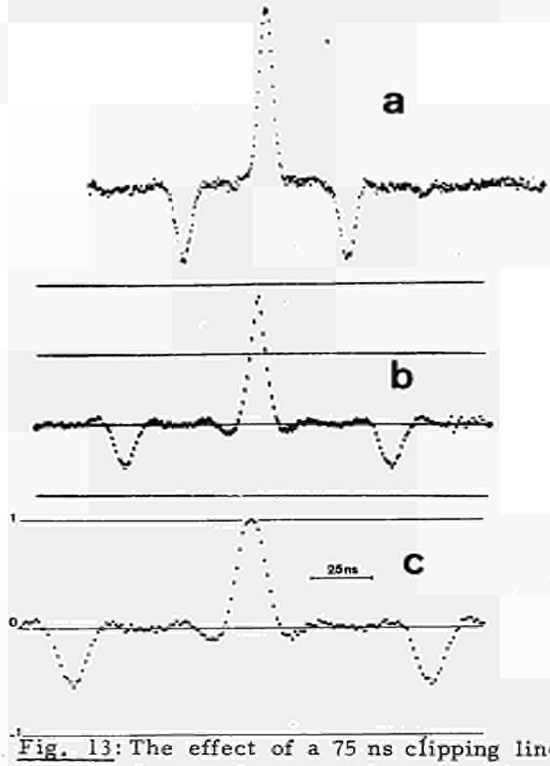

Fig. 13: The effect of a 75 ns clipping line on noise from a fast amplifier; a) $C(\tau)$, 1 ns/chan. b) $\psi(\tau)$ 1.25 ns/chan; c) $C(\tau)$ calculated from b).

Fig. 14 compares similar results obtained with the slow ORTEC amplifiers mentioned above. In fig. 14a the left branch of $C(\tau)$ could not be measured by conditional averaging as no long enough delay could be introduced in the signal path. The symmetrical curve in fig. 14b shows that no such problem arises for $\psi(\tau)$ as here the origin of the delays, τ_2, may be arbitrarily chosen on the auxiliary oscilloscope. The fact that in fig. 14a only one branch could be measured is a great drawback, as the best control of the correct operation of the alternate slope trigger used here is the measured symmetry of $C(\tau)$, like in fig. 13. Hence fig. 14 illustrates the usefulness of sign correlation in the microsecond range.

For sake of illustration we give here a

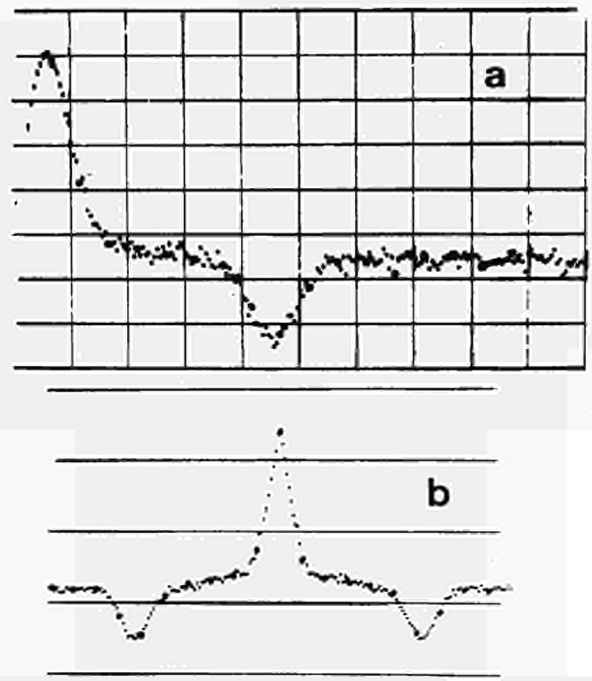

Fig. 14: The effect of a 0.8 μs clipping line on noise from a slow amplifier; input open; no integration. a) $C(\tau)$, 10 ns/chan. or 200 ns/div; b) $\psi(\tau)$, 125 ns/10 chan.

simple sign crosscorrelation obtained by applying a noise X(t) to one oscilloscope and its filtered image $Y(t)=X(t)*R(t)$ to the other. In fig. 15 X(t) was the noise from the slow amplifiers used above, with 0.1 μs differentiating time

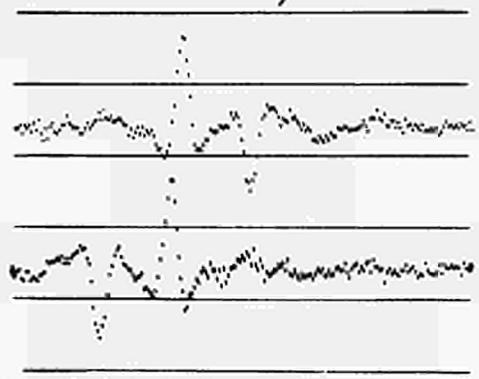

Fig. 15: A typical crosscorrelation. 25 ns/chan.

constant and Y(t) was obtained from X(t) by a 0.8 μs clipping line (unipolar and bipolar outputs of an ORTEC 410 amplifier). According to formula (4) the crosscorrelation is just the response of the clipping line to a signal which is $C_x(\tau)$. This is clearly apparent on the upper trace in fig. 15 from which $C_{xy}(\tau)$ can be deduced by (15). For crosscorrelation, $\psi_{xy}(0)$ is no longer necessarily unity and normalisation should be made by $\psi_{xy}(\infty)=\frac{1}{2}$. The lower trace in fig. 15 illustrates formula (5); inversion of X and Y leads to the reversal of the delay scale.

It should be emphasized that sign correlation keeps all its interest for non gaussian random processes. $\psi(\tau)$ is then not simply

connected to $r(\tau)$, but gives information on zero statistics and on level crossing properties. For random functions, gaussian or not, much information may be obtained on level crossing properties by intentionnaly displacing the reference levels from zero.

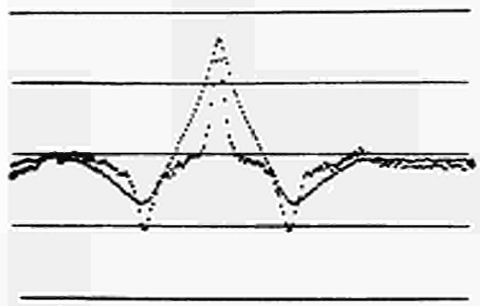

Fig. 16: A typical application to noise analysis for a low noise ORTEC 109A amplifier. Input open, 2 equal 0.8 µs delay lines, no integration. 25 ns/chan. $\psi(\tau)$ is shown for : broad curve, with protection diode at input; narrow curve, with FET only.

Fig. 16 shows a typical application to the determination of the noise properties of electronic components. It shows that the insertion of a diode to protect the input FET of a low noise amplifier completely changes the noise characteristics of the system : without protection first stage noise is the major component whereas with protection input noise is dominant.[1] The optimal pulse shaping time constants in the two cases are obviously quite different.

Although all the examples shown here pertain to nuclear instrumentation it is quite clear that the methods described may be applied to various problems in physics, like photon statistics, mean life distribution measurements, etc. They may be an alternative to frequency power spectrum measurements, with the known advantages of time domain analysis.

Acknowledgments

We wish to thank Professor A. BLANC-LAPIERRE for his constant support of this work.

References

1) G. Amsel, R. Bosshard, C. Zajde. IEEE Trans. Nucl. Sci. NS-14, N°1, p.1 (1967).

2) G. Amsel, Gatlinburg Conf. Semic. Det. May 1967. Nucl. Sci. Report N°44, NAS, Washington 1969 p. 590.

3) R. Bosshard, same publication, p. 603.

4) V. Radeka, same publication, p. 620.

5) G. Amsel, R. Bosshard, R. Rausch, M. Sauce and C. Zajde. 2° Colloque Traitement Signal, 5-10 May 1969, Nice (France). p.175

6) G. Amsel and R. Bosshard. Sampling and averaging techniques in the analysis of fast random signals; to be published.

7) A. Blanc-Lapierre and R. Fortet : "Theory of random functions", Gordon and Breit, New York (1964); A. Papoulis : Probability, random variables and stochastic processes, Mc Graw-Hill, N.Y. 1965.

DISCUSSION

Baldinger : - What is the precise meaning of the expression "fixed dead-time" of a scale of two, used in your lecture ?

Amsel : - Now, what we have done was to take a discriminator for the fixed dead time, that is of the nonparalyzable type. Once you have counted the pulse, you are blocked for a fixed time whatever happens, but in this case you can have two situations, either the dead time is constant, or it is not. Now, it is not constant when the discriminator is sensitive to the pulse height spectrum of the incoming pulses ; it should not be sensitive, but it generally and very often is, and that is why you have seen the difference between the two.
So we obtain the fixed dead time by putting in front of the discriminator the very fast discriminator, so as to feed the discriminator under study by standard pulses, but unfortunately we could not find any discriminator available in the laboratory which really had a fixed dead time for any kind of amplitude spectrums that you can apply to.
The scaler by itself had negligible dead time. I mean, it was the discriminator which had the main dead time.

Winter : - For the study of the noise behaviour of low noise amplifiers, it would perhaps be useful to measure directly the Fourier transform of the autocorrelation function that means the power spectrum, directly with a wave analyzer.

Amsel : Well, all our work was just to avoid this, because it is much more simple and direct to interpret the correlation functions than the Fourier transform. It is not so easy to measure these Fourier transforms in the very high frequency range, whereas sampling oscilloscopes go to an equivalent bandwidth of 12 GHz well easily, so that we could measure correlation functions within 1 or 2 nanoseconds. Obviously, there is a 1 to 1 correspondence between the two representations, but exactly in the same way as in the transient phenomena

analysis, more and more people don't use the Fourier transform, I think that time domain analyzis is much more powerful to interpret the noise characteristics of pulse amplifiers which are not narrowbanded.

Winter : - Well, so it is the question of available instrumentation. But if you start in the low frequency noise then if it is a 1/f behaviour or something like this, then the spectrum measurement would be, perhaps easier, or give perhaps easier and more rapid information. For the fast domain I agree with you.

Amsel : - For the low frequency range surely, the correlation function is not well adapted, then one has to use frequency analysis.

Radeka : - I would like to make just a comment on this. Actually, there are three methods of characterizing the noise or measuring it, and each one depends actually on the character of noise or its suitability. One is this with correlation functions, a second one is by measuring the spectra, and the third is by measuring the variance in the time domain in a particular physical measurement. All of these methods have their maximum sensitivity for a particular kind of noise. For all frequency noises which might be divergent, the correlations functions are even not well defined. They are defined for the differences, the finite differences only, and in that case the finite bandwidth methods are a little better, and the correlation function for 1/f noise would be a logarithmic one.

Amsel : - Spectral analysis may be better from the study of very slow noise components. The system shown here aims primarily to investigate short correlation times, from the subnanosecond to about 10 µs region. For slower components, slow real time correlators, which are very efficient and go up to seconds, or conventional frequency analysers might be used.

A NEW GENERAL PURPOSE CORRELATION FUNCTION COMPUTER

Ian H. Quayle
AIM Electronics Ltd.
Cambridge
England

Summary

A brief introduction to correlation technique is given, followed by a description of a hybrid correlation function computer.

Correlation Technique

Correlation is the process of judging the similarities between two things. In particular it gives us a measure of the degree of similarity. In signal recovery and processing the things which we wish to compare are generally voltage waveforms as a function of time, and it is the correlation of these waveforms which we will be considering in this paper.

The correlation coefficient is defined as the long term average of the product of the two waveforms. Thus at every moment in time, the instantaneous value of one of the waveforms must be multiplied by the instantaneous value of the other. It is relatively easy to see that, if the two waveforms have a great deal of similarity to one another, then they are likely to be both positive or both negative, at the same instant in time. This means that all the products appear as positive values. After averaging then, the correlation coefficient has a positive value. On the other hand, if the two waveforms are entirely dissimilar then chance positive products tend to be offset by negative products obtained by multiplying a positive value with a negative value. It can be shown that in this case the correlation coefficient will be zero. A third case exists where one of the waveforms is an inverted version of the other. This implies that the product at any instant in time will be made up of one positive value, and one negative value. Thus all the products will be negative and so will the correlation coefficient.

Now, in many practical experiments which involve correlation one of the waveforms may be treated as a reference, and the other as the signal, and there is usually some time delay between the two. This delay occurs as the signal is propagated through the experimental system. Simple evaluation of the correlation coefficient in this case is insufficient since it takes no account of the delay between the waveforms. A more meaningful approach is to apply a delay to the reference waveform, in order to compensate for the delay in the signal waveform, and then perform the correlation. Even more information may be gained by making the delay on the reference waveform, a variable one so that the correlation coefficient may be plotted as a function of the delay time. This plot is called the Cross Correlation Function and is expressed mathematically as

$$\phi_{12}(\tau) = \lim_{T\to\infty} \frac{1}{2T} \int_{-T}^{T} f_1(t) f_2(t+\tau)\, dt$$

Note that the limits of the integral here extend to all time. In practical correlation experiments a low pass filter is usually used for the integrator and provided that the time constant of this filter is an order of magnitude larger than the longest period occuring in the two waveforms, the error introduced is negligible.

We may qualitatively think of the cross correlation process in terms of FIG.1. Here we have two waveforms, $f_1(t)$ which is fixed in time. The second waveform, $f_2(t)$ has a variable delay applied to it and so it becomes $f_2(t+\tau)$. The limits of T, the integration time, comprise a time window through which we can look at the two waveforms. As the delay time is slowly varied we continuously compute the cross correlation coefficient and plot it as a function of τ. If at any value of τ, the waveforms have some similarity, then the value of the cross correlation function is positive. Thus the cross correlation function is a continuous assessment of the similarity of the two waveforms as the delayed one moves across the stationary one. Anstey describes this very nicely in saying that one waveform "is searching to find itself in the other". When it does so we have a positive peak in the correlation function. If it finds an inverted version of itself, we have a negative peak.

If we go back now and consider cross-correlation in the generalised experiment mentioned above, we can see that the correlation function will give a number of pieces of information about the system in the experiment. We can assess the propagation delays in the system and possibly discover and characterise multiple propagation paths. Further, since the action of the system upon the input waveform must be implicit in the type and degree of similarity between our signal and reference, we have the opportunity to completely specify the system by means of correlation process.

Classical methods of specifying the response of systems include the use of Bode or Nyquist plots which involve amplitude and phase measurements made at all frequencies within the bandwidth of the system. Another commonly used method is to examine the behaviour of the system in response to a delta function input. The Dirac delta function is a single impulse or 'spike' at time zero having infinite amplitude zero time duration and unit area. The practical difficulties of impulse response testing are sometimes very severe. The impulse function may be difficult to achieve in practice and some compromise has to be made. It is important that the power spectrum of the impulse, within the bandwidth of the system, is constant, and a practical impulse might not give this. Overload is another problem encountered in active systems which have a finite dynamic range. Further, system noise may cause difficulties in observation. Since all the classical methods require measurements to be made "off-line" they

could give rise to significant commercial losses where the optimisation of industrial process control systems is concerned. An approach, using correlation techniques, gives the impulse response of the system and at the same time avoids the problems outlined above.

The power density spectrum of white noise is theoretically the same as that of the impulse i.e. constant for all frequencies. If we then inject such a signal, having a constant power density spectrum, k, into our system and cross correlate this with the system output we find that we can obtain the impulse response of the system. This result is formalised in the Wiener-Lee relationship.

$$\phi_{io}(\tau) = \int_{-\infty}^{\infty} h(t)\,\phi_{ii}(\tau - t)\,dt$$

The cross correlation function is equal to the convolution of the auto-correlation function of the input, with the impulse response h(t) of the system. It can be shown that when the spectrum of the input signal is broad, relative to the bandwidth of the system, this reduces to the simple relation $\phi_{io}(\tau) = h(t)$ so that the cross correlation function of the input and output is the impulse response of the system. Note that the Wiener-Lee equation does not specify the type of input signal, but concentrates primarily on its spectrum. An example of a cross correlation computer in use in this type of application is shown in FIG. 2. Note also that since the Correlation Computer is only comparing the input and output of the system, the method is insensitive to noise generated within the system itself. Since this noise is independent of the input to the system it cannot have any correlation with it and it is simply averaged out in the correlation process.

FIG.1. The Cross-Correlation Process

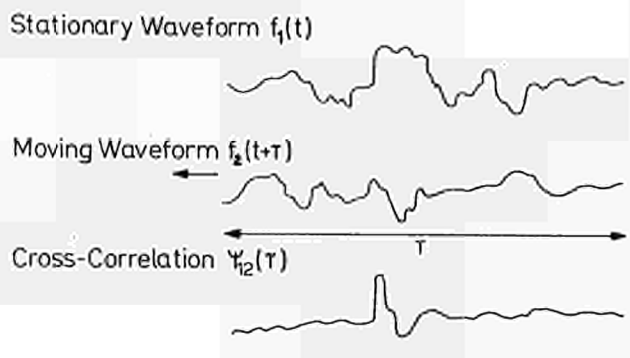

FIG. 2. Determination of the impulse response of a linear system by correlation, using white noise stimulation

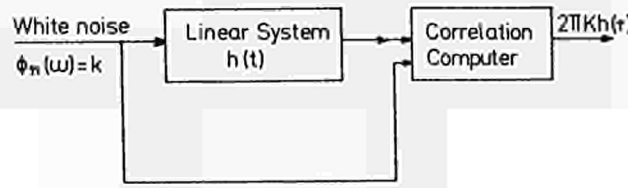

Auto-Correlation

In the looking at Wiener-Lee equation we briefly mentioned Auto-Correlation. We will now look at this in a little more detail. Auto-correlation is the process of correlating a waveform with itself. The auto-correlation function is expressed mathematically as

$$\phi_{ii}(\tau) = \lim_{T\to\infty} \frac{1}{2T} \int_{-T}^{T} f_i(t)\,f_i(t+\tau)\,dt$$

If we consider auto-correlation for both positive and negative values of delay, it is apparent that the function must be even, that is to say that it is symmetrical about the $\tau = 0$ axis. The particular merit of the auto-correlation function is that it is a time waveform which is displaying spectral information. One can accept this in a general way by considering a signal having a very narrow spectrum (e.g. a sine wave). This must always have a cyclic similarity with a time shifted version of itself. On the other hand, a signal having a broad spectrum (e.g. white noise) will only require a small time shift before all similarity is lost, because the instantaneous value of the signal is completely independent of the value at any other instant.

The Wiener theorem for auto-correlation formalises this

$$\phi_{ii}(\tau) = \int_{-\infty}^{\infty} \Phi_{ii}(\omega)\cos\omega\tau\,d\omega$$

AND

$$\Phi_{ii}(\omega) = \frac{1}{2\pi}\int_{-\infty}^{\infty} \phi_{ii}(\tau)\cos\omega\tau\,d\tau$$

The auto-correlation function of a waveform is thus related to its power spectrum by a Fourier cosine transform.

The auto-correlation function is a unique characteristic of a waveform. However, any auto-correlation could be derived from a whole family of waveforms. This is so because auto correlation ignores any phase information in the waveform, and concentrates only on the power spectrum.

Practical Correlators

The requirements of any correlator are shown in FIG 3.

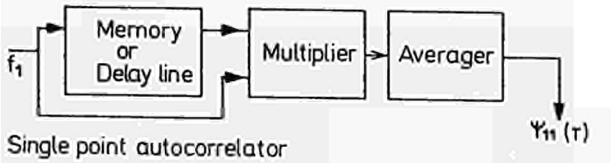

Single point autocorrelator

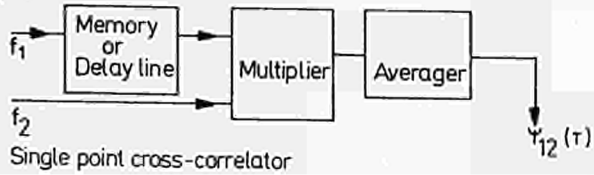

Single point cross-correlator

Block diagram of single point correlators

The only difference between an auto-correlator and a cross correlator is that in the first case the two inputs are connected together in parallel. The time delay τ at which the single point correlation is computed is provided by the memory or non-dispersive delay line. Negative delays with respect to the f_1 channel are achieved by switching the delay line to the f_2 channel. The multiplier involved should always be of the four quadrant type, and the averager is commonly a simple RC filter network.

In order to compute the whole correlation function, the delay line must be variable, and a practical example of this is shown in FIG 4.

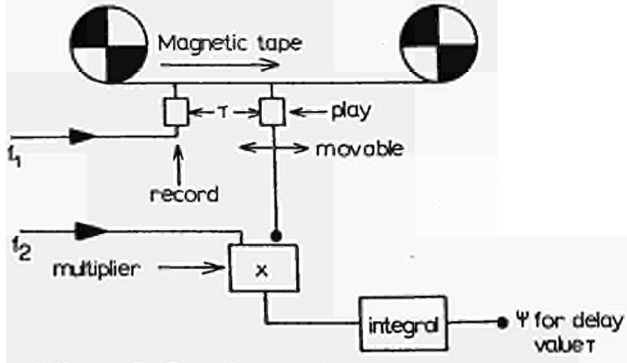

A Magnetic Tape Correlator

A magnetic tape recorder is used as the delay line. The input to be delayed, f_1 goes to the recording system. Separate record and playback heads are provided so that the interval between the signal appearing at the record head and being picked up by the playback head may be varied. Thus the delay time τ depends on the tape speed and the distance between the two heads. Due to mechanical problems it may be impractical to achieve zero delay, since there must be a limit to the smallest distance between the heads. In this case it would be necessary to use a second delay line in the second channel to provide a fixed negative delay offset. Since the value of the correlation function is likely to be different at each value of delay it follows that after each movement of the playback head sufficient time must elapse for the final value of the correlation function to settle in the output integrator before the value is plotted. Thus if reasonably long integration times are to be used it could take a very long time to plot the whole correlation function. This type of system cannot be said to operate in "real time".

The AIM general purpose correlation function computer

This computer fills a considerable need for a general purpose real time correlation system, at a reasonable price, and the development programme was aimed at producing an instrument which is both versatile and easy to use. The computer can be used for cross and auto correlation, and multi sweep signal averaging (or delta function correlation as it is often called). In addition, access to the internal memory is available so that transient phenomena may be stored and later non-destructively read out, at any rate.

The manufacturers specialise in modular instrumentation, particularly in the field of signal recovery. The standard racking system is ISEP but modules are also supplied in NIM. The correlation function computer can be referred to as modular for two reasons. Firstly it complements an existing modular range which can be used for extending the facilities of the instrument. Secondly the internal construction is modular. The internal delay and memory system is readily extendable and the cards which contain the peripherals may be changed in order to modify the input or output characteristics.

The basic block diagram of the correlation computer is shown in FIG 5. The delay line, or memory is a digital one consisting of a one hundred word shift register which is theoretically extendable up to and above 1000 words. Only three bits per word are used but the resolution of the system is improved by using special techniques in the analogue to digital conversion required to load the shift register.

FIG. 5. Block diagram of the AIM Correlation Function Computer

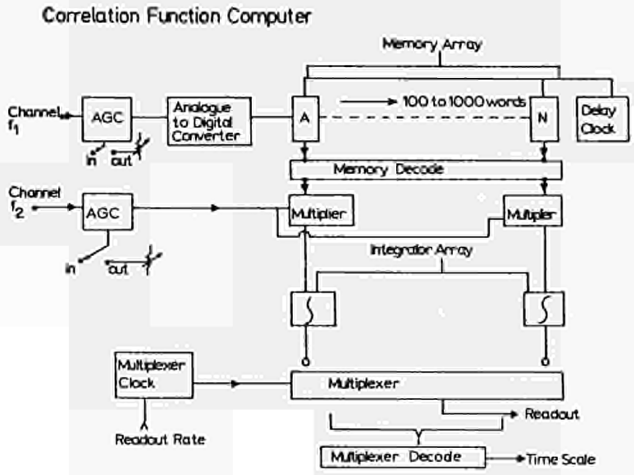

The shift register is clocked by the Delay Clock. Since the basic model has a one hundred word register, the maximum delay available at any rate of the Delay Clock is 100X the Delay Clock period. Thus after entering the register a particular binary word is transferred successively from one location to the next until it emerges from the shift register, and is lost, one hundred Delay Clock pulses later.

Each of the one hundred word memory elements consists of three J-K flip-flops. These are in integrated circuit form and use RTL type circuitry. Each of the hundred sets of three flip-flops are associated with a digital to analogue convertor comprising switched voltage sources and a resistive summation system. Thus from each of the hundred memory word locations the voltage analogue of the three bit binary word stored in that location, is available. The hundred outputs from these digital to analogue convertors go to one hundred four-quadrant multipliers having a common input derived from the second channel.

The multiplication is achieved using a pulse width modulation technique. This uses a 1MHz rectangular pulse train whose mark/space ratio is dependent on the instantaneous amplitude of the second channel. The amplitude of the pulse train is dependent on the output from any individual memory location. Thus the mean value of the pulse train at any time is equal to the mark-space ratio (channel 2) multiplied by the amplitude (channel 1).

It will be recalled that earlier we stressed that the multiplication performed should be of true four quadrant form, that is, both of the inputs, and the outputs, can have positive or negative values. Now a digital delay line such as the one described cannot readily carry bipolar information except by the addition of an extra bit to carry the sign of the binary number. To overcome this we add a d.c. offset to the channel 1 input before it is digitised by the analogue to digital convertor. This means that a binary word, in the register, greater than 100, is positive, a binary word of less than this is negative. The offset is subtracted in the digital analogue conversion at each memory location.

The output from each of the one hundred multipliers goes to a low pass RC filter having a time constant of ten seconds. This gives a noise equivalent bandwidth of 0.025Hz in each storage element. The voltage stored on the capacitor of each filter gives single point on the correlation function.

We may consider the operation of the correlator as a whole as we follow one word down the register. Let the Delay Clock period be t. At a time t the word finds itself in the first memory location. It is then multiplied with the value of the input to the second channel at this time, and the product fed to the output integrator of location 1. After N clock pulses the word finds itself at location N, at a time Nt. It is then multiplied by the value of the input to channel two. Note that this is the value of channel two at a time $(N-1)t$ after the first multiplication took place. In other words the multiplication occurs with a delay of Nt on channel two. It is not immediately obvious that channel two is having the effective delay applied to it, and not channel one.

The system then, really consists of one hundred separate single point correlators having one input common to channel two and the second input to the appropriate one of a hundred outputs from the digital delay line. All we need to do, to look at the complete correlation function is to scan across the hundred integrators successively.

Provided that the sampling of the voltage on the integrator capacitors can be done non-destructively we can perform this scan as rapidly or as slowly as we wish. If at the same time we can generate a second output voltage whose value depends on the location of the integrator output being sampled, we have available two voltages comprising the two axes of the correlation function.

In the AIM correlator, a two decade counter followed by a 1 in 100 diode decoding matrix is used to address each of the hundred integrators in succession. At the same time the outputs from the counter go to a BCD to analogue convertor. This generates a 100 step staircase for use as a delay time axis when displaying the correlation function on an oscilloscope or X-Y plotter.

Analogue to Digital Convertor

We mentioned earlier that although a word of only three bits was used in the digital delay line, the overall resolution of the system was much better than the 12% which one would normally expect from this. The enhanced accuracy is achieved by effectively pulse width modulating the least significant bit of the binary word. A triangular waveform is mixed with the signal input to the analogue to digital

convertor. The peak to peak amplitude of this triangular waveform is approximately equal to the resolution of the convertor, $\frac{1}{8}$X full scale. This causes the least significant bit from the convertor to change at a rate mainly dependent on the frequency of the triangular waveform. The frequency is nominally 1MHz but it is also frequency modulated in order to avoid beating with the Delay Time clock.

The operation of this technique for enhancing the convertor's resolution may be understood by considering the input voltage to be such that it is exactly midway between any two of the voltage thresholds at which the output may change. The action of the triangular wave superimposed on the input voltage is nil since it only just reaches the thresholds and cannot exceed them. However, if the input voltage now changes so as to approach one of the thresholds, the tip of the triangular wave now crosses the threshold for an instant. Therefore the output from the convertor assumes the new value for this time. Note that the nearer the input voltage gets to the threshold the longer the time during which the triangular wave is over the threshold and thus the longer the output from the convertor holds the new value. Since the correlator effectively averages this output it is evident that the use of a three bit word does not limit the resolution of the instrument.

The use of this technique for raising the resolution of the analogue to digital convertor is possible because of the speed of conversion obtainable. The basic convertor consists of seven integrated circuit comparators deriving their reference voltages from a potentiometric divider chain. The outputs from the comparators go to a matrix of gates used for decoding into binary. The decoding matrix was designed to give equal propagation delays to each bit so that the three bits changed simultaneously. Three bits appears to be the limit to this type of conversion method since one extra bit would require another eight comparators and much more complex decoding.

Input Stages

The two channels to the correlator each go to a special input stage which can operate in one of two ways. The requirement generally is for the input signal to be normalised so that it may use the whole dynamic range of both the analogue to digital convertor and the pulse width modulation multiplier.

Facilities are provided for achieving this normalisation automatically by means of an A.G.C. amplifier. This has a dynamic range of 60dB, and a high level/low level switch provides another 60dB. The gain control element is a field effect transistor used as a variable resistor. This forms part of the feedback loop of an amplifier and hence controls the overall gain. The signal applied to the FET is at a very low level in order to eliminate distortion due to the non-linear characteristics of the device.

In some applications, however, for example when the waveform to be correlated is arriving atrelatively long intervals, or when transient recording is required, the AGC cannot be given sufficient time to adjust the gain to a correct value. In a case like this it is convenient to be able to set the gain manually to a known value. This is achieved by switching out the A.G.C. and using an attenuator and fine vernier control to adjust the gain of each input amplifier. Associated with each input channel is a warning lamp to show if the gain is too high and the analogue to digital convertor or pulse width modulation multiplier is exceeding full scale.

Delta Function Correlation

Delta function correlation is a form of multi-sweep signal averaging. The AIM correlator is able to perform this by gating the Delay clock from a sync. pulse associated with the waveform to be averaged. The system operates like this. On arrival of a sync.pulse, the Delay Clock is started and clocks the delay register one hundred times. The register now has stored one hundred points on the waveform to be averaged. The same procedure may be used for recording transient phenomena. A delta function is then applied to channel 2. In practice the pulse width modulator is by-passed and the multipliers simply used as analogue gates which allow a sample of each point in the delay register to be entered into its appropriate integrator. The process is then repeated after the arrival of the next sync. pulse. Thus in the hundred integrators, one hundred points on the signal waveform are gradually built up as successive samples of the waveform are added to those already in the integrators. Any random element such as noise, in the signal, is averaged out leaving only components common to each sample. The averaged waveform may be viewed in the same way as for viewing a correlation function, by means of the output multiplexer.

Performance Specification

The frequency response of the computer is limited at low frequencies by the input coupling time constant. The present system can be used down to 0.1Hz. At high frequencies, the performance is limited by three factors. These are, the available bandwidth of the pulse width modulation multipliers, the speed of the analogue to digital convertor, and the maximum clocking rate of the shift register delay line. The maximum toggle frequency of the flip-flops used in the shift register is specified as 3MHz. In practice a maximum clock rate of 1MHz is used. The carrier frequency of the pulse width modulation multipliers is 1MHz. Frequencies higher than 250KHz may cause sub-harmonics of the carrier frequency to appear in the demodulated signal. For this reason the upper frequency response is specified at 250 KHz, although the system is capable of operating up to 500KHz. The input channels can accept signals from 10mV to 1000V peak to peak. Since the computer forms part of a modular range many features of its performance may be easily extended. For example there are a number of

low noise amplifiers available, capable of improving the input sensitivity providing differential input facilities, and giving input impedances above 10^{12}ohms. In addition the averaging time constant may be increased by interfacing the correlator with a small digital computer. A fast eight bit analogue to digital convertor having British Standard Interface is available. This may be used to multiplex the voltage from the hundred multipliers into the computer which then performs the integration digitally.

In addition, a modular waveform sampling adaptor, having a bandwidth of more than 1GHz may be used to extend the performance of the correlator into microwave frequencies.

Correlograms

The following series of oscilloscope photographs are correlograms taken using the prototype correlation function computer. The analysis required to derive some of these correlation functions can be found in the references given at the end of this paper.

In each of the correlograms the top trace shows the waveform to be correlated, the lower trace is the output from the correlator displayed on the oscilloscope. The top trace uses real time as the horizontal axis, the lower trace uses delay time . The computation of these correlograms was done in real time, the output of the computer settling in about 45 seconds.

Correlogram 1.

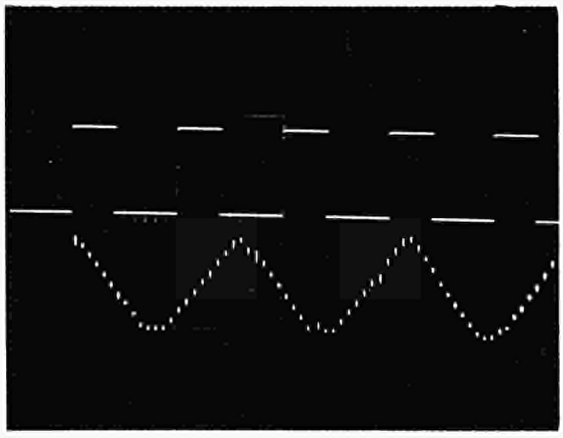

This is the autocorrelation of a rectangular waveform. The resulting correlation function is a triangular wave. This may be predicted graphically when one considers that at zero delay time the pulses overlap and hence all the auto correlation products are either zero or positive. As the delay time increases linearly, the area of overlap decreases linearly and hence the auto-correlation function is a linear ramp going to zero. When the delay time has increased sufficiently for the pulses to start to overlap again we obtain a linear rise up to the value obtained at zero delay time. Note that there is a flat bottom between the triangles. This is because the pulse train has a 2/3 mark/space ratio and this creates a delay period, of one fifth of the pulse repetition period, during which no overlap occurs. During this time the auto-correlation function must be zero.

Correlogram 2

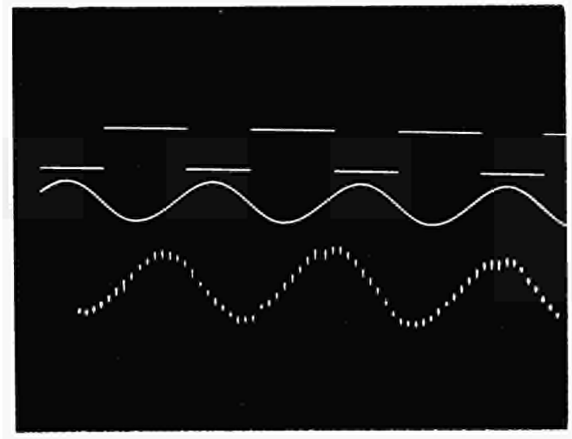

This is the cross-correlation of a rectangular pulse train with a sine wave of the same frequency. The sine wave is effectively locked 180^{o} out of phase with the fundamental component of the rectangular pulse train. The correlogram is a sine wave of the same angular frequency as the reference sinusoid. An identical correlogram would be produced from two similar sine waves locked in antiphase. This effectively demonstrates how the correlation process ignores components present in only one of the functions involved in cross-correlation. The odd harmonics present in the rectangular wave are simply averaged to zero. Note that since the two signals have a 180^{o} phase difference the correlogram has a negative value at $\tau = 0$.

Correlogram 3

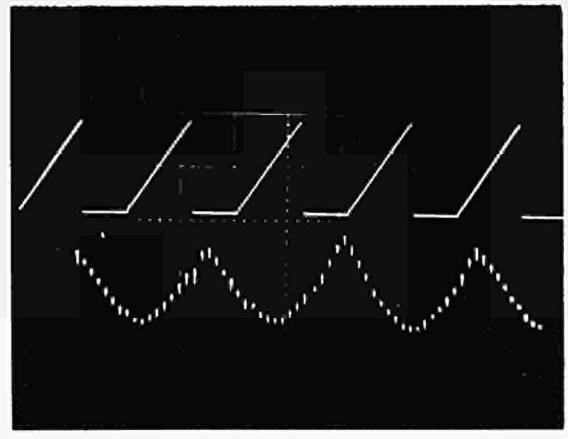

This is the auto-correlation of the triangular waveform shown. This has been treated analytically by Lee and the correlogram shows agreement with the theory.

Correlogram 4

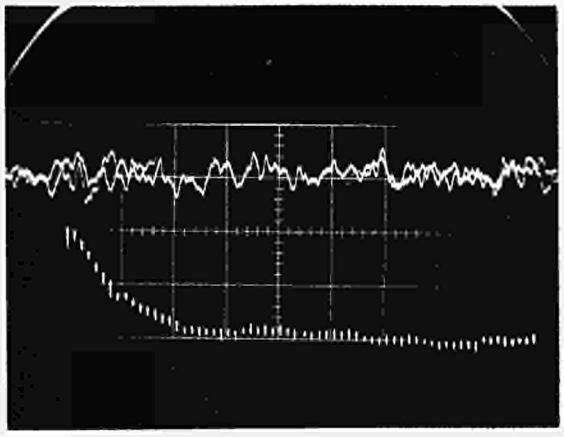

This shows the auto-correlation of band limited noise. If the noise had a bandwidth wider than the correlator then the function would simply be an impulse at $\tau = 0$, having an amplitude equal to the normalised mean power of the noise. Since the noise has been limited to less than the bandwidth of the computer, we obtain an exponential decay. The value at the point of the exponential gives the mean power of the noise and its time constant is the reciprocal of the bandwidth of the noise.

Correlogram 5

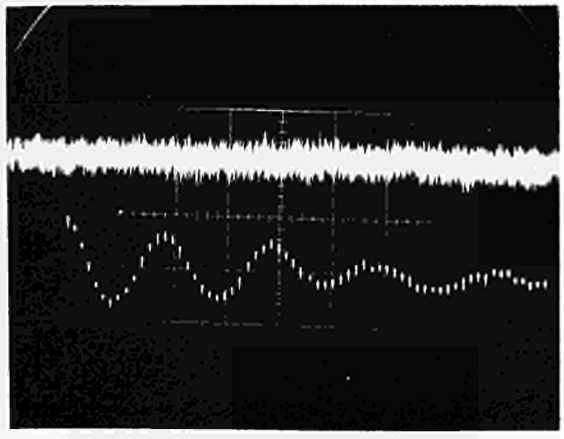

This shows the impulse response of an active filter which is part of an AIM modular instrumentation system. The filter was stimulated with white noise, shown above the correlogram. The output from the filter was cross correlated with the input to give the impulse response shown. It is possible to estimate the Q and centre frequency of the filter from this correlogram.

Acknowledgements

The author would like to thank Richard Cutting, who did most of the development work on the correlator and obtained the correlograms, for his assistance in the preparation of this paper, and Gordon Edge for his help and encouragement.

References

ANSTEY N.A. - An Introduction to Correlation Techniques (Data Correlation Division of Seismograph Services Ltd. 1963)

BENDAT J.S. - Principles and Applications of Random Noise Theory (Wiley 1958)

LEE J.W. - Statistical Theory of Communication (Wiley 1960)

DISCUSSION

Cooke-Yarborough : - I'am interested in the use of 100 analog separate integrators, because there is an attempt being made to do equivalent things for pulse height analysers. There have been pulse height analysers deviced with separate analog integrators for every channel and they appear not to have succeeded for a number of reasons, as far as I can make out, such as difficulty in equating the channels and just the sheer cost of these large analog elements. I would well like your comments on whether you feel that these elements have now advanced in quality and neatness so that their use in pulse-height analyser is now justified.

Quayle : - I am not familiar with pulse height analysers I'm afraid. The integrators, in the case of this correlator are simple RC networks and they are not operational integrators. The RC networks have a time constant of 10 sec. and in fact we have shown that the simple RC integrator for this particular application is adequate, so in fact the cost is quite small. It can be shown that the errors introduced in using a finite integration time, in this case, are quite small.

De Lotto : - I don't know if I have correctly understood all that you have said. I would like to know something about the multipliers. Can you explain how you take the product between digital quantity and the analog one ? I'm making this question as I have not seen in your block diagram any digital-to-analog converter for the upper quantity before the multiplier.

Quayle :- The digital to analog converter are actually part of the multiplier circuits and receive their inputs from the digital delay line. The pulse width modulator which operates on channel 2 can be regarded as a peripheral, serving the multipliers. Thus the output pulse train from the multipliers contains pulses whose width is dependent on channel 2 and whose amplitude can have one of eight discrete levels, given by the delayed, digitized, version of channel 1 . Thus the pulse area is the product of channel 1 and channel 2.

Miller : - I don't know whether it is in order to ask you about a competitor's product, but I think Princeton Applied Research make such a correlation computer. Now do they use the same technique, namely a digital shift register memory ?

Quayle : - I vaguely heard about the Princeton correlator. I believe they use a digital delay line. That's all I know about it I'am afraid, and it is also very expensive.

Miller : - I've heard rumours that it was all analog and I wanted to know if you knew, because it would be another possible way to do it. I've just heard the rumour that it was done by a capacitor system, a string of capacitors, which pass the sample along.

Quayle : - No, I don't think so. At the present state of the art, a digital delay-line is about the only way we can do it. We had quite a long development program, looking for an analog memory system and it is very difficult to do. I'm fairly sure that Princeton uses also a digital delay line.

Radeka : - I have one question only, possibly, two. For what frequency range is this system intended ?

Quayle : - The basic correlator will operate from 1 Hz to 100 KHz. But we can extend the range of the system putting in a sampling adaptor on the input, which effectively gives the bandwidth of 1 gigaherz.

Radeka : - I'm just wondering how one would compare this for high frequencies. It seems to me that the methods described in several reports by Amsel's group would be more suitable, actually for the frequency range above 10 KHz. For lower frequencies fast Fourier transform methods might be implemented with not much hardware if any.

Quayle : - Whilst agreeing that fast Fourier transform analysis methods can operate on the same range of frequencies as this correlation computer, they have the disadvantage that they require a large amount of expensive hardware.

Radeka : - Well, this system is actually quite complex too. So it might he worthwhile to evaluate it.

Quayle : - Well, actually it is not too complex. I did not intend to show a picture of the correlator because of time restrictions, but the whole system fits in a 19" rack and the depth is only about 11".

SWITCHING CIRCUITS OPTIMAL CONFIGURATION FOR AMPLITUDE DISCRIMINATION AND TIMING

N. Abbattista, V.L. Plantamura, G. Giannelli
Istituto di Fisica dell'Università di Bari, Bari, Italy
M. Coli
Laboratori Nazionali di Frascati del CNEN, Frascati (Roma), Italy

ABSTRACT

The switching circuits in their typical applications as amplitude discriminators and timing shapers were studied describing the output random process as a function of the input signal parameter random distributions. We show that the effect of the fluctuations of some input signal parameters randomly distributed may be reported to the input as a noise contribution to be added to the input signal noise. We propose then a deterministic model to allow the input to the output transformation. Finally, we discuss some circuit configurations suited to perform the optimal information treatment for amplitude discrimination and timing.

INTRODUCTION

We are dealing here with non linear regenerative circuits, in their typical applications as amplitude discriminators and timing shapers, with the purpose to describe the output random process as a function of the input signal parameter random distributions.

The noise contribution at the input of those circuits has to be though as a constant spectral power density covering the whole bandwidth of the switching device.

The purpose of this paper is to give a method based on a deterministic model suited to represent the noise contribution on a switching device, for the evaluation of complex configurations features and effective for the solution of their optimization problem.

THRESHOLD PROBABILITY FUNCTION

Following the procedure proposed in a previous paper[1], we suppose to have drawn experimentally the diagram of Fig. 1 on which, as a function of the input amplitude, the switching rate of the circuit under test, is reported.

We may interprete the curve as a cumulative probability function of the circuit threshold, Infact, if the input pulse amplitude S is assumed as a threshold value, the curve F(S) will give the probability that the circuit actual threshold lies between $-\infty$ and the value S under consideration.

The derivative of this curve is the probability density function of the threshold W(S).

To give the best approach for F(S) we simulate a tunnel diode monostable switching configuration on a digital computer. Input signals were step shaped pulses on which a telegraphic signal was superimposed, random amplitude and time being the two successive extractions of a Montecarlo set. Amplitude and time margins were of such a value to assure a given power and bandwidth for the input noise. The switching is established by the regenerative condition reported by many authors[2,3] as the "switching condition".

The results we obtained allow the following expressions for the cumulative probability function F(S) and for the probability density function W(S).

$$F(S) = \frac{1}{\sigma\sqrt{2\pi}} \int_{-\infty}^{S} e^{-\frac{(\xi - S_o)^2}{2\sigma^2}} d\xi$$

$$W(S) = \frac{1}{\sigma\sqrt{2\pi}} e^{-\frac{(S-S_o)^2}{2\sigma^2}}$$

These are the normal distribution functions. The value of σ is dependent on the actual power level acting on the circuit, that is indirectly, on the bandwidth of the whole switching configuration.

OUTPUT AMPLITUDE DISTRIBUTION

Now we may take advantage of the above definitions of input threshold characteristic functions, to obtain the amplitude distribution function at the output of the circuit.

We must start with the following considerations. The contribution to the output amplitudes due to the intrinsic regenerative mechanism is accounted for introducing a rigid gap in the output distribution. This is the result of a simple reasoning about an ideal device, capable of infinitely sharp discrimination from a state 1 (low) to a state 2 (high).

It is easy now to guess that the noise would modify only the hem between the two states, and increase the number of pulses (zero in the ideal device) whose amplitudes are within the gap interval.

We propose then to characterize this modification on the output number of pulses N(A) of a given amplitude A, with the same expression defining the number of switchings F(S) for a given input amplitude S. So the output amplitude distribution N(A) will result as follows:

$$N(A) = 1 - F[R(S-S_o)] + F[R(S-S_1)]$$

where R is a dimensional factor $[\Omega]$, $R(S_1-S_o)$

is the value of the regenerative gap of the active element considered in its circuital configuration.

The given interpretation of the phenomenon is in good agreement with the results obtained from the simulated experience on a digital computer as before referred. Fig. 2 shows how far this agreement is worthwhile.

NOISE FROM INPUT RISE TIME JITTER

The standard deviation σ of the threshold density function that is the extention range of the noise contribution on threshold probability function and output amplitude density, is dependent on the actual noise level p acting on the device characterized by its factor of merit K.

$$\sigma = f\,[\,p(K)\,]$$

We try then to find the expression of F(S) for the same switching configuration in absence of input equivalent noise, but triggered by pulses of random amplitude and randomly variable rise time τ, fast enough to be considered at the highest margin of the device bandwidth. We found again $\sigma \neq 0$ as in presence of noise.

In Fig. 3 we report the F(S) for input noise equivalent to the input randomly variable rise time. Obviously the effect on the output amplitude distribution can be determined with the same transformation,before suggested. The rise time jitter can then be referred as an input equivalent noisy power generator.

OUTPUT PULSE DELAY

One of the characteristic of the switching circuit commonly used is the delay of the output pulses as a function of the input pulse amplitudes. This too can be derived only with counting operations and taking into evidence a new cumulative switching probability diagram. We might follow the procedure hereafter: given a fixed input amplitude we draw the switching diagram varying the input pulse duration. The amplitude must be sufficiently great to assure the switching incertitude due to noise amplitude be negligible with respect to the pulse duration jitter.

As suggested before we reach a definition of the probability density W(D) of the circuit threshold relative to the pulse duration parameter together with the most probable value D_o of this threshold and its standard deviation.

The input pulse amplitude can then be associated with a delay of the output pulse equal to $D_o + T$ being T a fixed delay established by the point of reference used to measure the delay. Recurring the experience for many input amplitudes we can draw the diagram of the most probable delay and its jitter as a function of the input pulse amplitude.

PARALLEL AND CASCADE CONFIGURATIONS

Practically timing and discrimination are accomplished by parallel or cascade configurations of switching circuits. For the parallel configuration the output amplitude distributions convergence in an ideal coincidence circuit. We assume the intrinsic noise of the devices to be independent, and we ask for the cumulative probability of the threshold at the output of the coincidence $F^P(S)$.

For only two parallel channels of the same most probable threshold value, we have obviously:

$$F^P(S) = [F(S)]^2$$

It can be shown that the most probable threshold value, obtained by the distribution function, is shifted towards greater values of input amplitudes and that its standard deviation is sharply decreased.

The uncorrelated noise contribution (not on the input line) intrinsic to the devices goes to zero for the number of parallel channels going to infinity.

Given the cumulative probability F(D) of a single circuit, we consider the output coincidence a logical AND (resolving power equal to ∞). Evaluating the probability to obtain an output pulse within the time D we give, for the delay distribution function at the output of a double channel parallel configuration, the expression:

$$W^P(D) = 2\,W(D)\cdot F(D)$$

being the factor 2 worthwhile if the F(D) of the two circuits is the same.

Cascading two switching configurations the whole cumulative probability function $F^C(S)$, is the product of the output distribution function of the first circuit and the threshold probability function $F_2(S)$ of the second one.

Now again we can show an increase of the value of the most probable threshold (for two identical devices) and a sharp decrease in its standard deviation.

It might be possible to design the optimal configuration featuring the threshold with a very low standard deviation, but problems can arise from the absolute value of the whole sensitivity of the circuit.

Improvements in noise rejection attained by cascade configurations are established also for the input signal superimposed and not only for the device intrinsic component.

Regarding the distribution function of the first stage output for a given input signal amplitude and considering that the output pulses are standardised with respect to the time duration and have amplitude much greater than the threshold for infinite duration, we can conclude that the cascading modifies very little the delay distribution functions.

The foregoing examples can show how we have established a deterministic model of input output transformation to be exploited in problems of timing or discrimination. As far as this model might be adherent to the phenomena, it allows to evaluate on a computer the features of complex switching circuit configurations and to

start with their optimisation problems. Starting only from the information obtained by the curve defining the threshold as a statistical quantity, we deal now with mathematical calculations and quantitative evaluations of some more typical switching configuration are now in progress.

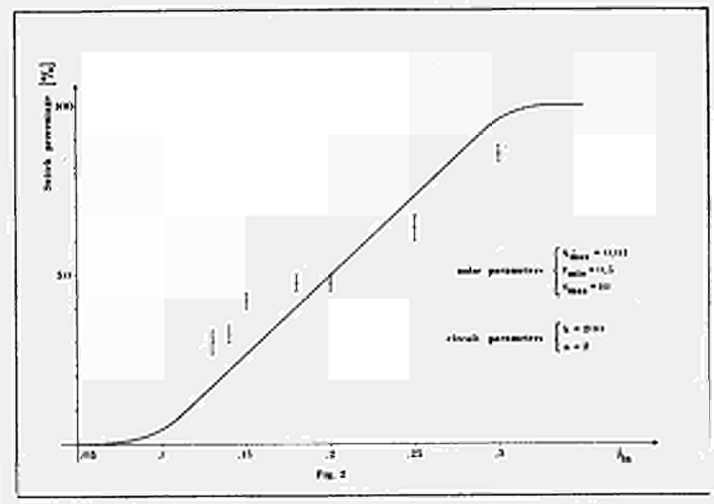

BIBLIOGRAPHY

1) N. Abbattista, M. Coli and V.L. Plantamura, Nucl. Instr. and Meth. 45, 157 (1966)

2) I. De Lotto and L. Stanchi, Rapport Euratom, EUR 430

3) I. De Lotto, P.F. Manfredi and L. Stanchi, Alta Frequenza 35, 830 (1966)

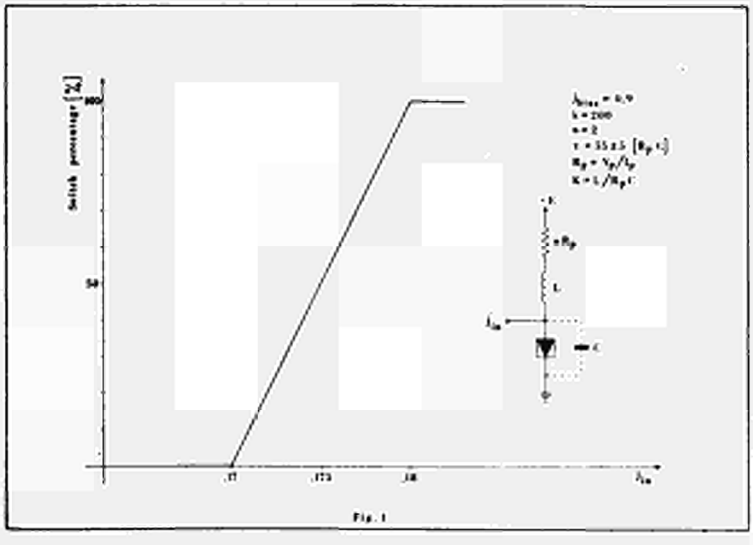

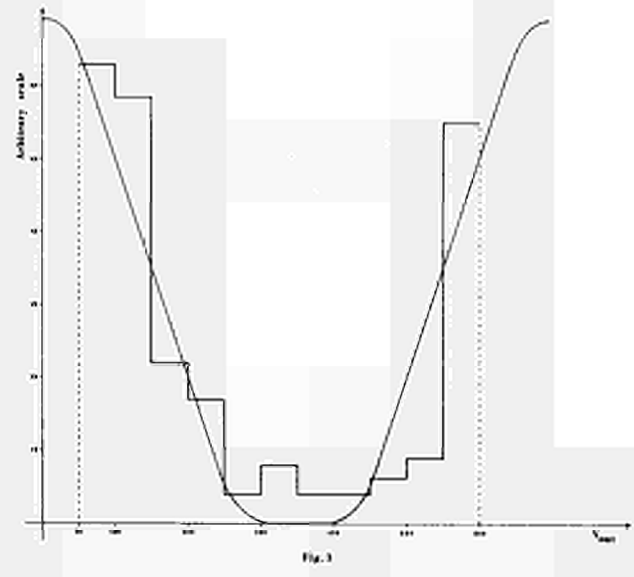

A METHOD FOR THE ANALYSIS OF COMPLEX GAMMA-RAY SPECTRA USING A COMPUTER

Tamon Inouye

Central Research Laboratory
Tokyo Shibaura Electric Co., Ltd.
Kawasaki 210, Japan

Summary

A computer method is developed for the analysis of complex gamma-ray spectra obtained by the Ge(Li) detector. The computer code by this method carries out smoothing, background subtraction and peak sorting of the multichannel pulse height distribution. By applying this method, 800 channel pulse height distributions of gamma-ray spectra have been analyzed.

I. Introduction

According to recent developments in lithium drifted germanium detectors, highly resolved gamma-ray spectra are available in the analysis of gamma-ray energy and intensity. This improved technique provides so highly resolved spectra that fine structures of the spectra can be observed. However, the spectra are so complicated by random statistical fluctuations and strange distributions of the background radiation that they are difficult to describe mathematically.

The author has developed a new mathematical method for the analysis of these complex gamma-ray spectra and made a computer code for the automatic reduction of such data.[1] The main mathematical procedures used in this method are as follows:

i) Smoothing of the spectra.
ii) Determination of the background distribution and subtraction of this component from the smoothed spectrum.
iii) Improvement of resolution.
iv) Sorting of the peaks.

As an application of this computer method, the author has analyzed an 800 channel pulse height distribution of the gamma-ray spectrum obtained from radionuclides produced by the fast neutron irradiation and successfully obtained many peaks automatically. This computer code contains calculations of all necessary corrections such as neutron intensity fluctuations. By this computer code, each complex spectrum can be processed within 10 seconds using a GE-635 computer.

II. Methods of Analysis

1) Smoothing of the Spectra

For the smoothing of the spectra, the method of the Fourier analysis is used. In principle, it may be explained as follows:

i) Transformation of the whole spectrum into the frequency space.
ii) Multiplication of a proper filter function to the frequency distribution function of the spectrum.
iii) Inverse transformation into the original energy space.

The raw data expressed by the function f(E), where the variable E is the energy expressed by the channel number of the pulse height analyzer, can be divided into the true distribution s(E) and the component of random fluctuations expressed by n(E) as follows:

$$f(E) = s(E) + n(E). \qquad (1)$$

The frequency (referred to as "energy frequency") component of these distributions is defined by using the Fourier transforms. Denoting the Fourier transformed functions by the corresponding capital letters, as

$$F(\omega) = \int_{-\infty}^{\infty} f(E) \exp(-i\omega E)\, dE, \text{ etc.},$$

eq. (1) is expressed in the frequency space as follows:

$$F(\omega) = S(\omega) + N(\omega). \qquad (2)$$

The extent of the frequency distribution is, roughly speaking, inversely proportional to the correlation length of the raw data, so we can approximately know the frequency distribution of $S(\omega)$ and $N(\omega)$. The function $S(\omega)$ is quite different from $N(\omega)$ because the original function s(E) in the energy space has a long range correlation up to several channels. However, the component n(E) is the independent event on each channel of the pulse height analyzer. Supposing that the function n(E) is a sort of the noise distribution, the correlation length of that may be regarded as 1 channel. Therefore, the frequency range of $N(\omega)$ extends up to nearly π radian/channel. However, the frequency component of the signal function, expressed by $S(\omega)$, has a frequency range up to $1 \sim 2$ radian/channel, because the correlation length extends to several channels usually. As a result of superposition of two different kinds of distributions, the whole frequency distribution $F(\omega)$ can be separated easily. An example is shown in fig. 1, where the absolute value of the

thus defined function $F(\omega)$ is shown. Here, the raw data $f(E)$ is a part of the gamma-ray spectrum from the radionuclides produced by the bombardment of aluminum by fast neutrons. As shown in the figure by dotted lines, the superposition of two distributions is easily observed, each of them extending to the above mentioned frequency ranges. From this fact, if the higher frequency component of the distribution is reduced, then the distribution with the smaller fluctuation will be obtained. Therefore, by applying a proper filter function $P(\omega)$ to the total frequency distribution $F(\omega)$ to reduce the higher frequency range, a frequency distribution of the smoothed spectrum, that may be very close to $s(E)$, will be obtained. By returning this frequency distribution into the original energy space, the smoothed version of the raw data, expressed by $s'(E)$, is calculated. Then we obtain

$$s'(E) = \frac{1}{2\pi} \int_{-\infty}^{\infty} F(\omega)\, P(\omega) \exp(i\omega E)\, d\omega. \qquad (3)$$

Typical examples are shown in fig. 2-A and fig. 2-B. Fig. 2-A is a part of the gamma-ray spectrum whose frequency distribution is shown in fig. 1. The pulse height distribution is converted into the Fourier transformed space and a Gaussian type filter function is multiplied to cut off higher frequency range than 2.1 radian/channel. This modulated frequency distribution is then inversely transformed into the original energy space. This is the smoothed spectrum shown in fig. 2-B.

2) Background Subtraction

After obtaining the smoothed spectra, the next problem is to determine the background distribution and to eliminate this component from the smoothed distribution. Here, we use a commonly regarded conception of the background distribution. We assume that the background distribution is a very slowly varying function that connects almost all minima of the spectrum. In this calculation, a criterion is placed to avoid picking up real valleys between peaks as points belonging to the background distribution. For this purpose, if the function $s'(E)$, that is the smoothed spectrum, has successively located minima at E_{i+1} and E_i, then the slope of the line that connects these adjacent minima, expressed by $\{s'(E_{i+1}) - s'(E_i)\} / \{E_{i+1} - E_i\}$, is checked, If this value is higher than that given in the input data for this comparison, then E_{i+1} is not taken into account for the points that construct the background distribution. This criterion is also effective for E_i. If the resulting slope is a negative value, whose absolute value is higher than the criterion, then E_i is not used as a background representing point. Determining the background distribution by this method and subtracting this component from the smoothed spectrum, the background subtracted distribution $g(E)$ is obtained. Fig. 2-C shows the spectrum, without background, whose original data is shown in fig. 2-A. The distribution seems to be in accordance with the customary regarded spectrum without the background component. Here, some multiple peaks are observed. This is a good example of the effect of the slope criterion.

3) Improvement of Resolution

This method can be applied by using a different filter function from that used for spectrum smoothing. Therefore, the same technique of the calculation for the smoothing can be used for this method with a different filter function which intensifies a higher energy frequency range. Details of this technique are described in the author's previous paper.[2]

4) Peak Sorting

Each peak is separated by finding a connected region where the background subtracted distribution $g(E)$ has a positive value. Therefore, separated peaks still appear in multiples. In this calculation, multiple peaks are separated when a downward convex region is found. The center position of the peak is determined by finding the part where the slope of $g(E)$ is zero. The area under the peak is simply calculated by integrating the area between adjacent zero points of $g(E)$. If the peak has several points where the curve is convex downwards, then the multiplicity of the peak is examined up to the threefold case. The center positions and the areas of these multiplets are determined by finding also the zero slope positions and the whole peak is constructed by superposing Gaussian functions of standard peak width at these energies. Fig. 2-D shows peak positions and areas under the peaks obtained from the smoothed spectrum shown in fig. 2-B determined by this method.

III. Application

A computer code has been made based on the methods described above to analyze the 800 channel pulse height distribution of gamma-rays emitted from the radionuclides produced by the bombardment of fast neutrons. The 14MeV fast neutron beam is generated by the neutron generator TOSHIBA NT-200. The gamma-ray spectra are obtained by using the ORTEC-8102-20 Ge(Li) detector. The 800 channel pulse height distribution of gamma-rays is recorded in computer cards. During the irradiation, neutron flux fluctuations are recorded and these data are also transferred into the computer cards.

Fig. 3 shows the flow chart of the calculation. In this experiment the energy resolution of the spectrum is comparatively good, so the technique for the resolution improvement is not needed. Therefore, this part is omitted in the calculation for data reduction. The main procedure of

data smoothing is the calculation of the Fourier transforms. In the case of a long spectrum, that includes more than several hundred data points, the calculation of the Fourier and inverse transform requires long computation time. For the digital calculation of the Fourier and inverse transform, the calculation time is proportional to N^2, where N is the number of sample points in the raw data. In this case, N = 800, then usual methods seem to take more than several minutes, so the technique of sectioning is adopted. If the whole length of the spectrum is divided into L parts, then the time needed for the Fourier and inverse transform is proportional to $(N/L)^2$. By reconstructing the whole spectrum, the total time for smoothing is proportional to N^2/L. Therefore, by sectioning the whole spectrum into L parts, the time for the calculation of the Fourier and inverse transform is reduced to 1/L. According to this principle, in this calculation, the 800-channel pulse height distribution is divided into 50 parts, each portion containing 16 channels. To this subregion are added 10 and 11 channels on both sides to avoid the transient effects of sectioning. The spectrum in this small section is transformed into the frequency space and mutliplied by a filter function and then transformed back into the original energy space. Thus obtained smoothed sections are connected together. The filter function is, in this case, a Gaussian distribution with a half width of 3 radian/channel and cut off frequency at ±2.1 radian/channel.

The center positions of the peaks are determined by finding the place where the slope is zero. Some comparisons have been made between the center of gravity of a single peak and the thus determined position. In usual cases, this difference is less than 0.5 channels. The total area is calculated simply by integrating count rates per channel over the whole separated peak. When a peak is identified as a multiplet, whose multiplicity is determined from the number of the places of downward convexities in the peak, each component is determined by assuming that it is the Gaussian distribution with the width determind from two eminent peaks in the standard material. The conversion from the channel number into the gamma-ray energy is also carried out by comparing with the spectrum of the standard material whose gamma-ray energies of the eminent peaks are known.

This computer code carries out the correction for the neutron generator output by calculating the following value:

$$J(\lambda)=(\Psi/\lambda)\{1-\exp(-\lambda T)\}/\int_0^T \phi(t)\exp\{-\lambda(T-t)\}dt, \quad (5)$$

where Ψ is the neutron flux under the standard condition, $\phi(t)$ is the monitored neutron flux intensity, λ is the decay constant of radionuclides produced by the bombardment and T is the irradiation time. This program prints out the energy, channel number, total counts per peak and corrected counts obtained by multiplying the value expressed by eq. (5). The whole calculation requires about 8 seconds using a GE-635 computer.

Thanks are to Dr. I. Fujii of the Central Research Laboratory of Tokyo Shibaura Electric Co., Ltd. for obtaining experimental data.

References

1) T. Inouye and N. C. Rasmussen, Trans. of the ANS. 10, (1967) 38.

2) T. Inouye, T. Harper and N. C. Rasmussen, Nucl. Instrum. and Methods 67 (1969) 125.

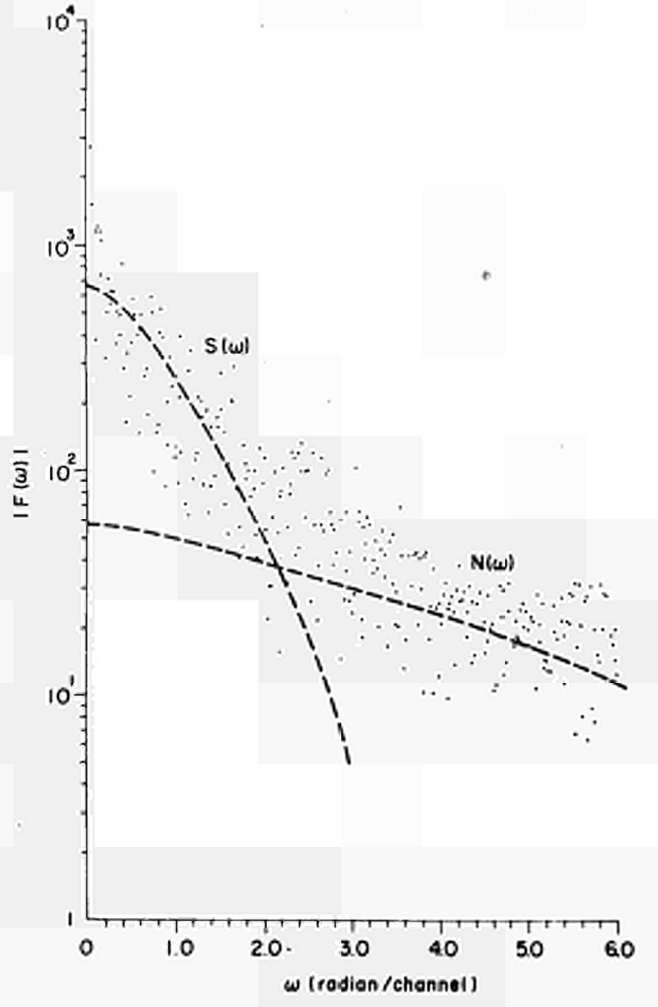

Fig. 1. An example of the energy frequency distribution of the gamma-ray spectrum.

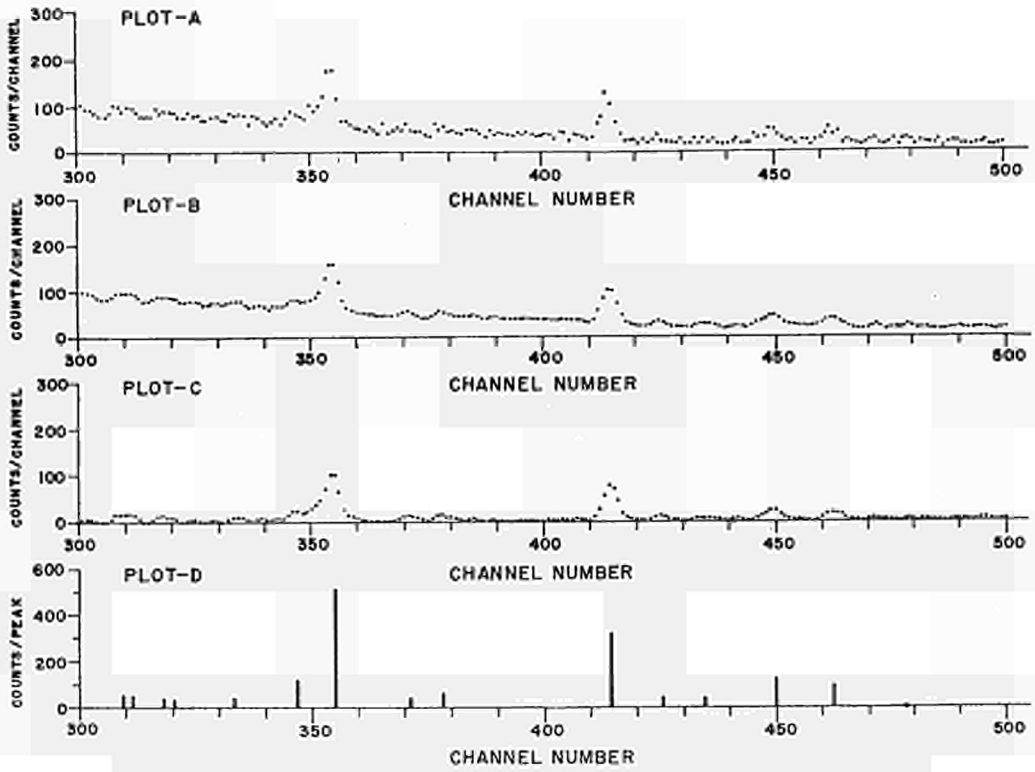

Fig. 2. An example of the data reduction in the fast neutron activation analysis.
Plot-A, Original spectrum
Plot-B, Smoothed spectrum
Plot-C, Background subtracted spectrum
Plot-D, Peak sorted distribution

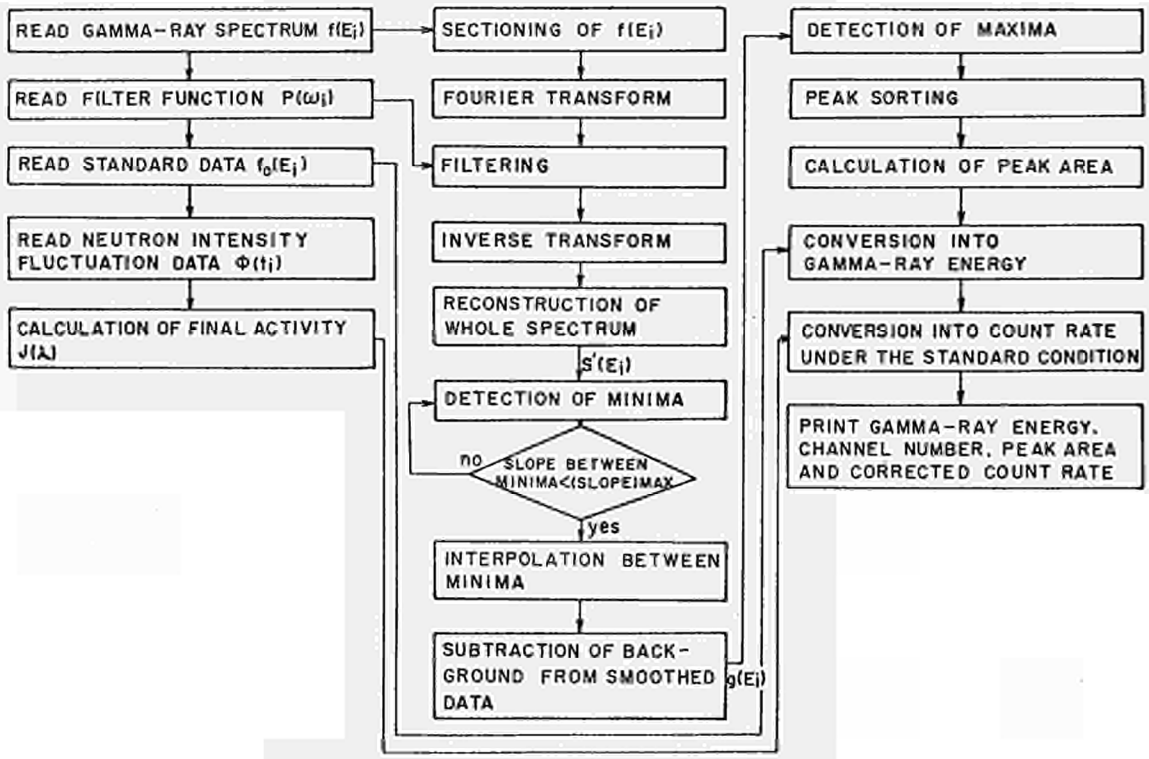

Fig. 3. Flow diagram of the calculation.

THE CAMAC SYSTEM OF MODULAR INSTRUMENTATION

R.C.M.Barnes and I.N.Hooton
Atomic Energy Research Establishment,
Harwell, England.

A new standard for modular instrumentation has been developed by the ESONE (European Standard of Nuclear Electronics) Committee and adopted by many European nuclear laboratories. The outstanding characteristic of this standard is a highway for the transfer of digital data and control information. This and other main features of the CAMAC specification are introduced in this paper. The use of CAMAC is illustrated by outlining the organisation of a typical small system in which CAMAC units are associated with a PDP-8 computer to operate as a multi-channel analyser.

Introduction

Origins of CAMAC

Many laboratories have adopted the practice of assembling instrumentation for nuclear experiments from modular equipment such as the ESONE system[1], the USAEC NIM system[2], and the Harwell 2000 series[3]. Within each system mechanical and electrical compatibility is achieved by specifying standards and codes of practice. However, there is no standardised means of transferring digital data within these systems, and individual laboratories have adopted ad hoc arrangements such as using the interfacing standards of a particular computer manufacturer.

The need for a new instrumentation standard, with a data transfer scheme independent of computer types as its central feature, was brought to the notice of the ESONE* Committee in 1966. As a result, a collaborative study was instituted, involving representatives from 26 laboratories. Working groups were set up to develop mechanical and electrical standards for a system directed towards instrumentation for data acquisition and control, constructed with closely packed integrated-circuit devices mounted on printed-circuit boards, and with few manually operated controls.

* ESONE (European Standard of Nuclear Electronics) is an informal forum of nucleonic instrumentation and data handling experts, drawn exclusively from national and international laboratories and universities in Europe, and was originally set up in 1960 on the initiative of the EURATOM Research Centre at Ispra.

Present Status of CAMAC

The main principles of the new system, now called CAMAC, were endorsed by the 1968 ESONE Conference in Rome. A formal announcement of the system was made in September, 1968,[4] preprints of the complete specification were available in January 1969, and the definitive English-language specification will shortly be issued by EURATOM[5]. A working group is preparing authorised translations in French, German and Italian.

At this stage the specification defines constructional standards for 'crates' and 'plug-in units', and electrical and logical standards for digital signals. The mandatory sections of these standards are in sufficient detail to ensure mechanical and electrical compatibility between equipment from different sources. Further detail is in the form of recommendations which allow some freedom of interpretation and implementation. Equipment which meets all the mandatory requirements of the specification is 'CAMAC Compatible', but there is also scope for lower levels of compatibility, for example, complying only with the mechanical aspects of CAMAC. The Secretariat and Executive Group of ESONE are able to advise and assist in matters concerning the interpretation of the specification. Working groups are now studying the standardisation of inter-crate connections in larger systems comprising more than one crate, and standards for external analogue signals.

The CAMAC specification may be used without licence or charge by any organisation or manufacturer. There is already widespread interest by laboratories and manufacturers in Europe and the U.S.A. Crates and a rapidly expanding range of plug-in units are becoming available from several commercial sources. The standard, if widely adopted, will simplify the task of designing and commissioning instrumentation systems for measurement and control, and will also permit manufacturers to sell their products in a wider market than has hitherto been possible. Although developed by representatives of nuclear laboratories, CAMAC was designed as a generalised data handling system for use in any field of digital instrumentation.

This paper is an informal presentation of selected features of CAMAC, which is fully defined in the CAMAC specification[5].

Mechanical Features

Crates and Plug-in Units

The CAMAC mechanical standards define a system of modular instrumentation in which plug-in units mount in a framework or 'crate'. The specification is mandatory for those mechanical dimensions which are essential for full compatibility between all crates and plug-in units. It does not include manufacturing drawings or define materials and finishes.

The Crate The crate has up to 25 mounting positions or stations, each having upper and lower guides for the runners of a plug-in unit, and an 86-way socket giving access to a multi-wire highway called the CAMAC Dataway. The crate is defined as a 19-inch rack-mounting unit with a minimum height of 5U ($8\frac{3}{4}$ inches), but this height may be increased as necessary, for example to include a ventilation aperture, and the crate may be constructed with less than 25 stations. The guides are on a pitch of 17.2 mm, which defines the minimum width of the plug-in unit.

Plug-in Units A plug-in unit consists basically of a vertical card with offset runners, an 86-way plug to suit the Dataway connector, and a front panel. A typical unit has a printed-circuit card which includes 86 printed plug contacts, 43 on each side of the card, but the use of an appropriate male plug connector on the rear of the unit is permitted. Units may occupy as many stations as they require, although they normally need access to the Dataway at only one or two stations.

NIM Compatibility

The guidance system and front panel height are compatible with those of the U.S.A.E.C. NIM system, which has a mounting pitch of 34.4 mm. Units in the NIM format fit into a CAMAC crate, with each NIM single-width unit occupying two CAMAC stations. A simple adaptor completes the connection between the AMP connector on the NIM unit and the CAMAC Dataway socket. There is liaison between the ESONE Executive Group and the NIM Committee of the U.S.A.

The Dataway

Construction

The Dataway is a standardised highway which links the 86-way sockets at all stations within the crate. The right hand station has a special function as the 'control station', but the remaining 'normal stations' are identical. The Dataway consists mainly of bus-lines joining corresponding pins of the sockets at all stations, or all normal stations, together with two individual lines between the socket of each normal station and that of the control station.

The physical construction of the Dataway is not specified, and local implementation may vary. For example, some laboratories and manufacturers are constructing the Dataway entirely by a printed-circuit 'motherboard', some entirely by wiring between pins of the Dataway connectors, and others by a combination of printed-circuits for signal lines and wiring for power supply lines.

Modules and Controllers

A data transfer takes place in a defined sequence of events constituting a Dataway Operation and involves at least two plug-in units, one of which acts as a 'controller' and the other as a controlled 'module'.

Use of Dataway Lines

Each line in the Dataway has a defined use. There are 24 Read data lines for transfers from modules to the controller, 24 Write data lines for transfers from the controller to modules, command lines for selecting the required data transfer or other operation, and lines to distribute power supplies. Five 'patch' pins at each station are not connected to Dataway lines but are freely available for special inter-connections and may, for example, be taken to terminals for patch leads. One signal bus line and two power lines are reserved for future requirements. The Dataway includes power lines for mandatory supplies at +24V, +6V, -6V and -24V, which can be assumed to be available in all CAMAC crates, and for additional supplies at +12V, -12V, +200V and 117V A.C. which need only be provided when they are actually required.

The Dataway Command

A command consists of signals on the appropriate Dataway lines to select a module or modules, a sub-section of the module, and the type of Dataway operation which is to be performed.

Station Number The modules are selected by signals on the individual station number (N) lines between the control station and each normal station. More than one station may be selected, so that the same command can be sent to several modules.

Sub-Address The required section of the module is selected by signals on four sub-address (A) bus lines. The sub-address may be used to indicate a specific data register, to define a status condition which is to be tested, or to direct operations such as 'Clear', 'Enable' or 'Disable' to the appropriate part of the module.

Function The operation is defined by signals on five Function (F) lines. Sixteen of the possible 32 functions are fully specified (four for Read operations, four for Write operations, and eight for operations which do not use the Read or Write lines). The functions are grouped so that simple decoding in the controller can determine, if necessary, the required direction of data transfer. Eight of the remaining functions are reserved for future extensions of the standard operations, and eight are available to meet the special needs of units or of local practice.

The Dataway Operation

During a Dataway Operation the controller generates command signals on the Sub-Address and Function bus-lines and on one or more individual Station Number lines. The command signals are accompanied by a signal on the Busy (B) bus-line, which is available at all stations to indicate that a Dataway operation is in progress.

If the addressed module recognises a Read command calling for a data transfer to the controller, it establishes data signals on the Read bus-lines. If the controller recognises a Write command calling for a data transfer to a module, it establishes data signals on the Write bus-lines. In addition, the module may transmit one bit of status information on the Response (Q) bus-line.

After allowing time for the data signals to become established, the controller then generates two timing signals, Strobes S1 and S2, in sequence on separate bus-lines. The first strobe, S1, is used by the addressed module to take data from the Dataway in a Write operation, or by the controller to take data from the Dataway in a Read operation and to accept the status information from the Q line. The two strobes may also initiate other actions in the controller and modules, but only S2 may initiate actions which change the state of signals on the Dataway.

The minimum time for a complete Dataway operation is 1 μs. During an initial period of at least 400 ns the command signals are established, the module responds to the command, and data signals are established. Then during a period of at least 300 ns the S1 strobe signal is generated, maintained for at least 100 ns, and removed. Similarly, the S2 strobe signal is generated during a second period of at least 300 ns. Although controllers are permitted to extend this cycle, or any part of it, the Dataway and modules must be capable of operating with the minimum time periods corresponding to the 1 μs. cycle.

Look-at-Me Signals

Each station has also an individual Look-at-Me (L) line to the control station. Whenever the absence of a Busy signal indicates that no Dataway operation is in progress any module may generate a signal on its L line to demand attention. The controller has access to all the L lines at the control station and may typically initiate a demand to a computer for a program interrupt or a direct access transfer, or may start a hardware-controlled sequence of operations.

Common Control Signals

Three common control signals are available at all stations, without requiring addressing by a command. They are used to initialise all units (Z) typically after switch-on, to clear data registers (C) and to inhibit features such as data taking (I). The common control signals Z and C are accompanied by S2, and should be gated with S2 in modules in order to reject noise.

Dataway Signals

The signal levels are specified so that they are compatible with commonly available DTL and TTL integrated circuit devices. All signals are generated from intrinsic OR outputs, typically free collectors, and are specified with negative logic to facilitate this. Hence the low level, near ground potential, represents logic '1' and the high level, near +3.5V, represents logic '0'. Each Dataway line is returned to the '0' state by a source of current from a positive potential. This 'pull-up current' source is generally located in the controller.

The loading and drive capability of most Dataway lines corresponds to one of two main classes. Those lines similar to the Read lines may be driven by any module but are only loaded by the input gates of the controller. In order to allow the features of the controller to be divided between several plug-in units the maximum signal loading is defined as four input gates. The drive capability demanded for signal outputs from modules can thus be achieved by inexpensive integrated circuit devices. Those lines similar to Write lines may be driven by a few outputs from the controller but may be loaded by signal inputs into every module. Only the controller needs this greater signal driving capability.

External Digital Signals

Two types of signal are recommended for use on coaxial or multi-way connectors mounted on the front panel of plug-in units or on the rear of units above the Dataway connector. The first is similar to Dataway signals, so that it can be derived from, and accepted by, DTL and TTL integrated circuits. Since it is transmitted over unterminated cables it is not suitable for fast signals. The second standard is similar to the NIM 50 ohm terminated signal, and is intended for more demanding situations and for inter-connections with many existing equipments which use the '16 mA into 50 ohm' signal standard.

Power Supplies

The specification distinguishes between Mandatory supplies (+24V, +6V, -6V, -24V), which can be assumed to be available in every installation, and Additional supplies which are only provided when they are required. It defines the stability of these power supplies and gives the maximum permitted current loading per station for plug-in units (2A for ± 6V and 1A for ± 24V) and as a total for the crate (25A for ± 6V and 6A for ± 24V). These current loadings cannot be reached simultaneously on all lines in a crate without forced ventilation, as this would seriously exceed the permitted power dissipation (see below). The current rating of the two Dataway connector pins carrying the 0V power return is 2 x 3A per station, and this may

also limit the current loading of a multi-width plug-in unit. In practice the power requirements of a crate of CAMAC equipment can vary widely, both in the total demand and in its distribution between the various supplies.

Dimensions

The physical location of the power supply unit is not defined, so that the arrangement best suited to a particular situation may be adopted, for example, a power supply unit mounted at the rear of each crate, a separate rack-mounted unit per crate, or a bulk power supply with or without final stabilisation at each crate.

Power supply units mounted on the back of the crate are restricted to a maximum height of 145 mm. to allow clear access to the rear of plug-in units above the Dataway. Their width should preferably be less than 430 mm. so that they can, if required, be mounted between rearward extensions of the side panels of the crate.

Power Dissipation

The CAMAC system is intended for use in environments typically associated with laboratory automation, such that plug-in units encounter an ambient temperature in the range 10^{o}C to 45^{o}C. The recommended maximum total power dissipation in a crate without forced ventilation is 200W. The dissipation at each station should not normally exceed 8W, but, with suitable precautions to ensure that the total dissipation for the crate is not excessive and is reasonably distributed, the dissipation in a plug-in unit may be increased to 25W per station.

A Typical Application of CAMAC

The CAMAC specification, which has been summarised above, defines how units interact with the Dataway. It does not directly define features such as the internal structure of units, the facilities which they provide, and the overall organisation of a CAMAC system. In order to give examples of a range of CAMAC units, their use of the standard features of CAMAC, and their role in a system, there follows a short description of a CAMAC system at Harwell. Two earlier versions[6] of this system are in use by Analytical Sciences Division at Harwell.

Specification of the System

The system was designed for gamma-ray spectrometry in analytical chemistry, particularly for activation analysis. The CAMAC units are associated with a PDP-8 computer to operate as a single-parameter pulse-height analyser or a multi-scaler, with a digital window on the input data if required. The data store is divided into 16 sections, each of 128 channels. The sections can contain individual spectra or may be combined to hold spectra with 256, 512, 1024 or 2048 channels.

Each data transfer from the analogue-to-digital converter is initiated by program interrupt, giving a dead-time of about 70 us., which is shorter than the average dead-time of the A.D.C. The computer background program, which is interrupted immediately a data word is ready, generates a live display of the current data area and also gives a second independent display channel so that spectra can be compared.

Data accumulation ceases when the first of a number of preset limit conditions is reached. The limit condition may be, for example, the count in a channel within a pre-determined block of channels, a preset live-time or a preset run-time.

The CAMAC units form the parts of the system (Figure 1) which:

a) Enable the computer to communicate with the experiment, by accepting data from an external analogue-to-digital converter and by controlling a sample changer.

b) Enable the user to communicate with the computer, via switches and lamps on a control panel outside the CAMAC crate.

c) Generate timing information, including run-time and live-time clock pulses.

Dataway Controller

This occupies the control station and two normal stations, and is an interface with the programmed input/output channel of the PDP-8 computer. It accepts command information from the computer, and generates command signals and strobe pulses on the Dataway. Data signals from the Read lines are routed through the controller to the accumulator input lines (AC) of the computer. Data signals from the Accumulator output lines (BAC) are routed to the Write lines. Dataway Look-at-Me signals (L) cause the controller to generate a 'Program Interrupt' signal to the computer, and the Dataway Response signal (Q) on certain commands causes it to generate a computer 'Skip' signal.

Input Data Gates and Drive Units

Communication with the user, via the control panel, is by means of four Input Gate Units and three Drive Units. Each Input Gate accepts 8 bits at Dataway signal levels from switches on the control panel, and gates these signals onto the Read lines in response to a Read command. The switches are used to select operating parameters such as the number of analyser channels in use. The computer program reads the state of all switches as part of a background task which also includes generating the monitor display.

Each Drive Unit has an 8-bit register, loaded by a Dataway Write operation, which controls the generation of corresponding signals on eight wires in a multi-way front panel connection. These signals drive lamps on the control panel and relays in the sample changer.

Data Input

Data from the analogue-to-digital converter is in the form of a serial pulse train which is counted by a 12-bit register in the A.D.C. Adaptor Unit. When the conversion is complete this unit generates a Look-at-Me signal, and the controller sends a Program Interrupt to the computer. A search program is entered to address Test commands to each source of L signals in turn. When the A.D.C. Adaptor which has been requesting attention receives a Test Command it generates a Response signal on the Q line and the controller sends a Skip signal to the computer. This causes the computer to enter a program which reads the contents of the register in the A.D.C. Adaptor (by a Dataway Read operation) and then increments the count in the corresponding analyser channel.

Timing Information

Clock Pulse Selection Timing signals are derived from a Clock Pulse Generator unit, which generates pulse trains at decade intervals from 1 MHz to 1 Hz. This unit uses only the power lines of the Dataway. One of the six outputs from the Clock Pulse Generator is selected, under program control, by the Choice Unit. This has eight front panel inputs, each of which is gated, by the appropriate bit of an 8-bit control register, to a common output connector. The register can be loaded by a Dataway Write operation with the appropriate bit-pattern to select the required clock pulses.

Run-Time and Live-Time The selected clock pulse is taken by a front panel connector to the AND gate unit, which contains two 4-input AND gates. An 8-bit control register, which can be loaded by a Dataway Write operation, pre-selects each gate input to be either a front panel signal or a continuous '1' state. One of these gates is used to produce a run-time clock, by gating the selected clock pulse with a 'counting' signal from the control panel. The other produces a live-time clock by gating the run-time pulses by a 'not busy' signal from the A.D.C. The run and live-time clock pulses, and also the 1 Hz clock pulse are taken by further front panel connections to inputs of the Flag Unit. This has eight inputs, each of which can set the corresponding bit of an 8-bit register and cause the unit to generate an L signal. When the computer program identifies the Flag Unit as a source of an L signal it reads the register by a Dataway Read operation and processes the 8-bit word in order to decide which servicing routines should be entered, for example, in order to increment the count in the run-time or live-time locations.

Initialising

The computer 'power clear' signal occurs at Switch-on and when the 'program start' key is operated. It causes the controller to generate the Dataway Initialise signal (Z), which sets the CAMAC system to a defined state.

References

1. ESONE System of Nuclear Electronics. EUR 1831e, EURATOM Ispra, October, 1964.

2. Standard Nuclear Instrument Modules. TID-20893 (Rev.2), U.S.A.E.C., January, 1968.

3. BISBY, H. The Design Principles and Rôle of a Comprehensive Unit System of Electronic Equipment. Radio Electron.Engr., Vol.29, pp.185 - 195, March, 1965.

4. BECKER, W. An Advanced Modular System of Nuclear Electronics for On-line Computer Applications. Nucl.Instrum.& Methods, Vol.64, pp.197 - 200, September, 1968.

5. CAMAC, A Modular Instrumentation System for Data Handling. EUR 4100e, EURATOM, to be published.

6. LEWIS, A. A Small Computer used as a Multi-Channel Analyser. AERE - R5844, H.M.S.O., July, 1968.

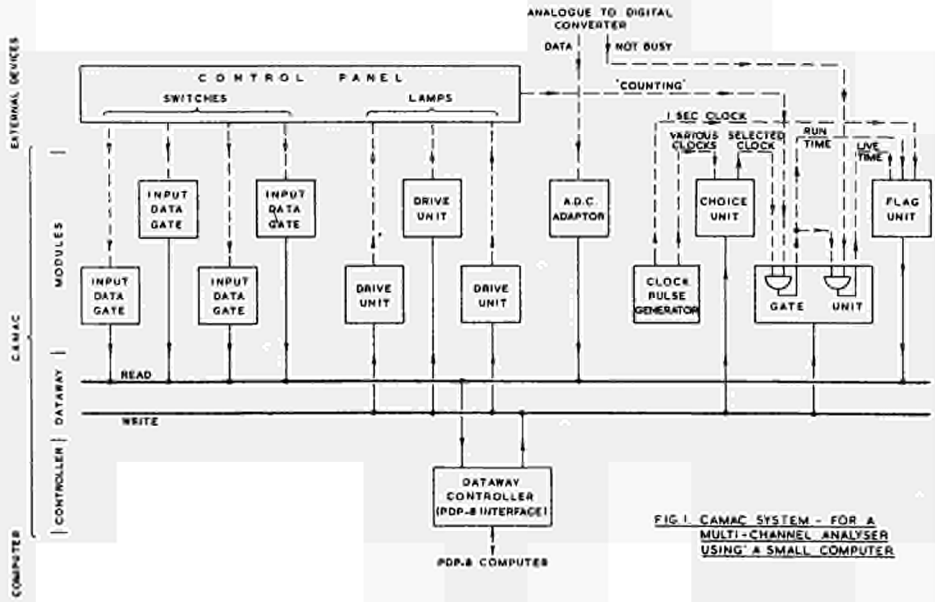

FIG 1 CAMAC SYSTEM - FOR A MULTI-CHANNEL ANALYSER USING A SMALL COMPUTER

PROJECT AGORA

Adaptative Network for Data Collection and Transmission

J.F. MOUGEL
Département d'Electronique Générale
Service d'Instrumentation Nucléaire

Centre d'Etudes Nucléaires de Saclay
91. Gif-sur-Yvette (France)

ABSTRACT

The aim of AGORA is to ensure all information transfers among three computers of different type (C.I.I. 10020 and PDP8). These transfers are automatically performed between the memories of computers and are controlled by the central unit of one of them. A high performance display is associated to the transmission network. A synthetic language is being written.

INTRODUCTION

The use of small or medium size computers in Nuclear Physics experiments, specially in high energy physics, needs a new determination of the place of the computer and of its integration in the processing : Data collection, transmission and analysis. Referring to an industrial process, we have a given structure generating data and accepting signals, a computer able to operate the sequential reading of status or data, and to give, on the other hand, the control signals needed to drive the process in good conditions. An important caracteristic of this system, is the permanence of the basic scheme. Particularly, the data transmission network, well adapted for a given structure, can be used, without any modification, during the same time the computer can perform its task satisfactorily (at least four of five years). The main problem, in this case, just after the reliability one, is of economic order : how to achieve the better network at the minimum price ?

In high energy physics, the question is quite different.

The data collection structure is not only established for a shorter period (six months to two or three years), but during this period, the basic scheme of the experiment can be modified according to the first results of the experiment, and the major problem, just after the choice of the computer, or sometimes on the same level, is to imagine a modular and adaptative network for the data and status transfer, in order to be able to follow in a minimum time interval (two or three weeks), the basic modification of the experimental structure, assuming that this modification has not a too large effect on the software. In short, we want to build a network :

a) which executes the data transfers at a high rate,

b) requiring a small software support,

c) for which the computer has only to give a small lot of orders to initiate the transfers, these transfers then beeing performed automatically with or without interference with the computer,

d) having a good compatibility with a large choice of data transmitters or receivers.

In order to fulfill these requirements, we designed a network module, called COPHYNUT (COupleur pour élément de PHYsique NUcléaire, in english : Link for Nuclear physic modules), and the first application planned, called AGORA, will permit the connection of three computers to several experiments, control stations or conversational display unit.

THE NETWORK CELL : COPHYNUT

The first study of this cell was carried in connection with a computer CAE 90-10 (or SDS 92). The main advantage of this machine is to have a programmed data channel working word by word or block by block (a block containing up to 4096 words). This permits tranfers rate up to 570 kilowords per second, in a programmed way.

To execute these block transfers, it is necessary to separate the test or order sequence and the true transfer sequence. For this, the peripheral device is adressed only in the order (or test) sequence. After that, it is supposed that the connection remain established during all the transmission sequence.

This transfer mode is fully compatible with the a and b requirements of the introduction : with only three computer instructions we can transfer up to 4096 words, 12 bits long, in a little more than 7 milliseconds. And we have decided to extend the sequential mode (test, order, transfer) along all the network, a modified 90-10 language becoming the COPHYNUT language.

But this simplicity do not give a sufficient reduction of the time during which the computer is busy (requirement c of the introduction). For that purpose and in order to have a modular and adaptative network, we have designed the structure shown on figure 1.

The network is constituted by a multiplicity of bidirectionnal bus lines, separated by addressable lock-switches. The first bus line is connected to the computer, while peripheral devices are linked to the external lines by an adressable lock-switch, or directly. Each ALS (Addressable lock-switch) can decode the whole or a part of the address sent by the computer with each order or test sequence ; and if this address, or part of address, corresponds to the one of the ALS, displayed by means of switches on its front panel, the signals can pass through the ALS gates during the presence of the address. Then, if the

peripheral device receiving an order has to transmit data, it generates a level AV (Aval, meaning downstream) ; if it has to receive data, it generatesa signal AM (Amont, meaning upstream). Reaching an ALS, this signal, AM or AV, turns on the gates of the ALS in the proper direction, as shown on figure 2.

These gates are open only if one of the two signals AM and AV reach them. If there is cofncidence between those signals, the gates are turned off and the part of network behind the ALS receiving the two signals is fully independant and can ensure a data transfer between two peripheral devices without any disturbance from or to the other part of the network. End of transmission sequence resets the levels AM and AV. One of the two peripheral devices has to supply the signals normally sent by the computer during the transfer sequence. In our case it is always the receiver which performs this function.

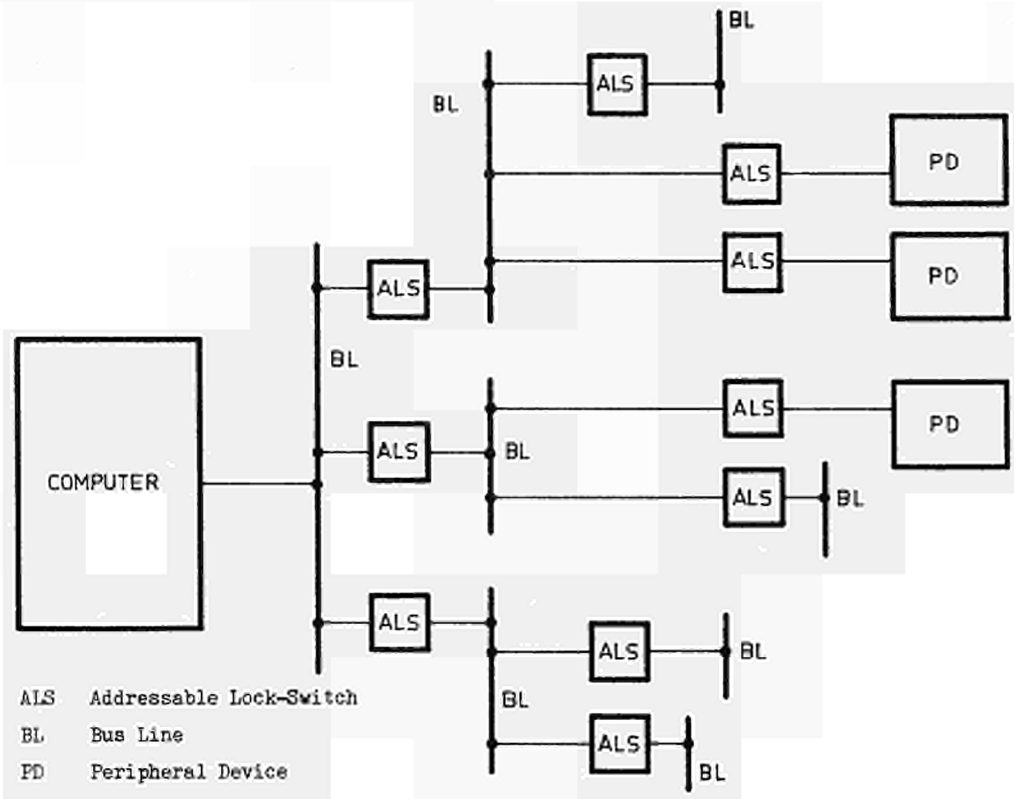

FIG. 1. COPHYNUT NETWORK

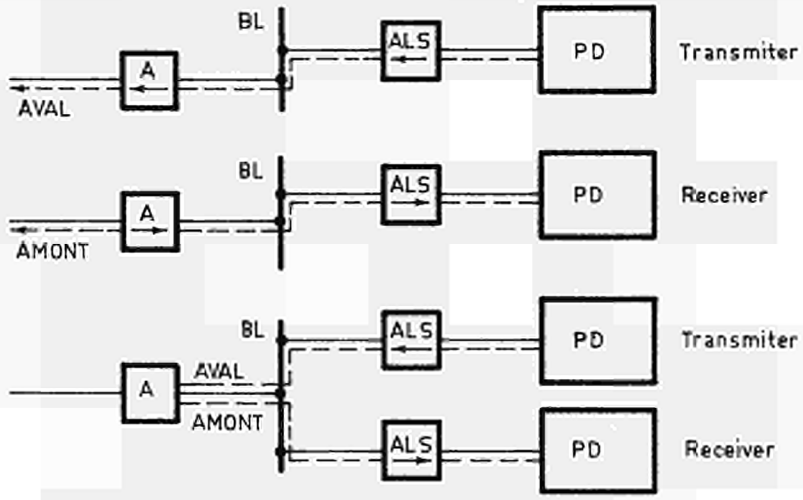

FIG. 2. TRANSFER DIRECTION IN LOCK-SWITCHES

In a COPHYNUT network, the programmed channel normally carries only the test and order sequences. The data transmission takes place between two peripheral devices, like scalers, encoders, pattern units (transmitters) or memory blocks, direct access to computer memory, automatic channels (normally receivers). For the 90-10 computer, the busy time of central unit to transfer 4096 words is only of the order of 30 μs, but the receiver and transmiter are chosen by software, and many data transmissions can take place simultaneously (up to 64).

In order to permit the use of 16 bits computers, the number of gates in ALS and wires in bus lines is 16. But the address is only 12 bits, and this is largely enough.

The figure 3 gives the schematic drawing of an ALS, but the address decoder can be suppressed and carried back to the peripheral device.

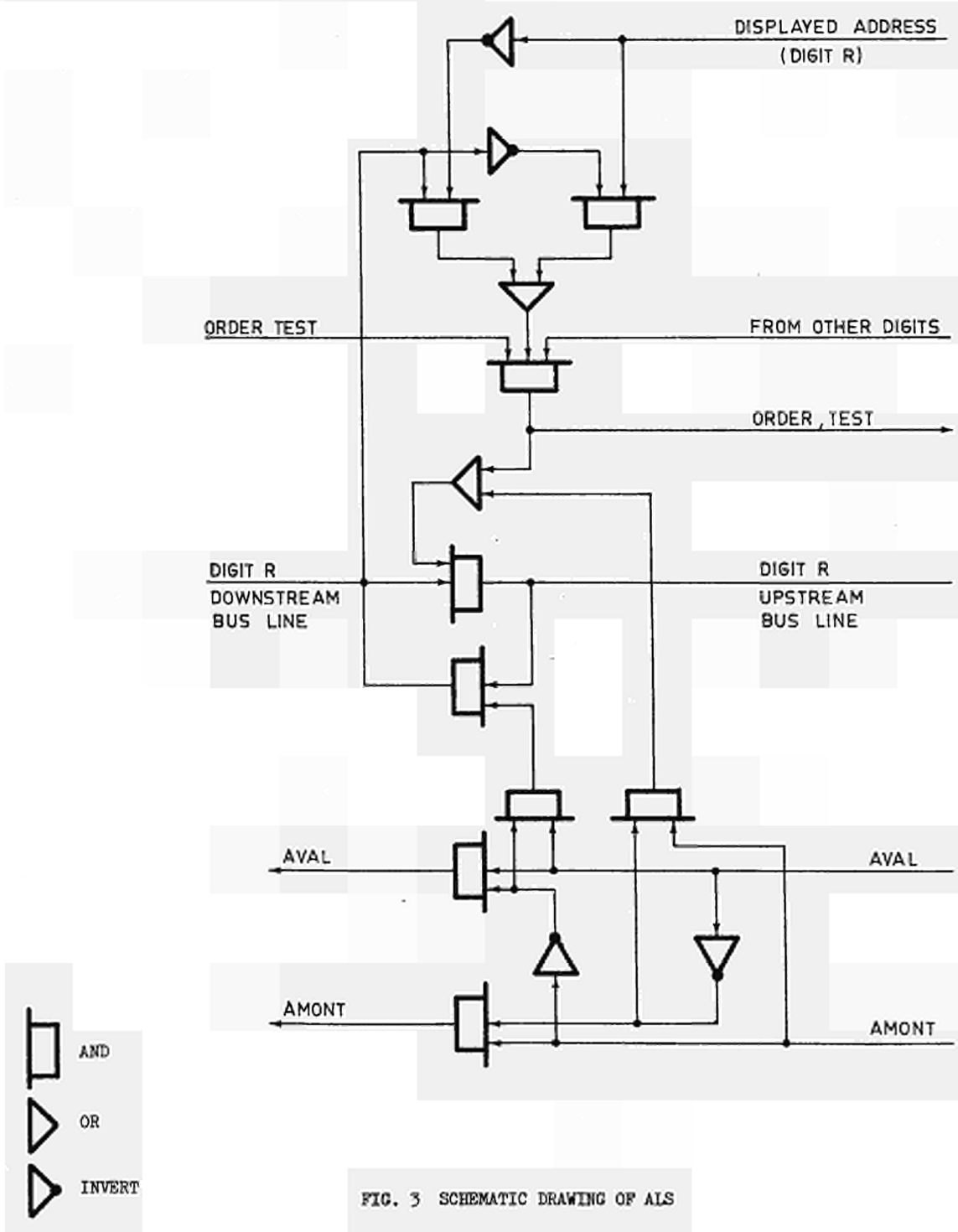

FIG. 3 SCHEMATIC DRAWING OF ALS

AN EXAMPLE OF APPLICATION OF THE COPHYNUT NETWORK : AGORA

Near the 300 MeV LINAC of Saclay, there will be three computers :

- One C.I.I. 10020 (SDS Sigma 2) used as a computing center and main machine.

- Two DEC PDP8 used for data collection with many experiments.

In addition, a conversational display unit will permit to the physicists to carry many tasks directly on spectra like peak-integration, back ground substraction, smoothing, edition, storage, etc ...

And in the two main experimental rooms, there will be a control station to permit to the physicist the survey and supervision of his experiment and first analysis. (See fig. 4)

The main computer, by its programmed channel (DI/O) establishes the network connections ; this channel can be used for data transfers if :

- The display unit enters a conversationnal mode.

- A physicist asks for a result from his control station.

But normally, all the data exchanges take place only between memories, or between memory and display :

- The 10020 memory is connected to the conversational display unit (picture regeneration).

- One of the PDP8 memory is connected to one of the control stations (spectrum mode).

Sometimes, a data collection sequence is ended on one of the PDP8 and a special interrupt occuring, a data transfer is initiated between the memory of this computer and the 10020 memory. Then, the normal connections are established again.

This minimum network can be enlarged to permit the direct connection of several experiments to the 10020 memory.

Just beside the 10020 DI/O, a consol assumes different functions :

- Level and logical adaptation between the DI/O and the COPHYNUT network.

- Generation of several specific orders or tests needed by the management of AGORA.

- Generation of several general purpose orders or tests needed by the physicists who use AGORA or one of the computer.

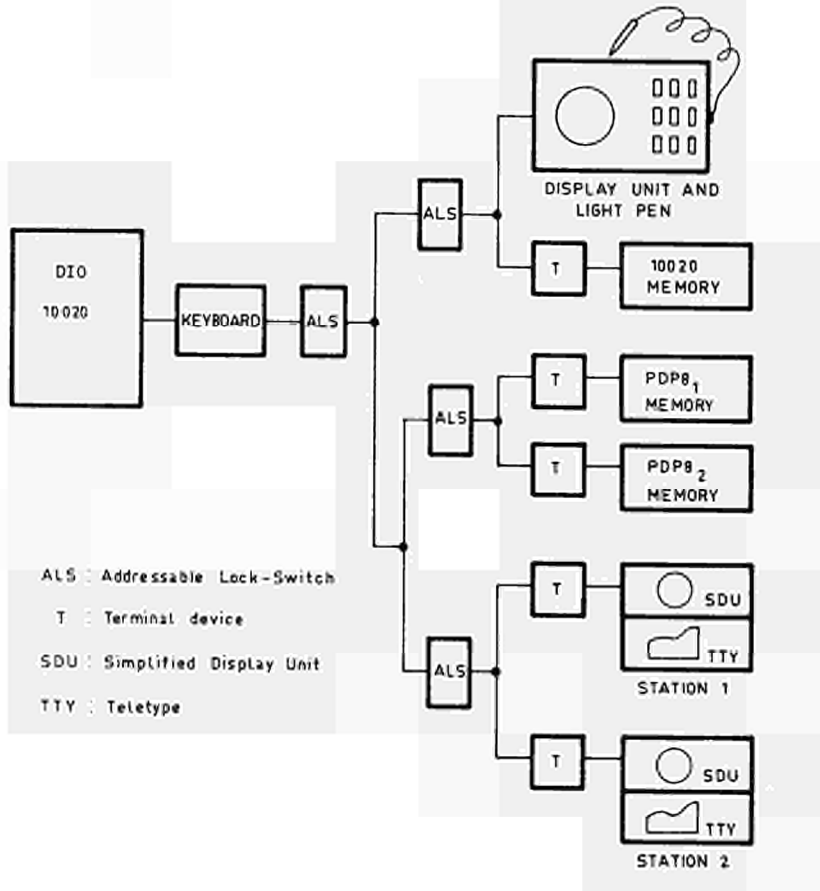

FIG. 4. AGORA NETWORK

Before each peripheral device, a terminal device assume the level and logical compatibility as well as the supply of orders needed by the interperipheral data transfer (see paragraph 2). In the case of display units, built specially for AGORA, this terminal is included in the peripheral device.

CONCLUSION

This modular network, built by connection of several identical lock-switches, flexible and adaptative, can be used for a lot of interconnection problems, provided a computer (or equivalent) be employed as the main control unit, not to operate the data transfers, but to manage the network itself.

Refering to AGORA, two units are now available :

- The lock-switch module, housed in a 3/25 mechanical CAMAC unit (86 pins connector and data way are not used, and cannot be used for this purpose). The front panel displays the address given to the lock-switch. All the interconnections (bus lines) go to or come from the back panel.

- The simplified display unit is housed in a crate, the left part of which is occupied by a 601 memory type Tektronix oscilloscope. The following functions are assumed by the associated electronic:

- Direct plotting (XY), with 1024 x 1024 points.

- Incremental plotting : each new value of Y, transmitted to the logic, triggers a plus one operation on the X register.

- Memory enabling and disabling, picture erasing.

The other parts of AGORA will be built, tested and assembled before April 1970.

CAMAC CRATE CONTROL FOR A PDP8 AND A CAMAC 24 BIT COUNTER

W.Attwenger,W.Egl,F.May,R.Patzelt,K.Petreczek,J.Schwarzer

Österreichische Studiengesellschaft für Atomenergie,
Reaktorzentrum - Seibersdorf, Elektronik - Institut

Abstract:

A Camac crate control for a PDP8 or a semi-automatic control system and a 24 bit preset counter for the Camac-system is described. Details of the use of four device addresses of the PDP8 and timing requirements are described. For the preset counter two methods are compared.

1. System philosophy

In many experiments more than one Camac crate must be controlled by one computer. In our special case a PDP8 will be used for this purpose. Digital Equipement provides only a limited number of device addresses, which are free for system-designers. We have decided to use four device addresses of the PDP8 to control up to eight crates. To be fully compatible with the Camac timing requirements a distinct separation between data transfers within the crate (Module and Crate control) and between crate and computer seems to be useful. It is obvious that the timing between Crate control and computer under these circumstances can use all data transfer features which are provided by the computer.

Furthermore it seems to be necessary that the crate controls can be influenced not only by a computer but also by more or less semi-automatic devices, e.g. a Teletype-Printer. Therefore several registers in the crate control are necessary. Since 12 bits for a dataword are not sufficient for data from experiments, our system uses the full width of dataway (24 bits). Further reason for using 24 bits will be given below.

Every crate control consists of two basic blocks, the control (logic) unit and the data unit. Two device addresses of the PDP8 (A and B) are reserved for the control unit and two device addresses (C and D) for the data unit. The crates themselves are addressed bythree bits of the "address word" via the datalines.

2. Registers in the Crate control:

2.1. Device Address A Register:

Information provided by this register which is set by the computer or the manual control is as follows:
bit 0 - 3 Camac Sub-Address (four bits)
bit 4 - 8 Camac Module Address (five bits)
bit 9 -11 Crate Address (three bits).
This register is oalled the address-register.

2.2. Device Address B-Register:

Information provided by the register which is set by the computer or the manual control is as follows:
bit 0 - 3 Crate Function (four bits)
bit 4 - 8 Camac Function (five bits)
bit 9 -11 Crate Function Modifier (three bits)
This register is called the instruction-register.

2.3. Read-Register:

In the read-register data received from the dataway are stored. Furthermore data from the LAM-lines and data from the Status-Response-Line (Q-line) can be transfered into this register. The first twelve bits of this register are addressed with device address C, the second twelve bits with device address D.

2.4. Write-Register:

In the write register data received from the computer or a manual control are stored. These data are sent to the module.

2.5. Q-Register:

If it seems desirable to have the possibility to give a skip-command to the computer after having read the status (Q-response) of a module this register must be provided. As indicated above the status response is normally written into the read-register. The use of this register will be explained in paragraph 3.3.

2.6. Inhibit-Register:

The inhibit-register is used for parallel control of the modules.

All registers in the crate control are overwritten and not set or cleared.

3. Actions initiated by the IOT1, IOT2 and IOT4 Pulses of the PDP8.

These pulses define three phases of the transfer cycle, they are used only for timing.

3.1. Device Address A:

IOT1: IOT1 is used in the search-routine to select the external device of the PDP8 which has set an Interrupt. If one of the eight crates using the same device address A has set an Interrupt-request, a skip-command is sent to the computer.

IOT2: Transferes the module-and subaddress-information into the address register. The decoded Camac address is stored in a Flip-Flop. IOT2 acts as a strobe-signal.
IOT4: starts the Camac-timing-cycle.

3.2. Device Address B:

IOT1: If the device address search routine has found that this group of crates has set an Interrupt-request, one crate (or more) can be identified. This is done in the following way:
The computer addresses with device address A the first crate in this group. If this crate has set an Interrupt-request a skip-command is returned to the computer.
IOT2: Transferes the information from the computer to the instruction register. (Strobe signal).
IOT4: starts the Camac timing cycle.

3.3. Device Address C:

IOT1: If the crate control has a separate Q-register as indicated in 2.5., this register can cause a skip-command, after device address C in combination with IOT1 has been called.
IOT2: strobes data.
IOT4: starts the Camac-timing-cycle.

3.4. Device Address D:

IOT1: is not used.
IOT2 and IOT4 are used as under 3.3.

4. Crate Function Codes:

CF0: "Camac function code only".
CF1: "Clear". The Camac function code "Clear" is generated and clears all modules.
CF2: "Initialize". With this instruction all modules receive an initialize command.
CF3: "Inhibit". This command is stored in a separate register that can control the function of all modules in the crate via bus-line of the dataway (inhibit-line)
CF4: "Reset-Inhibit". The above mentioned register is reseted.
CF5: "Read-LAM". With this instruction the LAM-information is strobed into the read-register. The strobing signal must be delayed with respect to IOT2. In our special case S1 as defined in the CAMAC-specification is used for this purpose. It is obvious that the busy-signal is not generated with the instruction.
CF6: "Read". With this command data of the read-register are transfered to the computer. This function will be usually combined with a read function code for the dataway. IOT4 and device addresses C and D define if either the information of a module is read into the crate control or information of the crate control is transfered into the computer.
CF7: "Write". For this instruction the same remarks as for CF6 "Read" are valid.
CF8: "Transfer". If it is necessary to transfer data from one module to another and the loss of time is insignificant this instruction can be used. Data that have been read from a module and are now stored in the read-register are put on the dataway writelines with CF8. The module which should receive the data must be addressed and the Camac function code "Write" must be given.

Fig. 1 shows the blockdiagramm of the Camac crate control.

5. A Twenty-four Bit Counter:

In data acquisition systems a preset counter is one of the most important functional modules. It must deliver an output signal if the accumulated number is equal or higher than a preset number. The preset number can be set electronically by a control unit (e.g. computer). Compatible with the maximum wordlength of the CAMAC-dataway a capacity of 24 bit is used, that is a good value to obtain results with a sufficiently low statistical uncertainty. The registers together with the input and output gates and the control-logic lead to a high number of functions. Only with an economical design it is possible to keep the number of IC-packages so low, that it is possible to place them on one CAMAC-board.

The simplest design consists of a register, that can be set directly, e.g., an upward counter set to the complement of the preset number. Therefore during normal operation the counter counts upwards until its full capacity is reached. The accumulated number equals the preset number and the additional overflow-bit is set and gives the output-signal. Only one register is necessary, but all Flip-Flops must have direct preset and clear inputs. During one counting action only one preset-number can be used and the number of the accumulated counts is not directly available.

Using complex 4-bit units for the counting-register, the preset number and the comparison logic it is possible to design with nearly the same amount of IC-packages a preset counter with two separate registers. This design avoids the restrictions mentioned above and is therefore definitely more versatile.

The following functions are included:
1. Inhibit I (for parallel control of all counters in one crate)
2. Initialize Z resets all registers.
3. Clear (clears only the counting register)
4. Enable FC 26 and Disable FC 24, switching an input-gate via a flip-flop-register (Enable register)
5. Read FC 0, Subaddress 1, reads the counting-register, Subaddress 2, reads the preset-register.
6. Overwrite FC 16, sets the preset register
7. Test FC 27, Subaddress 1, tests the Enable register
8. Test Status FC 27, Subaddress 2, tests the overflow-register
9. LAM is set as soon as the preset number is reached
10. Clear LAM register, FC 10.

To vaoid unnecessary decoding gates only "Read, FC 0 and FC 27" are accompanied by a sub-address. The subaddresses are not fully decoded. It is assumed that the central control unit must know the properties of the modules connected and can therefore avoid to send commands, that can be misunderstood because of incomplete decoding. By that many additional decoding gates are avoided.

In the counter IC dividing by 16 or 10 are used. Both types can not be preset. Therefore the first solution mentioned above is not possible. For the preset register quadruple D flip-flops are used (one bipolar active input per list). To keep the component costs low even with the high counting-rate of 10 mc the comparison of the count-and preset-register is made in two steps. The least significant decade information is added in a four bit adder to the complement of the preset number. The carry output of the full adder indicates that the two numbers are equal or that the preset-number is lower than the counted number.

The five higher significant decades compare their content with the preset-register in an equivalence circuit (5 bits with single rail inputs) which generates an output if equivalence has been reached. This signal sets a flip-flop. The output of the full adder and the flip-flop are sent to an "AND-GATE" and its output indicates that the preset number has been reached or exceeded. This output sets the LAM-flip-flop.

The decimal coded version is used if a decimal display or decimal printout is wanted.

IC Types used:	BCD Counter	SN 7490 N
	Binary Counter	SN 7493 N
	Full adder	SN 7483 N
	Quadruple D Flip-Flop	SN 7475 N
	Equivalence circuit	FCH 281
	Gates FCH 181 or FCH 191	
	Line Drivers	FCJ 141
	Fast Gate	SN 74H10N

Fig. 2 shows the main registers of the counter.

Further specifications of the counter:

The maximum counting frequency or pulse pair resolution is only depending on the first counting register. The minimum values are 10 mc and 100 nsec respectively, as specified for the IC used. For higher frequencies a prescaler will be used to keep the noise-imunity for the basic instrument as good as possible. The delay, after the preset-number has been reached until the LAM-signal is set, is in the order of 100 and 600 ns, depending on the value of the preset-number.

The input-signal must be compatible with DTL-requirements, pulse width min. 20 ns. Enable and Disable Inputs respond to the same levels, pulse width min. 100 ns.

6. Further Remarks concerning the Crate control

From 16 possible crate function codes only 9 have been used in this system which will be in operation at the end of May. Using the modifier-bits the number of possible function codes can be considerably increased.

With an increased amount of hardware in the crate controls it would be possible to shorten the search-routines for the crates or the modules which have set an Interrupt. To achieve this, the crates must be able to generate LAM-patterns which would be read by the computer. An example illustrates the possibility: Assume that with crate address "zero" all crates are addressed. Using crate function code 10, defined as "Read LAM pattern" every crate would load information on the readlines. Crate 1 would give its status on the first three bits of the data word, crate 2 must use the two next bits and so on. By this the computer would have the status information of all the crates connected.

The three modifier bits could also be interpreted as sub-addresses of crates allowing an increased number of crates to be controlled.

In a special neutron scattering experiment the problem has been raised that the three 24 bit counters must be read and cleared in minimum time. We therefore decided to transfer the content of each counter in a storage-register (separate module) using patch-pins of the dataway to send the instructions to storage register that is not addressed during operation (via the dataway). Since the system uses the full width of the CAMAC dataway this transfer can be done in three CAMAC timing cycles only. Since the counting time for each counter is larger than 100 sec, the three storage registers can be read even with a Teletype Printer during each counting cycle.

Acknowledgement:

The authors are indebted to Mr. H. Halling for many useful discussions. Mr. Halling designed a semi-automatic system which allows the control of a Camac-crate-control. Design features of this system have been published at the meeting of the "Fachausschuß Elektronik im Physikalischen Experiment", 24.3.-29.3.1969, Subject:"Steuerlogik für Computer, Kompatibles System (CAMAC). The meeting was held in Berlin.

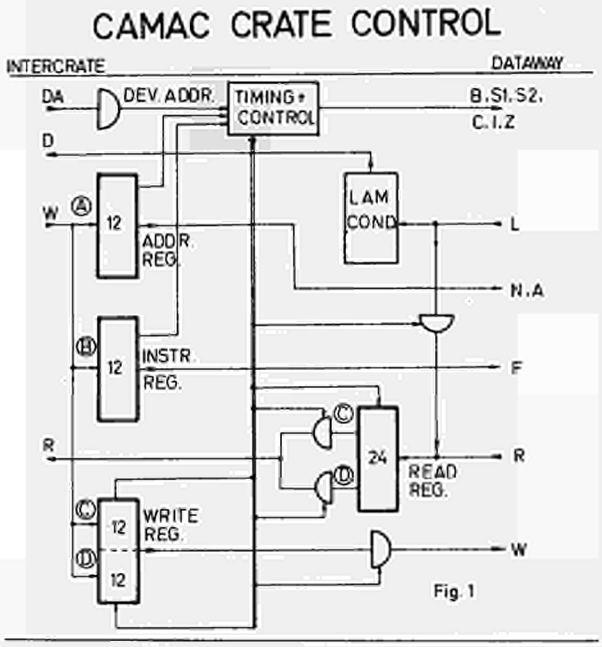

Fig. 1. Blockdiagramm of the Camac crate control

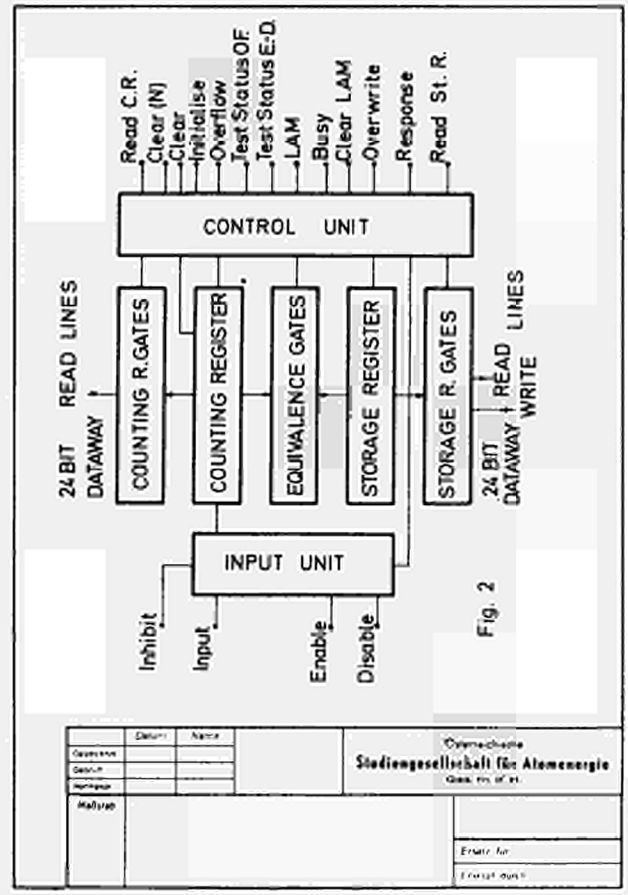

Fig. 2. Blockdiagramm of the Camac 24 bit counter

PROGRAMMED CONTROL OF AUTONOMOUS TRANSFERS IN A CAMAC SYSTEM

J.M.Richards and L.D.Ward
Atomic Energy Research Establishment
Harwell, England.

The transfer of data under the control of a CAMAC installation is essential in many applications. The programmed control of these transfers can provide very desirable flexibility. This is illustrated by the Programmed Command Generator 7038 which is an autonomous transfer controller in the Harwell 7000 Series of CAMAC units.

Introduction

Many applications require the transfer of data between a CAMAC installation and a computer in a cycle-stealing mode. These autonomous transfers must be organised by hardware in the CAMAC system. The hardware organising the autonomous transfers should not normally be part of a particular computer interface, since this would reduce the range of application both of the computer interface and of the autonomous hardware. For this reason a class of units known as Command Generators has been devised in one implementation of CAMAC (The Harwell 7000 Series) to control autonomous transfers. Command generators can be linked in a standard manner to control autonomous transfers through various computer interfaces.

Command Generators

If a command generator is to exploit all the features of the 7000 Series it must be able to provide the following control data:

Crate Address	3 bits
Station Address	5 bits
Sub-Address	4 bits
Function Code	5 bits
Channel Code	4 bits
Full Command	21 bits

The crate address, station address, sub-address and function code enable the command generator to specify any module and function in the system. The channel code specifies the type of autonomous transfer between the CAMAC interface and the computer. The full channel code is of 5 bits, but the most significant bit is the same as the F16 bit of the function code. The interpretation of the channel code is determined by the computer interface, and can differ in different interfaces. Thus, in one example, channel code 4 specifies the transfer of 16 bits of data to a particular computer input, while channel code 5 specifies the same computer input but transfers a full 24-bit word in two computer transfers.

Defined Channel Codes

Channel codes 0 and 16 will always specify non-computer dataway operations, such as module to module transfers or a dataless function. Channel codes 1 and 17 can be used to interrupt the computer at the end of a block of data transfers.

Sequencing Autonomous Commands

The separation of the function of autonomous command generation from other controller functions does not limit the method of organising the sequence of autonomous commands to any specific approach. Some feasible methods of sequencing are listed below:-

a) An L signal may trigger a single transfer to readout the module generating L.

b) The command generator may readout from a number of sub-addresses from successive stations in a block of stations.

c) The command generator may scan a block of registers and readout all those which generate Q when addressed.

d) The command generator may organise a sequence of autonomous transfers specified by a program of instructions.

Advantages of Programmed Control

Method d) above, the programmed control of autonomous transfers, has the following advantages.

a) It is very flexible and imposes no additional restrictions on module design.

b) The order of addressing modules is not tied to module position.

c) Several different autonomous sequences can be provided by one command generator. These sequences can include the readout of one or more common modules.

d) No autonomous operations are required to search for modules requiring readout.

e) The program of autonomous transfers could be loaded from the computer, so that the autonomous data collection program can be stored with the analysis program and modified under computer control.

f) The transfer sequence will not normally be altered by the failure, removal, or addition of a module. Thus data from each module will retain the same position in the readout sequence, fault finding will be simplified and changes in the analysis program, to allow for changes in the modules available, will be minimised.

Disadvantages of Programmed Control

The two main disadvantages of the programmed control of autonomous transfers are:-

a) A programmed command generator may be more expensive than a less flexible system of command generation.

b) It may take longer to establish successive commands than some other kinds of command generation because of limited store speeds, and possible intermediate program steps.

The Programmed Command Generator 7038

This unit provides an example of a command generator controlled by a program store. It is designed to control sequences of autonomous transfers and is programmed by 24-bit instructions. The command generator is a double-width CAMAC module, but it requires a separate store of instructions, which may be a free-standing diode plugboard or a store module. The command generator can accept up to 256 words of program store, but 32 words will be sufficient for many applications.

The unit has four trigger inputs, these are in fixed priority-order and start the program from addresses 0, 1, 2 and 3. The unit may also be started at any address by dataway instruction.

The program word is made up from 21 bits which normally specify the command, and a 3-bit instruction code, which specifies instructions such as Transfer and Transfer and End.

A Simple Program

The simplest form of program involves only these two types of instruction, e.g.,

Transfer	First register.
Transfer	Second register.
Transfer	Third register.
Transfer and End	Fourth register.

Use of the Q Signal

The Conditional Skip instruction code provides a means of testing Q. It can be used for controlling block transfers from a module, provided that each transfer can be tested by Q. A program to read a block of data from one module might be:-

1. Conditional Skip Station 20 Sub-Address 0
   Function 8 Channel Code 0

   This instruction jumps to instruction 3 if Q is set to indicate that a word is ready for transfer otherwise instruction 2 is executed.

2. Transfer and End Station 26 Channel Code 1

   This instruction completes the block transfer by calling for a computer interrupt. The command generator then waits for another trigger pulse.

3. Transfer Station 20 Sub-address 0
   Function 2 Channel Code 4

   This instruction reads a word from the module addressed.

4. Jump to Instruction 1.

Sequential Readout

Blocks of registers in successive modules can also be readout using a few instructions, by the use of the module address register which holds the current Crate address, station address and sub-address. This module address register can be incremented or loaded by appropriate instructions, and the current state of the register can be tested by Conditional Jump instructions. The full instruction set of the programmed command generator can be illustrated by the following program which will read the module in station 1, will then read and clear four registers in the modules at each of the stations 4, 6, 8, 10, 12, 14, 16 and 18, and will preset a scaler in station 2 so that the sequence can be re-triggered after, say, the preset number of clock pulses.

1. Transfer Crate 0 Station 1
   Sub-address 0 Function 0
   Channel Code 4

   This instruction reads data from the first module.

2. Load Station 4 Sub-address 0

   This instruction sets the module address to the start of the block of modules.

3. Transfer Current Address Function 2
   Channel Code 5

   This instruction reads and clears the register at the current address.

4. Increase and Transfer + Sub-address 1
   Function 2 Channel Code 5

   This instruction reads and clears data from the next register.

5. Conditional Jump Sub-address 3
   Instruction 4

   Instruction 4 is repeated until the register at Sub-address 3 has been read and cleared.

6. Increase + Station 2 Sub-address 0

   This instruction selects the next module, Sub-address 0.

7. Conditional Jump Station 18 Instruction 3

   The sequence jumps to Instruction 3 to read the next module and continues the process until module 18 has been read.

8. Write Data Station 2 Sub-address 0
   Data 60

   This instruction overwrites 60 into module 2.

9. End

   This unit halts until the sequence or another autonomous transfer sequence is re-triggered.

Thus these nine instructions program a sequence in which 33 registers are read and one register is loaded.

Conclusions

It is desirable that autonomous transfers in a CAMAC system should be controlled by command generators independent of particular computer interfaces, rather than by hardware built into each computer interface.

There are also considerable advantages in controlling command generation by program rather than by an inflexible sequence.

These points are illustrated by the Programmed Command Generator 7038, one of the command generators in the Harwell 7000 Series of CAMAC compatible modules.

CAMAC and Modular Instrumentation

A report on the discussion edited by :
H. Bisby, AERE, Harwell, U.K.
W. Becker, EURATOM, Ispra, Italy
R.C.M. Barnes, AERE, Harwell, U.K.

In introducing the descriptive paper by Barnes and Hooton (7.1. "The CAMAC System of Modular Instrumentation"), Bisby (Chairman ESONE Committee) reviewed the derivation of the CAMAC standard by reference to a chronological sequence of dates which had marked significant progress towards reaching international agreement by the ESONE Committee. The period started in May 1965 when a proposal was first discussed for a new standard to anticipate the introduction of integrated circuit components and the techniques of printed circuits and on-line data acquisition and control of experiments by small scientific computers. Bisby also gave a conservative estimate of the approximate "effective" cost of deriving the CAMAC standard as $ 700, 000, so far, and that completion of further levels of compatibility could raise this to $ 1 M.

In replying to questions on his paper, Barnes made the following points :
1. Several large establishments (Harwell, Rutherford, CERN, etc.) had devised tempo - rary schemes for inter-crate connection of the dataway because the CAMAC specification did not specify this facility. The topic was under intensive discussion by the ESONE Committee and an agreed method could possibly be reached by late September 1969.
2. The principal reason for separate "Read" and "Write" lines on the dataway was to satisfy the design principle that "modules", of which these would be many, should be kept as simple as possible even at the sacrifice of increased complexity in "controllers", which would be fewer in number. Thus by the use of separate lines, "modules" in the Read operation need only drive into 4 gates (max) in the "Controller", whereas "controllers" in the Write operation must be capable of driving into 23 input gates (max).
3. Driver modules for peripheral equipment (Teletypes Printers, Punches, etc.) were being developed, however if the computer had interface facilities for these output devices, this would reduce the need for such CAMAC modules.

Three project application papers were presented and may be summarized.

J.F. MOUGEL : Project AGORA

A system was described which allowed information transfers between three computers of different types (C.I.I. 10020 and 2 PDP8's) under the control of one of them. A high performance interactive display was included in the system. The logic function of the system were modular and interconnected on a high-way system.

W. ATTWENGER, W. EGL, F. MAY, R. PATZELT, K. PETRECZEK, J. SCHWARZER

A CAMAC Crate Controller for a PDP8 Computer.

The controller design was such that it could be used with a computer or a non-com-puter semi-automatic system. This provided a very flexible unit having a 24-bit presettable data register and was fully compatible with the CAMAC system. The logic design described the instructions needed for data transfer between the CAMAC crate and the computer.

J.M. RICHARDS, L.D. WARD : Programmed Control of Autonomous Transfers in a CAMAC System.

This described a technique for the autonomous transfer of data into a computer controlled by a Programme Command Generator Module in a CAMAC application. The flexible programme could be contained on a patch-board in the module, or on a most complex programme patch-board external to the module or in a small core-memory in a module. In the latter case, the programme routine could be changed on instruction from the computer itself.

In response to an invitation from the Chairman for participants to present additional project applications of CAMAC which are being developed or considered the following statements were made :

F. ISELIN : CAMAC had now been accepted for as many as possible of the data processing applications in Nuclear Physics Division.+) An intercrate highway system was described together with its controllers and a range of general purpose modules such as a 4-channel

+) CERN, Geneva

16-bit binary scaler and scaler display, binary to decimal converter, print controller, executive L-sorter, etc. A major principle adopted in all these cases was to encourage commercial companies to supply the needs of the N.P. Division.

D.N. MACLENNON : A data processing system for installation with a control processor (PDP8) on a Fisheries Research Ship was described and utilized the CAMAC system. This was being developed and would handle analogue and digital signals from temperature pressure or other physical transducers and telemeter (sonic and electromagnetic) signals from transducers on buoys and trawl nets etc.

P.C. VAN DEN BERG : The CAMAC system was being employed in the instrumentation of the fast - thermal reactor experiment STEK in which absorbtion X-sections of fission products were to be measured. To minimize measurement time, an on-line computer (DDP516) was to be used. The measurements included absorbtion X-sections, fast neutron spectra using a proton re-coil counter and a time of flight method, reactor safety levels using ionization chambers and pulsed neutron source methods. A range of CAMAC modules were described and included a time analyzer, clock--pulse generator, 24-bit input gate, demand (L) sorter and 5 other general purpose modules.

G. HUGHES : A beam current monitoring system at Daresbury was planned and contained a fast-gated current integrator. This would accept currents in the range 10^{-3} - 10^{-9} A and integrating times as low as 1 μs. This unit, although in NIM format would be used in a CAMAC digital data processing scheme.

H. KLESSMAN : A preliminary system, very similar to CAMAC was described for a time of flight experiment using a PDP8 computer. Emphasis was placed on the development of software in a modular concept, to cover typical sub--routines common to various types of experiment. Further systems under development will employ CAMAC wherever possible.

M.C.B. RUSSELL : Positional control of crystal spectrometers can be achieved using stepping-motors and schemes were being worked out for this purpose and also the speed-control of large motors, using the CAMAC system in a computer controlled experiment.

During the afternoon discussion period there was actively interchange of comment on the potential applications of CAMAC in respect of power supplies analogue signal problems, signal processing functions, the rationalization of system software and the economics of using CAMAC. The following principal comments may serve to form the basis of a summary of the discussion.

Power Supplies

Several participants believed that the power supply schemes, available from commercial companies, should incorporate supplies compatible with the NIM system in order to complement the mechanical compatibility of NIM with CAMAC.

A discussion on the reasons for the choice of + 6 V for CAMAC left most of the potential users of CAMAC satisfied that a wise choice had been made.

Arguments for and against the use of bulk power supplies, having final stabilization in the separate crates were not resolved. The need for unexpensive supplies for single crate systems was clearly established. The Chairman pointed out that CAMAC deliberately did not specify the methods to be used for providing the standard voltages and therefore many solutions were both possible and feasible. These solutions would need to take into account short-circuit, out-of-tolerance and over--voltage conditions according to user requirements.

Signal Processing Functions (Hardware)

Several participants, particularly from the firms supplying CAMAC equipment, commented on their products and the wide range of hardware being generated to meet laboratory demands. There were obvious financial savings for smaller laboratories, such as those in University departments etc , in taking advantage of the developments, arising in the larger laboratories, which were now becoming commercially available.

The discussion showed that there was considerable interest in using the data processing facilities now being generated in CAMAC for nuclear applications, in other fields of measurement and control and R an D (medical electronics, telecommunications, broadcasting, etc.).

Several speakers believed that the CAMAC system had a powerful potential in many fields of application by virtue of the redundancy which the system allowed in controllers and crate assemblies.

To the question of whether commercial companies would supply the more specific processing hardware and not therefore in great demand, the company representatives replied that they could do this by defraying their development costs over the more general purpose units provided the latter were in sufficient demand. An appeal, in this context, was made for a rationalization of user needs, for the more popular units, eg. scalers, multiplexers, A-D and D-A converters.

Analogue Signals

The use of analogue and signal amplitude sensitive circuits in a CAMAC crate was described. Several proposals were made for reducing the possible interference created by digital transfers on the dataway. It was pointed out that experience with NIM on this earthing of front panels had been reasonably satisfactory and CAMAC used the same method. To avoid front panel earthing problems, a suggestion was made that analogue signals could be fed in on balanced twisted pairs through the front panel and then unbalanced inside the module. Alternatively, it was essential if coaxial feeds were employed to ensure adequate connection of outer screens to the front panel.

A general preference was registered for standardizing analogue signals in the 0 - 10 V range rather than 0 - 5 V ; although it was pointed out that the former increases the reverse bias requirements, for transistors, which might not therefore be readily achieved.

Software Problems

It was generally accepted that some form of software rationalization for CAMAC applications would be advantageous and may bring about greater cost savings in project applications than might even be possible with hardware rationalization.

Software modularity by task or phase of the experiment (reference paper Best and Hooton) not necessarily with a 1:1 correspondence between software and hardware modules was being investigated at several laboratories (HMI, Berlin ; Harwell, etc.) because this was thought to be feasible and would offer the possibility of allowing system software to be set up by users who are not and need not be software experienced. The use of complex languages may be a rather inefficient way to approach rationalization for real-time small computer systems.

General Comment

Participants expressed the hope that a conference or symposium could be organized on an annual basis which would bring together both users and commercial companies who were in the CAMAC business. Some felt that the present CAMAC discussion followed too closely on the issue of the CAMAC specification and they therefore would like to have been more experienced on the CAMAC system and its interpretation.

Reprinted from the proceedings

Ispra Nuclear Electronics Symposium

6-9.5.1969

Report EUR 4289 e

TIME-OF-FLIGHT INSTRUMENTATION FOR A QUASIELASTIC CRITICAL NEUTRON-SCATTERING EXPERIMENT

by

E. Mose Christiansen, Palle Christensen

Danish Atomic Energy Commission
Research Establishment Risö
Electronics Department

Summary

The instrumentation for a quasielastic critical neutron time-of-flight experiment is described. On the basis of an experiment using a sinusoidal modulating chopper and a position-sensitive neutron detector, a combined time-of-flight and scattering-angle analysis is performed by means of a 1024-channel analyser. A digital delay generator delays the phase reference pulses from the chopper for a period equal to the mean flight time of the neutrons. As this may be much longer than the time separation between the reference pulses a special working principle was required. This paper describes in some detail the delay generator and the changes made in the standard pulse-height analyser to perform the position- and the time-of-flight analysis.

Introduction

In a quasielastic critical neutron-scattering experiment a monochromatic neutron beam is directed at the sample, and the scattered neutrons are analysed according to their energy and scattering angle. With the instrumentation described herein the energy analysis is performed by the time-of-flight technique, a sinusoidal modulated neutron beam being used, while the scattering angles are determined by means of a position-sensitive neutron detector.

During the last few years various methods[1,2] of increasing the low efficiency of the standard time-of-flight technique have come into use. One of these methods involves the use of a sinusoidal modulated neutron beam. The standard time-of-flight spectrum may be regarded as the response of the scattering system to an impulse signal, and the scattering parameters are determined from this response function, f(t), but they may be equally well determined from the response of the system to a number of different impressed sinusoidal signals, that is, from the frequency response, $F(\omega)$, of the system.

The method is fully exploited by the use of several neutron detectors or, as in the present work, a position-sensitive neutron detector making simultaneous analysis of the scattering angles possible.

This paper describes the experimental equipment, particularly the electronics used for the time-of-flight- and the scattering-angle analysis.

Experimental Equipment

General Arrangement

Fig. 1 shows a functional diagram of the experimental arrangement. The sinusoidal intensity modulation of the monochromatic neutron beam is effected by means of a high-speed chopper, the rotor disk of which contains a total of 24 uniformly spaced neutron-absorbing sections. The neutrons are detected by the position-sensitive neutron detector after they have been scattered by the sample and have passed through the flight path. This detector is of the type that employs a resistive anode as charge divider, and the position of impact of a neutron is determined from the ratio of the charge accumulated at one end of the detector to the total charge generated by the detection process. The detector[3] consists of a 50 cm long cylindrical brass tube with an anode of 0.3 mm glass wire, coated with colloidal carbon giving a resistance of approximately 45 kilo-ohms. The detector gas is a mixture containing He^3.

The signals from the two ends of the detector are each amplified by a charge-sensitive preamplifier (Nuclear Enterprises, type NE 5287). One signal is further amplified and shaped before being sent to the analogue-to-digital converter (ADC) of the 1024-channel analyser (TMC type CN-1024). The sum of the signals from the two preamplifiers is shaped and amplified in the same way to go finally to the ADC of the analyser.

The ADC was modified to analyse the two signals according to their ratio and thus according to the position of impact of the detected neutron. A single-channel pulse-height selector operating on the sum signal excludes, in connection with the coincidence facility of the ADC, signals that do not originate from the detection of neutrons. Suitable delays were inserted in the two signal paths to give the coincidence circuit of the analyser time for its operation. 128 channels, employing the seven least signifi-

cant bits of the address, are used for the position analysis. The last three bits are set according to time, making up eight phase channels representing in all one period of the modulating signal. From the contents of the phase channels the attenuation and phase shift of the modulating signal are determined.

The phase counter is advanced by pulses generated by the chopper system. A pattern engraved along the rim of the rotor disk is detected by an opto-electronic system giving out eight pulses per period of the modulating signal. To ensure timing accuracy, a balanced detector-amplifier system was used in connection with a zero cross-over trigger. A second pattern and opto-electronic system generate a reset pulse for every eighth pulse from the first pattern to preserve the synchronism between the chopper and the phase counter. The flight time of the neutrons will contribute to the phase shift a term that increases linearly with frequency. In order to compensate for this and thereby reduce the stability demand on the chopper, the reference pulses from the chopper are delayed for a period equal to the mean flight time of the neutrons. A digital delay generator provides this delay.

To take full advantage of the resolution capabilities of the measuring facility, modulation frequencies up to 20 kHz are required. With the 24 periods per revolution this gives a chopper speed of 50 000 r.p.m. The chopper is actuated by a high-frequency motor (C.O. Öberg and Co., type VM 17), fed from a rotating high-frequency generator. The stability obtained by this system without any feedback is 0.5% for several hours. At the lower modulation frequencies this will be sufficient. At the higher frequencies a better stability may, however, be required in order that the delay generator may function correctly. A voltage generated by the delay generator may be used for the stabilization of the chopper.

Digital Delay Generator

Design Parameters. The mean flight-time of the neutrons is a few milliseconds with the present flight path. To fit in with this and also to comply with future requirements, the delay generator was given a maximum delay of 10 msec, adjustable in steps of 1 μsec. The delay generator must be able to delay all the pulses from the chopper by the set period, even though for most modulation frequencies this will be much longer than the time separation between the pulses. Because of the special operating principle needed to achieve this, and in order to keep the time jitter of the delay within a fraction of the setting accuracy, a clock frequency of 10 MHz was chosen. Thus the time jitter will be within 0.3 μsec. The clock oscillator is crystal controlled, giving the delay generator a long-term stability of 20 p.p.m.

Operating Principle. In order to delay pulses for periods longer than those that separate them, the digital delay generator currently measures the difference between the set delay and the total of pulse periods that is just less than the delay. This difference is then used as the preset for the delay counter operating on every input pulse. A specific value of the difference is used as the preset for the delay counter until a new measurement of the difference has been performed, whereupon the preset is corrected in accordance with this. The principle outlined above will delay all pulses for the correct time provided that the totals of any fixed numbers of pulse periods are equal and only change slowly.

A functional diagram of the delay generator is shown in fig. 2. The time difference used as the preset for the delay counter is measured by a five-decade up/down synchronous counter. By pushing the CLEAR- and START-buttons the control logic is reset, and the counter is preset with the delay, set in a four-decade thumb-wheel switch register. The first reference pulse to arrive from the chopper initiates counting-down by clock pulses. If no more reference pulses have arrived when the counter passes zero, an output pulse is generated, the counter is preset with the delay, and the procedure is repeated for every reference pulse from the chopper.

If one or more reference pulses have arrived during the counting-down to zero, the counting is continued. At the arrival of the first reference pulse from the chopper after the expiration of the delay, the counting direction is reversed, and during the following period until the next reference pulse arrives, the clock pulses count the up/down counter up. Then the counting is stopped, and the contents of the counter, which are now equal to the difference between the set delay and the total of reference pulse periods that is just less than the delay, are transferred to a five-decade memory register. The up/down counter is preset to the delay, and the whole procedure is restarted at the next reference pulse.

From the memory register the difference is transferred to the five-decade delay counter. At every reference pulse the counting-down by clock pulses is started. When the contents of the register equal zero, an output pulse is generated, and the delay counter is again preset with the difference contained in the memory register.

The time required for the operation of the control logic and for the transfer of the measured time difference from the up/down counter to the memory register and from this to the delay counter, in-

hibits the generation of an output pulse a few tenths of a microsecond about the time of arrival of the reference pulses. This limits the allowable relative variations of the chopper speed to the ratio between one period of the reference pulse signal and the total delay. Only at the higher speeds may the stability of the chopper be inadequate. An error voltage may, however, be derived from the control logic of the delay generator to be used for the stabilization of the chopper.

The reset pulse for the phase counter in the multi-channel analyser is generated synchronously with the delayed reference pulse that follows next to the arrival of the reset pulse from the chopper system. This means that the measured phase may be wrong by one to seven eighths of a period of the modulating signal. It will, however, always be possible to correct this when the delay and the modulation frequency are known.

Design. The circuits[4] are based on the application of the transistor-transistor-logic integrated digital networks. The two counters as well as the control logic were designed for synchronous operation. Fig. 3 shows the up/down counter, and fig. 4 shows the connections between the registers for a single decade. The design of the decades is approximately as found[5] by using the 1, 2, 4, 8 code. Fig. 5 shows the control logic. A total of 108 dual-in-line network packages were applied, all mounted on a single printed circuit board.

Multichannel Analyser

Position Analysis. The calculation of the charge ratio for determination of the position of impact of a detected neutron is performed by means of the analogue-to-digital converter (ADC, TMC model 213) of the multichannel analyser. The converter is of the Wilkinson type in which a capacitor is charged to a voltage proportional to the pulse to be analysed and then discharged by a constant current. The discharge time and thus the number of gated address advance pulses is then proportional to the pulse height. For the computation of the charge ratio the ADC is altered in such a way that the capacitor is discharged by a current proportional to the denominator of the ratio. The number of address advance pulses is now proportional to the charge ratio.

To make the discharge current proportional to the denominator of the charge ratio, that is the sum pulse, a linear gate, a pulse stretcher and a current generator were added to the ADC (see fig. 6). The linear gate is controlled by the same UNCLAMP signal that controls the gate at the input of the converter circuit. The output from the pulse stretcher and thus the discharge current are sustained until the end of the conversion process. In order to make this particular ADC work, the current generator must supply it with at least 0.2 mA. This sets a lower limit for the sum pulses that might be accepted for analysis. As, however, the minor sum pulses have to be rejected because they do not originate from detected neutrons, this limit is unimportant for our purpose.

The charge ratio is digitized with a resolution of seven bits. Fig. 7 shows the results of a linearity test on the converter. The 128 channels used for the position analysis should be compared with the approximately 2% spatial resolution of the detector. This is illustrated in fig. 8, which shows the performance of the total position analysis system, using a narrow, collimated beam of thermal neutrons. The different intensities of the particular peaks are due to varying gas multiplication along the detector.

Phase Analysis. A separate three-bit phase counter was added to the computer unit to perform the phase analysis. The counter is advanced by the delayed phase reference pulses. At every eighth pulse the counter is reset by the delayed reset pulse in order to keep up the synchronism with the chopper. When a detector pulse has been accepted for analysis, the state of the phase counter is transferred to the three last bits of the address register. The first seven bits are set according to the charge ratio as determined by the ADC. As in normal pulse-height analysis, the memory cycle is initiated at the end of the conversion process. If a detector pulse is coincident with a phase reference pulse, the memory cycle is inhibited as the state of the phase counter is indefinite at that moment. This is effected by using the late anticoincidence facility of the ADC in connection with two one-shot multivibrators to define the resolution time. The multivibrators are triggered by the phase reference pulses and by the phase transfer pulse respectively. The memory cycle is also inhibited by the address overflow signal, taken from the seventh binary.

Conclusion

The instrumentation has been in operation for only a short time, so its performance has not yet been completely evaluated. It has, however, proved its capability in giving spectra with a spatial resolution equal to the theoretically possible for the detector. Fig 9 shows an example of the type of spectra measured by the instrumentation. The individual peaks represent the angular distribution of neutrons scattered by the sample, while the ensemble of peaks gives

the distribution according to the phase. The flight path was 4.45 m, and the measurement was performed at a modulation frequency of 4444 Hz.

Extension of the instrumentation is already foreseen as the instrumentation is going to be governed from the control system of an automatic neutron spectrometer. The stabilization of the chopper as mentioned in this paper is also being prepared in connection with a system to change the chopper speed on command from the control system.

Acknowledgements

The authors wish to thank J. Kjems of the Physics Department for the encouraging co-operation and the patience with which he has awaited the completion of this instrumentation, as well as for the results presented in figs. 8 and 9. Thanks are due to T. Hviid for the design of the logic and the circuitry of the delay generator and for helpful suggestions and assistance with the work. We also wish to acknowledge the work of A. Sloth on the opto-electronic system for the reference pulse generation.

References

1. I.F. Colwell et al., A New High Efficiency Time-of-Flight System. IAEA Symposium, Copenhagen 1968. Paper SM-104/77.

2. F. Gompf et al., The Use of a Pseudostatistical Chopper for Time-of-Flight Measurements. IAEA Symposium, Copenhagen 1969. Paper SM-104/67.

3. I. Kjems, Risö, Denmark, personal communication, 1969.

4. T. Hviid, Risö, Denmark, unpublished work 1969.

5. Texas Instruments: Integrated Circuits Applications Manual.

DISCUSSION

Miller : - I would like to ask what is the limit for accuracy of your dividing circuitry for using it for seven decades of accuracy.

Christensen : - 2% .

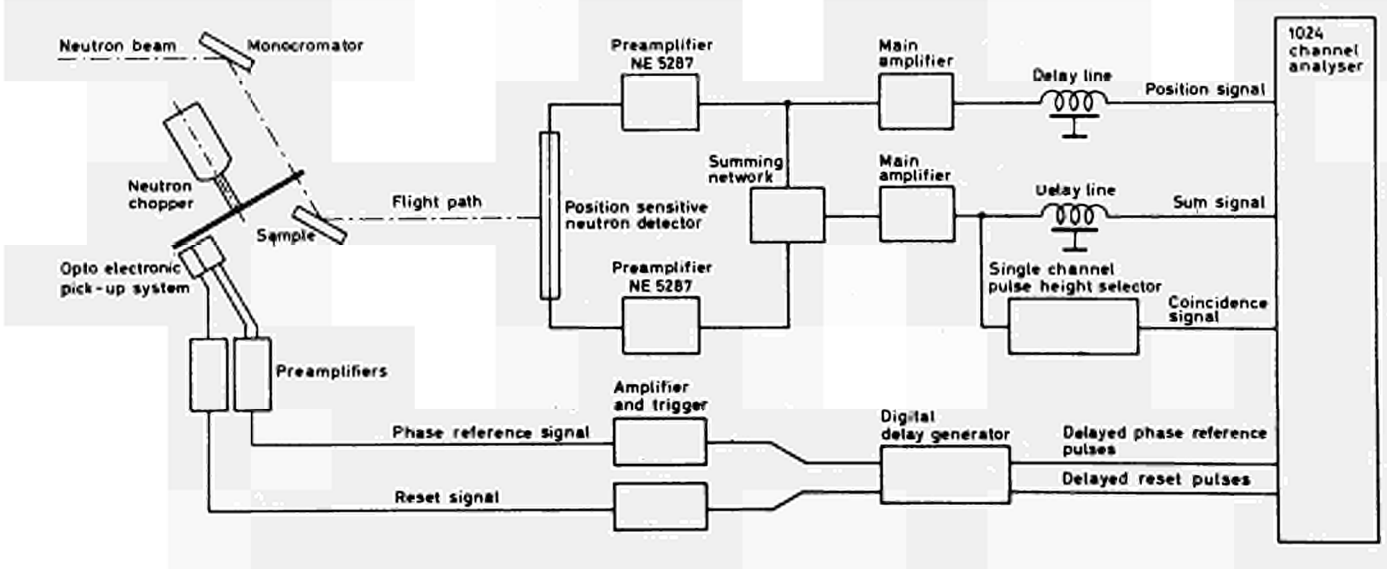

Fig. 1 - Experimental arrangement, functional diagram.

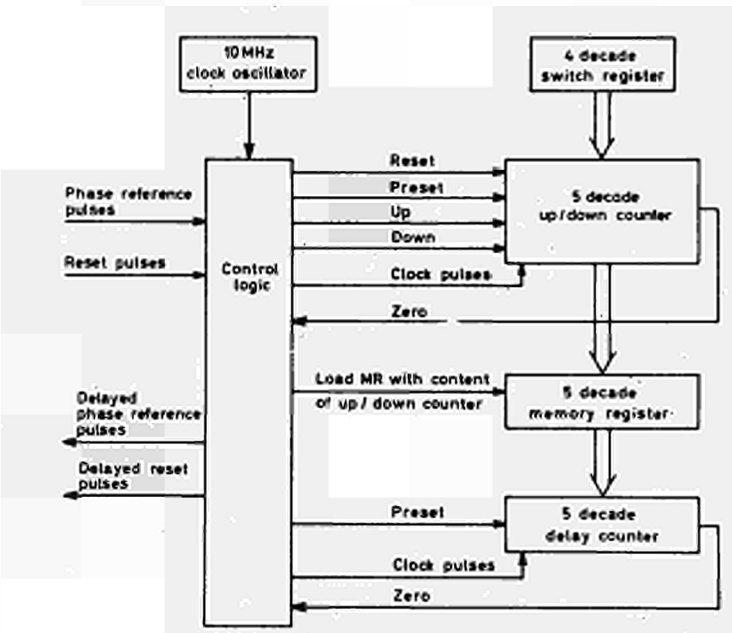

Fig. 2 - Delay generator, functionnal diagram.

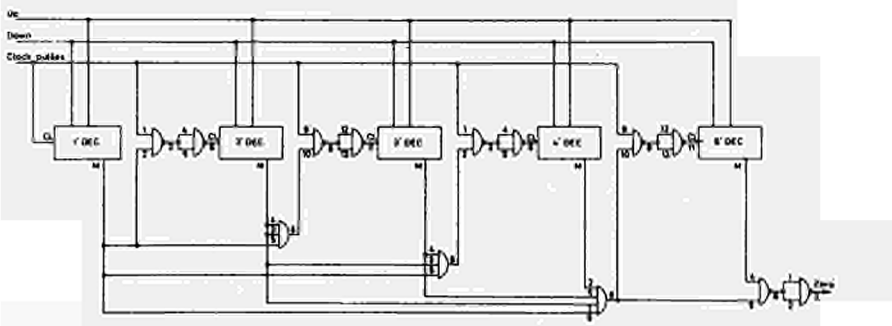

Fig. 3 - Delay generator, block diagram of up/down counter.

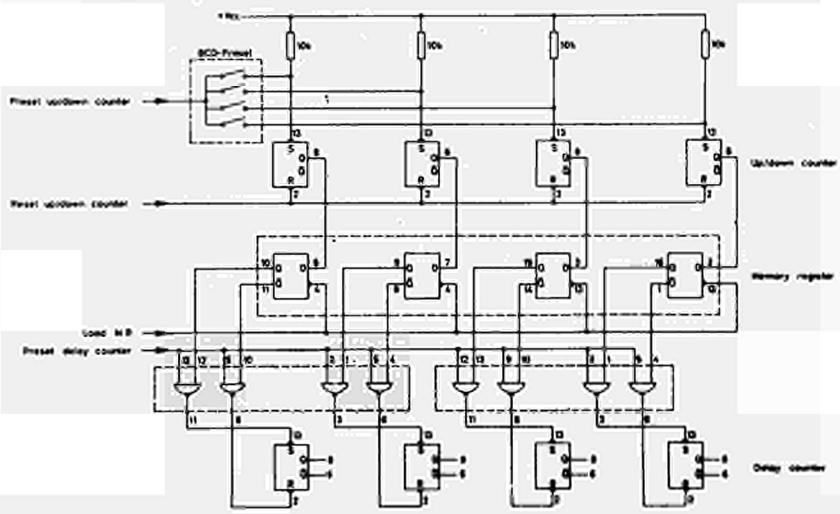

Fig. 4 - Delay generator, block diagram of connections between the registers, one decade shown.

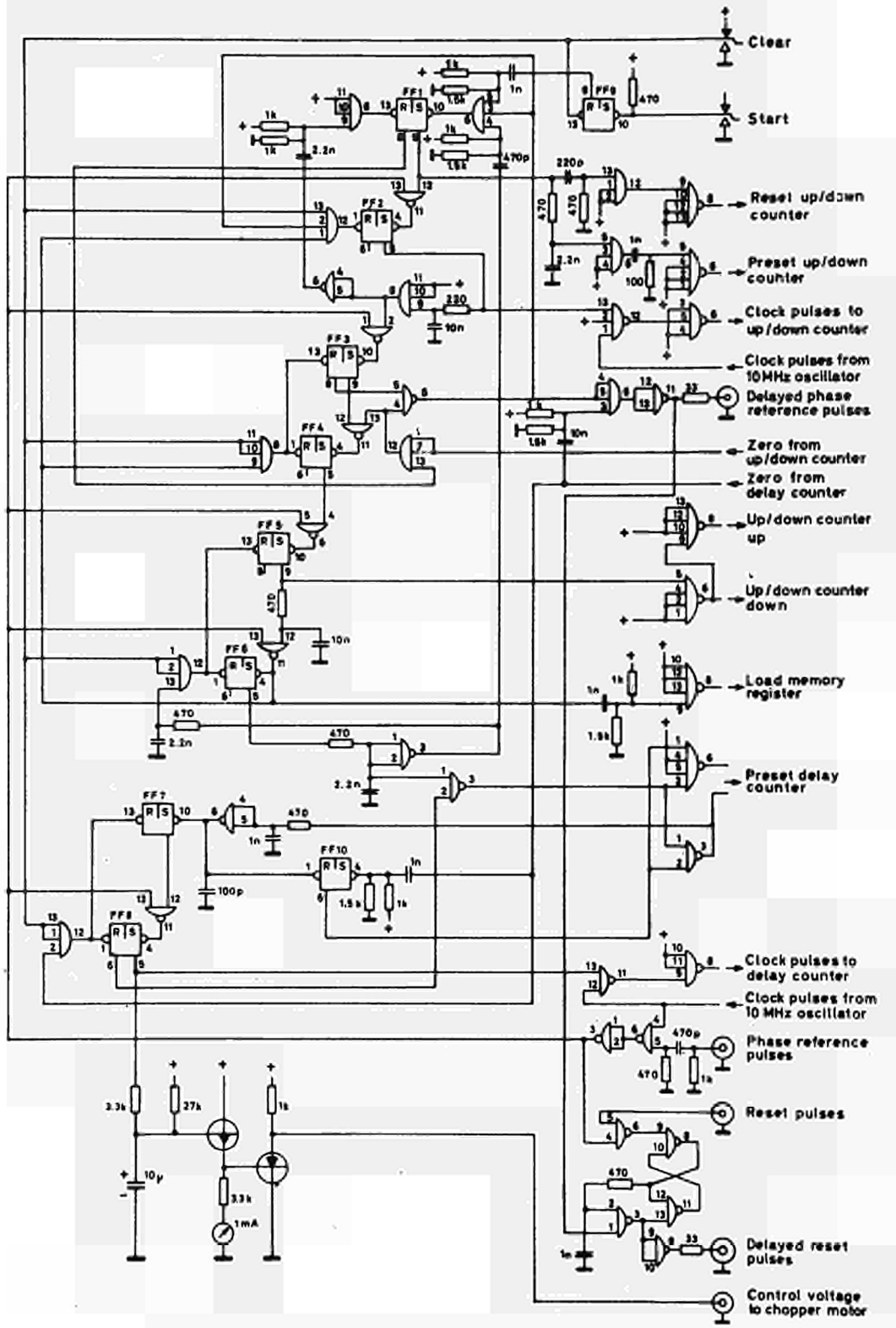

Fig. 5. Delay generator, block diagram of control logic.

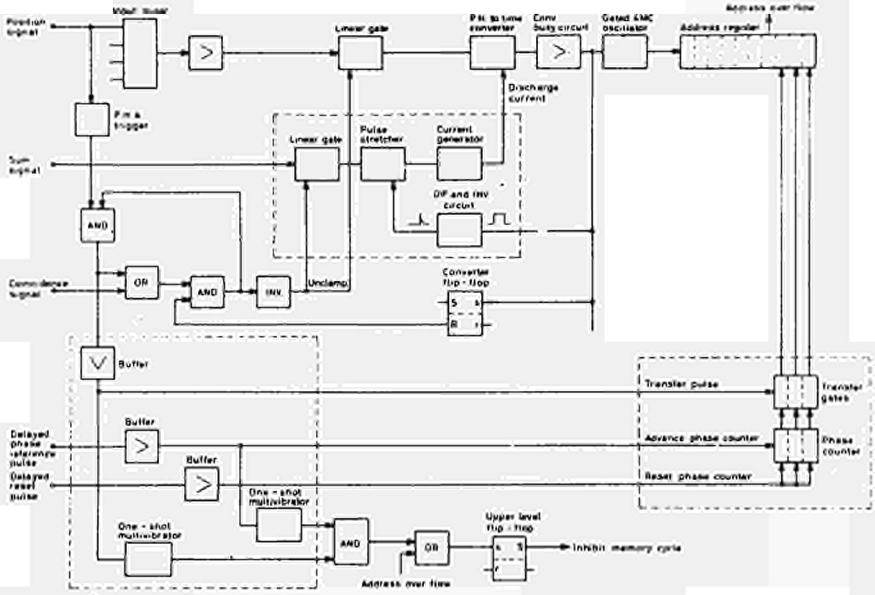

Fig. 6.

1024-channel analyser, simplified block diagram of circuits used for position and phase analysis. The circuits added to the original design are surrounded by a dashed line.

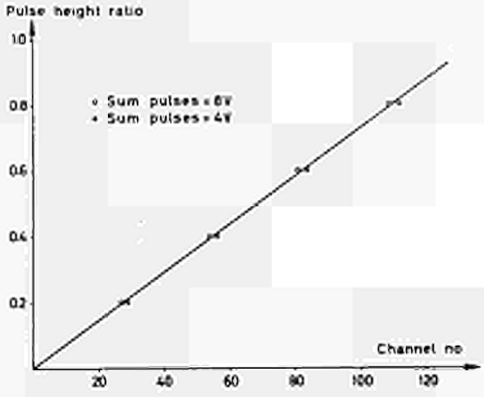

Fig. 7.

Result of linearity test on the pulse-ratio converter.

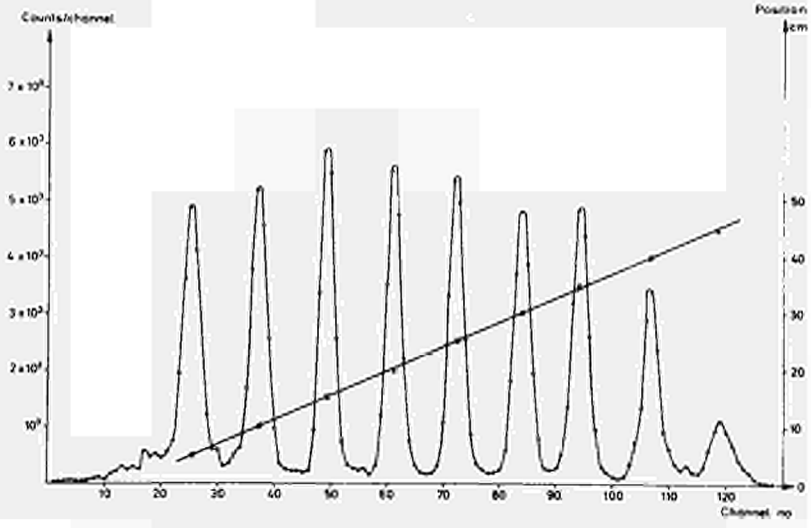

Fig. 8. Result of linearity test on the total position-analysis system by means of a 3 mm collimated beam of thermal neutrons.

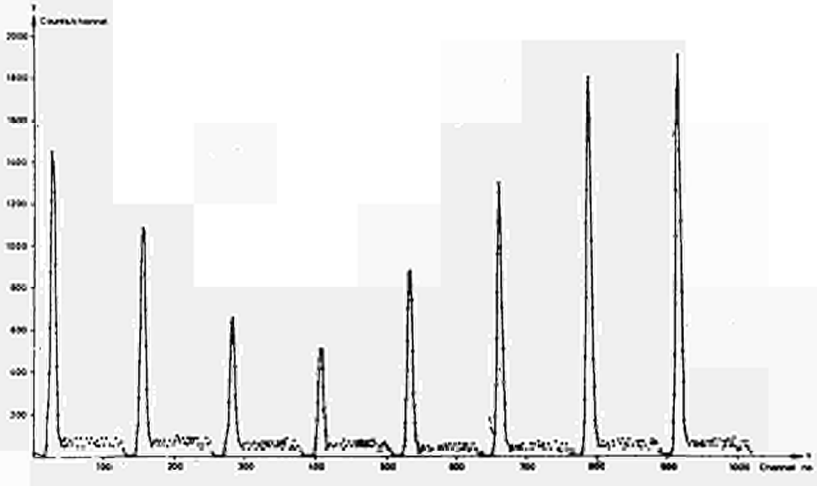

Fig. 9.

Scattering angle/phase spectrum. Flight path 4.45 m; modulation frequency 4444 Hz.

Reprinted from the proceedings

Ispra Nuclear Electronics Symposium

6-9.5.1969

Report EUR 4289 e

TIME-OF-FLIGHT INSTRUMENTATION FOR A QUASIELASTIC CRITICAL NEUTRON-SCATTERING EXPERIMENT

by

E. Mose Christiansen, Palle Christensen

Danish Atomic Energy Commission
Research Establishment Risö
Electronics Department

Summary

The instrumentation for a quasielastic critical neutron time-of-flight experiment is described. On the basis of an experiment using a sinusoidal modulating chopper and a position-sensitive neutron detector, a combined time-of-flight and scattering-angle analysis is performed by means of a 1024-channel analyser. A digital delay generator delays the phase reference pulses from the chopper for a period equal to the mean flight time of the neutrons. As this may be much longer than the time separation between the reference pulses a special working principle was required. This paper describes in some detail the delay generator and the changes made in the standard pulse-height analyser to perform the position- and the time-of-flight analysis.

Introduction

In a quasielastic critical neutron-scattering experiment a monochromatic neutron beam is directed at the sample, and the scattered neutrons are analysed according to their energy and scattering angle. With the instrumentation described herein the energy analysis is performed by the time-of-flight technique, a sinusoidal modulated neutron beam being used, while the scattering angles are determined by means of a position-sensitive neutron detector.

During the last few years various methods[1,2] of increasing the low efficiency of the standard time-of-flight technique have come into use. One of these methods involves the use of a sinusoidal modulated neutron beam. The standard time-of-flight spectrum may be regarded as the response of the scattering system to an impulse signal, and the scattering parameters are determined from this response function, f(t), but they may be equally well determined from the response of the system to a number of different impressed sinusoidal signals, that is, from the frequency response, $F(\omega)$, of the system.

The method is fully exploited by the use of several neutron detectors or, as in the present work, a position-sensitive neutron detector making simultaneous analysis of the scattering angles possible.

This paper describes the experimental equipment, particularly the electronics used for the time-of-flight- and the scattering-angle analysis.

Experimental Equipment

General Arrangement

Fig. 1 shows a functional diagram of the experimental arrangement. The sinusoidal intensity modulation of the monochromatic neutron beam is effected by means of a high-speed chopper, the rotor disk of which contains a total of 24 uniformly spaced neutron-absorbing sections. The neutrons are detected by the position-sensitive neutron detector after they have been scattered by the sample and have passed through the flight path. This detector is of the type that employs a resistive anode as charge divider, and the position of impact of a neutron is determined from the ratio of the charge accumulated at one end of the detector to the total charge generated by the detection process. The detector[3] consists of a 50 cm long cylindrical brass tube with an anode of 0.3 mm glass wire, coated with colloidal carbon giving a resistance of approximately 45 kilo-ohms. The detector gas is a mixture containing He^3.

The signals from the two ends of the detector are each amplified by a charge-sensitive preamplifier (Nuclear Enterprises, type NE 5287). One signal is further amplified and shaped before being sent to the analogue-to-digital converter (ADC) of the 1024-channel analyser (TMC type CN-1024). The sum of the signals from the two preamplifiers is shaped and amplified in the same way to go finally to the ADC of the analyser.

The ADC was modified to analyse the two signals according to their ratio and thus according to the position of impact of the detected neutron. A single-channel pulse-height selector operating on the sum signal excludes, in connection with the coincidence facility of the ADC, signals that do not originate from the detection of neutrons. Suitable delays were inserted in the two signal paths to give the coincidence circuit of the analyser time for its operation. 128 channels, employing the seven least signifi-

cant bits of the address, are used for the position analysis. The last three bits are set according to time, making up eight phase channels representing in all one period of the modulating signal. From the contents of the phase channels the attenuation and phase shift of the modulating signal are determined.

The phase counter is advanced by pulses generated by the chopper system. A pattern engraved along the rim of the rotor disk is detected by an opto-electronic system giving out eight pulses per period of the modulating signal. To ensure timing accuracy, a balanced detector-amplifier system was used in connection with a zero cross-over trigger. A second pattern and opto-electronic system generate a reset pulse for every eighth pulse from the first pattern to preserve the synchronism between the chopper and the phase counter. The flight time of the neutrons will contribute to the phase shift a term that increases linearly with frequency. In order to compensate for this and thereby reduce the stability demand on the chopper, the reference pulses from the chopper are delayed for a period equal to the mean flight time of the neutrons. A digital delay generator provides this delay.

To take full advantage of the resolution capabilities of the measuring facility, modulation frequencies up to 20 kHz are required. With the 24 periods per revolution this gives a chopper speed of 50 000 r.p.m. The chopper is actuated by a high-frequency motor (C.O. Öberg and Co., type VM 17), fed from a rotating high-frequency generator. The stability obtained by this system without any feedback is 0.5% for several hours. At the lower modulation frequencies this will be sufficient. At the higher frequencies a better stability may, however, be required in order that the delay generator may function correctly. A voltage generated by the delay generator may be used for the stabilization of the chopper.

Digital Delay Generator

Design Parameters. The mean flight-time of the neutrons is a few milliseconds with the present flight path. To fit in with this and also to comply with future requirements, the delay generator was given a maximum delay of 10 msec, adjustable in steps of 1 μsec. The delay generator must be able to delay all the pulses from the chopper by the set period, even though for most modulation frequencies this will be much longer than the time separation between the pulses. Because of the special operating principle needed to achieve this, and in order to keep the time jitter of the delay within a fraction of the setting accuracy, a clock frequency of 10 MHz was chosen. Thus the time jitter will be within 0.3 μsec. The clock oscillator is crystal controlled, giving the delay generator a long-term stability of 20 p.p.m.

Operating Principle. In order to delay pulses for periods longer than those that separate them, the digital delay generator currently measures the difference between the set delay and the total of pulse periods that is just less than the delay. This difference is then used as the preset for the delay counter operating on every input pulse. A specific value of the difference is used as the preset for the delay counter until a new measurement of the difference has been performed, whereupon the preset is corrected in accordance with this. The principle outlined above will delay all pulses for the correct time provided that the totals of any fixed numbers of pulse periods are equal and only change slowly.

A functional diagram of the delay generator is shown in fig. 2. The time difference used as the preset for the delay counter is measured by a five-decade up/down synchronous counter. By pushing the CLEAR- and START-buttons the control logic is reset, and the counter is preset with the delay, set in a four-decade thumb-wheel switch register. The first reference pulse to arrive from the chopper initiates counting-down by clock pulses. If no more reference pulses have arrived when the counter passes zero, an output pulse is generated, the counter is preset with the delay, and the procedure is repeated for every reference pulse from the chopper.

If one or more reference pulses have arrived during the counting-down to zero, the counting is continued. At the arrival of the first reference pulse from the chopper after the expiration of the delay, the counting direction is reversed, and during the following period until the next reference pulse arrives, the clock pulses count the up/down counter up. Then the counting is stopped, and the contents of the counter, which are now equal to the difference between the set delay and the total of reference pulse periods that is just less than the delay, are transferred to a five-decade memory register. The up/down counter is preset to the delay, and the whole procedure is restarted at the next reference pulse.

From the memory register the difference is transferred to the five-decade delay counter. At every reference pulse the counting-down by clock pulses is started. When the contents of the register equal zero, an output pulse is generated, and the delay counter is again preset with the difference contained in the memory register.

The time required for the operation of the control logic and for the transfer of the measured time difference from the up/down counter to the memory register and from this to the delay counter, in-

hibits the generation of an output pulse a few tenths of a microsecond about the time of arrival of the reference pulses. This limits the allowable relative variations of the chopper speed to the ratio between one period of the reference pulse signal and the total delay. Only at the higher speeds may the stability of the chopper be inadequate. An error voltage may, however, be derived from the control logic of the delay generator to be used for the stabilization of the chopper.

The reset pulse for the phase counter in the multi-channel analyser is generated synchronously with the delayed reference pulse that follows next to the arrival of the reset pulse from the chopper system. This means that the measured phase may be wrong by one to seven eighths of a period of the modulating signal. It will, however, always be possible to correct this when the delay and the modulation frequency are known.

Design. The circuits[4] are based on the application of the transistor-transistor-logic integrated digital networks. The two counters as well as the control logic were designed for synchronous operation. Fig. 3 shows the up/down counter, and fig. 4 shows the connections between the registers for a single decade. The design of the decades is approximately as found[5] by using the 1, 2, 4, 8 code. Fig. 5 shows the control logic. A total of 108 dual-in-line network packages were applied, all mounted on a single printed circuit board.

Multichannel Analyser

Position Analysis. The calculation of the charge ratio for determination of the position of impact of a detected neutron is performed by means of the analogue-to-digital converter (ADC, TMC model 213) of the multichannel analyser. The converter is of the Wilkinson type in which a capacitor is charged to a voltage proportional to the pulse to be analysed and then discharged by a constant current. The discharge time and thus the number of gated address advance pulses is then proportional to the pulse height. For the computation of the charge ratio the ADC is altered in such a way that the capacitor is discharged by a current proportional to the denominator of the ratio. The number of address advance pulses is now proportional to the charge ratio.

To make the discharge current proportional to the denominator of the charge ratio, that is the sum pulse, a linear gate, a pulse stretcher and a current generator were added to the ADC (see fig. 6). The linear gate is controlled by the same UNCLAMP signal that controls the gate at the input of the converter circuit. The output from the pulse stretcher and thus the discharge current are sustained until the end of the conversion process. In order to make this particular ADC work, the current generator must supply it with at least 0.2 mA. This sets a lower limit for the sum pulses that might be accepted for analysis. As, however, the minor sum pulses have to be rejected because they do not originate from detected neutrons, this limit is unimportant for our purpose.

The charge ratio is digitized with a resolution of seven bits. Fig. 7 shows the results of a linearity test on the converter. The 128 channels used for the position analysis should be compared with the approximately 2% spatial resolution of the detector. This is illustrated in fig. 8, which shows the performance of the total position analysis system, using a narrow, collimated beam of thermal neutrons. The different intensities of the particular peaks are due to varying gas multiplication along the detector.

Phase Analysis. A separate three-bit phase counter was added to the computer unit to perform the phase analysis. The counter is advanced by the delayed phase reference pulses. At every eighth pulse the counter is reset by the delayed reset pulse in order to keep up the synchronism with the chopper. When a detector pulse has been accepted for analysis, the state of the phase counter is transferred to the three last bits of the address register. The first seven bits are set according to the charge ratio as determined by the ADC. As in normal pulse-height analysis, the memory cycle is initiated at the end of the conversion process. If a detector pulse is coincident with a phase reference pulse, the memory cycle is inhibited as the state of the phase counter is indefinite at that moment. This is effected by using the late anticoincidence facility of the ADC in connection with two one-shot multivibrators to define the resolution time. The multivibrators are triggered by the phase reference pulses and by the phase transfer pulse respectively. The memory cycle is also inhibited by the address overflow signal, taken from the seventh binary.

Conclusion

The instrumentation has been in operation for only a short time, so its performance has not yet been completely evaluated. It has, however, proved its capability in giving spectra with a spatial resolution equal to the theoretically possible for the detector. Fig 9 shows an example of the type of spectra measured by the instrumentation. The individual peaks represent the angular distribution of neutrons scattered by the sample, while the ensemble of peaks gives

the distribution according to the phase. The flight path was 4.45 m, and the measurement was performed at a modulation frequency of 4444 Hz.

Extension of the instrumentation is already foreseen as the instrumentation is going to be governed from the control system of an automatic neutron spectrometer. The stabilization of the chopper as mentioned in this paper is also being prepared in connection with a system to change the chopper speed on command from the control system.

Acknowledgements

The authors wish to thank J. Kjems of the Physics Department for the encouraging co-operation and the patience with which he has awaited the completion of this instrumentation, as well as for the results presented in figs. 8 and 9. Thanks are due to T. Hviid for the design of the logic and the circuitry of the delay generator and for helpful suggestions and assistance with the work. We also wish to acknowledge the work of A. Sloth on the opto-electronic system for the reference pulse generation.

References

1. I.F. Colwell et al., A New High Efficiency Time-of-Flight System. IAEA Symposium, Copenhagen 1968. Paper SM-104/77.
2. F. Gompf et al., The Use of a Pseudostatistical Chopper for Time-of-Flight Measurements. IAEA Symposium, Copenhagen 1969. Paper SM-104/67.
3. I. Kjems, Risö, Denmark, personal communication, 1969.
4. T. Hviid, Risö, Denmark, unpublished work 1969.
5. Texas Instruments: Integrated Circuits Applications Manual.

DISCUSSION

Miller : - I would like to ask what is the limit for accuracy of your dividing circuitry for using it for seven decades of accuracy.

Christensen : - 2% .

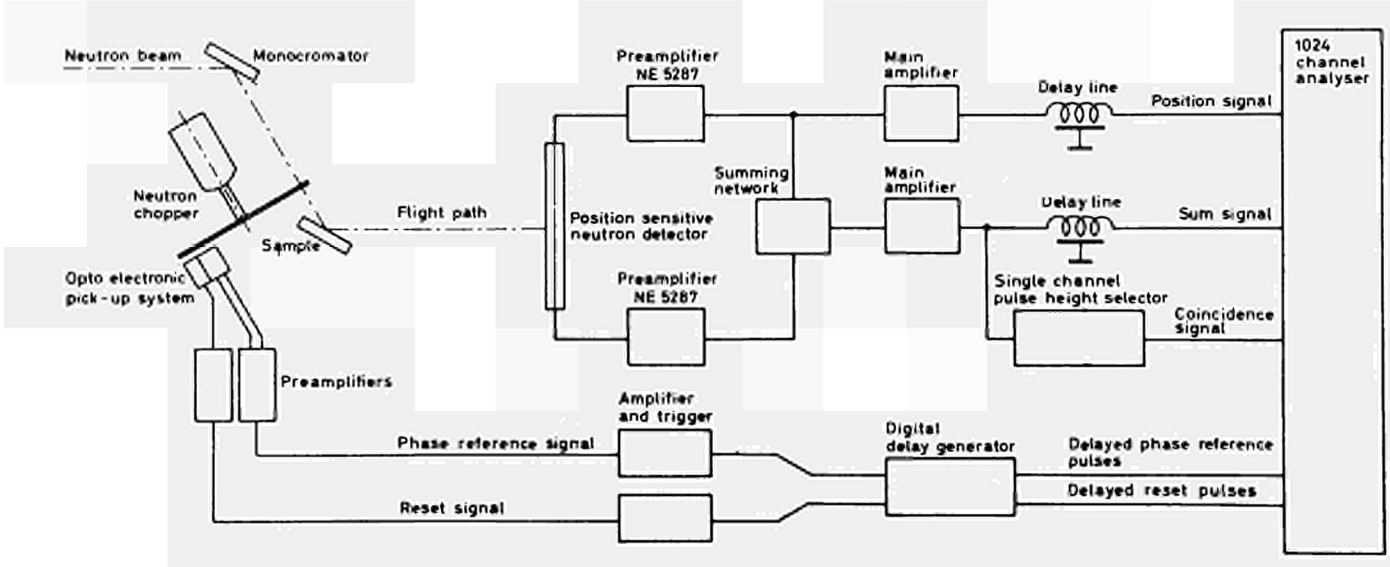

Fig. 1 - Experimental arrangement, functional diagram.

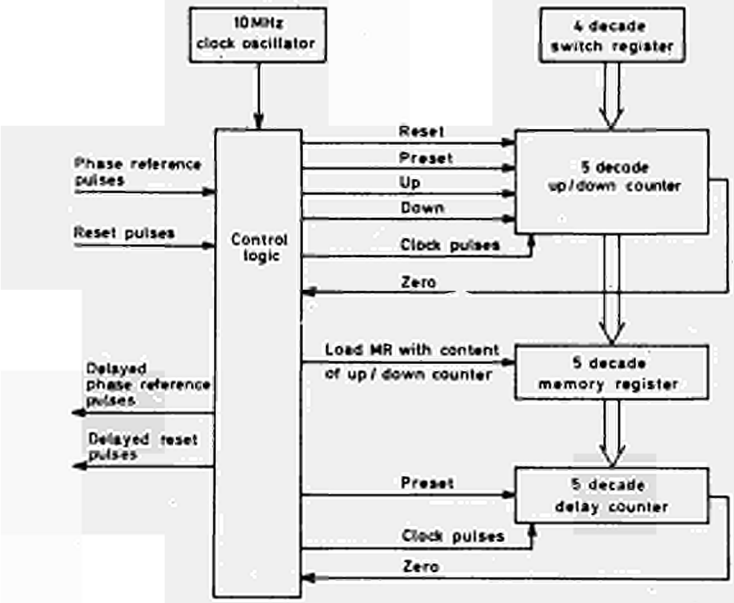

Fig. 2 - Delay generator, functional diagram.

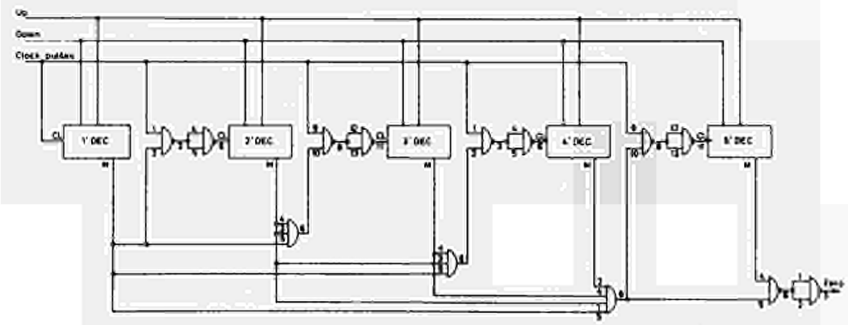

Fig. 3 - Delay generator, block diagram of up/down counter.

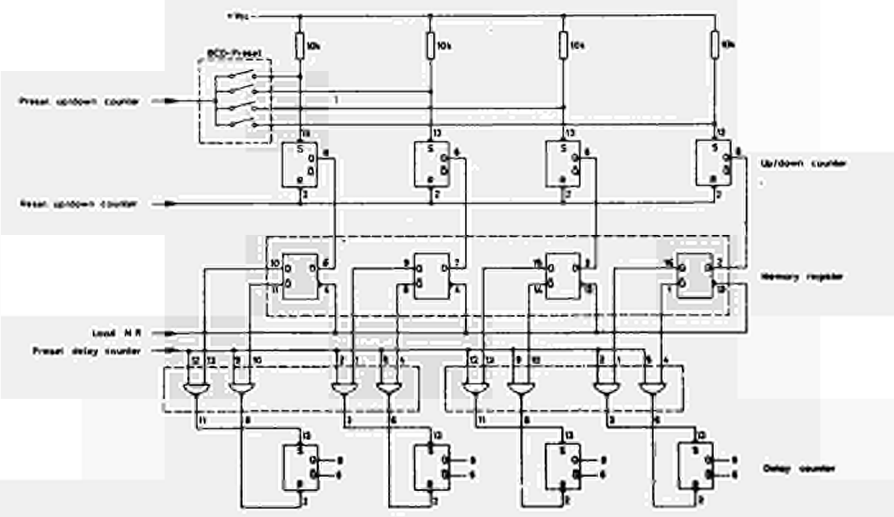

Fig. 4 - Delay generator, block diagram of connections between the registers, one decade shown.

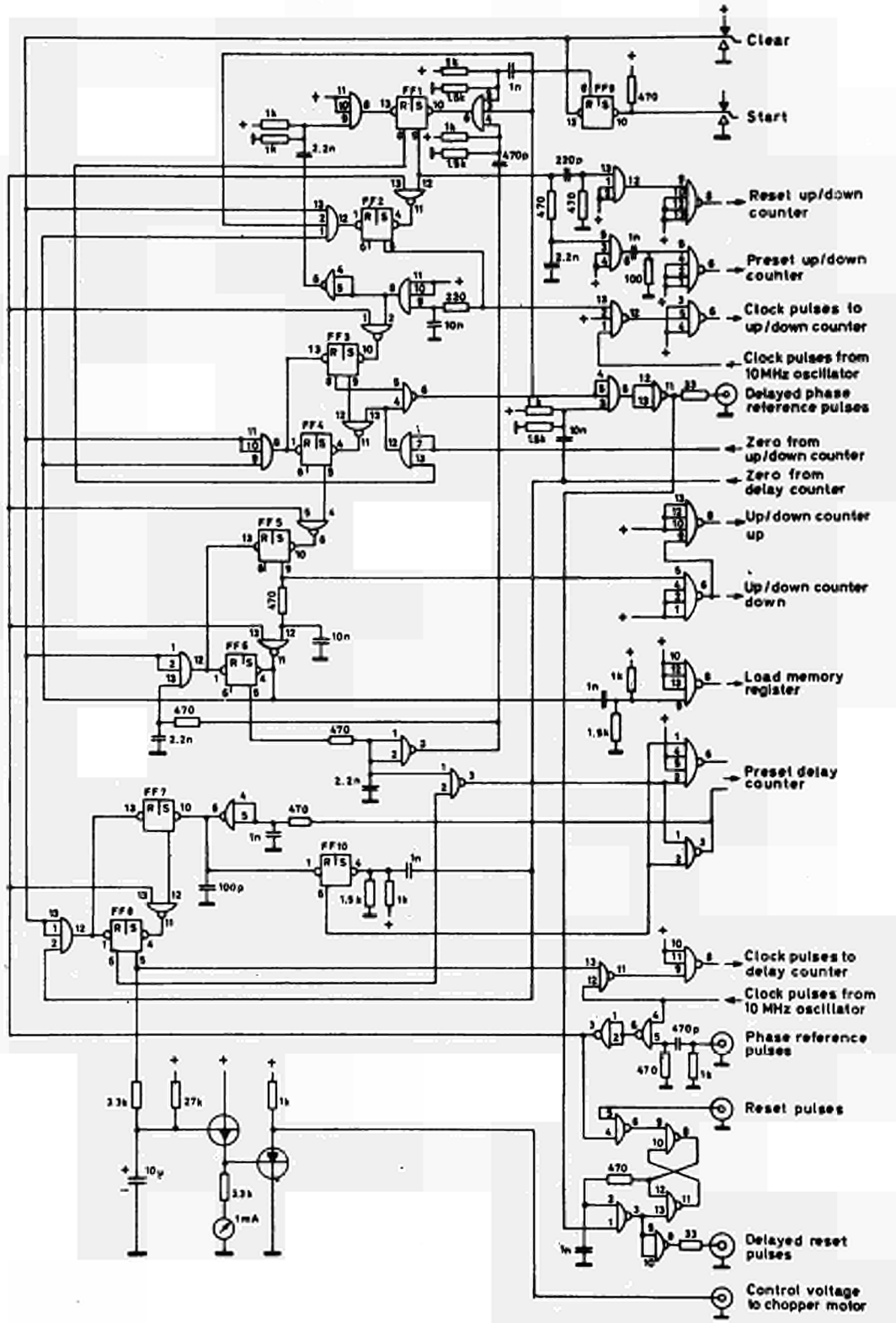

Fig. 5. Delay generator, block diagram of control logic.

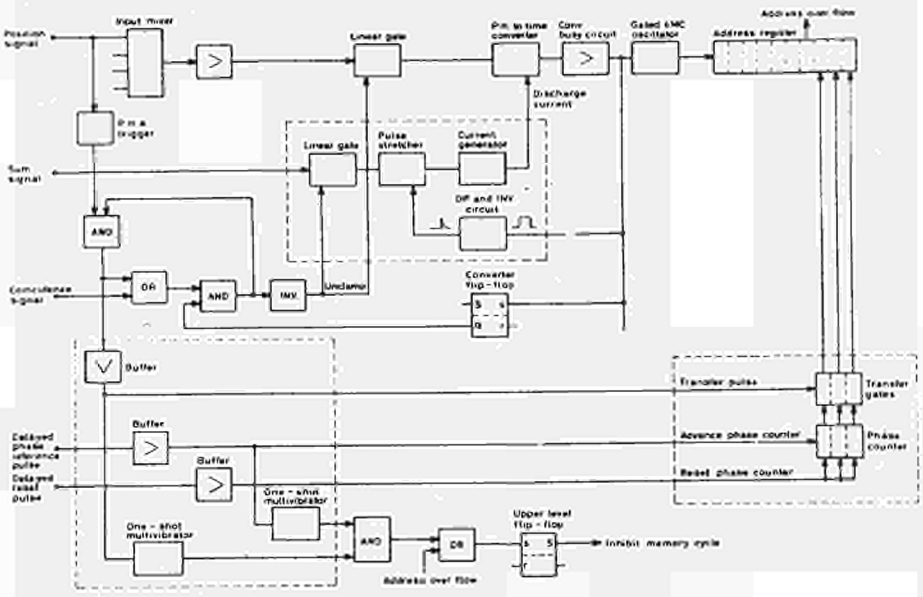

Fig. 6.

1024-channel analyser, simplified block diagram of circuits used for position and phase analysis. The circuits added to the original design are surrounded by a dashed line.

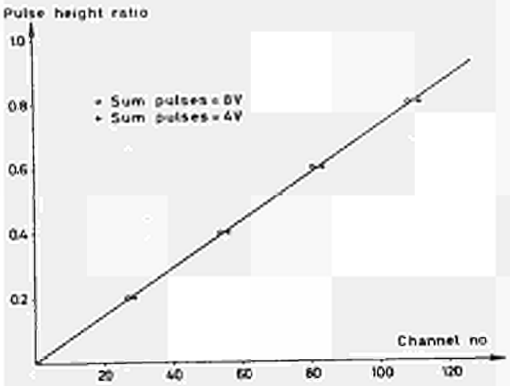

Fig. 7.

Result of linearity test on the pulse-ratio converter.

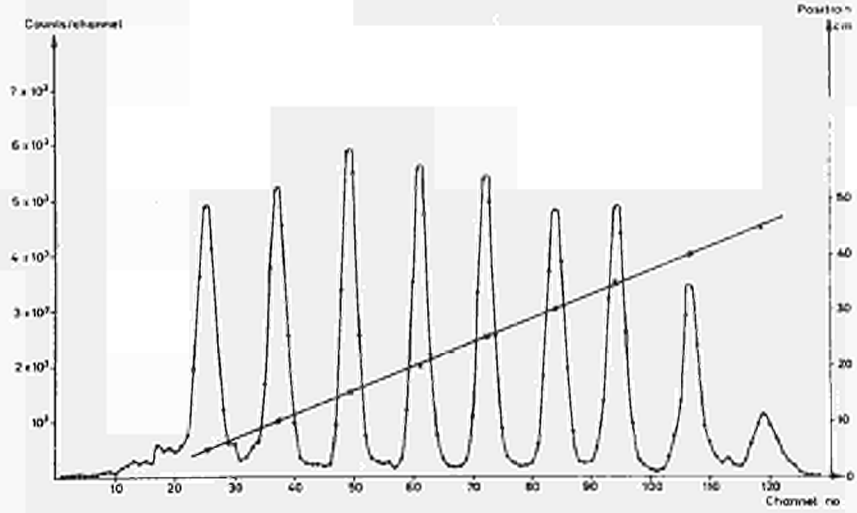

Fig. 8. Result of linearity test on the total position-analysis system by means of a 3 mm collimated beam of thermal neutrons.

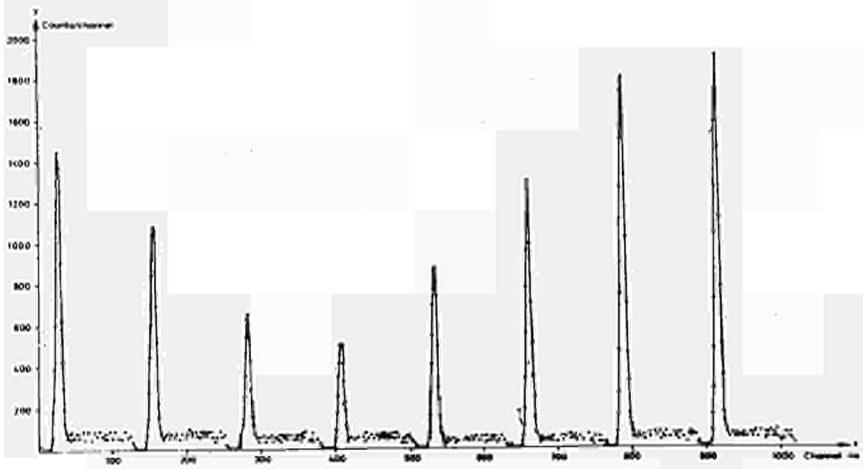

Fig. 9.

Scattering angle/phase spectrum. Flight path 4.45 m; modulation frequency 4444 Hz.

NOTICE TO THE READER

All Euratom reports are announced, as and when they are issued, in the monthly periodical **EURATOM INFORMATION,** edited by the Centre for Information and Documentation (CID). For subscription (1 year: US$ 15, £5.7) or free specimen copies please write to:

Handelsblatt GmbH
« Euratom Information »
Postfach 1102
D.4 Düsseldorf (Germany)

or

Centrale de vente des publications
des Communautés européennes
37, rue Glesener
Luxembourg

All Euratom reports are on sale at the offices listed below (when ordering, specify clearly the EUR number and the title of the report, which are shown on the internal title page).

CENTRALE DE VENTE DES PUBLICATIONS DES COMMUNAUTÉS EUROPÉENNES

37, rue Glesener, Luxembourg (Compte chèque postal N° 191-90)

BELGIQUE — BELGIË
MONITEUR BELGE
40-42, rue de Louvain - Bruxelles
BELGISCH STAATSBLAD
Leuvenseweg 40-42 - Brussel

DEUTSCHLAND
BUNDESANZEIGER
Postfach - Köln 1

FRANCE
SERVICE DE VENTE EN FRANCE
DES PUBLICATIONS DES
COMMUNAUTÉS EUROPÉENNES
26, rue Desaix - Paris 15e

ITALIA
LIBRERIA DELLO STATO
Piazza G. Verdi, 10 - Roma

LUXEMBOURG
CENTRALE DE VENTE
DES PUBLICATIONS DES
COMMUNAUTÉS EUROPÉENNES
37, rue Glesener - Luxembourg

NEDERLAND
STAATSDRUKKERIJ
Christoffel Plantijnstraat - Den Haag

UNITED KINGDOM
H.M. STATIONERY OFFICE
P.O. Box 569 - London S.E.I.

DM 48	FB 600	FF 60	Lit. 7 500	Fl. 43,50	$ 12